

KUVEMPU  **UNIVERSITY**

Department of P.G. Studies and Research in Chemistry,
Jnanasahyadri, Shankaraghatta-577451

Thesis submitted to the Faculty of Science, Kuvempu University

For the award of

DOCTOR OF PHILOSOPHY IN CHEMISTRY

**“Synthesis and biological evaluation of some new
heterocyclic compounds containing Nitrogen and Oxygen
atoms”**

Submitted by

Ms. Sukanya S.H. M.Sc.

Research Scholar

Department of P.G. Studies and Research in Chemistry,
Kuvempu University, Jnanasahyadri,
Shankaraghatta-577451

Under the guidance of

Dr. Talavara Venkatesh M.Sc., Ph.D.

Assistant Professor

Department of P.G. Studies and Research in Chemistry,
Kuvempu University, Jnanasahyadri,
Shankaraghatta-577451

2022

KUVEMPU  **UNIVERSITY**

Department of P.G. Studies and Research in Chemistry,
Jnanasahyadri, Shankaraghatta-577451

Thesis submitted to the Faculty of Science, Kuvempu University

For the award of

DOCTOR OF PHILOSOPHY IN CHEMISTRY

**“Synthesis and biological evaluation of some new
heterocyclic compounds containing Nitrogen and Oxygen
atoms”**

Submitted by

Ms. Sukanya S.H. M.Sc.

Research Scholar

Department of P.G. Studies and Research in Chemistry,
Kuvempu University, Jnanasahyadri,
Shankaraghatta-577451

Under the guidance of

Dr. Talavara Venkatesh M.Sc., Ph.D.

Assistant Professor

Department of P.G. Studies and Research in Chemistry,
Kuvempu University, Jnanasahyadri,
Shankaraghatta-577451

2022

Ms. Sukanya S.H. M.Sc.

Research Scholar

Department of P.G. Studies and Research in Chemistry,

Kuvempu University, Jnanasahyadri,

Shankaraghatta-577451

Email: sukanyash8@gmail.com

DECLARATION

I hereby declare that the research work presented in this thesis entitled **“Synthesis and biological evaluation of some new heterocyclic compounds containing Nitrogen and Oxygen atoms”** is submitted to the department of Chemistry, Kuvempu University for the award of the degree of **Doctor of Philosophy in Chemistry** is a bonafide research work carried out by me under the supervision of **Dr. Talavara Venkatesh**, Assistant Professor, Department of Chemistry, Kuvempu University, Jnanasahyadri, Shankaraghatta, Shimoga-577541.

I further declare that, the contents presented in this thesis or any part thereof has not been submitted elsewhere for any other degree, diploma of similar title in any other universities.

Date: 17/11/2022

Place: Shankaraghatta

Sukanya S.H.
Ms. SUKANYA S. H.

KUVEMPU UNIVERSITY

Dr. TALAVARA VENKATESH M.Sc., Ph.D.
Assistant Professor

Department of P.G. Studies and
Research in Chemistry, Jnanasahyadri,
Kuvempu University,
Shankaraghatta-577451
Shivamogga (Dist), Karnataka, INDIA
Mobile No: +917259417026
Email: venkateshatalwar@gmail.com

CERTIFICATE

This is to certify that the work reported in this thesis entitled “**Synthesis and biological evaluation of some new heterocyclic compounds containing Nitrogen and Oxygen atoms**” submitted by **Ms. Sukanya S.H.**, to the Faculty of Science, Kuvempu University, for the award of **Doctor of Philosophy in Chemistry** is a record of the bonafide and original research work carried out by her under my guidance and direct supervision. The work reported in this thesis has not formed the basis for the award of any degree or diploma or any other similar title in any institution or university.

Date: 17/11/2022

Place: Shankaraghatta



Dr. TALAVARA VENKATESH

(Research Supervisor)

ACKNOWLEDGEMENT

It gives me great pleasure to acknowledge all the persons who came in contact in the way with helping hands, during my research tenure.

At this moment of accomplishment, first of all I pay extremely indebted to my advisor **Dr. Talavara Venkatesh**, Assistant Professor, Department of P.G. Studies and Research in Chemistry, Kuvempu University, Jnanasahyadri, Shankaraghatta-577451, for his guidance and support. I am grateful to him for giving an opportunity to work under his team and it is with high regards that, I thank him for his inspiring guidance, endless encouragement and constructive criticism during my stay in his research group.

I would like to express my special thanks to **Prof. Y. Arthoba Nayaka**, Chairman, Department of P.G. Studies and Research in Chemistry, Kuvempu University, Jnanasahyadri, Shankaraghatta, for providing his fullest support which led to complete my work.

It is my pleasure to thank **Prof. Yadav D. Bodke** and **Prof. J. Keshavayya**, Professor, Department of P.G. Studies and Research in Chemistry, Kuvempu University, Jnanasahyadri, Shankaraghatta, for their kind cooperation during my research work. I also thank all the Faculty members of Department of Chemistry, Kuvempu University, Jnanasahyadri, Shankaraghatta, for their constant encouragement.

I am lovingly acknowledging the moral support of my mother **Dr. Renukamma** and my brother **Pradeep S.H.** who put the fundamental learning character, their valued education, inseparable support, prayers and spent hours with my research work and helping me with my studies. I also thank all my family members for their constant encouragement throughout my career.

I am very much thankful to my research group **Upendranath K, Priyarani R.S, Megha G.V, Manjunatha B, Navneethgowda P.V, Anjan Kumar G.C** and **Dr. Nagaraj O**, for their kind co-operation and encouragement during the course of my research work.

I would like to express my thanks to teaching and non-teaching staffs of Department of Chemistry, Kuvempu University for their support during my research period.

I am very much thankful to **Aditya Rao S.J**, Kimberlite chemicals India Pvt. Ltd, KIADB III Phase, Doddaballapur, Bangalore-561203, Karnataka, India, **Ravi Kumar S**, Department of Biotechnology Kuvempu University and **Shanavaz H**, Department of Chemistry, Faculty of engineering and technology, Jain University, who helped in evaluating the molecular docking and ADME-T studies. I also thank to **Anup Pandith**, Assistant Professor, Taipei Medical University, **Muthipeedika Nibin Joy**, Senior Researcher, Ural Federal University and **N. Shivakumara**, Department of Chemistry, Ramaiah Institute of Technology, who helped in evaluating the DFT and DNA binding studies for my research work.

I wish to extend my sincere thanks to my wonderful primary and high school teachers respectively who inspired me to study.

I am very much grateful to SAIF, Mysore University, Karnataka University, Dharwad and Mangalore University, Mangalagangothri, Karnataka for providing the spectral data. I also thankful to Department of Microbiology, Maratha Mandal's NGH Institute of Dental Sciences & Research Centre, Belgaum, Karnataka and LAYA Workstation, Haveri and Alekhya agro solutions, Mysore for their support in getting biological studies.

I thank to **Kuvempu University** for providing all facilities for the completion of my research work. I also thankful to **OBC fellowship, Government of Karnataka**, for providing financial support to carry out the research work.

Last but not the least I would like to render my great fullness for all **my beloved friends**, who co-operated with us to best possible extent.

Ms. SUKANYA S.H.



Dedicated to....

*Respected guide, my beloved
parents, lecturers, friends
and all my supportives.*

CONTENTS

	Page No.
Chapter-1: Introduction	1-33
1.1. Benefits of synthetic drugs	3
1.2. Pyrimidine	4
1.2.1. Electrophilic and nucleophilic substitution on pyrimidine nucleus	5
1.2.2. Biological significance of pyrimidine derivatives	6
1.2.3. Pharmaceuticals importance of pyrimidine derivatives	8
1.2.4. Antibacterial agent	10
1.2.5. Antifungal agent	11
1.2.6. Antiviral agent	12
1.2.7. Anticancer agent	13
1.2.8. Anti-inflammatory agent	14
1.2.9. Anti-mycobacterial agent	15
1.2.10. Antioxidants	15
1.2.11. Anti- HIV agent	16
1.2.12. Anticonvulsant and Anti-Depressants	17
1.2.13. Anti-malarial agent	17
1.3. Isoxazole	18
1.3.1. Electrophilic substitution on isoxazoles	19
1.3.2. Significance of isoxazole derivatives	19
1.3.3. Antibacterial agent	20
1.3.4. Antifungal agent	21
1.3.5. Antiviral agent	22
1.3.6. Anticancer agent	23
1.3.7. Anti-inflammatory agent	24
1.3.8. Anti-mycobacterial agent	25
1.3.9. Antioxidants	25
1.3.10. Anti- HIV agent	26
1.3.11. Anti-Depressant and Antianxiety agent	27
1.4. Plan of work	28
1.5. References	29

Chapter-2:	34-66
Section-2A: Facile TiO₂ NPs catalyzed synthesis of substituted-4-hydroxy/methoxy benzylidene derivatives as potent antioxidant and anti-tubercular agents	
2A.1. Introduction	34
2A.2. Present work	38
2A.3. Experimental	45
2A.4. Absorption property	49
2A.5. Pharmacological studies	50
2A.6. Results and discussion	52
2A.7. Conclusion	64
2A.8. References	65
Section-2B: Facile synthesis of some 5-(3-substituted-thiophene)-pyrimidine derivatives and their pharmacological and computational studies	67-99
2B.1. Introduction	67
2B.2. Present work	70
2B.3. Experimental	76
2B.4. Absorption property	78
2B.5. Pharmacological studies	79
2B.6. Results and discussion	82
2B.7. Conclusion	96
2B.8. References	97
Chapter-3:	100-136
Efficient L-Proline catalyzed synthesis of some new (4-substituted-phenyl)-1,5-dihydro-2H-pyrimido[4,5-<i>d</i>][1,3]thiazolo[3,2<i>a</i>]-pyrimidine-2,4(3<i>H</i>)-diones bearing thiazolopyrimidine derivatives and evaluation of their pharmacological activities	
3.1. Introduction	100
3.2. Present work	106
3.3. Experimental	114
3.4. Pharmacological studies	118
3.5. Results and discussion	120
3.6. Conclusion	132

3.7. References	133
Chapter-4:	137-180
Section-4A: An efficient <i>p</i>-TSA catalyzed synthesis of some new substituted-(5-hydroxy-3-phenylisoxazol-4-yl)-1,3-dimethyl-1<i>H</i>-chromeno[2,3-<i>d</i>]pyrimidine-2,4(3<i>H</i>,5<i>H</i>)-dione derivatives and evaluation of their pharmacological and computational investigations	
4A.1. Introduction	137
4A.2. Present work	141
4A.3. 2D ¹ H - ¹³ C HSQC NMR	148
4A.4. Experimental	150
4A.5. Electronic absorption study	153
4A.6. Powder-XRD analysis	156
4A.7. Pharmacological studies	157
4A.8. Results and discussion	160
4A.9. Conclusion	176
4A.10. References	177
Section-4B: An efficient <i>p</i>-TSA catalyzed synthesis of some new substituted-(5-hydroxy-3-phenylisoxazol-4-yl)-3,3-dimethyl-2<i>H</i>-xanthen-1(9<i>H</i>)-one scaffolds and evaluation of their pharmacological and computational investigations	181-215
4B.1. Introduction	181
4B.2. Present work	184
4B.3. 2D ¹ H - ¹³ C HSQC NMR	190
4B.4. Experimental	192
4B.5. Electronic absorption study	195
4B.6. Powder-XRD analysis	198
4B.7. Pharmacological studies	199
4B.8. Results and discussion	199
4B.9. Conclusion	212
4B.10. References	213

Chapter-5:	216-259
Synthesis, <i>in-vitro</i> evaluation and docking studies of novel 6-amino-4-substituted-pyrano[3,2-<i>d</i>]isoxazole-5-carbonitrile derivatives as potential anti-diabetic and anticancer agents	
5.1. Introduction	216
5.2. Present work	221
5.3. Experimental	228
5.4. Absorption property	233
5.5. Pharmacological studies	235
5.6. Results and discussion	236
5.7. Conclusion	256
5.8. References	257
 Chapter-6:	 260-290
Section-6A: Synthesis, <i>in-vitro</i> evaluation, docking and ADME studies of novel 5-[3-(4-chlorophenyl)-substituted-6-hydroxypyrimidine-2,4(1<i>H</i>,3<i>H</i>)-dione derivatives as potential anti-diabetic and anticancer agents	
6A.1. Introduction	260
6A.2. Present work	263
6A.3. Experimental	270
6A.4. Absorption property	273
6A.5. Pharmacological studies	274
6A.6. Results and discussion	274
6A.7. Conclusion	288
6A.8. References	289
 Section-6B: Synthesis, <i>in-vitro</i> evaluation, docking and ADME studies of novel 5-[3-(4-chlorophenyl)-substituted-1,3-dimethylpyrimidine-2,4,6(1<i>H</i>,3<i>H</i>,5<i>H</i>)-trione derivatives as potential anti-diabetic and anticancer agents	 291-319
6B.1. Introduction	291
6B.2. Present work	294
6B.3. Experimental	299
6B.4. Absorption property	302
6B.5. Pharmacological studies	303

6B.6. Results and discussion	303
6B.7. Conclusion	317
6B.8. References	318
Chapter-7:	320-345
Synthesis, characterization and biological evaluation of some new 2-[(4-hydroxy-6-methylpyrimidin-2-yl)amino]-1-(4-substituted)ethanone derivatives.	
7.1. Introduction	320
7.2. Present work	324
7.3. Experimental	330
7.4. Pharmacological studies	332
7.5. Results and discussion	332
7.6. Conclusion	343
7.7. References	344
List of Publications	346-348

1. Introduction

Synthetic organic chemistry is the branch of chemistry which deals with the study of building-up bioactive-organic compounds from smaller entities. It has found application in the preparation of novel, potential and commercially active compounds [1]. Organic synthesis plays an important role in chemistry, biochemistry, medicine, agriculture, molecular biology, physics, materials science, electronics and engineering field by allowing for the creation of specific molecules for scientific and technological investigations. The heart of organic synthesis is designing synthetic routes and strategies for the synthesis of bioactive molecules [2].

Heterocyclic chemistry is dealing with the study of synthesis, properties and applications of heterocycles. A heterocyclic compound is a cyclic compound that has atoms of at least two different elements as members of in its rings. Although heterocyclic compounds may be inorganic, most contain at least one carbon. Since in organic chemistry non-carbons like oxygen, nitrogen and sulphur usually are considered to replace carbon atoms, they are called heteroatom [3].

Heterocyclic compounds are widely distributed in nature. They are essential to life and play vital role in the metabolism of the living cells. Most of the sugars such as glucose, fructose, sucrose and their derivatives exist largely in the form of five membered or six membered rings containing one oxygen atom. Most members of the vitamin B group *viz* thiamine (vitamin B1), riboflavin (vitamin B2), niacin (vitamin B3), pantothenic acid (vitamin B5), pyridoxine (vitamin B6) and cobalamin (vitamin B12) possess one or more nitrogen containing heterocyclic rings. Pyrimidine and purine heterocyclic compounds are the base components of genetic material DNA. Most of the alkaloids which are nitrogenous bases occurring in plants and antibiotics including tetracyclines, sulfonamides and penicillin also contain heterocyclic ring systems. Synthetic heterocyclic compounds have valuable

properties as chemotherapeutic agents, drugs, dyestuffs, copolymers and energy materials etc [4].

Most of heterocyclic compounds which display the aromatic behaviour of benzene are called as aromatic heterocycles. Huckel's rule is followed by these compounds to state cyclization, conjugation and planar structures having $(4n+2) \pi$ electrons [5].

Heterocyclic compounds can be useful to classify based on their electronic structure. The saturated heterocycles behave like the acyclic derivatives [6, 7]. Thus, piperidine and tetrahydrofuran are used as conventional amines and ethers, with modified steric profiles. Therefore, the study of heterocyclic chemistry focuses especially on unsaturated derivatives and the superiority of work and applications involves unstrained five and six-membered rings such as thiophene, pyrrole, furan, isoxazole, pyridine and pyrimidine etc [8]. Another large class of heterocycles are fused to benzene ring, which are quinoline, benzothiophene, indole and benzofuran etc [9].

Synthesis of heterocycles has evolved as a powerful tool for producing new compounds applicable for drug invention. Heterocycles forms scaffolds of potent and selective pharmacophores [10]. Heterocyclic compounds containing two nitrogen atoms such as pyrimidine, pyrazole, imidazole exhibited important biological properties. The nitrogen and oxygen containing heterocyclic compounds such as isoxazole and phenylisoxazole achieved a great importance in pharmacological field. They are obtained from various natural resources and synthetic reactions. Among the privileged class of various heterocyclic compounds, nitrogen and oxygen derivatives are key moieties in medicinal chemistry. They have drawn much attention due to its biological properties like antimicrobial, antidiabetic, herbicidal, anticancer, anti-TB, antibiotics, anti-inflammatory, antidepressant and anti-HIV etc [11, 12] as well as photophysical properties such as latent fingerprints (LFPs), opto-electronics, fluorescence sensors and energy materials [13, 14].

Role of multicomponent reactions (MCRs) in synthesis of heterocyclic compounds

Multi-component reactions (MCRs) afford an exceptionally valuable tool within the field of synthetic and medicinal chemistry. They are upstanding as tool for synthesizing polyfunctional molecules with high competence over multistep synthesis. Globally, it has been explored as an efficient tool for preparing several active drugs [15]. MCRs offer many advantages such as they avoid unnecessary purification, wastages, byproducts, toxic reagents, solvents consumption and they also followed the easy workup, shorter reaction time high atom economy and cost effectiveness [16].

1.1. Benefits of synthetic drugs

Synthetic heterocyclic products have delight in a long history of consumption, frequently proposing solo resource and uses, the notable gains of unnaturally developed compounds are,

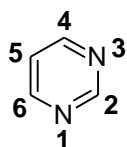
- Accessible in uncontaminated forms
- Developed stroke because of reformed compounds structures
- Protracted living half-life
- Enhanced corpulent solubility
- Superior drug deliberation
- Cost effective products
- Knowledge of manufacturing conditions
- Strong hold in the manufacturing process [17]

In view of these facts, we have synthesized some novel nitrogen and oxygen containing derivatives and investigated their biological and computational studies.

Nitrogen containing heterocyclic compounds

1.2. Pyrimidine

Pyrimidine is a six membered heterocyclic aromatic compound containing two nitrogen atoms at 1, 3- position of the ring. It is a colourless compound, having molecular formula of $C_4H_4N_2$ and molecular weight of 80.09 g/mol having melting point 22.5 °C and boiling point 124 °C. In pyrimidine ring has less π -electron density develops less energy; therefore electrophilic substitution is more difficult while nucleophilic substitution is facilitated. It is a weaker base than pyridine & imidazole as addition of a proton does not increase the resonance energy. In pyrimidine N-alkylation and N-oxidation are difficult as compared to pyridine. The pK_a value for protonated pyrimidine is 1.23, it is less basic than pyridine ($pK_a=5.23$). Only one nitrogen atom of the pyrimidine can be alkylated by alkylating agent, but with triethyloxoniumborofluoride both nitrogen atoms can be alkylated.

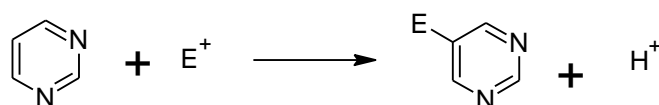


Pyrimidine has been great attention to organic researcher due to their wide range of chemical and pharmacological properties. It is abundant in many natural products, antibiotics such as pyrimethamine, trimethoprim, triflouridine, idoxuridine and propylthiouracil etc. It is a part of nucleic acids, RNA and DNA, which are the most commonly recognized pyrimidine bases. Moreover DNA which is the transporter of genetics covers the nitrogen incorporated heterocyclic adenine and guanines are purine bases, as well as cytosine and thymines are pyrimidine bases. Uracil in RNA involves the pyrimidine base. The most important functional groups of pyrimidine ring are nitrogen, carbonyl group and exocyclic amino group. Hydrogen bond interactions involving the amino and carbonyl groups are the second important mode of interaction between bases. Hydrogen bonds between bases permit a

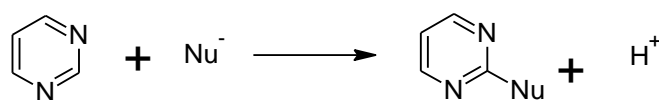
complementary association of two and occasionally three strands of nucleic acids [18]. Pyrimidine incorporated heterocycles have remarkable applications in pharmacological and substantial sciences [19].

1.2.1. Electrophilic and nucleophilic substitution on pyrimidine nucleus

Electrophiles mainly attacks at C-5 position which is least electron leaving site on pyrimidine ring.



Nucleophilic attacks at C-2, C-4 & C-6 position on pyrimidine ring with the negative charge of the intermediate delocalised over both nitrogen atoms.



Common methods for the synthesis of pyrimidine derivatives

I. Knoevenagel condensation reaction

German chemist, Emil Knoevenagel synthesized α,β -unsaturated compounds by the reaction of condensation between an aldehyde/ketone with an active methylene compound in the presence of basic catalyst or Lew's acid (**Fig. 1**) [20].

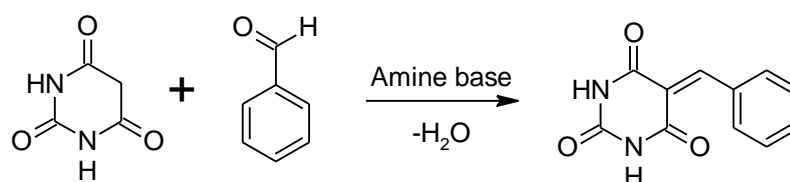


Fig. 1. Knoevenagel condensation reaction.

II. Biginelli-type/ Traube-Schwartz reaction

In 1899, Traube and Schwartz reported multicomponent reaction of ethyl acetoacetate, aryl aldehyde and urea/amine to produce 3,4-dihydropyrimidin-2(1*H*)- ones (**Fig. 2**) [21].

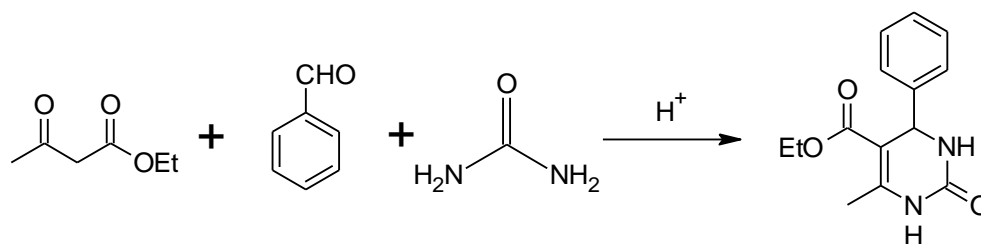


Fig. 2. Biginelli-type/ Traube-Schwartz reaction.

III. Michael addition reaction

American organic chemist, Arthur Michael discovered the Michael addition reaction. It is a nucleophilic addition reaction involving the addition of a carbanion or nucleophile to an α,β -unsaturated carbonyl compound, which is electron-withdrawing in nature to form a new carbon-carbon bonds. Carbanion is the Michael donor and alkene is the Michael acceptor (**Fig. 3**) [22].

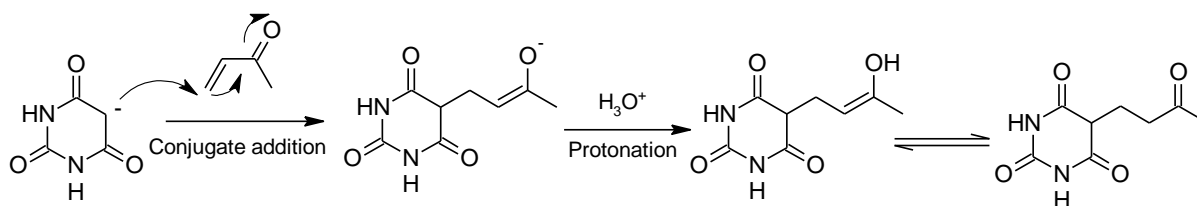
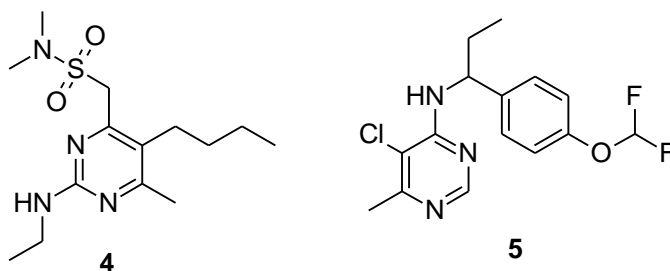


Fig. 3. Michael addition reaction.

1.2.2. Biological significance of pyrimidine derivatives

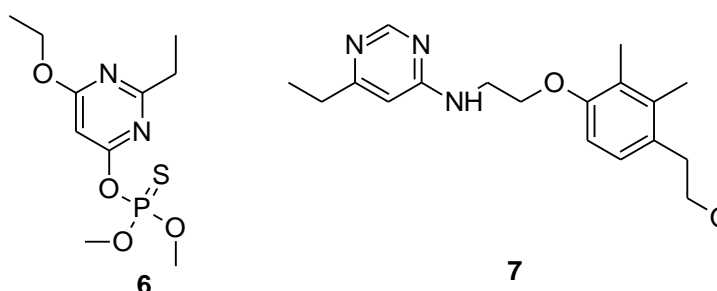
1.2.2.1. Fungicidal agents

The compounds were used to kill or inhibit the growth of fungi or fungal spores are known as fungicides. Bupirimate (**4**) is a fungicide and it belongs to the chemical family of pyrimidine sulfamates. It is used to treat a variety of fungal infections, mainly inhibiting sporulation and control of powdery mildew of fruits, roses, ornamental flowers and other crops [23]. Diflumetorim (**5**) is another fungicide and used to control the white rust (*Puccinia horiana*) and inhibits the fungal growth from germination of conidiophores [24].



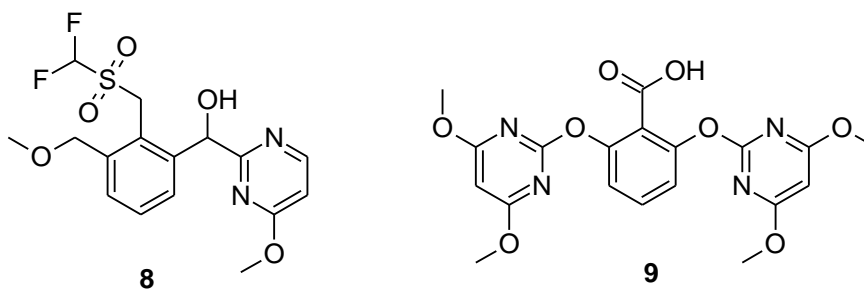
1.2.2.2. Insecticidal agents

The chemical substance used to control or kill the pest population in crops is known as insecticides. Heterocycles are high potential towards insecticidal activity. Etrimphos (**6**) is an organophosphate pyrimidine insecticide and also called “Satisfar”. It is used to control of *Acarus siro* (Flour mites) and *Glycyphagus destructor* (Long hairy mites) from crops [25]. Pyrimidifen (**7**) is an insecticide and it is used to control the mites on fruits and vegetables, mainly control the spider mites, African red mites and diamondback moth in citrus, strawberries, tomatoes, apples and vegetables etc [26].



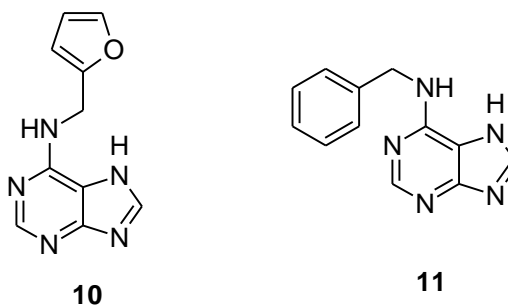
1.2.2.3. Herbicidal agents

Pesticides used to kill the unwanted plants are known as herbicides. They are also known as weed killer. Pyrimisulfan (**8**) is a herbicide used for pre and post-emergence weed control in turf, broadleaf, sedge and kyllinga species [27]. Bispyribac (**9**) is a post-emergence herbicide; it is used to control grasses, sedges and broad-leaved weeds in paddy rice and other crops [28].



1.2.2.4. Growth regulators

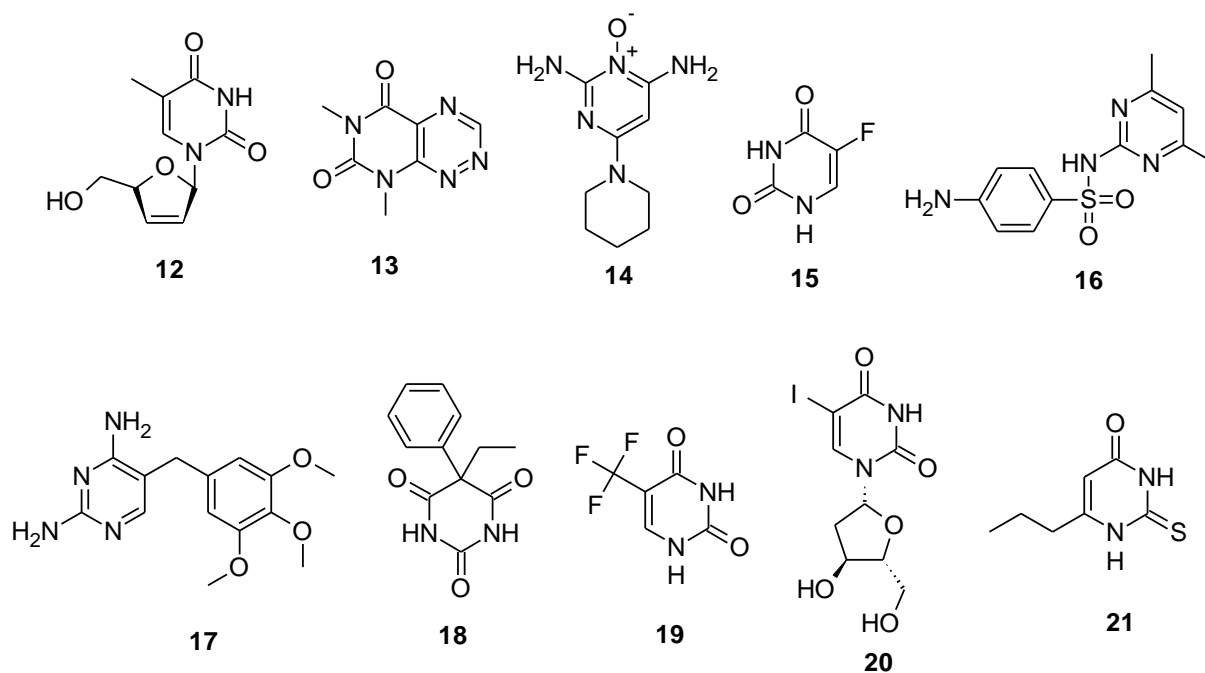
The chemical substances were used to influence the development of cells, tissues and organs in plants are known as growth regulators. Heterocyclic compounds are recognized as agrochemicals growth regulators. Kinetin (**10**) containing a pyrimidine nucleus, it is a type of cytokinin and come under class of plant hormone. It has ability to induce cell division; hence, it is used in plant tissue culture [29]. Benzyladenine (**11**) is a first generated synthetic cytokinin, it stimulate the plant growth by cell division and act as an inhibitor of respiratory kinase in plants and increases post-harvest life of green vegetables [30].



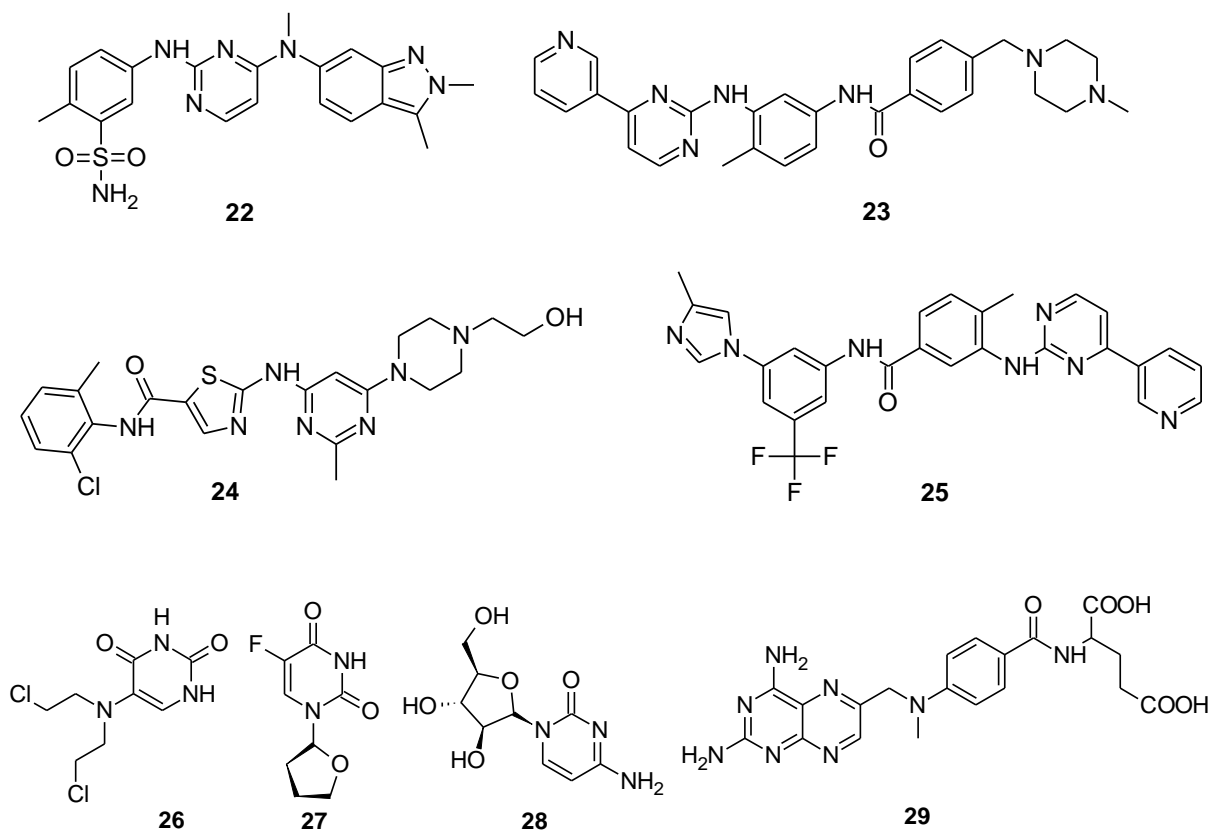
1.2.3. Pharmaceuticals importance of pyrimidine derivatives

Some of the drugs available in the market that have pyrimidine analogs in their rings are used for treatment of several disorders. For example, stavudine (**12**) is used as anti-HIV agent, fervernuline (**13**) as antibiotic, minoxidil (**14**) is used as antihypertensive agent, 5-flourouracil (**15**) is used for treatment of cancer, sulfamethiazine (**16**) & trimethoprim (**17**) are used for treatment against bacterial diseases. Also phenobarbitone (**18**) is used as a sedative-hypnotic as well as anticonvulsant agent, triflouridine (**19**) & idoxuridine (**20**) are

used in treatment of various viral infections and propylthiouracil (**21**) is used as antithyroid agent [31].



Triazolopyrimidines, pyridopyrimidines, pteridines, purines, furopyrimidines, pyrimidoazepines, pyrrolopyrimidines and quinazolines are a class of fused pyrimidine scaffolds that exhibit good pharmacological properties. Hence, improve the activity of heterocyclic compounds by fusing the pyrimidine analogs with different heterocyclic moieties [32]. Many fused pyrimidines have been used as cancer therapy against various types of cancers as approved by the US Food and Drug Administration. Pazopanib (**22**), imatinib (**23**), dasatinib (**24**), nilotinib (**25**), uramustine (**26**), tegafur (**27**), cytarabine (**28**) and methotrexate (**29**) are a few examples of drugs that contain pyrimidine nucleus used as anticancer agents.

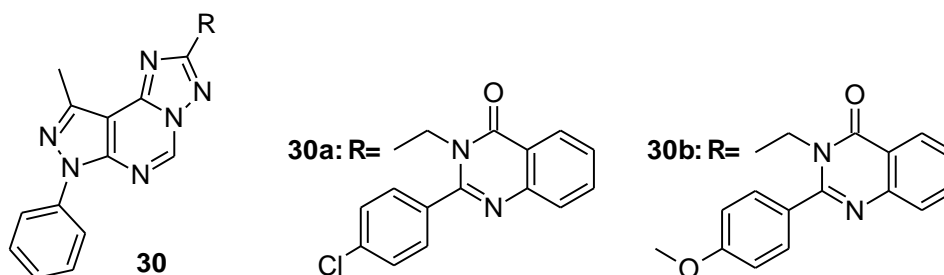


By considering these recent findings, researchers are focusing on the synthesis of new fused pyrimidine analogs and screening them against various biological activities [33, 34]. In medicinal chemistry, pyrimidine derivatives have been recognized for their therapeutic applications. During the last few decades, several pyrimidine derivatives have been developed as chemotherapeutic agents and have found wide clinical applications. Some of the reported bio-active pyrimidine derivatives are discussed below.

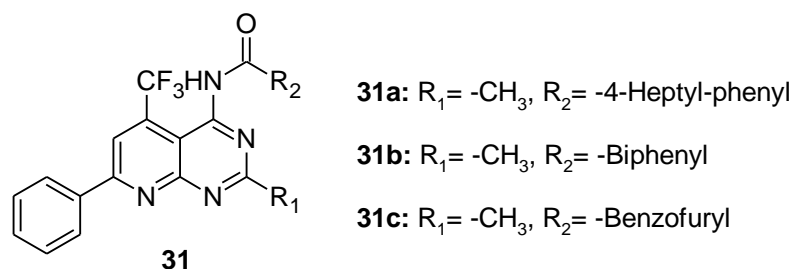
1.2.4. Antibacterial agents

In 2020, M. Horchani *et al.*, reported a series of new pyrazolo-triazolo-pyrimidine derivatives (**30**) as an antibacterial agent. The compounds were screened against four Gram-negative strains such as *E. coli*, *P. aeruginosa*, *P. mirabilis*, *C. freundii* and two Gram-positive strains *E. faecalis* and *S. aureus*. Among them, **30a** compound displayed MIC of 6.25 μM against *S. aureus* and 25 μM against *E. coli*, *P. aeruginosa*, *P. mirabilis* & *C.*

freundii. The compound **30b** showed a MIC of 12.5 μ M against *E. coli*, *P. aeruginosa* & *P. mirabilis* bacterial strains [35].

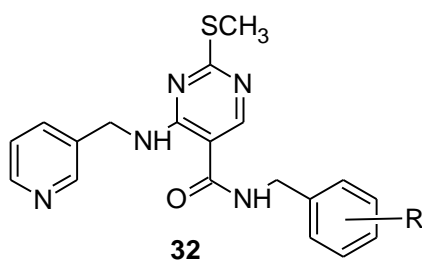


A series of novel pyrido[2,3-*d*]pyrimidine derivatives (**31**) were synthesized by B. Chandrasekaran *et. al.*, and screened for antibacterial activity. Among all the synthesized compounds, **31a**, **31b** & **31c** were displayed good antibacterial activity with MIC of 12.5 μ g/mL against *S. aureus* and *B. subtilis* [36].



1.2.5. Antifungal agents

A series of novel N-(substituted-phenyl/benzyl)-2-methylthio-4-((pyridin-3-ylmethyl)amino)pyrimidine-5-carboxamides (**32**) have been synthesized by S.C. Wang and co-authors in 2018. The compounds were screened for antifungal activity against two fungi such as *B. cinerea* and *S. Sclerotiorum*. Among all the derivatives, **32a**, **32b**, **32c** & **32d** exhibited good % of inhibition at 73, 71.6, 71.2 & 71.1 respectively against *B. cinerea*. The compounds **32b**, **32d**, **32e**, **32f** & **32g** displayed highest % of inhibition at 95.2, 96.7, 96.2, 96.6 & 96.1 respectively against *S. Sclerotiorum* [37].



32a: R= 4-CH₃

32b: R= 4-F

32c: R= 4-Cl

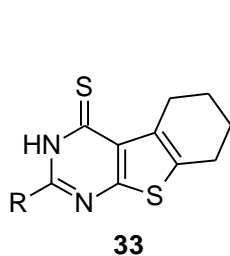
32d: R= 4-Br

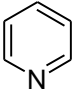
32e: R= H

32f: R= 4-CH(CH₃)₂

32g: R= 3-Cl

S.B. Bari and N.G. Haswani reported a series of thienopyrimidin-4(3*H*)-thiones (**33**) and evaluated *in vitro* antifungal activity against *C. albicans*, *A. niger* and *P. chrysogenum*. The compounds **33a**, **33b**, **33c** & **33d** exhibited potent antifungal activity with MIC value of 4, 2 & 2 µg/mL against *C. albicans*, *A. niger* and *P. chrysogenum* respectively [38].



33a: R= 

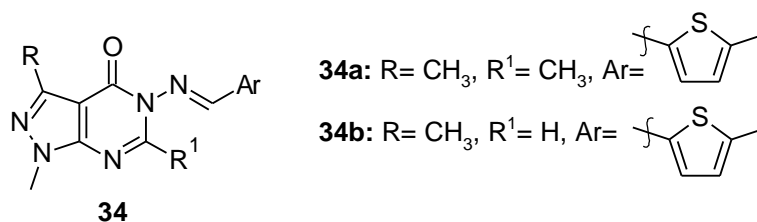
33b: R= S-C₂H₅

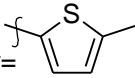
33c: R= S-C₄H₉

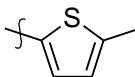
33d: R= SH

1.2.6. Antiviral agents

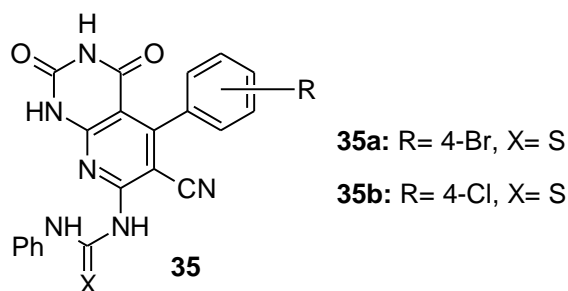
In 2018, Y.Y. Wang and co-authors reported a pyrazolo[3,4-*d*]pyrimidine derivatives (**34**) and evaluated for their antiviral activity against tobacco mosaic virus (TMV). The study results indicated that, compounds **34a** and **34b** displayed excellent antiviral activity against TMV with half maximal effective concentration (EC₅₀) values of 70.3 and 53.65 µg/mL respectively [39].



34a: R= CH₃, R¹= CH₃, Ar= 

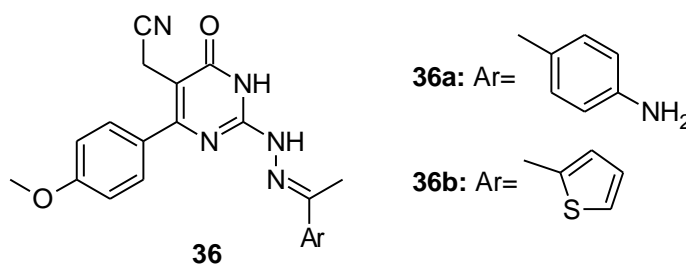
34b: R= CH₃, R¹= H, Ar= 

In 2002, a series of novel pyrido[2,3-*d*]pyrimidine derivatives (**35**) has been synthesized by M.N. Nasr *et. al.*, and investigated as an antiviral agent against herpes simplex virus (HSV). Among all the synthesized compounds, **35a** with 4-bromo & **35b** with 4-chloro substitution were exhibited most potent antiviral activity with least IC₅₀ values of 4 & 8 µg/mL respectively [40].



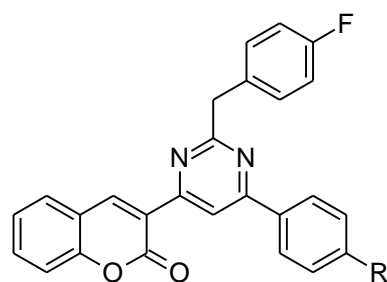
1.2.7. Anticancer agents

E.M. Abbass *et. al.*, synthesized a new series of pyrimidine derivatives (**36**) were demonstrated for cytotoxic activity against HepG2 and HCT116 cell lines. Compounds **36a** and **36b** showed a very strong efficacy against HepG2 cell line with IC₅₀ value of 8.76±0.9 µM & 11.31±1.2 µM respectively and also exhibited potent cytotoxicity against HCT-116 cell line with IC₅₀ value of 10.46±1.6 µM & 13.65±1.1 µM respectively [41].



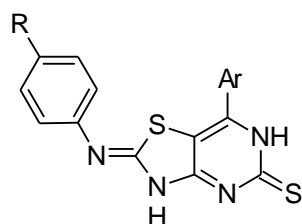
In 2015, a series of 3-(2-(4-fluorobenzyl)-6-(substituted phenyl) pyrimidin-4-yl)-2Hchromen-2-one derivatives (**37**) have been synthesized by K.M. Hosamani *et. al.*, and they were evaluated for their anticancer activity against two human cancer cell lines *viz.*, A-549 (human lung carcinoma) and MDA-MB-231 (human adenocarcinoma mammary gland). Among them, **37a** exhibited most potent activity against A-549 cell line with IC₅₀ value of

2.15±0.12 μM and **37b** was found to be extremely active against MDA-MB-231 cell line with IC_{50} value of 2.23±0.19 μM respectively [42].

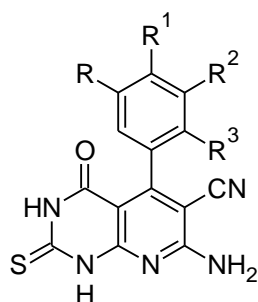
**37****37a:** R= Cl**37b:** R= OCH₃

1.2.8. Anti-inflammatory agents

A novel derivatives of thiazolo[4,5-*d*]pyrimidines (**38**) were synthesized by R.B. Bakr *et. al.*, reported as anti-inflammatory activity. In that, compound **38a** was the most active derivative with 57 %, 88 % and 88 % inhibition of inflammation after 1, 3 and 5 h, respectively as compared to standard drug celecoxib [43].

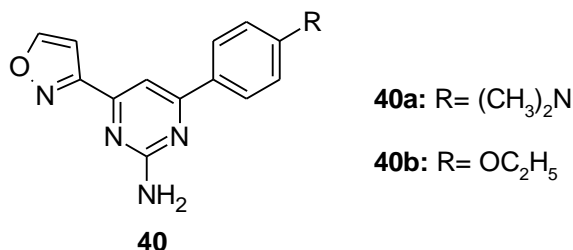
**38****38a:** R= COCH₃, Ar= NO₂-C₆H₄

In 2018, M.A. Abdelgawad and co-workers reported a series of tetrahydropyrido[2,3-*d*]pyrimidine-6-carbonitrile derivatives (**39**) as an anti-inflammatory agent. Among all the synthesized compounds, **39a** exhibited highest anti-inflammatory activity with 74 %, 76 % and 57 % inhibition after 1, 3 and 5 h respectively [44].

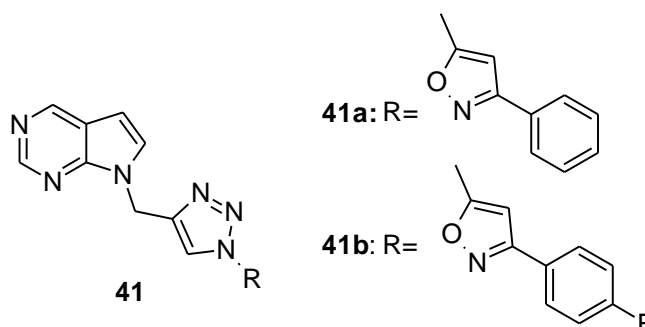
**39****39a:** R= OCH₃, R¹= OCH₃, R²= OCH₃, R³= H

1.2.9. Anti-TB agents

N. Pappula *et. al.*, reported a series of novel pyrimidine-linked isoxazole derivatives (**40**) and screened for their anti-mycobacterial activity. Compounds **40a** and **40b** showed excellent activity with MIC of 0.78 $\mu\text{g/mL}$, these compounds shows potent anti-TB activity than pyrazinamide (3.125 $\mu\text{g/mL}$) [45].

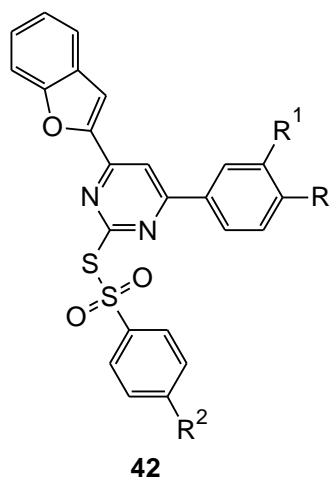


A series of novel 1*H*-pyrrolo[2,3-*d*]pyrimidine-1,2,3-triazole derivatives (**41**) have been synthesized by K.S. Raju *et. al.*, and reported as antimycobacterial agent. The compounds **41a** and **41b** were displayed excellent anti-TB efficacy with MIC of 0.78 $\mu\text{g/mL}$ [46].



1.2.10. Antioxidants

A series of benzofuran-gathered C-2,4,6-substituted pyrimidine derivatives (**42**) has been developed by J. Rangaswamy *et. al.*, and screened for anti-oxidant activity using *in vitro* assays such as DPPH and DMPD radical scavenging methods. The results showed that, the compounds **42a**, **42b**, **42c** and **42d** produced significant antioxidant activity with IC_{50} values of 8 & 15, 18 & 29, 10 & 18 and 24 & 22 μM for DPPH and DMPD radical scavenging activity respectively [47].



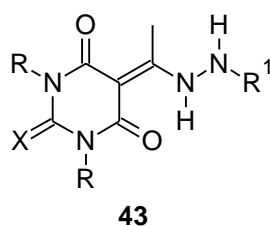
42a: R= OH, R¹= OCH₃, R²= OH

42b: R= OH, R¹= OCH₃, R²= OCH₃

42c: R= OH, R¹= H, R²= OH

42d: R= OH, R¹= H, R²= OCH₃

In 2018, J. Figueiredo *et al.*, synthesized a series of trisubstituted barbiturates and thiobarbiturates (**43**) and evaluated their antioxidant activity. Among the series, **43a**, **43b** & **43c** displayed potent DPPH radical scavenging activity with IC₅₀ values of 18.8, 20.4 & 23.8 μM respectively [48].



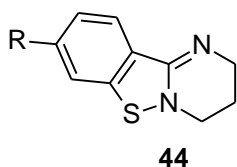
43a: X= O, R= CH₃, R¹= C₆H₅

43b: X= O, R= H, R¹= C₆H₅

43c: X= O, R= CH₃, R¹= 4-NO₂C₆H₄

1.2.11. Anti-HIV agents

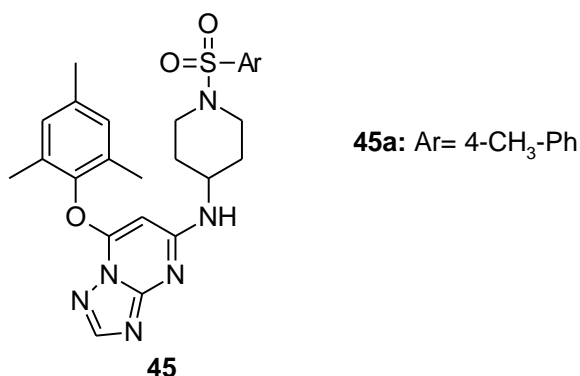
S. Okazaki and co-workers synthesized a series of novel benzo[4,5]isothiazolo[2,3-*a*]pyrimidine scaffolds (**44**) and reported as anti-HIV agents. Compound **44a** exhibited potent anti-HIV activity with least EC₅₀ (50 % effective concentration) value of 0.10±0.03 μM [49].



44a: R= *m*-anisyl

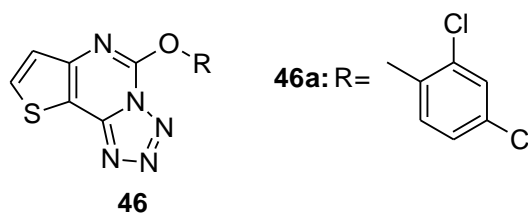
In 2021, a series of piperidiny-substituted [1,2,4]triazolo[1,5-*a*]pyrimidines (**45**) have been synthesized by B. Huang *et al.*, and evaluated their anti-HIV activity. Out of all the

synthesized compounds, **45a** was the most active compound and exhibited excellent anti-HIV efficacy with EC₅₀ value of 4.29 μM [50].



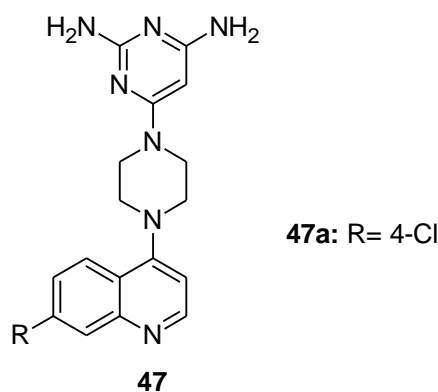
1.2.12. Anticonvulsant and Anti-depressants

A series of 5-alkoxytetrazolo[1,5-*c*]thieno[2,3-*e*]pyrimidine derivatives (**46**) were synthesized by S.B. Wang *et. al.*, and reported as anticonvulsant and antidepressant activities. Compound **46a** was recognized as most active compound, which decreased the immobility time by 51.62 % at a dose of 100 mg/kg [51].



1.2.13. Anti-malarial agents

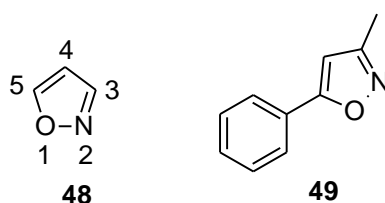
In 2013, S.I. Pretorius *et. al.*, synthesized a sequence of quinoline-pyrimidine hybrids (**47**) and reported as antimalarial agent against chloroquine-susceptible (CQS) D10 and chloroquine-resistant (CQR) Dd2 strains of *Plasmodium falciparum*. Out of all the compounds, **47a** was displayed potent efficacy with IC₅₀ value of 0.070±0.017 μg/mL against D10 and Dd2 strains [52].



Nitrogen and Oxygen incorporated heterocyclic compounds

1.3. Isoxazole

Isoxazole (**48**) is a five-membered electron-rich azole having two heteroatoms such as oxygen and nitrogen at 1 and 2 adjacent position of the ring. It is a yellow coloured compound, having molecular formula of C_3H_3NO and molecular weight of 69.06 g/mol having melting point 93-95 °C, boiling point 95 °C and pK_a value is -3.0 for conjugated acid. Two carbon-carbon double bonds contribute to the unsaturated property of the molecule. The structural features of isoxazole make it possible for multiple non-covalent interactions, especially hydrogen bonds (hydrogen bond acceptor N and O), pi-pi stack (unsaturated five-membered ring) and hydrophilic interactions [53]. Isoxazole was first discovered by Claisen in 1888 [54, 55] who synthesized the 3-methyl-5-phenylisoxazole (**49**) in 1903, by oxylation of propargylaldehyde acetal. Later, Quilico in 1946, who investigated the synthesis of the isoxazole ring by reaction of N-oxides with acetylenic compounds [56].

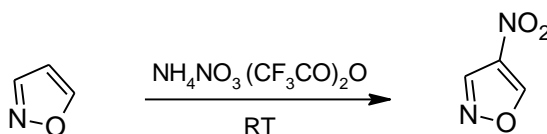


Isoxazole moieties represent a class of unique pharmacophores, it is abundant in many natural products include ibotenic acid, muscimol etc. It is a constituent units of diverse

therapeutic agents *viz* antimicrobial [57], anti-HIV [58], anti-TB [59], anti-inflammatory [60], anti-diabetic [61], anticancer [62], antidepressant [63], peptidase inhibitors [64] etc. Therefore, it attracted the attention of researchers in the development of new drug leads in pharmaceutical chemistry. Various methods to synthesize substituted isoxazoles have been published including approaches based on condensation of 1,3-dicarbonyl compounds with hydroxylamine [65] addition of nitrile oxides to supported alkynes [66], intermolecular cycloadditions [67] condensations [68] and intramolecular cyclizations of amino acids [69] etc.

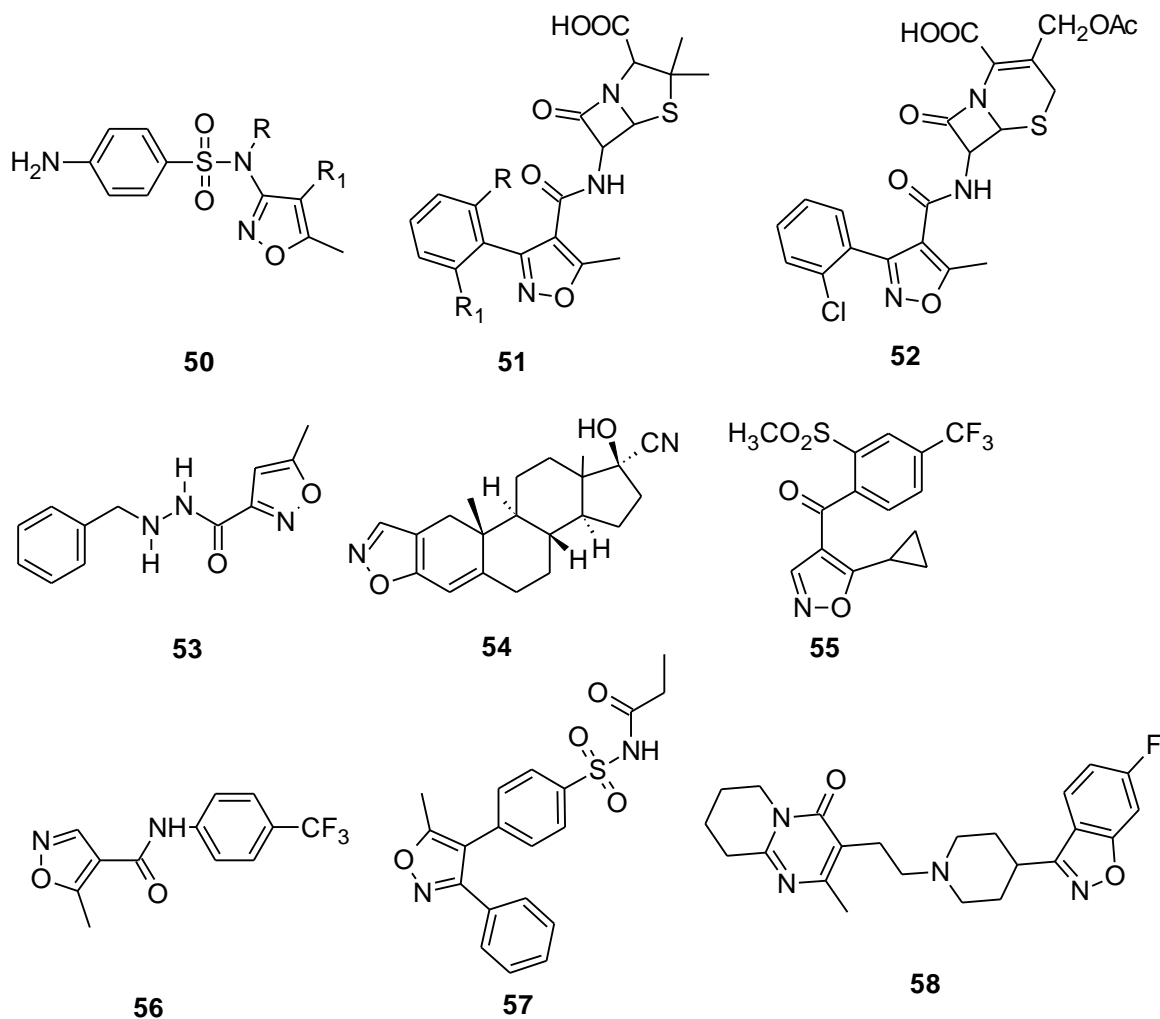
1.3.1. Electrophilic substitution on isoxazoles

The π -electron density distribution of unsubstituted isoxazole shows higher at the 4th position, followed by 5th and 3rd position on the ring. The experimental observation shows the 4th position being the preferred site for electrophilic substitution reactions [70, 71].



1.3.2. Significance of isoxazole derivatives

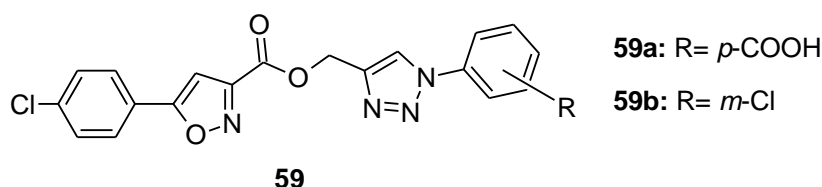
Some of important pharmacologically active drugs containing an isoxazole core are sulfamethoxazole (**50**) (PABA antagonist, antibacterial), oxacillin (**51**) and cephalosporin (**52**) (β -lactam antibiotics), isocarboxazide (**53**) (MAO inhibitor, antidepressant), anabolic steroid (**54**), isoxaflutole (**55**) (4-HPPD Inhibitor, herbicide), leflunomide (**56**) (DHODH inhibitor, immunosuppressant, anti-rheumatic), parecoxib (**57**) (COX-2 inhibitor, FANS), risperidone (**58**) (dopamine antagonist, antipsychotic).



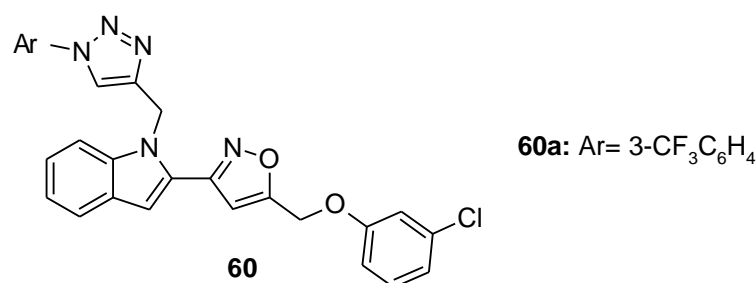
The discovery of synthetic strategies relying on their chemistry as well as significant biological activities displayed by isoxazole derivatives makes interest in research field. Therefore, we discussed some reported bio-active isoxazole derivatives as below.

1.3.3. Antibacterial agents

In 2020, F. Habib and co-authors reported isoxazole-triazole conjugated derivatives (**59**) and screened them for *in vitro* antibacterial activity. Compound **59a** shows least IC_{50} value of 67.60 $\mu\text{g/mL}$ against *P. aeruginosa* and **59b** displayed potent IC_{50} values of 92.25, 165.19, 74.13, 44.66, 105.92, 87.17 $\mu\text{g/mL}$ against *P. aeruginosa*, *S. typhimurium*, *S. pneumoniae*, *E. faecalis*, *K. pneumoniae* & *E. coli* bacterial strains respectively [72].

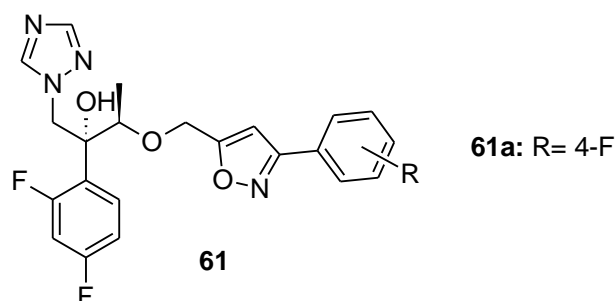


A series of 5-((3-chlorophenoxy)methyl)-3-(1-((1-(aryl)-1*H*-1,2,3-triazol-4-yl)methyl)-1*H*indol-2-yl)isoxazole derivatives (**60**) has been developed by M. Prashanthi *et. al.*, and reported as antibacterial activity. Compound **60a** displayed potent antibacterial efficacy with MIC value of 3.12 ± 0.22 , 3.12 ± 0.14 and 6.25 ± 0.83 $\mu\text{g/mL}$ against *B. subtilis*, *S. aureus* and *E. coli* respectively [73].



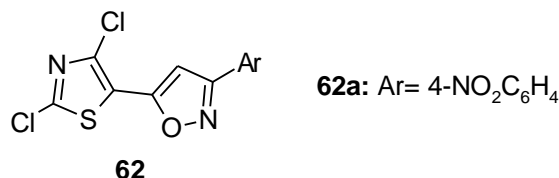
1.3.4. Antifungal agents

Synthesis and antifungal evaluation of (2*R*,3*R*)-3-((3-substituted-isoxazol-5-yl)methoxy)-2-(2,4-difluorophenyl)-1-(1*H*-1,2,4-triazol-1-yl) butan-2-ol derivatives (**61**) was reported by F. Xie *et. al.*, in 2020. Compound **61a** showed excellent inhibitory activity against *C. albicans*, *C. parapsilosis*, *C. neoformans* and *C. glabrata* with MIC value of 0.0313, 0.0625, 0.0313 and 0.125 $\mu\text{g/mL}$ respectively [74].



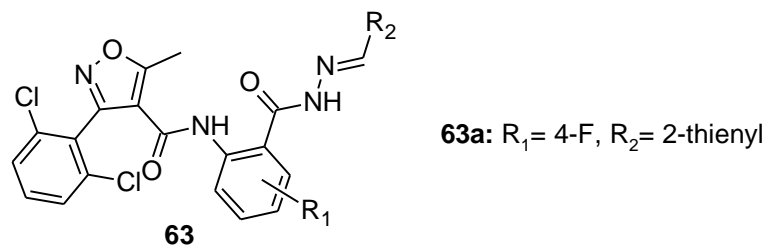
S.S. Basha and co-workers synthesized a series of thiazolyl-isoxazole derivatives (**62**) and reported as antifungal activity against *A. niger* and *P. chrysogenum*. Compound **62a**

exhibited excellent fungal activity with highest zone of inhibition of 29 ± 1 , 31 ± 6 , 33 ± 4 , 36 ± 3 mm and 33 ± 3 , 35 ± 1 , 36 ± 2 , 38 ± 3 mm with respect to concentrations of 12.5, 25, 50 & 100 $\mu\text{g/mL}$ against *A. niger* and *P. chrysogenum* respectively [75].

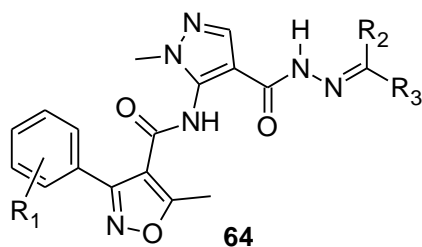


1.3.5. Antiviral agents

Z.B. Yang and co-workers developed a series of novel isoxazole-amide derivatives (**63**) and reported as antiviral activity against tobacco mosaic virus (TMV) and cucumber mosaic virus (CMV). The bioassay results indicated that, **63a** compound exhibited excellent curative and protection activity against TMV and CMV, with the 50 % effective concentration (EC₅₀) values of 168.5, 157.6 and 197.9, 168.4 mg/L respectively. This compound exhibited best curative, protection and inactivation activities against TMV and CMV which were superior to standard Ningnanmycin (NNM) [76].



A series of novel pyrazole-hydrazone containing isoxazole derivatives (**64**) have been synthesized by Z. Yang *et. al.*, and reported as antiviral activity against tobacco mosaic virus (TMV). Compounds **64a**, **64b** and **64c** exhibited the best curative activity, protection activity and inactivation activity against TMV with EC₅₀ values of 240.8 ± 2.2 , 287.4 ± 2.3 , 172.3 ± 2.1 , 342.6 ± 4.3 , 148.4 ± 3.3 , 62.2 ± 1.6 and 37.3 ± 1.9 mg/L respectively [77].



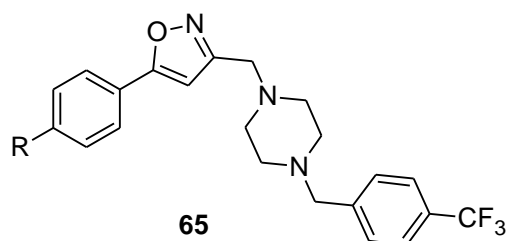
64a: R₁= 2-Cl, R₂= H, R₃= 4-Cl-Ph

64b: R₁= 2-Cl, R₂= H, R₃= 2-Br-Ph

64c: R₁= 2,6-diCl, R₂= H, R₃= Furyl

1.3.6. Anticancer agents

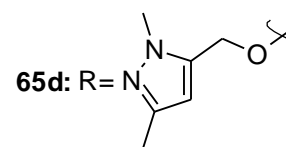
In 2018, B. Caliskan *et. al.*, synthesized and evaluated cytotoxicity of novel isoxazole-piperazine hybrids (**65**) against human liver and breast cancer cell lines. Among the series, compounds **65(a-d)** showed the most potent cytotoxicity on both the cell lines with IC₅₀ values in the range of 0.3-3.7 μ M [78].



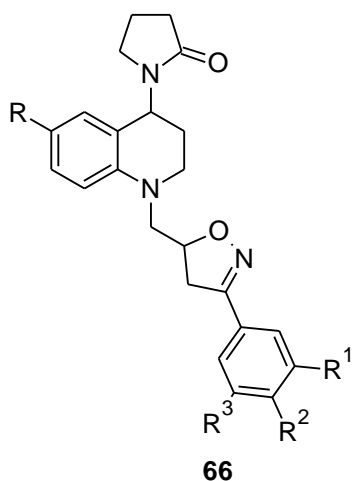
65a: R=

65b: R=

65c: R=



In 2020, a new series of tetrahydroquinoline-isoxazoline hybrid derivatives (**66**) were synthesized by C.C. Bernal *et. al.*, and screened against different cancer cell lines *viz* human breast adenocarcinoma, human liver carcinoma, human lung adenocarcinoma, cervical cancer and murine melanoma. In that, compounds **66a** (CC₅₀=11.37 μ M) and **66b** (CC₅₀=25.59 μ M) showed potent anticancer activity against murine melanoma cell line. Compound **66c** showed excellent activity on cervical cancer cell line with cytotoxic concentration (CC₅₀) value of 10.21 μ M [79].



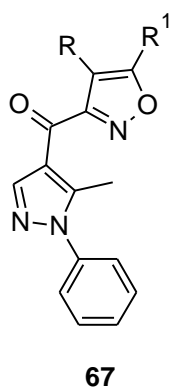
66a: $R^1 = H, R^2 = H, R^3 = H, R^4 = H$

66b: $R^1 = OCH_3, R^2 = H, R^3 = H, R^4 = H$

66c: $R^1 = CH_3, R^2 = OCH_3, R^3 = OCH_3, R^4 = OCH_3$

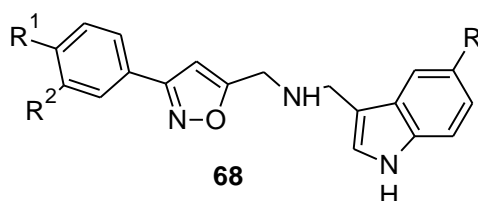
1.3.7. Anti-inflammatory agents

In 2020, E.K. Abdelall synthesized a series of novel isoxazole derivatives (**67**) and reported as anti-inflammatory activity. Among the series, compound **67a** shows potent anti-inflammatory efficacy with ED_{50} value of 45 mg/kg, nearly the same as that of standard drug celecoxib (40 mg/kg) [80].



67a: $R = COCH_3, R^1 = CH_3$

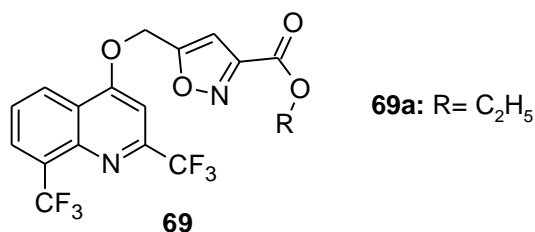
A series of new indole containing isoxazole derivatives (**68**) has been synthesized by S.R. Pedada *et. al.*, and investigated as anti-inflammatory activity. Compound **68a** showed potent anti-inflammatory efficacy with highest % of edema inhibition of 75.67 ± 4.21 and 76.54 ± 3.1 at 3rd and 4th hour respectively [81].



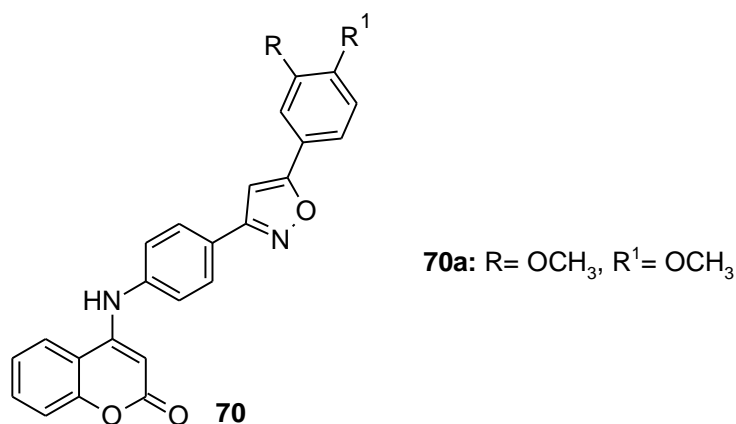
68a: $R = CH_3, R^1 = F, R^2 = CF_3$

1.3.8. Anti-mycobacterial agents

A series of 5-(2,8-bis(trifluoromethyl)quinolin-4-yloxymethyl)isoxazole-3-carboxylic acid ethyl ester derivatives (**69**) are excellent anti-TB agent and was reported by J. Mao *et. al.* The compound **69a** was found to be active against *M. tuberculosis* both intracellularly and extracellularly with a MIC value of 0.9 μM and 12.2 μM respectively [82].

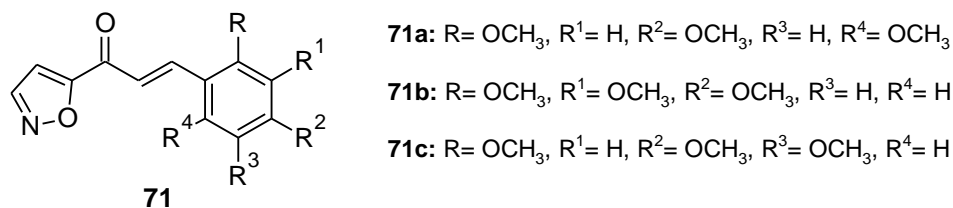


In 2014, D. Patel and co-authors synthesized coumarin based isoxazoles (**70**) and study their anti-mycobacterial activity against MTB H37Rv. Compound **70a**, which had a methoxy group, showed strong anti-mycobacterial action with a MIC of 62.5 $\mu\text{g/mL}$ and 99 % inhibition rate [83].

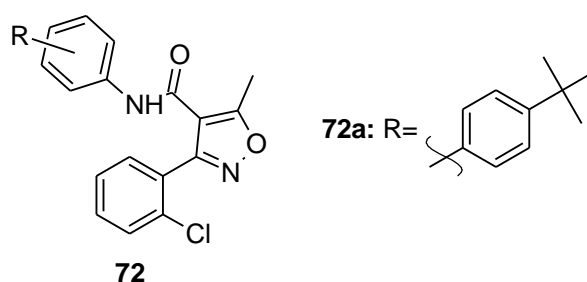


1.3.9. Antioxidants

In 2020, a series of isoxazole ring-containing chalcones (**71**) has been synthesized by A. Shaik *et. al.* and reported as antioxidant activity. Among the synthesized compounds, **71a**, **71b** & **71c** exhibited potent DPPH free radical scavenging assay with least IC₅₀ values of 5 \pm 1, 6 \pm 1 & 7 \pm 2 $\mu\text{g/mL}$ respectively [84].

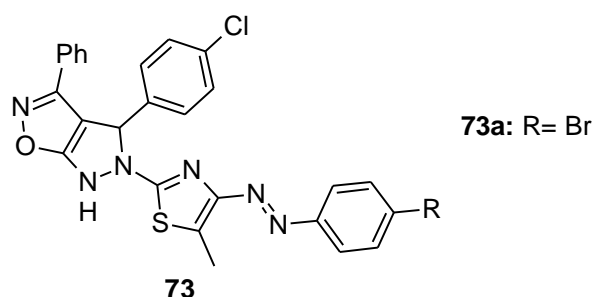


In 2021, A.M. Eid *et al.*, synthesized and evaluated antioxidant activity of isoxazole-carboxamide derivatives (**72**). Compound **72a** was the most active as antioxidant agent with IC₅₀ value of 7.8±1.21 µg/mL [85].



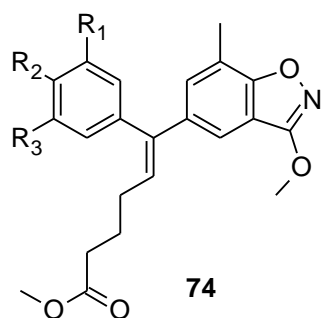
1.3.10. Anti-HIV agents

In 2014, a series of thiazol-2-ylpyrazolo[4,3-*d*]isoxazole diazenyl derivatives (**73**) has been synthesized by S.M. Gomha *et al.* and reported as anti-HIV activity against the HIV-1 viral enzyme reverse transcriptase (RT). Compound **73a** exhibited very potent inhibitory power against HIV-1 viral RT with IC₅₀ value of 0.016 µM [86].



In 2009, B.L. Deng and his-workers synthesized a series of alkenyldiarylmethanes containing benzo[*d*]isoxazole and oxazolidine-2-one rings (**74**) and investigated anti-HIV activity. Compound **74a** recognized as potent non-nucleoside HIV-1 reverse transcriptase

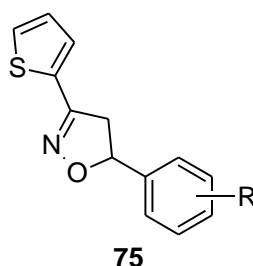
inhibitors and showed most promising efficacy with EC_{50} values of $0.04 \mu\text{M}$ (vs HIV-1RF) and $0.02 \mu\text{M}$ (vs HIV-1IIIB) [87].



74a: $R_1 = \text{CH}_3$, $R_2 = \text{OCH}_3$, $R_3 = \text{COOCH}_3$

1.3.11. Anti-depressant and Antianxiety agents

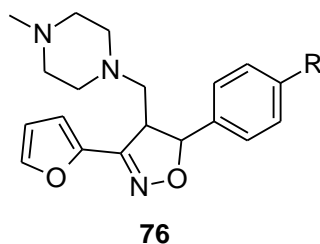
A series of 5-substituted phenyl-3-(thiophen-2-yl)-4,5-dihydro-1,2-oxazoles (**75**) was synthesized by J. Kumar *et al.* and reported as antidepressant and antianxiety activities. The compound **75a** exhibited good antidepressant activity in terms of immobility time 173 ± 5 sec and **75b** showed highest antianxiety activity of 20.44 % preference to open arm [88].



75a: $R = 4\text{-N}(\text{CH}_3)_2$

75b: $R = 4\text{-F}$

J. Kumar *et al.*, (2017) synthesized a series of 3,4,5-trisubstituted isoxazoles including the furan and piperazine moiety (**76**) and reported as antidepressant efficacy in albino mice and antianxiety activity. Compounds **76a** & **76b** reduced the duration of immobility times of 152.00-152.33 % at 10 mg/kg dose level [89].



76a: $R = \text{H}$

76b: $R = \text{N}(\text{CH}_3)_2$

1.4. Plan of work

The research work entitled “**Synthesis and biological evaluation of some new heterocyclic compounds containing Nitrogen and Oxygen atoms**” is systematically presented in seven chapters and are given below:

Chapter-1: Introduction

Chapter-2: This chapter has been divided into two sections.

Section-2A: Facile TiO₂ NPs catalyzed synthesis of substituted-4-hydroxy/methoxy benzylidene derivatives as potent antioxidant and anti-tubercular agents.

Section-2B: Facile synthesis of some 5-(3-substituted-thiophene)-pyrimidine derivatives and their pharmacological and computational studies.

Chapter-3: Efficient L-Proline catalyzed synthesis of some new (4-substituted-phenyl)-1,5-dihydro-2*H*-pyrimido[4,5-*d*][1,3]thiazolo[3,2*a*]-pyrimidine-2,4(3*H*)-diones bearing thiazolopyrimidine derivatives and evaluation of their pharmacological activities.

Chapter-4: This chapter has been divided into two sections.

Section-4A: An efficient *p*-TSA catalyzed synthesis of some new substituted-(5-hydroxy-3-phenylisoxazol-4-yl)-1,3-dimethyl-1*H*-chromeno[2,3-*d*]pyrimidine-2,4(3*H*,5*H*)-dione derivatives and evaluation of their pharmacological and computational investigations.

Section-4B: An efficient *p*-TSA catalyzed synthesis of some new substituted-(5-hydroxy-3-phenylisoxazol-4-yl)-3,3-dimethyl-2*H*-xanthen-1(9*H*)-one scaffolds and evaluation of their pharmacological and computational investigations.

Chapter-5: Synthesis, *in-vitro* evaluation and docking studies of novel 6-amino-4-substituted-pyrano[3,2-*d*]isoxazole-5-carbonitrile derivatives as potential anti-diabetic and anticancer agents.

Chapter-6: This chapter has been divided into two sections.

Section-6A: Synthesis, *in-vitro* evaluation, docking and ADME studies of novel 5-[3-(4-chlorophenyl)-substituted-6-hydroxypyrimidine-2,4(1*H*,3*H*)-dione derivatives as potential anti-diabetic and anticancer agents.

Section-6B: Synthesis, *in-vitro* evaluation, docking and ADME studies of novel 5-[3-(4-chlorophenyl)-substituted-1,3-dimethylpyrimidine-2,4,6(1*H*,3*H*,5*H*)-trione derivatives as potential anti-diabetic and anticancer agents.

Chapter-7: Synthesis, characterization and biological evaluation of some new 2-[(4-hydroxy-6-methylpyrimidin-2-yl)amino]-1-(4-substituted)ethanone derivatives.

1.5. References

1. N. Dege, M.A. Raza, O.E. Dogan, T. Agar, M.W. Mumtaz, *J. Iran. Chem. Soc.*, **2021**, 18, 2345-2368.
2. D. Robert, *Organic synthesis*, **2018**, 1-5.
3. A.R. Katritzky and J.A. Boulton, *Advances in Heterocyclic Chemistry*, (Ed.), Academic Press, New York, **1963-1980**, Vol-1 to 27, 1-400.
4. A. Pandith, R.G. Siddappa, Y.J. Seo, *J. Photochem. Photobiol. C: Photochem. Rev.*, **2019**, 40, 81-116.
5. M. Garcia-Valverde, Torroba, *Molecules*, **2005**, 10, 318-320.
6. P.K. Singh, O. Silakari, *Med. Chem.*, **2018**, 13, 1071-1087.
7. S. Pathania, R.K. Narang, R K. Rawal, *Eur. J. Med. Chem.*, **2019**, 180, 486-508.
8. T. Venkatesh, K. Upendranath, Y.A. Nayaka, *J. Solid State Electrochem.*, **2021**, 25, 1237-1244.
9. A. Pandith, A. Kumar, H.S. Kim, *RSC Adv.*, **2015**, 5, 81808-81816.
10. A. Weissberger, *The Chemistry of Heterocyclic Compounds*, (Ed.), Wiley Interscience, New York, **1950-1975**, Vol-1 to 29, 1-100.
11. N. Depa and H. Erothu, *Rasayan J. Chem.*, **2022**, 15, 1-9.
12. J. Zhu, J. Mo, H.Z. Lin, Y. Chen, H.P. Sun, *Bioorg. Med. Chem.*, **2018**, 26, 3065-3075.
13. K. Upendranath, T. Venkatesh, M. Shashank, G. Nagaraju, K.M. Pasha, *J. Mol. Struct.*, **2022**, 1250, 1-14.

14. B. Manjunatha, Y.D. Bodke, R. Sandeepkumar Jain, T.N. Lohith, M.A. Sridhar, *J. Mol. Struct.*, **2021**, 1244, 1-9.
15. C. Simon, T. Constantieux, J. Rodriguez, *Eur. J. Org. Chem.*, **2004**, 24, 4957-4980.
16. K. Pramod Sahu, K. Praveen Sahu, S.M. Kaurav, M. Messali, S.M. Almutairi, P.L. Sahu, D.D. Agarwal, *ACS Omega*, **2018**, 3, 15035-15042.
17. R. Rydzewski, *Real World Drug Discovery*, Elsevier, 1st Edition, **2008**, 1-350.
18. E. Zarenezhad, M. Farjam, A. Iraji, *J. Mol. Struct.*, **2021**, 1230, 1-24.
19. J. Xu, V. Chmela, N.J. Green, D.A. Russell, M.J. Janicki, R.W. Gora, J.D. Sutherland, *Nature*, **2020**, 582, 60-66.
20. E. Knoevenagel, *Ber. Dtsch. Chem. Ges.*, **1898**, 31, 2596-2619.
21. C.O. Kappe and A. Stadler, *The Biginelli Dihydropyrimidine Synthesis-Organic reactions*, **2004**, 63, 1-116.
22. B.D. Mather, K. Viswanathan, K.M. Miller, T.E. Long, *Prog. Polym. Sci.*, **2006**, 31, 487-531.
23. D. Bellon-Gomez, D. Vela-Corcia, A. Perez-Garcia, J.A. Tores, *Pest Manag. Sci.*, **2015**, 71, 1407-1413.
24. J. Yang, A. Guan, Z. Li, P. Zhang, C. Liu, *J. Agric. Food Chem.*, **2020**, 68, 6485-6492.
25. V.S. Kolekar, D.D. Wakure, P.N. Raut, S.C. Utture, *Acta Hortic.*, **2011**, 890, 547-555.
26. D. Marcic, *J. Pest Sci.*, **2012**, 85, 395-408.
27. T. Yoshimura, T. Ikeuchi, S. Ohno, S. Asakura, Y. Hamada, *Pestic. Sci.*, **2013**, 38, 1-2.
28. R. Veeraputhiran, R. Balasubramanian, *Indian J. Weed Sci.*, **2013**, 45, 12-15.
29. R.E. Marquez-Lopez, A.O. Quintana-Escobar, V.M. Loyola-Vargas, *Phytochem. Rev.*, **2019**, 18, 1387-1408.
30. M.K. Gora, H. Jat, K.C. Jakhar, H. Jat, A. Shivran, *J. Pharmacogn. Phytochem.*, **2018**, 7, 3383-3385.
31. M. Diaz-Gavilan, J.A. Gomez-Vidal, F. Rodriguez-Serrano, J.A. Marchal, O. Caba, A. Aranega, M.A. Gallo, A. Espinosa, J.M. Campos, *Bioorg. Med. Chem. Lett.*, **2008**, 18, 1457-1460.
32. S.V. Dinakaran, B. Bhargavi, K.K. Srinivasan, *Pharm. Chem.*, **2012**, 4, 255-265.
33. D.A. Aboul El-Ella, M.M. Ghorab, E. Noaman, H.I. Heiba, A.I. Khalil, *Bioorg. Med. Chem. Lett.*, **2008**, 16, 2391-2402.
34. J.E. Gready, C. McKinlay, M.G. Gebauer, *Eur. J. Med. Chem.*, **2003**, 38, 719-728.
35. M. Horchani, A. Hajlaoui, A.H. Harrath, L. Mansour, H.B. Jannet, A. Romdhane, *J. Mol. Struct.*, **2020**, 1199, 1-9.

36. B. Chandrasekaran, S. Cherukupalli, S. Karunanidhi, A. Kajee, R.R. Aleti, N. Sayyad, R. Karpoornath, *J. Mol. Struct.*, **2019**, 1183, 246-255.
37. S.C. Wang, F.X. Wan, S. Liu, S. Zhang, L. Jiang, *J. Chin. Chem. Soc.*, **2018**, 65, 445-451.
38. S.B. Bari & N.G. Haswani, *J. Saudi Chem. Soc.*, **2017**, 21, 264-274.
39. Y.Y. Wang, F.Z. Xu, Y.Y. Zhu, B. Song, D. Luo, G. Yu, J. Wu, *Bioorg. Med. Chem. Lett.*, **2018**, 28, 2979-2984.
40. M.N. Nasr & M.M. Gineinah, *Arch. Pharm. Pharm. Med. Chem.*, **2002**, 6, 289-295.
41. E.M. Abbass, A.K. Khalil, A.M. El-Naggar, *J. Heterocycl. Chem.*, **2020**, 57, 1154-1164.
42. K.M. Hosamani, D.S. Reddy, H.C. Devarajegowda, *RSC Adv.*, **2015**, 5, 11261-11271.
43. R.B. Bakr, A.A. Ghoneim, A.A. Azouz, *Bioorg. Chem.*, **2019**, 88, 1-35.
44. M.A. Abdelgawad, R.B. Bakr, A.A. Azouz, *Bioorg. Chem.*, **2018**, 77, 339-348.
45. N. Pappula & R. Sharabu, *J. Pharm. Res. Int.*, **2021**, 33, 69-79.
46. K.S. Raju, S. AnkiReddy, G. Sabitha, V.S. Krishna, D. Sriram, K.B. Reddy, S.R. Sagurthi, *Bioorg. Med. Chem. Lett.*, **2019**, 29, 284-290.
47. J. Rangaswamy, H.V. Kumar, S.T. Harini, N. Naik, *J. Heterocycl. Chem.*, **2015**, 52, 1349-1360.
48. J. Figueiredo, J.L. Serrano, E. Cavalheiro, L. Keurulainen, J. Yli-Kauhaluoma, V. M. Moreira, P. Almeida, *Eur. J. Med. Chem.*, **2018**, 143, 829-842.
49. S. Okazaki, T. Mizuhara, K. Shimura, H. Murayama, H. Ohno, S. Oishi, N. Fujii, *Bioorg. Med. Chem.*, **2015**, 23, 1447-1452.
50. B. Huang, D. Kang, Y. Tian, D. Daelemans, E. De Clercq, C. Pannecouque, X. Liu, *Chem. Bio. Drug Des.*, **2021**, 97, 67-76.
51. S.B. Wang, X.Q. Deng, Y. Zheng, Y.P. Yuan, Z.S. Quan, L.P. Guan, *Eur. J. Med. Chem.*, **2012**, 56, 139-144.
52. S.I. Pretorius, W.J. Breytenbach, C. De Kock, P.J. Smith, D.D. N'Da, *Bioorg. Med. Chem.*, **2013**, 21, 269-277.
53. J. Zhu, J. Mo, H.Z. Lin, Y. Chen, H.P. Sun, *Bioorg. Med. Chem.*, **2018**, 26, 3065-3075.
54. L. Claisen, O. Lowman, *Berichte der deutschen chemischen Gesellschaft*, **1888**, 21, 1149-1157.
55. L. Claisen, *Berichte der deutschen chemischen Gesellschaft*, **1891**, 24, 3900-3918.
56. A.M. Quilico, C. Gazz, *Chim. Ital.*, **1942**, 72, 399-405.
57. V.V. Dabholkar, F.Y. Ansari, *J. Serb. Chem. Soc.*, **2009**, 74, 1219-1228.

58. J. Trivedi, A. Parveen, F. Rozy, A. Mitra, C. Bal, D. Mitra, A. Sharon, *Eur. J. Med. Chem.*, **2019**, 183, 1-9.
59. B. Manjunatha, Y.D. Bodke, R. Sandeepkumar Jain, T.N. Lohith, M.A. Sridhar, *J. Mol. Struct.*, **2021**, 1244, 1-9.
60. E.K.A. Abdelall, *Bioorg. Chem.*, **2020**, 94, 1-42.
61. I. Saidi, M. Manachou, M. Znati, J. Bouajilac, H.B. Jannet, *J. Mol. Struct.*, **2022**, 1247, 1-16.
62. S.R. Pedada, N.S. Yarla, P.J. Tambade, D.B. Lakkappa, A. Bishayee, K.M. Arunasree, G.H. Philip, G. Dharmapuri, G. Aliev, S. Putta, G. Rangaiah, *Eur. J. Med. Chem.*, **2016**, 1-33.
63. M.A. Barmade, P.R. Murumkar, M. Kumar Sharma, M. Ram Yadav, *Curr. Top. Med. Chem.*, **2016**, 16, 2863-2883.
64. W.T. Ashton, R.M. Sisco, H. Dong, K.A. Lyons, H. He, G.A. Doss, B. Leiting, R.A. Patel, J.K. Wu, F. Marsilio, N.A. Thornberry, A.E. Weber, *Bioorg. Med. Chem. Lett.*, **2005**, 15, 2253-2258.
65. D.M. Shen, M. Shu, K.T. Chapman, *Org. Lett.*, **2000**, 2, 2789-2792.
66. V. Yedidia, C.C. Leznoff, *Can. J. Chem.*, **1980**, 58, 1144-1150.
67. J.C. Lee, T. Hong, *Tetrahedron Lett.*, **1997**, 38, 8959-8960.
68. F. Freeman, T. Chen, J.B. Van der Linden, *Synthesis*, **1997**, 861-862.
69. G.T. Kondrateva, M.A. Aitzhanova, V.S. Bogdanov, Z.N. Ivanova, *Bull. Acad. Sci. USSR Div. Chem. Sci.*, **1978**, 27, 773-777.
70. R.E. Wasylshen, J.B. Rowbotham, T. Schaefer, *Can. J. Chem.*, **1974**, 52, 833-837.
71. G. Berthier, G. Del Re, *J. Chem. Soc.*, **1965**, 3109-3117.
72. F. Habib, S. Alam, A. Hussain, B. Aneja, M. Irfan, M.F. Alajmi, M. Abid, *J. Mol. Struct.*, **2020**, 1201, 1-35.
73. M. Prashanthi, H.R. Babu, J.U. Rani, *Rus. J. Bioorg. Chem.*, **2021**, 47, 601-608.
74. F. Xie, T. Ni, Z. Ding, Y. Hao, R. Wang, R. Wang, D. Zhang, *Bioorg. Chem.*, **2020**, 101, 1-15.
75. S.S. Basha, K. Divya, A. Padmaja, V. Padmavathi, *Res. Chem. Intermed.*, **2015**, 41, 10067-10083.
76. Z.B. Yang, P. Li & Y.J. He, *Molecules*, **2019**, 24, 1-17.
77. Z. Yang, P. Li & X. Gan, *Molecules*, **2018**, 23, 1-12.
78. B. Caliskan, E. Sinoplu, K. Ibis, E. Akhan Guzelcan, R. Cetin Atalay, E. Banoglu, *J. Enzyme Inhib. Med. Chem.*, **2018**, 33, 1352-1361.

-
79. C.C. Bernal, L.C. Vesga, S.C. Mendez-Sanchez, A.R. Romero Bohorquez, *Med. Chem. Res.*, **2020**, 29, 675-689.
80. E.K. Abdelall, *Bioorg. Chem.*, **2020**, 94, 1-42.
81. S.R. Pedada, N.S. Yarla, P.J. Tambade, B.L. Dhananjaya, A. Bishayee, K.M. Arunasree, G. Rangaiah, *Eur. J. Med. Chem.*, **2016**, 112, 289-297.
82. J. Mao, H. Yuan, Y. Wang, B. Wan, D. Pak, R. He, S.G. Franzblau, *Bioorg. Med. Chem. Lett.*, **2010**, 20, 1263-1268.
83. D. Patel, P. Kumari & N.B. Patel, *Arab. J. Chem.*, **2017**, 10, 3990-4001.
84. A. Shaik, R.R. Bhandare, K. Palleapati, S. Nissankararao, V. Kancharlapalli, S. Shaik, *Molecules*, **2020**, 25, 1-11.
85. A.M. Eid, M. Hawash, J. Amer, A. Jarrar, S. Qadri, I. Alnimer, A. Mousa, *Bio. Med. Res. Int.*, **2021**, 1-9.
86. S.M. Gomha, M.G. Badrey, M.M. Abdalla, R.K. Arafa, *Med. Chem. Comm.*, **2014**, 5, 1685-1692.
87. B.L. Deng, Y. Zhao, T.L. Hartman, K. Watson, R.W. Buckheit Jr, C., Pannecouque, M. Cushman, *Eur. J. Med. Chem.*, **2009**, 44, 1210-1214.
88. J. Kumar, M. Akhtar, C. Ranjan, G. Chawla, *Int. J. Pharm. Chem. Anal.*, **2015**, 14, 274-283.
89. J. Kumar, G. Chawla, M. Akhtar, K. Sahu, V. Rathore, S. Sahu, *Arab. J. Chem.*, **2017**, 10, 141-149.

2A.1. Introduction

The nitrogen and oxygen-containing heterocyclic compounds achieve great importance due to their wide range of pharmacological activities. They are obtained from various natural resources and synthetic reactions in medicinal chemistry. Pyrimidine, pyrazole and isoxazole derivatives have drawn much attention due to their biological importance as antimicrobial, anticancer, anti-inflammatory, anti-diabetic, anti-tubercular, antioxidant, antiparasitic, anti-convulsants, anti-depressants, analgesic, gastro protectors and kinase inhibitors [1-6].

Knoevenagel reaction is widely used for C=C bond formation using conventional catalysts such as acetic acid, $\text{Bi}(\text{NO}_3)_3 \cdot 5\text{H}_2\text{O}$, Lewis acids like $\text{ZrOCl}_2 \cdot 8\text{H}_2\text{O}$, Nano- Fe_3O_4 , β -alanine, CAS ((\pm)-Camphor-10-Sulfonic Acid), L-valine and L-tyrosine [7-11] etc. Among them, nanocatalysis is a rapidly growing field that often employs nanoparticles in a variety of organic and inorganic reactions [12, 13]. Titanium oxide nanoparticles (TiO_2 NPs) are used in various industrial processes, organic catalyst [14-16], bactericides [17], gas sensors [18], environmental protections [19], dielectric ceramics [20], photovoltaic solar cells [21] and absorbents [22] etc.

Tuberculosis (TB) is a dominant infectious disease that affects the broader population. This disease is caused by *Mycobacterium tuberculosis* (MTB). According to the World Health Organization's (WHO) Global Tuberculosis (2019), about 10 million people were affected and approximately 1.4 million deaths were caused by TB [23]. The excess production of free radicals (nitric oxide, superoxide and hydroxyl) can cause damage to biomolecules such as lipids, proteins, enzymes and DNA in cells and tissues; this may lead to several disorders such as cancer, diabetes, cardiovascular, autoimmune diseases, neurodegenerative disorders, aging and other diseases [24-26]. Antioxidants are capable of interacting with free radicals and stopping their chain reactions before essential vital molecules are damaged. To overcome these problems further investigation of novel drugs are

more essential. Pyrimidine, pyrazole and isoxazole derivatives have properties that are potentially useful in fighting against various diseases. Some of the reported biologically active drugs have been mentioned in **Fig. 1**.

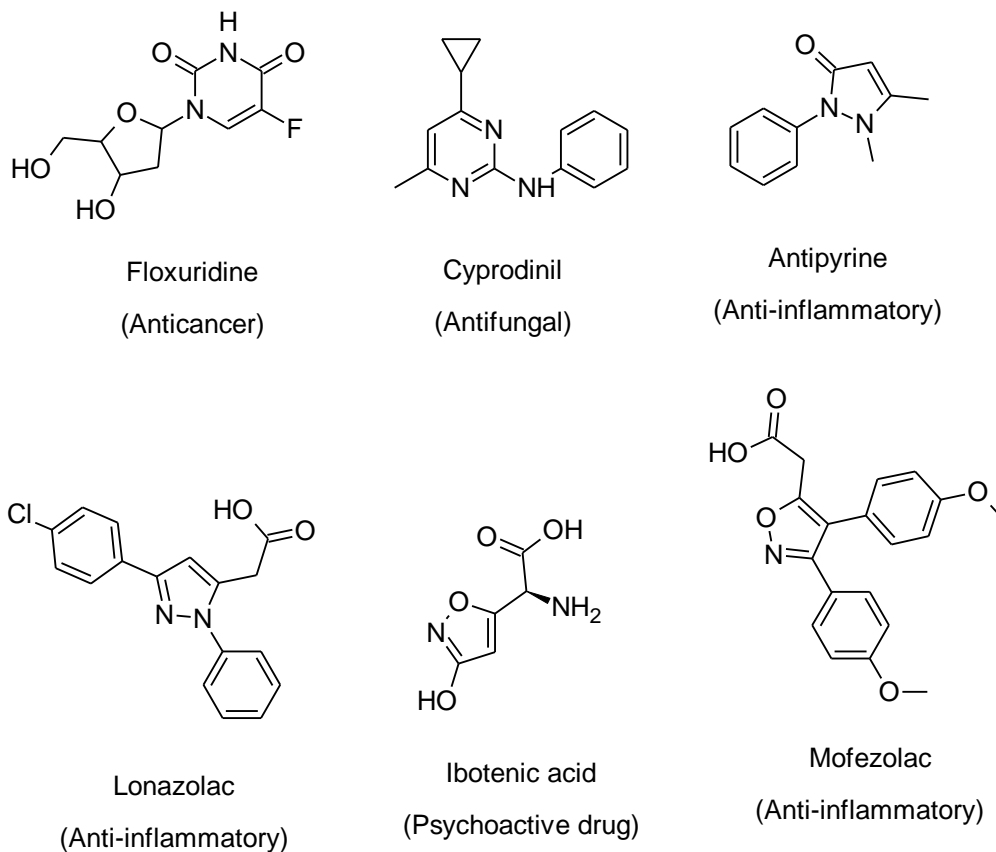
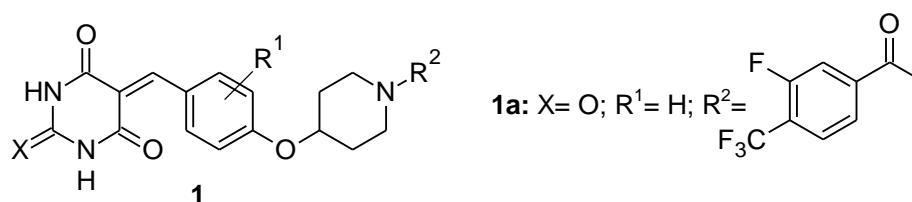
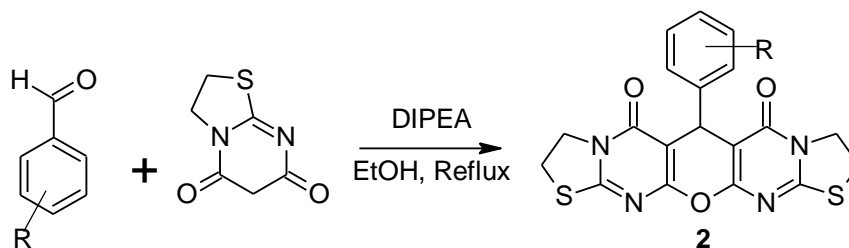


Fig. 1. Biologically active drugs containing pyrimidine, pyrazole and isoxazole nucleus.

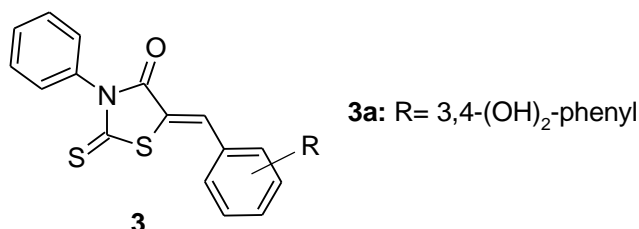
L. Ma *et. al.*, reported a series of 5-benzylidenepyrimidine 2,4,6(1*H*,3*H*,5*H*)-trione derivatives (**1**), among all the compounds, **1a** exhibited potent glucose-lowering effects on insulin-resistant HepG2 cells and regulated adiponectin and leptin expression in 3T3-L1 adipocytes [27].



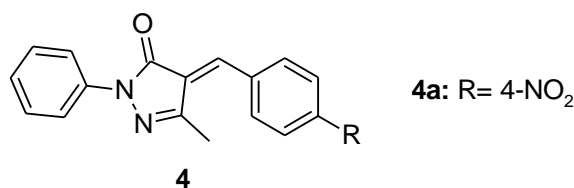
In 2021, A.A. Esmaeili and co-workers reported 5-aryl-2,3,7,8-tetrahydro-5H-11-oxa-1,9-dithia-3a,6a,10,12-tetraaza-dicyclopenta[*b,i*]anthracene-4,6-diones derivatives (**2**) via cyclocondensation reaction of 2,3-dihydro-thiazolo[3,2-*a*]pyrimidine-5,7-dione and aromatic aldehyde derivatives in the presence of diisopropylethylamine as an organo-base catalyst [28].



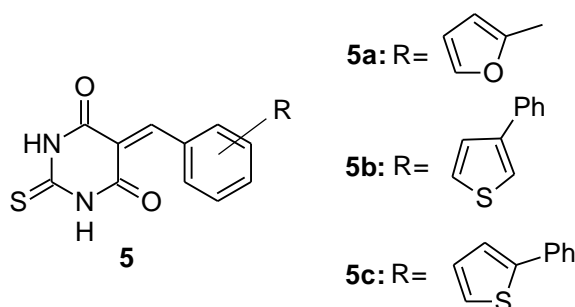
A series of rhodanine/5-benzylidene-3-phenyl-2-thioxo-1,3-thiazolidin-4-one derivatives (**3**) was synthesized via Knoevenagel condensation reaction. Among the benzylidene derivatives, **3a** with two hydroxyl groups at 3,4-position on phenyl ring, showed the highest antioxidant property of 71.2 % of inhibition have been reported by M. Molnar *et al.*, [29].



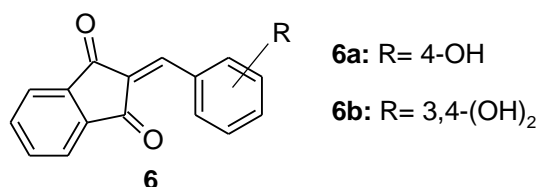
In 2018, substituted 2-phenyl-5-methyl-pyrazol-3-one derivatives (**4**) have been reported by V.M. Lunagariya *et al.*, as potential antibacterial and anticancer agents. Compound **4a** having electron withdrawing NO₂ group at para position of the phenyl ring shows good anticancer activity with IC₅₀ value of 52.44±1 µg/mL [30].



In 2018, M. Shabeer and his-workers reported a 5-benzylidene-2-thioxodihydropyrimidine-4,6(1*H*,5*H*)-dione derivatives (**5**) as potential antifungal agents. Compounds **5a**, **5b** and **5c** showed potent fungal activity against *C. parapsilosis*, *C. tropicalis* and *C. neoformans* with IC₅₀ value of <1.95 µg/mL and compound **5b** exhibited least IC₅₀ values of 1.95, 9.39 and 6.18 µg/mL against *C. albicans*, *C. dubliniensis* and *C. lusitaniae* fungal strains respectively [31].



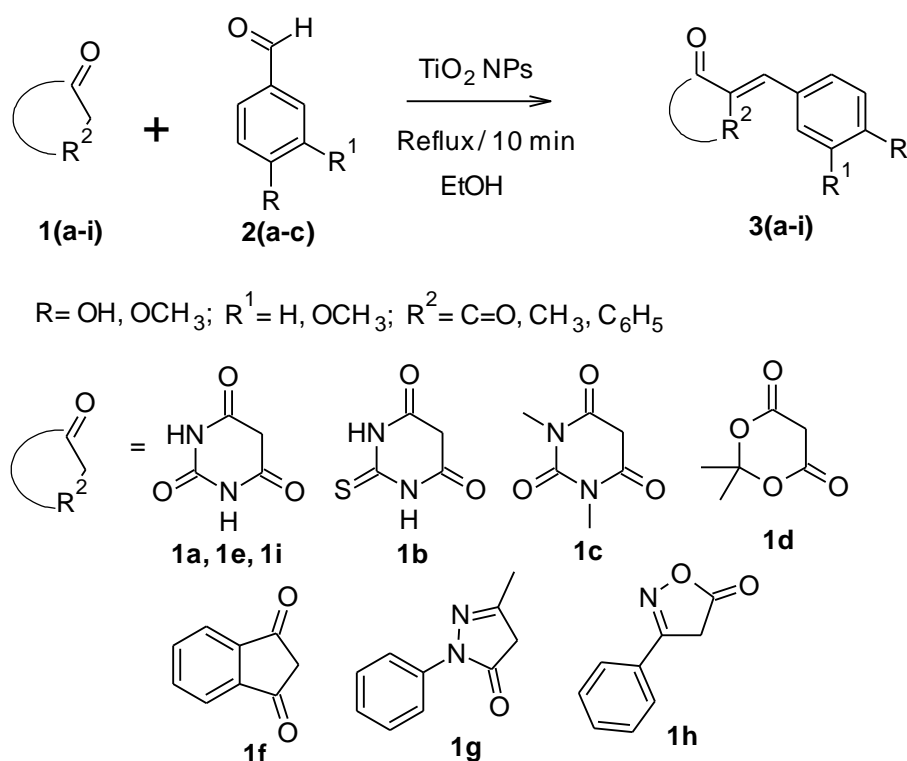
Zirconium catalyzed 2-arylidene indan-1,3-diones derivatives (**6**) have been reported by F. Oliveira *et. al.*, and were evaluated as inhibitors of the NS2B-NS3 protease of West Nile Virus. The most active hydroxylated derivatives **6a** and **6b** exhibited as noncompetitive enzymes inhibitors with IC₅₀ values of 11 µmol L⁻¹ and 3 µmol L⁻¹, respectively [32].



Based on the above investigations, we have reported substituted-4-hydroxy/methoxy benzylidene derivatives and have examined their antioxidant, anti-TB and molecular docking studies against Human peroxiredoxin 5 and Enoyl-ACP reductase as target enzymes, respectively.

2A.2. Present work

In this chapter, we described a simple and convenient method for the synthesis of substituted-4-hydroxy/methoxy benzylidene derivatives **3(a-i)** via Knoevenagel condensation reaction of different active methylene compounds (**1**) with 4-hydroxy/methoxy benzaldehyde (**2**) in aqueous ethanol in the presence of TiO₂ NPs as a catalyst and the reaction pathway of the synthesized compounds has been given in **Scheme 1**.



Scheme 1. Synthesis of substituted-4-hydroxy/methoxy benzylidene derivatives **3(a-i)**.

The synthetic strategy involves in the following steps:

- The reaction was initiated by the formation of enol (**1**) from an active methylene compound.
- TiO₂ NPs are coordinated to the oxygen atom of the aromatic aldehyde (**2**) and then activated for nucleophilic attack.
- Enol (**1**) attacks the carbonyl group of aldehyde (**2**) and affords an intermediate (**3**), which undergoes subsequent dehydration to desired Knoevenagel products (**4**).

- A possible mechanism for the formation of substituted-4-hydroxy/methoxy benzylidene derivatives has been shown in **Fig. 2**.

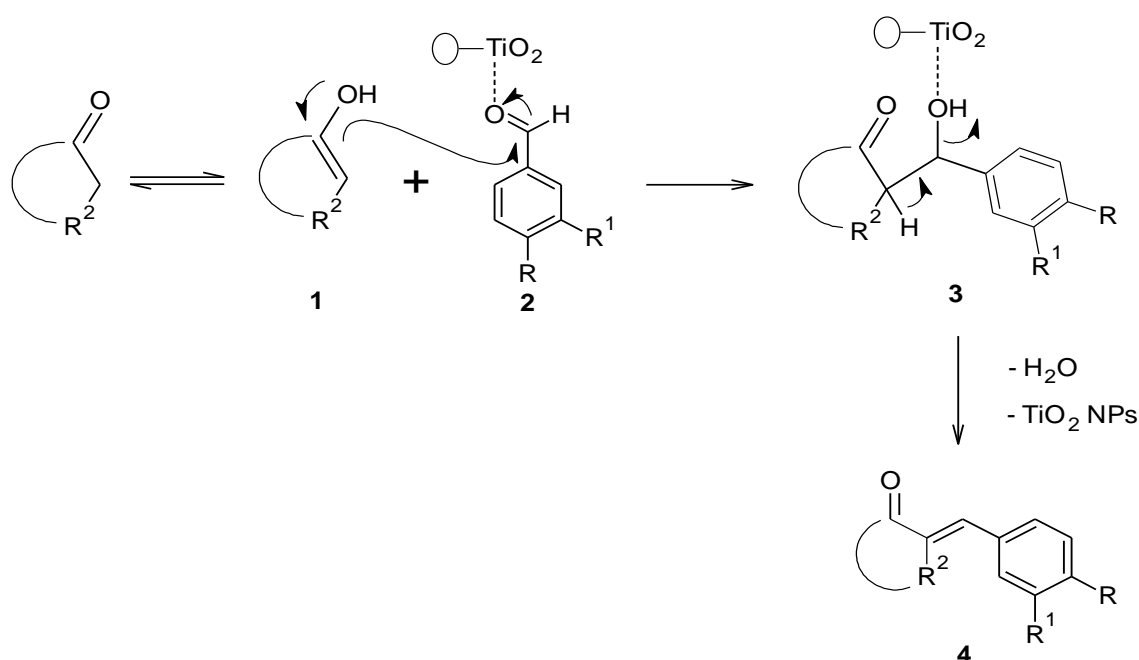


Fig. 2. Possible mechanism of synthesized compounds **3(a-i)**.

Firstly, we studied the effect of the catalyst on the reaction. In the previous reports, the reaction was carried out in the presence of different catalysts such as acetic acid, Bi(NO₃)₃·5H₂O, ZrOCl₂·8H₂O, Nano-Fe₃O₄, β-alanine, CAS ((±)-Camphor-10-Sulfonic Acid), L-valine and L-tyrosine (**Table 1**). We have screened the TiO₂ NPs catalyst to find the progress of the reaction as well as the increase in product yield of compound **3a**. By using this catalyst, the result was very encouraging with a short reaction time and good yield.

Table 1. Effect of different catalysts on synthesized compound **3a**.

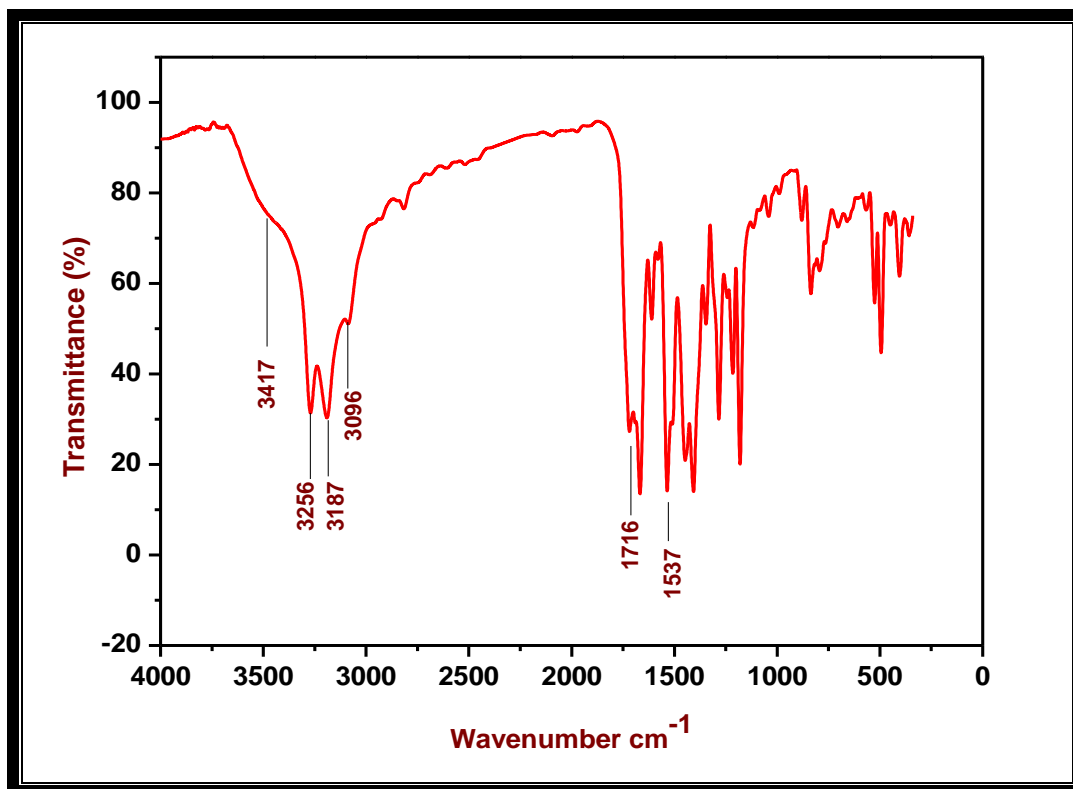
Entry	Catalyst	Solvent	Temperature (°C)	Time (min)	Yield (%)
1	TiO ₂ NPs	EtOH:H ₂ O	Reflux	10	98
2	ACOH	EtOH	Reflux	180	85 ^[30]
3	Bi(NO ₃) ₃ ·5H ₂ O	EtOH	Reflux	20	95 ^[31]
4	ZrOCl ₂ ·8H ₂ O	H ₂ O	Reflux	120	86 ^[32]
5	Fe ₃ O ₄ NPs	EtOH	Reflux	30	70 ^[7]
6	β-alanine	ACOH	Reflux	180	71 ^[8]
8	CAS	EtOH:H ₂ O	Reflux	35	85 ^[9]
9	L-valine	EtOH	Reflux	10	93 ^[10]
10	L-tyrosine	H ₂ O	RT	16	93 ^[11]
11	-	H ₂ O	Reflux	12 h	93 ^[33]

The structures of the desired substituted-4-hydroxy/methoxy benzylidene derivatives **3(a-i)** were confirmed by recording UV-Visible, IR, ^1H NMR, ^{13}C NMR and Mass spectral data.

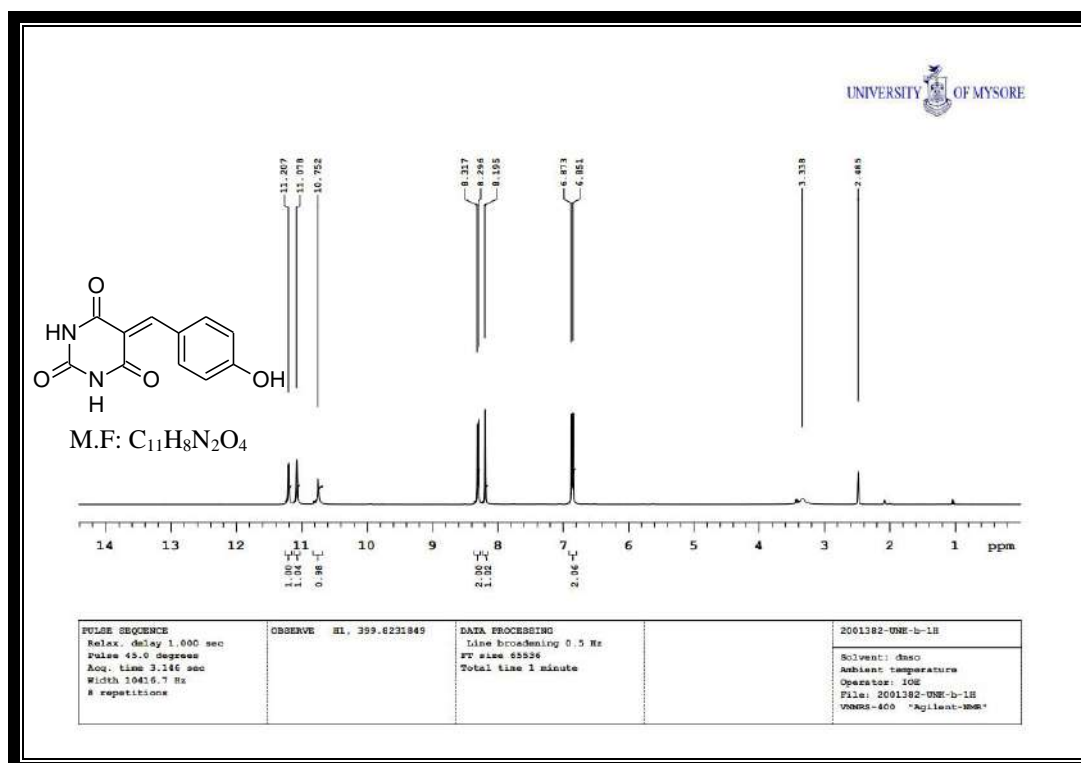
In the IR spectrum, the compound **3a** showed a stretching vibration band at 3417 cm^{-1} due to the hydroxyl group and another vibration band at 3256 cm^{-1} corresponding to amide functionality. 3096 cm^{-1} due to CH group and 1716 cm^{-1} correspond to stretching vibration frequency of the carbonyl group (C=O). The ^1H NMR spectrum of compound **3a** exhibited two singlet peaks at δ 11.20 ppm and 11.07 ppm, which corresponds to two NH protons of the pyrimidine core (s, 2H, NH) and another singlet peak at δ 10.75 ppm due to OH proton (s, 1H, OH). A doublet peak at 8.31-8.29 ppm corresponds to two aromatic protons (d, $J= 8\text{ Hz}$, 2H, Ar-H), a singlet peak at δ 8.19 ppm due to CH proton (s, 1H, CH) and another doublet peak at 6.87-6.85 ppm corresponds to two aromatic protons (d, $J= 8\text{ Hz}$, 2H, Ar-H). In ^{13}C NMR spectrum of the compound **3a**, the signals appear at 162.82 and 164.16 ppm corresponds to carbonyl carbons (C=O).

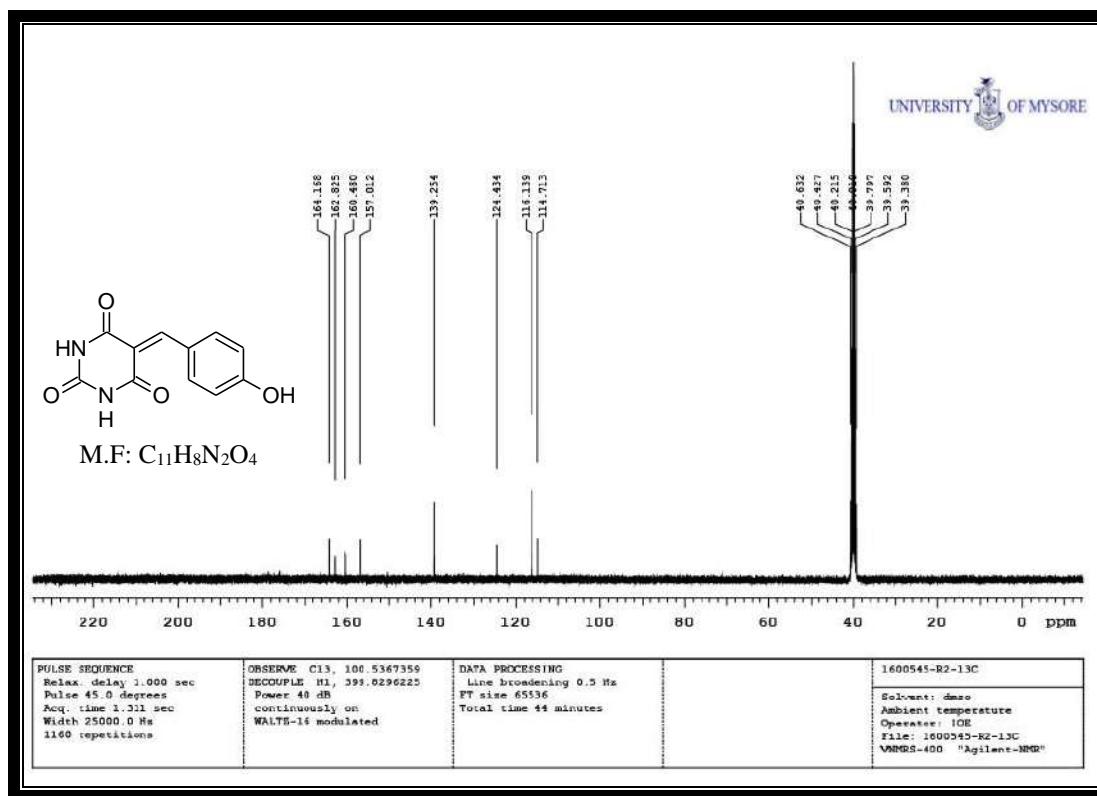
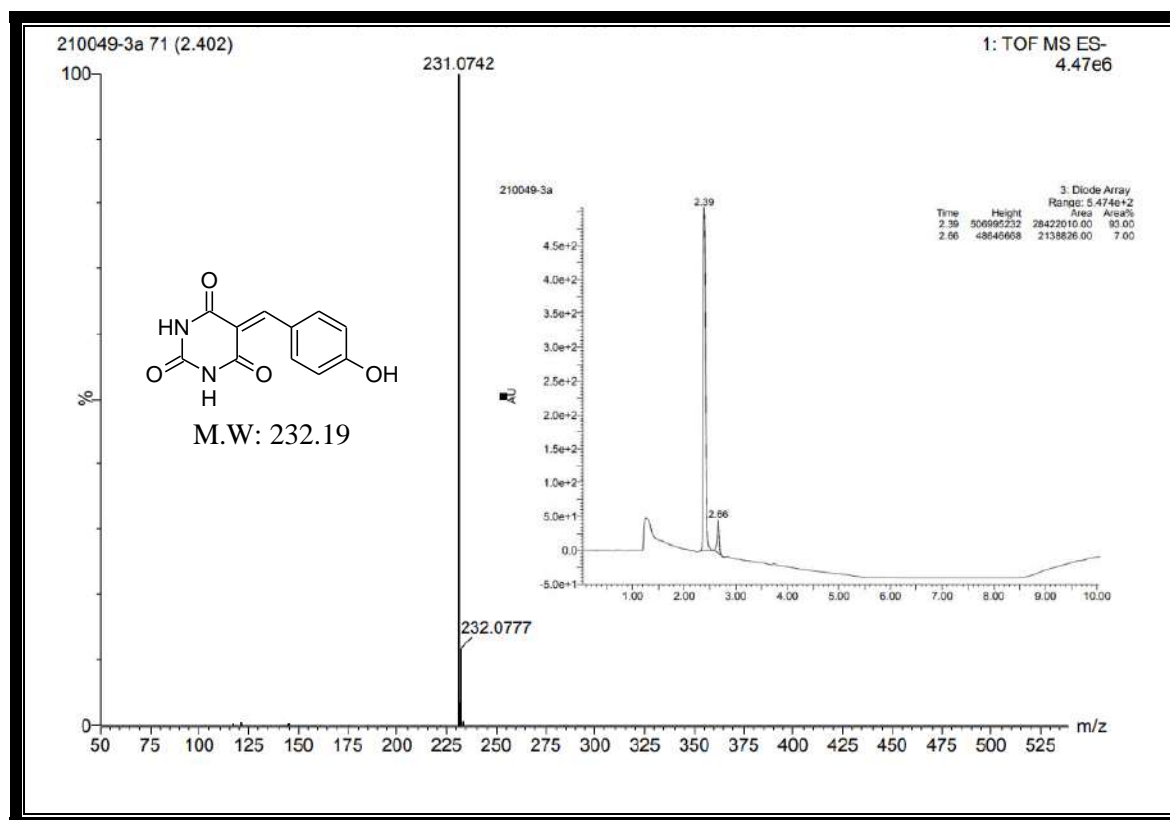
The mass spectrum showed a molecular ion peak m/z at 231.0742 [M^+-1], which corresponds to the molecular weight of the compound **3a**.

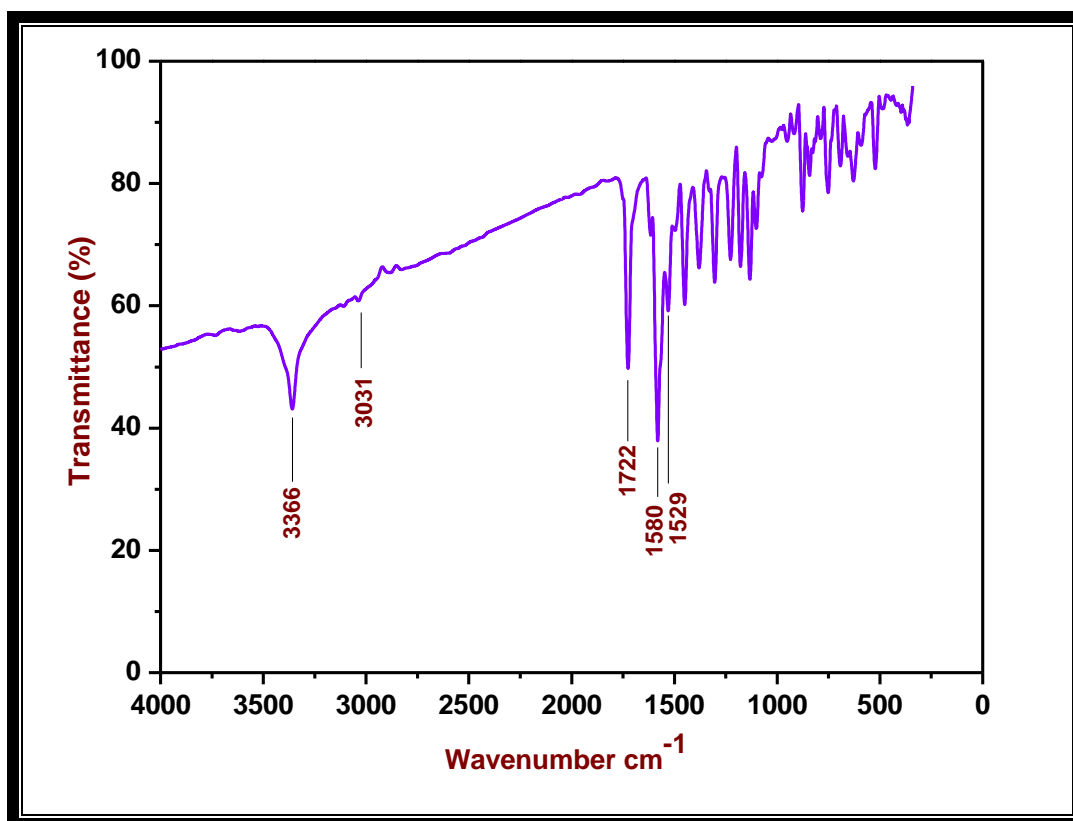
Characterization:



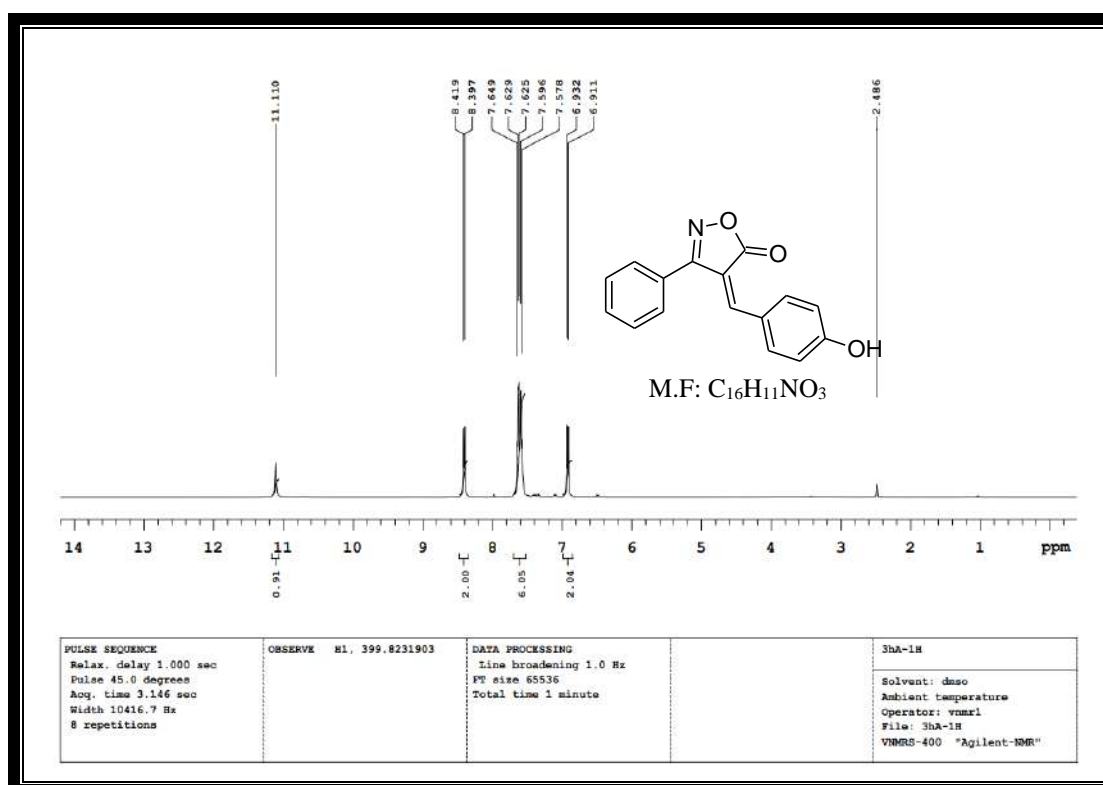
IR spectrum of compound 3a

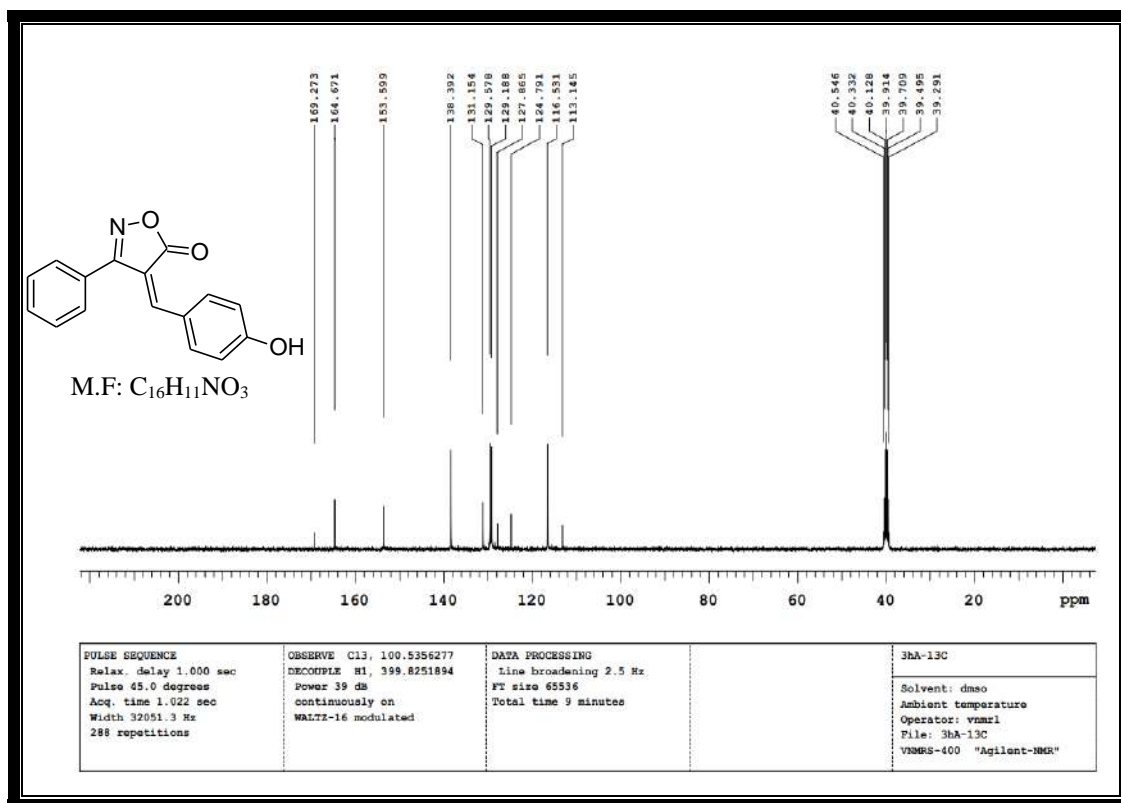
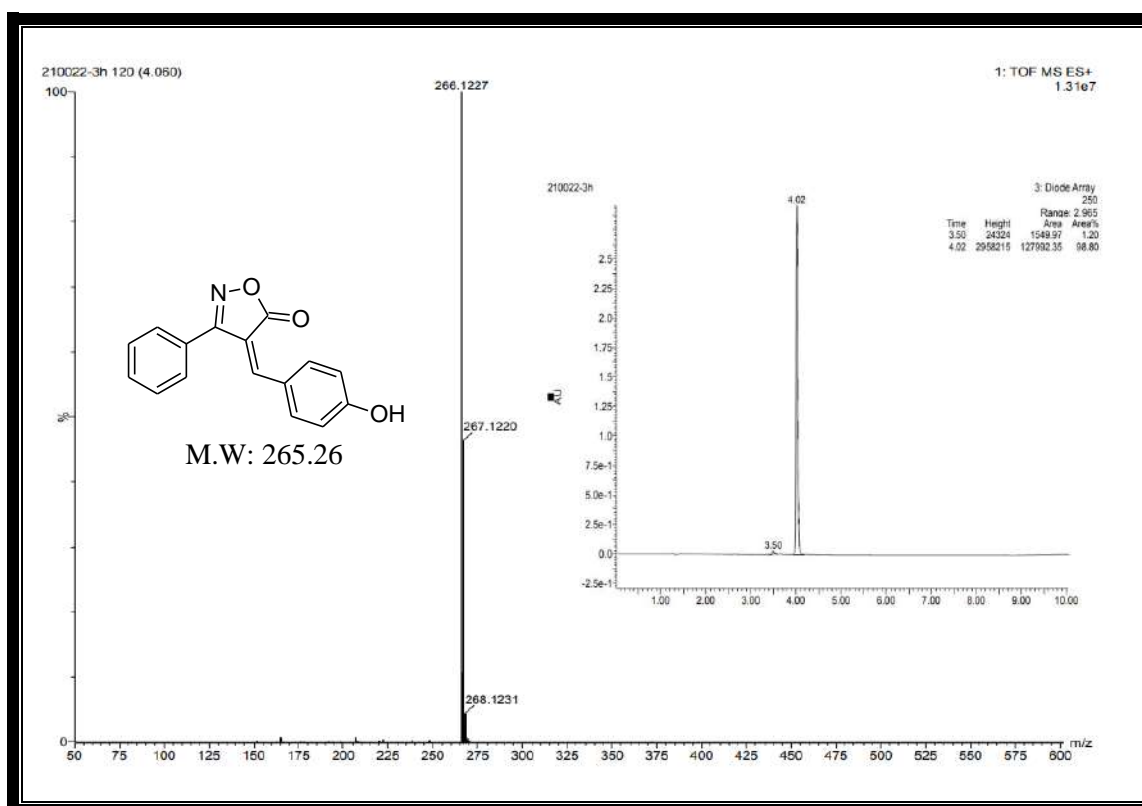
¹H NMR spectrum of compound 3a

**¹³CNMR spectrum of compound 3a****MASS spectrum of compound 3a**



IR spectrum of compound 3h

 ^1H NMR spectrum of compound 3h

¹³CNMR spectrum of compound 3h

MASS spectrum of compound 3h

2A.3. Experimental

2A.3.1. General information:

The reagents and solvents were commercially purchased from Sigma Aldrich and are used without further purification. TLC was used to monitor the progress of the reactions using E. Merck silica gel GF254 precoated on aluminium coated plates. Visualization of the developed chromatogram was performed by UV light (254 and 356 nm). The melting point ranges of solid compounds were determined in open capillary tubes and uncorrected. The absorption spectra of the synthesized compounds were recorded by using HR 4000 UV-Visible Spectrophotometer and DMSO was used as a solvent. The FTIR spectra were obtained using KBr pellets on Bruker FTIR Alpha spectrometer. The ^1H NMR and ^{13}C NMR spectra were recorded on Bruker 400 MHz and 100 MHz in DMSO-d_6 as a solvent respectively and TMS was used as internal standard. Mass spectral data were obtained by Agilent 1200 series LC & Micromass Q spectrometry.

2A.3.2. Procedure for synthesis of substituted-4-hydroxy/methoxy benzylidene derivatives 3(a-i):

A mixture of different active methylene compounds (**1**) (1 mmol) with 4-hydroxy/methoxy benzaldehyde (**2**) (1 mmol) in 15 mL of aqueous ethanol using TiO_2 NPs as a catalyst and was refluxed with constant stirring for about 10 min. Simultaneously, the reaction was monitored by TLC (ethyl acetate: petroleum ether). After completion of reaction, the reaction mixture was cooled to room temperature and poured into the 100 mL of flake ice with vigorous stirring to extract the solid precipitate, which was then filtered, washed with distilled ethanol and dried to yield pure solid products **3(a-i)**.

5-(4-Hydroxybenzylidene)pyrimidine-2,4,6(1H,3H,5H)-trione (3a):

Yellow solid; Yield: 98 %; MP: 300-305 °C; Mol. Formula: C₁₁H₈N₂O₄; UV (nm) λ_{\max} (log ϵ): 468 (3.64), 382 (3.99), 297 (3.93) and 464 (3.74), 377 (3.78), 300 (4.01); FTIR (ν cm⁻¹): 3417 (OH), 3256 (NH), 3096 (CH), 1716 (C=O), 1537 (C=C); ¹H NMR (δ ppm): 11.20 (s, 1H, NH), 11.07 (s, 1H, NH), 10.75 (s, 1H, OH), 8.31-8.29 (d, J = 8 Hz, 2H, Ar-H), 8.19 (s, 1H, CH), 6.87-6.85 (d, J = 8 Hz, 2H, Ar-H); ¹³C NMR (δ ppm): 164.16, 162.82, 160.48, 157.01, 139.25, 124.43, 116.13, 114.71; HRMS: m/z 231.0742 [M⁺-1]; Anal. Calcd: C 56.90, H 3.47 & N 12.06 %, Found: C 56.85, H 3.42 & N 12.02 %.

5-(4-Hydroxybenzylidene)-2-thioxodihydropyrimidine-4,6(1H,5H)-dione (3b):

Orange solid; Yield: 98 %; MP: 330-335 °C; Mol. Formula: C₁₁H₈N₂O₃S; UV (nm) λ_{\max} (log ϵ): 493 (3.57), 413 (3.49) and 490 (3.36), 311 (3.72); FTIR (ν cm⁻¹): 3402 (OH), 3272 (NH), 3011 (CH), 1705 (C=O), 1565 (C=C), 1354 (C=S); ¹H NMR (δ ppm): 12.29 (s, 1H, NH), 12.19 (s, 1H, NH), 10.95 (s, 1H, OH), 8.38-8.36 (d, J = 8 Hz, 2H, Ar-H), 8.23 (s, 1H, CH), 6.90-6.88 (d, J = 8 Hz, 2H, Ar-H); ¹³C NMR (δ ppm): 178.60, 164.16, 162.84, 160.47, 157.05, 139.27, 124.42, 116.14, 114.68; HRMS: m/z 248.9160 [M⁺]; Anal. Calcd: C 53.22, H 3.25 & N 11.28 %, Found: C 53.18, H 3.20 & N 11.22 %.

5-(4-Hydroxybenzylidene)-1,3-dimethylpyrimidine-2,4,6(1H,3H,5H)-trione (3c):

Yellow solid; Yield: 95 %; MP: 295-298 °C; Mol. Formula: C₁₃H₁₂N₂O₄; UV (nm) λ_{\max} (log ϵ): 470 (3.44), 382 (4.18), 296 (3.94) and 467 (3.99), 380 (3.98), 300 (4.04); FTIR (ν cm⁻¹): 3491 (OH), 3001 (CH), 2899 (N-CH₃), 1699 (C=O), 1569 (C=C); ¹H NMR (δ ppm): 10.82 (s, 1H, OH), 8.30-8.28 (d, J = 8 Hz, 2H, Ar-H), 8.25 (s, 1H, CH), 6.88-6.86 (d, J = 8 Hz, 2H, Ar-H), 3.20-3.18 (d, J = 8 Hz, 6H, N-CH₃); ¹³C NMR (δ ppm): 163.49, 163.12, 161.22, 156.73, 151.46, 138.64, 124.16, 115.87, 114.28, 28.97, 28.35; HRMS: m/z 261.0570 [M⁺+1]; Anal. Calcd: C 60.00, H 4.65 & N 10.76 %, Found: C 60.00, H 4.61 & N 10.71 %.

5-(4-Hydroxybenzylidene)-2,2-dimethyl-1,3-dioxane-4,6-dione (3d):

Pale yellow solid; Yield: 85 %; MP: 195-199 °C; Mol. Formula: C₁₃H₁₂O₅; UV (nm) λ_{\max} (log ϵ): 456 (3.47), 372 (3.57) and 450 (3.89), 368 (3.57); FTIR (ν cm⁻¹): 3362 (OH), 3015 (CH), 1692 (C=O), 1564 (C=C); ¹H NMR (δ ppm): 10.91 (s, 1H, OH), 8.24 (s, 1H, CH), 8.15-8.17 (d, J = 8 Hz, 2H, Ar-H), 6.87-6.89 (d, J = 8 Hz, 2H, Ar-H), 1.70 (s, 6H, CH₃); ¹³C NMR (δ ppm): 164.39, 164.13, 158.12, 156.43, 150.44, 137.44, 123.15, 114.57, 113.18, 24.66, 24.05; HRMS: m/z 248.9160 [M⁺]. Anal. Calcd: C 62.90, H 4.87 %, Found: C 62.85, H 4.82 %.

5-(4-Hydroxy-3-methoxybenzylidene)pyrimidine-2,4,6(1H,3H,5H)-trione (3e):

Yellow solid; Yield: 89 %; MP: 240-242 °C; Mol. Formula: C₁₂H₁₀N₂O₅; UV (nm) λ_{\max} (log ϵ): 484 (3.79), 404 (3.67), 294 (3.96) and 481 (4.10), 300 (4.03); FTIR (ν cm⁻¹): 3490 (OH), 3252 (NH), 3008 (CH), 2820 (OCH₃), 1674 (C=O), 1554 (C=C); ¹H NMR (δ ppm): 11.22 (s, 1H, NH), 11.09 (s, 1H, NH), 10.51 (s, 1H, OH), 8.45 (s, 1H, Ar-H), 8.20 (s, 1H, CH), 7.79-7.76 (m, 1H, Ar-H), 6.89-6.87 (d, J = 8 Hz, 1H, Ar-H), 3.81 (s, 3H, OCH₃); ¹³C NMR (δ ppm): 163.45, 163.95, 162.64, 146.29, 146.11, 136.77, 128.80, 116.24, 112.03, 50.233; HRMS: m/z 261.9065 [M⁺-1]; Anal. Calcd: C 54.97, H 3.84 & N 10.68 %, Found: C 54.93, H 3.79 & N 10.62 %.

2-(4-Hydroxybenzylidene)-1H-indene-1,3(2H)-dione (3f):

Green solid; Yield: 93 %; MP: 238-240 °C; Mol. Formula: C₁₆H₁₀O₃; UV (nm) λ_{\max} (log ϵ): 506 (3.91), 400 (3.73) and 506 (3.77), 393 (3.86); FTIR (ν cm⁻¹): 3499 (OH), 3011 (CH), 1672 (C=O), 1557 (C=C); ¹H NMR (δ ppm): 10.84 (s, 1H, OH), 8.51-8.49 (d, J = 8 Hz, 2H, Ar-H), 7.90-7.88 (d, J = 8 Hz, 4H, Ar-H), 7.71 (s, 1H, CH), 6.93-6.91 (d, J = 8 Hz, 2H, Ar-H); ¹³C NMR (δ ppm): 190.34, 189.38, 163.68, 146.66, 142.04, 139.61, 137.98, 135.90, 135.73, 125.57, 125.00, 123.11, 123.06, 116.38; HRMS: m/z 250.0856 [M⁺]; Anal. Calcd: C 76.79, H 4.03 %, Found: C 76.72, H 4.00 %.

4-(4-Hydroxybenzylidene)-5-methyl-2-phenyl-2,4-dihydro-3H-pyrazol-3-one (3g):

Orange solid; Yield: 85 %; MP: 132-135 °C; Mol. Formula: C₁₇H₁₄N₂O₂; UV (nm) λ_{max} (log ε): 372 (4.09) and 488 (3.36), 368 (4.05), 301 (4.04); FTIR (ν cm⁻¹): 3356 (OH), 3010 (CH), 1678 (C=O), 1601 (C=N), 1553 (C=C); ¹H NMR (δ ppm): 10.79 (s, 1H, OH), 8.63-8.61 (d, *J* = 8 Hz, 2H, Ar-H), 7.92-7.90 (d, *J* = 8 Hz, 2H, Ar-H), 7.68 (s, 1H, CH), 7.43-7.39 (t, 2H, Ar-H), 7.18-7.14 (t, 1H, Ar-H), 6.93-6.91 (d, *J* = 8 Hz, 2H, Ar-H), 2.32-2.30 (d, *J* = 8 Hz, 3H, CH₃); ¹³C NMR (δ ppm): 190.34, 169.45, 157.45, 144.13, 140.11, 137.41, 136.72, 132.41, 131.42, 129.21, 128.40, 123.14, 117.47, 113.48, 20.82; HRMS: *m/z* 279.1800 [M⁺+1]. Anal. Calcd: C 73.37, H 5.07 & N 10.07 %, Found: C 73.31, H 5.01 & N 10.02 %.

4-(4-Hydroxybenzylidene)-3-phenylisoxazol-5(4H)-one (3h):

Yellow solid; Yield: 90 %; MP: 210-212 °C; Mol. Formula: C₁₆H₁₁NO₃; UV (nm) λ_{max} (log ε): 482 (3.80), 400 (3.27) and 481 (4.22), 320 (3.51); FTIR (ν cm⁻¹): 3366 (OH), 3031 (CH), 1722 (C=O), 1580 (C=N), 1529 (C=C); ¹H NMR (δ ppm): 11.11 (s, 1H, OH), 8.41-8.39 (d, *J* = 8 Hz, 2H, Ar-H), 7.64-7.57 (m, 6H, Ar-H), 6.93-6.91 (d, *J* = 8 Hz, 2H, Ar-H); ¹³C NMR (δ ppm): 169.27, 164.67, 153.59, 138.39, 131.15, 129.57, 129.18, 127.86, 124.79, 116.53, 113.14; HRMS: *m/z* 266.1227 [M⁺+1]; Anal. Calcd: C 72.45, H 4.18 & N 5.28 %, Found: C 72.41, H 4.12 & N 5.21 %.

5-(4-Methoxybenzylidene)pyrimidine-2,4,6(1H,3H,5H)-trione (3i):

Pale yellow solid; Yield: 89 %; MP: 295-297 °C; Mol. Formula: C₁₂H₁₀N₂O₄; UV (nm) λ_{max} (log ε): 372 (4.15), 298 (3.94) and 368 (4.13), 300 (4.05); FTIR (ν cm⁻¹): 3260 (NH), 3018 (CH), 2838 (OCH₃), 1678 (C=O), 1556 (C=C); ¹H NMR (δ ppm): 11.27 (s, 1H, NH), 11.14 (s, 1H, NH), 8.36-8.34 (d, *J* = 8 Hz, 2H, Ar-H), 8.23 (s, 1H, CH), 7.06-7.04 (d, *J* = 8 Hz, 2H, Ar-H), 3.86 (s, 3H, OCH₃); ¹³C NMR (δ ppm): 164.48, 164.24, 162.98, 160.54, 157.52, 139.42, 124.24, 116.13, 114.34, 55.96; HRMS: *m/z* 247.1104 [M⁺+1]; Anal. Calcd: C 58.54, H 4.09 & N 11.38 %, Found: C 58.50, H 4.02 & N 11.32 %.

2A.4. Absorption property

The UV-Visible spectra of compounds **3(a-i)** were recorded in two different solvents (DMSO & DMF) at 10^{-5} M concentration using UV-Visible spectrophotometer. The λ_{\max} and molar absorption coefficient values were appended in **Table 2**. All the synthesized compounds exhibited 2 to 3 absorption maxima (λ_{\max}) in the range of 294-506 nm in DMSO and 300-506 nm in DMF solvents due to the $\pi-\pi^*$ & $n-\pi^*$ transitions (**Fig. 3**) [34]. Among them, compound **3f** shows highest absorption maxima at 400, 506 & 393, 506 nm in DMSO and DMF respectively.

Table 2. Electronic absorption data of the synthesized compounds **3(a-i)** in DMSO & DMF solvents.

Compd.	DMSO		DMF	
	$\lambda_{\max}(\text{nm})$	Log ϵ	$\lambda_{\max}(\text{nm})$	Log ϵ
3a	297	3.93	300	4.01
	382	3.99	377	3.78
	468	3.64	464	3.74
3b	413	3.49	311	3.72
	493	3.57	490	3.36
3c	296	3.94	300	4.04
	382	4.18	380	3.98
	470	3.44	467	3.99
3d	372	3.57	368	3.57
	456	3.47	450	3.89
3e	294	3.96	300	4.03
	404	3.67	481	4.10
	484	3.79	-	-
3f	400	3.73	393	3.86
	506	3.91	506	3.77
3g	372	4.09	301	4.04
	-	-	368	4.05
	-	-	488	3.36
3h	400	3.27	320	3.51
	482	3.80	481	4.22
3i	298	3.94	300	4.05
	372	4.15	368	4.13

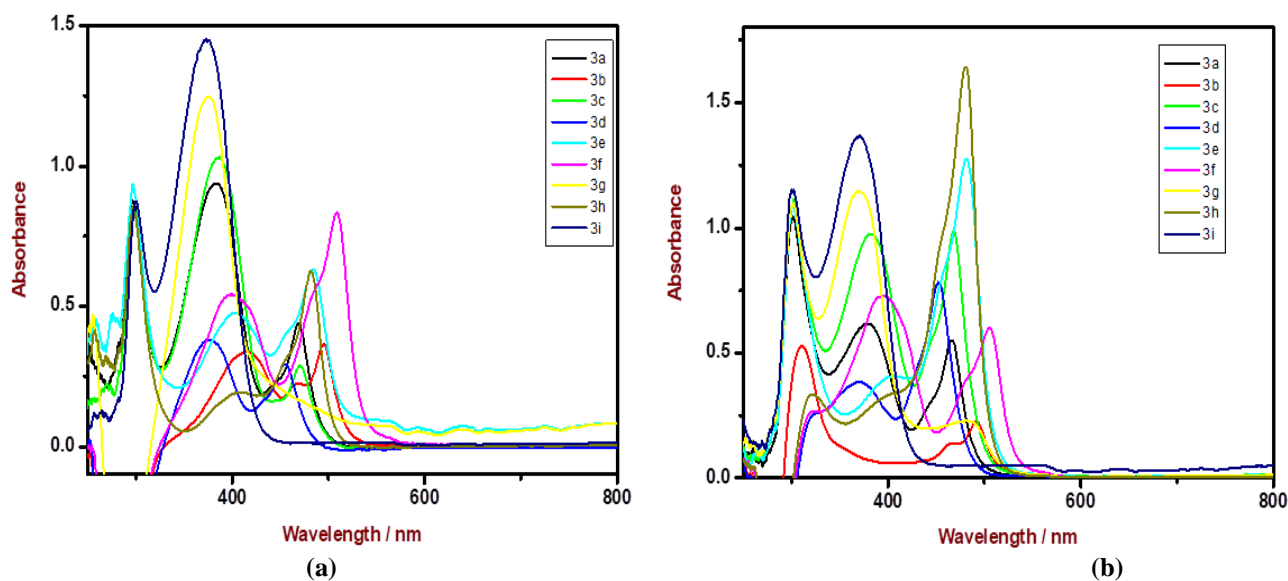


Fig. 3. UV-Visible spectrum of synthesized compounds **3(a-i)** in DMSO (a) & DMF (b).

2A.5. Pharmacological studies

2A.5.1. DPPH and Nitric oxide radical scavenging activities

Evaluation of antioxidant activity of obtained compounds **3(a-i)** was done by spectrophotometrically using two different radical scavenging assays *viz.* DPPH [35] and nitric oxide [36]. The DPPH is a stable free radical with maximum absorption at 517 nm and is reduced to a corresponding hydrazine when it reacts with hydrogen donors. When DPPH reacts with an antioxidant agent, it can donate hydrogen get reduced and deep violet colour of DPPH change to yellow, showing a considerable decreased in absorption at 517 nm. DPPH solution (3 $\mu\text{g/mL}$) was prepared in methanol (methanol: DPPH in 1:1) for blank reference. Here we used two different concentrations (100 & 200 $\mu\text{g/mL}$) of synthesized compounds and standard BHT (in methanol). Then 1 mL of each concentration of synthesized compounds and standard was added to 1 mL of DPPH solution. The solution mixture was shaken vigorously and kept in dark place for 30 min at room temperature. After that, the absorbance was measured by UV at 517 nm.

Nitric oxide (NO) scavenging activity was carried out by Garrat method based on the diazotization reaction described by Griess. The assay uses sodium nitroprusside as the source

of NO and sulfanilamide and *N*-1-naphthylethylenediamine dihydrochloride under acidic conditions to detect NO_2^- generated at the expense of NO by the antioxidant system. Here also used two different concentrations (100 & 200 $\mu\text{g/mL}$) of synthesized compounds in DMSO were mixed with 20 mM sodium nitroprusside solution. Total volume was made up to 1,000 μL with 200 mM Phosphate buffer, pH 7.4. The contents were mixed well and incubated at 37 °C for 2 h followed by addition of Griess reagent (100 μL). The mixture was kept at room temperature for 20 min. Optical density (OD) of the coloured solution formed was measured at 528 nm. Ascorbic acid was used as the positive control. Radical scavenging activities were calculated using the formula.

$$\% \text{ inhibition} = [(A_{\text{control}} - A_{\text{test}}) / A_{\text{control}}] \times 100$$

Where A_{control} is the absorbance of the control reaction and A_{test} is the absorbance of the synthesized compound. IC_{50} value was calculated using the formula:

$$\text{IC}_{50} = [(\Sigma C / \Sigma I) \times 50]$$

Where ΣC is the sum of synthesized compound concentrations used to test and ΣI is the sum of % of inhibition at different concentration. Each value is expressed as mean \pm SD of three replicates.

2A.5.2. Anti-tubercular activity

Anti-tubercular activity of all the synthesized compounds was carried out by Microplate Alamar Blue assay (MABA) method and using eight different concentrations (0.8, 1.6, 3.12, 6.25, 12.5, 25, 50 & 100 $\mu\text{g/mL}$) for analysis against *M. tuberculosis* (H37RV strain) [37]. About 200 μL of sterile deionized water was added to all outer perimeter wells of sterile 96 wells plate to minimized evaporation of medium in the test wells during incubation. The 96-wells plate received 100 μL of the Middlebrook 7H9 broth and serial dilution of compounds were made directly on a plate. About 0.8 to 100 $\mu\text{g/mL}$ concentration of synthesized compounds were tested. Plates were covered and sealed with parafilm and incubated at 37 °C

for five days. After that, 25 μ L of freshly prepared 1:1 mixture of Almar Blue reagent and 10 % tween 80 was added to the plate and incubated for 24 hrs. A blue color in the well was interpreted as no bacterial growth and pink color was scored as growth. The results were explained in terms of minimum inhibitory concentration (MIC) and Isoniazid, Ethambutol, Pyrazinamide, Rifampicin and Streptomycin were used as standard drugs for comparison.

2A.5.3. *in silico* molecular docking study

in silico molecular docking study was used to predict the binding affinity of the compounds and also used to assess the orientation of inhibitors bound in the active pockets of receptors. The antioxidant and anti-tubercular activity results of synthesized compounds were subjected to molecular docking studies using Auto Dock (version 4.2) with the Lamarckian genetic algorithm. The synthesized compounds having 2D structures were converted to energy minimized 3D structures and were further used for *in silico* protein-ligand docking [38]. The obtained compounds were used as ligand and docking receptors are Human peroxiredoxin 5 (PDB ID: 1HD2) and InhA(enoyl-ACP reductase) (PT70 PDB ID: 2X22) respectively [39].

2A.6. Results and discussion

2A.6.1. Antioxidant activity

The synthesized compounds **3(a-i)** were screened for their free radical scavenging activity by DPPH and nitric oxide methods. All the compounds showed varied free radical scavenging capacity in assessment with the standard BHT. Among all the synthesized compounds, **3e** demonstrated the most effective antioxidant efficacy with an IC_{50} value of 105.48 μ g/mL when compared to the reference standard BHT (IC_{50} 91.23 μ g/mL) and compounds **3d**, **3f**, **3g** and **3i** with an IC_{50} value range of 113.45-123.30 μ g/mL have showed

promising antioxidant activity and rest of the compounds shows moderate scavenging activity and as shown in **Fig. 4(a)**.

Nitric oxide radical scavenging activity results of the synthesized compounds **3(a-i)** have been shown in **Fig. 4(b)**. From the activity results, compounds **3g** and **3h** (IC_{50} value 139.12 and 129.72 $\mu\text{g/mL}$) showed effective scavenging activity as compared to the reference standard ascorbic acid (IC_{50} 117.91 $\mu\text{g/mL}$). Rest of the compounds also showed good to moderate antioxidant activity with IC_{50} value range of 129.72-180.07 $\mu\text{g/mL}$. Therefore, all the synthesized compounds **3(a-i)** exhibited more effective antioxidant efficacy due to the presence of the electron donating group (OH) at para position of the phenyl ring [40] and the results have been appended in the **Table 3**.

Table 3. DPPH and Nitric oxide radical scavenging activity of synthesized compounds **3(a-i)**.

Compd.	DPPH radical scavenging activity		IC_{50} ($\mu\text{g/mL}$)	Nitric oxide radical scavenging activity		IC_{50} ($\mu\text{g/mL}$)
	% of inhibition			% of inhibition		
	100 $\mu\text{g/mL}$	200 $\mu\text{g/mL}$		100 $\mu\text{g/mL}$	200 $\mu\text{g/mL}$	
3a	38.94 \pm 0.17	61.58 \pm 0.15	149.22	35.39 \pm 0.17	68.92 \pm 0.25	143.80
3b	36.45 \pm 0.25	74.12 \pm 0.17	135.66	32.24 \pm 0.10	64.23 \pm 0.25	152.33
3c	29.20 \pm 0.25	64.22 \pm 0.35	160.56	25.98 \pm 0.20	57.32 \pm 0.10	180.07
3d	39.97 \pm 0.45	81.87 \pm 0.10	123.11	32.58 \pm 0.20	71.54 \pm 0.15	144.06
3e	54.27 \pm 0.10	87.93 \pm 0.17	105.48	34.28 \pm 0.10	61.89 \pm 0.17	155.97
3f	48.24 \pm 0.20	83.97 \pm 0.15	113.45	28.97 \pm 0.15	61.39 \pm 0.25	166.00
3g	51.21 \pm 0.15	79.24 \pm 0.25	114.98	34.84 \pm 0.20	72.98 \pm 0.10	139.12
3h	30.42 \pm 0.15	59.23 \pm 0.25	167.31	41.25 \pm 0.10	74.38 \pm 0.17	129.72
3i	41.51 \pm 0.10	80.14 \pm 0.20	123.30	31.24 \pm 0.10	64.33 \pm 0.20	156.95
Standard^{a, b}			91.23			117.91

Each value is expressed as mean \pm SD of three replicates

Standard^a: BHT used as reference standard for DPPH method

Standard^b: Ascorbic acid used as reference standard for Nitric oxide method.

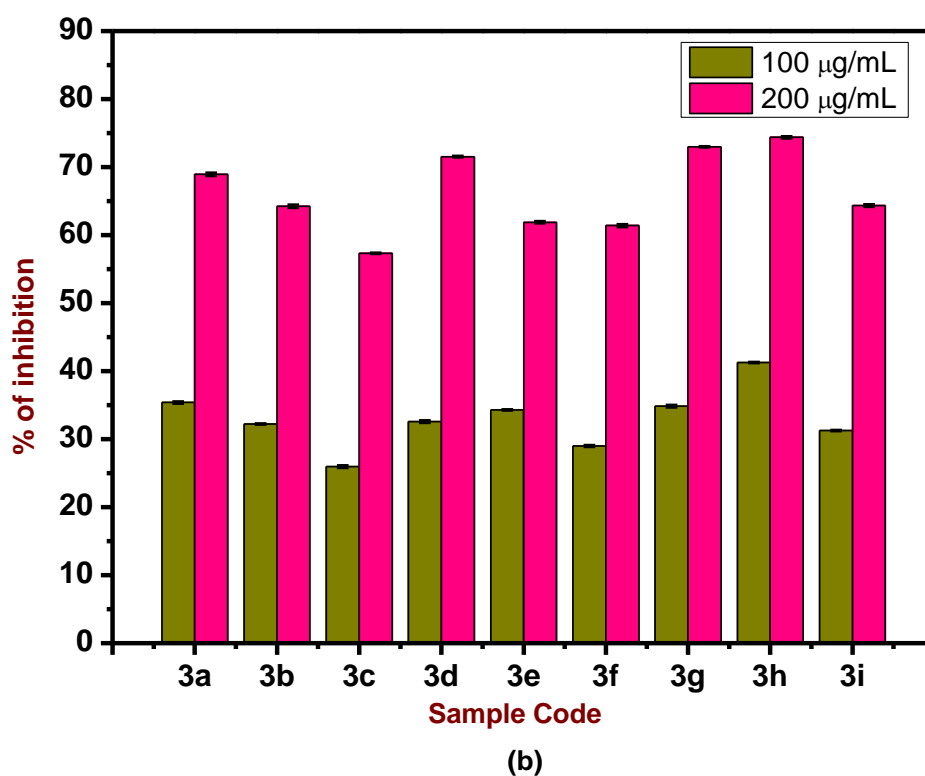
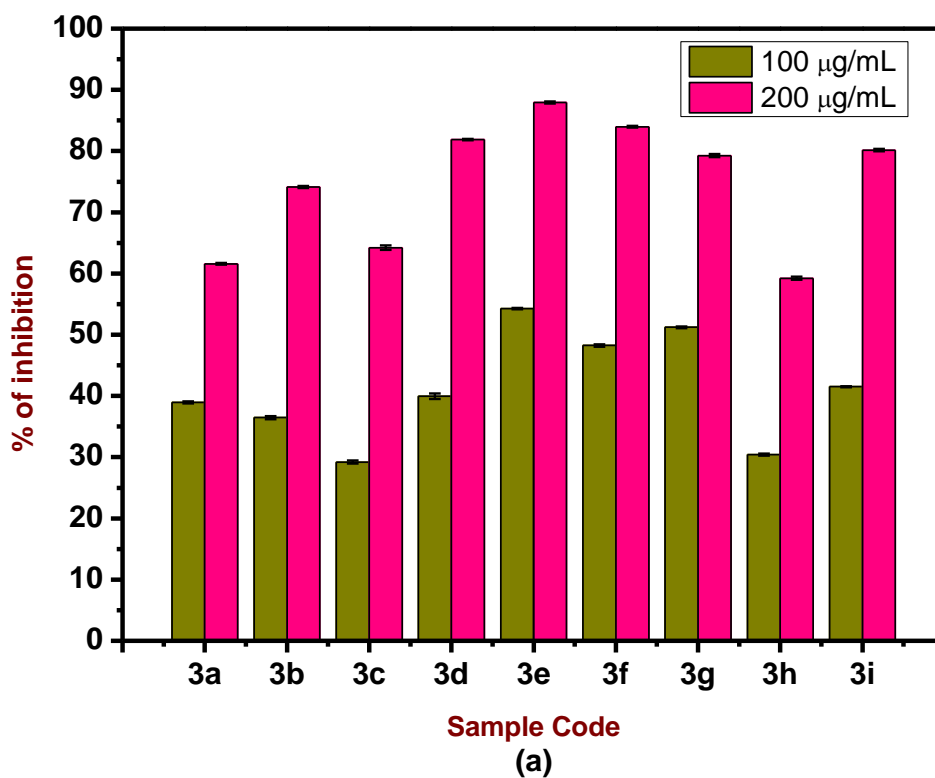


Fig. 4. Antioxidant activity of synthesized compounds 3(a-i) by DPPH method (a) and Nitric oxide radical method (b).

2A.6.2. Anti-tubercular activity

The synthesized compounds were also screened for anti-TB activity against H37RV strain. Among the tested compounds, compound **3b** exhibited good anti-TB efficacy with MIC value of 25 $\mu\text{g/mL}$ due to the presence of thioxo group (C=S) and rest of the compounds showed moderate activity with MIC value range of 50-100 $\mu\text{g/mL}$ as compared to anti-TB standard drugs (**Table 4** and **Fig. 5**). The presence of the electron withdrawing group at the para position was highly favourable to the MTB growth inhibition, while electron donating group leads to inactive or decreases in the growth inhibition [41]. Our synthesized compounds having electron donating group (-OH) at the para position of the phenyl ring, due to this reason growth inhibition occurs at higher concentration as compared to standard drugs.

Table 4. Anti-tubercular activity results of synthesized compounds **3(a-i)**.

Compd.	100 $\mu\text{g/mL}$	50 $\mu\text{g/mL}$	25 $\mu\text{g/mL}$	12.5 $\mu\text{g/mL}$	6.25 $\mu\text{g/mL}$	3.12 $\mu\text{g/mL}$	1.6 $\mu\text{g/mL}$	0.8 $\mu\text{g/mL}$
3a	S	S	R	R	R	R	R	R
3b	S	S	S	R	R	R	R	R
3c	S	S	R	R	R	R	R	R
3d	S	S	R	R	R	R	R	R
3e	S	S	R	R	R	R	R	R
3f	S	S	R	R	R	R	R	R
3g	S	S	R	R	R	R	R	R
3h	S	S	R	R	R	R	R	R
3i	S	S	R	R	R	R	R	R
Std^a	S	S	S	S	S	S	S	R
Std^b	S	S	S	S	S	S	S	R
Std^c	S	S	S	S	S	S	R	R
Std^d	S	S	S	S	S	S	S	S
Std^e	S	S	S	S	S	S	S	S

S-Sensitive, **R**- Resistant, **Std^a**- Isoniazid, **Std^b**- Ethambutol, **Std^c**- Pyrazinamide, **Std^d**- Rifampicin, **Std^e**- Streptomycin

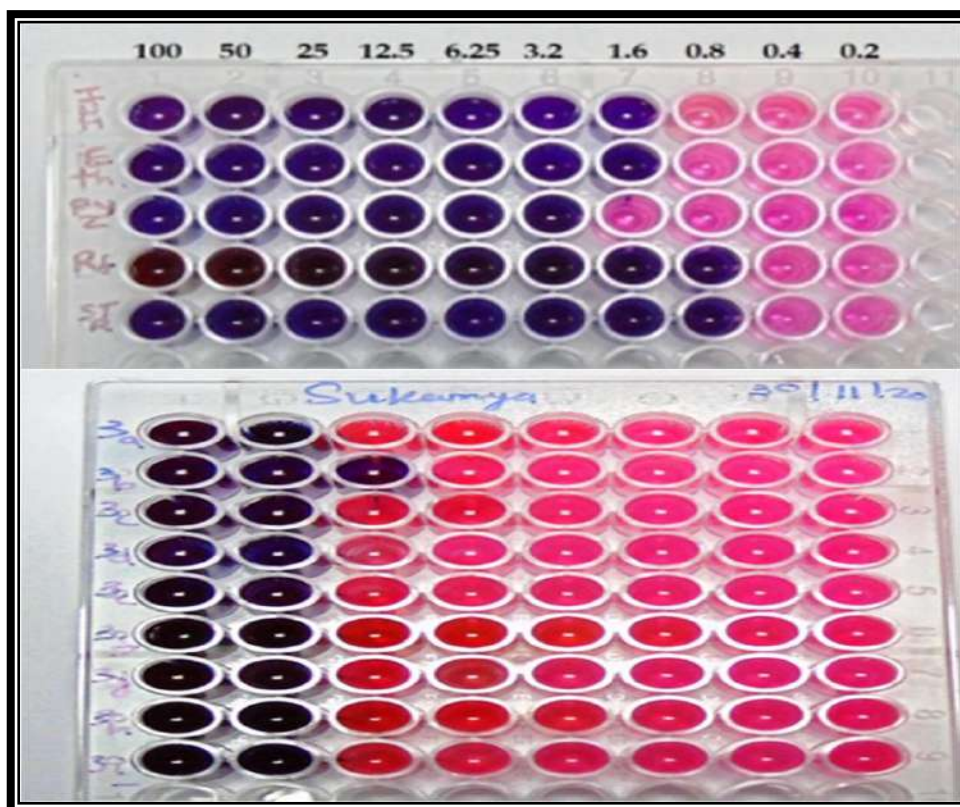


Fig. 5. Images of anti-TB activity results of the synthesized compounds **3(a-i)**.

2A.6.3. *in silico* molecular docking study

The docking of receptors Human peroxiredoxin 5 for antioxidant activity with **3(a-i)** and InhA(enoyl-ACP reductase) for anti-tubercular activity with obtained compound **3b** exhibited well-established bonds with amino acids (Thr44, Gly46, Cys47, Ile119 and Ile194, Gly96, Leu197, Ser94, Ala198, Ala22 & Thr196) in the receptor active pocket (**Fig. 6 & 7**).

The docking results of antioxidant activity revealed that the compounds **3(a-i)** had significant binding modes, with docking scores ranging from -4.7 to -5.8 kcal/mol and 3-4 hydrogen bonds respectively as compared with the reference standard ascorbic acid (-6.5 kcal/mol). In that, the compound **3h** showed least binding energy -5.8 kcal/mol has almost near dock score compared with the reference standard ascorbic acid (-6.5 kcal/mol) as shown in **Table 5 & Fig. 6**.

The anti-tubercular activity of synthesized compound **3b** showed good sensitivity; therefore, it was selected for an *in-silico* molecular docking study with InhA (enoyl-ACP reductase) as an inhibitor. The docking analysis suggested an encouraging complement of compound **3b** and standard drugs with ACP reductase. The compound **3b** was interacted with ACP reductase active site with least binding energy of -8.0 kcal/mol and three hydrogen bonds when compared with standard drugs Streptomycin, Pyrazinamide and Isoniazide (-9.3, -8.9 and -6.9 kcal/mol respectively). Hence, **3b** showed almost a near dock score compared with the standard drug Pyrazinamide (-8.9 kcal/mol) as shown in **Table 6 & Fig. 7**.

Table 5. *in silico* molecular docking results for antioxidant activity of synthesized compounds **3(a-i)** and standard drug (ascorbic acid).

Compd.	Affinity (kcal/mol)	H-bonds	H-bond length (Å)	H-bond with amino acids	Hydrophobic interactions
3a	-5.1	3	2.76	1HD2:Thr44:: 3a :O4	Pro45, Leu116, Ile119, Arg127, Thr147
			2.88	1HD2:Gly46:: 3a :O4	
			3.20	1HD2:Cys47:: 3a :O4	
3b	-5.0	4	2.77	1HD2:Thr44:: 3b :O3	Pro45, Leu116, Ile119, Arg127, Thr147
			2.90	1HD2:Gly46:: 3b :O4	
			3.18	1HD2:Cys47:: 3b :O4	
3c	-5.1	3	2.75	1HD2:Thr44:: 3c :O4	Pro45, Leu116, Ile119, Arg127, Thr147
			2.92	1HD2:Gly46:: 3c :O4	
			3.21	1HD2:Cys47:: 3c :O4	
3d	-5.2	3	2.77	1HD2:Thr44:: 3d :O3	Pro45, Leu116, Ile119, Arg127, Thr147
			2.88	1HD2:Cys47:: 3d :O3	
			3.19	1HD2:Gly46:: 3d :O3	
3e	-5.3	3	2.81	1HD2:Thr44:: 3e :O5	Leu116, Ile119, Arg127, Thr147
			2.93	1HD2:Cys47:: 3e :O5	
			3.25	1HD2:Gly46:: 3e :O5	
3f	-5.4	3	2.85	1HD2:Thr44:: 3f :O3	Pro45, Leu116, Ile119, Phe120, Arg127, Thr147
			2.88	1HD2:Cys47:: 3f :O3	
			3.18	1HD2:Gly46:: 3f :O3	
3g	-5.5	1	3.14	1HD2:Ile119:: 3g :O2	Pro40, Thr44, Phe120, Arg127, Thr147
3h	-5.8	3	2.91	1HD2:Thr44:: 3h :O3	Leu116, Phe120, Arg127, Thr147
			3.06	1HD2:Gly46:: 3h :O3	
			3.34	1HD2:Cys47:: 3h :O3	

3i	-4.7	2	3.25	1HD2:Gly46:: 3i :O2	Pro40, Cys47, Leu116, Ile119, Phe120, Arg127, Thr147
			3.31	1HD2:Thr44:: 3i :O2	
Ascorbic Acid	-6.5	5	2.80	1HD2:Gly46:: Aca :O5	Pro40, Pro45, Phe120, Arg127, Thr147
			2.80	1HD2:Thr44:: Aca :O5	
			3.01	1HD2:Thr44:: Aca :O6	
			3.15	1HD2:Gly46:: Aca :O4	
			3.17	1HD2:Cys47:: Aca :O5	

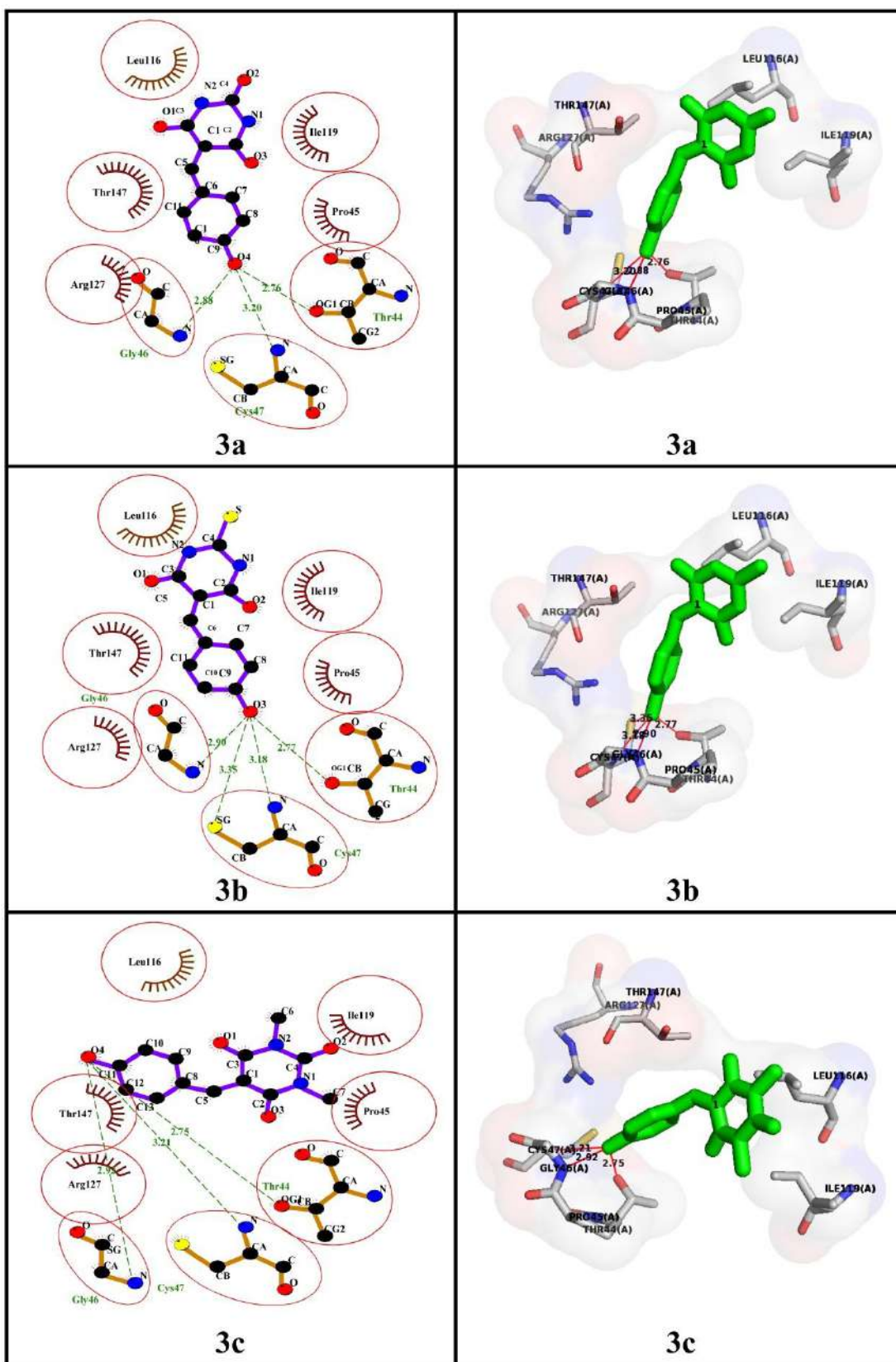
Protein Name: Crystal structure of Human peroxiredoxin 5 (PDB ID: 1HD2).

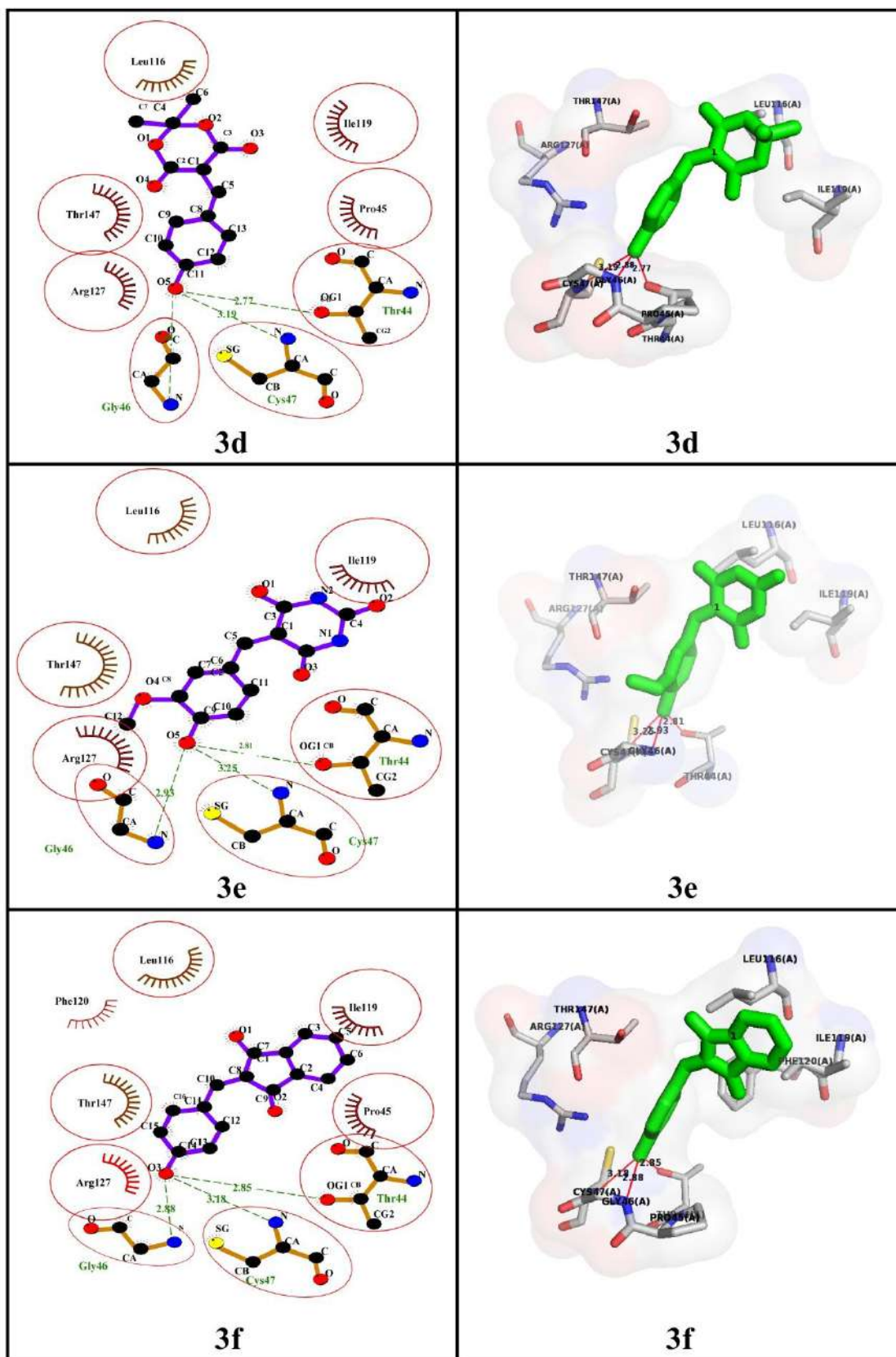
Table 6. *in silico* molecular docking results for Anti-TB activity of synthesized compound **3b** and Standard drugs (Streptomycin, Pyrazinamide and Isoniazid).

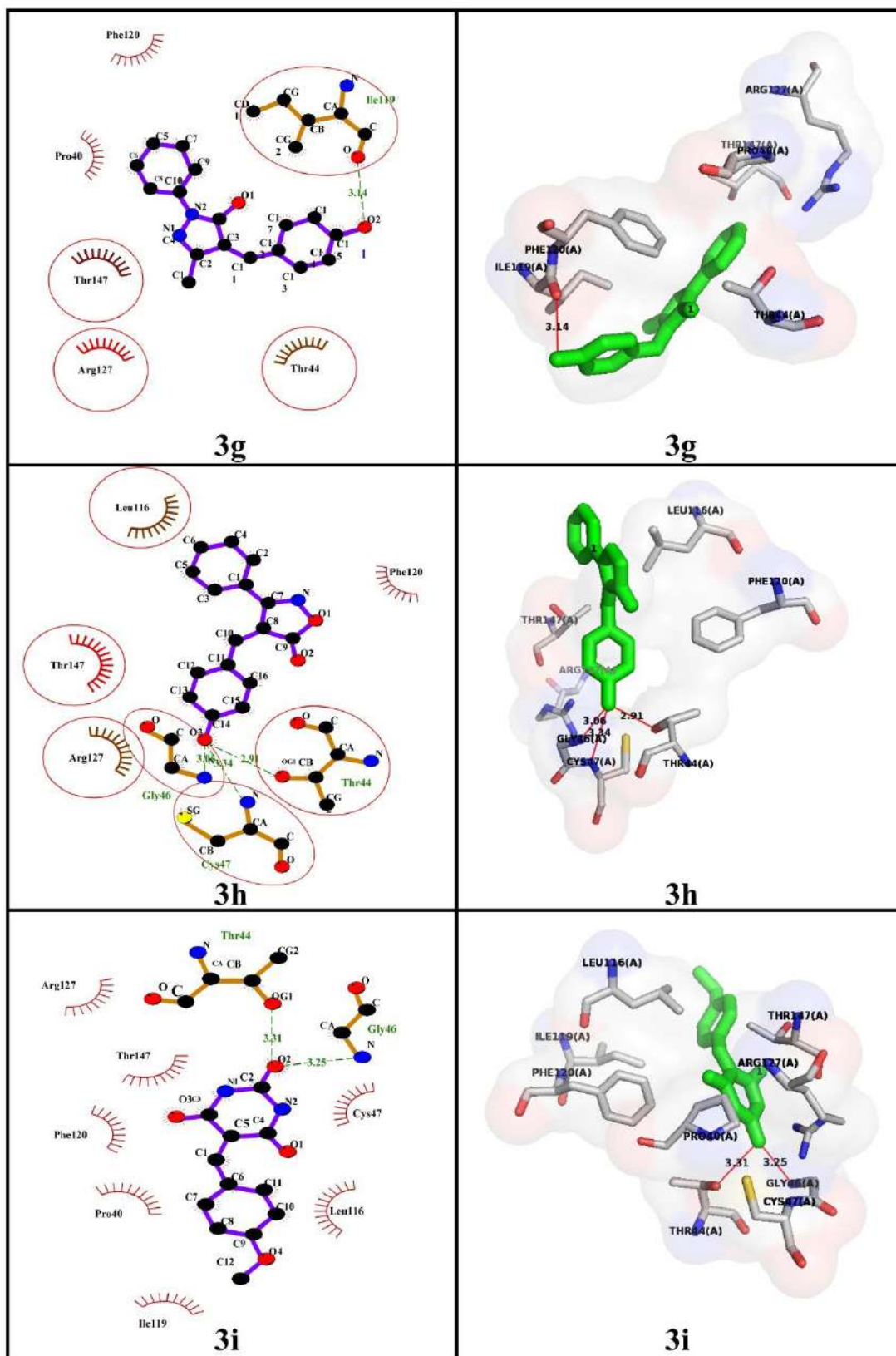
Compd.	Affinity (kcal/mol)	H-bonds	H-bond length (Å)	H-bond with amino acids	Hydrophobic interactions
3b	-8.0	3	2.89	2X22:Ser94:: 3b :O3	Ser20, Ile21, Ala198
			3.17	2X22:Ala22:: 3b :O3	
			3.24	2X22:Thr196:: 3b :O2	
STR	-9.3	5	2.90	2X22:Ile194:: STR :OAB	Ile16, Ser20, Ile21, Ile95, Met147, Asp148, Phe149, Tyr158, Met161, Lys165, Gly192, Thr196, Met199, Ile202, Val203,
			2.96	2X22:Gly96:: STR :O3	
			3.07	2X22:Leu197:: STR :O6	
			3.11	2X22:Ser94:: STR :O3	
			3.29	2X22:Ala198:: STR :O6	
PZY	-8.9	1	2.96	2X22:Ser94:: PZY :N3	Gly14, Ser20, Ile21, Ala22, Ile95, Gly96
IZA	-6.9	2	2.97	2X22:Gly96:: IZA :N3	Phe41, Leu63, Asp64, Val65, Ile95, Ile122
			3.06	2X22:Gly96:: IZA :N2	

STR: Streptomycin; **PZY:** Pyrazinamide; **IZA:** Isoniazid

Protein Name: Crystal structure of *M. tuberculosis* InhA (enoyl-ACP reductase) inhibited by PT70 (PDB ID: 2X22).







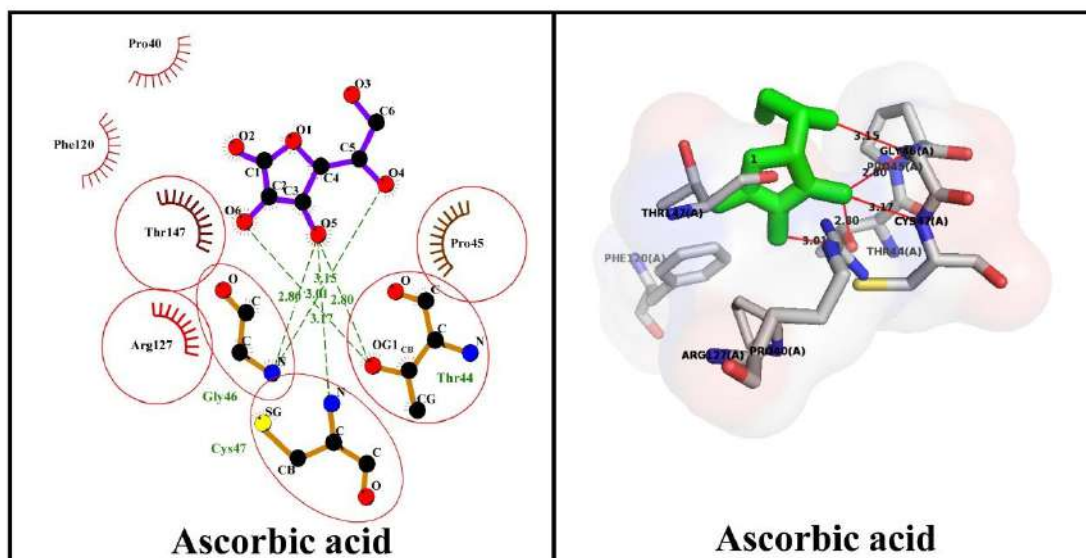


Fig. 6. 2D & 3D interaction of synthesized compounds **3(a-i)** and reference standard (ascorbic acid) with Human peroxiredoxin 5.

2A.7. Conclusion

In this chapter, we developed a simple and efficient method for the synthesis of substituted-4-hydroxy/methoxy benzylidene derivatives **3(a-i)** as a potent antioxidant and anti-TB agents. It is a facile synthetic approach for environment-friendly, mild reaction conditions, simple work-up procedure, shorter reaction time and excellent yield. Also, activity results suggested that, compound **3e** showed more potent DPPH scavenging activity and **3h** exhibited very effective nitric oxide radical scavenging activity as compared to reference standard BHT and ascorbic acid, respectively. Anti-TB activity results suggested that, the compound **3b** exhibited more potent efficacy with MIC value of 25 $\mu\text{g/mL}$. Moreover, docking results for antioxidant and anti-tubercular activity of synthesized compounds revealed that, the compounds **3h** and **3b** showed least binding energy of -5.8 and -8.0 kcal/mol almost near dock scores compared with the reference standards ascorbic acid and Pyrazinamide (-6.5 kcal/mol and -8.9 kcal/mol) respectively. Therefore we conclude that, these compounds are more potent antioxidant and anti-TB agents.

2A.8. References

1. S. Pinheiro, M.C. Erick Pinheiro, M.F. Estela Muri, C. Jaqueline Pessoa, A. Mayara, *Med. Chem. Res.*, **2020**, 29, 1751-1776.
2. K.M. Elattar, B.D. Mert, M. Moniera, A. El-Mekabaty, *RSC Adv.*, **2020**, 10, 15461-15492.
3. M. Faisal, A. Saeed, S. Hussain, P. Dar, F. Ali Larik, *J. Chem. Sci.*, **2019**, 70, 1-30.
4. K. Karrouchi, S. Radi, Y. Ramli, J. Taoufik, Y.N. Mabkhot, F.A. Al-aizari, M. Ansar, *Molecules*, **2018**, 23, 1-86.
5. S. Kakkar and B. Narasimhan, *BMC Chem.*, **2019**, 13, 1-24.
6. J. Zhua, J. Moa, H. Lina, Y. Chenb, H. Sun, *Bioorg. Med. Chem.*, **2018**, 26, 3065-3075.
7. M. Fattahi, A. Davoodnia, M. Pordel, *Russ. J. Gen. Chem.*, **2017**, 87, 863-867.
8. Y. Luo, L. Ma, H. Zheng, L. Chen, R. Li, C. He, S. Yang, X. Ye, Z. Chen, Z. Li, Y. Gao, J. Han, Gu He, Li Yang, Y. Wei, *J. Med. Chem.*, **2010**, 53, 273-281.
9. D. Kumbhar, R. Patil, D. Patil, A. Patravale, D. Chandam, S. Jadhav, M. Deshmukh, *Synth. Commun.*, **2016**, 46, 85-92.
10. P. Kour, M. Ahuja, P. Sharma, A. Kumar, *J. Chem. Sci.*, **2020**, 108, 1-10.
11. G. Thirupathi, M. Venkatanarayana, P.K. Dubey, Y.B. Kumari, *Chem. Sci. Trans.*, **2013**, 2, 441-446.
12. B. Baghernejad, *Bulg. Chem. Commun.*, **2015**, 47, 497-501.
13. B.M.A. Shehri, M.R. Shabaan, M. Shkir, A. Kaushik, M.S. Hamdy, *J. Nanostructure Chem.*, **2020**, 1-11.
14. J.Z. Guo, H. Cui, W. Zhou, *J. Photochem. Photobiol. A: Chem.*, **2008**, 193, 89-96.
15. D.N. Thanh, O. Kikhtyanin, R. Ramos, M. Kothari, P. Ulbrich, T. Munshi, D. Kubicka, *Catal. Today*, **2016**, 277, 97-107.
16. D. Friedmann, A. Hakki, H. Kim, W. Choi, D. Bahnemann, *Green Chem.*, **2016**, 18, 5391-5411.
17. H.M. Coleman, C.P. Marquis, J.A. Scott, *Chem. Eng. J.*, **2005**, 113, 55-63.
18. V. Guidi, M.C. Caratta, M. Ferroni, *Sens. Actuators B: Chem.*, **1999**, 57, 197-200.
19. C.H. Ao, S.C. Lee, *Chem. Eng. Sci.*, **2005**, 60, 103-109.
20. A.A. Titov, V.A. Krokhin, N.K. Zhulanov, *J. Mater. Process. Technol.*, **1995**, 55, 249-253.
21. C.L. Huisman, A. Goossens, *Synth. Met.*, **2003**, 138, 237-241.
22. S.M. Abdelbasir, A.E. Shalan, *Korean J. Chem. Eng.*, **2019**, 36, 1209-1225.

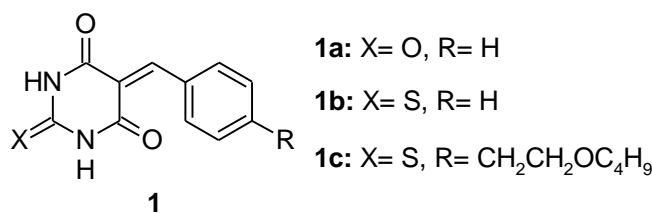
23. WHO. Global tuberculosis report, Geneva; Available from **2019**.
24. A. Torreggiani, M. Tamba, *Trends. Het. Chem.*, **2005**, 10, 115-137.
25. N. Karali, O. Guzel, N. Ozsoy, *Eur. J. Med. Chem.*, **2010**, 45, 1068-1077.
26. V.P. Patil, V.L. Markad, K.M. Kodam, *Bioorg. Med. Chem. Lett.*, **2013**, 23, 6259-6263.
27. L. Ma, C. Xie, Y. Ran, X. Liang, L. Huang, H. Pei, L. Chen, *J. Med. Chem.*, **2012**, 55, 9958-9972.
28. A.A. Esmaeili, F. Mesbah, A. Moradi, A. Khojastehnezhad, M. Khalili, *Phosphorus Sulfur Silicon Relat. Elem.*, **2021**, 196, 819-825.
29. M. Molnar, H. Brahmabhatt, V. Rastija, V. Pavic, M. Komar, M., Karnas, J. Babic, *Molecules*, **2018**, 23, 1-15.
30. V.M. Lunagariya, P.K. Thakor, N. Darshana, Kanthecha, M.N. Patel, *J. Organomet. Chem.*, **2018**, 854, 49-63.
31. M. Shabeer, L.C.A. Barbosa, M. Karak, A.C.S. Coelho, A. Jacqueline, Takahashi, *Med. Chem. Res.*, **2018**, 27, 1043-1049.
32. F. Oliveira, M. De-Souza, A.S. Oliveira, L.M. Silva, F.M. Oliveira, E.G. Santos, P. Silva, R.S. Ferreira, F.S. Villela, F.T. Martins, H.S. Leal, B.G. Vaz, R.R. Teixeira, S.O. Paula, *Eur. J. Med. Chem.*, **2018**, 18, 1-28.
33. N. Zidar, D. Kikelj, *Acta Chim. Slov.*, **2011**, 58, 151-157.
34. A. Pandith, G. Hazra, H.S. Kim, *Spectrochim. Acta A Mol. Biomol. Spectrosc.*, **2017**, 178, 151-159.
35. J. Rani, M. Saini, S. Kumar, P.K. Verma, *Chem. Cent. J.*, **2017**, 11, 1-11.
36. Y. Gull, N. Rasool, M. Noreen, F.U.H. Nasim, A. Yaqoob, S. Kousar, M.S. Islam, *Molecules*, **2013**, 18, 8845-8857.
37. R. Rishikesan, R.P. Karuvalam, J.M. Nibin, A.M. Sajith, K.R. Eeda, R. Pakkath, K.R. Haridas, V. Bhaskar, K. Narasimhamurthy, A. Muralidharan, *J. Chem. Sci.*, **2021**, 133, 1-12.
38. A. Pandith, A. Kumar, H.S. Kim, *RSC Adv.*, **2015**, 5, 81808-81816.
39. A.M. Vijesh, A.M. Isloor, S. Telkar, T. Arulmoli, H.K. Fun, *Arab. J. Chem.*, **2013**, 6, 197-204.
40. M.N. Joy, Y.D. Bodke, S. Telkar, *Chem. Nat. Compd.*, **2020**, 56, 614-620.
41. K.N. Venugopala, C. Tratat, M. Pillay, S. Chandrashekarappa, M. Attimarad, O.I. Alwassil, A.B. Nair, N. Sreeharsha, R. Venugopala, M.A. Morsy, M. Haroun, H.M. Kumalo, B. Odhav, K. Mlisana, *Drug Des. Dev. Ther.*, **2020**, 14, 1027-1039.

2B.1. Introduction

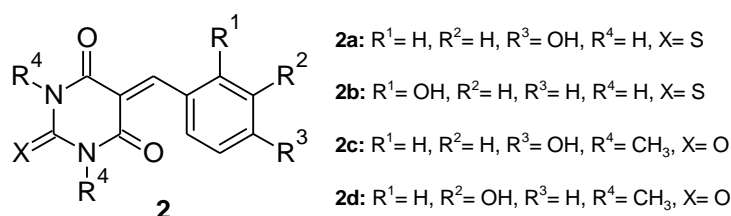
Heterocyclic compounds play a predominant role in medicinal chemistry and synthetic organic chemistry due to their massive biological importance. The synthesis of nitrogen and sulphur containing heterocyclic compounds are multi-structures in one molecule has attracted the attention of medicinal chemists and researchers because of their multifaceted pharmacological activities [1-2]. Among them, pyrimidine and thiophene have been recognized as key scaffolds owing to their important biological significance and interesting therapeutic properties which includes anti-tubercular [3], anticancer [4], anti-HIV [5], antibacterial [6], antifungal [7], antitumor [8], EGFR inhibitor [9, 10], protein kinase inhibitors [11-14] and 5-HT7 receptor [15] etc.

Moreover, the heterocyclic compounds increase the strength of the molecules by forming hydrogen bonds with DNA. Hence, the interactive study of heterocyclic moieties with DNA is essential for estimating their anticancer activity and elucidating the viable mechanism of their action. Therefore, DNA binding is considered as an essential experimental step to measure anticancer drug activity because most of the anticancer drugs specifically target DNA [16]. These compounds appear to be the most effective against various cancers. Around 60 % of the medicines used for cancer treatment are based on heterocyclic moieties. Among the various heterocyclic moieties, nitrogen and sulphur-based compounds are effective against different types of cancer [17-19]. Some of the reported biologically important heterocyclic compounds have been discussed below.

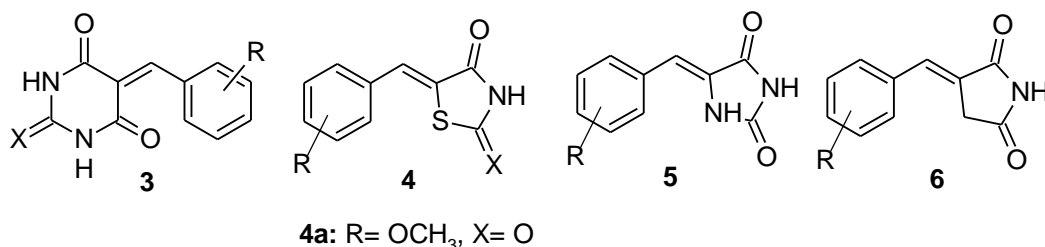
Q. Yan *et. al.*, synthesized a series of novel 5-benzylidene barbiturate and thiobarbiturate derivatives (**1**) and determined their tyrosinase inhibitors and antibacterial activity. The compounds **1a** and **1b** were found to be the most potent inhibitors with IC₅₀ values of 13.98 μ M and 14.49 μ M respectively. The compounds **1b** and **1c** exhibited a MIC of 3.1 μ g/mL against Gram-positive *S. aureus* strain [20].



In 2013, B.B. Sokmen and co-workers developed substituted barbiturates and thiobarbiturates (**2**) and reported as antibacterial, anti-urease and antioxidant activities. The results showed that all compounds exhibited anti-urease and antioxidant activities. Among the targets, **2a** and **2b** are the most active reducing agent. Compounds **2c** and **2d** have found highest anti-urease activity with an IC₅₀ value of 0.036 & 0.033 μM. [21].

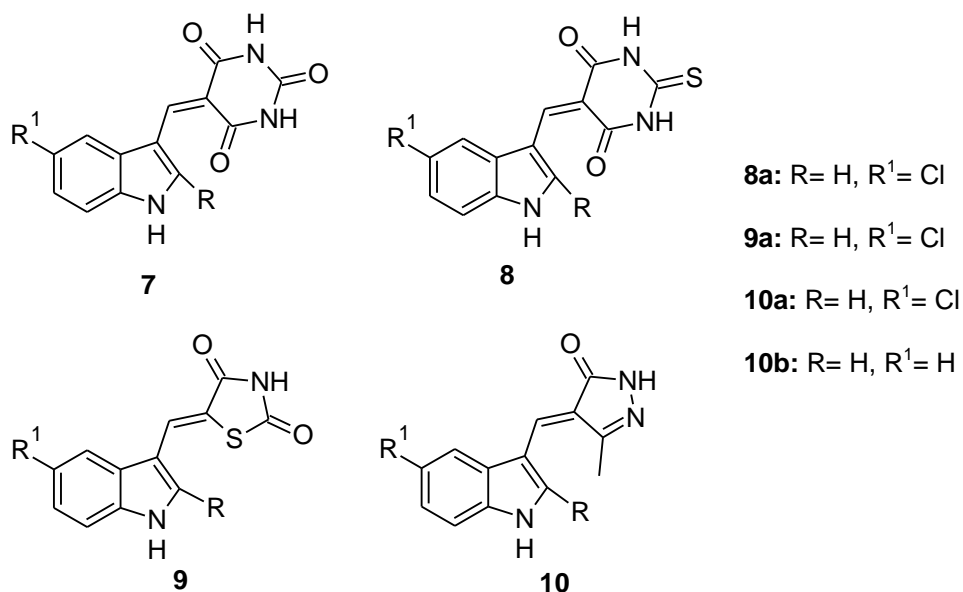


Barbituric or thiobarbituric acid derivatives (**3**), 2-iminothiazolidin-4-one or 2,4-thiazolidinedione derivatives (**4**), phenylmethylehydantoin compounds (**5**) and phenylmethylenepyrrolidine 2,5-dione compounds (**6**) was reported by Y. Luo *et. al.*, and evaluated their *in vitro* inhibitory effects on MCP1-mediated chemotaxis, coincubation of murine macrophage-like cell line. Among them, 5-(4-methoxybenzylidene) thiazolidine-2,4-dione (**4a**) shows most potent inhibitory effect of 57.8±3.4 % against chemotaxis at concentration of 25 μg/mL [22].

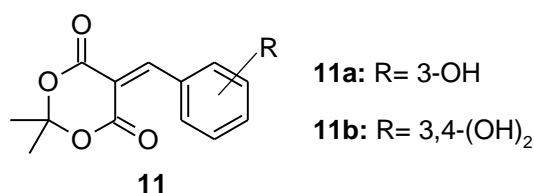


Substituted 5-(1*H*-indol-3-ylmethylidene)pyrimidine-2,4,6(1*H*,3*H*,5*H*)-triones (**7**), 5-(1*H*-indol-3-ylmethylidene)-2-thioxodihydropyrimidine-4,6(1*H*,5*H*)-diones (**8**), 5-(1*H*-indol-

3-ylmethylidene)-1,3-thiazolidine-2,4-diones (**9**) and 4-(1*H*-indol-3-ylmethylidene)-5-methyl-2,4-dihydro-3*H*-pyrazol-3-one derivatives (**10**) was reported by J.S. Biradar & B.S. Sasidhar in 2011 and evaluated *in vitro* antioxidant, cytotoxic activities against three tumor cell lines. Among the screened compounds **8a**, **9a**, **10a** and **10b** exhibited excellent antioxidant activity. Compounds **9a**, **10a** and **10b** have shown strong cytotoxicity [23].



O.C. Sanchez *et al.*, reported a 5-benzylidene-2,2-dimethyl-1,3-dioxane-4,6- dione derivatives (**11**) and evaluated their antimicrobial activity. Among the series, hydroxyls derivatives were selected against *E. coli*, *S. aureus* and *P. aeruginosa*, 3-hydroxyl and 3,4-dihydroxyl (**11a** & **11b**) derivatives were active against all the three bacterial strains [24].

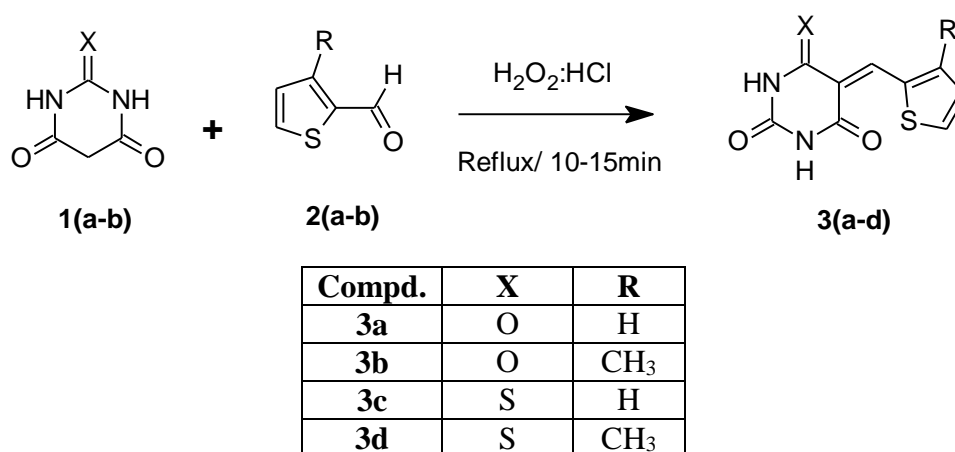


Based on the above findings, we herein report the application of H₂O₂:HCl as a green halogenating catalyst for the synthesis of 5-(3-substituted-thiophene)-pyrimidine derivatives and investigation of their antibacterial, anticancer, DNA binding, ADME-T and molecular docking studies to predict the inhibitory effects as well as interactions of the synthesized

compounds against pathogens, enzymes and also subjected to computational study to know about their chemical reactivity parameters.

2B.2. Present work

In this chapter, we described the convenient and straightforward method for the synthesis of 5-(3-substituted-thiophene)-pyrimidine derivatives **3(a-d)** *via* Knoevenagel condensation of barbituric/thiobarbituric acid (**1**) with 3-substituted-thiophene-2-carboxaldehyde (**2**) in aqueous ethanol using $\text{H}_2\text{O}_2:\text{HCl}$ as catalyst. The reaction pathway has been given in **Scheme 2**.



Scheme 2. Synthesis of 5-(3-substituted-thiophene)-pyrimidine derivatives **3(a-d)**.

Initially, we studied the effect of catalyst on the reaction. In the previous reports, the same reaction was carried out in the presence of different catalysts such as CuO NPs, PVP-Ni NPs, Fe₃O₄ NPs, L-tyrosine, NH₂SO₃H, EAN, Bi(NO₃)₃.5H₂O and also in the absence of catalyst (**Table 1**). We have carry out the reaction using hypochlorous acid (HOCl) as a catalyst to determine the progress of the reaction as well as product yield of **3a** compound. By using this catalyst the result was very encouraging with a short reaction time and good yield. Consequently, to study the effect of temperature on synthesized compound **3a**, we carried out a reaction at room temperature, 50 °C and 80 °C (**Table 2**). As a result, an

increase in the reaction temperature decreased the reaction time from 60 to 20 and 20 to 10 min, respectively, but the product yield was not affected by change in temperature.

Table 1. Effect of catalysts on synthesized compound **3a**.

Entry	Catalyst	Solvent	Temperature (°C)	Time (min)	Yield (%)
1	H₂O₂: HCl	EtOH: H₂O	Reflux	10	96
2	CuO NPs	-	RT	10	93 ^[25]
3	PVP-Ni NPs	Ethylene glycol	Reflux	10	87 ^[26]
4	Fe ₃ O ₄ NPs	EtOH	Reflux	30	70 ^[27]
5	L-tyrosine	H ₂ O	RT	16	93 ^[28]
6	NH ₂ SO ₃ H	-	Grinding	120	96 ^[29]
7	-	Ionic liquids	RT	10	96 ^[30]
8	Bi(NO ₃) ₃ .5H ₂ O	EtOH	Reflux	20	95 ^[31]
9	-	EtOH	Reflux	120	89 ^[20]

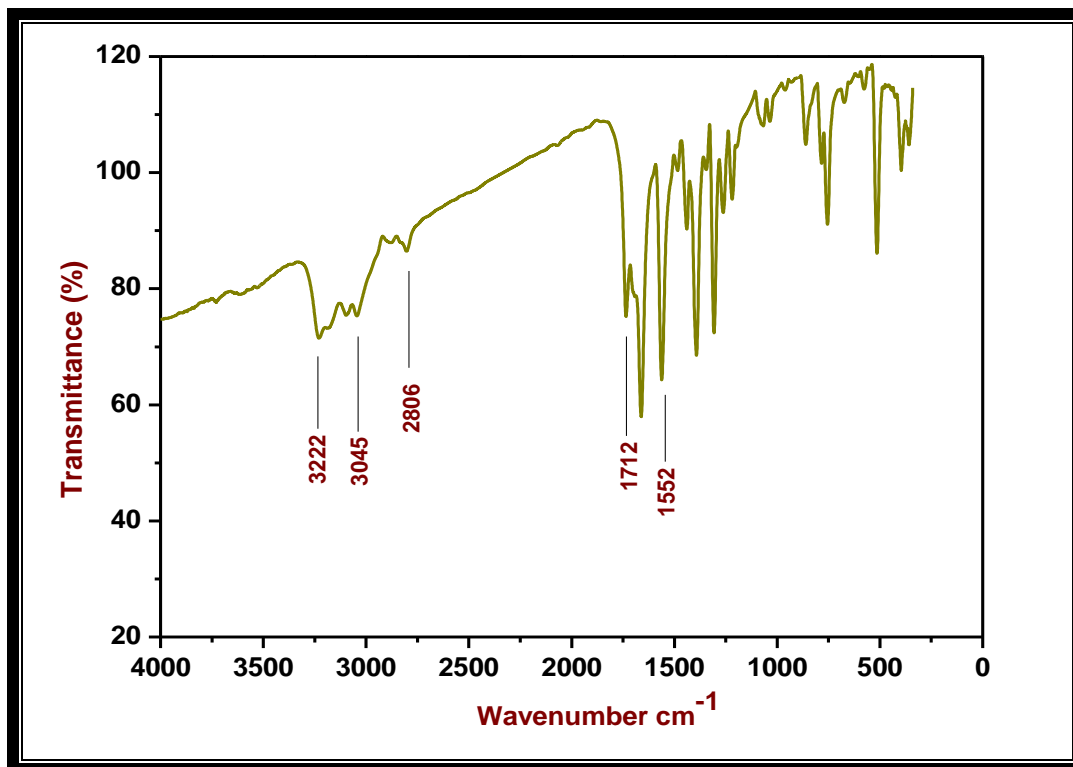
Table 2. Effect of temperature on synthesized compound **3a**.

Entry	Temperature (°C)	Time (min)	Yield (%)
1	RT	60	96
2	50	20	96
3	80	10	96

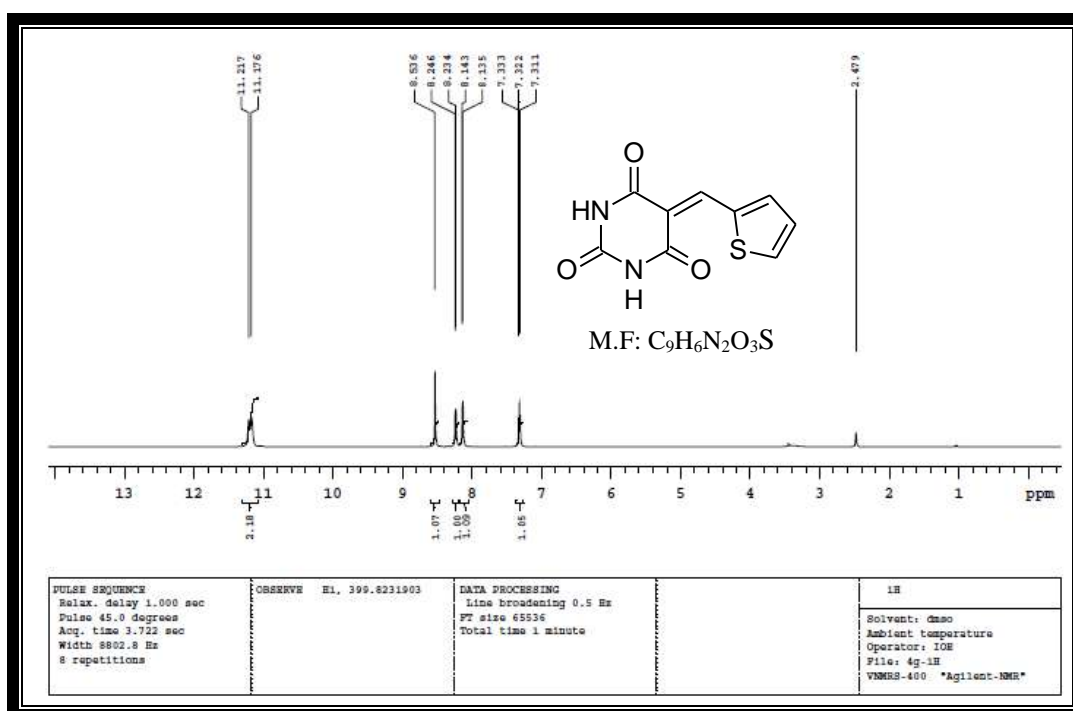
Further, the structures of the intended 5-(3-substituted-thiophene)-pyrimidine derivatives **3(a-d)** were confirmed by IR, ¹H NMR, ¹³C NMR and HRMS spectral data. IR spectrum of compound **3a** showed the absorption band in the region of 3222 cm⁻¹ is attributed to the amide stretching vibration, 3045 cm⁻¹ due to CH group and the absorption band at 1712 cm⁻¹ correspond to stretching vibration of the carbonyl group (C=O). Another stretching vibrational band at 1552 cm⁻¹ correspond to C=C bond. The ¹H NMR spectrum of compound **3a** exhibited two singlet peaks at δ 11.21 and 11.17 ppm, which corresponds to two NH protons of pyrimidine nucleus (s, 2H, NH) and another singlet peak at δ 8.53 ppm due to CH proton (s, 1H, CH). Multiplet peak was observed in the range of δ 8.24-8.13 ppm, corresponds to two aromatic protons (m, 2H, Ar-H) and a triplet peak at δ 7.33-7.31 ppm due to one aromatic proton (t, *J*= 8 Hz, 1H, Ar-H). In addition, the ¹³C NMR spectrum of compound **3a** exhibited peaks at δ 163.95 and 163.45 ppm, which corresponds to carbonyl carbons.

The mass spectrum showed a molecular ion peak m/z at 221.9054 [M^+-1], which corresponds to the molecular weight of compound **3a**.

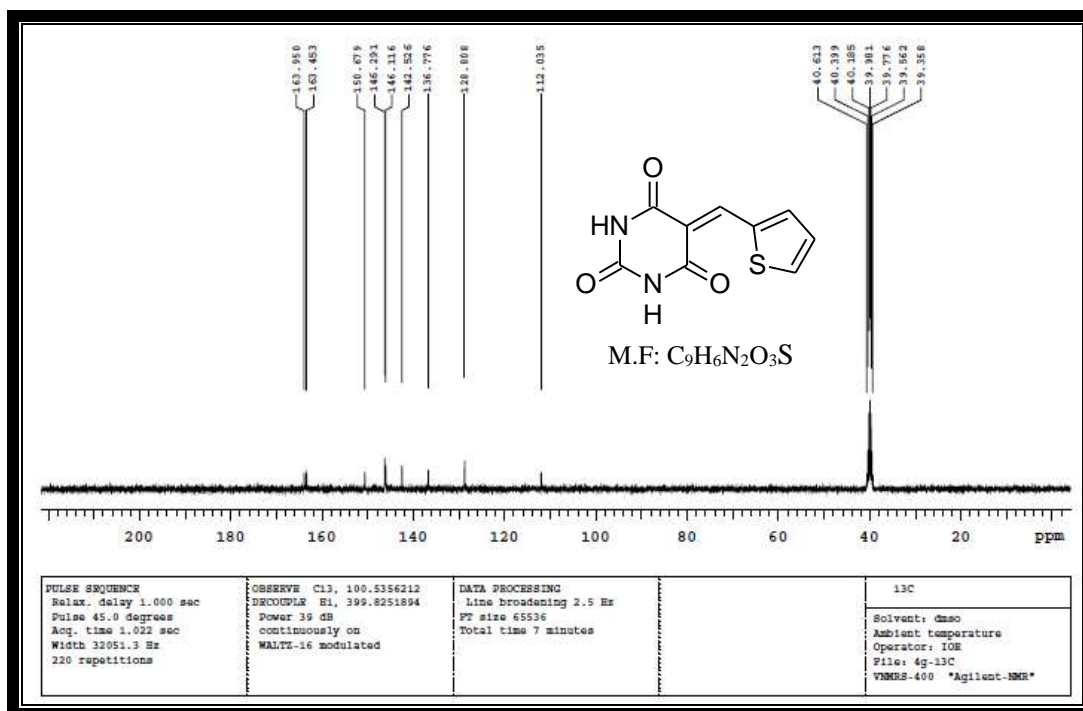
Characterization:



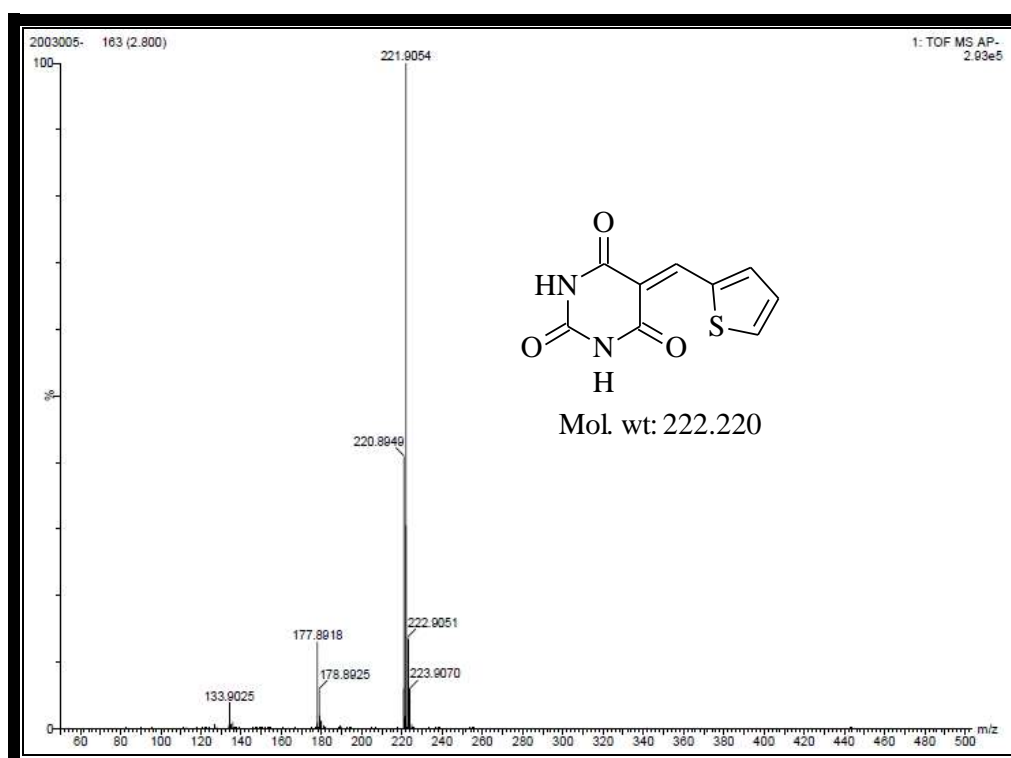
IR spectrum of compound **3a**



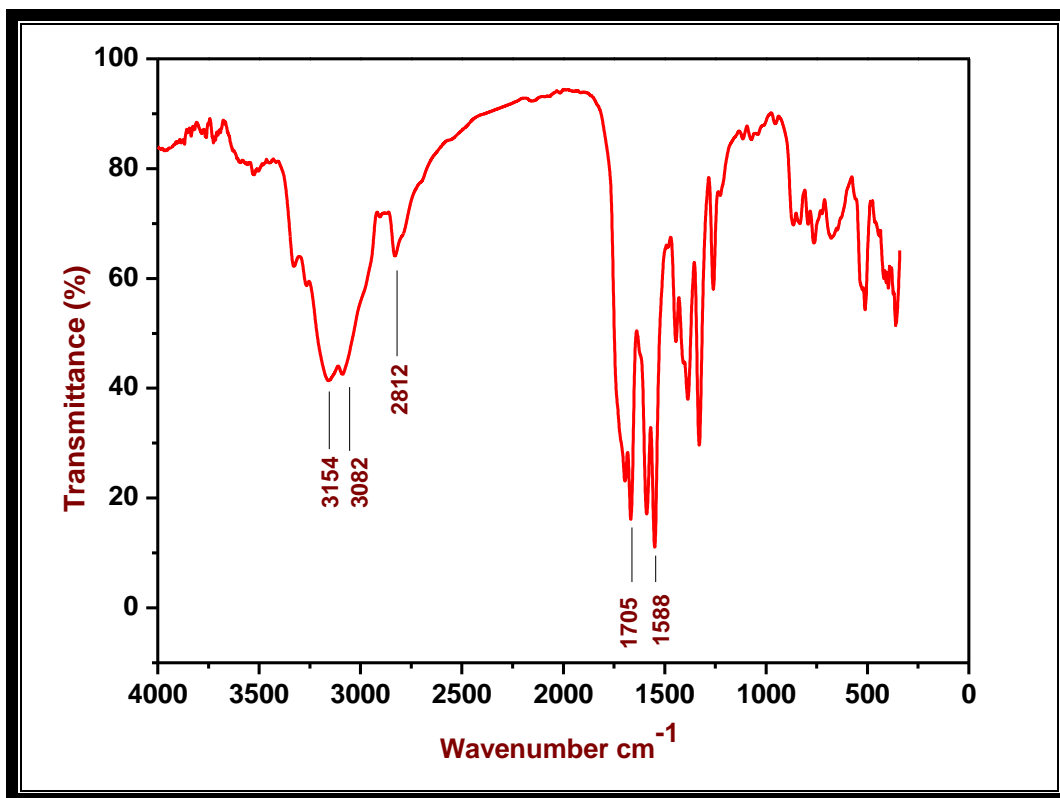
^1H NMR spectrum of compound **3a**



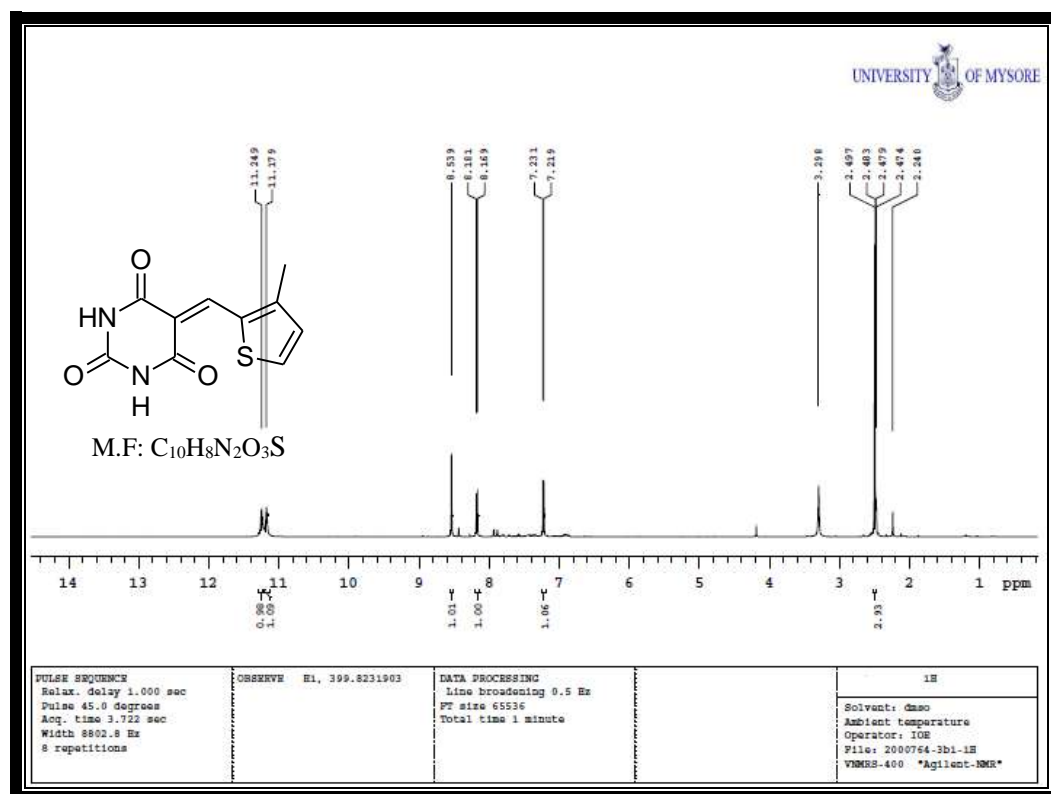
¹³CNMR spectrum of compound 3a

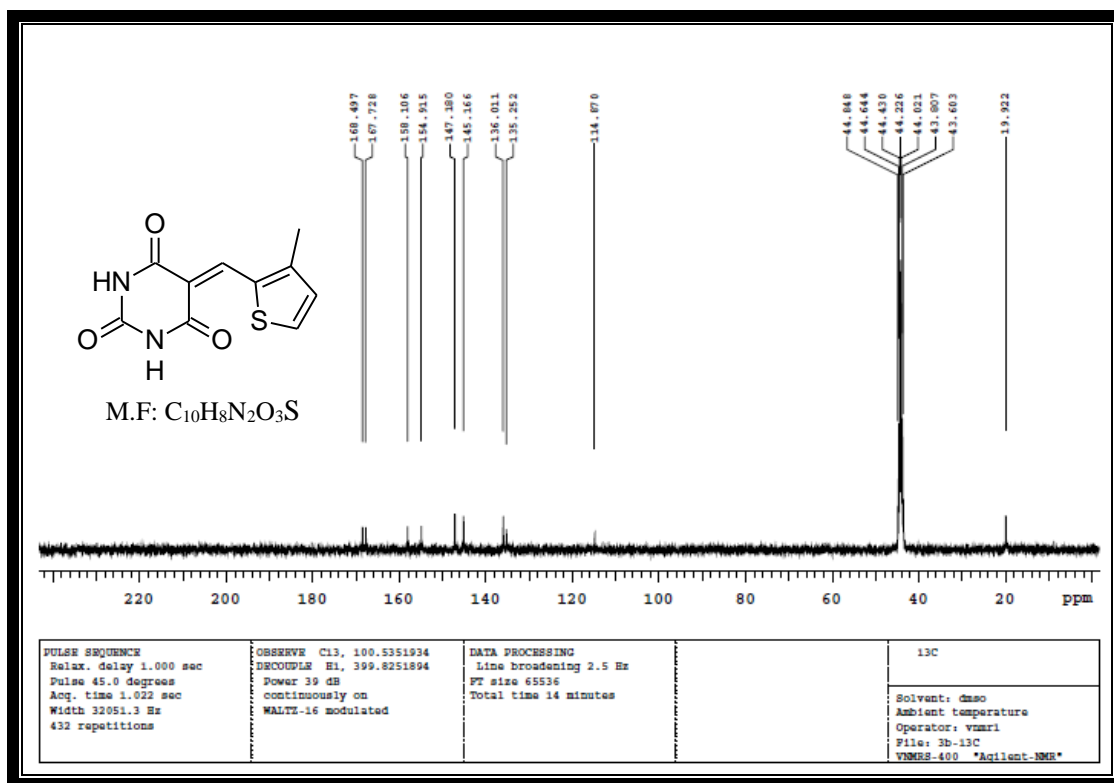
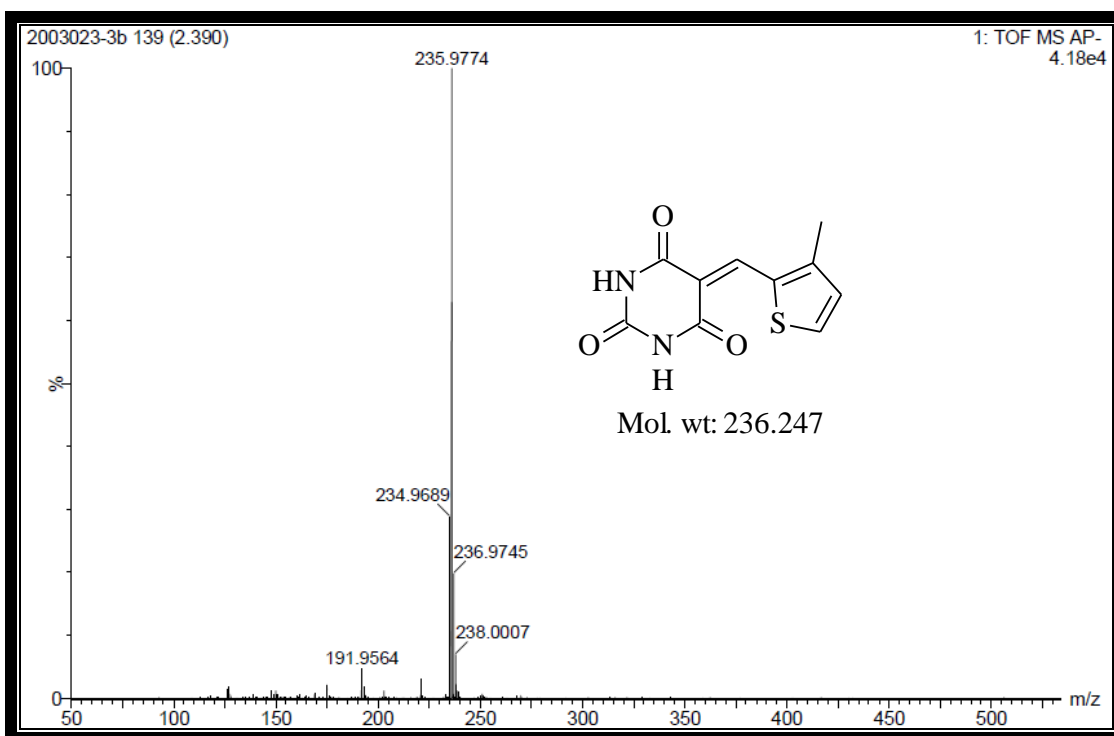


MASS spectrum of compound 3a



IR spectrum of compound 3b

¹H NMR spectrum of compound 3b

¹³CNMR spectrum of compound 3b

MASS spectrum of compound 3b

2B.3. Experimental

2B.3.1. General information:

The general information regarding the different solvents, reagents and instruments etc., used for the analysis has been previously discussed in the experimental section (2A.3.1) of Chapter-2A.

2B.3.2. General procedure for the synthesis of 5-(3-substituted-thiophene)-pyrimidine derivatives 3(a-d):

The synthesis of 5-(3-substituted-thiophene)-pyrimidine derivatives **3(a-d)** was carried out by the reaction of barbituric/thiobarbituric acid (**1**, 1mmol) with 3-substituted-thiophene-2-carboxaldehyde (**2**, 1mmol) in the presence of 15 mL aqueous ethanol using 6 % H₂O₂:HCl (2:1) as a catalyst. The reaction mixture was refluxed at 80 °C for about 10-15 min and progress of the reaction was monitored by TLC (Ethyl acetate & Petroleum ether). After the completion of reaction, the mixture was cooled to room temperature and poured into the 100 mL flake ice with vigorous stirring to get solid precipitated out. The crude mixture was filtered, washed and recrystallized with absolute ethanol to afford pure solid products **3(a-d)**.

5-(Thiophen-2-ylmethylidene)pyrimidine-2,4,6(1H,3H,5H)-trione (3a):

Yellow solid; Yield: 96 %; MP: 280-282 °C; Mol. Formula: C₉H₆N₂O₃S; UV (nm) λ_{max} (log ε): 366 (4.31), 280 (4.30); FTIR (ν cm⁻¹): 3222 (NH), 3045 (CH), 1712 (C=O), 1552 (C=C); ¹H NMR (δ ppm): 11.21 (s, 1H, NH), 11.17 (s, 1H, NH), 8.53 (s, 1H, CH), 8.24-8.13 (m, 2H, Ar-H), 7.33-7.31 (t, *J* = 8 Hz, 1H, Ar-H); ¹³C NMR (δ ppm): 163.95, 163.45, 150.67, 146.29, 146.11, 142.52, 136.77, 128.80, 112.03; HRMS: *m/z* 221.9054 [M⁺-1]; Anal. Calcd: C 48.64, H 2.72 & N 12.61 %, Found: C 48.59, H 2.68 & N 12.53 %.

5-[(3-Methylthiophen-2-yl)methylidene]pyrimidine-2,4,6(1H,3H,5H)-trione (3b):

Yellow solid; Yield: 94 %; MP: 302-306 °C; Mol. Formula: C₁₀H₈N₂O₃S; UV (nm) λ_{\max} (log ϵ): 380 (4.00), 286 (4.29); FTIR (ν cm⁻¹): 3154 (NH), 3082 (CH), 2812 (CH₃), 1705 (C=O), 1588 (C=C); ¹H NMR (δ ppm): 11.24 (s, 1H, NH), 11.17 (s, 1H, NH), 8.53 (s, 1H, CH), 8.18-8.16 (d, J = 8 Hz, 1H, Ar-H), 7.23-7.21 (d, J = 8 Hz, 1H, Ar-H), 2.24 (s, 3H, CH₃); ¹³C NMR (δ ppm): 168.49, 167.72, 158.10, 154.91, 147.18, 145.16, 136.01, 135.25, 114.87, 19.92; HRMS: m/z 235.9774 [M⁺-1]; Anal. Calcd: C 50.84, H 3.41 & N 11.86 %, Found: C 50.79, H 3.36 & N 11.80 %.

5-(Thiophen-2-ylmethylidene)-2-thioxodihydropyrimidine-4,6(1H,5H)-dione (3c):

Green solid; Yield: 93 %; MP: 320-322 °C; Mol. Formula: C₉H₆N₂O₂S₂; UV (nm) λ_{\max} (log ϵ): 396 (3.14), 286 (4.28); FTIR (ν cm⁻¹): 3206 (NH), 3012 (CH), 1710 (C=O), 1559 (C=C), 1156 (C=S); ¹H NMR (δ ppm): 12.30 (s, 1H, NH), 12.20 (s, 1H, NH), 8.36-8.34 (d, J = 8 Hz, 2H, Ar-H), 8.20 (s, 1H, CH), 6.88-6.86 (d, J = 8 Hz, 1H, Ar-H); ¹³C NMR (δ ppm): 178.61, 164.16, 162.82, 160.48, 157.01, 139.25, 124.43, 116.13, 114.71; HRMS: m/z 237.9467 [M⁺-1]; Anal. Calcd: C 45.36, H 2.54 & N 11.76 %, Found: C 45.30, H 2.49 & N 11.71 %.

5-[(3-Methylthiophen-2-yl)methylidene]-2-thioxodihydropyrimidine-4,6(1H,5H)-dione (3d):

Green solid; Yield: 95 %; MP: 310-312 °C; Mol. Formula: C₁₀H₈N₂O₂S₂; UV (nm) λ_{\max} (log ϵ): 404 (3.23), 286 (4.29); FTIR (ν cm⁻¹): 3208 (NH), 3024 (CH), 2852 (CH₃), 1704 (C=O), 1556 (C=C), 1200 (C=S); ¹H NMR (δ ppm): 11.25 (s, 1H, NH), 11.18 (s, 1H, NH), 8.54 (s, 1H, CH), 8.19-8.17 (d, J = 8 Hz, 1H, Ar-H), 7.24-7.22 (d, J = 8 Hz, 1H, Ar-H), 2.24 (s, 3H, CH₃); ¹³C NMR (δ ppm): 173.35, 163.55, 142.47, 130.89, 130.39, 129.86, 128.90, 128.03, 114.28, 26.80; HRMS: m/z 251.9608 [M⁺-1]; Anal. Calcd: C 47.60, H 3.20 & N 11.10 %, Found: C 47.55, H 3.16 & N 11.06 %.

2B.4. Absorption property

The UV-Visible spectra of compounds **3(a-d)** were recorded in DMSO solvent at 10^{-5} M concentration using UV-Visible spectrophotometer. The λ_{\max} and molar absorption coefficient values were appended in **Table 3**. Synthesized compounds exhibited two absorption maxima (λ_{\max}) in the range of 280-286 nm and 366-404 nm in DMSO solvent due to the π - π^* & n - π^* transitions (**Fig. 1**) [32]. Among them, compound **3d** shows the highest absorption maxima at 286 and 404 nm.

Table 3. Electronic absorption data of the synthesized compounds **3(a-d)** in DMSO solvent.

Compd.	DMSO	
	λ_{\max} (nm)	Log ϵ
3a	280	4.30
	366	4.31
3b	286	4.29
	380	4.00
3c	286	4.28
	396	3.14
3d	286	4.29
	404	3.23

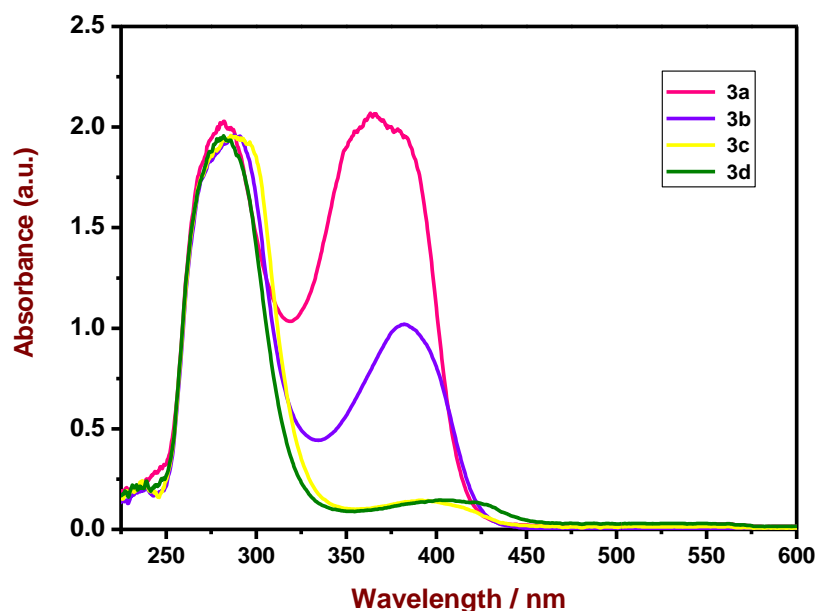


Fig. 1. A graph of UV-Visible spectrum of synthesized compounds **3(a-d)** in DMSO solvent.

2B.5. Pharmacological studies

2B.5.1. Antibacterial activity

Antibacterial activity of the synthesized compounds **3(a-d)** was carried out by the agar well diffusion method [33] using Gram-negative strain *Escherichia coli* (MTCC-1559) and Gram-positive strain *Staphylococcus aureus* (MTCC-902). The test compounds were dissolved in DMSO at two different concentrations, 20 & 40 µg/mL. Petridishes were prepared by pouring 20 mL of sterilized NA media under aseptic condition and allowed to solidify. After solidification of the media, 100 µL of standardized test microbial inoculums of *E. coli* and *S. aureus* were spreaded uniformly using sterile cotton swabs. 6 mm diameter agar is drawn from plate to form a well using sterile cork borer. Ciprofloxacin was used as positive control and DMSO used as negative control. After keeping at 4 °C for 4 hours for the diffusion of antibacterial metabolites, thereafter plates were incubated at 37 °C for 24 h. The diameter of the inhibition zone around the well is measured in millimeter (mm) and the average of three repeated agar discs were taken to assess the strength of antibacterial activity.

2B.5.2. *In vitro* cytotoxicity

In vitro cytotoxicity was assessed by MTT assay method [34] against MCF-7 (Human breast cancer) cell line. The cells were seeded in a 96-well flat-bottom microplate and maintained at 37 °C in 95 % humidity and 5 % CO₂ overnight. Different concentrations (200, 100, 50, 25, 12.5 and 6.25 µg/mL) of samples were treated. The cells were incubated for another 48 h, and the wells were washed twice with PBS. 20 µL of MTT staining solution was added to each well, and the plate was incubated at 37 °C. After 4 h, 100 µL of DMSO was added to each well to dissolve the formazan crystals, and absorbance was recorded at 570 nm using a microplate reader. The percentage of cell survival was calculated by using the following formula.

$$\% \text{ of cell survival} = \frac{\text{Mean OD of test compound}}{\text{Mean OD of Negative control}} \times 100$$

2B.5.3. DNA binding study

DNA binding study was assessed by using electronic spectroscopy. A solution of CT-DNA in 50 mM Tris-HCl/50 mM NaCl buffer solution was prepared at pH 6.9-7.01. In buffer solution, the ratio of absorption values of CT-DNA at 260 and 280 nm is 1.8-1.9, indicates that DNA was free of proteins [35]. Then a concentrated stock solution of DNA was prepared in 50 mM Tris-HCl, 50 mM NaCl in double distilled water at pH 6.9-7.01. The concentration of CT-DNA was determined per nucleotide by taking the absorption coefficient ($6600 \text{ dm}^3 \text{ mol}^{-1} \text{ cm}^{-1}$) at 260 nm [36]. Stock solutions were stored at 4°C . 2 mL of the solution was taken containing a fixed concentration of the compounds **3(a-d)** with CT-DNA (0 to 350 μL of a $0.5025\text{-}6.0670 \times 10^{-7}$ M stock CT-DNA solution). A blank solution containing the same concentration of DNA was used as a reference. Solutions were prepared by mixing the compound and CT-DNA in DMSO medium and then recording the UV absorption spectra by adding 25 to 350 μL DNA to the compound. The spectra were recorded against a blank solution containing the same concentration of DNA ($4.0909 \times 10^{-6} \text{ molL}^{-1}$). The intrinsic binding constant K_b was obtained by using the following equation [37].

$$\frac{[\text{DNA}]}{(\epsilon_A - \epsilon_B)} = \frac{[\text{DNA}]}{(\epsilon_B - \epsilon_F)} + \frac{1}{K_b(\epsilon_B - \epsilon_F)}$$

Where, ϵ_A , ϵ_B and ϵ_F corresponds to the apparent, bound and free compound extinction coefficients, respectively. A plot of $\frac{[\text{DNA}]}{(\epsilon_A - \epsilon_F)}$ versus $[\text{DNA}]$ gave a slope of $\frac{1}{(\epsilon_B - \epsilon_F)}$ and Y-intercept equal to $\frac{1}{K_b(\epsilon_B - \epsilon_F)}$. Hence K_b is the ratio of slope to intercept. The % of hyperchromicity or hypochromicity (% H) for the CT-DNA/[Ligand] was obtained from $(\epsilon_a - \epsilon_f)/\epsilon_f \times 100$.

2B.5.4. *in silico* molecular docking study

The docking of the synthesized compounds to the binding pocket of glucosamine-6-phosphate synthase (GlcN-6-P) and P38 MAP kinase was carried out using the AutodockVina program [38]. The co-crystallized structure of GlcN-6-P (PDB ID: 2VF5) and P38 MAP kinase (PDB ID: 1OUK) were retrieved from protein databank and their substrate binding sites were identified using pdbsum server [39, 40]. A grid box of dimensions 40 x 50 x 40 Å with X, Y & Z coordinates at 32.198, 16.709 and -3.151 for GlcN-6-P and 56 x 60 x 48 Å with X, Y & Z coordinates at 44.746, 34.234 and 32.603 for P38 MAPk were created respectively. For the obtained molecules, all the torsions were allowed to rotate during docking. The grid box was set around the residues forming the active pocket. The binding interactions were visualized using Biovia Discovery Studio Visualizer V.20.1 and Schrodinger-Maestro V.12.7. The *in silico* studies were performed on a local machine equipped with AMD Ryzen 5 six-core 3.4 GHz processor, 8 G.B. graphics and 16 GB RAM with Microsoft Windows 10 operating system.

2B.5.5. *in silico* oral bioavailability assessment and ADME-toxicology study

The oral bioavailability of the synthetic molecules **3(a-d)** can be predicted by considering their structural properties to screen based on the Rule of five or Lipinski rule-of-five (RO5) filter [41]. Rule of five employs the molecular properties necessary to filter candidate drug's pharmacokinetics (PK) and pharmacodynamics (PD) [42-44].

Oral bioavailability assessment was done using Osiris Data warrior V.4.4.3 [45] based on total molecular weight, ClogP, H-acceptors, H-donors, rotatable bonds as part of RO5 filters, along with TPSA (Topological polar surface area) and drug-likeness assessment [46]. Pharmacodynamic properties like mutagenicity, tumorigenicity, reproductive effects, irritancy, toxicity and hepatotoxicity were predicted using the admetSAR server. Bioactivity scores were predicted using the molinspiration server for GPCR ligand, ion channel

modulator, kinase inhibitor, nuclear receptor inhibitor, protease inhibitor, enzyme inhibitor. Pharmacokinetic properties like blood-brain barrier penetration, human intestinal absorption, Caco-2 permeability and CYP450 2D6 substrate were predicted by submitting each molecule individually to the admetSAR server [47].

2B.5.6. Computational study

Computational studies of synthesized compounds **3(a-d)** was conducted by using the Gaussian 09 software [48] with the help of the density functional theory at Becke-3-Lee-Yang-parr (DFT)/B3LYP level with 6-31G (d,p) basis set [49]. The energy minimization process has been conducted at the same level in the gas phase to obtain a stable structure. The 3D representation of the optimized structure was presented in a molecular visualization program Gauss view 5.0 and the output was processed using the Avogadro software [50].

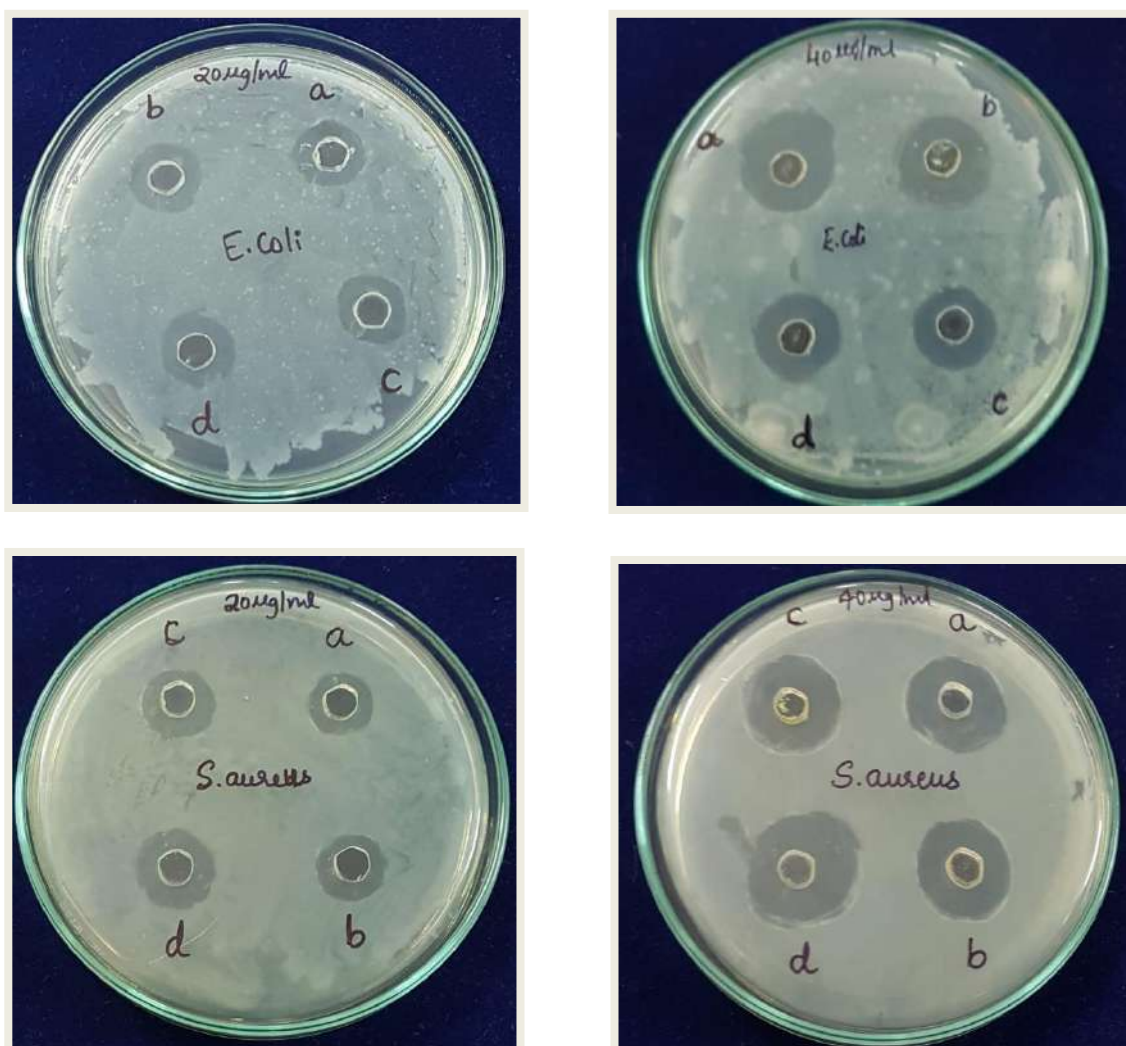
2B.6. Results and discussion

2B.6.1. Antibacterial activity

The synthesized 5-(3-substituted-thiophene)-pyrimidine derivatives **3(a-d)** were screened for their *in vitro* antibacterial activity at two different concentrations (20 & 40 $\mu\text{g/mL}$). All four compounds showed appreciable antibacterial activity with a varied zone of inhibition in the range of 3.3 ± 0.15 to 7.8 ± 0.14 mm for *E. coli* and 3.0 ± 0.11 to 7.9 ± 0.44 mm for *S. aureus* (**Table 4**). The results revealed that, compounds **3b** (3.8 ± 0.12 and 7.8 ± 0.79 mm) and **3d** (3.7 ± 0.84 and 7.9 ± 0.44 mm) having an electron-donating group (methyl) on C-3 of the thiophene ring exhibited the most inhibitory effect against bacterial strains *E. coli* & *S. aureus*, respectively and as compared to standard drug Ciprofloxacin (**Fig. 2**).

Table 4. Antibacterial activity results of synthesized compounds **3(a-d)**.

Compd.	Zone of inhibition in mm			
	<i>Escherichia coli</i>		<i>Staphylococcus aureus</i>	
	20 $\mu\text{g/mL}$	40 $\mu\text{g/mL}$	20 $\mu\text{g/mL}$	40 $\mu\text{g/mL}$
3a	3.5 \pm 0.76	7.8 \pm 0.14	3.0 \pm 0.11	7.5 \pm 0.46
3b	3.8 \pm 0.12	7.8 \pm 0.79	3.1 \pm 0.67	7.6 \pm 0.82
3c	3.3 \pm 0.15	7.2 \pm 0.46	3.5 \pm 0.48	7.4 \pm 0.64
3d	3.4 \pm 0.44	7.1 \pm 0.38	3.7 \pm 0.84	7.9 \pm 0.44
Ciprofloxacin	4.0 \pm 0.58	8.0 \pm 0.76	4.2 \pm 0.12	8.4 \pm 0.98

**Fig. 2.** Images of antibacterial activity of the synthesized compounds **3(a-d)**.

2B.6.2. *In vitro* cytotoxicity

All four synthesized compounds were investigated for their *in vitro* cytotoxicity against MCF-7 (Breast cancer) cell line (**Fig. 3**). The plot details compound concentration versus the survival fraction (**Fig. 4**). The percentages of cell survival of the tested compounds are listed in **Table 5**.

In vitro cytotoxicity results revealed that, all four compounds displayed a superior selectivity against the MCF-7 cell line. Among the tested compounds, compound **3a** exhibited promising cytotoxicity with a minimum cell survival range of 23.68 to 44.16 % at the concentration range of 200 to 6.25 $\mu\text{g/mL}$ and IC_{50} value of 1.15 ± 0.57 $\mu\text{g/mL}$. Whereas **3b**, **3c** & **3d** displayed reliable selectivity at all the concentrations with cell survival ranges of 29.00 to 50.93 %, 31.31 to 66.82 % and 26.95 to 53.12 %, respectively and IC_{50} value in the range of 8.55 ± 0.40 to 26.84 ± 0.61 $\mu\text{g/mL}$.

Table 5. Percentage of cell viability of compounds **3(a-d)** against MCF-7 cell line.

Concentration in $\mu\text{g/mL}$	Mean cell viability of MCF-7				
	3a	3b	3c	3d	5-Fluorouracil
6.25	44.16 \pm 0.76	50.93 \pm 0.42	66.82 \pm 0.41	53.12 \pm 0.34	-
12.5	38.11 \pm 0.82	48.68 \pm 0.31	58.1 \pm 0.13	46.88 \pm 0.52	-
25	34.09 \pm 1.2	43.72 \pm 0.52	48.6 \pm 0.23	43.93 \pm 0.42	-
50	32.37 \pm 0.82	40.23 \pm 0.61	40.03 \pm 0.82	40.03 \pm 0.62	-
100	30.06 \pm 0.62	36.8 \pm 0.20	37.38 \pm 0.61	37.85 \pm 0.34	-
200	23.68 \pm 0.41	29 \pm 0.16	31.31 \pm 0.42	26.95 \pm 0.52	-
IC₅₀	1.15 \pm 0.57	8.55 \pm 0.40	26.84 \pm 0.61	9.39 \pm 0.54	41.51 \pm 1.57

Values are Mean \pm SE, N=3, *P<0.01 vs. Control

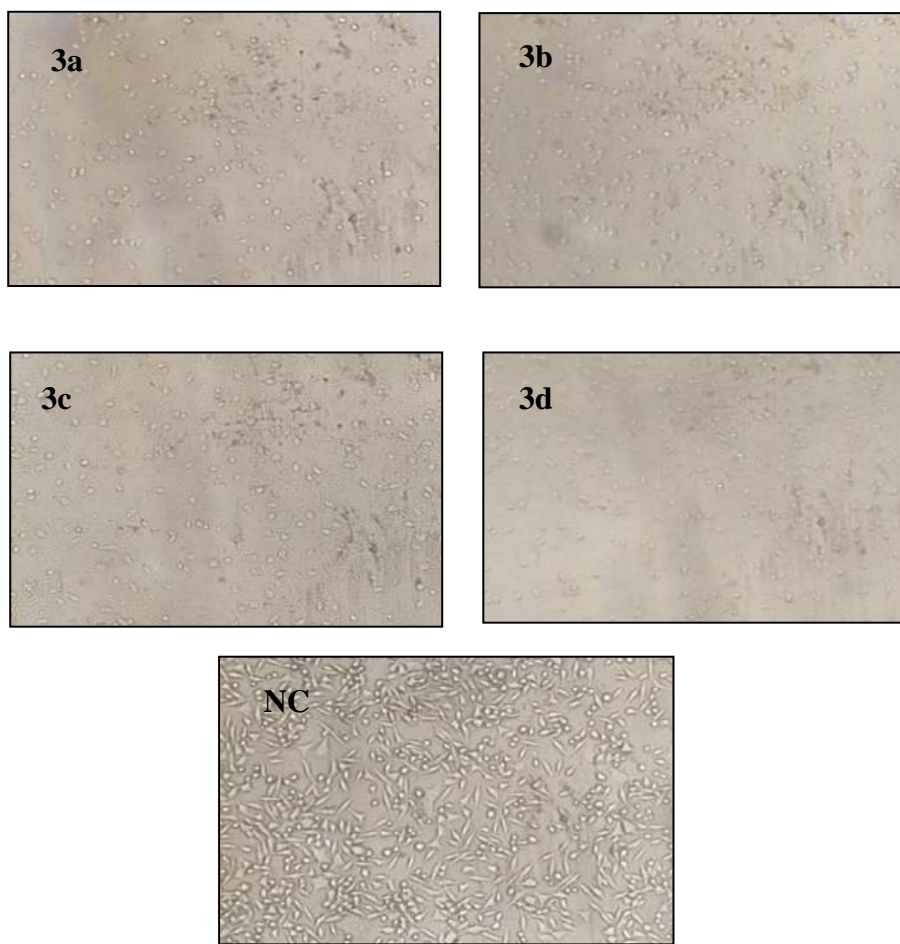


Fig. 3. Images of cytotoxic effect of the synthesized compounds **3(a-d)**.

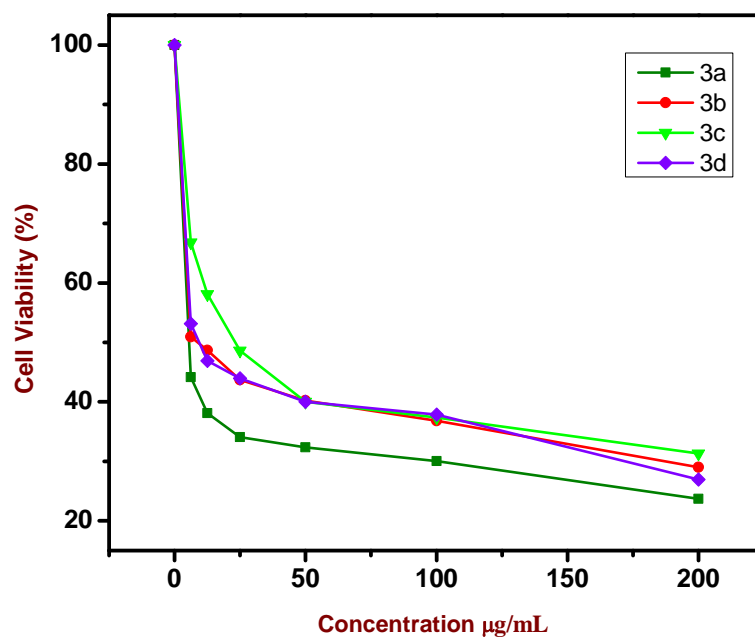


Fig. 4. A graph of % of surviving cells of compounds **3(a-d)** at different concentration against MCF-7 cell line.

2B.6.3. DNA binding study

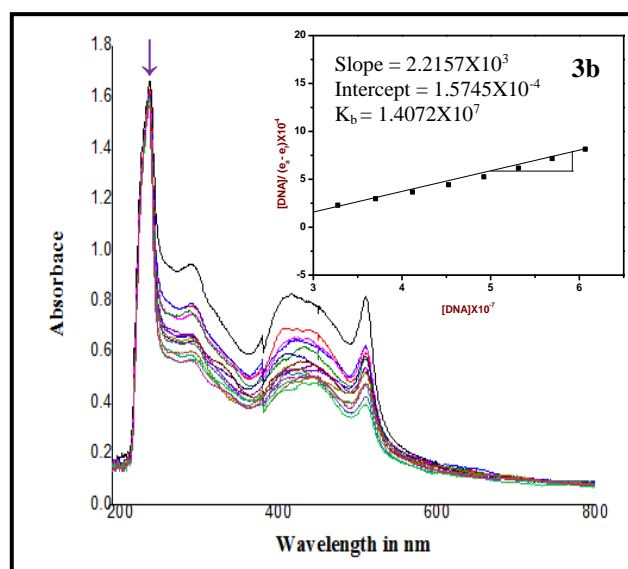
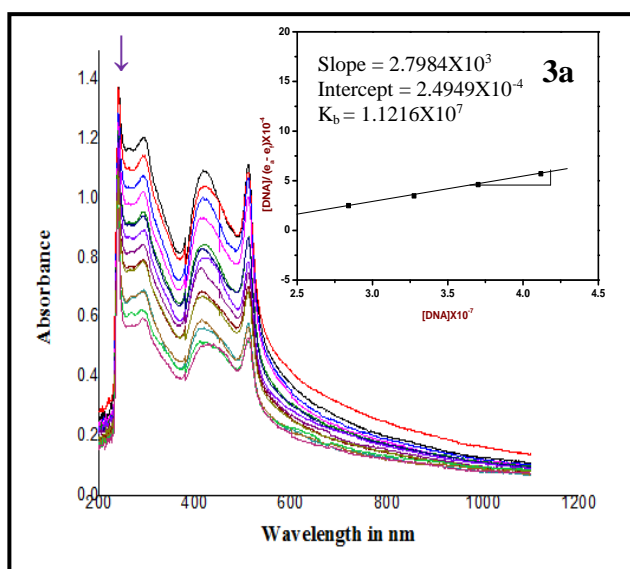
DNA binding was assessed using electronic spectroscopy. The UV-absorption spectral studies were employed to examine the binding mode of compounds to CT-DNA, which involves changes in absorbance and wavelength [51]. The molecules bind to DNA with two modes (covalent or non-covalent binding). Covalent bonding led to bathochromism and hyperchromism due to breaking the DNA structure when a compound interacted with DNA covalently. While in non-covalent binding, there are "electrostatic", "groove", and "intercalative" types of interactions. Decreased absorption (hypochromic shifts) and redshift (bathochromic shift) revealed the intercalative binding of compounds with DNA. The lower hypochromic/hyperchromic effect with no or negligible bathochromic shift led to the electrostatic binding. Minor/no effect, with the exception of some hyperchromism indicating groove binding [52, 53].

The DNA binding efficiency of synthesized compounds **3(a-d)** was monitored by comparing their absorption spectra with and without CT-DNA. The absorption spectra were carried out at a fixed concentration of synthesized compounds and varied with DNA concentrations (25-350 μL of 0.5025×10^{-7} to 6.0670×10^{-7} molL^{-1}) under the physiological condition of pH 7.01. The absorption spectra of all the synthesized compounds **3(a-d)** exhibited absorption bands at 235 to 240 nm due to π - π^* transitions (**Fig. 5**). The K_b values of compounds **3(a-d)** are found to be 1.1216×10^7 , 1.4072×10^7 , 1.0634×10^7 and 3.4872×10^7 respectively appear in **Table 6**. These K_b values confirm that all the synthesized compounds interacted strongly with CT-DNA. Among the four compounds, compound **3d** showed a prominent binding ability with CT-DNA compared to other compounds. The absorption bands of the compounds were affected due to the gradual increase of CT-DNA concentration resulting hyperchromism/hypochromism. No/or negligible blue/red shift indicates strong interaction of the compounds with CT-DNA mainly through electrostatic or groove binding

[54]. The kinetics and thermodynamics of compounds-DNA interaction in terms of binding constant (K_b) and Gibbs free energy change (ΔG) were evaluated using the classical Van't Hoff's equation, $\Delta G = -2.303RT \log K_b$. The negative ΔG values confirmed the spontaneous binding of compounds with CT-DNA through the formation of stable complexes.

Table 6. DNA binding results of synthesized compounds **3(a-d)**.

Compd.	λ_{\max} (nm)		$\Delta\lambda_{\max}$ (nm)	% H	K_b (M^{-1})	ΔG (kJ/mol)
	Free	Bound				
3a	240	239	1	6.1879×10^{-4}	1.1216×10^7	-40.205
3b	236	236	0	6.0157×10^{-4}	1.4072×10^7	-40.767
3c	239	239	0	1.1560×10^{-3}	1.0634×10^7	-40.073
3d	236	236	0	1.2388×10^{-3}	3.4872×10^7	-43.015



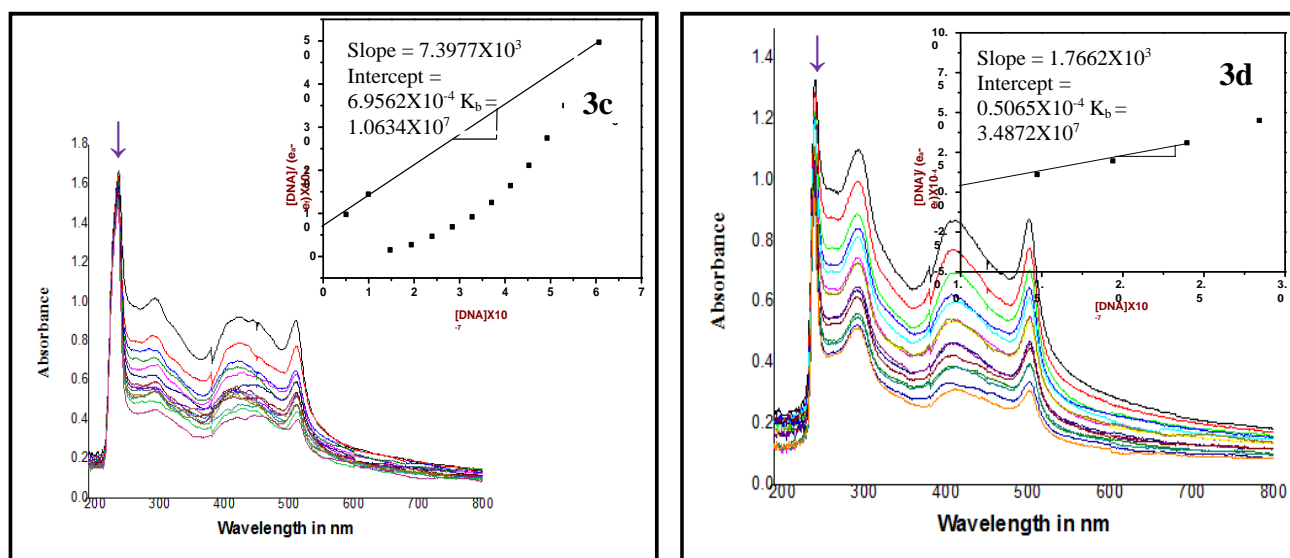


Fig. 5. The electronic absorption spectra of compounds **3(a-d)** in the absence and presence of increasing amounts of CT-DNA. Arrow (\downarrow) shows the change in the absorbance with increase the DNA concentration. Inset: plot of $[DNA]/(\epsilon_a - \epsilon_f)$ vs $[DNA]$.

2B.6.4. Structure-activity relationship (SAR) study

The evaluation of the antibacterial activity of the newly synthesized compounds **3(a-d)** revealed that, the presence of electron-donating group has a significant effect on enhancing their potency. The compounds **3b** and **3d** have a methyl group at C-3 of the thiophene ring. This could have improved their cell permeability, which improved their activity profile compared to **3a** and **3c**. The combination of heterocyclic rings like pyrimidine and thiophene is presumed to be the main reason for the profound cytotoxicity of the newly synthesized compounds **3(a-d)**. Furthermore, the presence of the urea group in the pyrimidine ring could have significantly contributed to the superior cytotoxicity of **3a** and **3b** compounds as compared to other synthesized molecules [55].

2B.6.5. *in silico* molecular docking study

Molecular docking results revealed that, compound **3b** bound with GlcN-6-P and P38 MAPk with a minimum binding energy of -7.9 and -6.4 kcal/mol, respectively. **3a**, **3d** and **3c** interacted with a binding energy of -7.6 and -6.4 kcal/mol, -7.4 and -6.2 kcal/mol and -7.4 and

-6.0 kcal/mol with GlcN-6-P and P38 MAPk targets respectively. The interaction of all the molecules with GlcN-6-P and P38 MAPk were compared with antibacterial agent Ciprofloxacin (-7.7 kcal/mol) and anticancer agent 5-fluorouracil (-4.7 kcal/mol) (**Table 7 & Fig. 6**). The computational methods in drug discovery have gained enormous importance in modern drug research. They play a critical role in reducing the virtual chemical space in synthesizing, modifying, and screening chemical drugs against a specific disease target. Their effectiveness can be validated using microbial pathogens due to their simpler and clearer cellular understandings. Similarly, cell death modalities can also be studied using in vitro cell culture studies, particularly focusing on necrosis, apoptosis, necroptosis, autophagic cell death, etc. In the present study, *in silico* molecular docking studies were performed to predict the most effective binding among the synthesized molecules to appropriate targets [56]. The studied molecules showed remarkable binding interactions with the selected target proteins, supporting their remarkable antimicrobial and anticancer effects.

Table 7. Binding energies of synthesized compounds **3(a-d)** with GlcN-6-P and P38 MAPk targets.

Antibacterial activity		Anticancer activity	
Compd.	Binding energy in kcal/mol	Compd.	Binding energy in kcal/mol
3a	-7.6	3a	-6.4
3b	-7.9	3b	-6.4
3c	-7.4	3c	-6.0
3d	-7.4	3d	-6.2
Ciprofloxacin	-7.7	5-Fluorouracil	-4.7

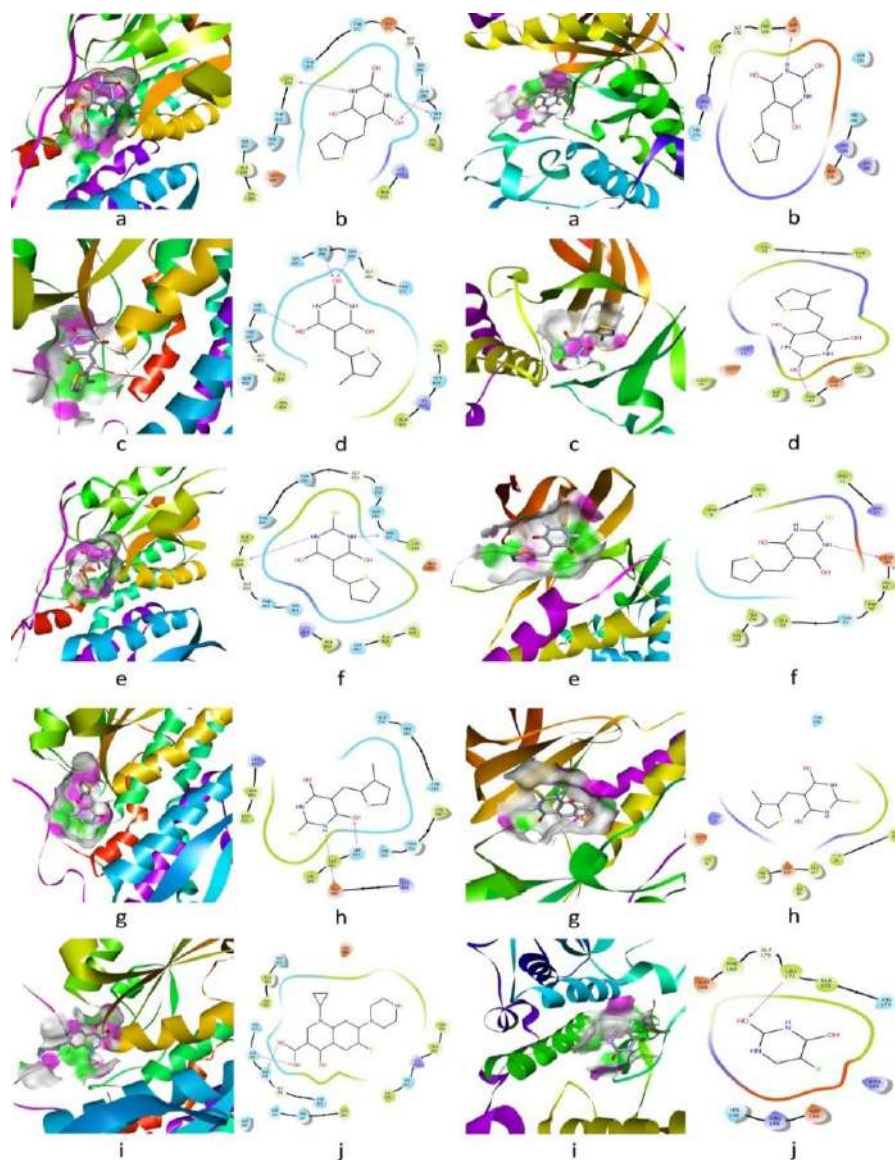


Fig. 6. Binding interaction of compounds **3a** (a&b), **3b** (c&d), **3c** (e&f) & **3d** (g&h) with GlcN-6-P along with standard drug ciprofloxacin (i&j) (a) & Binding interaction of compounds **3a** (a&b), **3b** (c&d), **3c** (e&f) & **3d** (g&h) with P38 MAPk along with standard drug 5-fluorouracil (i&j) (b).

2B.6.6. *in silico* ADME-toxicology study

The bioavailability and drug-likeness were estimated for all the synthesized compounds **3(a-d)** based on the molecular properties. The results indicated that, all four compounds under study could pass through Lipinski's filter without any violations, demonstrating a positive drug-likeness score indicating their suitability as drug-leads. *in silico* pharmacokinetic studies showed that all the molecules under investigation could penetrate the blood-brain barrier and

are readily absorbed by the human intestine while they are impermeable to Caco-2, and non-substrate Cytochromes P450 (CYP450) group of enzymes (**Table 8**).

in silico pharmacodynamics studies revealed that, all four molecules are non-mutagenic, non-tumorigenic, non-irritant and AMES non-toxic with high reproductive effects with possible hepatotoxicity. The bioactivity assessment indicated that the molecules do not belong to the GPCR group of ligands, do not modulate ion channels, non-kinase inhibitors, non-nuclear receptor ligands, non-protease and non-enzyme inhibitors (**Table 9**).

Table 8. Bioavailability, drug likeness and *in silico* pharmacokinetic assessment of synthesized compounds **3(a-d)**.

Compd.	Bioavailability and Drug likeness							<i>in silico</i> Pharmacokinetics			
	Total Molecular weight	cLogP	H-Acceptors	H-Donors	Rotatable Bonds	Polar Surface Area	Drug likeness	Human intestinal absorption	Caco-2 permeability	Blood brain barrier	CYP450 2D6 substrate
3a	222.224	0.2739	5	2	1	103.51	5.2698	+0.982	-0.779	+0.982	-0.873
3b	236.251	0.6178	5	2	1	103.51	4.9763	+0.728	-0.753	+0.980	-0.889
3c	238.291	0.6344	4	2	1	118.53	4.2229	+0.979	-0.698	+0.977	-0.871
3d	252.318	0.9783	4	2	1	118.53	3.9143	+0.987	-0.673	+0.976	-0.886

Table 9. *in silico* pharmacodynamics and bioactivity assessment of synthesized compounds **3(a-d)**.

Compd.	<i>in silico</i> Pharmacodynamics							Bioactivity score					
	Mutagenic	Tumorigenic	Reproductive Effective	Irritant	Aerobic biodegradability	Ames toxicity	Hepatotoxicity	GPCR ligand	Ion channel modulator	Kinase inhibitor	Nuclear receptor ligand	Protease inhibitor	Enzyme inhibitor
3a	NONE	NONE	HIGH	NONE	-0.590	-0.706	+0.925	-1.12	-1.58	-0.86	-1.26	-1.30	-0.69
3b	NONE	NONE	HIGH	NONE	-0.562	-0.694	+0.950	-1.07	-1.44	-0.90	-0.91	-1.32	-0.73
3c	HIGH	NONE	HIGH	NONE	-0.859	-0.731	+0.900	-1.43	-1.77	-1.41	-1.73	-1.32	-1.00
3d	HIGH	NONE	HIGH	NONE	-0.843	-0.711	+0.850	-1.35	-1.62	-1.42	-1.35	-1.34	-1.03

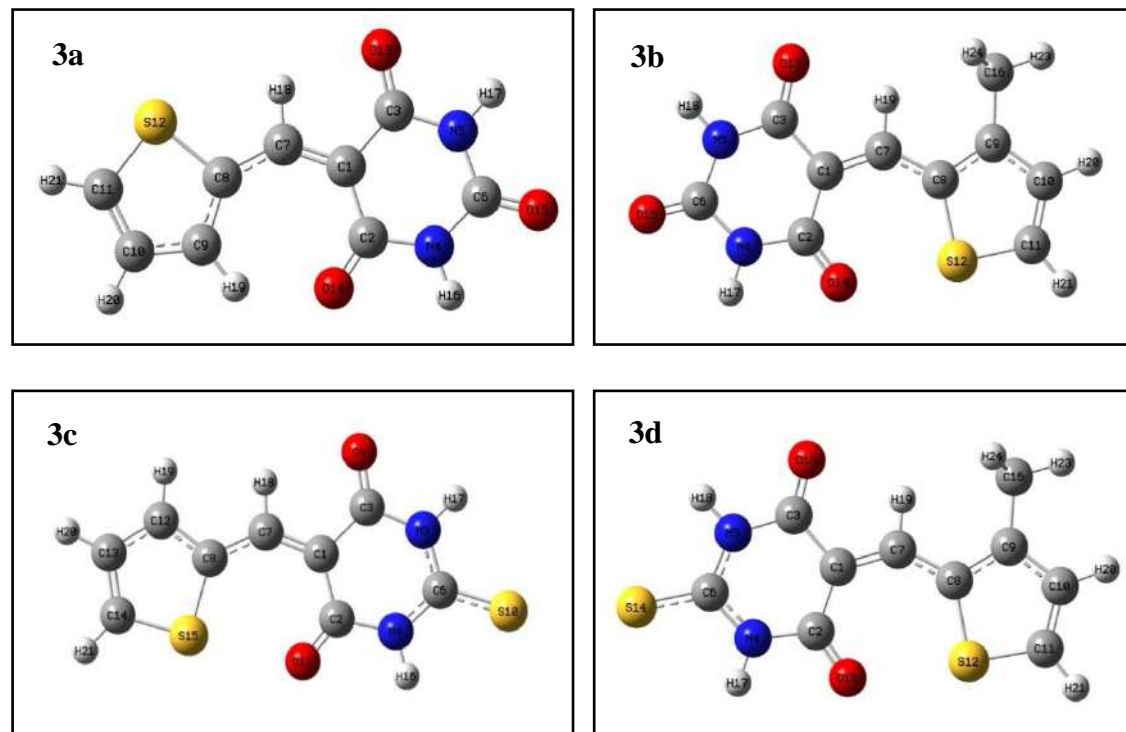
2B.6.7. DFT study

Frontier molecular orbitals (FMOs) containing the highest occupied molecular orbital (HOMO) and lowest unoccupied molecular orbital (LUMO), as well as the energy gap ($\Delta E = E_{HOMO} - E_{LUMO}$) were considered to be very effective parameters in chemical quantum chemistry. FMOs also delivered important information about chemical reactivity, biological activity and kinetic stability of the molecules. The optimized HOMO and LUMO structures of synthesized compounds **3(a-d)** are shown in **Fig. 7 & 8**. The HOMO and LUMO of compounds were helpful in determining various global reactivity parameters such as ionization energy ($I = -E_{HOMO}$), electron affinity ($A = -E_{LUMO}$), chemical hardness ($\eta = 1/2 (I - A)$), chemical softness ($\sigma = 1/\eta$), electronegativity ($\chi = 1/2 (I + A)$), chemical potential ($\mu = -\chi$), and electrophilicity index ($\omega = \mu^2/2\eta$) helps to study about donor-acceptor interaction and intramolecular charge transfer (ICT) ability of synthesized compounds [57].

The calculated HOMO-LUMO energies and global reactivity parameters of the synthesized compounds **3(a-d)** are displayed in **Table 10**. A smaller HOMO-LUMO energy gap (ΔE) indicates a soft molecule, while a larger gap indicates a hard molecule. Lower energy gap, less ionization potential, electron affinity, chemical hardness, electronegativity, electrophilicity index values and more softness values indicates that molecule with more chemically and biologically active with low kinetic stability [58]. DFT study data reveals that, the energy gap (ΔE) of compounds **3a**, **3b**, **3c** and **3d** are 0.16038 eV, 0.15988 eV, 0.12799 eV and 0.12636 eV respectively. **3a**, **3b** and **3c**, **3d** molecules show nearly similar energy gaps due to the similar structure. Among them **3d** molecule shows less energy gap (0.12636 eV) and more softness value (15.8277 eV). Hence, it is chemically more reactive as compared to other molecules. **3a** molecule having more electronegative value (0.19923 eV), hence it has more tendency to attract a bonding electron pairs as compared to other molecules.

Table 10. Chemical parameters of synthesized compounds **3(a-d)**.

Entry	E_{HOMO} (eV)	E_{LUMO} (eV)	ΔE $E_{\text{HOMO}} - E_{\text{LUMO}}$ (eV)	I (eV)	A (eV)	η (eV)	σ (eV)	χ (eV)	μ (eV)	ω (eV)	D (Debye)
3a	-0.27942	-0.11904	0.16038	0.27942	0.11904	0.08019	12.4703	0.19923	-0.19923	0.24749	4.6744
3b	-0.27411	-0.11423	0.15988	0.27411	0.11423	0.07994	12.5093	0.19417	-0.19417	0.23581	5.2238
3c	-0.25095	-0.12296	0.12799	0.25095	0.12296	0.06399	15.6274	0.18695	-0.18695	0.27310	5.4300
3d	-0.24793	-0.12157	0.12636	0.24793	0.12157	0.06318	15.8277	0.18475	-0.18475	0.27012	5.9267

**Fig. 7.** Optimized structures of synthesized compounds **3(a-d)**.

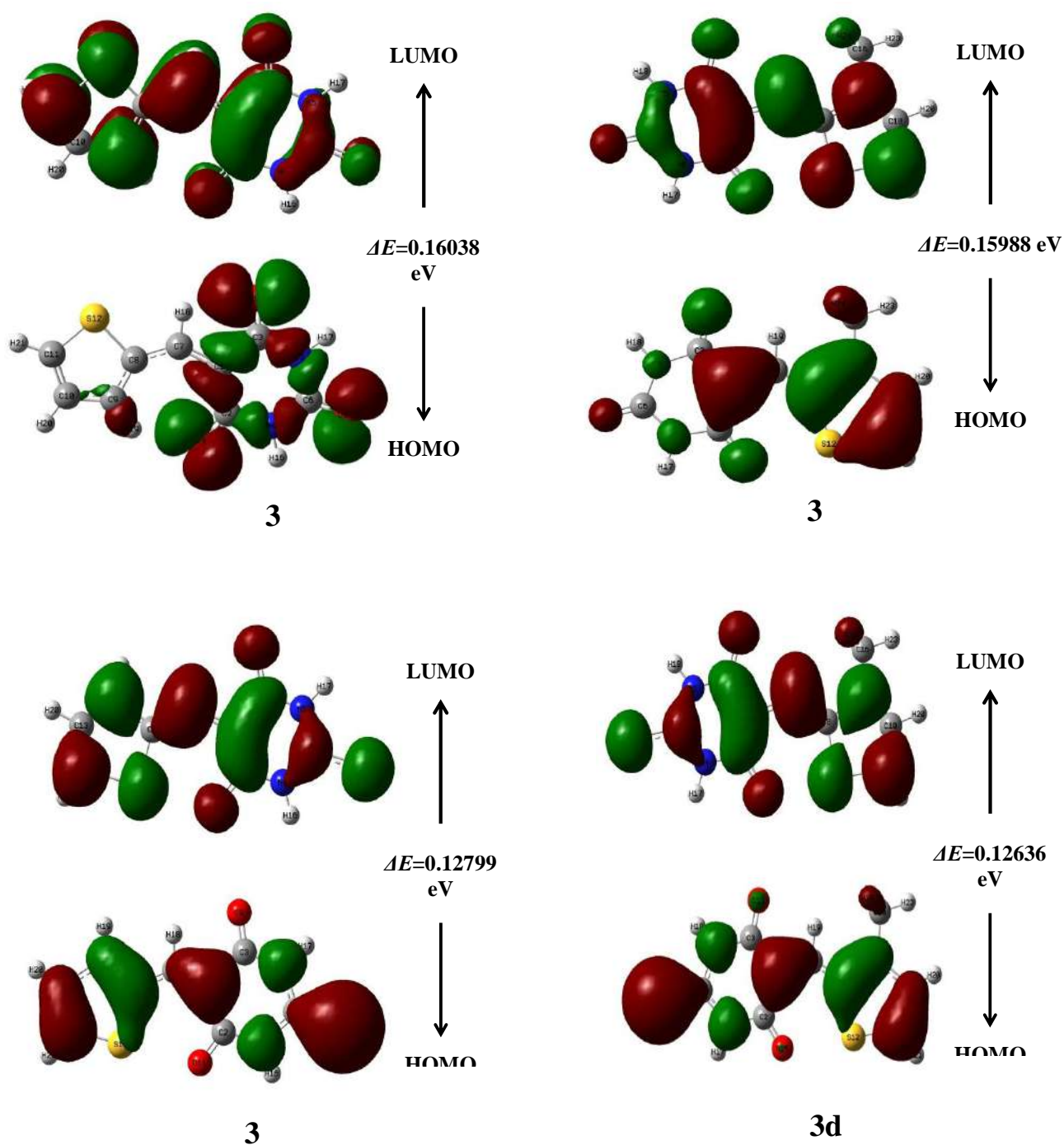


Fig. 8. HOMO-LUMO structures of synthesized compounds 3(a-d).

2B.7. Conclusion

We have described a mild, easy and green protocol for synthesizing 5-(3-substituted-thiophene)-pyrimidine derivatives **3(a-d)** using $\text{H}_2\text{O}_2\text{:HCl}$ as a catalyst under reflux condition. This synthetic approach has a short reaction time, excellent yield, and clean reactions make this procedure a magnificent alternative to the existing methods. Moreover, the activity results revealed that, compounds **3b** and **3d** exhibited more potent antibacterial activity against *E. coli* & *S. aureus* than the standard drug Ciprofloxacin. *In vitro* cytotoxicity results disclosed the outstanding selectivity on MCF-7 cell line, mainly compound **3a** exhibiting the most effective cytotoxicity with a minimum cell survival range of 23.68 to 44.16 %. DNA binding results indicate that, all the synthesized compounds interacted strongly with CT-DNA and compound-DNA complexes were stabilized by electrostatic or groove binding. *In silico* ADME-toxicology results showed that, the compounds obeyed all the five rules with good bioavailability. Hence, there was no possibility of causing harmful toxicants, thus indicating their suitability as drug-leads. *in silico* molecular docking results suggested that, compound **3b** bound with GlcN-6-P and P38 MAPk with a least binding energy of -7.9 and -6.4 kcal/mol, respectively. DFT results indicates, compound **3d** was chemically and biologically more reactive with low kinetic stability due to smaller energy gap.

2B.8. References

1. P.K. Singh, O. Silakari, *Med. Chem.*, **2018**, 13, 1071-1087.
2. S. Pathania, R.K. Narang, R.K. Rawal, *Eur. J. Med. Chem.*, **2019**, 180, 486-908.
3. T. Venkatesh, Y.D. Bodke, B. Manjunatha, S.R. Kumar, *Nucleosides, Nucleotides and Nucleic Acids*, **2021**, 1-13.
4. B. Sravanthi, L. Kaviarasan, T.K. Praveen, P. Sai Kiran, C. Pavankumar, B. Gowramma, *J. Iran. Chem. Soc.*, **2020**, 17, 2359-2370.
5. D. Kang, D. Feng, T. Ginex, J. Zou, F. Wei, T. Zhao, B. Huang, Y. Sun, S. Desta, E.D. Clercq, C. Pannecouque, P. Zhan, X. Liu, *Acta Pharm. Sin. B.*, **2020**, 10, 878-894.
6. P. Prasad, G.K. Anirudhdha, M.P. Patel, *New J. Chem.*, **2018**, 42, 12666-12676.
7. U.H.K. Zia, U.K. Arif, W. Pingyu, C. Yongmei, K. Dandan, K. Shafiullah, T. Kamran, *Nat. Prod. Res.*, **2015**, 29, 933-938.
8. S.M. Ghada, *Polycycl. Aromat. Compd.*, **2021**, 1-17.
9. X. Zhen, C. Cilong, Z. Lingjia, Z. Zhihui, Z. Qian, Y. Feiyi, Y. Zunhua, Z. Pengwu, X. Shan, Z. Wufu, *Bioorg. Med. Chem.*, **2020**, 28, 1-13.
10. X. Zhen, Z. Zhihui, C. Cilong, Z. Qian, Z. Lingjia, Y. Zunhua, X. Li, L. Yu, Z. Pengwu, S. Xu, Z. Wufu, *Eur. J. Med. Chem.*, **2020**, 203, 1-43.
11. I.E. Elshayma, *J. Heterocyclic. Chem.*, **2020**, 57, 2067-2078.
12. A.K. Nadia, M.A. Eman, F.Z. Ashraf, S.E.Z. Mona, A.S. Eman, *Eur. J. Med. Chem.*, **2020**, 187, 1-56.
13. A.S. Sergei and E.R. Aleksandr, *J. Org. Chem.*, **2019**, 84, 15788-15796.
14. S. Lei, C. Chengjuan, H. Xueting, H. Hao, W. Manman, Z. Jianqiu, Y. Yile, L. Jianming, Z. Tiantai, Z. Dayong, *Eur. J. Med. Chem.*, **2020**, 191, 1-18.
15. R. Giuseppe, S. Loredana, P. Valeria, C. Marialuisa, I. Sebastiano, A. Emanuele, S. Mario, C. Alfredo, R. Antonio, F. Giuseppe, N.M. Maria, *Eur. J. Med. Chem.*, **2019**, 183, 1-16.
16. I. Ali, W.A. Wani, K. Saleem, M.F. Hsieh, *RSC Adv.*, **2014**, 4, 29629-29641.
17. A. Aarti, K. Archana, K.A. Dr. Amarjit, C. Dr. Nithish, S. Yudhvir. *Int. J. Pharm. Sci. Rev. Res.*, **2019**, 58, 104-113.
18. A. Jawaid, A.K. Ahsan, A. Zulphikar, H. Rafi, Y.M. Shahar, *Eur. J. Med. Chem.*, **2017**, 125, 143-189.
19. C.S. Prabodh, K.B. Kushal, S. Archana, S. Diksha, D. Aakash. *Eur. J. Med. Chem.*, **2020**, 188, 1-47.

20. Q. Yan, R. Cao, W. Yi, Z. Chen, H. Wen, L. Ma, H. Song, *Eur. J. Med. Chem.*, **2009**, 44, 4235-4243.
21. B.B. Sokmen, S. Ugras, H.Y. Sarikaya, H.I. Ugras, R. Yanardag, *Appl. Biochem. Biotechnol.*, **2013**, 171, 2030-2039.
22. Y. Luo, L. Ma, H. Zheng, L. Chen, R. Li, C. He, S. Yang, X. Ye, Z. Chen, Z. Li, Y. Gao, J. Han, Gu He, Li Yang, Y. Wei, *J. Med. Chem.*, **2010**, 53, 273-281.
23. J.S. Biradar, B.S. Sasidhar, *Eur. J. Med. Chem.*, **2011**, 46, 6112-6118.
24. O.C. Sanchez, R.R. Cairo, Y.V. Reyes, R. Rojas, E.O. Rodriguez, E.D. Peralta, Y. Nunez, *Sociedade Brasileira de Quimica*, **2011**, 1-2.
25. N.R. Dighore, P.L. Anandgaonker, S.T. Gaikwad and A.S. Rajbhoj, *Res. J. Chem. Sci.*, **2014**, 4, 93-98.
26. J.M. Khurana and V. Kanika, *Catal. Lett.*, **2010**, 138, 104-110.
27. M. Fattahi, A. Davoodnia, M. Pordel, *Russ. J. Gen. Chem.*, **2017**, 87, 863-867.
28. G. Thirupathi, M. Venkatanarayana, P.K. Dubey, Y. Bharathi Kumari, *Chem. Sci. Trans.*, **2013**, 2, 441-446.
29. J. Tai Li, H. Guang Dai, D. Liu, T. Shuang Li, *Synth. Commun.*, **2006**, 36, 789-794.
30. Y. Hu, Z.C. Chen, Z.G. Le, Q.G. Zheng, *Synth. Commun.*, **2004**, 34, 4521-4529.
31. M. Shabeer, L.C.A. Barbosa, M. Karak, A.C.S. Coelho, *Med. Chem. Res.*, **2018**, 27, 1043-1049.
32. A. Pandith, G. Hazra, H.S. Kim, *Spectrochim. Acta A Mol. Biomol. Spectrosc.*, **2017**, 178, 151-159.
33. T. Venkatesh, Y.D. Bodke, N.M. Joy, B.M. Vinoda, Y. Shiralgi, B.L. Dhananjaya, *Lett. Org. Chem.*, **2016**, 13, 661-671.
34. S.H. Sukanya, T. Venkatesh, S.J. Aditya Rao, M.N. Joy, *J. Mol. Struct.*, **2021**, 1247, 1-13.
35. N. Shivakumara, P. Murali Krishna, *Curr. Chem. Lett.*, **2019**, 8, 157-168.
36. I. Ali, S.D. Mukhtar, M.F. Hsieh, Z.A. Alothman, A. Alwarthan, *RSC Adv.*, **2018**, 8, 37905-37914.
37. A. Wolfe, G.H. Shimer, Jr and T. Meehan, *Biochemistry*, **1987**, 26, 6392-6396.
38. O. Trott, J.A. Olson, *J. Comput. Chem.*, **2010**, 31, 455-461.
39. S.J. Aditya Rao, C.K. Ramesh, S. Raghavendra, M. Paramesha, *Curr. Comput. Aided Drug Des.*, **2020**, 16, 231-237.
40. S.J. Aditya Rao, S.M. Shivayogi, J.K. Satyanarayana, R.C. Kumaran, *Bioimpacts*, **2021**, 11, 1-11.

41. C.A. Lipinski, F. Lombardo, B.W. Dominy, P.J. Feeney. *Adv. Drug Deliv. Rev.*, **1997**, 23, 3-25.
42. R. Aditya, T. Venugopal, N. Jayanna, M. Paramesha, C. Ramesh, *Lett. Drug Des. Discov.*, **2020**, 17, 1-9.
43. A. Jarrahpour, M. Motamedifar, M. Zarei, M.H. Youssoufi, M. Mimouni, Z.H. Chohan, *Phosphorus Sulfur Silicon Relat Elem.*, **2010**, 185, 491-497.
44. S. Raghavendra, S.J. Aditya Rao, V. Kumar, C.K. Ramesh, *Comput. Biol. Chem.*, **2015**, 59, 81-86.
45. T. Sander, J. Freyss, M. Von Korff, C. Rufener, *J. Chem. Inf. Model*, **2015**, 55, 460-473.
46. T. Venkatesh, Y.D. Bodke, S.J. Aditya Rao, *Chem. Data Collect.*, **2020**, 25, 1-13.
47. F. Cheng, W. Li, Y. Zhou, J. Shen, Z. Wu, G. Liu, *J. Chem. Inf. Model*, **2012**, 52, 3099-3105.
48. M.J.E.A. Frisch, G.W. Trucks, H.B. Schlegel, G.E. Scuseria, M.A. Robb, J.R. Cheeseman, H. Nakatsuji, *Gaussian. Inc. Wallingford CT*, **2009**, 201-205.
49. A.D. Becke, *J. Chem. Phys.*, **1993**, 98, 1372-1377.
50. M.D. Hanwell, D.E. Curtis, D.C. Lonie, T. Vandermeersch, E. Zurek, G.R. Hutchison, *Aust. J. Chem.*, **2012**, 4, 01-33.
51. G. Ramesh, S. Daravath, N. Ganji, A. Rambabu, K. Venkateswarlu, Shivaraj. *J. Mol. Struct.*, **2019**, 1202, 1-41.
52. I. Ali, A. Haque, K. Saleem, M.F. Hsieh, *Bioorg. Med. Chem.*, **2013**, 21, 3808-3820.
53. R. Indumathy, M. Kanthimathi, T. Weyhermuller, B.U. Nair, *Polyhedron*, **2008**, 27, 3443-3450.
54. R. Hajian, E. Ekhlasi, R. Daneshvar, *J. Chem.*, **2012**, 9, 1587-1598.
55. J. Yao, J. Chen, Z. He, W. Sun, W. Xu, *Bioorg. Med. Chem.*, **2012**, 20, 2923-2929.
56. M. Campillos, M. Kuhn, A.C. Gavin, L.J. Jensen, P. Bork, *Science*, **2008**, 321, 263-266.
57. A. Pandith, Y.J. Seo. *J. Inorg. Biochem.*, **2020**, 203, 1-41.
58. J. George, J.C. Prasana, S. Muthu, T.K. Kuruvilla, S. Savanthi, R.S. Saji, *J. Mol. Struct.*, **2018**, 1171, 268-278.

3.1. Introduction

Multi-component reactions (MCRs) afford an extremely valuable tool within the field of synthetic and medicinal chemistry. They consider as an important tool for the synthesis of polyfunctional molecules with high competence over multistep synthesis. Globally, it has been explored as an efficient tool for preparing several active drugs [1]. MCRs offer many advantages such as they avoid unnecessary purification, wastages, byproducts, toxic reagents, solvents consumption, and they also followed the easy workup, shorter reaction time and high atom economy [2, 3].

Proline is a bifunctional chiral homogenous organocatalyst that is cost-effective, efficient, and more readily available than any other catalyst [4]. L-Proline has both acidic ($-\text{COOH}$) and basic ($-\text{NH}$) functionality and catalyzes chemical transformations similar to enzyme catalysis [5]. It is efficient in catalyzing various organic transformations [6], Knoevenagel-type condensation [7], Biginelli reaction [8], Mannich [9], Michael [10], Diels-Alder [11], α -amination reaction [12] and asymmetric Hantzsch reaction [13].

Heterocyclic compounds play a predominant role in the field of medicinal as well as synthetic organic chemistry due to their broad biological importance. They always attract the attention of medicinal chemists and researchers due to their multiform pharmacological activities [14, 15]. Pyrimidine and thiazole are important scaffolds in drug discovery, combining these pharmacophores into a single entity could enhance their pharmacological properties such as antitumor [16], anti-inflammatory [17], anti-tubercular [18], anticancer [19], antioxidant [20], antimicrobial [21], antipsychotic [22], anxiolytic and antidepressant [23] etc. Rationalizing this hypothesis by synthesizing a series of thiazolopyrimidine derivatives could result in novel molecules displaying considerable pharmacological potential.

Cancer is a global malignant disease causing severe health problems and even death. It is generally characterized by the rapid and uncontrolled proliferation of cells, thereby leading

to the invasiveness of various tissues. The advancements in the medical field have given good insights into the inheritance of cancer. However, seeking a proper cure for cancer is still a major unsolved challenge to the scientific community [24]. A defensive response of the body that minimizes tissue damage by inducing physiological adaptations can be termed as inflammation. There are different inflammatory disorders such as retinitis, multiple sclerosis, psoriasis, atherosclerosis, inflammatory bowel diseases, osteoarthritis, and rheumatoid arthritis [25]. Although the significant effects of inflammation do not look critical *prima facie*, chronic inflammation is a vital contributory factor in mortality and morbidity. These observations emphasize the importance of developing potent anticancer and anti-inflammatory agents with minimum side effects. In this aspect, the concept of synthesizing novel heterocyclic compounds is rational as a majority of available anticancer and anti-inflammatory agents contain one or more heterocyclic groups [26, 27]. The significance of pyrimidine and thiazole-based compounds are underlined by their presence in various drugs available in the market (**Fig. 1**) and some reported biologically important cyclocondensation compounds have been discussed below.

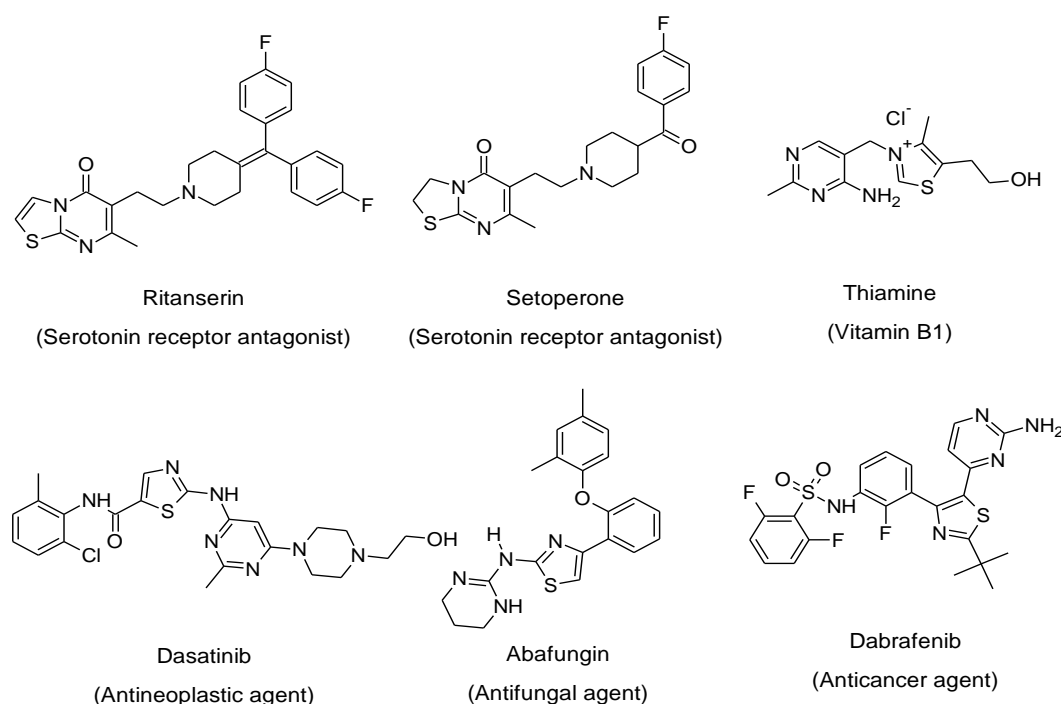
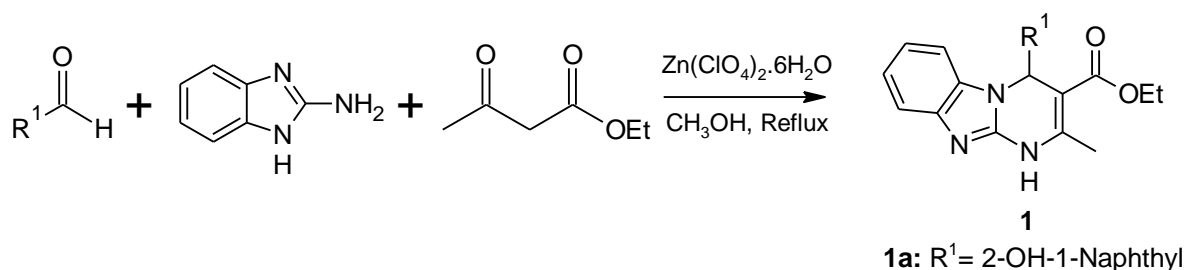
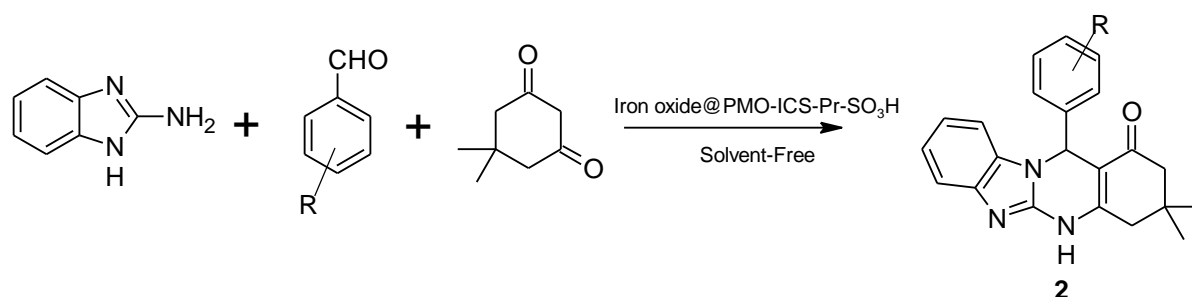


Fig. 1. Some of the drugs containing pyrimidine and thiazole moieties.

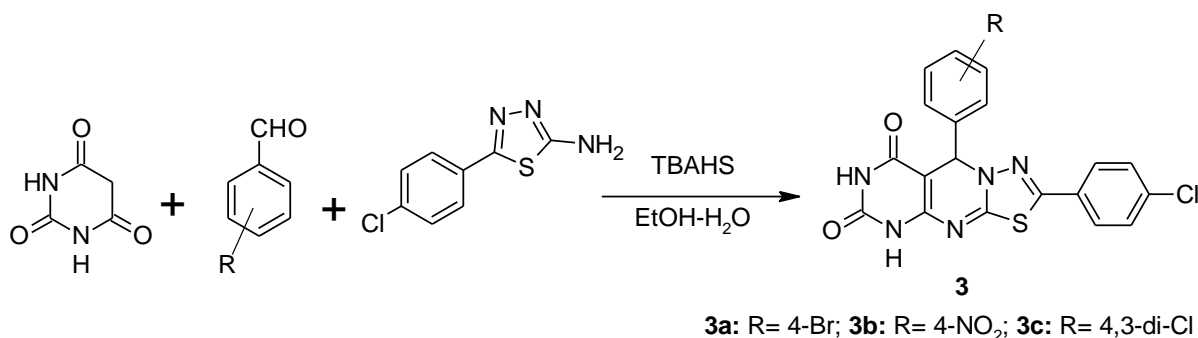
In 2015, N. Kaur *et. al.*, have been reported a series of tricyclic dihydropyrimidine derivatives (**1**) through Traube-Schwarz reaction in the presence of $Zn(ClO_4)_2 \cdot 6H_2O$ as a catalyst and evaluated for their *in vitro* anticancer activity. Out of all the tested compounds, **1a** possessed the highest cytotoxicity in PC3 and NCI-H1299 cancer cell lines, with an IC_{50} value of 37 μM in PC3 and 40 μM in NCI-H1299 cell lines [28].



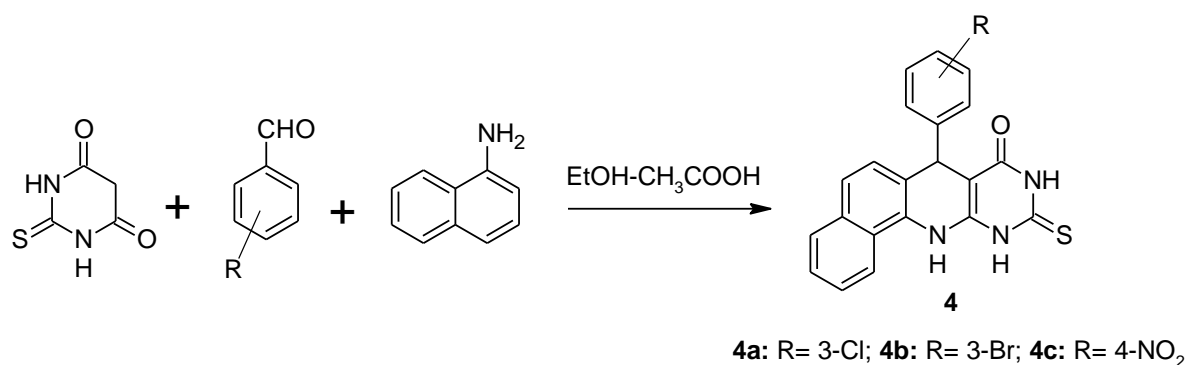
A series of substituted-3,3-dimethyl-3,4,5,12-tetrahydrobenzo[4,5]imidazo[1,2-*b*]quinazolin-1(2*H*)-one derivatives (**2**) have been reported by A. Akbari *et. al.*, in 2020 using mesoporous organosilica magnetic nanoparticles due to shorter reaction time, excellent yields, low catalyst loading, cost-effectiveness and catalyst recyclability [29].



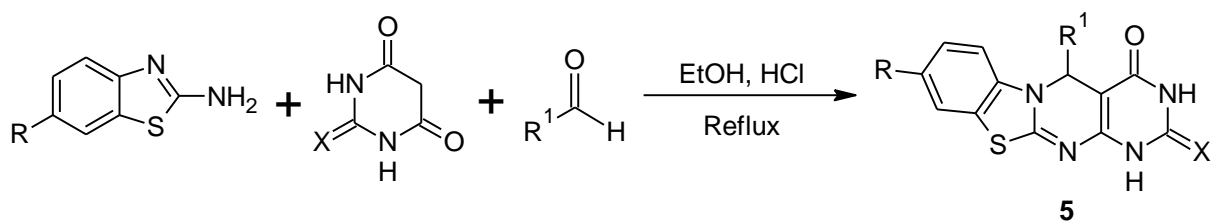
In 2019, S.G. Khansole *et. al.*, have been reported a pyrimido [4,5-*d*] [1,3,4] thiadiazolo [3,2-*a*] pyrimidinedione derivatives (**3**) using tetrabutyl ammonium hydrogen sulphate (TBAHS) as a green catalyst and screened for their antioxidant activity. The compounds **3a** & **3b** showed good DDPH radical scavenging activity with % of inhibition is 86.2 ± 1.06 & 84.6 ± 1.26 , the compounds **3a**, **3b** & **3c** exhibited excellent OH radical scavenging activity with % of inhibition 84.1 ± 0.44 , 85.2 ± 1.06 and 85.0 ± 1.98 respectively [30].



A series of 7-aryl-10-thioxo-7,10,11,12-tetrahydro-9H-benzo[H]pyrimido[4,5-b]quinoline-8-one derivatives (**4**) was reported by D. Kumbhar *et. al.*, and investigated as an antimicrobial agent against pathogenic fungi such as *C. truncatum*, *U. maydis* and bacterial strains *viz* *B. megaterium* and *P. vulgaris*. Electron withdrawing groups containing compounds such as **4a**, **4b** and **4c** shows good antifungal and promising antibacterial activity [31].



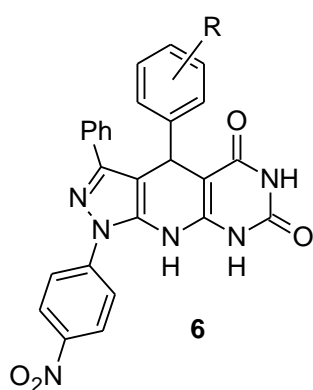
In 2018, T. Venkatesh and co-authors synthesized substituted phenyl-1,5-dihydro-2H-benzo[4,5]thiazolo[3,2-*a*]pyrimido[4,5-*d*]pyrimidine derivatives (**5**) and reported as antimicrobial activity against various microbial strains, at different concentrations. Compounds **5b** and **5c** were found to be more active against bacterial strains *E. coli*, *P. syringae* and *S. aureus* with MIC value of 50 µg/mL and compounds **5a**, **5b** and **5d** were shows MIC value of 150 µg/mL against fungal strains *F. oxysporum*, *A. flavus* and *A. solani* respectively [32].



5a: X= O; R= H; R¹= 4-Cl C₆H₄; **5b:** X= O; R= H; R¹= C₆H₅

5c: X= S; R= H; R¹= C₆H₅; **5d:** X= S; R= H; R¹= 4-Cl C₆H₄

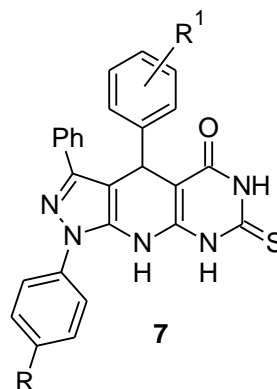
A. Bazgira *et. al.*, have been described a series of pyrazolo[4,3:5,6]pyrido[2,3-*d*]pyrimidine-dione derivatives (**6 & 7**) and evaluated *in vitro* antibacterial activity. The compounds **6(a-e)** shows good MIC value in the range of 18-32 $\mu\text{g/mL}$ and 20-32 $\mu\text{g/mL}$ against *S. epidermidis* and *P. aeruginosa* respectively and compounds **7(a-f)** displayed MIC value range of 12-32 $\mu\text{g/mL}$ against *P. aeruginosa* bacterial strain [33].



6a: R= C₆H₅; **6b:** R= 4-Cl-C₆H₄

6c: R= 4-Br-C₆H₄; **6d:** R= 4-CH₃-C₆H₄

6e: R= 3-NO₂-C₆H₄

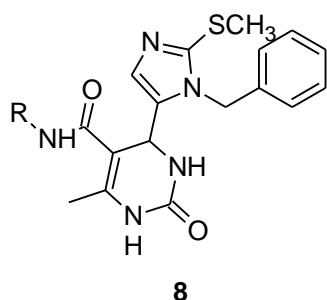
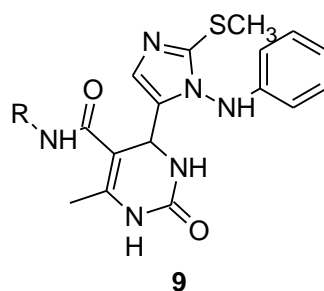
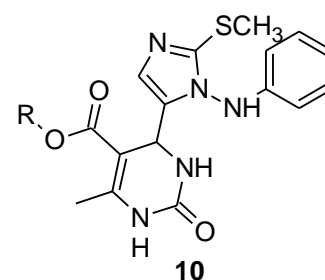


7a: R= H; R¹= C₆H₅; **7b:** R= H; R¹= 4-Cl-C₆H₄

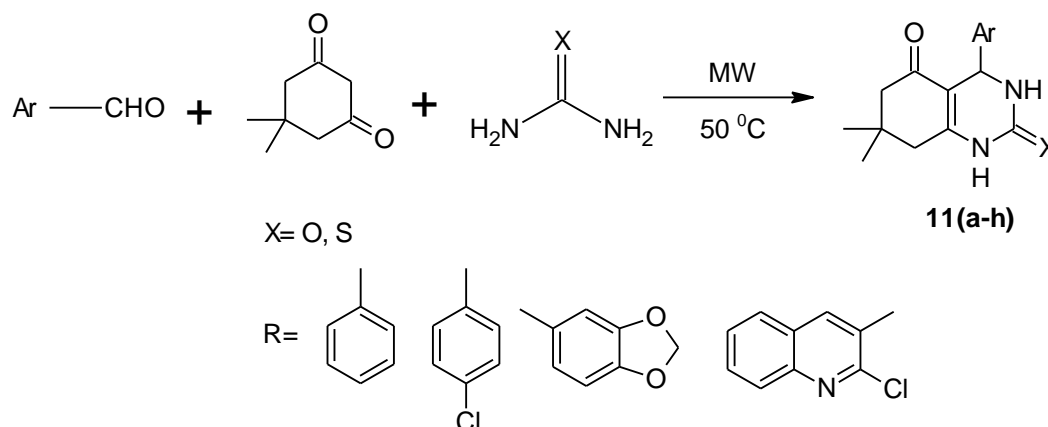
7c: R= H; R¹= 4-NO₂-C₆H₄; **7d:** R= NO₂; R¹= C₆H₅

7e: R= NO₂; R¹= 4-Cl-C₆H₄; **7f:** R= NO₂; R¹= 4-NO₂-C₆H₄

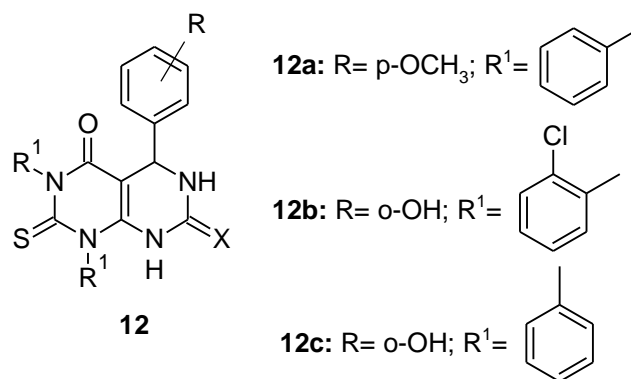
In 2012, a series of novel substituted 6-methyl-2-oxo-*N*,4-diphenyl-1,2,3,4-tetrahydropyrimidine-5-carboxamide derivatives (**8, 9 & 10**) was prepared by B. Sedaghati *et. al.* and evaluated for antimicrobial activity. The compounds **8a & 10a** shows MIC value of 128 $\mu\text{g/mL}$ against *S. aureus* and *P. aeruginosa* strains respectively. Compounds **9a, 9b** and **9c** showed MIC value of 32 $\mu\text{g/mL}$ against *C. albicans* fungal strain [34].

**8a:** R= 3-Chlorophenyl**9a:** R= 4-Chlorophenyl**9b:** R= 2-Pyridyl**9c:** R= 3-Pyridyl**10a:** R= Ethyl

M. Kidwai *et. al.*, developed a convenient synthetic route for the preparation of 4-aryl-7,7-dimethyl-1,2,3,4,5,6,7,8-octahydroquinazoline-2-one/thione-5-one (**11**) in the absence of solvent and catalyst, under microwave irradiation and reported as antibacterial activity against *S. aureus*, *E. coli* and *P. aeruginosa*. All compounds were susceptible at concentration of 32 & 64 $\mu\text{g/mL}$ as compared to standard drug Norfloxacin [35].



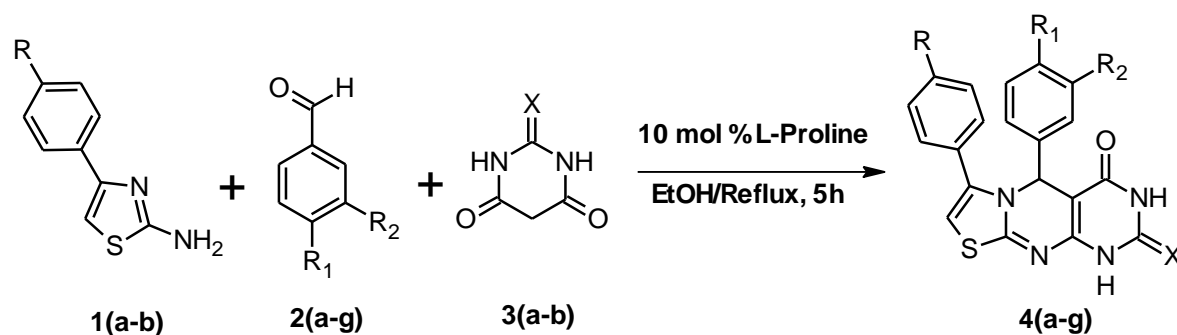
In 2010, V.V. Dabholkar and co-workers reported a substituted dihydropyrimidinones (**12**) as antibacterial agents. All the synthesized compounds were subjected to bacterial strains *S. aureus*, *C. diphtheria*, *P. aeruginosa* and *E. coli*. Among them, **12a** shows maximum zone of inhibition at 22 mm against *S. aureus*, **12b** shows highest % inhibition of 27 & 32 mm against *C. diphtheria* and *E. coli*, **12c** exhibits highest inhibition at 30 mm against *P. aeruginosa* strain [36].



Based on the above investigations, we reported (4-substituted-phenyl)-1,5-dihydro-2*H*-pyrimido[4,5-*d*][1,3]thiazolo[3,2*a*]-pyrimidine-2,4(3*H*)-dione derivatives and examined their *in vitro* cytotoxicity, anti-inflammatory and *in silico* studies using P38 MAP kinase and MMP-9 proteins as target enzymes.

3.2. Present work

In this chapter, we explained a simple, convenient and eco-friendly method for the synthesis of some new (4-substituted-phenyl)-1,5-dihydro-2*H*-pyrimido[4,5-*d*][1,3]thiazolo[3,2*a*]-pyrimidine-2,4(3*H*)-dione derivatives **4(a-g)** via one-pot three-component reaction of 2-amino-4-(4-substituted-phenyl)thiazoles (**1**), substituted benzaldehyde (**2**) and barbituric/thiobarbituric acid (**3**) in aqueous ethanol using 10 mol % of L-Proline as a catalyst to affords solid targets and the reaction pathway has been given in **Scheme 3**.



Compd.	R	R ₁	R ₂	X
4a	OCH ₃	H	NO ₂	O
4b	OCH ₃	OH	H	O

4c	OCH ₃	OH	OCH ₃	O
4d	OCH ₃	N(CH ₃) ₂	H	O
4e	OCH ₃	OCH ₃	H	O
4f	NO ₂	OH	H	S
4g	NO ₂	Cl	NO ₂	S

Scheme 3. Synthesis of (4-substituted-phenyl)-1,5-dihydro-2*H*-pyrimido[4,5-*d*][1,3]thiazolo[3,2*a*]-pyrimidine-2,4(3*H*)-dione derivatives **4(a-g)**.

The synthetic strategy involves in the following steps:

- The reaction was initiated by the formation of enol **II** from barbituric/thiobarbituric acid **I**.
- L-Proline was coordinated through a hydrogen bond to the oxygen atom of the substituted benzaldehyde **III** and then it was activated for nucleophilic attack.
- Enol **II** attacks the carbonyl group of the activated benzaldehyde **III** and affords Knoevenagel intermediate **IV**.
- It undergoes Michael addition with 2-amino-4-(4-substituted-phenyl) thiazole **V**, afford intermediates **VI** & **VII**, followed by cyclocondensation giving the final products **VIII**.
- The plausible mechanism for the formation of new (4-substituted-phenyl)-1,5-dihydro-2*H*-pyrimido[4,5-*d*][1,3]thiazolo[3,2*a*]-pyrimidine-2,4(3*H*)-dione derivatives has been proposed in **Fig. 2**.

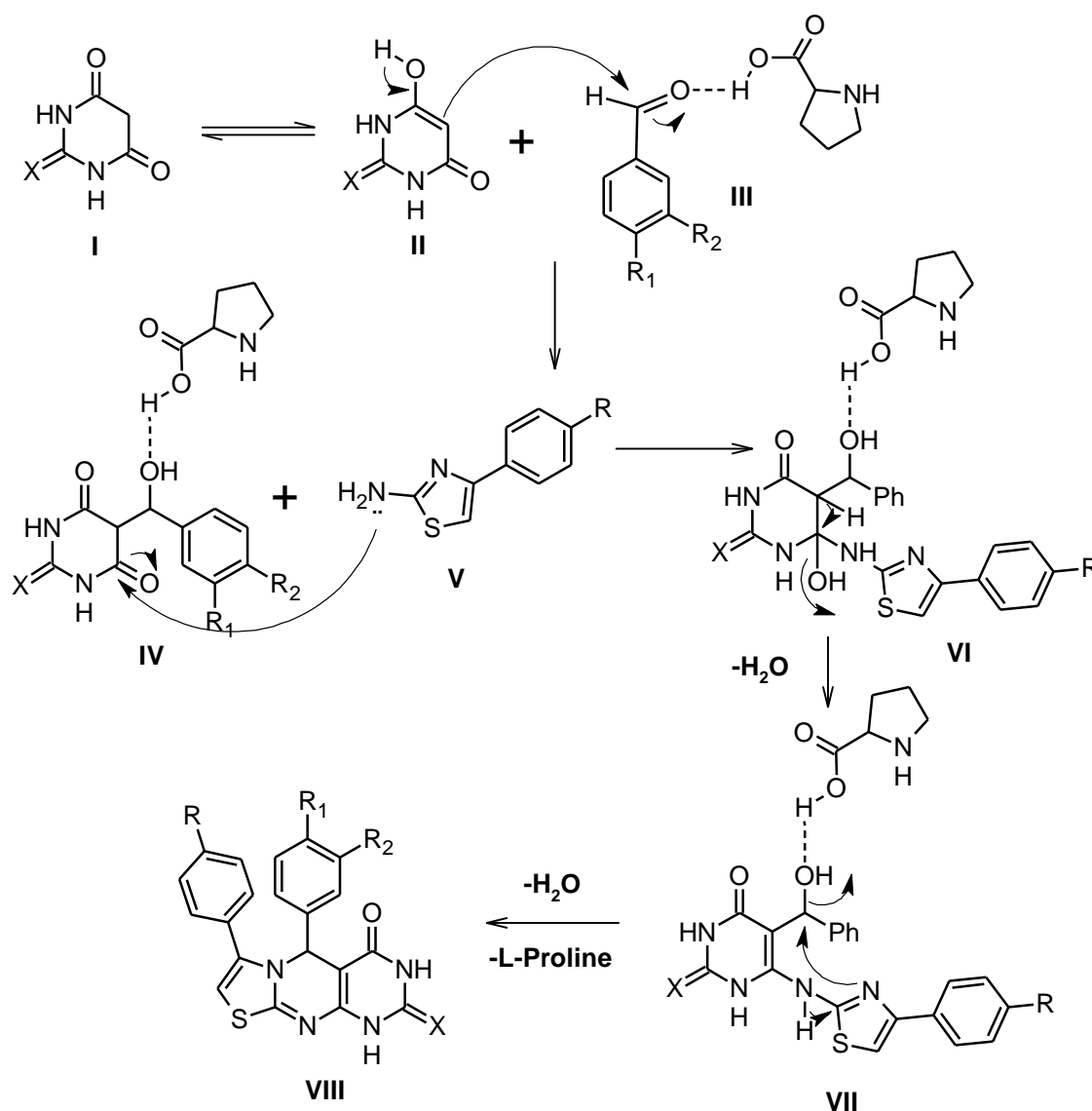


Fig. 2. Plausible mechanism of synthesized compounds **4(a-g)**.

Firstly, we studied the effect of catalyst on the reaction. In the previous reports, this method was carried out in the presence of different catalysts such as HCl, TBAHS, $Zn(ClO_4)_2 \cdot 6H_2O$, TMGT, $InCl_3$, *p*-TSA, ZnO NPs and also in the absence of catalyst (**Table 1**). Further, we screened different conditions to find the influence of catalyst on progress of the reaction as well as on the increase of product yield by using different mol % of L-Proline i.e., 5, 10, 15 and 20 mol % was examined on the compound **4a**. The best result was obtained in the presence of 10 mol %, whereas a further increase in the quantity of catalyst does not have any significant effect on the reaction kinetics (**Table 2**).

Table 1. Effect of different catalysts on synthesized compound **4a**.

Entry	Catalyst	Solvent	Temperature (°C)	Time (hours)	Yield (%)
1	L-Proline	EtOH: H₂O	Reflux	5	90
2	HCl	EtOH	Reflux	8	90 ^[32]
3	TBAHS	EtOH: H ₂ O	Reflux	3	84 ^[30]
4	-	EtOH: acetic acid	Reflux	8	89 ^[31]
5	Zn(ClO ₄) ₂ . 6H ₂ O	MeOH	Reflux	8	78 ^[37]
6	TMGT	Ionic liquid	Reflux	5	77 ^[38]
7	InCl ₃	EtOH/H ₂ O	Reflux	1	87 ^[39]
8	p-TSA	Solvent-free	Reflux	4	95 ^[33]
9	ZnO NPs	Ball milling	RT	40 min	82 ^[40]

Table 2. Effect of mol % of L-Proline catalyst on synthesized compound **4a**.

Entry	Catalyst	Mol (%)	Time	Yield (%)
1	-	-	10 h	60
2	L-Proline	5	9 h	76
3	L-Proline	10	5 h	90
4	L-Proline	15	5 h	90
5	L-Proline	20	5 h	88

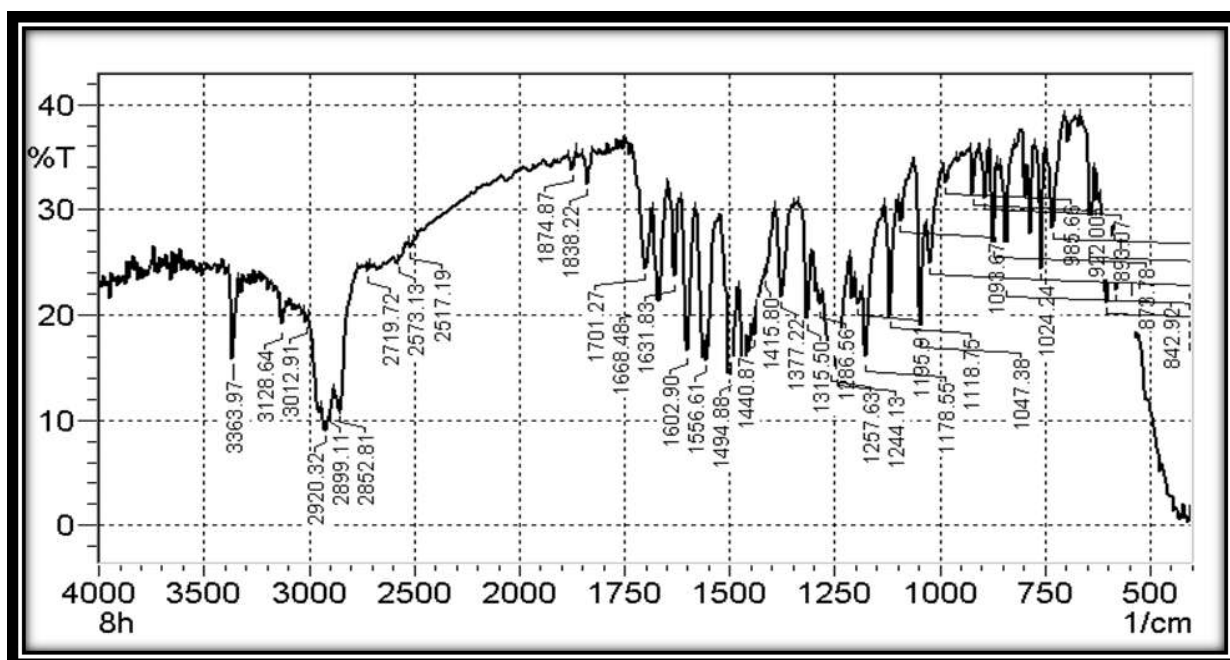
The structures of newly (4-substituted-phenyl)-1,5-dihydro-2*H*-pyrimido[4,5-*d*][1,3]thiazolo[3,2*a*]-pyrimidine-2,4(3*H*)-dione derivatives **4(a-g)** were confirmed by recording their IR, ¹H NMR, ¹³C NMR, and Mass spectral data.

IR spectrum of compound **4a** showed the absorption band in the region of 3363 cm⁻¹ that can be attributed to the amide stretching vibration, 2920 cm⁻¹ correspond to methoxy group (OCH₃), and the absorption band at 1668 cm⁻¹ correspond to stretching vibration of the carbonyl group (C=O). Another stretching vibrational band at 1602 cm⁻¹ correspond to the C=N bond. The ¹H NMR spectrum of compound **4a** exhibited two singlet peaks at δ 9.99 and 9.01 ppm, which corresponds to two NH protons of pyrimidine nucleus (s, 2H, NH) and another doublet peak at δ 7.98 ppm (d, *J* = 8 Hz, 1H, Ar-H) correspond to aromatic proton. Singlet peak at δ 7.87 ppm correspond to the CH proton of the thiazole core (s, 1H, Ar-CH). Multiplet peak was observed in the range of δ 7.55-7.36 ppm corresponds to five aromatic

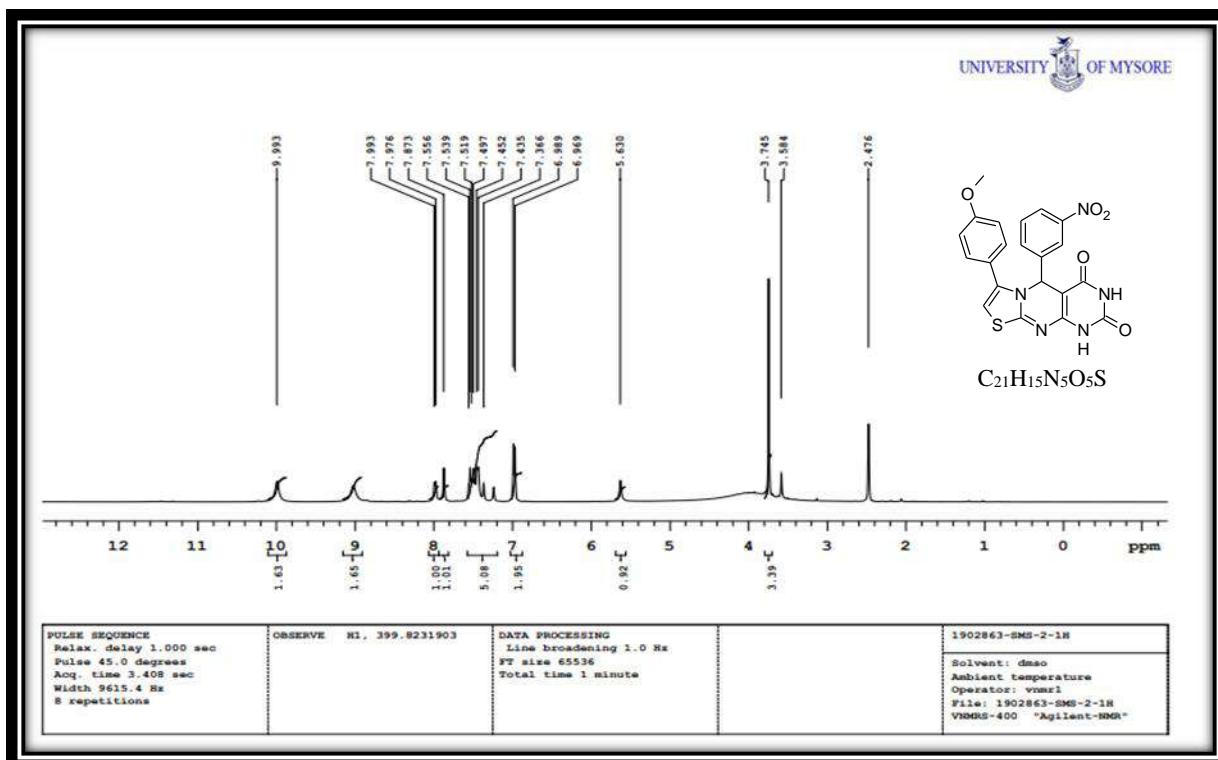
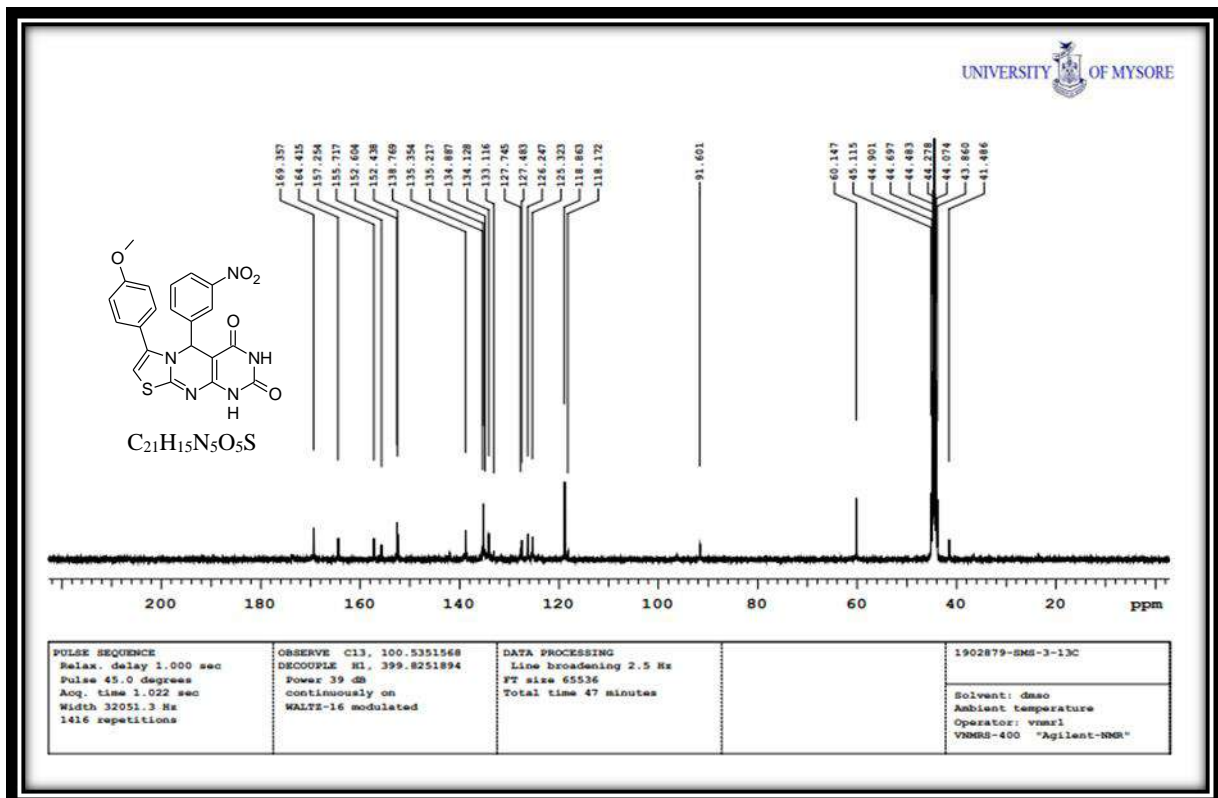
protons (m, 5H, Ar-H) and a doublet peak appeared in the range of δ 6.98-6.96 ppm is due to two aromatic protons (d, $J=8$ Hz, 2H, Ar-H). A singlet peak at δ 5.63 ppm due to CH proton (s, 1H, CH) and another singlet that appeared at δ 3.74 ppm correspond to methoxy protons (s, 3H, OCH₃). In addition, the ¹³C NMR spectrum of compound **4a** exhibited a peak at δ 169.35 and 164.41 ppm, which correspond to carbonyl carbons and peaks at δ 60.14 ppm due to methoxy carbon.

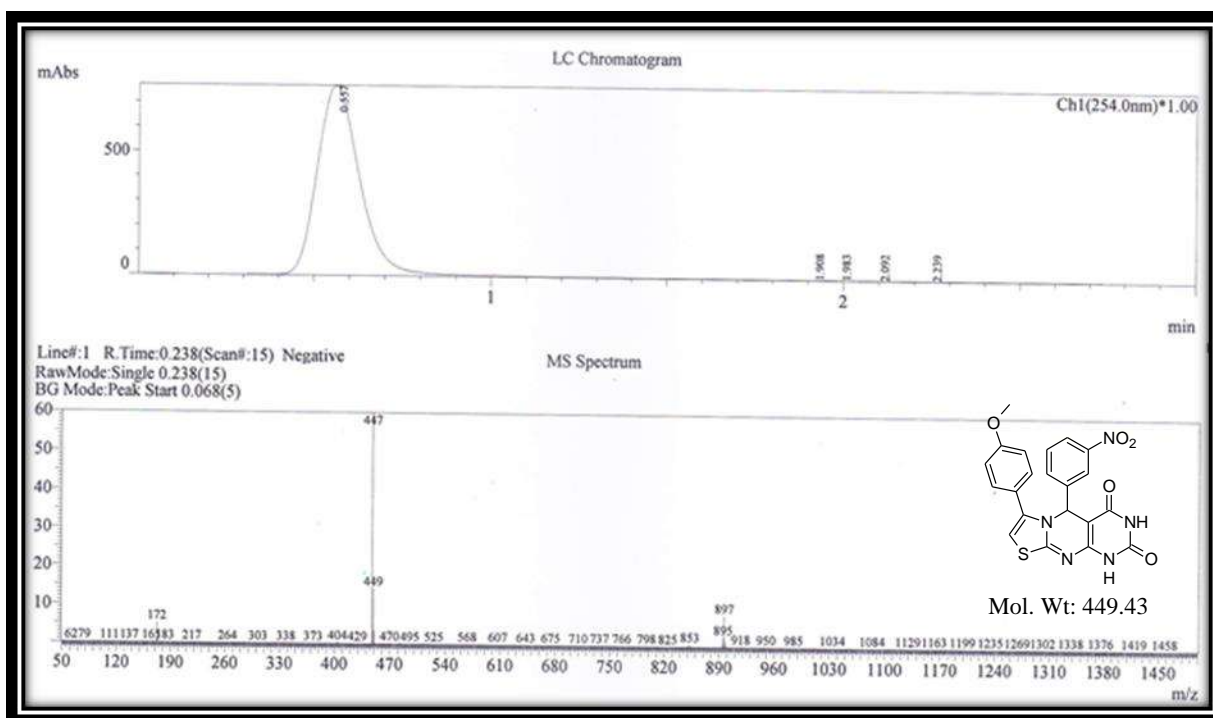
The mass spectrum showed a molecular ion peak m/z at 449 [M⁺], which corresponds to the molecular weight of the compound **4a**.

Characterization:

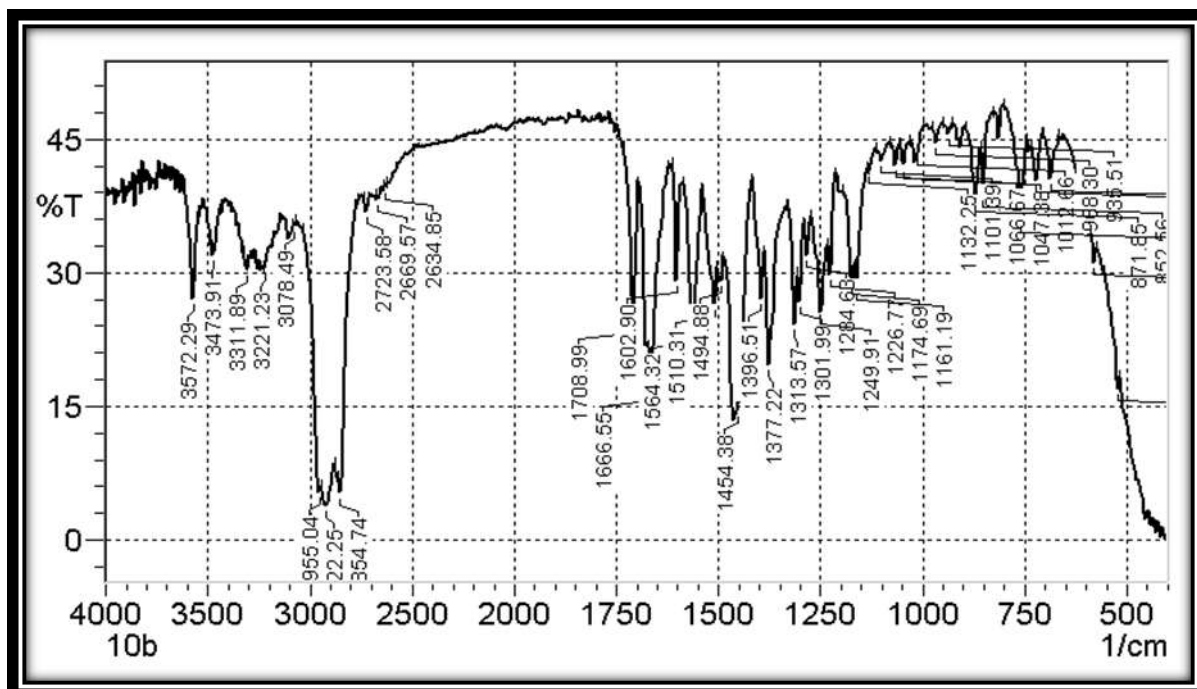


IR spectrum of compound **4a**

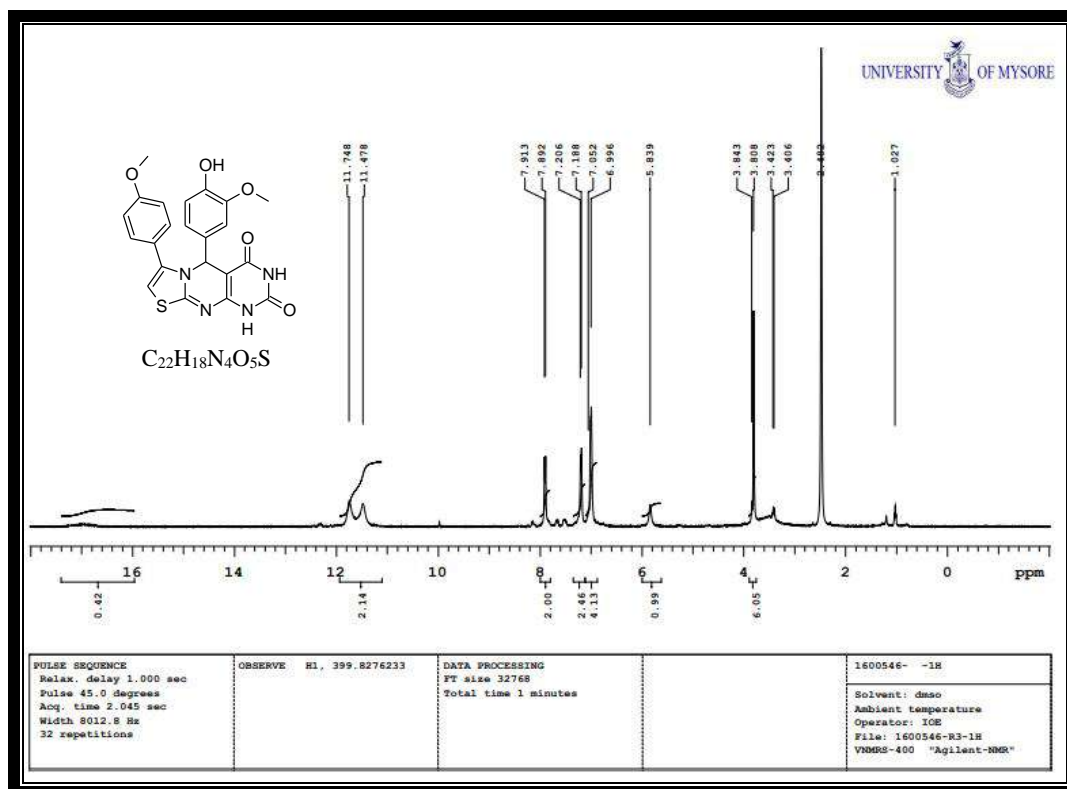
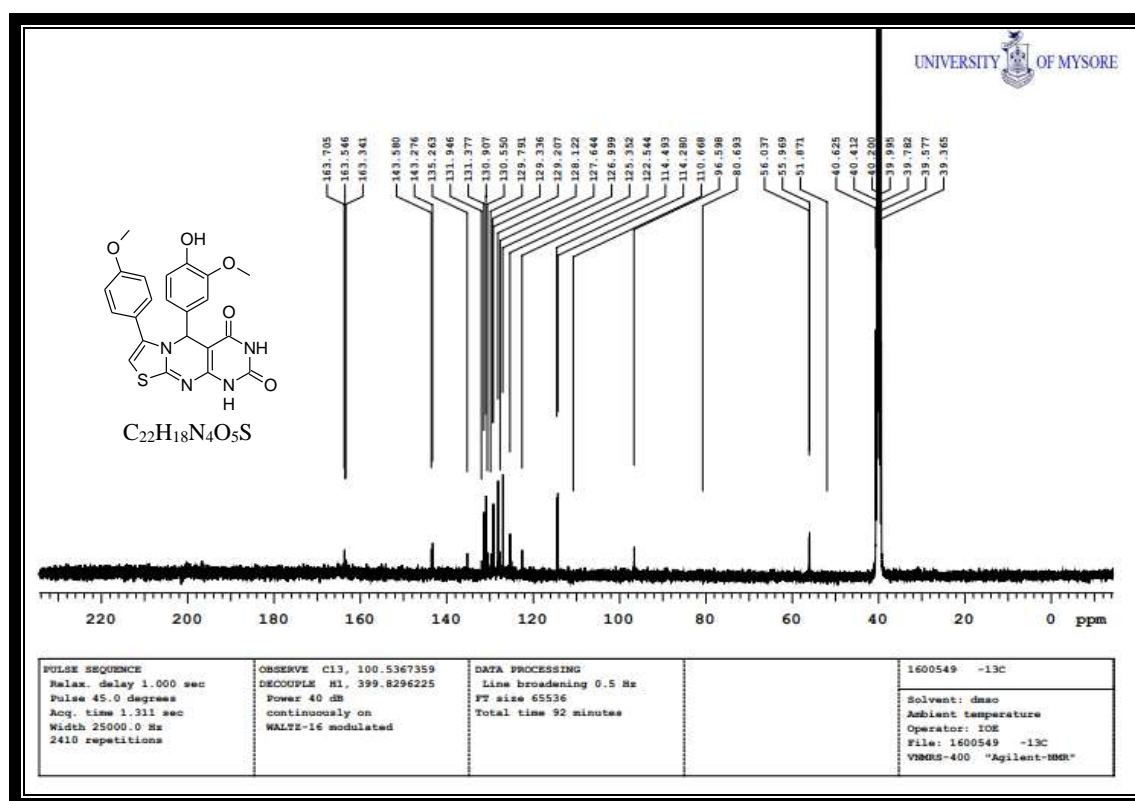
¹H NMR spectrum of compound 4a¹³C NMR spectrum of compound 4a

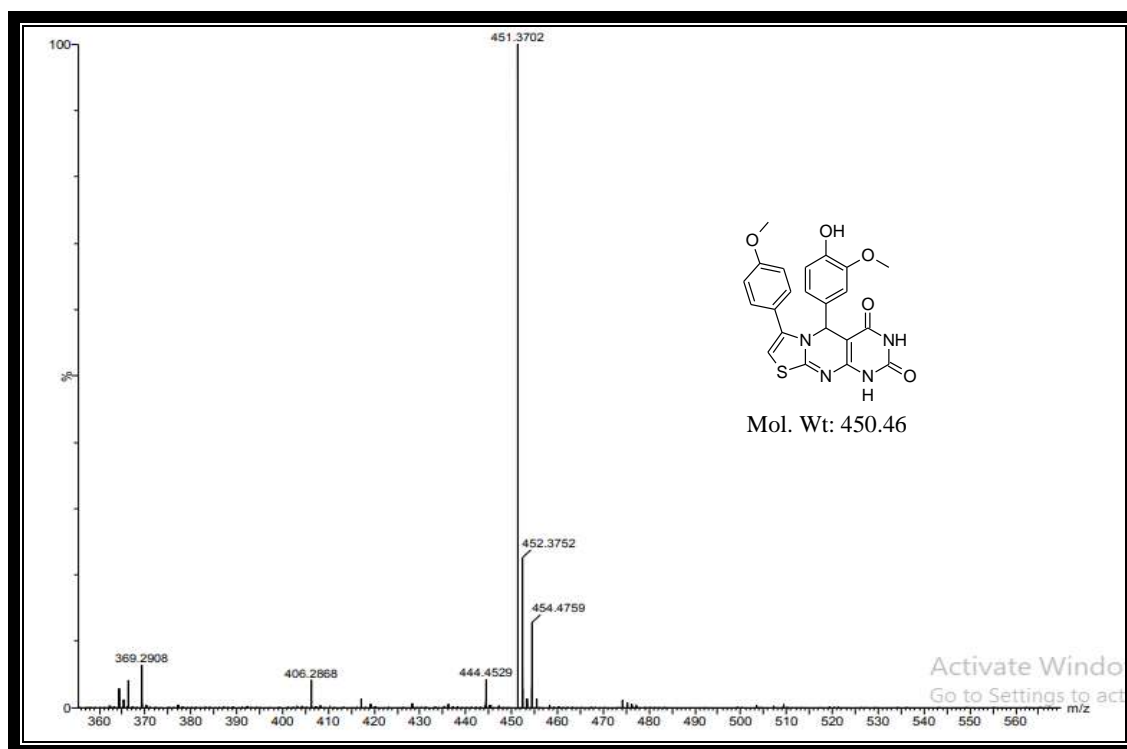


MASS spectrum of compound 4a



IR spectrum of compound 4c

¹H NMR spectrum of compound 4c¹³C NMR spectrum of compound 4c



MASS spectrum of compound 4c

3.3. Experimental

3.3.1. General information:

The general information regarding the different solvents, reagents and instruments etc., used for the analysis has been discussed detailed in the experimental section (2A.3.1) of **Chapter-2A**.

3.3.2. General procedure for the synthesis of (4-substituted-phenyl)-1,5-dihydro-2H-pyrimido[4,5-*d*][1,3]thiazolo[3,2*a*]-pyrimidine-2,4(3*H*)-dione derivatives 4(a-g):

An equimolar quantity of 2-amino-4-(4-substituted-phenyl)thiazoles (**1a/b**, 1 mmol), substituted benzaldehyde (**2**, 1 mmol), and barbituric/thiobarbituric acid (**3**, 1 mmol) in the presence of aqueous ethanol using 10 mol % of L-Proline as a catalyst and refluxed with constant stirring for about 4-5 hours. Simultaneously, the reaction was monitored by TLC (Ethyl acetate & petroleum ether). After completion of the reaction, the reaction mixture was cooled to room temperature and poured into the 100 mL flake ice with vigorous stirring to get

solid precipitate. Then, it was filtered, washed, recrystallized from absolute ethanol, and dried to afford pure solid products (**4a-g**).

7-(4-Methoxyphenyl)-5-(3-nitrophenyl)-1,5-dihydro-2H-pyrimido[4,5-d][1,3]

thiazolo[3,2-a]pyrimidine-2,4(3H)-dione (4a):

Yellow solid; Yield: 82 %; MP: 290-292 °C; Mol. Formula: C₂₁H₁₅N₅O₅S; FTIR (ν cm⁻¹): 3363 (NH), 2920 (OCH₃), 1668 (C=O) & 1602 (C=N); ¹H NMR (δ ppm): 9.99 (s, 1H, NH), 9.01 (s, 1H, NH), 7.99-7.97 (d, *J* = 8 Hz, 1H, Ar-H), 7.87 (s, 1H, CH), 7.55-7.36 (m, 5H, Ar-H), 6.98-6.96 (d, *J* = 8 Hz, 2H, Ar-H), 5.63 (s, 1H, CH), 3.74 (s, 3H, OCH₃); ¹³C NMR (δ ppm): 169.35, 164.41, 157.25, 155.71, 152.60, 152.43, 138.76, 135.35, 135.21, 134.88, 134.12, 133.11, 127.74, 127.48, 126.24, 125.32, 118.86, 118.17, 91.60 & 60.14; LCMS: *m/z* 449 [M⁺]; Anal. Calcd: C 56.12, H 3.36, N 15.58 %, Found: C 56.05, H 3.12, N 15.47 %.

5-(4-Hydroxyphenyl)-7-(4-methoxyphenyl)-1,5-dihydro-2H-pyrimido[4,5-d][1,3]

thiazolo[3,2-a]pyrimidine-2,4(3H)-dione (4b):

Yellow solid; Yield: 80 %; MP: 295-298 °C; Mol. Formula: C₂₁H₁₆N₄O₄S; FTIR (ν cm⁻¹): 3452 (OH), 3273 (NH), 2955 (OCH₃), 1678 (C=O) & 1597 (C=N); ¹H NMR (δ ppm): 12.00 (s, 1H, OH), 11.28 (s, 1H, NH), 11.16 (s, 1H, NH), 8.27 (s, 1H, Ar-H), 7.85-7.83 (d, *J*=8 Hz, 1H, Ar-H), 7.31-7.29 (t, *J* = 8 Hz, 1H, Ar-H), 7.23-6.99 (m, 3H, Ar-H), 6.86 (s, 1H, Ar-H), 6.68-6.66 (d, *J* = 8 Hz, 2H, Ar-H), 5.36 (s, 1H, CH), 3.78 (s, 3H, OCH₃); ¹³C NMR (δ ppm): 163.61, 160.47, 158.79, 154.60, 154.18, 152.06, 149.60, 135.14, 134.28, 133.97, 133.07, 132.96, 131.48, 130.70, 129.42, 121.40, 118.80, 93.11 & 60.11; LCMS: *m/z* 422 [M⁺+2]; Anal. Calcd: C 59.99, H 3.84, N 13.33 %, Found: C 59.93, H 3.82, N 13.28 %.

5-(4-Hydroxy-3-methoxyphenyl)-7-(4-methoxyphenyl)-1,5-dihydro-2H-pyrimido[4,5-d][1,3]thiazolo[3,2-a]pyrimidine-2,4(3H)-dione (4c):

Yellow solid; Yield: 81 %; MP: 267-270 °C; Mol. Formula: C₂₂H₁₈N₄O₅S; FTIR (ν cm⁻¹): 3473 (OH), 3221 (NH), 2922 (OCH₃), 1666 (C=O) & 1602 (C=N); ¹H NMR (δ ppm):

12.13 (s, 1H, OH), 11.74 (s, 1H, NH), 11.47 (s, 1H, NH), 7.91-7.89 (d, $J=8$ Hz, 2H, Ar-H), 7.20-7.18 (d, $J=8$ Hz, 2H, Ar-H), 7.05-6.99 (m, 4H, Ar-H), 5.83 (s, 1H, CH), 3.84 (s, 6H, OCH₃); ¹³C NMR (δ ppm): 163.70, 163.34, 143.58, 143.27, 135.26, 131.94, 131.37, 130.55, 129.79, 129.20, 128.12, 127.64, 126.99, 125.35, 122.54, 114.49, 114.28, 110.66, 96.59, 80.69, 56.03 & 55.96; HRMS: m/z 451.3702 [M^++1]; Anal. Calcd: C 58.66, H 4.03, N 12.44 %, Found: C 58.63, H 3.98, N 12.38 %.

5-(4-N-dimethylphenyl)-7-(4-methoxyphenyl)-1,5-dihydro-2H-pyrimido[4,5-d][1,3]thiazolo[3,2-a]pyrimidine-2,4(3H)-dione (4d):

Orange red solid; Yield: 79 %; MP: 275-278 °C; Mol. Formula: C₂₃H₂₁N₅O₃S; FTIR (ν cm⁻¹): 3322 (NH), 2832 (CH₃), 1673 (C=O) & 1598 (C=N); ¹H NMR (δ ppm): 11.32 (s, 1H, NH), 11.20 (s, 1H, NH), 8.26 (s, 1H, Ar-H), 7.85-7.83 (d, $J=8$ Hz, 1H, Ar-H), 7.34-7.32 (t, $J=8$ Hz, 1H, Ar-H), 7.29-7.03 (m, 3H, Ar-H), 6.89 (s, 1H, Ar-H), 6.68-6.66 (d, $J=8$ Hz, 2H, Ar-H), 5.43 (s, 1H, CH), 3.78 (s, 3H, OCH₃), 2.43 (s, 6H, CH₃); ¹³C NMR (δ ppm): 163.61, 160.47, 158.87, 155.62, 154.03, 151.98, 149.24, 135.94, 134.19, 133.68, 133.08, 132.35, 131.28, 130.60, 130.01, 129.63, 128.40, 122.18, 117.20, 96.24, 56.18 & 22.01; HRMS: m/z 449 [M^++2]; Anal. Calcd for: C 61.78, H 4.73, N 15.65 %, Found: C 61.71, H 4.68, N 15.58 %.

5,7-Bis(4-methoxyphenyl)-1,5-dihydro-2H-pyrimido[4,5-d][1,3]thiazolo[3,2a]pyrimidine-2,4(3H)-dione (4e):

Light yellow solid; Yield: 81 %; MP: 285-290 °C; Mol. Formula: C₂₂H₁₈N₄O₅S; FTIR (ν cm⁻¹): 3228 (NH), 2962 (OCH₃), 1666 (C=O) & 1592 (C=N); ¹H NMR (δ ppm): 11.34 (s, 1H, NH), 11.23 (s, 1H, NH), 8.28 (s, 1H, Ar-H), 7.85-7.83 (d, $J=8$ Hz, 1H, Ar-H), 7.33-7.31 (t, $J=8$ Hz, 1H, Ar-H), 7.28-7.00 (m, 3H, Ar-H), 6.88 (s, 1H, Ar-H), 6.70-6.68 (d, $J=8$ Hz, 2H, Ar-H), 5.39 (s, 1H, CH), 3.84 (s, 6H, OCH₃); ¹³C NMR (δ ppm): 162.32, 160.43, 158.68, 155.12, 154.23, 150.03, 149.01, 136.12, 135.16, 134.08, 133.89, 133.34, 132.08, 130.21,

129.08, 128.32, 121.21, 118.12, 94.23, 59.45 & 56.78; HRMS: m/z 436 $[M^+ + 2]$; Anal. Calcd: C 60.82, H 4.18, N 12.90 %, Found: C 60.79, H 4.13, N 12.88 %.

5-(4-Hydroxyphenyl)-7-(4-nitrophenyl)-2-thioxo-1,2,3,5-tetrahydro-4H-pyrimido[4,5-d][1,3]thiazolo[3,2-a]pyrimidin-4-one (4f):

Yellow solid; Yield: 81 %; MP: 280-284 °C; Mol. Formula: $C_{20}H_{13}N_5O_4S_2$; FTIR (ν cm^{-1}): 3471 (OH), 3294 (NH), 1666 (C=O) & 1591 (C=N); 1H NMR (δ ppm): 12.32 (s, 1H, NH), 12.23 (s, 1H, NH), 11.50 (s, 1H, OH), 8.72 (s, 1H, Ar-H), 8.22-8.18 (t, 2H, Ar-H), 7.84-7.82 (d, $J=8$ Hz, 2H, Ar-H), 7.87 (s, 1H, Ar-H), 6.82-6.80 (d, $J=8$ Hz, 1H, Ar-H), 6.54-6.52 (d, $J=8$ Hz, 2H, Ar-H), 5.46 (s, 1H, CH); ^{13}C NMR (δ ppm): 173.06, 169.57, 163.77, 162.57, 155.84, 155.08, 147.92, 146.69, 132.74, 130.91, 128.86, 128.31, 127.86, 126.91, 124.59, 116.37, 115.21, 107.30 & 96.72; HRMS: m/z 452.3012 $[M+1]^+$; Anal. Calcd: C 53.21, H 2.90, N 15.51 %, Found: C 53.17, H 2.87, N 15.47 %.

5-(4-Chloro-3-nitrophenyl)-7-(4-nitrophenyl)-2-thioxo-1,2,3,5-tetrahydro-4H-pyrimido[4,5-d][1,3]thiazolo[3,2-a]pyrimidin-4-one (4g):

Yellow solid; Yield: 79 %; MP: 304-308 °C; Mol. Formula: $C_{20}H_{11}ClN_6O_5S_2$; FTIR (ν cm^{-1}): 3284 (NH), 1666 (C=O) & 1608 (C=N); 1H NMR (δ ppm): 10.89 (s, 2H, NH), 8.26-8.18 (m, 2H, Ar-H), 8.00-7.98 (d, $J=8$ Hz, 1H, Ar-H), 7.87-7.85 (d, $J=8$ Hz, 1H, Ar-H), 7.65 (s, 1H, Ar-H), 7.53-7.51 (d, $J=8$ Hz, 1H, Ar-H), 7.34-7.32 (d, $J=8$ Hz, 2H, Ar-H), 5.57 (s, 1H, CH); ^{13}C NMR (δ ppm): 174.38, 169.75, 169.19, 162.64, 148.02, 147.86, 146.48, 144.98, 141.08, 132.60, 131.37, 131.09, 126.82, 125.32, 124.55, 124.20, 123.86, 122.37, 107.18 & 90.57; HRMS: m/z 513.1334 $[M^+ - 1]$ and 511.1325 $[M^+ - 2]$; Anal. Calcd: C 46.65, H 2.15, N 16.32 %, Found: C 46.60, H 2.11, N 16.28 %.

3.4. Pharmacological studies

3.4.1. *In vitro* cytotoxicity

In vitro cytotoxicity was evaluated by MTT assay method and followed by according to the procedure Kumbar *et. al.*, [41] against MCF-7 (Human breast cancer) cell line and detailed procedure has been explained in the experimental section 2B.5.2 of **Chapter-2B**. Compounds at six different concentrations (200, 100, 50, 25, 12.5 & 6.25 µg/mL) were used for the analysis. Paclitaxel (PTX) was used as standard drug for comparison.

3.4.2. Anti-inflammatory activity

The anti-inflammatory activity of the synthesized compounds was investigated by the Gelatin Zymography electrophoresis method [42]. 50 µL of matrix metalloproteinase (MMP) sample was mixed with 50 µL of the synthesized compounds and incubated for 1 hour at RT. MMP sample with Tetracycline hydrochloride served as positive control while MMP sample alone served as a negative control. After incubation, an equal quantity of non-reducing buffer was added to the above samples, mixed well, and 30 µL of each sample was loaded into the gel. The electrophoresis was run at 50 V for 15 min and later increased to 100 V until the bromophenol blue reaches the bottom of the plate. After electrophoresis, the gel was washed with SDS (sodium dodecyl sulfate) surfactant followed by zymogram renaturing buffer for 1 hour to remove the remaining surfactant from the gel and allowed the gel for renaturing of the proteins. The gel was further incubated in zymogram incubation buffer overnight at 37 °C. Finally, the gel was stained with Coomassie blue R-250, and the development of white bands indicated the presence of gelatinases with the lower bands representing gelatinases-A (MMP-2) which are about 72 kD, while the upper bands are gelatinases-B (MMP-9) which are about 95 kD [43].

3.4.3. *in silico* molecular docking studies

Automated docking was used to study the interactions of synthesized compounds at the binding pocket of the target proteins. The mode of cell death can be studied by considering necrosis, apoptosis, necroptosis, autophagic cell death, etc. The inhibition of P38 MAP kinase is likely to affect cellular proliferation accounting for cell toxicity [44, 45]. This can be used as a test for mitochondrial respiration indirectly connected by cellular toxicity [46]. Similarly, Matrix metalloproteinases (MMPs) play important roles in the interaction between inflammatory cells [47] and MMP-9, specifically involved in several cancers associated with inflammation [48]. Inhibitors of metalloproteinase (TIMP) can be used to control the elevated expression of MMP-9 to control pathological conditions such as cancer and inflammation [49]. In the present study, the molecular interactions of the synthesized compounds at the binding pocket of P38 MAP kinase and MMP-9 targets [50] were studied using automated docking by employing the Autodock Vina program [51]. The co-crystallized structure of P38 MAP kinase (PDB ID: 1OUK) and MMP-9 (PDB ID: 5CUH) were retrieved from the protein databank, and their substrate binding sites were identified using pdbsum server [52]. A grid box of dimensions 56 x 60 x 48 Å with X, Y & Z coordinates at 44.746, 34.234 and 32.603 for P38 MAPk and 44 x 52 x 48 Å with X, Y & Z coordinates at 15.463, 23.591 and -1.658 for MMP-9 were created respectively. All the torsions were allowed to rotate for synthesized compounds during docking. The grid box was set around the residues forming the active pocket. The binding interactions were visualized using Biovia Discovery Studio Visualizer V.20.1.

3.4.4. *in silico* oral bioavailability assessment and ADME-toxicology studies

The oral bioavailability of the synthetic molecules **4(a-g)** was predicted using the Lipinski rule-of-five (RO5) filter [53] to derive the candidate drug's pharmacokinetic (PK) and pharmacodynamics (PD) [54]. The structural properties used in the RO5 filter are derived

using Osiris Data warrior V.4.4.3 software [55]. Different parameters describing the pharmacodynamics and pharmacokinetic properties were assessed using the admetSAR server [56]. The bioavailability scores were predicted using the molinspiration server [57].

3.5. Results and discussion

3.5.1. Cytotoxicity study

The *in vitro* cytotoxicity of the synthesized compounds **4(a-g)** was evaluated against MCF-7 (Breast cancer) cell line (**Fig. 3**). A graph detailing the concentration versus survival fraction of the compounds was plotted (**Fig. 4**), and the results were expressed as the half-maximal inhibitory concentrations (IC_{50}). Paclitaxel used as a reference standard showed an IC_{50} value of $298.86 \pm 6.35 \mu\text{g/mL}$ (**Table 3**).

The cytotoxicity results suggested that, the tested compounds have a very good selectivity against the MCF-7 cell line compared to the reference standard and compounds **4f** & **4g** possessed significant IC_{50} values of 1.15 ± 0.49 & $8.55 \pm 2.05 \mu\text{g/mL}$ respectively. The remaining compounds also displayed reliable selectivity with an IC_{50} value in the range of 18.90 ± 0.69 to $115.00 \pm 1.27 \mu\text{g/mL}$ compared to reference standard Paclitaxel. The compounds **4f** & **4g** demonstrated highly promising cell viability at $6.25 \mu\text{g/mL}$ concentration. The presence of electron-withdrawing nitro and chloro groups on the phenyl ring was supposed to be the reason for the superior activity profile of the compounds [58].

Table 3. % of cell viability against MCF-7 cell line of synthesized compounds **4(a-g)**.

Compd.	Mean cell Viability of MCF-7 Concentration in $\mu\text{g/mL}$							IC_{50} in $\mu\text{g/mL}$
	NC	6.25	12.5	25	50	100	200	
4a	100	96.57 ± 0.66	93.15 ± 1.21	92.37 ± 1.54	73.21 ± 1.44	45.79 ± 1.55	23.21 ± 0.99	93.68 ± 1.20
4b		99.22 ± 1.10	90.03 ± 1.21	76.79 ± 2.09	70.56 ± 0.55	47.82 ± 0.66	27.88 ± 1.44	93.60 ± 2.37
4c		90.65 ± 1.22	89.72 ± 0.88	82.24 ± 0.66	80.84 ± 0.77	53.89 ± 1.87	31.62 ± 1.10	115.00 ± 1.27
4d		76.95 ± 0.88	64.17 ± 1.87	29.44 ± 1.10	26.79 ± 1.65	23.83 ± 0.55	19.00 ± 0.44	18.90 ± 0.69
4e		93.77 ± 0.55	73.05 ± 2.21	62.46 ± 1.32	49.53 ± 1.10	40.81 ± 1.54	29.60 ± 1.32	57.63 ± 1.47
4f		40.72 ± 2.58	23.98 ± 0.64	22.17 ± 0.96	20.48 ± 0.47	19.68 ± 0.64	19.00 ± 0.64	1.15 ± 0.49
4g		64.03 ± 0.96	44.00 ± 1.44	40.84 ± 1.44	38.35 ± 0.80	36.99 ± 0.48	34.50 ± 1.12	8.55 ± 2.05
Std		-	-	-	-	-	-	-

Std- Paclitaxel (PTX), **NC-** Negative control

Values are Mean \pm SE, N=3, *P<0.01 vs. Control

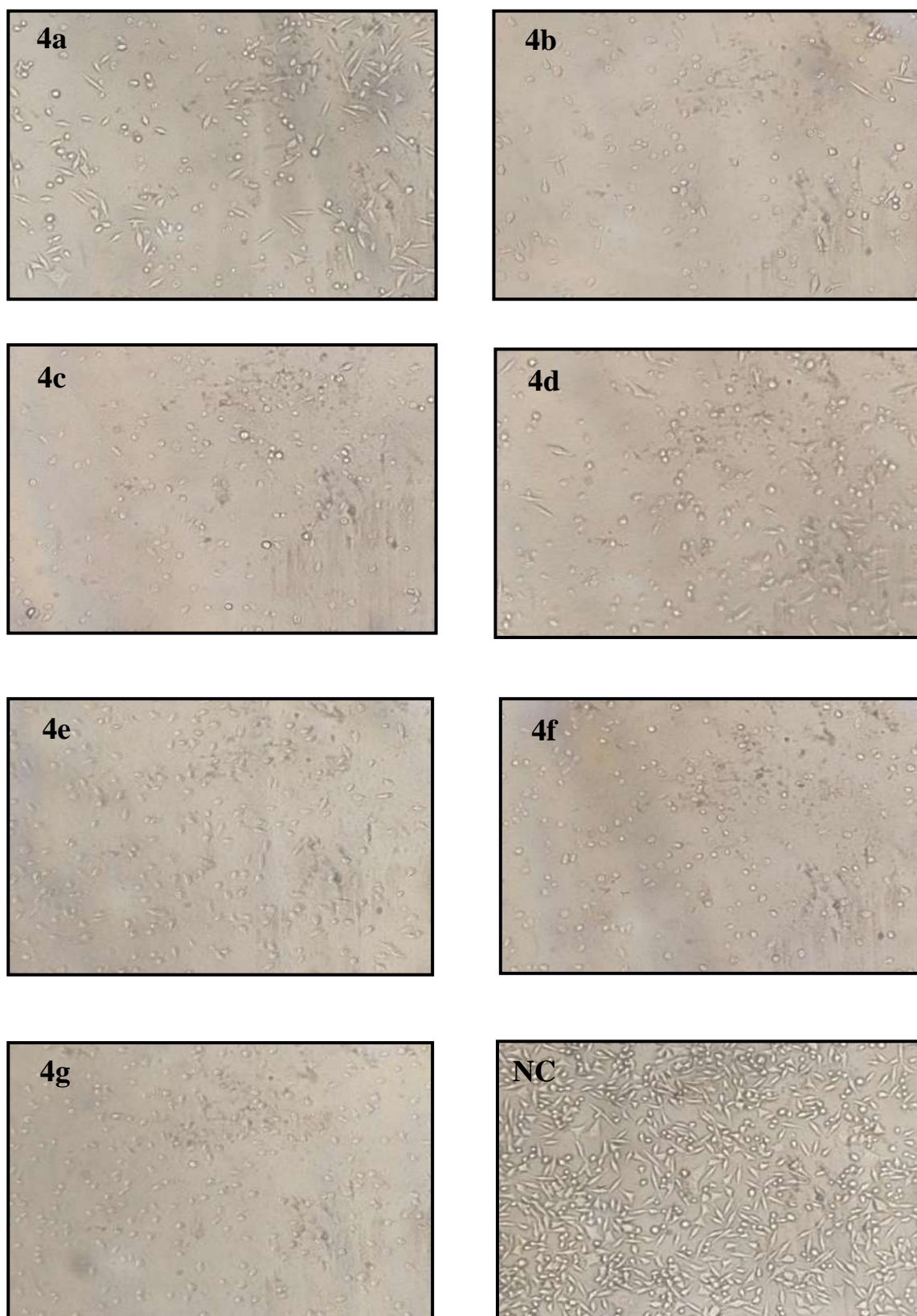


Fig. 3. Images of anticancer study of the synthesized compounds **4(a-g)** and **NC**.

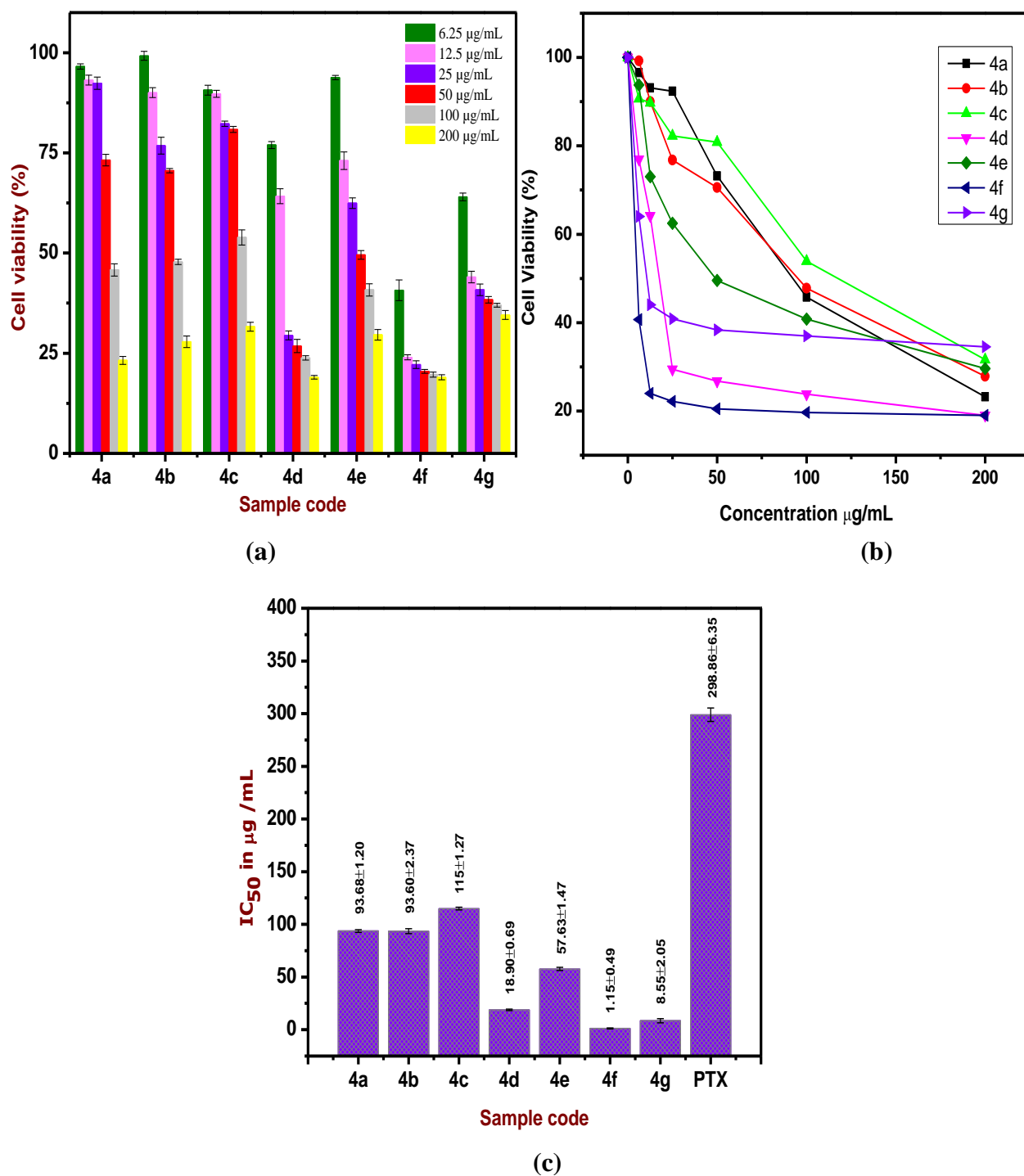


Fig. 4. A graph of % of survival cells of compounds **4(a-g)** at different concentration (**a** & **b**), A graph of IC₅₀ value of compounds **4(a-g)** against MCF-7 cell line (**c**).

3.5.2. Anti-inflammatory activity

Gelatin zymography is the most sensitive and widely used assay for detecting the percentage inhibition of compounds against two enzymes MMP-2 and MMP-9 (Fig. 5 & 6). The anti-inflammatory activity results revealed that, compounds **4a** & **4g** exhibited a noticeable activity in terms of % inhibition when compared to other compounds. Compounds **4a** & **4g** displayed encouraging anti-inflammatory activity against matrix metalloproteinase-2 (MMP-2) with % inhibition value of 90 ± 0.41 & 85 ± 0.34 and moderate anti-inflammatory activity against matrix metalloproteinase-9 (MMP-9) with % inhibition value of 45 ± 0.38 & 35 ± 0.54 as compared to positive control (99 ± 0.51 & 95 ± 0.35 %), (Table 4) respectively. The probable reason behind the anti-inflammatory effects displayed by the synthesized molecules **4a** and **4g** may be due to the presence of electron-withdrawing nitro groups in their ring structures [59].

Table 4. Anti-inflammatory activity results of synthesized compounds **4(a-g)**.

Entry	Compound	Anti-inflammatory activity against MMP-2 (% Inhibition)	Anti-inflammatory activity against MMP-9 (% Inhibition)
1	4a	90 ± 0.41	45 ± 0.38
2	4b	50 ± 0.48	5 ± 0.25
3	4c	37 ± 0.37	5 ± 0.41
4	4d	33 ± 0.38	5 ± 0.42
5	4e	45 ± 0.36	22 ± 0.47
6	4f	78 ± 0.32	20 ± 0.61
7	4g	85 ± 0.34	35 ± 0.54
8	PC	99 ± 0.51	95 ± 0.35
9	NC	-	-

PC-Positive control, NC-Negative control

Values are Mean \pm SE, N=3, *P<0.01 vs. Control

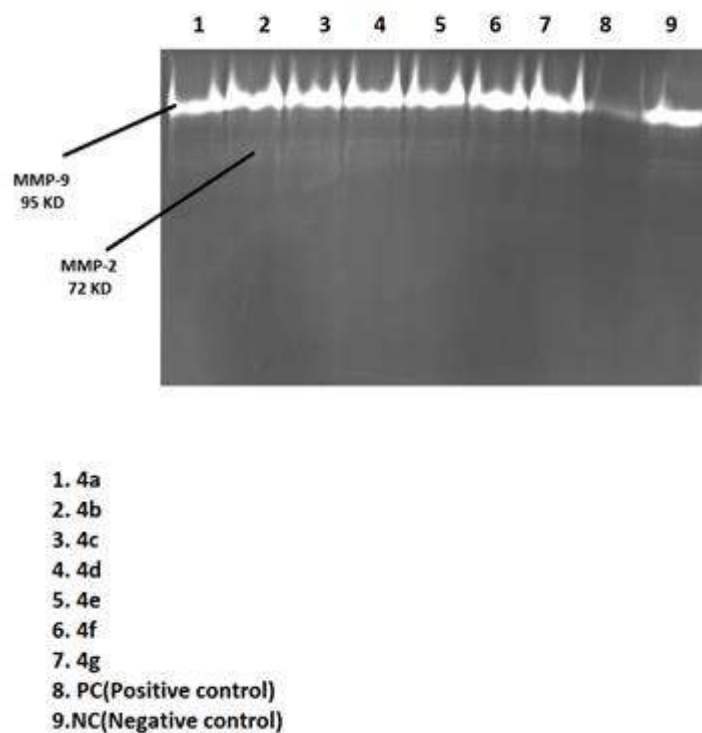


Fig. 5. Electrophoresis bands for anti-inflammatory activity of compounds 4(a-g).

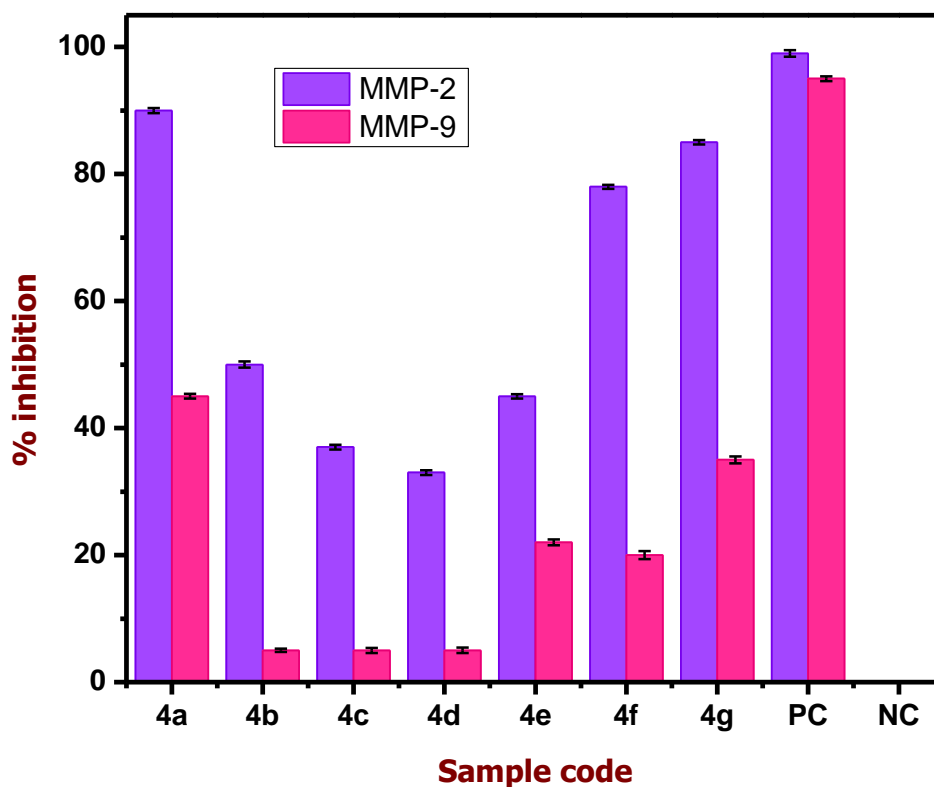


Fig. 6. A graph of % inhibition effect of anti-inflammatory activity of compounds 4(a-g).

3.5.3. SAR study

The SAR study has been carefully carried out for the newly synthesized compounds **4(a-g)**. All the newly synthesized compounds exhibited remarkable anticancer activity as compared to the reference standard Paclitaxel. Among the tested compounds, **4f** and **4g** displayed prominent IC₅₀ values and promising cell viability at 6.25 µg/mL concentration due to presence of electron-withdrawing nitro and chloro groups is presumed to be the main reason for the superior activity profile of these compounds [58]. However, the combined effect of the electron-donating hydroxyl group and the electron-withdrawing nitro group could be the possible reason for the superior potency of the **4f** compound.

The anti-inflammatory activity against MMP-2 and MMP-9 revealed the vital presence of electron-withdrawing groups for superior potency [59]. The compounds **4a** and **4g** demonstrated a prominent anti-inflammatory effect due to the presence of EW nitro group in the phenyl ring as compared with other molecules. The electron-withdrawing functionalities are known to increase lipophilicity, which enhances the cell-permeability of the synthesized compounds. This could be the possible reason for the improved activity profile of these compounds [60].

3.5.4. *in silico* molecular docking study

Molecular interactions between the synthesized molecules and an appropriate target protein were studied using the *in silico* molecular docking method [61]. The binding interactions were compared with standard drugs and expressed as kcal/mol. In the present study, P38 MAPk was used as a target for synthesized compounds to correlate their anticancer effects. P38 MAPk acts as a measure of mitochondrial respiration, indirectly corresponding to cellular toxicity. By inhibiting P38 MAPk, the effect of inhibitors on cell proliferation can be measured. The preventive mechanisms behind such cancer-preventive effects may range from the inhibition of genotoxic effects, increased antioxidants and anti-inflammatory activity,

inhibition of proteases and cell proliferation, protection of intracellular communications to modulate apoptosis, and signal transduction pathways [62]. Similarly, Matrix metalloproteinases (MMPs) play important roles in the interaction between inflammatory cells. MMP9, along with other MMPs, is expressed in inflammatory cells and is involved in the regulation of inflammation and other tissue responses [63] by deteriorating the extracellular matrix (ECM) proteins and helping in the remodelling of the extracellular matrix. MMP-9 also has a crucial role in several cancers associated with inflammation. An imbalance in the activation and inhibition of MMPs plays a vital role in cancer pathophysiology [64]. Inhibitors of metalloproteinase (TIMP) can be used to control the elevated expression of MMP-9 to control pathological conditions such as cancer and inflammation.

The interactions of P38 MAPk with compound **4f** displayed the least binding energy of -8.7 kcal/mol followed by **4g** (-8.4 kcal/mol) (**Fig. 7**). The compounds **4a**, **4c**, **4b**, **4e** and **4d** have bound with the minimum binding energies of -8.3, -8.3, -8.1, -7.9, and -7.5 kcal/mol with P38 MAPk protein respectively (**Fig. 8**). Similarly, the synthesized compound **4g** has bound to the target protein MMP-9 with a binding energy of -9.3 kcal/mol forming 5 hydrogen bonds. The rest of the synthesized compounds interacted with MMP-9 protein with binding energies ranging from -8.6 to -7.8 kcal/mol. The interaction energies of each molecule with the number of hydrogen bonds formed with different residues of the appropriate target proteins are presented in **Table 5**.

Table 5. *in silico* molecular docking results for anticancer and anti-inflammatory activity of synthesized compounds **4(a-g)** and standard drugs Paclitaxel and Tetracycline.

Anticancer activity				Anti-inflammatory activity			
Compd.	Binding energy in kcal/mol	H-bonds	Residues	Compd.	Binding energy in kcal/mol	H-bonds	Residues
4a	-8.3	04	TYR35, LYS53, MET109, GLU71	4a	-8.6	04	HIS226, HIS230, HIS236, TYR248
4b	-8.1	04	TYR35, LYS53, MET109, ASP168	4b	-7.9	03	HIS226, HIS230, HIS236
4c	-8.3	03	GLY170, ARG189, ASP168	4c	-7.8	02	HIS236, TYR248
4d	-7.5	02	GLY170, ASP168	4d	-7.9	03	HIS226, HIS230, HIS236
4e	-7.9	02	GLY170, ASP168	4e	-8.0	03	HIS226, HIS230, HIS236,
4f	-8.7	03	TYR35, MET109, ASP168	4f	-8.0	01	TYR248
4g	-8.4	03	TYR35, LYS53, MET109	4g	-9.3	05	HIS226, HIS230, HIS236, TYR248, ALA191
Paclitaxel	-8.0	03	TYR35, LYS53, ASP168	Tetracycline	-7.3	04	TYR251, LEU256, PRO254, PRO255

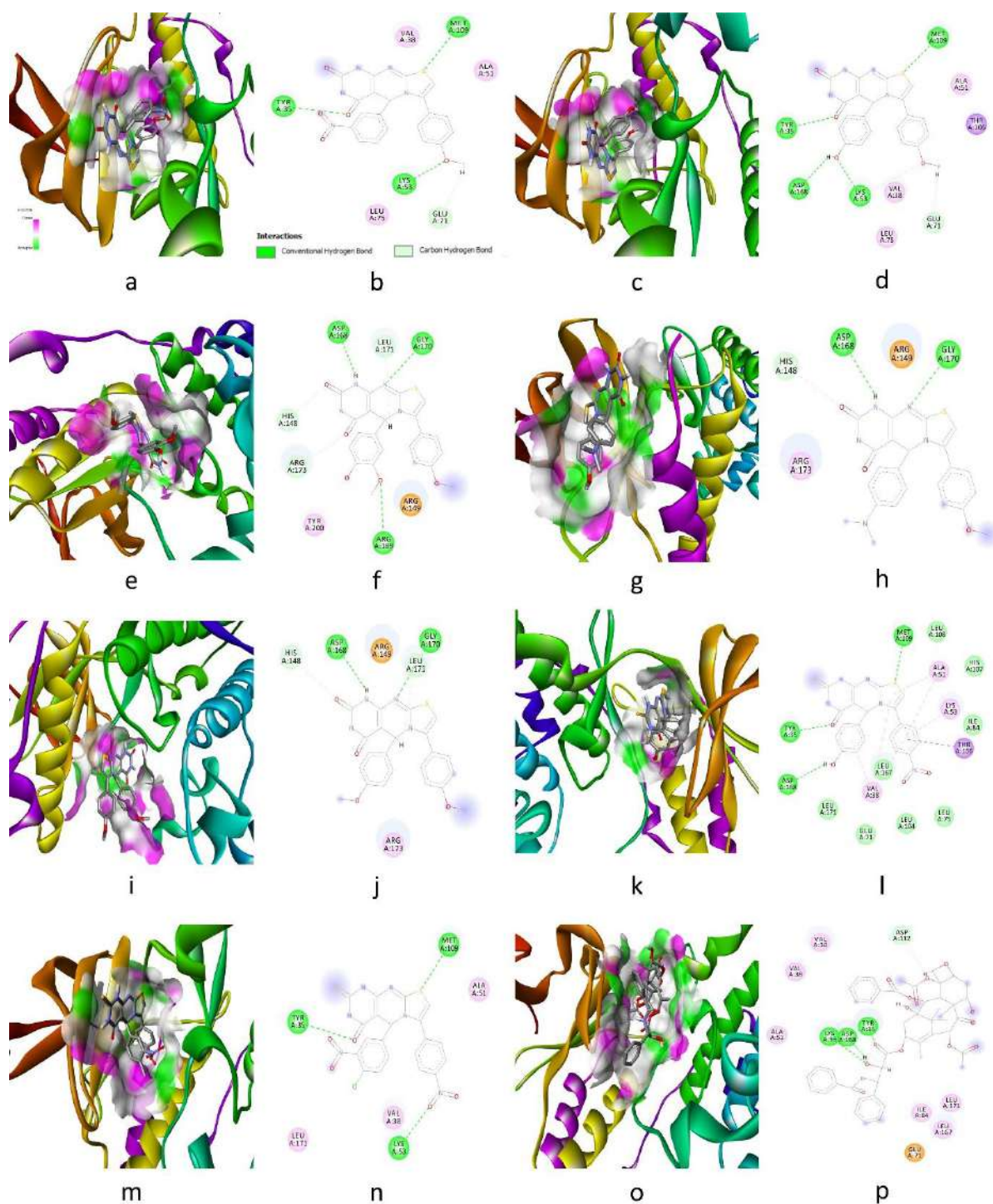


Fig. 7. 3D and 2D representations of molecular interactions between p38 MAPK target protein and synthesised compounds **4a** (a, b), **4b** (c, d), **4c** (e, f), **4d** (g, h), **4e** (i, j), **4f** (k, l), **4g** (m, n) and reference drug Paclitaxel (o, p).

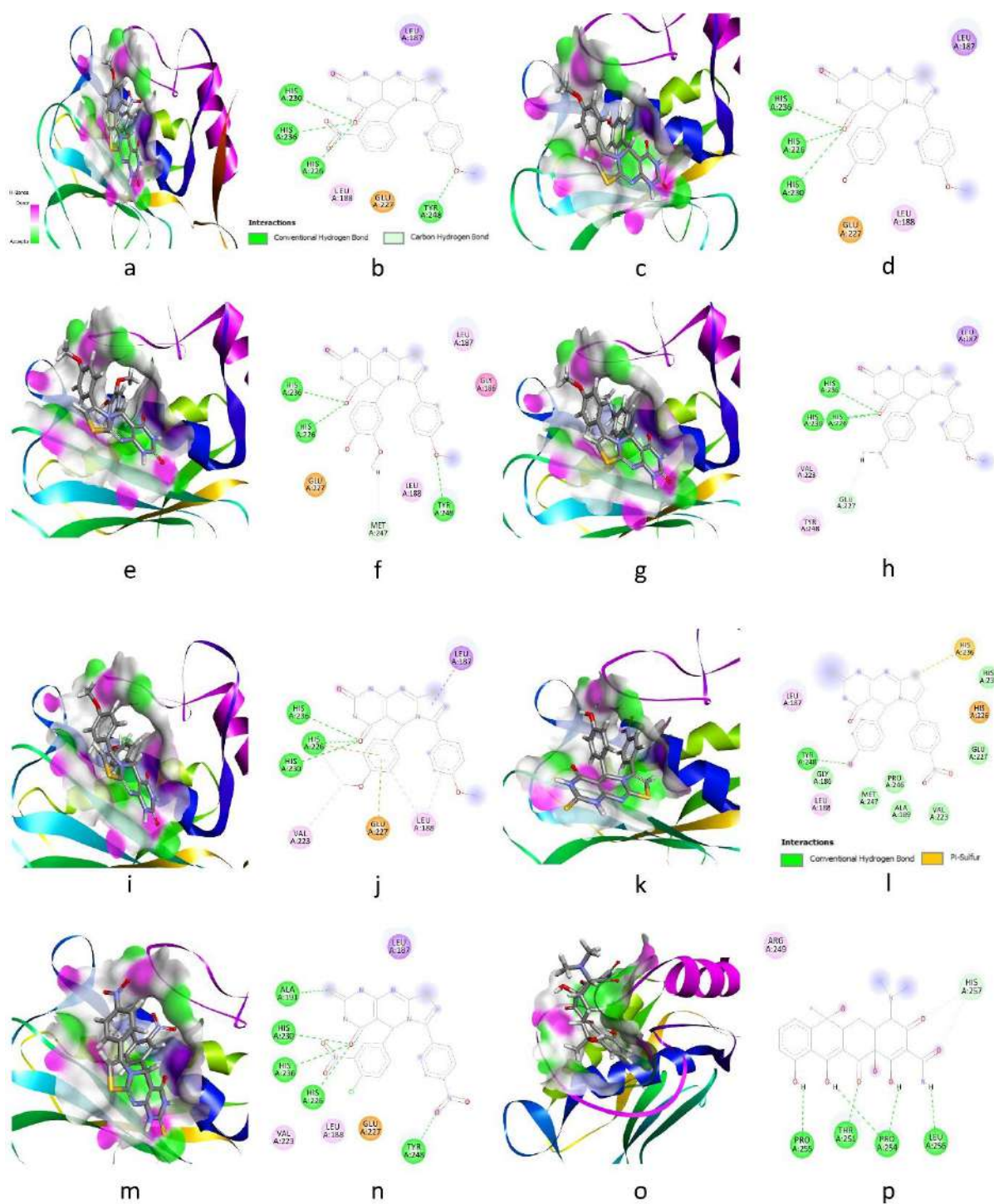


Fig. 8. 3D and 2D representations of molecular interactions between MMP-9 target protein and synthesised compounds **4a** (a, b), **4b** (c, d), **4c** (e, f), **4d** (g, h), **4e** (i, j), **4f** (k, l), **4g** (m, n) and reference drug Tetracycline (o, p).

3.5.5. *in silico* ADME-toxicology studies

Assessment of absorption, distribution, metabolism, excretion and toxicity (ADME-T) studies has the crucial step in high throughput screening [65] and the *in silico* methods are proven to be a reliable approach. The bioavailability and drug-likeness of all the synthesized compounds **4(a-g)** were assessed based on their molecular properties. The results indicated that, all the compounds under study passed through Lipinski's filter without any violation. *In silico* pharmacokinetic studies suggested that, the synthesized molecules could penetrate the blood-brain barrier and human intestinal barrier but were impermeable to Caco-2 (**Table 6**).

in silico pharmacodynamics studies indicated non-mutagenic, non-tumorigenic, non-irritant, AMES non-toxic with high reproductive effects and possible hepatotoxicity effects for all synthesized molecules. The bioactivity scores higher than 0 are considered biologically active, whereas the values between -0.50 to 0.0 are considered to be moderately active and below -0.5 to be inactive [66]. The bioactivity assessment indicated that the molecules do not belong to the GPCR group of molecules, do not modulate ion channels, non-kinase inhibitors, non-nuclear receptor ligands, non-protease and non-enzyme inhibitors (**Table 7**).

Table 6. Bioavailability, drug likeness and *in silico* pharmacokinetic assessment of synthesized compounds **4(a-g)**.

Compounds	Bioavailability and Drug likeness							<i>in silico</i> Pharmacokinetics			
	Total Molecular weight	cLogP	H-Acceptors	H-Donors	Rotatable Bonds	Polar Surface Area	Drug likeness	Human intestinal absorption	Caco-2 permeability	Blood brain barrier	CYP450 2D6 substrate
4a	449.446	2.1585	10	2	4	154.15	0.37683	0.863+	0.656-	0.972+	0.853-
4b	420.448	2.7934	8	3	3	128.56	4.658	0.893+	0.637-	0.969+	0.861-
4c	450.474	2.7234	9	3	4	137.79	4.658	0.893+	0.601-	0.966+	0.861-
4d	447.518	3.0355	8	2	4	111.57	5.3679	0.918+	0.575-	0.972+	0.842-
4e	434.475	3.0691	8	2	4	117.56	4.6405	0.900+	0.515-	0.971+	0.865-
4f	451.486	2.2433	9	3	3	180.17	-1.1518	0.832+	0.723-	0.972+	0.868-
4g	514.929	2.2734	11	2	4	205.76	-1.1113	0.846+	0.805-	0.973+	0.872-

Table 7. *in silico* pharmacodynamics and bioactivity assessment of synthesized compounds **4(a-g)**.

Compounds	<i>In silico</i> Pharmacodynamics							Bioactivity assessment					
	Mutagenic	Tumorigenic	Reproductive Effective	Irritant	Aerobic biodegradability	Ames toxicity	Hepatotoxicity	GPCR ligand	Ion channel modulator	Kinase inhibitor	Nuclear receptor ligand	Protease inhibitor	Enzyme inhibitor
4	NON	NON	NON	NON	0.95-	0.703	0.875	-	-	-	-	-	-
4	NON	NON	NON	NON	0.99	0.593	0.900	-	-	-	-	-	0.0
4	NON	NON	NON	NON	1.00-	0.588	0.850	-	-	-	-	-	-
4	NON	HIG	NON	NON	0.99	0.567	0.850	-	0.6	-	-	-	-
4	NON	NON	NON	NON	0.99	0.587	0.850	-	-	-	-	-	-
4f	NON	NON	HIG	NON	0.99	0.700	0.825	-	-	-	-	-	-
4	NON	NON	HIG	NON	1.00-	0.712	0.850	-	-	-	-	-	-

3.6. Conclusion

In summary, we have successfully synthesized new (4-substituted-phenyl)-1,5-dihydro-2*H*-pyrimido[4,5-*d*][1,3]thiazolo[3,2*a*]-pyrimidine-2,4(3*H*)-dione derivatives with good yield and evaluated for their *in vitro* cytotoxicity and anti-inflammatory effects. Among the newly synthesized molecules, the compounds **4f** and **4g** were identified as the most active anticancer agents, whereas the compounds **4a** and **4g** were found to exhibit promising anti-inflammatory activity. This was also supported by the *in silico* interaction studies. SAR study revealed the importance of electron-withdrawing groups in enhancing the potency of these more active compounds. *In silico* ADME-toxicology results suggested that, all the compounds are non-toxic and have good oral bioavailability and the drug-likeness score indicated that they are suitable as drug leads. *in silico* molecular docking results suggested that, compounds **4f** and **4g** have bound with P38 MAPk with a minimal binding energy of -8.7 and -8.4 kcal/mol, respectively, while the effective anti-inflammatory compounds, **4g** and **4a** have bound with MMP-9 protein with minimal binding energy of -9.3 and -8.6 kcal/mol, respectively.

3.7. References

1. C. Simon, T. Constantieux, J. Rodriguez, *Eur. J. Org. Chem.*, **2004**, 24, 4957-4980.
2. T. Venkatesh, Y.D. Bodke, K. Nagaraj, S.R. Kumar, *Med. Chem.*, **2018**, 8, 1-7.
3. T. Venkatesh, Y.D. Bodke, B. Manjunatha, S.R. Kumar, *Nucleosides, Nucleotides and Nucleic Acids*, **2021**, 1-13.
4. B. List, R.A. Lerner, C.F. Barbas, *J. Am. Chem. Soc.*, **2000**, 122, 2395-2396.
5. S. Balalaie, M. Bararjanian, A.M. Amani, B. Movassagh, *Synlett.*, **2006**, 2, 263-266.
6. M. Srinivasan, S. Perumal, S. Selvaraj, *ARKIVOC*, **2005**, 9, 201-208.
7. N. Obaiiah, Y.D. Bodke and S. Telkar, *ChemistrySelect*, **2020**, 5, 178-184.
8. J. Mabry and B. Ganem, *Tetrahedron Lett.*, **2006**, 47, 55-56.
9. B. List, P. Pojarliev, W.T. Biller, H.J. Martin, *J. Am. Chem. Soc.*, **2002**, 124, 827-833.
10. P. Kotrusz and S. Toma, *ARKIVOC*, **2006**, 5, 100-109.
11. D.B. Ramachary, N.S. Chowdari, C.F. Barbas, *Angew. Chem. Int. Ed.*, **2003**, 115, 4365-4369.
12. A. Bøgevig, N. Kumaragurubaran, K. Juhl, W. Zhuang, K.A. Jørgensen, *Angew. Chem. Int. Ed.*, **2002**, 41, 1790-1793.
13. A. Kumar and R.A. Maurya, *Tetrahedron*, **2007**, 63, 1946-1952.
14. C. Simon, T. Constantieux, J. Rodriguez, *Eur. J. Org. Chem.*, **2004**, 24, 4957-4980.
15. S.H. Sukanya, T. Venkatesh, S.J. Aditya Rao, N. Shivakumara, M.N. Joy, *Chim. Techno Acta*, **2021**, 8, 1-13.
16. H.T. Fahmy, S.A. Rostom, A.A. Bekhit, *Arch. Pharm.*, **2002**, 335, 213-222.
17. S.A. Abdel-Aziz, E.S. Taher, P. Lan, G.F. Asaad, H.A. Gomaa, N.A. El-Koussi, B.G. Youssif, *Bioorg. Chem.*, **2021**, 111, 1-14.
18. Y. Ouyang, H. Yang, P. Zhang, Y. Wang, S. Kaur, X. Zhu, H. Wang, *Molecules*, **2017**, 22, 1-27.
19. C. Madasu, Y.M. Xu, E.M. Wijeratne, M.X. Liu, I. Molnar, A.A. Gunatilaka, *Med. Chem. Res.*, **2022**, 1-11.
20. R.M. Mohareb, F. Al-Omran, R.A. Azzam, *Steroids*, **2014**, 84, 46-56.
21. S.T. Asundaria, K.C. Patel, *Pharm. Chem. J.*, **2012**, 45, 725-731.
22. M.S.K. Youssef, R.A. Ahmed, M.S. Abbady, S.A. Abdel-Mohsen, A.A. Omar, *Monatsh. Chem.*, **2008**, 139, 553-559.
23. J.P. Beck, M.A. Curry, R.J. Chorvat, L.W. Fitzgerald, P.J. Gilligan, R. Zaczek, G.L. Trainor, *Bioorg. Med. Chem. Lett.*, **1999**, 9, 1185-1188.

24. J. Akhtar, A.A. Khan, Z. Ali, R. Haider, M.S. Yar, *Eur. J. Med. Chem.*, **2016**, 125, 143-189.
25. Q. Xin, R. Yuan, W. Shi, Z. Zhu, Y. Wang, W. Cong, *Life Sciences*, **2019**, 237, 1-24.
26. R. Ranjith, *J. Chem. Pharm. Res.*, **2016**, 8, 505-526.
27. S. Sharma, D. Kumar, G. Singh, V. Monga, B. Kumar, *Eur. J. Med. Chem.*, **2020**, 200, 1-72.
28. N. Kaur, K. Kaur, T. Raj, G. Kaur, A. Singh, T. Aree, D.O. Jang, *Tetrahedron*, **2015**, 71, 332-337.
29. A. Akbari, M.G. Dekamin, A. Yaghoubi, M.R. Naimi-Jamal, *Scientific Reports*, **2020**, 10, 1-16.
30. S.G. Khansole, J.A. Angulwar, V.N. Bhosale, S.S. Choudhare, *IJRAR*, **2019**, 6, 525-530.
31. D. Kumbhar, D. Chandam, R. Patil, S. Jadhav, D. Patil, A. Patravale and M. Deshmukh, *J. Heterocycl. Chem.*, **2018**, 55, 692-698.
32. T. Venkatesh, Y.D. Bodke, K. Nagaraj and S.R. Kumar, *Med. Chem.*, **2018**, 8, 1-7.
33. A. Bazgira, M.M. Khanaposhtani, A.A. Soorki, *Bioorg. Med. Chem. Lett.*, **2008**, 18, 5800-5803.
34. B. Sedaghati, A. Fassihi, S. Arbabi, M. Ranjbar, H. R. Memarian, L Saghaie, D. Abedi, *Med. Chem. Res.*, **2012**, 21, 3973-3983.
35. M. Kidwai, S. Saxena, M.K.R. Khan, S.S. Thukral, *Eur. J. Med. Chem.*, **2005**, 40, 816-819.
36. V.V. Dabholkar, T.D.J. Ravi, *Serb. Chem. Soc.*, **2010**, 75, 1033-1040.
37. T. Raj, P. Saluja, N. Singh, *Sens. Actuators B Chem.*, **2015**, 206, 98-106.
38. A. Shaabani, A. Rahmati and S. Naderi, *Bioorg. Med. Chem. Lett.*, **2005**, 15, 5553-5557.
39. J.M. Khurana, A. Chaudhary, B. Nand, A. Lumb, *Tetrahedron Lett.*, **2012**, 53, 3018-3022.
40. T. Raj, H. Sharma, Mayank, A. Singh, T. Aree, N. Kaur, N. Singh and D.O. Jang, *ACS Sustain. Chem. Eng.*, **2017**, 5, 1468-1475.
41. V.M. Kumbar, M.R. Peram, M.S. Kugaji, T. Shah, S.P. Patil, U.M. Muddapur, K.G. Bhat, *Odontology*, **2020**, 1, 148-156.
42. C.D. Souza-Tarla, J.A. Uzuelli, A.A. Machado, R.F. Gerlach, J.E. Tanus-Santos, *Clin. Biochem.*, **2005**, 38, 410-414.
43. V. Kumar and J. Keshavayya, *J. Mol. Struct.*, **2019**, 1186, 404-412.

44. M.D. Kavitha, K.G.M. Mallikarjun, S.J. Aditya Rao, T.S. Shilpa, S.N. Prasad and R. Sarada, *Biotechnol. Lett.*, **2019**, 41, 91-106.
45. P. Maher, *J. Biol. Chem.*, **1999**, 274, 17491-17498.
46. S.J. Aditya Rao, S.M. Shivayogi, J.K. Satyanarayana, R.C. Kumaran, *Bioimpacts*, **2021**, 11, 187-197.
47. F. Grbovic, M.S. Stankovic, M. Curcic, N. Dordevic, D. Seklic, M. Topuzovic, *Plants*, **2013**, 2, 371-378.
48. M. Bjorklund and E. Koivunen, *Biochim. Biophys. Acta (BBA) - Rev. Cancer*, **2005**, 1755, 37-69.
49. S. Mondal, N. Adhikari, S. Banerjee, S.A. Amin, T. Jha, *Eur. J. Med. Chem.*, **2020**, 194, 1-20.
50. Q. Gao, Y. Wang, J. Hou, Q. Yao, J. Zhang, *J. Comput. Aided. Mol. Des.*, **2017**, 31, 625-641.
51. O. Trott, J.A. Olson, *J. Comput. Chem.*, **2010**, 31, 455-461.
52. S.J. Aditya Rao, C.K. Ramesh, S. Raghavendra, M. Paramesha, *Curr. Comput. Aided Drug Des.*, **2020**, 16, 231-237.
53. C.A. Lipinski, F. Lombardo, B.W. Dominy, P.J. Feeney, *Adv. Drug Deliv. Rev.*, **1997**, 23, 3-25.
54. S. Raghavendra, S.J. Aditya Rao, V. Kumar, C.K. Ramesh, *Comput. Biol. Chem.*, **2015**, 59, 81-86.
55. T. Sander, J. Freyss, M. Von Korff, C. Rufener, *J. Chem. Inf. Model*, **2015**, 55, 460-473.
56. F. Cheng, W. Li, Y. Zhou, J. Shen, Z. Wu, G. Liu, *J. Chem. Inf. Model*, **2012**, 52, 3099-3105.
57. A. Jarrahpour, M. Motamedifar, M. Zarei, M.H. Youssoufi, M. Mimouni, Z.H. Chohan, *Phosphorus Sulfur Silicon Relat. Elem.*, **2010**, 185, 491-497.
58. A. Mrozek-Wilczkiewicz, M. Kuczak, K. Malarz, W. Cieslik, E. Spaczynska, R. Musiol, *Eur. J. Med. Chem.*, **2019**, 177, 338-349.
59. S. Sharma, D. Kumar, G. Singh, V. Monga, B. Kumar, *Eur. J. Med. Chem.*, **2020**, 200, 1-72.
60. J.B. Zawilska, J. Wojcieszak, A.B. Olejniczak, *Pharmacol. Rep.*, **2013**, 65, 1-14.
61. M.J. Keiser, B.L. Roth, B.N. Armbruster, P. Ernsberger, J.J. Irwin, B.K. Shoichet, *Nat. Biotechnol.*, **2007**, 25, 197-206.

62. Soobrattee, Muhammad, Theeshan Bahorun, O.I. Aruoma, *BioFactors*, **2006**, 27, 19-35.
63. X. Wang, Y.Y. Yu, S. Lieu, F. Yang, J. Lang, C. Lu, *Bone*, **2013**, 52, 111-119.
64. D.B. Corry, A. Kiss, L.Z. Song, L. Song, J. Xu, S.H. Lee, Z. Werb, F. Kheradmand, *FASEB J.*, **2004**, 18, 995-997.
65. S.J. Aditya Rao, B. Jeevitha, R. Smitha, C.K. Ramesh, M. Paramesha, K.S. Jamuna, *Int. J. Res. Dev. Pharm. Life Sci.*, **2015**, 4, 1686-1696.
66. A. Husain, A. Ahmad, S.A. Khan, M. Asif, R. Bhutani, F.A. Al-Abbasi, *Saudi Pharm. J.*, **2016**, 24, 104-114.

4A.1. Introduction

Heterocyclic compounds are widely used in the medicinal field because of their bio-active structural variety. Among them, pyrimidine and its derivatives play an important role in drug discovery due to their chemical significance and diverse biological potential [1]. Pyrimidine is a six-membered unsaturated compound composed of carbon and nitrogen atoms at positions 1 and 3. They are found in many natural compounds such as nucleotides, nucleic acid, vitamins, liposacharides and antibiotics etc., [2]. It is used as a starting material for the synthesis of bio-active heterocyclic compounds and as raw material for drug synthesis [3]. It has been found to be associated with broad range of biological activities such as antihypertensive [4], anticancer [5], antimicrobial [6], anti-inflammatory [7], antioxidant [8], antitumor [9], anti-tubercular [10], antipsychotic [11], anxiolytic and antidepressant [12] etc. These wide applications create an interest in researchers on pyrimidine derivatives.

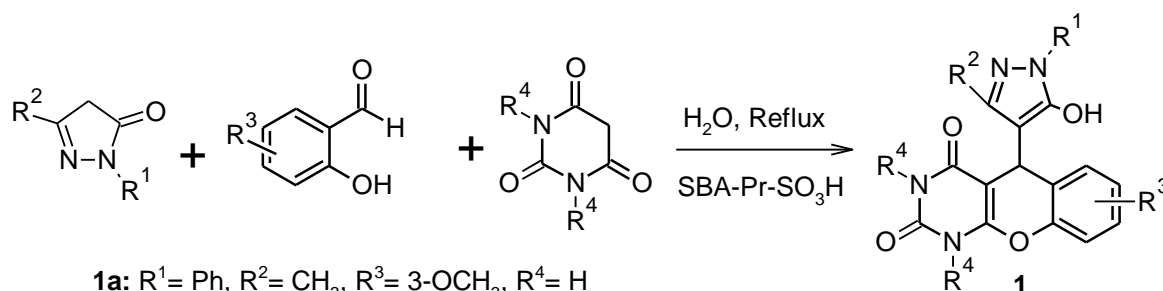
Among the life-threatening diseases faced by humankind, cancer predominates the list. Cancers are generally caused by the combined genetic and non-genetic changes induced by environmental factors that trigger inappropriate activation or inactivation of specific genes leading to neoplastic transformations or abnormal cell growth. Cancer is a heterogeneous disease that comes in several clinical and histological forms [13]. There are different treatment methods for cancer, including surgery and radiation, chemotherapy, and hormonal therapy. Surgery and radiation therapies either removes (destroy) or control cancer cells in specific areas, but chemotherapy and hormonal therapy destroy or control cancer spread across the body [14]. Current chemotherapies suffer from major limitations of side effects and drug resistance. Therefore, the constant search for novel and safer anticancer drugs remains essential [15]. With the advancements in rational drug discovery approaches, more accurate and reliable drug targets have been identified. One such cellular target majorly studied in the treatment of cancer is the mitogen-activated protein (MAP) kinases [16]. The MAP kinase

(MAPK) mediates a wide variety of cellular behaviors in response to extracellular stimuli. One of the members of this family, the P38 MAP kinase, is an important enzyme involved in signal transduction and plays a vital role in numerous biological processes [17]. The inhibition of P38 MAP kinase is likely to affect cellular proliferation accounting for cell toxicity [18]. This can be used to test mitochondrial respiration, which indirectly linked to cellular toxicity [19].

Tuberculosis (TB) is a bacterial infection caused by *Mycobacterium tuberculosis* (MTB), and it is an aerial transferable and contagious disease with comparatively high mortality worldwide. TB predominantly affects the lungs and other parts of the body, including kidneys, brain, vertebral column & other vital organ systems [20]. Treatment for Rifampicin-resistant TB (RR-TB), Multidrug-resistant TB (MDR-TB), and extensively drug-resistant TB (XDR-TB) requires a longer period of time (up to 2 years) with more expensive and toxic medicines [21]. To overcome these problems, there is a need to discover effective novel anti-tuberculosis drugs for the treatment of infectious diseases. The most widely studied molecular mechanism behind the anti-tuberculosis effect includes the involvement of InhA-Enoyl-Acyl Carrier Protein Reductase enzyme. The InhA enzyme is involved in mycolic acids biosynthesis and has been recognized as a promising target for novel anti-mycobacterial drugs [22]. Therefore, the development of drug-leads justifying the structural demands of InhA-Enoyl-Acyl Carrier Protein Reductase inhibitors will result in the development of an effective strategy to control tuberculosis, a disease that kills more than two million people each year [23]. Some of the reported biologically important heterocyclic compounds have been discussed below.

In 2017, G.M. Ziarani and co-authors reported a series of pyrazol-chromeno[2,3-*d*]pyrimidinones (**1**) using nanocatalyst and screened for antimicrobial activity. Among the synthesized compounds **1a** & **1b** shows highest zone of inhibitions at 11 & 14 mm against *B.*

subtilis and compounds **1a** & **1c** shows inhibitions at 11 & 13 mm against *S. aureus* respectively [24].

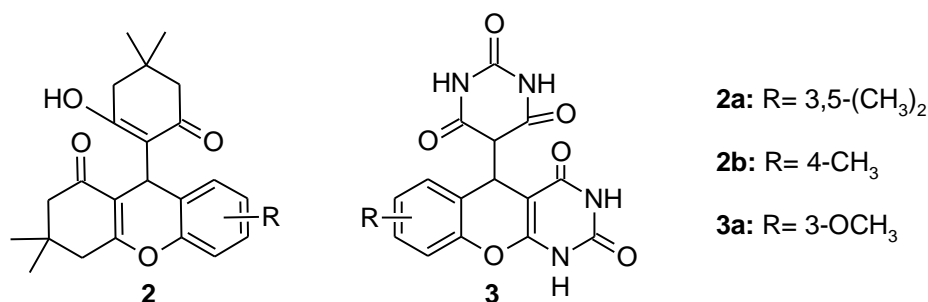


1a: $R^1 = \text{Ph}$, $R^2 = \text{CH}_3$, $R^3 = 3\text{-OCH}_3$, $R^4 = \text{H}$

1b: $R^1 = 4\text{-NO}_2\text{Ph}$, $R^2 = \text{CH}_3$, $R^3 = \text{H}$, $R^4 = \text{H}$

1c: $R^1 = \text{CH}_3$, $R^2 = \text{H}$, $R^3 = \text{H}$, $R^4 = \text{CH}_3$

R.M. Naidu *et al.*, synthesized 3,4-dihydro-9-(2-hydroxy-4,4-dimethyl-6-oxocyclohex-1-enyl)-3,3-dimethyl-2H-xanthen-1(9H)-ones (**2**) and 5-(2,4-dioxo-1,3,4,5-tetrahydro-2H-chromeno[2,3-*d*]pyrimidin-5-yl)pyrimidine-2,4,6(1*H*,3*H*,5*H*)-triones (**3**) and screened for their antioxidant activity against DPPH and FRAP assays. Compounds **2a** and **3a** are excellent free radical scavengers toward DPPH free radicals and compounds **2b** and **3a** shows good in FRAP assay due to the presence of ED hydroxyl group in their structure [25].

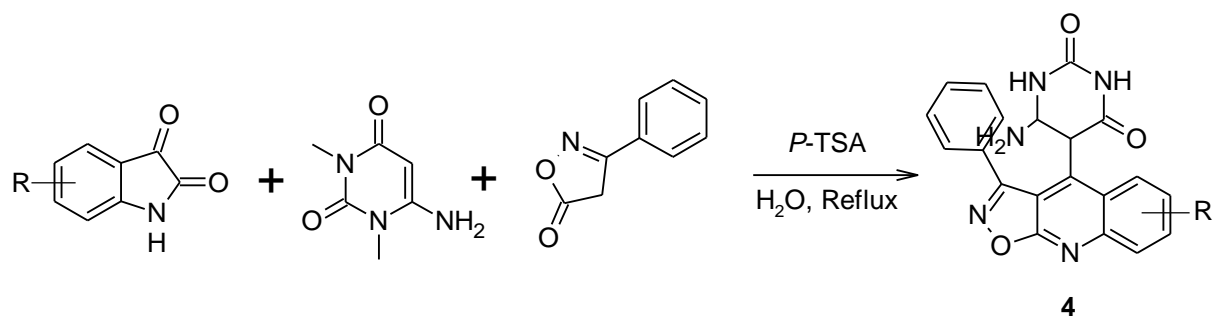


2a: $R = 3,5\text{-(CH}_3)_2$

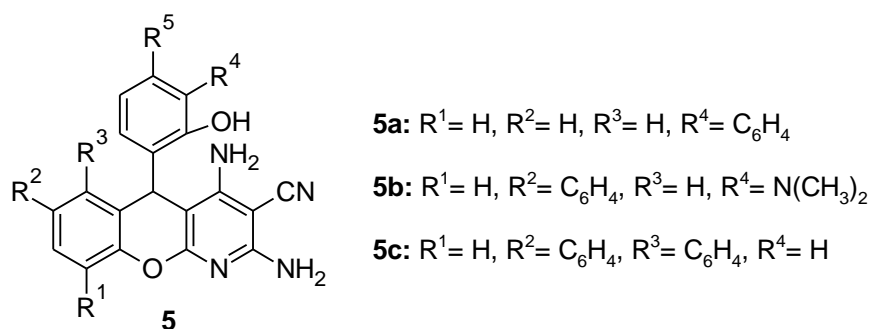
2b: $R = 4\text{-CH}_3$

3a: $R = 3\text{-OCH}_3$

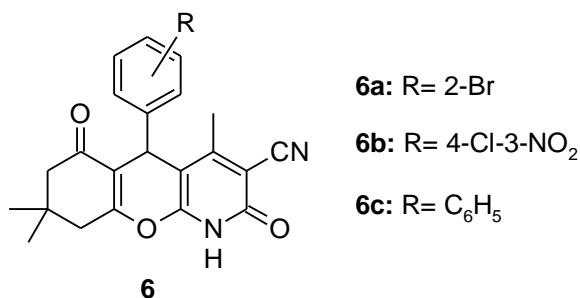
In 2015, isoxazolo[5,4-*b*]quinolin-4-yl)pyrimidine 2,4(1*H*,3*H*)-dione derivatives (**4**) was reported by N. Poomathi and co-authors *via* cleavage of the isatin C-N bond followed by ring expansion reaction using *p*-TSA as the catalyst [26].



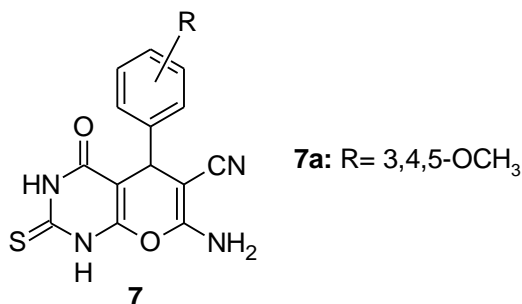
S.T. Chung *et al.*, synthesized a series of 4*H*-chromene and chromeno[2,3-*b*]pyridine derivatives (**5**) and reported as anti-inflammatory activity. Among them, **5a**, **5b** and **5c** compounds exhibited significant anti-inflammatory activity with IC₅₀ values of 6.9±0.3, 7.6±1.3 & 7.6±0.1 μM for human chondrocytes and 6.1±1.0, 8.8±1.1 & 8.0±0.1 μM for porcine chondrocytes respectively [27].



A series of some new chromeno[2,3-*b*]pyridine derivatives (**6**) was reported by D. Azarifar and co-authors in 2022 and screened for their DPPH free radical scavenging and antifungal activity. The compounds **6a**, **6b** & **6c** exhibited highest % inhibition of 95.7±1.9, 95.3±2.3 & 92.3±1.7 respectively for DPPH radical activity and almost all the compounds showed excellent antifungal activity in the range 44.2 to 99.1 % against *F. oxysporum* fungal strain [28].



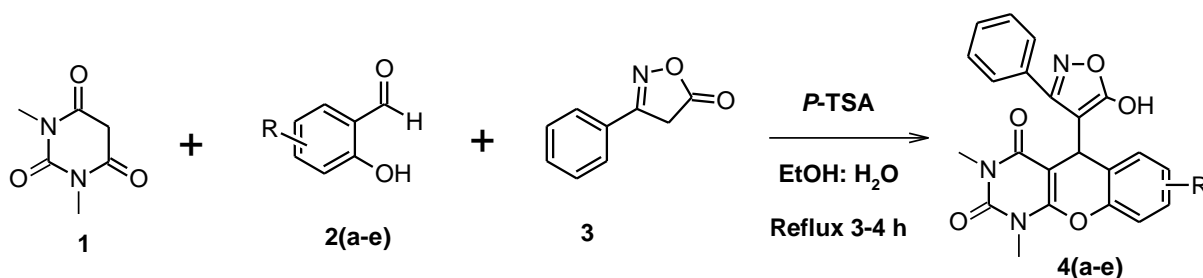
In 2012, H.M. Aly and co-workers synthesized a novel chromeno[2,3-*d*]pyrimidine derivatives (**7**) and investigated as antimicrobial activity. The compound **7a** showed good antimicrobial activity against *P. aeruginosa*, *S. aureus*, *A. flavus* & *C. albicans* microbial strains [29].



From the above investigations, we herein reported a series of substituted-(5-hydroxy-3-phenylisoxazol-4-yl)-1,3-dimethyl-1*H*-chromeno[2,3-*d*]pyrimidine-2,4(3*H*,5*H*)-dione derivatives and evaluation of their pharmacological activities (cytotoxicity & anti-TB), *in silico* molecular docking and DFT study.

4A.2. Present work

A series of some novel substituted-(5-hydroxy-3-phenylisoxazol-4-yl)-1,3-dimethyl-1*H*-chromeno[2,3-*d*]pyrimidine-2,4(3*H*,5*H*)-dione derivatives **4(a-e)** were reported in this chapter, by the reaction of 1,3-dimethylbarbituric acid (**1**), substituted salicylaldehyde/2-hydroxy-nepthaldehyde (**2**) and 3-phenyl-5-isoxazolone (**3**) was administered in refluxed temperature in the presence of *p*-TSA as a catalyst in aqueous ethanol. The synthetic pathway of the synthesized compounds has been given in **Scheme 4**.



Compd.	R
4a	H
4b	3-OCH ₃
4c	C ₄ H ₄
4d	5-NO ₂
4e	5-Br

Scheme 4. Synthesis of substituted-(5-hydroxy-3-phenylisoxazol-4-yl)-1,3-dimethyl-1*H*-chromeno[2,3-*d*]pyrimidine-2,4(3*H*,5*H*)-dione derivatives **4(a-e)**.

The possible mechanism for forming a new substituted-(5-hydroxy-3-phenylisoxazol-4-yl)-1,3-dimethyl-1*H*-chromeno[2,3-*d*]pyrimidine-2,4(3*H*,5*H*)-dione derivatives **4(a-e)** as given in **Fig. 1**. The reaction was initiated by the formation of enol (**II**) from the active methylene compound (**I**). Enol (**II**) attacks the carbonyl group of the substituted salicylaldehyde (**III**) and affords Knoevenagel intermediates (**IV**) & (**V**). Then it undergoes an intramolecular nucleophilic cyclization by the elimination of water molecules to afford an intermediate (**VI**). Finally, Michael addition with 3-phenyl-5-isoxazolone affords the final product (**VIII**).

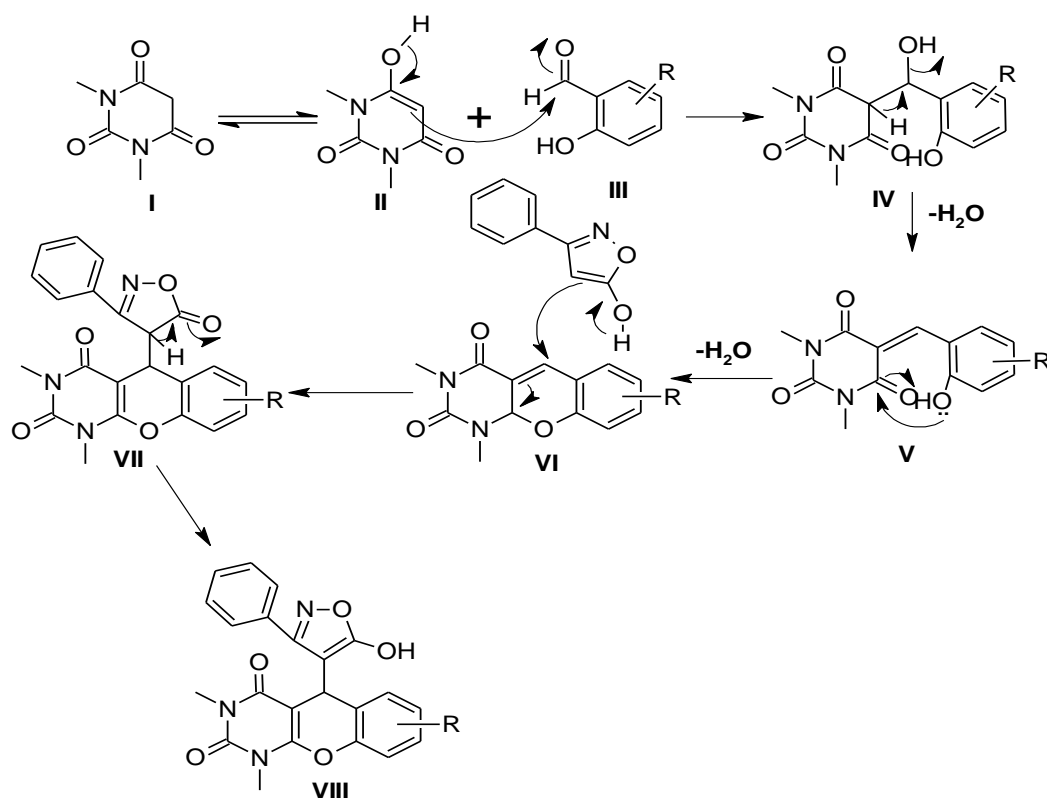
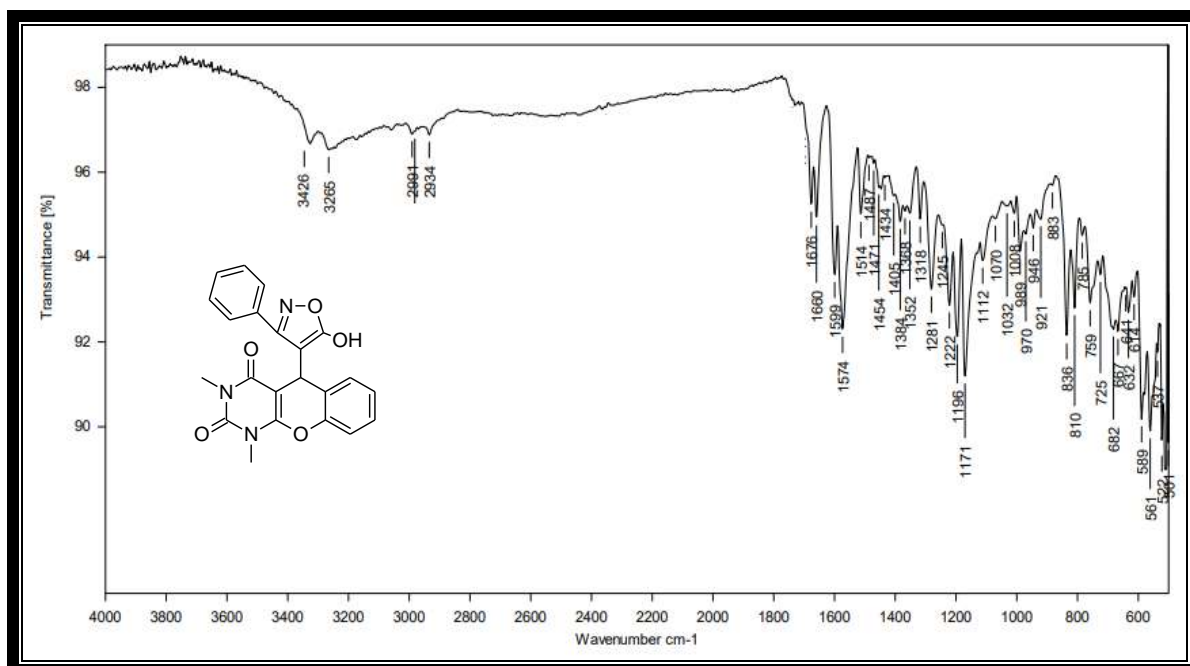


Fig. 1. Possible mechanism of synthesized compounds **4(a-e)**.

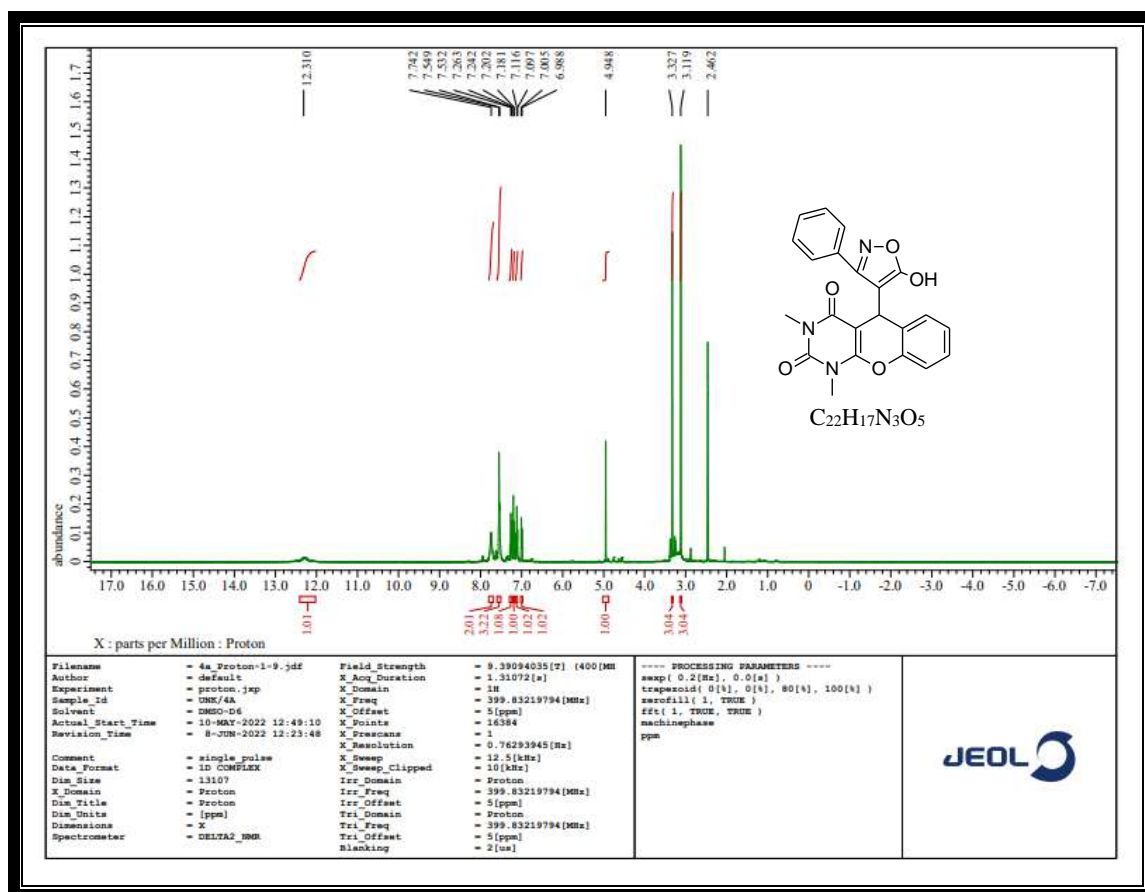
The structures of newly substituted-(5-hydroxy-3-phenylisoxazol-4-yl)-1,3-dimethyl-1*H*-chromeno[2,3-*d*]pyrimidine-2,4(3*H*,5*H*)-dione derivatives **4(a-e)** were confirmed by recording their IR, ¹H NMR, ¹³C NMR and Mass spectral data. IR spectrum of compound **4a** showed the absorption band in the region 3426 cm⁻¹ is attributed to the OH stretching vibration, 2934 cm⁻¹ correspond to N-methyl functionality and the absorption band at 1676 cm⁻¹ correspond to the stretching vibration of the carbonyl group (C=O). Another stretching vibrational band at 1599 cm⁻¹ correspond to the azomethine group (C=N). The ¹H NMR spectrum of compound **4a** exhibited a singlet peak at δ 12.31 ppm corresponding to OH proton of isoxazole nucleus (s, 1H, OH), and multiplet peaks at δ 7.74-7.53 ppm corresponds to five aromatic protons (m, 5H, Ar-H). A doublet peaks at δ 7.26-7.24, 7.20-7.18, 7.11-7.09 & 7.00-6.98 ppm which corresponds to four aromatic protons (d, *J*= 8 Hz, 4H, Ar-H). A singlet peak at δ 4.94 due to CH proton (s, 1H, CH) and another two singlet peaks at δ 3.32 and 3.11 ppm corresponds to two methyl protons (s, 6H, CH₃). In addition, the ¹³C NMR spectrum of compound **4a** exhibited peaks at δ 171.06, 161.73 and 161.67 ppm, which corresponds to carbonyl carbons and peaks at δ 29.24 and 28.17 ppm due to methyl carbons.

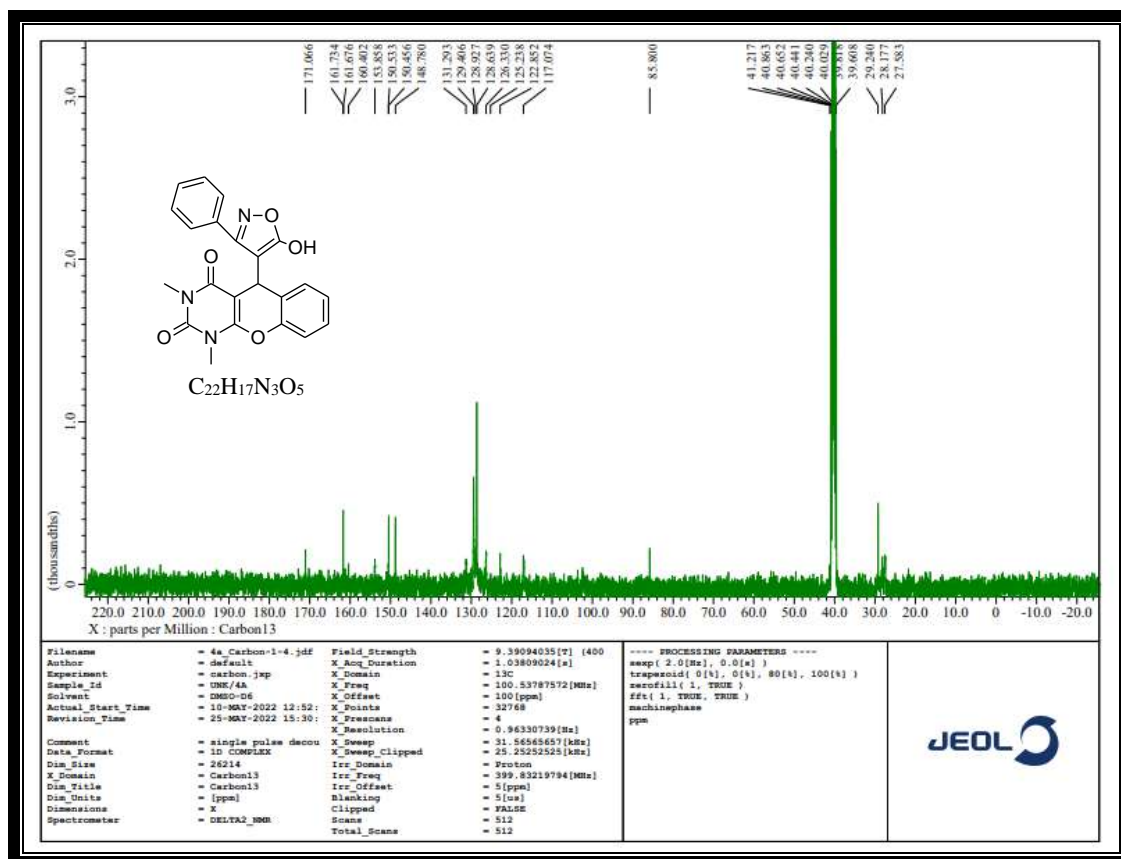
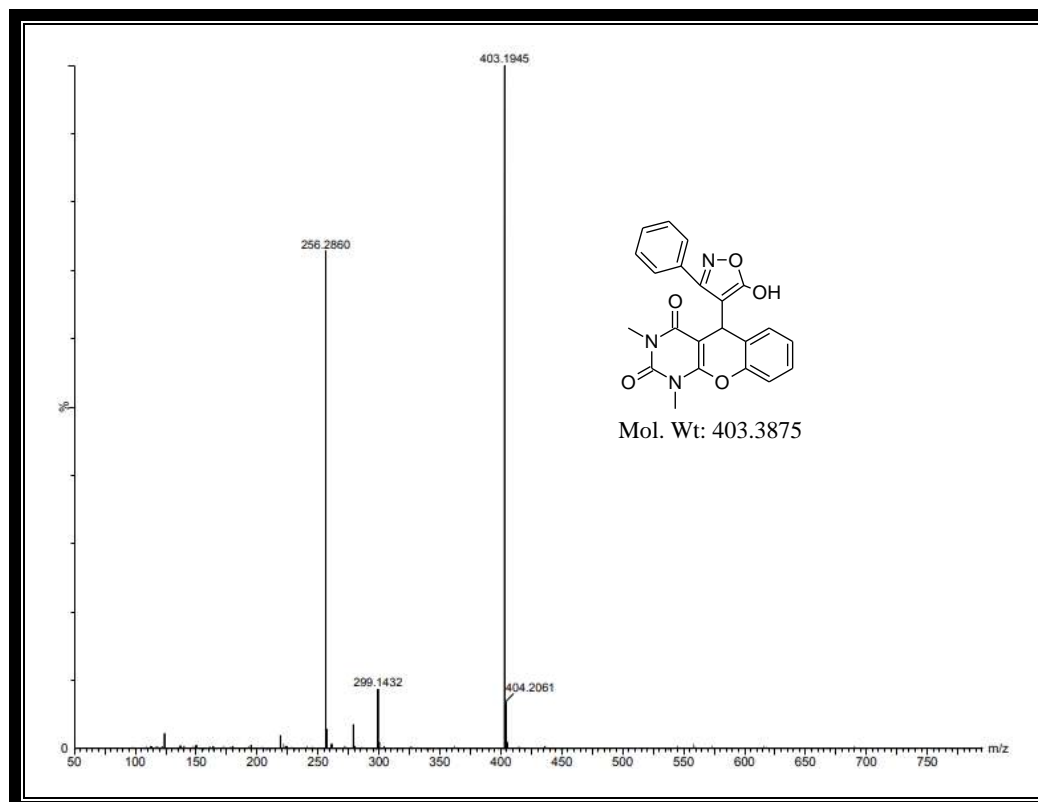
In the mass spectrum, a molecular ion peak *m/z* at 403.1945 [M⁺] is due to molecular weight of the compound **4a**.

Characterization:

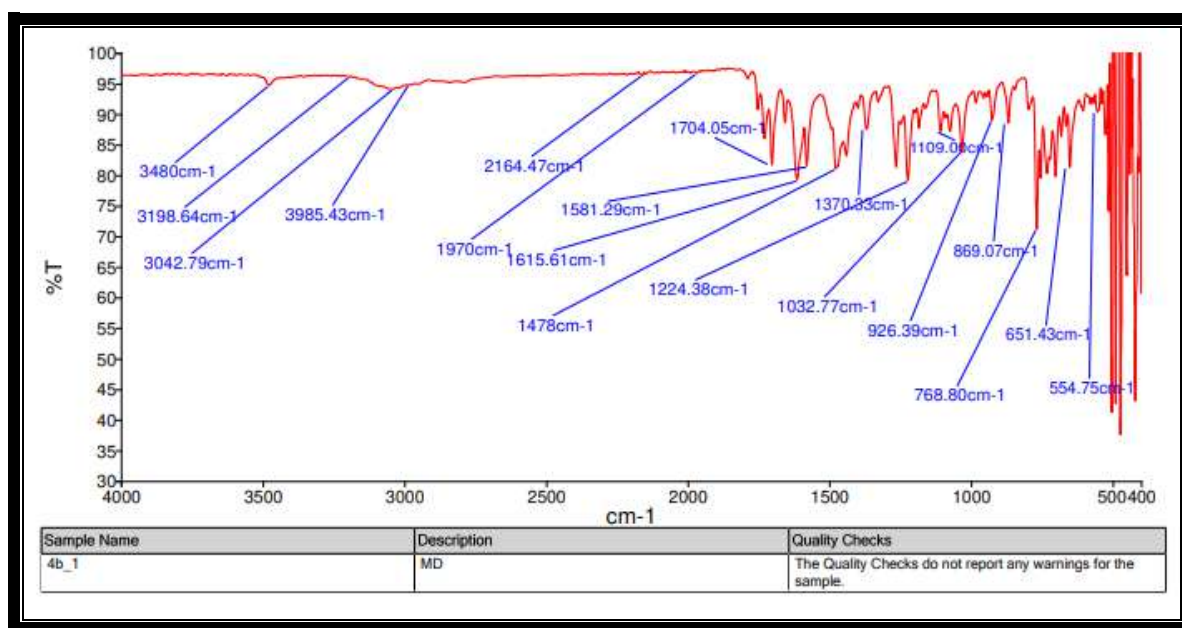


IR spectrum of compound 4a

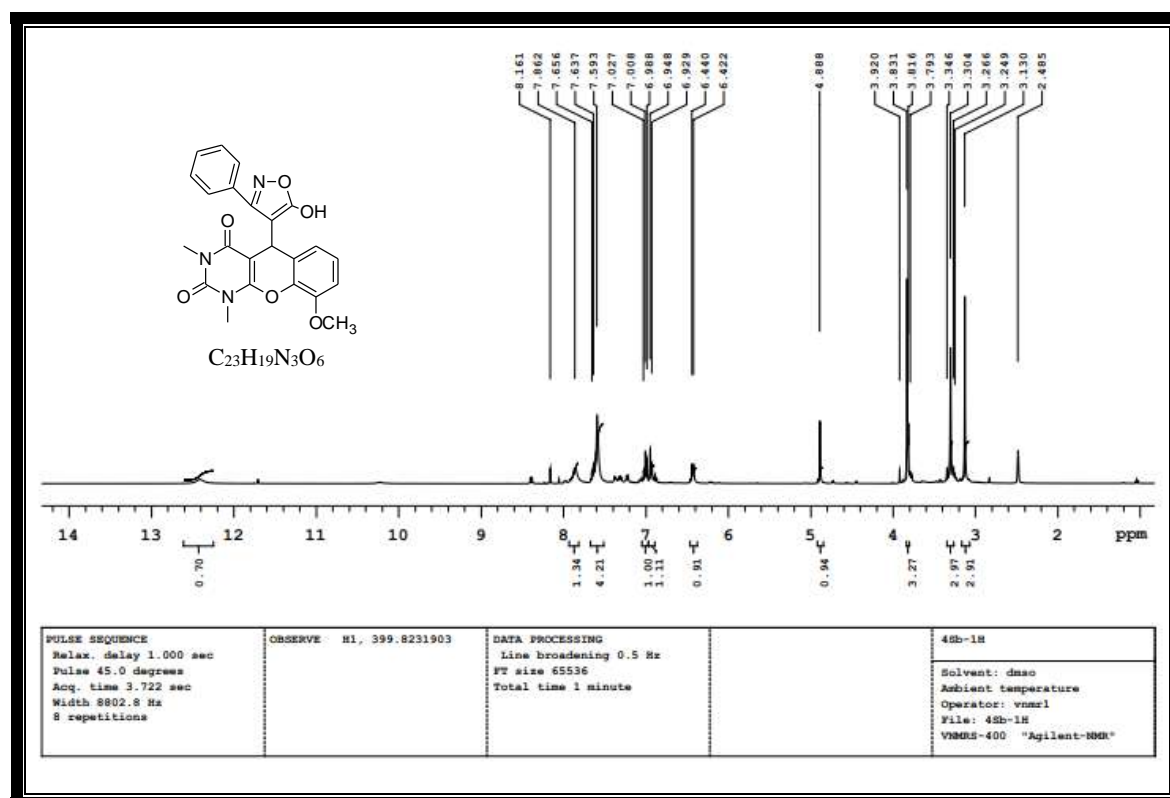
¹H NMR spectrum of compound 4a

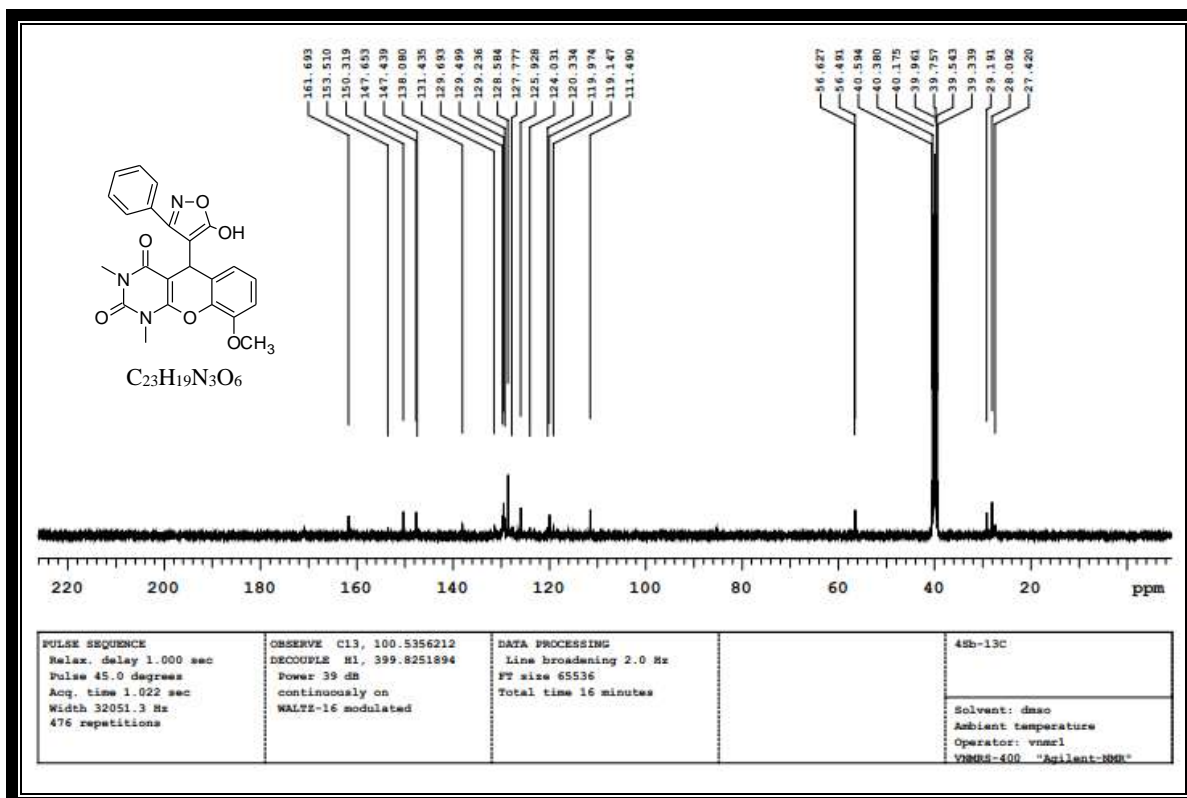
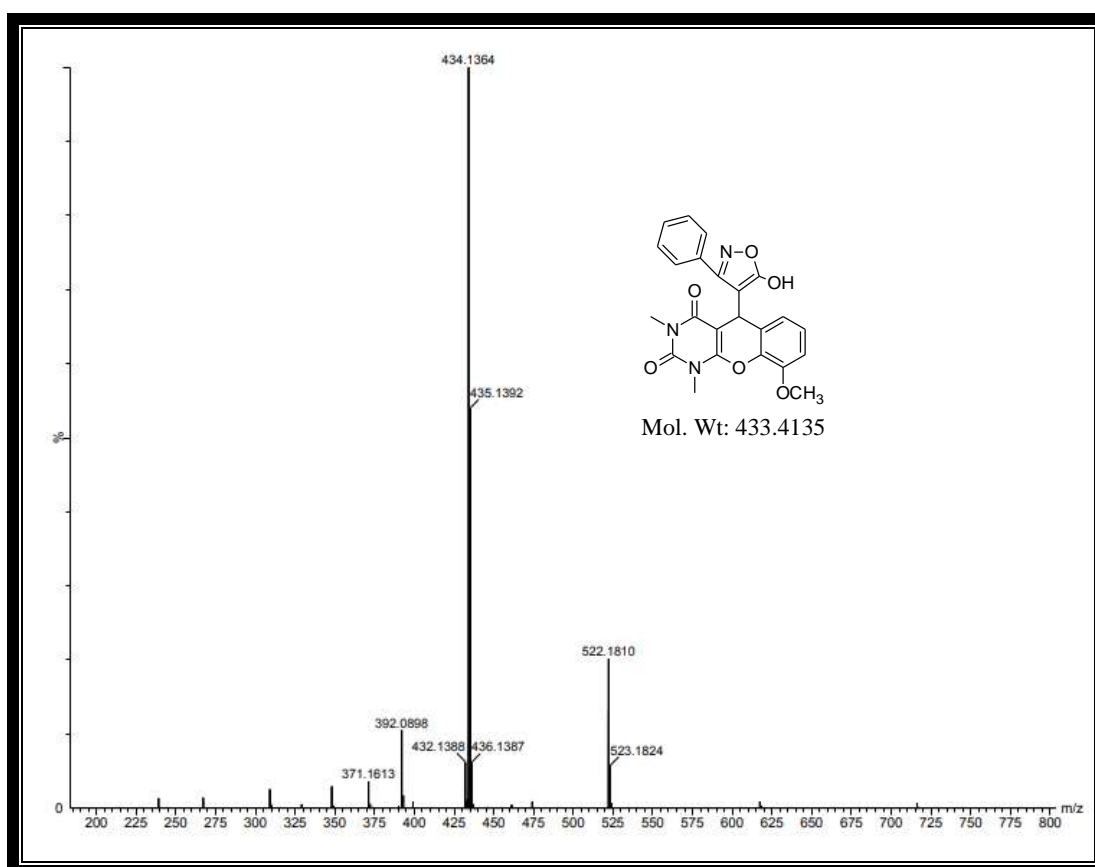
 ^{13}C NMR spectrum of compound 4a

MASS spectrum of compound 4a



IR spectrum of compound 4b

¹H NMR spectrum of compound 4b

 **^{13}C NMR spectrum of compound 4b****MASS spectrum of compound 4b**

4A.3. 2D ^1H - ^{13}C HSQC NMR

The ^1H NMR spectrum of compound **4a** exhibited two singlet peaks at δ 3.11 (H_1) and 3.32 (H_2) ppm correspond to methyl protons (s, 6H, CH_3) and another singlet peak at δ 4.94 (H_3) ppm due to CH proton (s, 1H, CH). A doublet peaks at δ 6.98-7.00 (H_4), 7.09-7.11 (H_5), 7.18-7.20 (H_6) & 7.24-7.26 (H_7) ppm which corresponds to four aromatic protons (d, $J=8$ Hz, 4H, Ar-H) and multiplet peaks at δ 7.53-7.74 (H_8 - H_{12}) ppm corresponds to five aromatic protons (m, 5H, Ar-H). The ^{13}C NMR spectrum of compound **4a** exhibited peaks at δ 27.58 (C_3), 28.17 (C_1) & 29.24 (C_2) ppm correspond to CH & CH_3 carbons. Peaks at δ 117.07 (C_7), 122.58 (C_5) & 126.33 (C_4 , C_6) ppm due to four aromatic carbons. Other peaks at δ 128.63 (C_{10}), 129.40 (C_9 , C_{11}) & 131.29 (C_8 , C_{12}) ppm corresponds to five aromatic carbons (^1H & ^{13}C NMR of compound **4a**).

Heteronuclear single quantum coherence or correlation (HSQC) experiment explained the ^1H - ^{13}C single bond correlation. 2D ^1H - ^{13}C HSQC NMR spectrum of compound **4a** was recorded in DMSO- d_6 solvent. The horizontal axis indicates the ^1H NMR and vertical axis indicated ^{13}C NMR. HSQC of compound **4a** explained that, ^1H - ^{13}C correlation between H_1 (δ 3.11) & C_1 (δ 28.17), H_2 (δ 3.32) & C_2 (δ 29.24), H_3 (δ 4.94) & C_3 (δ 27.58), H_4 (δ 6.98) & C_4 (δ 126.33), H_5 (δ 7.09) & C_5 (δ 122.58), H_6 (δ 7.18) & C_6 (δ 126.33), H_7 (δ 7.24) & C_7 (δ 117.07), H_8 (δ 7.74) & C_8 (δ 131.29), H_9 (δ 7.54) & C_9 (δ 129.40), H_{10} (δ 7.53) & C_{10} (δ 128.63), H_{11} (δ 7.54) & C_{11} (δ 129.40), H_{12} (δ 7.74) & C_{12} (δ 131.29). In addition, δ 12.31 ppm which does not shows HSQC correlation to any carbon, it indicated the OH proton & δ 148.78, 150.45, 153.85, 160.40, 161.67, 161.73 & 171.06 ppm which does not shows HSQC correlations to other protons. This confirmed the structure of 5-(5-Hydroxy-3-phenylisoxazol-4-yl)-1,3-dimethyl-1*H*-chromeno[2,3-*d*]pyrimidine-2,4(3*H*,5*H*)-dione (**Fig. 2**).

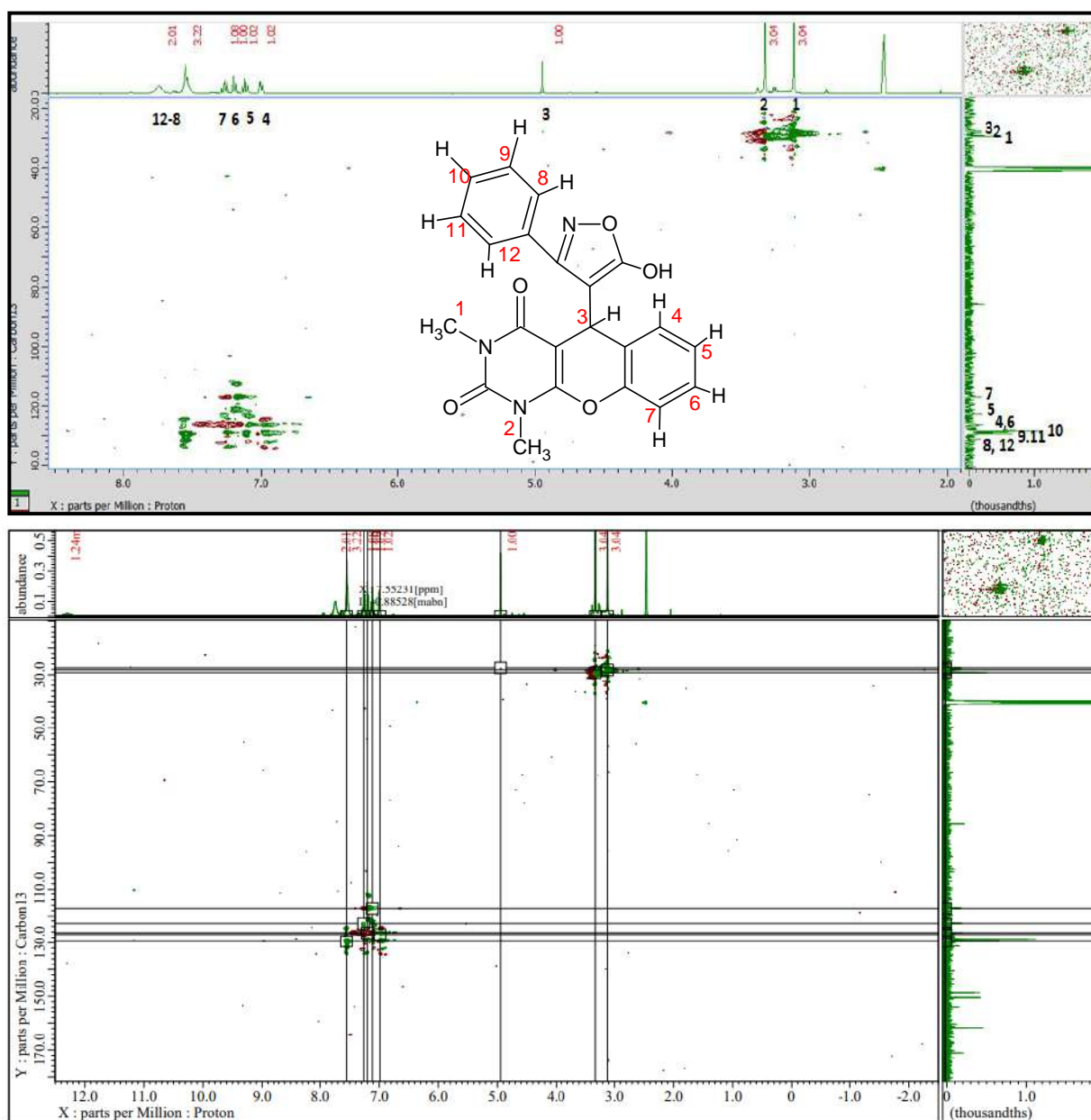


Fig. 2. 2D ^1H - ^{13}C HSQC NMR spectrum of compound **4a** recorded in DMSO- d_6 solvent.

4A.4. Experimental

4A.4.1. General information:

The general information regarding the different solvents, reagents and instruments etc., used for the analysis has been discussed previously in the experimental section (2A.3.1) of **Chapter-2A**. The anticancer and anti-TB activities were carried out in the Dept. of Microbiology, Maratha Mandal's NGH Institute of Dental Sciences & Research Centre, Belgaum, Karnataka. The computational studies were carried out by density functional theory (DFT)/B3LYP method by Gaussian 09 software using 6-31G (d,p) basis set at gaseous phase.

4A.4.2. Procedure for the synthesis of substituted-(5-hydroxy-3-phenylisoxazol-4-yl)-1,3-dimethyl-1*H*-chromeno[2,3-*d*]pyrimidine-2,4(3*H*,5*H*)-dione derivatives 4(a-e):

A mixture of 1,3-dimethylbarbituric acid (**1**, 1 mmol), substituted salicylaldehyde/2-hydroxy-naphthaldehyde (**2**, 1 mmol) and *p*-TSA (10 mol %) in ethanol/water (1:1) was stirred under refluxed condition. After 5 min, 3-phenyl-5-isoxazolone (**3**, 1 mmol) was added to it and refluxed at temperature with constant stirring for about 3-4 h. simultaneously, the reaction was monitored by TLC (Ethyl acetate & Pet ether). After completion of the reaction, the reaction mixture was cooled to room temperature and poured into the 100 mL flake ice with vigorous stirring to get a solid precipitate. Then, it was filtered, washed, recrystallized from absolute ethanol and dried to afford pure solid products **4(a-e)**.

5-(5-Hydroxy-3-phenylisoxazol-4-yl)-1,3-dimethyl-1*H*-chromeno[2,3-*d*]pyrimidine-2,4(3*H*,5*H*)-dione (**4a**):

Pale yellow solid; Yield: 92 %; MP: 234-238 °C; Mol. Formula: C₂₂H₁₇N₃O₅; UV (nm) λ_{max} (log ε): 413 (2.95) & 311 (4.01); FTIR (ν cm⁻¹): 3426 (OH), 2934 (N-CH₃), 1676 (C=O) & 1599 (C=N); ¹H NMR (δ ppm): 12.31 (s, 1H, OH), 7.74-7.53 (m, 5H, Ar-H), 7.26-7.24 (d, *J*= 8 Hz, 1H, Ar-H), 7.20-7.18 (d, *J*= 8 Hz, 1H, Ar-H), 7.11-7.09 (d, *J*= 8 Hz, 1H, Ar-H),

7.00-6.98 (d, $J=8$ Hz, 1H, Ar-H), 4.94 (s, 1H, CH), 3.32 (s, 3H, CH₃), 3.11 (s, 3H, CH₃); ¹³C NMR (δ ppm): 171.06, 161.73, 161.67, 160.40, 153.85, 150.53, 150.45, 148.78, 131.29, 129.40, 128.92, 128.63, 126.33, 125.23, 122.85, 117.07, 85.80, 29.24, 28.17, 27.58; HRMS: m/z 403.1945 [M^+]; Anal. Calcd: C 65.50, H 4.25, N 10.42 %, Found: C 65.45, H 4.20, N 10.39 %.

5-(5-Hydroxy-3-phenylisoxazol-4-yl)-9-methoxy-1,3-dimethyl-1H-chromeno[2,3-d]pyrimidine-2,4(3H,5H)-dione (4b):

Yellow solid; Yield: 89 %; MP: 220-222 °C; Mol. Formula: C₂₃H₁₉N₃O₆; UV (nm) λ_{\max} (log ϵ): 371 (3.99) & 318 (4.11); FTIR (ν cm⁻¹): 3480 (OH), 3042 (OCH₃), 2985 (N-CH₃), 1704 (C=O) & 1615 (C=N); ¹H NMR (δ ppm): 12.40 (s, 1H, OH), 7.86 (s, 1H, Ar-H), 7.65-7.63 (d, $J=8$ Hz, 4H, Ar-H), 7.02-6.92 (m, 2H, Ar-H), 6.44-6.42 (d, $J=8$ Hz, 1H, Ar-H), 4.88 (s, 1H, CH), 3.83 (s, 3H, OCH₃), 3.30 (s, 3H, CH₃), 3.13 (s, 3H, CH₃); ¹³C NMR (δ ppm): 161.69, 153.51, 150.31, 147.65, 147.43, 138.08, 131.43, 129.69, 129.49, 128.58, 127.77, 125.92, 124.03, 120.33, 119.97, 119.14, 111.49, 56.62, 29.86, 29.19, 28.09; HRMS: m/z 434.1364 [M^++1]; Anal. Calcd: C 63.74, H 4.42, N 9.70 %, Found: C 63.71, H 4.38, N 9.66 %.

5-(5-Hydroxy-3-phenylisoxazol-4-yl)-1,3-dimethyl-4H-benzo[g]chromeno[2,3-d]pyrimidine-2,4(3H,5H)-dione (4c):

Pale yellow solid; Yield: 85 %; MP: 228-230 °C; Mol. Formula: C₂₆H₁₉N₃O₅; UV (nm) λ_{\max} (log ϵ): 355 (4.03) & 318 (4.17); FTIR (ν cm⁻¹): 3465 (OH), 2820 (N-CH₃), 1702 (C=O) & 1597 (C=N); ¹H NMR (δ ppm): 12.46 (s, 1H, OH), 8.12 (s, 1H, Ar-H), 7.85-7.82 (m, 4H, Ar-H), 7.60 (s, 1H, Ar-H), 7.39-7.31 (m, 3H, Ar-H), 6.98-6.96 (d, $J=8$ Hz, 2H, Ar-H), 5.30 (s, 1H, CH), 3.39 (s, 3H, CH₃), 3.23 (s, 3H, CH₃); ¹³C NMR (δ ppm): 170.70, 161.98, 160.69, 158.20, 153.74, 151.02, 150.40, 146.96, 140.12, 135.33, 134.03, 131.44, 130.42, 129.69, 129.22, 128.36, 127.01, 126.63, 125.47, 123.07, 121.68, 117.15, 114.20, 113.23, 29.84, 29.27,

28.31; HRMS: m/z 452.3012 [$M^+ - 1$]; Anal. Calcd: C 68.87, H 4.22, N 9.27 %, Found: C 68.83, H 4.17, N 9.24 %.

5-(5-Hydroxy-3-phenylisoxazol-4-yl)-1,3-dimethyl-7-nitro-1H-chromeno[2,3-d] pyrimidine-2,4(3H,5H)-dione (4d):

Yellow solid; Yield: 82 %; MP: 180-182 °C; Mol. Formula: $C_{22}H_{16}N_4O_7$; UV (nm) λ_{max} (log ϵ): 543 (2.90) & 325 (4.14); FTIR (ν cm^{-1}): 3398 (OH), 2845 (N-CH₃), 1678 (C=O) & 1599 (C=N); 1H NMR (δ ppm): 12.42 (s, 1H, OH), 7.92 (s, 1H, Ar-H), 7.45-7.43 (d, J = 8 Hz, 4H, Ar-H), 6.98-6.72 (m, 2H, Ar-H), 6.38-6.36 (d, J = 8 Hz, 1H, Ar-H), 4.72 (s, 1H, CH), 3.26 (s, 3H, CH₃), 3.18 (s, 3H, CH₃), ^{13}C NMR (δ ppm): 162.88, 154.54, 150.46, 148.66, 147.52, 138.34, 131.52, 129.82, 129.24, 128.76, 127.64, 126.86, 124.72, 122.36, 120.96, 120.12, 112.52, 29.95, 29.06, 28.46; HRMS: m/z 448.1238 [M^+]; Anal. Calcd: C 58.93, H 3.60, N 12.50 %, Found: C 58.89, H 3.57, N 12.46 %.

7-Bromo-5-(5-hydroxy-3-phenylisoxazol-4-yl)-1,3-dimethyl-1H-chromeno[2,3-d] pyrimidine -2,4(3H,5H)-dione (4e):

Orange solid; Yield: 80 %; MP: 166-168 °C; Mol. Formula: $C_{22}H_{16}BrN_3O_5$; UV (nm) λ_{max} (log ϵ): 419 (3.95) & 314 (4.01); FTIR (ν cm^{-1}): 3388 (OH), 2848 (N-CH₃), 1683 (C=O) & 1591 (C=N); 1H NMR (δ ppm): 12.44 (s, 1H, OH), 7.88 (s, 1H, Ar-H), 7.40-7.38 (d, J = 8 Hz, 4H, Ar-H), 7.02-6.88 (m, 2H, Ar-H), 6.34-6.32 (d, J = 8 Hz, 1H, Ar-H), 4.54 (s, 1H, CH), 3.18 (s, 3H, CH₃), 3.12 (s, 3H, CH₃); ^{13}C NMR (δ ppm): 162.83, 156.55, 150.43, 148.61, 147.49, 138.25, 131.48, 129.75, 129.21, 128.63, 127.58, 126.80, 124.52, 122.28, 120.82, 120.16, 112.46, 29.86, 29.02, 28.42; HRMS: m/z 482.2012 [M^+] & 484.2041 [$M^+ + 2$]; Anal. Calcd: C 54.79, H 3.34, N 8.71 %, Found: C 54.75, H 3.30, N 8.66 %.

4A.5. Electronic absorption study

The UV- Visible spectra of the newly synthesized compounds **4(a-e)** were recorded in six different solvents, such as methanol and ethanol as polar protic solvents, acetonitrile and DMSO as polar aprotic solvents, 1,4-dioxane and chloroform as nonpolar solvents in 10^{-5} M concentration using HR 4000 UV-Visible Spectrophotometer. The λ_{max} and molar absorption coefficient values were tabulated in **Table 1** and UV-Vis spectra of the compounds were displayed in **Fig. 3**. All the synthesized compounds exhibited two absorption maxima (λ_{max}) in the range of 305-414 nm in methanol, 300-416 nm in ethanol, 302-508 nm in acetonitrile, 311-543 nm in DMSO, 302-400 nm in 1,4-dioxane and 301-414 nm in chloroform due to the π - π^* & n - π^* transitions. Among six solvents, most of the compounds exhibited maximum bathochromic/redshift towards the longer wavelength in DMSO solvent. It indicates that, as the polarity of the solvent increases, the absorption maxima (λ_{max}) a shift towards a longer wavelength in the synthesized compounds. This is due to the effective interaction between the solvent molecules and the lone pair of electrons [30]. Apart from these, compound **4d** displayed a large redshift at 325 and 543 nm in DMSO solvent as compared to other compounds.

Table 1. Electronic absorption data of the synthesized compounds **4(a-e)** in six different solvents.

Compd.	Solvents											
	Methanol		Ethanol		Acetonitrile		DMSO		1, 4-dioxane		Chloroform	
	$\lambda_{\max}(\text{nm})$	Log ϵ	$\lambda_{\max}(\text{nm})$	Log ϵ	$\lambda_{\max}(\text{nm})$	Log ϵ	$\lambda_{\max}(\text{nm})$	Log ϵ	$\lambda_{\max}(\text{nm})$	Log ϵ	$\lambda_{\max}(\text{nm})$	Log ϵ
4a	306	4.11	300	3.84	302	4.03	311	4.01	302	3.98	301	3.80
	404	3.66	402	3.51	411	3.38	413	2.95	400	3.17	408	3.00
4b	315	4.06	321	4.11	307	4.06	318	4.11	302	4.02	323	4.23
	365	4.12	364	4.16	360	3.94	371	3.99	360	3.69	356	4.18
4c	305	3.99	321	4.04	321	4.02	318	4.17	309	4.13	322	4.20
	356	3.89	355	4.11	356	4.07	355	4.03	353	3.95	358	4.18
4d	308	3.98	311	4.15	316	4.20	325	4.14	309	4.08	316	4.18
	-	-	-	-	508	2.84	543	2.90	-	-	-	-
4e	307	4.13	309	4.19	304	4.07	314	4.01	307	4.07	307	4.14
	414	3.93	416	4.07	414	3.88	419	3.95	396	3.92	414	4.05

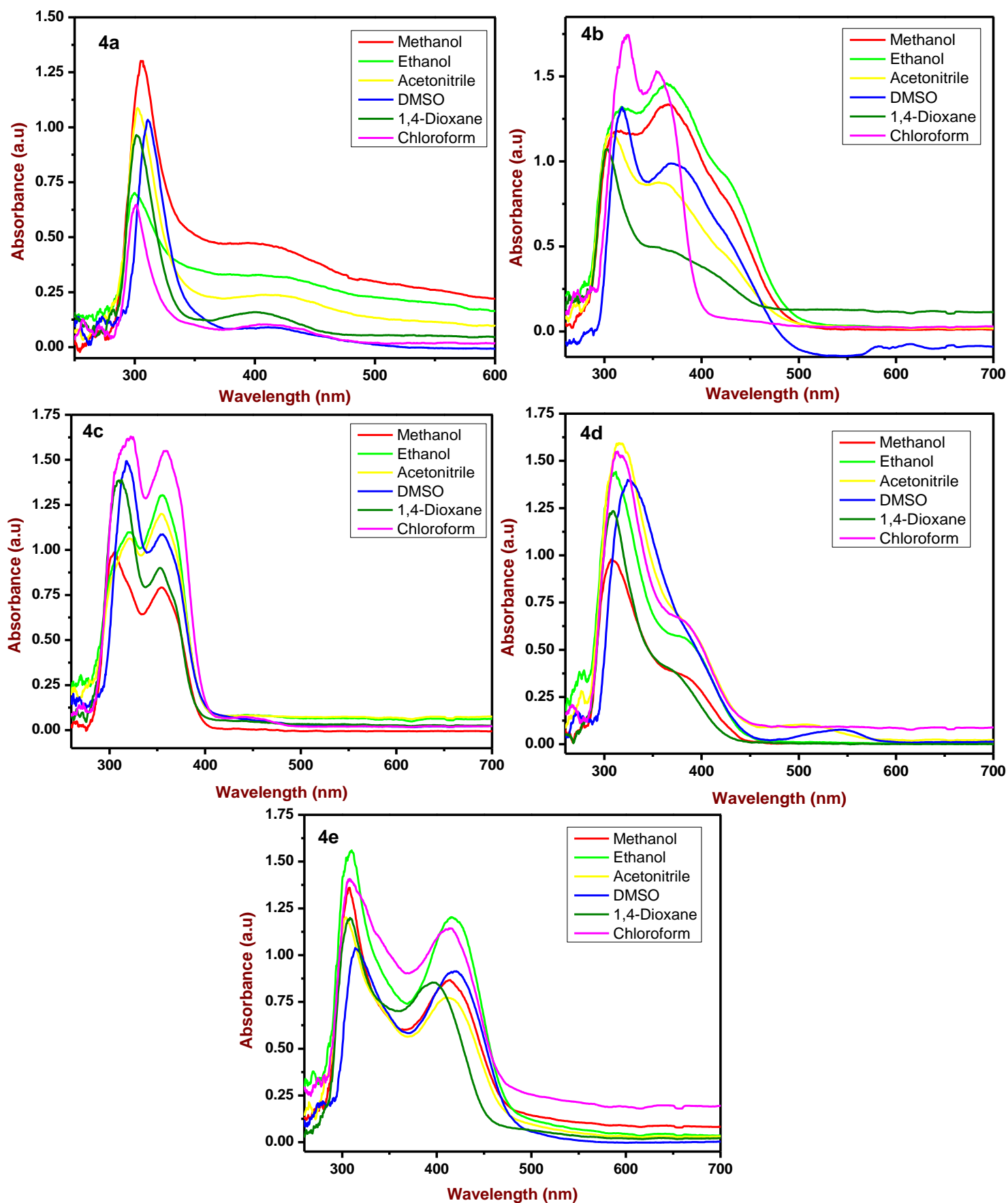


Fig. 3. A graph of UV-Visible spectra of the synthesized compounds **4(a-e)** in six different solvents.

4A.6. Powder-XRD analysis

In order to study the crystalline nature and lattice parameter of synthesized compounds have been evaluated using the powder X-ray diffraction method. The analysis has been done at the 2θ range of $5-80^\circ$ and wavelength 1.5406 \AA . The compound **4a** was selected for P-XRD analysis, it has 6 reflections at the range of $10-80^\circ$ with the intense peaks and lattice parameters are associated with compound and has been determined by the h, k and l of miller indices values [31]. The crystalline size was calculated using Debye-Scherrer Eq. (1). Where β is the full width at half maxima in radians, λ is the wavelength of $\text{CuK}\alpha$ X-ray radiation used ($\lambda = 0.154 \text{ nm}$) and θ is the Bragg's diffraction angle in degree [32].

$$D = 0.9\lambda/\beta\cos\theta \quad \text{--- (1)}$$

From the **Fig. 4**, the compound **4a** has sharp intense peaks at 100 to 210 , hence this confirm the crystalline in nature. It has six reflections with one intense peak at 200 ; hence this compound has monocyclic crystalline nature. Considering the intense peaks from the graph, the unit cell parameters and miller indices have been calculated and from the calculation, **4a** compound is monocyclic and crystalline in nature and results were listed in **Table 2**.

Table 2. Calculated Powder-XRD structural data of synthesized compound **4a**.

Compd.	Peak	2θ	$\theta/2$	$\text{Sin } \theta$	$\text{Sin}^2 \theta$	$\text{Sin}^2 \theta \times 1000$	$h^2+k^2+l^2$	h.k.l
4a	1	12.37	6.18	0.107	0.0115	11.58	1	100
	2	13.52	6.76	0.117	0.0138	13.85	1.19	100
	3	15.94	7.97	0.138	0.0192	19.22	1.66	110
	4	19.25	9.62	0.167	0.0279	27.92	2.40	111
	5	25.73	12.86	0.222	0.0495	49.53	4.2	200
	6	27.39	13.69	0.236	0.0560	56.01	4.8	210

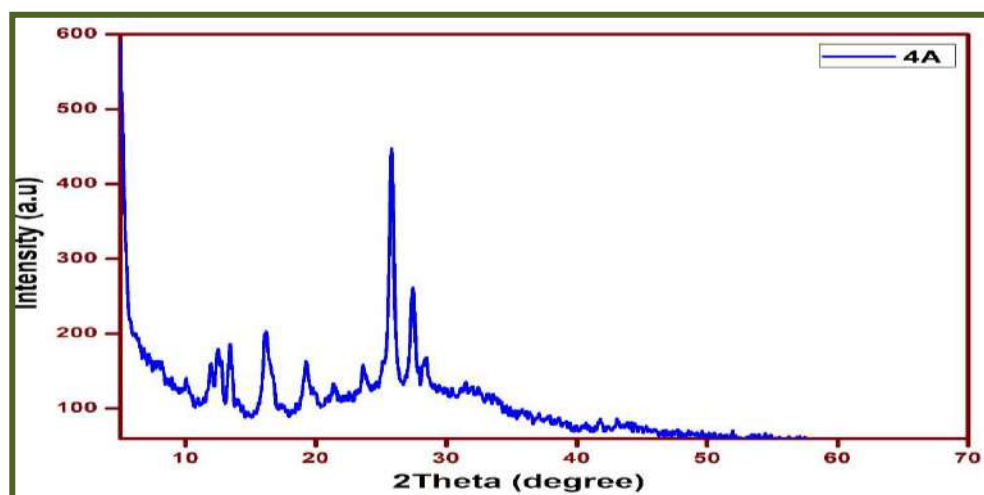


Fig. 4. A graph of Powder-XRD of synthesized compound **4a**.

4A.7. Pharmacological studies

4A.7.1. Cytotoxicity

In vitro cytotoxicity was evaluated by MTT assay method according to the procedure Kumbar *et. al.*, [33] against MCF-7 (Human breast cancer) cell line and anastrozole and folic acid was used as standard drugs for comparison. The detailed procedure has been explained in the experimental section 2B.5.2 of **Chapter-2B**.

4A.7.2. Anti-mycobacterial activity

The anti-mycobacterial activity of synthesized compounds was assessed against *M. tuberculosis* using the Micro Plate Alamar Blue assay (MABA) method as described by the reported literature [34] and detailed procedure has been explained in the experimental section 2A.5.2 of **Chapter-2A**.

4A.7.3. *in silico* analysis

In silico studies were performed to assess the therapeutic potentials of synthesized compounds as P38 MAP kinase and InhA-Enoyl-Acyl Carrier Protein Reductase inhibitors. In this avenue, the molecular interactions of synthesized compounds with P38 MAP kinase and InhA-Enoyl-Acyl Carrier Protein Reductase were assessed using molecular docking

studies. The structural alterations imposed by the synthesized compounds upon binding with target proteins were assessed using molecular dynamics simulation studies.

4A.7.4. Preparation of target molecules

The crystal structure of P38 MAP kinase (PDB ID: 1OUK) and InhA-Enoyl-Acyl Carrier Protein Reductase (PDB ID: 2X22) were acquired from Protein Data Bank (www.rcsb.org). The optimization of the protein was carried out using Autodock 4.2 tools. Briefly, the crystal structure of proteins was edited by removing the heteroatoms and adding with C-terminal oxygen, polar hydrogen and Kollman charges [35].

4A.7.5. Preparation of ligands

The 3D structures of synthesized compounds were prepared using Chems sketch v12.01 (ACD/labs). The structures were optimized and converted to .pdbqt format using open babel [36] and later utilized for molecular docking studies.

4A.7.6. Molecular Docking

The docking of synthesized compounds to the binding pocket of P38 MAP kinase and InhA-Enoyl-Acyl Carrier Protein Reductase was carried out by employing the Broyden-Fletcher-Goldfarb-Shanno algorithm implemented in the Autodock Vina program [37]. By using the co-crystallized structures, the substrate-binding site of each target was identified, and a grid box of dimensions 56 x 60 x 48 Å with X Y Z coordinates at 44.746, 34.234 and 32.603 was set for P38 MAP kinase and a grid box of dimensions 48 x 60 x 52 Å with X Y Z coordinates at -15.003, -35.911 and 14.697 was set for InhA-Enoyl-Acyl Carrier Protein Reductase, were generated, respectively. The Docking results were analyzed with Biovia Discovery Studio Visualizer 20.1.0 to compute the protein-ligand interactions.

4A.7.7. Molecular dynamic (MD) simulation

The molecular dynamics (MD) simulation studies detail the physical movement of atoms and molecules in a virtual environment. The MD simulations of protein-ligand complexes were studied for a duration of 50 ns by applying CHARMM36 all-atom force field [38] of GROMACS package [39], version 2018. Briefly, the simple point charge (SPC) model [40] was utilized to solvate the system and was neutralized using sodium or chloride ions. The energy minimization was done by the steepest descent method. V-rescale thermostat [41] in NVT ensemble and Parrinello Rahman barostat [42] in NPT ensemble were used to maintain a constant temperature (300 K) and pressure (1 bar). LINCS algorithm [43] and particle mesh ewald (PME) method [44] were applied to constrain the bond length and calculated electrostatic interactions, respectively. Finally, in the periodic boundary conditions (PBC), the generation of simulation trajectories for the individual complex was started at a time step of 1000 ps (1 ns) and run for a duration of 50000 ps (50 ns). The produced MD trajectories were analyzed using *gmx energy*, *gmx rms*, *gmx rmsf*, *gmx gyrate*, and *gmx sasa* modules of GROMACS. Further, the binding free energy components were calculated by employing the Molecular mechanics/Poisson-Boltzmann surface area (MMPBSA) module [45].

4A.7.8. DFT study

The geometry of compounds was optimized at the B3LYP/6-31G (d, p) level of theory. The quantum mechanical method gradient-correlated density functional theory (DFT) was used as the Becke three-parameter exchange functional and the Lee-Yang-Parr correlation functional (B3LYP) incarnation as implemented in the Spartan 20 professional software [46, 47].

4A.8. Results and discussion

4A.8.1. Cytotoxicity study

The *in vitro* cytotoxicity of the synthesized compounds **4(a-e)** was evaluated against MCF-7 cell line (**Fig. 5**). A graph describing the concentration versus survival fraction of the compounds was plotted (**Fig. 6**) and the results were expressed as the half-maximal inhibitory concentrations (IC₅₀) (**Table 3**). Standards anastrozole and folic acid exhibited an IC₅₀ value of 99.47±1.57 & 139.20±1.42 µg/mL respectively.

The cytotoxicity results suggested that, the test compounds have very good selectivity against the MCF-7 cell line and results revealed that, compounds **4c** & **4e** possessed significant cytotoxicity with IC₅₀ values of 4.44±0.20 & 1.34±0.31 µg/mL respectively, and they demonstrated cell viability at 6.25 µg/mL. Remaining compounds were displayed reliable selectivity with IC₅₀ value in the range of 25.44±2.64 to 182.70±13.15 µg/mL compared to reference standards anastrozole and folic acid. Presence of an additional phenyl nucleus in **4c** and an EW bromo group in **4e** was supposed to be the main reason for the superior activity of these compounds. Therefore, the tested compounds have very good selectivity against MCF-7 cell line as compared to reference standards.

Table 3. Percentage of cell viability against MCF-7 cell line of the synthesized compounds **4(a-e)**.

Compd.	Mean cell viability of MCF-7 Concentration in µg/mL							IC ₅₀ in µg/mL
	NC	6.25	12.5	25	50	100	200	
4a	100	92.58±1.01	86.12±1.35	80.62±1.68	77.03±1.35	64.35±1.01	44.97±2.02	182.70±13.15
4b		63.87±1.01	58.37±2.02	47.37±1.35	41.15±0.67	37.56±0.33	34.93±1.35	25.44±2.64
4c		49.88±2.08	43.43±1.44	39.43±1.07	36.32±0.73	33.73±0.33	31.58±0.67	4.44±0.20
4d		65.79±1.69	51.67±0.67	48.56±1.68	44.25±2.36	43.3±1.01	41.39±1.01	30.59±5.83
4e		46.45±0.74	42.34±0.33	40.28±0.67	38.54±0.36	37.08±0.33	35.64±1.68	1.34±0.31
Std^a		74.60±1.39	72.24±0.27	69.68±1.11	66.93±1.11	55.71±1.95	30.90±1.39	99.47±1.57
Std^b		85.82±1.11	82.48±0.83	78.15±1.38	74.01±1.67	61.02±0.56	36.61±0.55	139.20±1.42

Std^a- Anastrozole (AZ), **Std^b**- Folic acid (FA), **NC**- Negative control
Values are Mean ±SE, N=3, *P<0.01 vs. Control

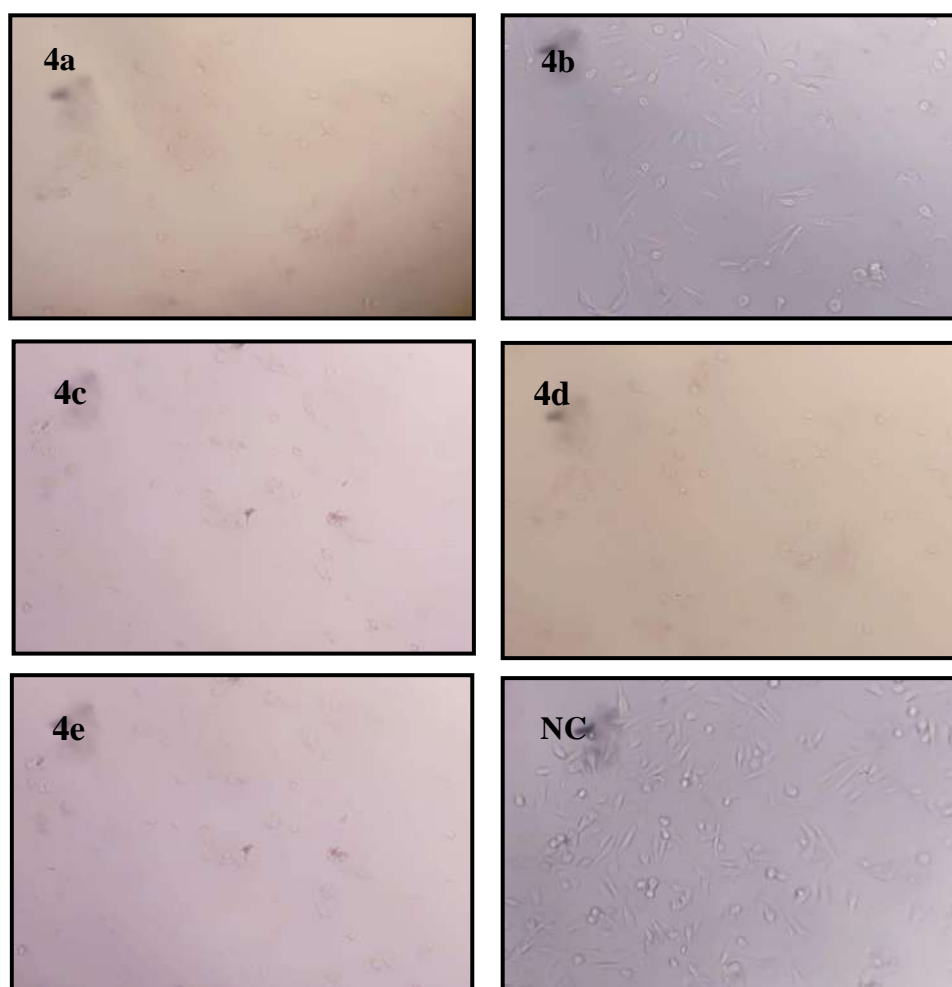


Fig. 5. Images of anticancer activity of the synthesized compounds **4(a-e)** and Negative control (**NC**).

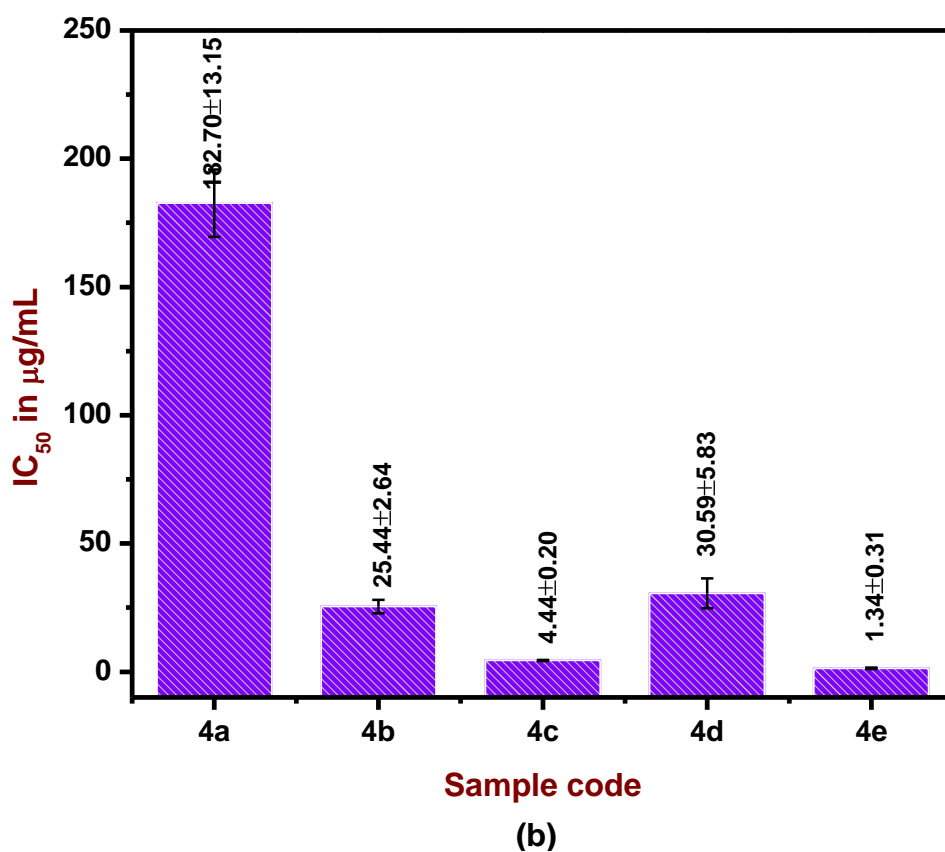
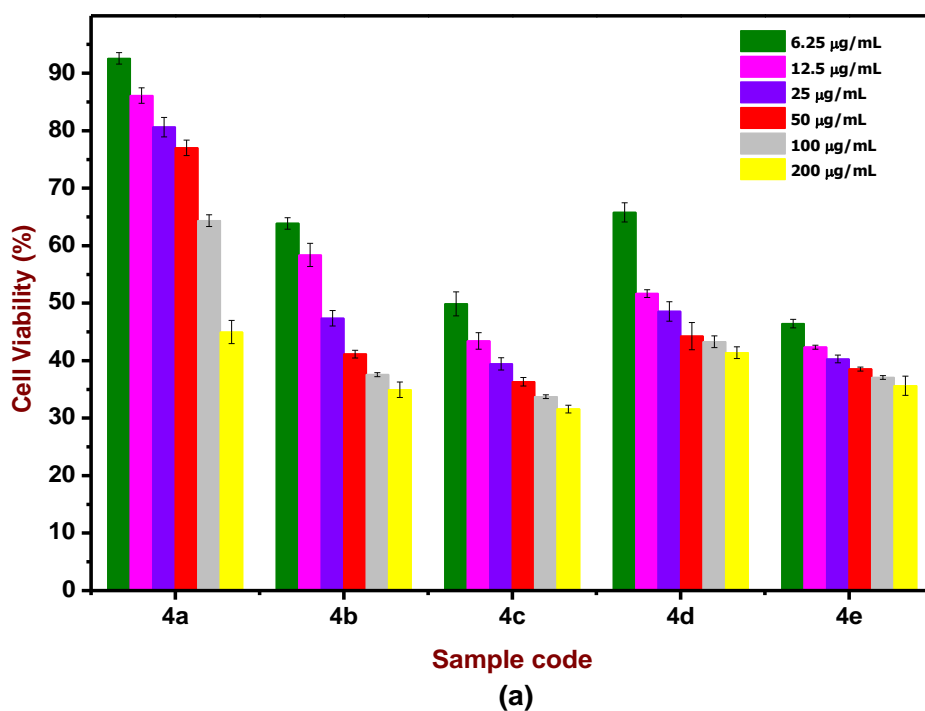


Fig. 6. A graph of % of survival cells of synthesized compounds **4(a-e)** at different concentration (a); a graph of IC₅₀ value of compounds **4(a-e)** against MCF-7 cell line (b).

4A.8.2. Anti-tubercular activity

The anti-TB activity of the synthesized compounds **4(a-e)** was evaluated against H37RV strain using five different reference standards (Isoniazid, Ethambutol, Pyrazinamide, Rifampicin & Streptomycin) showed MIC values at 1.6, 1.6, 3.12, 0.8, 0.8 $\mu\text{g/mL}$ respectively. The activity results suggested that, the compounds **4c** & **4d** exhibited higher sensitivity with MIC value of 12.5 $\mu\text{g/mL}$ and remaining compounds also displayed reliable sensitivity with MIC value range of 25-100 $\mu\text{g/mL}$ as compared to reference standards (**Table 4 and Fig. 7**). The presence of an additional phenyl nucleus in **4c** and EW nitro group in **4d** was supposed to be the main reason for the admirable anti-TB activity.

Table 4. Anti-tubercular activity results of synthesized compounds **4(a-e)**.

Compd.	Concentration in $\mu\text{g/mL}$							
	100	50	25	12.5	6.25	3.12	1.6	0.8
4a	S	R	R	R	R	R	R	R
4b	S	S	S	R	R	R	R	R
4c	S	S	S	S	R	R	R	R
4d	S	S	S	S	R	R	R	R
4e	S	S	S	R	R	R	R	R
Std^a	S	S	S	S	S	S	S	R
Std^b	S	S	S	S	S	S	S	R
Std^c	S	S	S	S	S	S	R	R
Std^d	S	S	S	S	S	S	S	S
Std^e	S	S	S	S	S	S	S	S

S-Sensitive, **R**-Resistant, **Std^a**- Isoniazid, **Std^b**- Ethambutol, **Std^c**- Pyrazinamide, **Std^d**- Rifampicin, **Std^e**- Streptomycin.

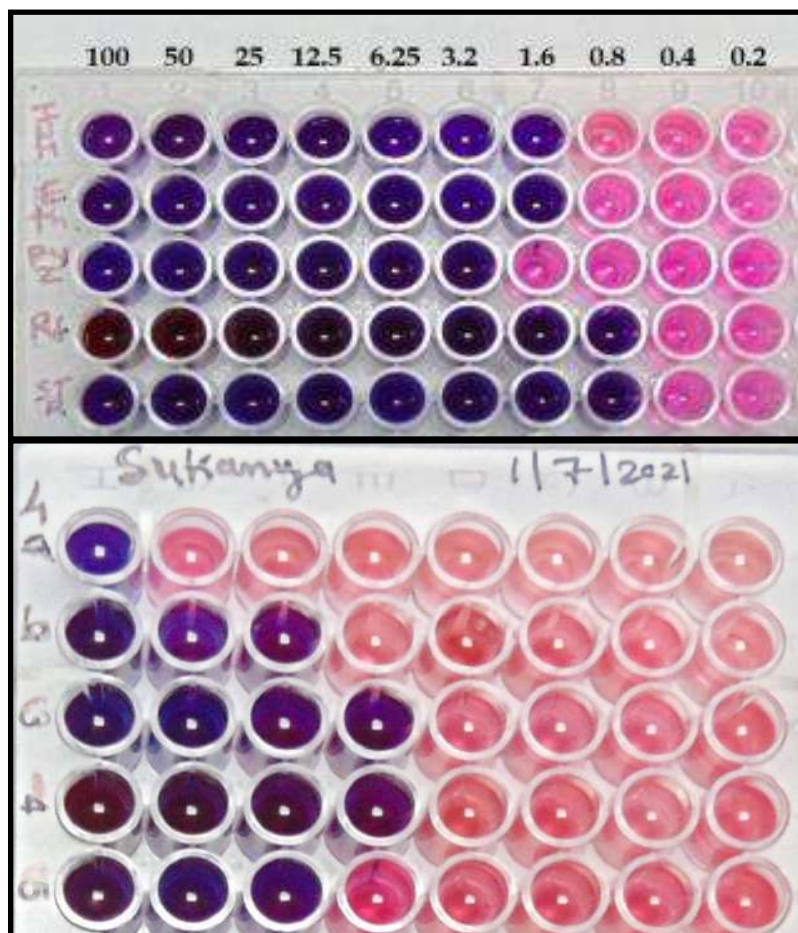


Fig. 7. Image of anti-TB activity results of the synthesized compounds **4(a-e)**.

4A.8.3. Structure-activity relationship (SAR)

The SAR study has been carried out for the newly synthesized compounds **4(a-e)**. All newly synthesized targets exhibited remarkable anticancer activity as compared to the standard drugs anastrozole and folic acid. Among the tested compounds **4c** & **4e** displayed outstanding IC_{50} values and promising cell viability at 6.25 $\mu\text{g}/\text{mL}$ concentration compared to other members of the series due to the presence of an additional phenyl nucleus in **4c** and an electron-withdrawing bromo group in **4e**, which is supposed to be the main reason for the superior activity of the compounds [48].

The anti-TB activity studies against H37RV strain revealed that, compounds **4c** & **4d** demonstrated better efficacy than other compounds. The compound **4c** possess an additional

phenyl nucleus, whereas **4d** possesses electron-withdrawing nitro group could be the possible reason for the improved activity profile of these compounds [49].

4A.8.4. *in silico* molecular docking study

The computational methods in drug discovery have gained enormous importance in the rational drug discovery pipeline. In recent times, new and improved methods have been developed to enhance accuracy and reliability [50]. In most computational drug discovery experiments, cellular targets are majorly exploited to explore the potential effects of test compounds. For example, the modification of cell death can be studied by measuring the mitochondrial respiration that indirectly correlates with cellular toxicity imposed by such compounds by inhibiting the activity of P38 MAPk protein [51, 52]. Similarly, InhA-Enoyl-Acyl Carrier Protein Reductase is a pivotal enzyme involved in the synthesis of mycolic acids (MA) [53]. Any alterations in the InhA gene result in resistance to first-line drugs such as isoniazid, making it a suitable target for drug discovery [54, 55]. The superior interaction displayed by the synthesized compounds with both the target proteins is primarily due to their structural and automatic composition [56]. Therefore, the most effectively interacting molecules were selected to assess their impact on the structural stability of their respective target proteins.

In this study, *in silico* molecular docking was performed to predict the most effective binding of obtained compounds with appropriate target enzymes (**Fig. 8**) [57, 58]. The synthesized compounds **4(b-e)** were docked into the binding pocket of P38 MAP kinase. Among the docked structures, compound **4c** demonstrated the most negative binding energy of -10.9 kcal/mol forming two hydrogen bonds with ARG149 and GLY170. The binding interactions were compared with Folic acid and Anastrozole which demonstrated binding energy of -8.7 and -7.0 kcal/mol respectively (**Table 5**). The interactions of synthesized compounds (**4c & 4d**) with InhA-Enoyl-Acyl Carrier Protein Reductase demonstrated that, **4c**

& **4d** interacted with the target protein with negative binding energy of -9.3 & -9.4 kcal/mol respectively (**Table 6**). The interactions were compared with Isoniazid (-5.8 kcal/mol), Pyrazinamide (-5.1 kcal/mol), Rifampicin (-8.0 kcal/mol) and Streptomycin (-8.4 kcal/mol) respectively.

Table 5. Molecular interactions between synthesized compounds **4(b-e)** & standards with P38 MAP kinase protein.

Compd.	Binding energy in kcal/mol	H-bonds	Interacting Residues
4b	-9.1	03	ARG70, GLY170, LEU171
4c	-10.9	02	ARG149, GLY170
4d	-8.4	03	ASP112, ASN115, MET109
4e	-8.8	-	-
Anastrozole	-7.0	03	TYR35, LYS53, MET109
Folic acid	-8.7	-	-

Table 6. Molecular interactions between synthesized compounds **4c, 4d** & standards with InhA-Enoyl-Acyl Carrier Reductase Protein.

Compd.	Binding energy in kcal/mol	H-bonds	Interacting Residues
4c	-9.3	-	-
4d	-9.4	-	-
Isoniazid	-5.8	02	VAL65, LEU63
Pyrazinamide	-5.1	05	ILE21, ALA22, SER94, GLY96, GLY14
Rifampicin	-8.0	04	ARG225, MET155, LEU268, LEU 217
Streptomycin	-8.4	05	GLY14, ILE15, PHE41, ILE95, SER94

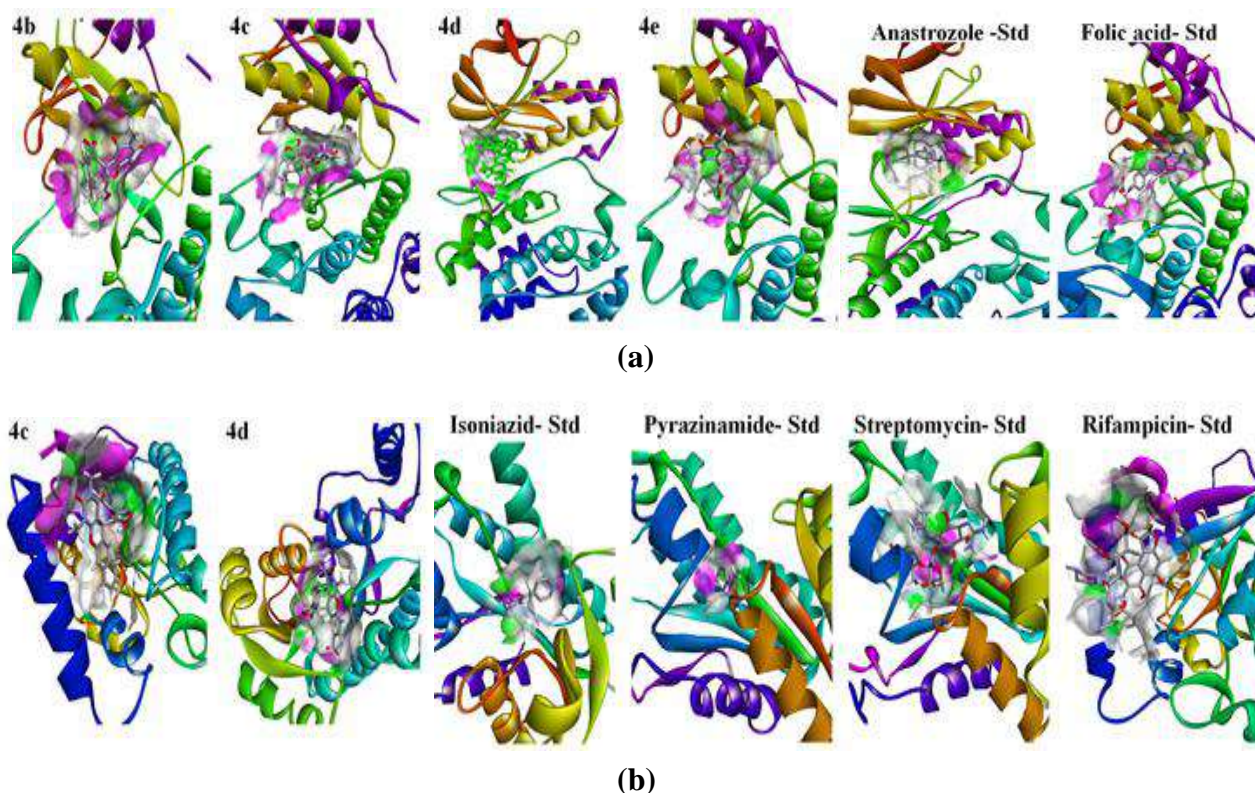


Fig. 8. Molecular interaction of synthesized compounds **4(b-e)** & standards with P38 MAP kinase **(a)**; **4c, 4d** & standards with InhA-Enoyl-Acyl Carrier Protein Reductase **(b)**.

4A.8.5. Molecular dynamics simulation

The conformational changes imposed by the test compounds upon binding with respective targets were assessed using MD simulations [59]. Among the docked structures, the structure with the most negative binding energy was selected for the MD simulation studies. Thus, the compound **4c** (-10.9 kcal/mol) bound structure of P38 MAP kinase was selected. The MD simulated structures displayed stable conformational changes acquired by the target protein upon binding with the ligand (**Fig. 9**). The relative potential energy can be used to compare conformations and configurations of the same molecular system. However, there will be no consideration of the entropic term in the calculation of the final MD value of the potential energy [60]. A general rule is that larger the relative potential energy more be the flexible or less stability. Therefore, the structural stability of the unbound and bound

structures was assessed by considering the root mean square deviations (RMSD) of C α atoms of the protein from their backbone and the root mean square fluctuations (RMSF) describing the fluctuations associated with the amino acid residues during the simulation [61]. Theoretically, a decreased RMSF represents decreased flexibility of the macromolecule or increased stability of the macromolecule. Likewise, reduced the Radius of gyration between the C α atoms indicates higher compactness or higher stability [62]. Similarly, a lower value of the protein SASA indicates lesser structural relaxation and hence higher protein stability [63]. Therefore, RMSD, RMSF, Rg and SASA analyses are used to measure the stability or flexibility of the macromolecule.

The average potential energy of the synthesized compound **4c** bound P38 MAP kinase structure was found to be -1.3326×10^{-6} kJ/mol, which was compared with anastrozole-bound (-1.2481×10^{-6} kJ/mol) and unbound structure (-1.2268×10^{-6} kJ/mol) (**Table 7**). The MD trajectory analysis for RMSD and RMSF revealed that, the synthesized compound **4c** stabilized the macromolecular structure as compared to free and anastrozole-bound structures. The RMS deviations are found to be within 0.2 nm with an average value of 0.1349 nm. There were no drastic conformational changes observed in the macromolecular structure throughout the simulation upon binding with compound **4c**. The results are compared with anastrozole-bound structure that has an average RMS deviation of 0.1797 nm. Lesser fluctuations were observed in terms of RMSF, indicating the macromolecule has attained conformational stability upon binding with the synthetic compound **4c**. The Radius of gyration (Rg) describes the packageability of the macromolecule. It is greatly influenced by the binding of ligand molecules [64], supporting the conformational changes acquired by the macromolecule upon binding with the ligand. The Rg plot showed a decreasing curve for ligand-bound and unbound structures, indicating that the macromolecule has folded itself into stable conformation as the simulation advanced. The average Rg value of 2.2240 nm for

compound **4c** bound structure indicated a tighter packageability as compared to unbound (2.2595 nm) and Anastrozole-bound structure (2.2413 nm). The conformational changes acquired by the macromolecule also influence the solvent-accessible surface area (SASA) of the surface residues. The SASA studies describe the contribution of hydrophobic interactions of nonpolar amino acids in attaining structural stability in the solvent environment [65]. The SASA studies corroborated the conformational stability as described by the Rg analysis.

Table 7. Calculated MD parameters of compound **4c** and **anastrozole** for native and ligand-bound P38 MAP kinase along with binding energies and the contributing energy terms calculated using *g_mmpbsa* module.

		P38 MAP kinase		
Gromacs Modules		Native Protein	Compound 4c	Anastrozole-Standard
	Potential Energy ($\times 10^{-6}$) (kJ/mol)	-1.2268	-1.3326	-1.2481
	RMSD (nm)	0.2583	0.1349	0.1797
	RMSF (nm)	0.1380	0.0725	0.0953
	Rg (nm)	2.2595	2.2240	2.2413
	SASA (nm ²)	181.286	176.292	178.809
MMPBSA Module	Binding Energy (kJ/mol)	-	-23.536	-60.137
	SASA Energy (kJ/mol)	-	-0.127	-13.744
	Polar Solvation Energy (kJ/mol)	-	-23.514	74.769
	Electrostatic Energy (kJ/mol)	-	0.310	-13.132
	van der WAALS Energy (kJ/mol)	-	-0.205	-108.03

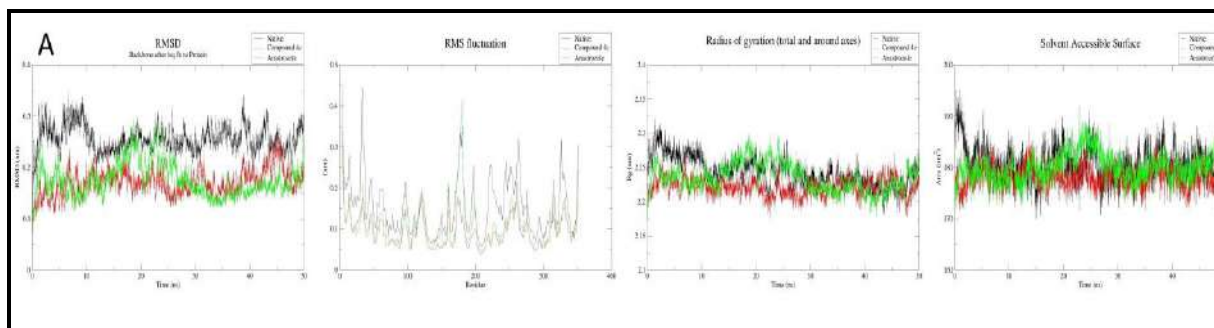


Fig. 9. RMSD, RMSF, Rg and SASA, plots obtained from MD trajectories analysis of **4c** and **anastrozole** for unbound and bound structures of P38 MAP kinase.

4A.8.6. DFT study

On the basis of distribution pattern of frontier molecular orbitals (FMOs), optical properties of the molecules and also their electronic properties were specified. It containing HOMO and LUMO, as well as the energy gap ($\Delta E = E_{HOMO} - E_{LUMO}$), were considered to be very effective parameters to understand the chemical reactivity, biological activity and kinetic stability of the molecules [66, 67]. The FMO orbitals & HOMO-LUMO energy gap of the compounds **4(a-e)** as shown in **Fig. 10**; electrostatic potential map explains the charge distribution on the molecules (**Fig. 11**), chemical functional descriptors (CFDs) are generally used to identify the hydrogen bonding donor and acceptors of the molecules (**Fig. 12**) and optimized structures of targets as shown in **Fig. 13**. Energy gap of the compounds were helps to understand the donor-acceptor interaction and intramolecular charge transfer (ICT) ability of synthesized compounds. Global reactivity parameters were calculated by using the following formulae.

$$I = -E_{HOMO} \quad (\text{Ionization energy})$$

$$A = -E_{LUMO} \quad (\text{Electron affinity})$$

$$\eta = 1/2 (I - A) \quad (\text{Chemical hardness})$$

$$\sigma = 1/\eta \quad (\text{Chemical softness})$$

$$\chi = 1/2 (I + A) \quad (\text{Electronegativity})$$

$$(\mu = -\chi) \quad (\text{Chemical potential})$$

$$\omega = \mu^2/2\eta \quad (\text{Electrophilicity index})$$

The calculated HOMO-LUMO energies and global reactivity parameters of the synthesized compounds **4(a-e)** are displayed in **Table 8**. A smaller HOMO-LUMO energy gap (ΔE) indicates a soft molecule, while a larger gap indicates a hard molecule. Lower energy gap, lesser chemical hardness, and more softness values indicate that molecule with more chemically and biologically active with low kinetic stability [68]. DFT results revealed

that, the energy gap (ΔE) of compounds **4(a-e)** in the range of 3.91 eV to 5.20 eV. Among them, the compound **4d** shows less energy gap (3.91 eV) and more softness value (0.51 eV). Hence, compound **4d** is chemically more reactive compared to other molecules. Also, the compound **4d** has more electronegative value (4.59 eV); hence, they tend to attract a bonding electron pair compared to other molecules.

Table 8. Chemical parameters of synthesized compounds **4(a-e)**.

Compd.	E_{HOMO} (eV)	E_{LUMO} (eV)	ΔE $E_{\text{HOMO}} - E_{\text{LUMO}}$ (eV)	I (eV)	A (eV)	η (eV)	σ (eV)	χ (eV)	μ (eV)	ω (eV)	D (Debye)
4a	-6.20	-1.00	5.20	6.20	1.00	2.6	0.38	3.6	-3.6	2.49	4.45
4b	-6.05	-0.93	5.12	6.05	0.93	2.56	0.39	3.49	-3.49	2.37	6.04
4c	-5.99	-1.45	4.54	5.99	1.45	2.27	0.44	3.72	-3.72	3.04	5.14
4d	-6.55	-2.64	3.91	6.55	2.64	1.95	0.51	4.59	-4.59	5.40	4.35
4e	-6.39	-1.21	5.18	6.39	1.21	2.59	0.38	3.8	-3.8	2.78	4.04

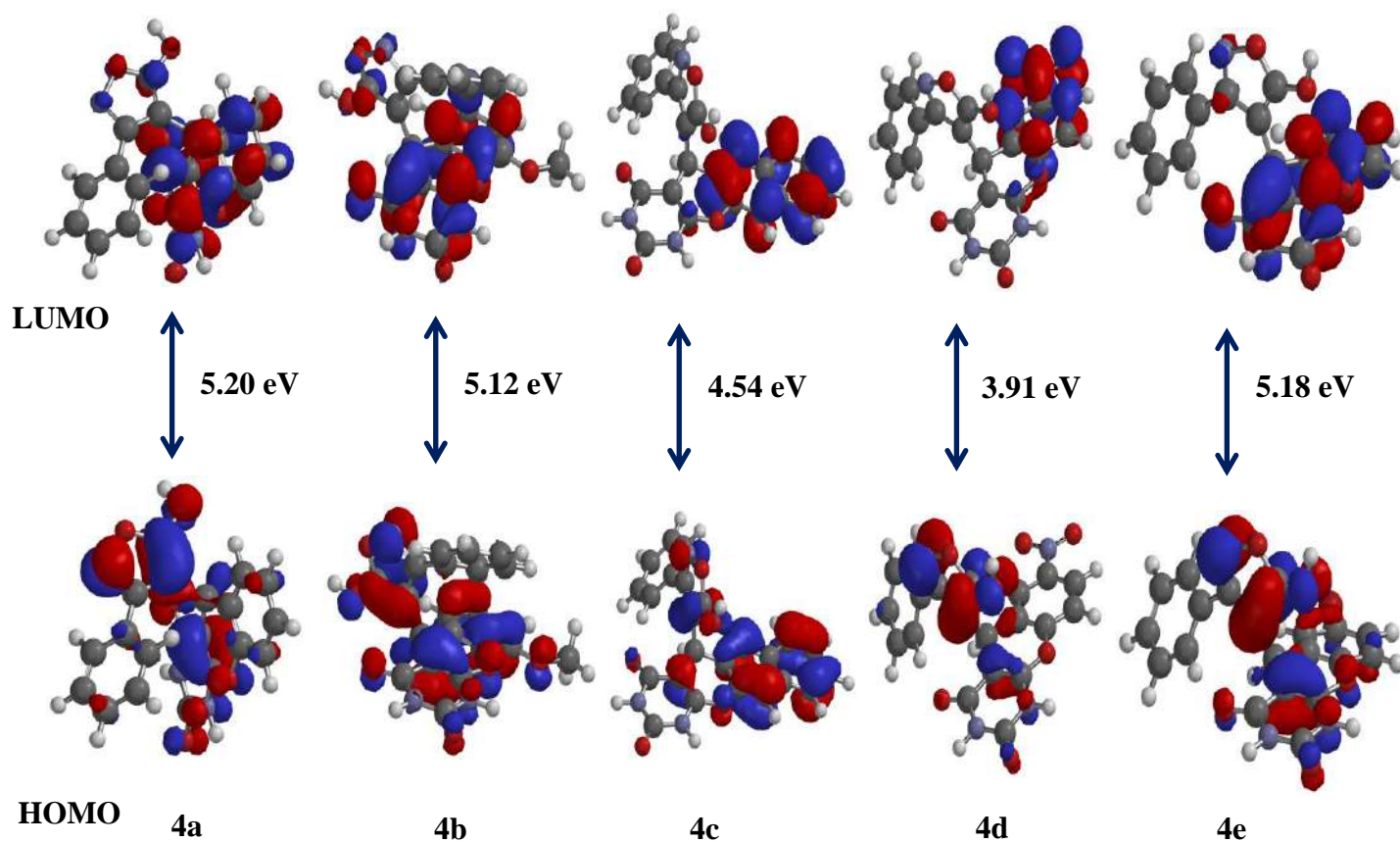


Fig. 10. FMO orbitals & HOMO-LUMO energy gap of the synthesized compounds **4(a-e)**.

4A.8.7. Molecular Electrostatic potential

The molecular electrostatic potential (MEP) explains the charge distribution on the molecules and it helps to identify the electrophilic and nucleophilic sites of the compounds. The MEP of obtained compounds **4(a-e)** was represented in **Fig 11**. The negative potential is expressed in red colour, which is the electron-rich region and acts as a nucleophilic centre of the compounds, and it is the vital region to form hydrogen bonds with proteins. The positive potential is expressed in the blue colour, which is the electron-deficient region and acts as the electrophilic centre of the compounds, and the green colour represents zero potential [69]. The negative potential is produced in the oxygen functionalities (C=O, OH and OCH₃) of the compounds [70]. This region is responsible for hydrogen bonding interaction and analysis proves that, the compound **4d** has a more electronegative value (4.59 eV) due to the presence of electron-withdrawing nitro group on the phenyl ring and an electron-donating hydroxyl group on isoxazole nucleus. Hence, these compounds have a greater tendency to attract a bonding electron pair as compared to other molecules.

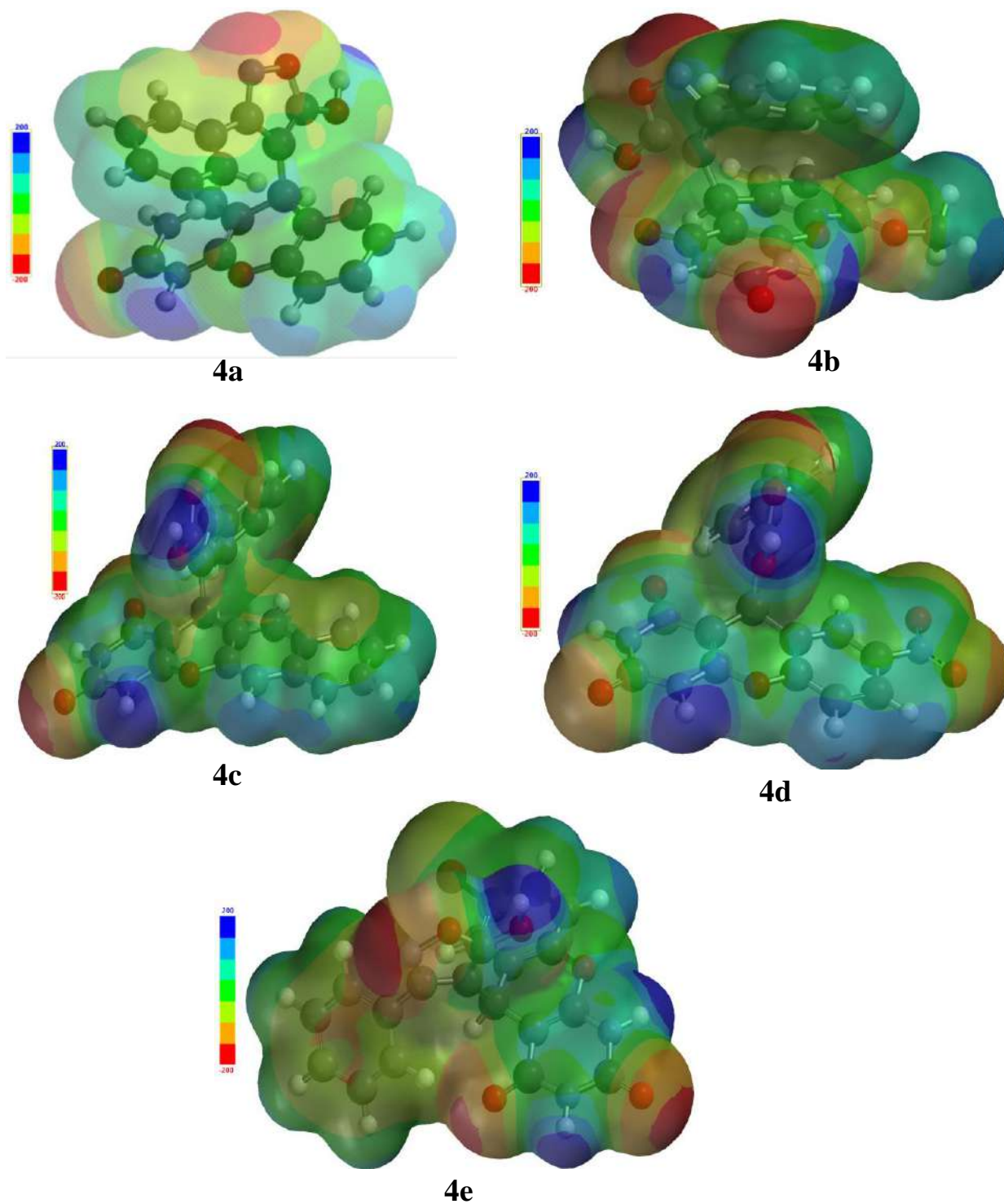


Fig. 11. Images of molecular electrostatic potential map (-200 to +200 kJ) of the synthesized compounds 4(a-e).

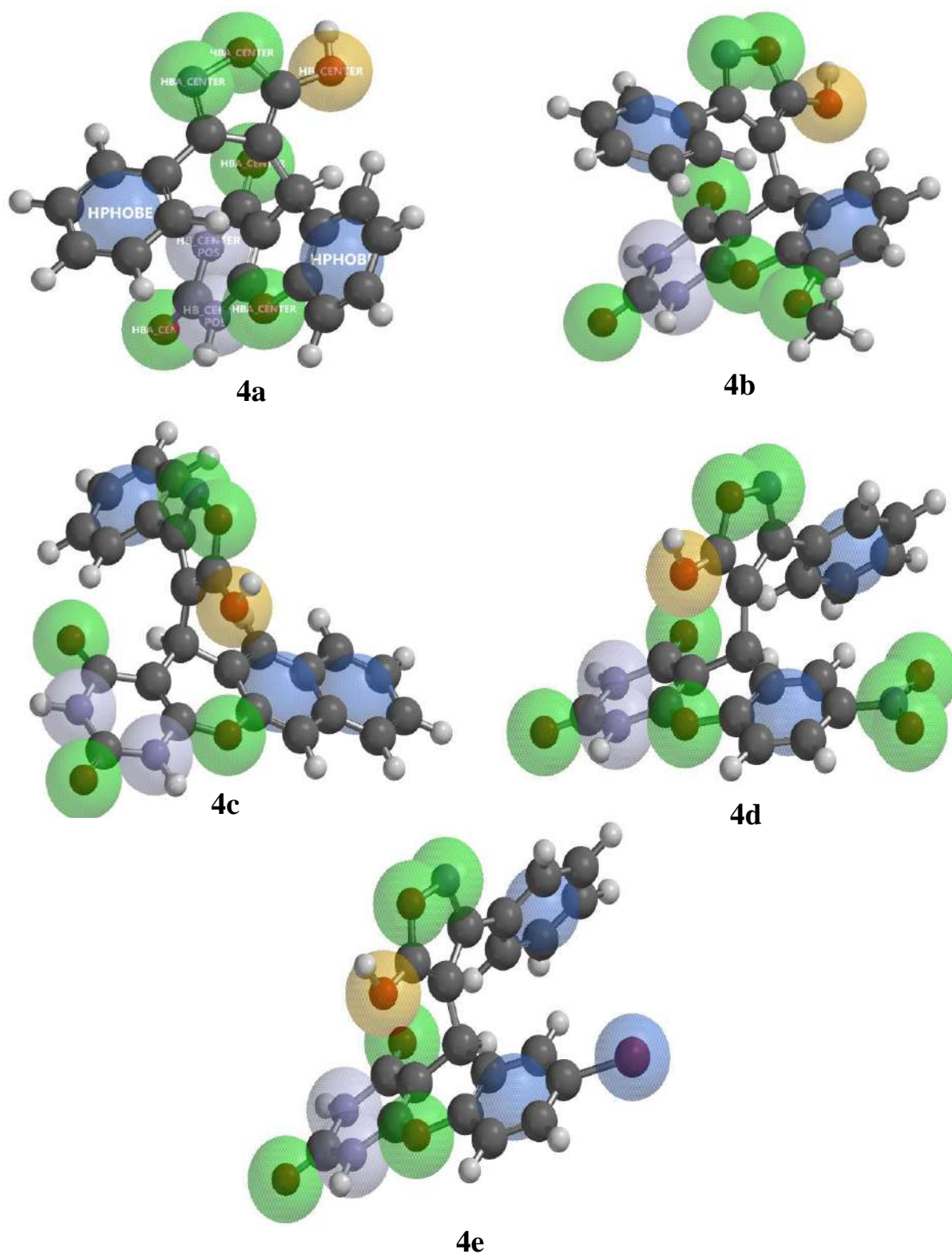


Fig. 12. Images of chemical functional descriptors (CFDs) of the synthesized compounds **4(a-e)**.

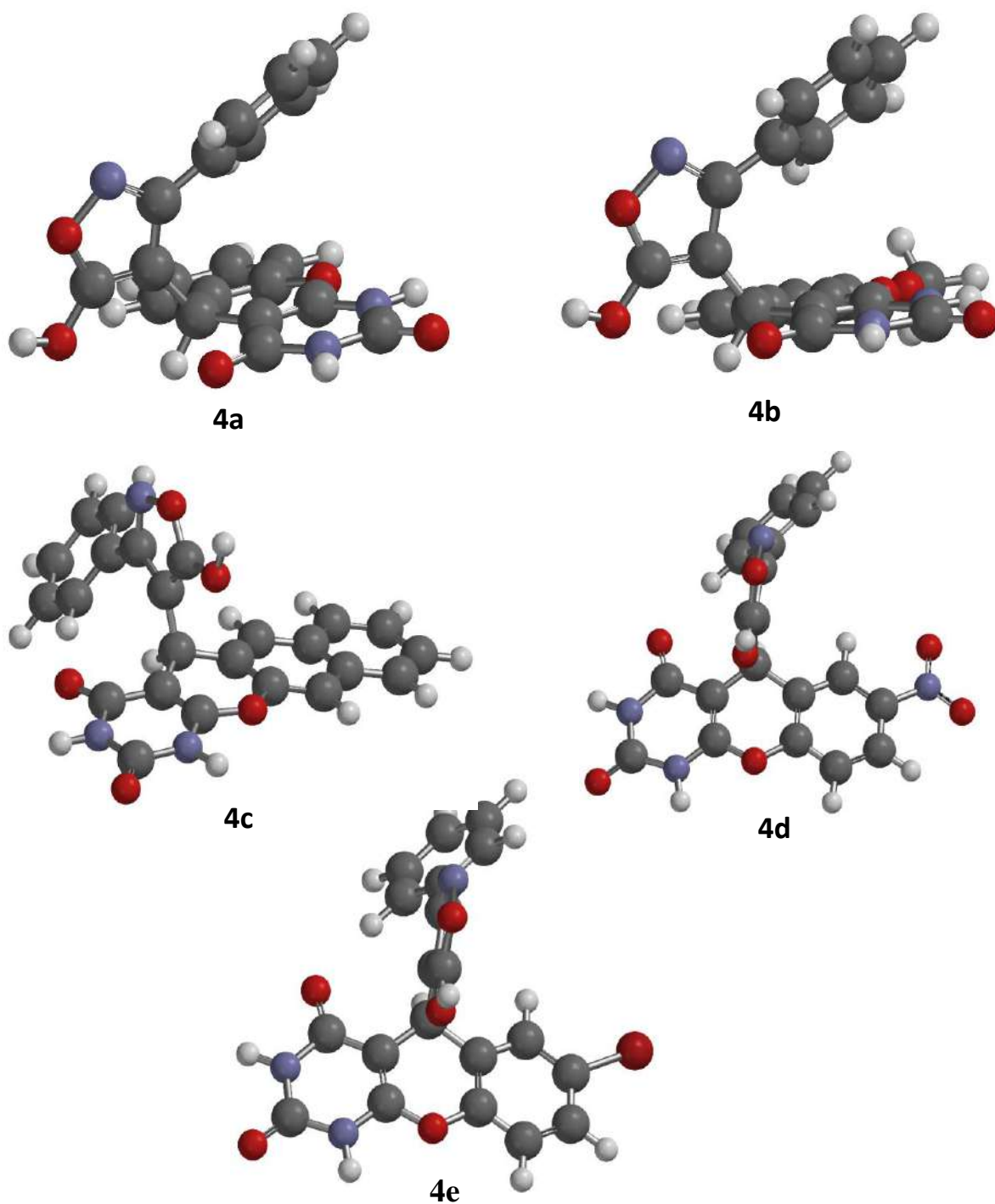


Fig. 13. Optimized structures of the synthesized compounds **4(a-e)**.

4A.9. Conclusion

In summary, we have developed an eco-friendly and concise method for the synthesis of some new substituted-(5-hydroxy-3-phenylisoxazol-4-yl)-1,3-dimethyl-1*H*-chromeno[2,3-*d*]pyrimidine-2,4(3*H*,5*H*)-dione derivatives and screened for pharmacological and computational investigations. From the absorption study, all the compounds exhibited a maximum bathochromic shift towards the longer wavelength in DMSO solvent. Compounds **4c** & **4e** possessed significant cytotoxicity with IC₅₀ value of 4.44±0.20 & 1.34±0.31 µg/mL respectively and compounds **4c** & **4d** showed good anti-TB sensitivity at 12.5 µg/mL as compared to reference standards. Moreover, the SAR study indicates the importance of an electron-withdrawing group and an additional phenyl nucleus in enhancing the biological potency of the synthesized compounds. Molecular docking study suggested that, compound **4c** showed least binding energy of -10.9 kcal/mol with P38 MAPk protein. From the DFT study, the synthesized compounds are chemically and biologically more reactive with low kinetic stability due to smaller energy gap.

4A.10. References

1. J. Rani, S. Kumar, M. Saini, J. Mundlia, P.K. Verma, *Res. Chem. Intermed.*, **2016**, 42, 6777-6804.
2. T. Rajamani & S. Muthu, *Spectrochim. Acta A Mol. Biomol. Spectrosc.*, **2013**, 115, 654-666.
3. S. Achelle & N. Ple, *Curr. Org. Synth.*, **2012**, 9, 163-187.
4. A.M. Farghaly, O.M. Aboul Wafa, Y.A. Elshaier, W.A. Badawi, H.H. Haridy, H.A. Mubarak, *Med. Chem. Res.*, **2019**, 28, 360-379.
5. R. Dudhe, P.K. Sharma, P. Verma, A. Chaudhary, *J. Adv. Sci. Res.*, **2011**, 2, 10-17.
6. M.A. Radwan, M.A. Alshubramy, M. Abdel-Motaal, B.A. Hemdan, D.S. El-Kady, *Bioorg. Chem.*, **2020**, 96, 1-44.
7. H. Rashid, M.A.U. Martines, A.P. Duarte, J. Jorge, S. Rasool, R. Muhammad, M.N. Umar, *RSC adv.*, **2021**, 11, 6060-6098.
8. S. Lahmidi, M. El Hafi, M. Boulhaoua, A. Ejjoummany, M. El Jemli, E.M. Essassi, J.T. Mague, *J. Mol. Struct.*, **2019**, 1177, 131-142.
9. M. Fares, S.M. Abou-Seri, H.A. Abdel-Aziz, S.E.S. Abbas, M.M. Youssef, R.A. Eladwy, *Eur. J. Med. Chem.*, **2014**, 83, 155-166.
10. Y. Ouyang, H. Yang, P. Zhang, Y. Wang, S. Kaur, X. Zhu, H. Wang, *Molecules*, **2017**, 22, 1-27.
11. M.S.K. Youssef, R.A. Ahmed, M.S. Abbady, S.A. Abdel-Mohsen, A.A. Omar, *Monatsh. Chem.*, **2008**, 139, 553-559.
12. J.P. Beck, M.A. Curry, R.J. Chorvat, L.W. Fitzgerald, P.J. Gilligan, R. Zaczek, G.L. Trainor, *Bioorg. Med. Chem. Lett.*, **1999**, 9, 1185-1188.
13. F. Bertucci & D. Birnbaum, *J. Biol.*, **2008**, 7, 1-4.
14. M.M. Ghorab, M.G. El-Gazzar, M.S. Alsaid, *Int. J. Mol. Sci.*, **2014**, 15, 5582-5595.
15. J. Akhtar, A.A. Khan, Z. Ali, R. Haider, M.S. Yar, *Eur. J. Med. Chem.*, **2016**, 125, 143-189.
16. I. Collins & P. Workman, *Nat. Chem. Biol.*, **2006**, 2, 689-700.
17. T. Zarubin & J. Han, *Cell Res.*, **2005**, 15, 11-18.
18. P. Maher, *J. Biol. Chem.*, **1999**, 274, 17491-17498.
19. S.J. Aditya Rao, S.M. Shivayogi, J.K. Satyanarayana, R.C. Kumaran, *Bioimpacts*, **2021**, 11, 187-197.

20. M.A. Khedr, M. Pillay, S. Chandrashekharappa, D. Chopra, B.E. Aldhubiab, M. Attimarad, O.I. Alwassil, K. Mlisana, B. Odhav, K.N. Venugopala, *J. Biomol. Struct. Dyn.*, **2018**, 36, 1-48.
21. A. Dutta & D. Sarma, *Tuberculosis*, **2020**, 124, 1-19.
22. O. Holas, P. Ondrejcek, M. Dolezal, *J. Enzyme Inhib. Med. Chem.*, **2015**, 30, 629-648.
23. S.R. Luckner, *J. Biol. Chem.*, **2010**, 285, 14330-14337.
24. G.M. Ziarani, F. Saidian, P. Gholamzadeh, A. Badiei, A.A. Soorki, *Iran. J. Chem. Chem. Eng.*, **2017**, 36, 39-48.
25. R.M. Naidu Kalla, R.S. Karunakaran, M. Balaji, I. Kim, *ChemistrySelect*, **2019**, 2, 644-649.
26. N. Poomathi, S. Mayakrishnan, D. Muralidharan, R. Srinivasan, P.T. Perumal, *Green Chem.*, **2015**, 17, 3362-3372.
27. S.T. Chung, W.H. Huang, C.K. Huang, F.C. Liu, R.Y. Huang, C.C. Wu, A.R. Lee, *Res. Chem. Intermed.*, **2016**, 42, 1195-1215.
28. D. Azarifar, M. Ghaemi, M. Jaymand, R. Karamian, M. Asadbegy, F. Ghasemlou, *Mol. Divers.*, **2022**, 26, 891-902.
29. H.M. Aly & M.M. Kamal, *Eur. J. Med. Chem.*, **2012**, 47, 18-23.
30. O. Nagaraja, Y.D. Bodke, I. Pushpavathi, S. Ravi Kumar, *Heliyon*, **2020**, 6, 1-11.
31. K. Upendranath, T. Venkatesh, Y.A. Nayaka, M. Shashank, G. Nagaraju, *Inorg. Chem. Commun.*, **2022**, 139, 1-14.
32. G. Ramesh, S. Daravath, N. Ganji, A. Rambabu, K. Venkateswarlu, *J. Mol. Struct.*, **2020**, 1202, 1-41.
33. S.H. Sukanya, T. Venkatesh, S.R. Kumar, Y.D. Bodke, *Chem. Data Collect.*, **2021**, 33, 1-16.
34. S. Raghavendra, S.J. Aditya Rao, Vadlapudi Kumar, C.K. Ramesh, *Comput. Biol. Chem.*, **2015**, 59, 1-20.
35. S.J. Aditya Rao, T. Venugopal, N. Jayanna, M. Paramesha, C. Ramesh, *Lett. Drug Des. Discov.*, **2021**, 18, 445-453.
36. N.M.O. Boyle, M. Banck, C.A. James, C. Morley, T. Vandermeersch, G.R. Hutchison, *J. Cheminformatics*, **2011**, 3, 1-14.
37. O. Trott and A.J. Olson, *J. Comput. Chem.*, **2010**, 31, 455-461.
38. R.B. Best, X. Zhu, J. Shim, P.E.M. Lopes, J. Mittal, M. Feig, A.D. MacKerell, *J. Chem. Theory Comput.*, **2012**, 8, 3257-3273.

39. M.J. Abraham, T. Murtola, R. Schulz, S. Pall, J.C. Smith, B. Hess, E. Lindahl, *SoftwareX*, **2015**, 1, 19-25.
40. H.J.C. Berendsen, J.P.M. Postma, W.F. Van Gunsteren, J. Hermans, *Forces*, **1981**, 331-342.
41. G. Bussi, D. Donadio, M. Parrinello, *J. Chem. Phys.*, **2007**, 126, 1-8.
42. M. Parrinello and A. Rahman, *J. Appl. Phys.*, **1981**, 52, 7182-7190.
43. B. Hess, H. Bekker, H.J.C. Berendsen, J.G.E.M. Fraaije, *J. Comput. Chem.*, **1997**, 18, 1463-1472.
44. U. Essmann, L. Perera, and M.L. Berkowitz, T. Darden, H. Lee and L.G. Pedersen, *J. Chem. Phys.*, **1995**, 103, 8577-8593.
45. R. Kumari, R. Kumar, O.S.D.D. Consortium, A. Lynn, *J. Chem. Inf. Model*, **2014**, 54, 1951-1962.
46. A. Pandith, C. Dasagrandhi, H.R. Kim, H.S. Kim, *Sens. Actuators B Chem.*, **2017**, 1-37.
47. A. Pandith, A. Kumar and H.S. Kim, *RSC Adv.*, **2015**, 1-25.
48. K. Kaur & V. Jaitak, *Anti-Cancer Agents in Med. Chem.*, **2019**, 19, 962-983.
49. R.S. Keri & S.A. Patil, *Biomed. Pharmacother.*, **2014**, 68, 1161-1175.
50. S.J. Aditya Rao, C.K. Ramesh, S. Raghavendra, M. Paramesha, *Curr. Comput. Aided Drug Des.*, **2020**, 16, 231-237.
51. P. Maher, *J. Biol. Chem.*, **1999**, 274, 17491-17498.
52. S.H. Sukanya, T. Venkatesh, S.J. Aditya Rao, M.N. Joy, *J. Mol. Struct.*, **2021**, 1247, 1-13.
53. A. Dessen, A. Quemard, J.S. Blanchard, W.R. Jacobs, Jr. and J.C. Sacchettini, *Science*, **1995**, 267, 1638-1641.
54. S.K. Halder and F. Elma, *J. Clinical Tuberculosis and Other Mycobacterial Diseases*, **2021**, 24, 1-15.
55. H.M.A. Hameed, M.M. Islam, C. Chhotaray, C. Wang, Y. Liu, Y. Tan, X. Li, S. Tan, V. Delorme, W.W. Yew, J. Liu, T. Zhang, *Front. Cell. Infect. Microbiol.*, **2018**, 8, 1-21.
56. G. Schneider, *Adaptive Systems in Drug Design*, **2002**, 115-145.
57. M.D. Kavitha, K.G. Mallikarjun Gouda, S.J. Aditya Rao, T.S. Shilpa, N.P. Shetty, Ravi Sarada, *Biotechnol. Lett.*, **2019**, 41, 91-106.
58. K.N. Venugopala, S. Chandrashekharappa, *J. Enzyme Inhib. Med. Chem.*, **2021**, 36, 1472-1487.
59. S.J. Aditya Rao and P. Nandini Shetty, *Life Sci.*, **2021**, 281, 1-11.

-
60. M. Levitt, M. Hirshberg, R. Sharon, V. Daggett, *Comput. Phys. Commun.*, **1995**, 91, 215-231.
 61. K. Malathi, A. Anbarasu and S. Ramaiah, *J. Biomol. Struct. Dyn.*, **2019**, 37, 4601-4613.
 62. M.B. Boroujeni, M.S. Dastjerdeh, M.A. Shokrgozar, H. Rahimi, E. Omidinia, *Inform. Med. Unlocked*, **2021**, 23, 1-9.
 63. A. Damjanovic, B.R. Brooks and E.B. Garcia-Moreno, *J. Phys. Chem.*, **2011**, 115, 4042-4053.
 64. V. Gramany, F.I. Khan, A. Govender, K. Bisetty, S. Singh, K. Permaul, *J. Biomol. Struct. Dyn.*, **2016**, 34, 1681-1692.
 65. X. Zhang, J. Yan, H. Wang, Y. Wang, J. Wang, D. Zhao, Molecular docking, *J. Biomol. Struct. Dyn.*, **2021**, 39, 1189-1202.
 66. A. Ali, M. Khalid, M.F. Rehman, S. Haq, A. Ali, M.N. Tahir, M. Ashfaq, F. Rasool, and A.A.C. Braga, *ACS Omega*, **2020**, 5, 15115-15128.
 67. C. Ooretir, N. Kaniskan, *Recent Experimental and Computational Advances in Molecular Spectroscopy*, **1993**, 351-367.
 68. J. George, J.C. Prasana, S. Muthu, T.K. Kuruvilla, S. Savanthi, R.S. Saji, *J. Mol. Struct.*, **2018**, 1171, 268-278.
 69. F. Erdemir, D.B. Celepci, A. Aktas, Y. Gok, *J. Mol. Struct.*, **2020**, 1204, 1-25.
 70. R. Kavitha, S. Nirmala, R. Nithyabalaji, R. Sribalan, *J. Mol. Struct.*, **2020**, 1204, 1-32.

4B.1. Introduction

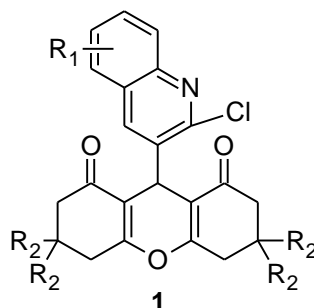
Isoxazole is an important heterocyclic nucleus, commonly found in various pharmacologically active natural products, clinical drugs and lead compounds [1]. Isoxazole derivatives are paid attention to the development of heterocyclic chemistry due to their broad spectrum of biological activities such as antimicrobial [2], anticancer [3], anti-HIV [4], anti-tuberculosis [5], anti-inflammatory [6], neuroprotective [7], anti-diabetic [8] and antidepressant activities [9]. On the other hand, isoxazole and its derivatives have also been recognized as important and useful synthons in organic synthesis [10, 11] and as organic materials in optoelectronics [12, 13].

Pyran is an oxygen-containing heterocyclic compound found in various natural products as well as synthetic drugs such as coumarins, benzopyrans, sugars, flavonoids, xanthenes, β -lapachone, Zanamivir and Laninamivir etc., [14, 15]. A literature survey revealed that, benzopyrans and fused pyran-based bio-active structural moieties, which exhibits various pharmacological uses such as antiviral [16], anticonvulsant [17], antimicrobial [18], antileishmanial [19], antiproliferative [20], anti-HIV [21], anti-TB [22], antifungal [23], anti-diabetic [24] and also act as inhibitors [25] etc. Because of wide range of pharmacological applications, contraction of bio-active isoxazole and pyran moieties are an important goal for chemists.

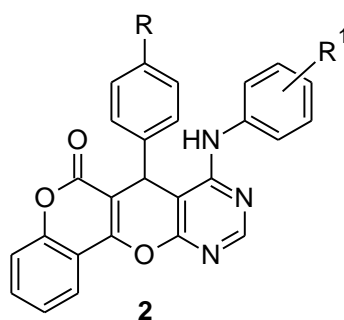
Density functional theory (DFT) was used to study the quantum-mechanical (QM) method, electronic structure of atoms, molecules and solids [26]. Furthermore, FMO analysis can provide important information about electronic properties, chemical reactivity, biological activity and kinetic stability of the molecules [27]. The HOMO and LUMO of compounds were helpful in determining various global reactivity parameters, donor-acceptor interaction and intramolecular charge transfer (ICT) ability of compounds [28, 29]. Hence, we subjected the synthesized compounds to DFT studies to examine the chemical reactivity, biological and

kinetic stability of the compounds. Some of the reported biologically active heterocyclic compounds have been discussed below.

V. Krishnakumar *et al.*, reported a series of 3,4,6,7-tetrahydro-9-(1,2-dihydro-2-oxoquinolin-3-yl)-2*H*-xanthene-1,8(5*H*,9*H*)-diones (**1**), it offers a catalyst free cascade-tandem reaction with high yield and operational simplicity [30].



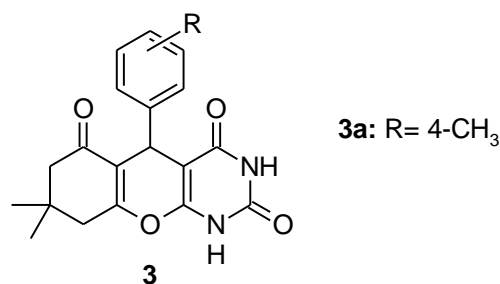
In 2017, L. Suresh and his co-workers reported a chromenopyrano[2,3-*d*]pyrimidine derivatives (**2**) and evaluated their antibacterial activity. Compounds **2a** and **2b** were identified as lead molecules due to the presence of EW NO₂ group in ring structure, which established promising activity against bacterial strains *S. aureus* and *B. subtilis* with MIC of 15.6 & 31.2 µg/mL respectively [31].



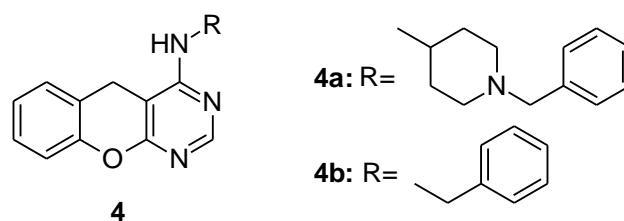
2a: R= CH₃, R¹= 3-NO₂

2b: R= CH₃, R¹= 4-NO₂

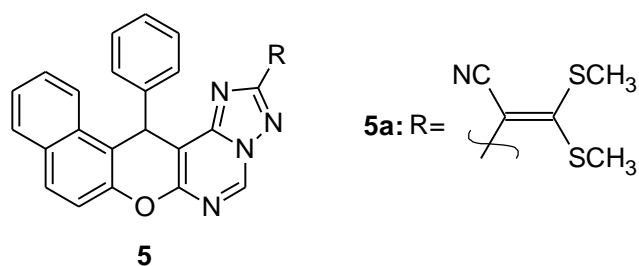
In 2020, A. Singh *et al.*, synthesized a series of chromeno-pyrimidine derivatives (**3**) and reported as potential corrosion inhibitors. **3a** shows effective corrosion inhibition with efficiency of 96.4 % at 200 mg/mL concentration [32].



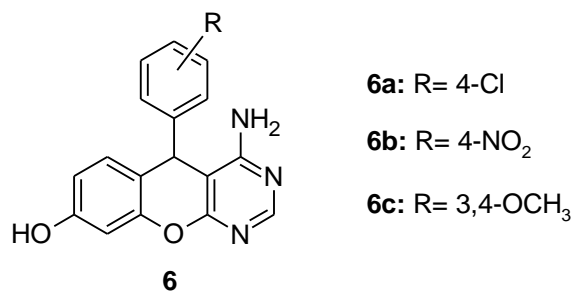
In 2010, a series of novel chromeno[2,3-*b*]-pyrimidine derivatives (**4**) was synthesized by U.S. Rai *et. al.*, and screened for antimicrobial activity. Compounds, **4a** & **4b** showed excellent antibacterial activity with MIC value of 1.612 µg/mL against *S. aureus* bacteria as compared to the standard drug Ceftriaxone (3.125 µg/mL) [33].



F.S. Abu and co-workers reported a novel substituted chromenotriazolo[1,5-*c*]pyrimidine derivatives (**5**) and designed as potential anti-proliferative agents. In that, compound **5a** had significant and selective anti-proliferative activity against liver and breast cell lines with IC₅₀ values of 9.23±0.9 and 10.25±1.0 µM respectively [34].



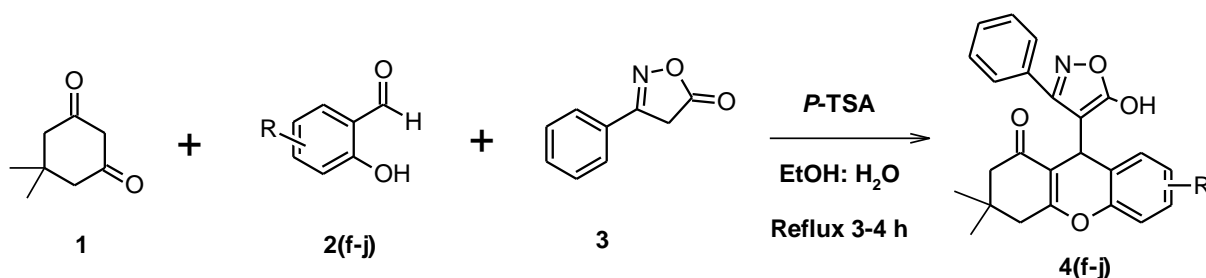
S. Poola *et. al.*, reported a pyrano[2,3-*d*] pyrimidine derivatives (**6**) and screened for their antioxidant and antimicrobial activity. The compounds **6a** & **6b** exhibited higher free radical scavenging activity with IC₅₀ value of 36.82±1.38 & 34.42±1.21 µg/mL respectively. Compound **6c** showed higher antibacterial activity of 21, 19, 19 & 20 mm against *B. subtilis*, *S. aureus*, *P. aeruginosa* & *E. coli* respectively at concentration of 100 µg/mL [35].



In this avenue, the current study aims to synthesize novel substituted-(5-hydroxy-3-phenylisoxazol-4-yl)-3,3-dimethyl-2*H*-xanthen-1(9*H*)-one derivatives and evaluate some of their computational and biological activities (cytotoxicity and anti-TB). Also, the study was extended to predict the binding interactions of synthesized molecules against target enzymes P38 MAP kinase and InhA-Enoyl-Acyl Carrier Protein Reductase proteins along with their structural stability assessment using molecular dynamics (MD) simulations.

4B.2. Present work

This chapter contains a novel substituted-(5-hydroxy-3-phenylisoxazol-4-yl)-3,3-dimethyl-2*H*-xanthen-1(9*H*)-one derivatives **4(f-j)** was synthesized by the reaction of dimedone (**1**) with substituted salicylaldehyde/2-hydroxy-nepthaldehyde (**2**) and 3-phenyl-5-isoxazolone (**3**) in aqueous ethanol using *p*-TSA as a catalyst. The synthetic route of the synthesized compounds has been shown in **Scheme 5**.



Compd.	R
4f	H
4g	3-OCH ₃
4h	C ₄ H ₄
4i	5-NO ₂
4j	5-Br

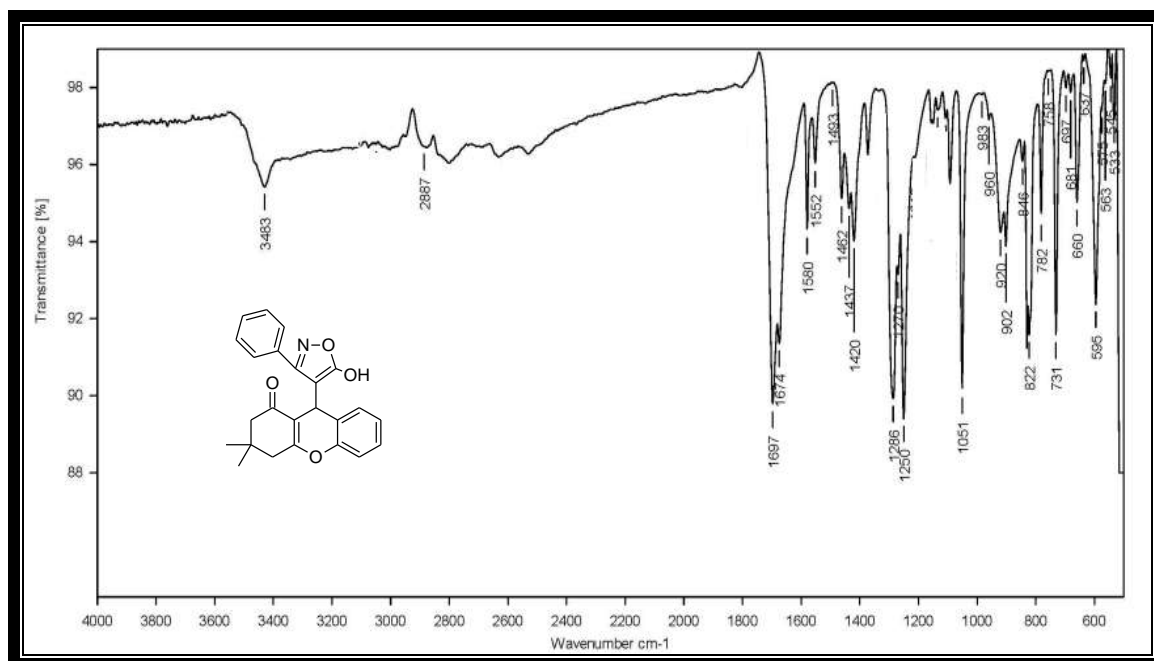
Scheme 5. Synthesis of substituted-(5-hydroxy-3-phenylisoxazol-4-yl)-3,3-dimethyl-2*H*-xanthen-1(9*H*)-one derivatives **4(f-j)**.

Further, the structures of newly substituted-(5-hydroxy-3-phenylisoxazol-4-yl)-3,3-dimethyl-2*H*-xanthen-1(9*H*)-one derivatives **4(f-j)** were confirmed by recording their IR, ¹H NMR, ¹³C NMR and Mass spectral data.

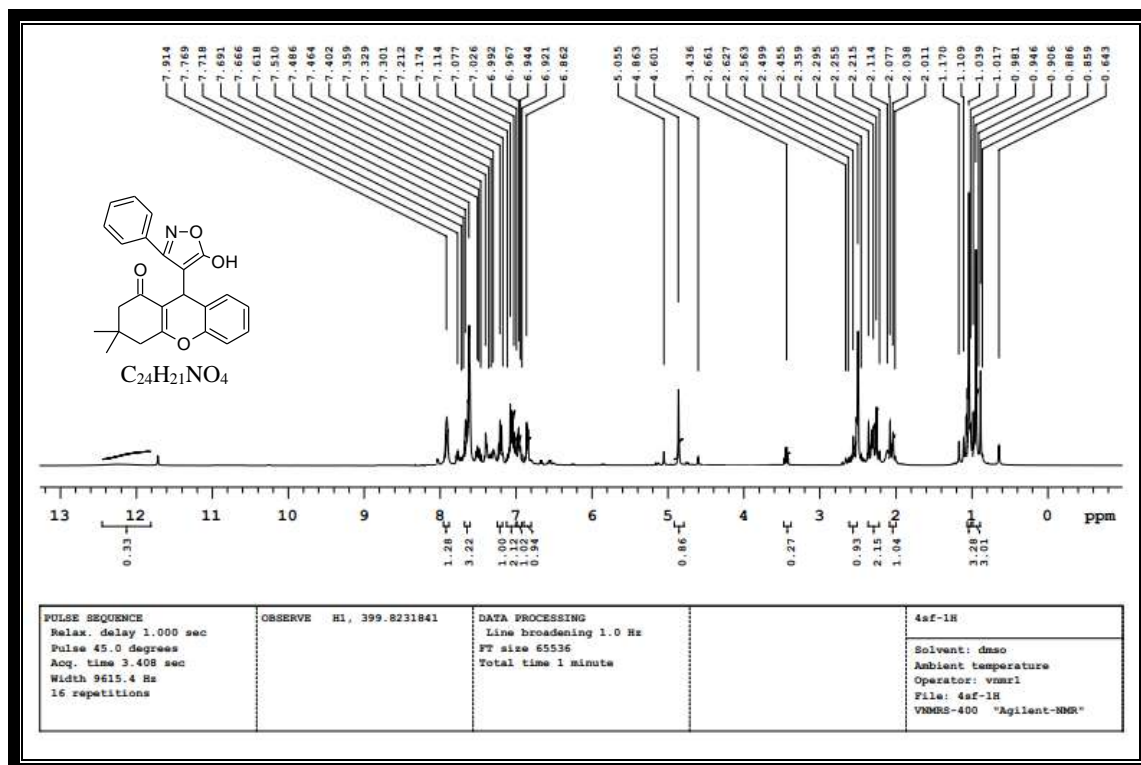
The IR spectrum of compound **4g** showed the absorption band in the region of 3464 cm⁻¹ is attributed to the OH stretching vibration, 2854 cm⁻¹ correspond to OCH₃ functionality and the absorption band at 1763 cm⁻¹ correspond to the stretching vibration of the carbonyl group (C=O). Another stretching vibrational band at 1599 cm⁻¹ correspond to the C=N group. The ¹H NMR spectrum of compound **4g** exhibited a singlet peak at δ 12.23 ppm due to OH proton of isoxazolone nucleus (s, 1H, OH), two singlet peaks at δ 7.94 & 7.62 ppm corresponds to five aromatic protons (s, 5H, Ar-H). A doublet peak at δ 6.96-6.94, 6.90-6.88 & 6.37-6.35 ppm corresponds to three aromatic protons (d, *J*= 8 Hz, 3H, Ar-H). A singlet peak at δ 4.84 ppm due to CH proton (s, 1H, CH) and another singlet at 3.81 ppm due to methoxy protons (s, 3H, OCH₃). Four singlet peaks at 2.52, 2.29, 2.25 & 2.09 ppm corresponds to CH₂ protons (s, 4H, CH₂) and another two singlet peaks at δ 1.04 and 0.96 ppm corresponds to methyl protons (s, 6H, CH₃). In addition, the ¹³C NMR spectrum of compound **4g** exhibited peak at δ 165.86 ppm which correspond to carbonyl carbon and peaks at δ 55.65 ppm due to OCH₃, 50.22 & 40.61 due to CH₂, 31.53 & 28.71 ppm due to CH₃ carbons.

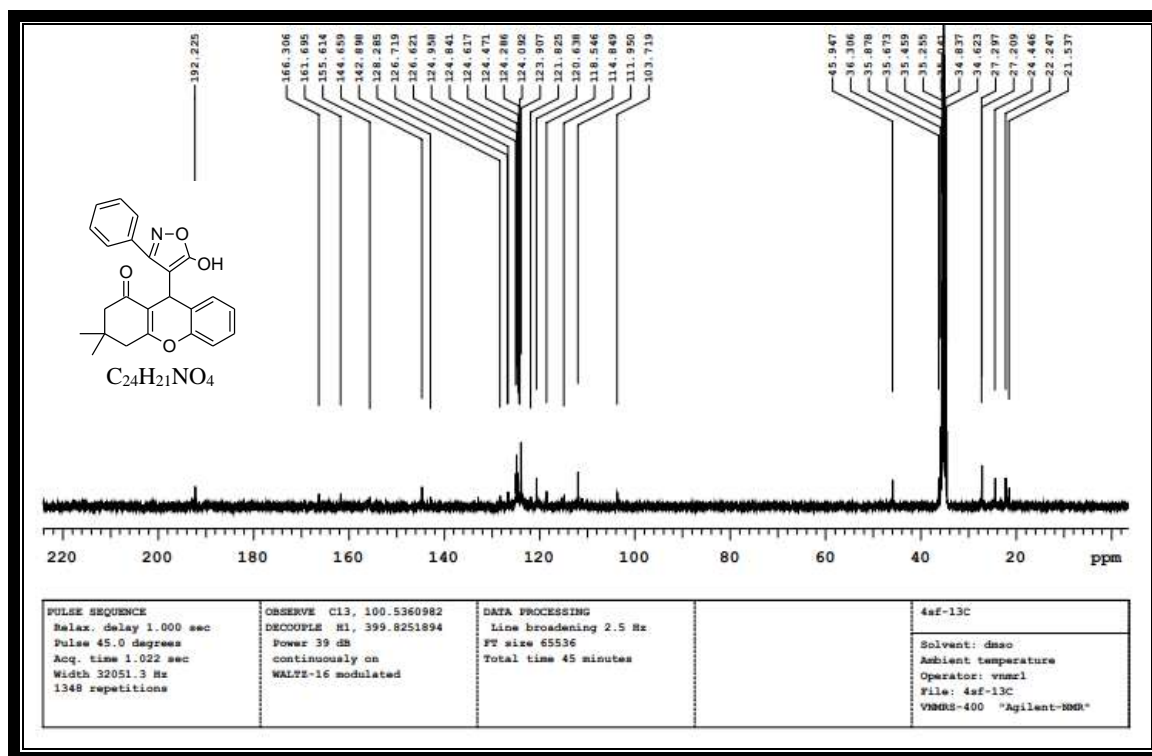
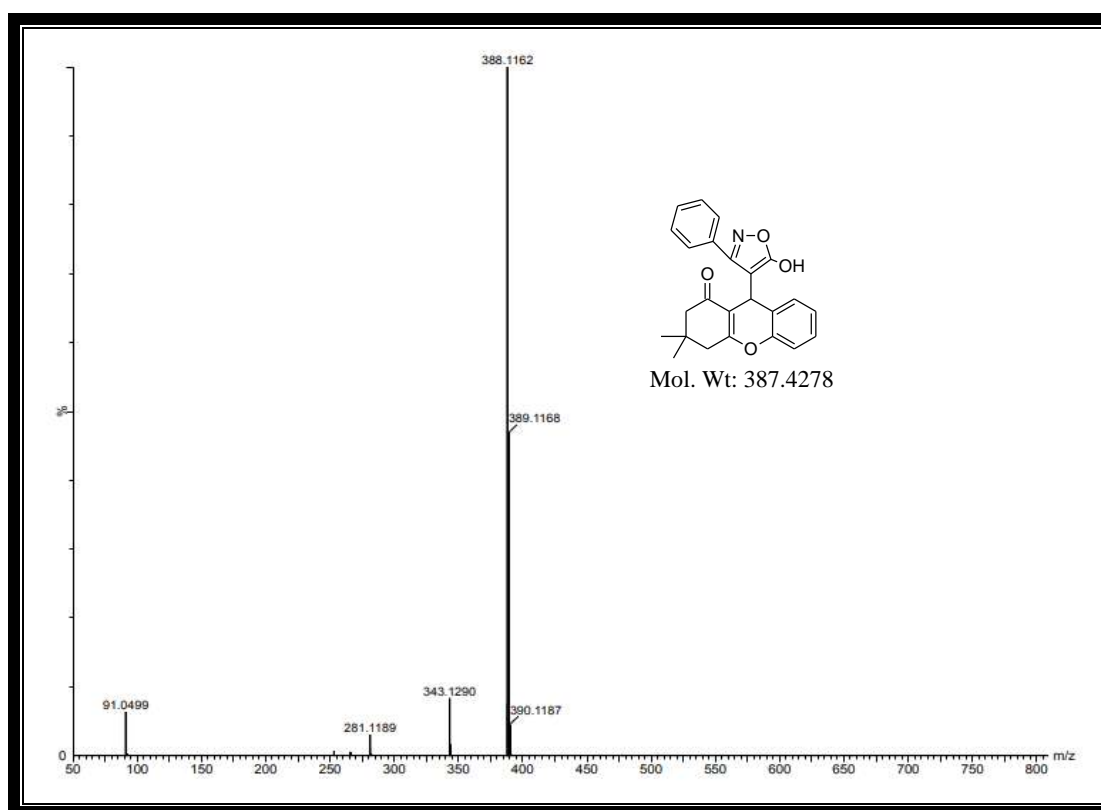
The mass spectrum showed a molecular ion peak *m/z* at 418.1750 due to [M⁺+1], which corresponds to the molecular weight of the compound **4g**.

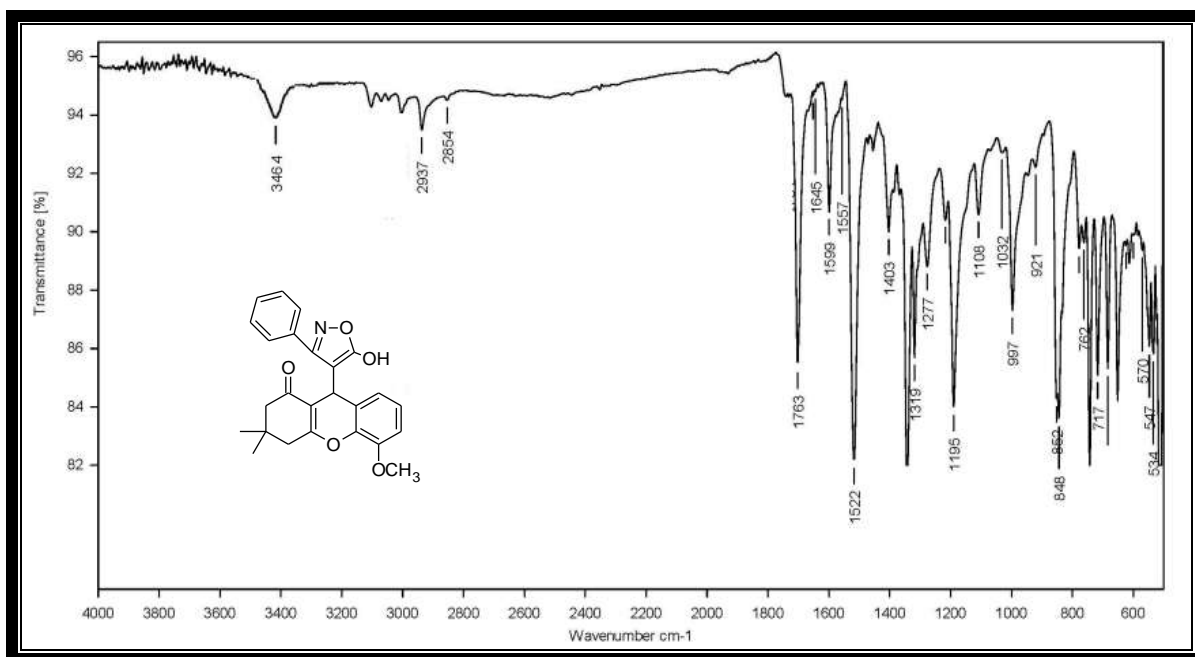
Characterization:



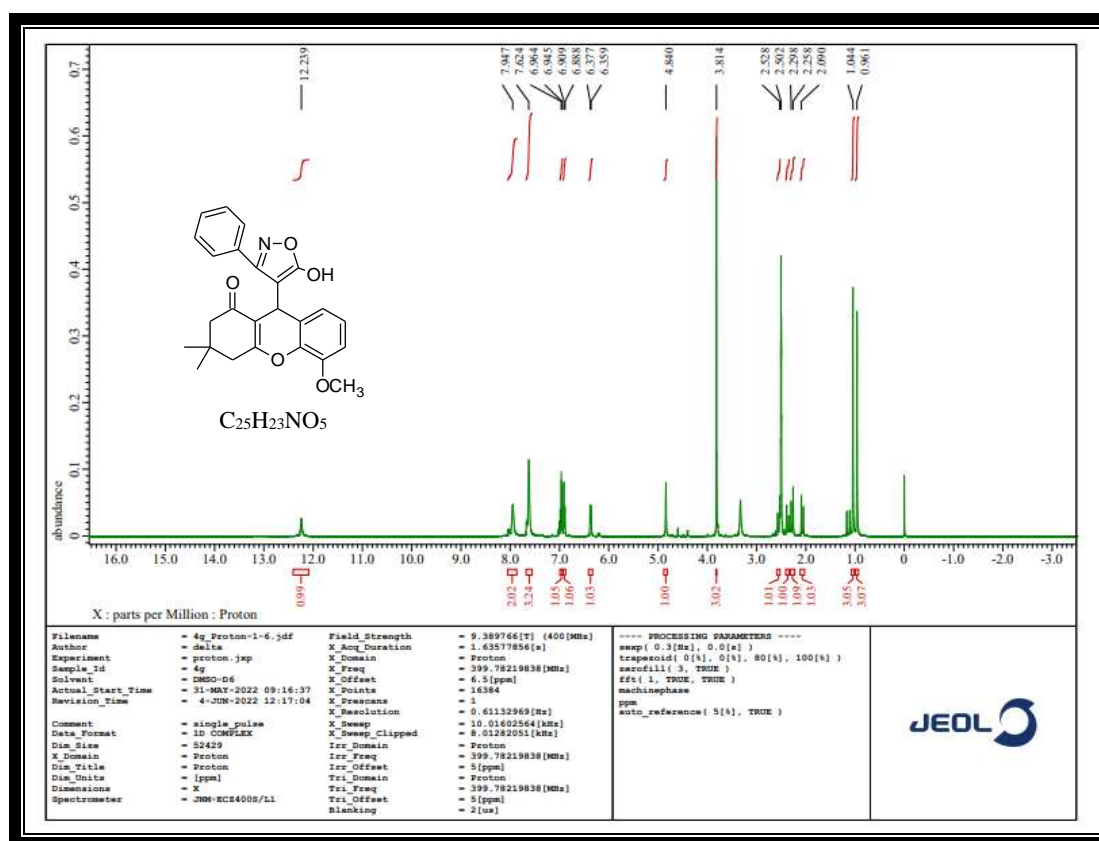
IR spectrum of compound 4f

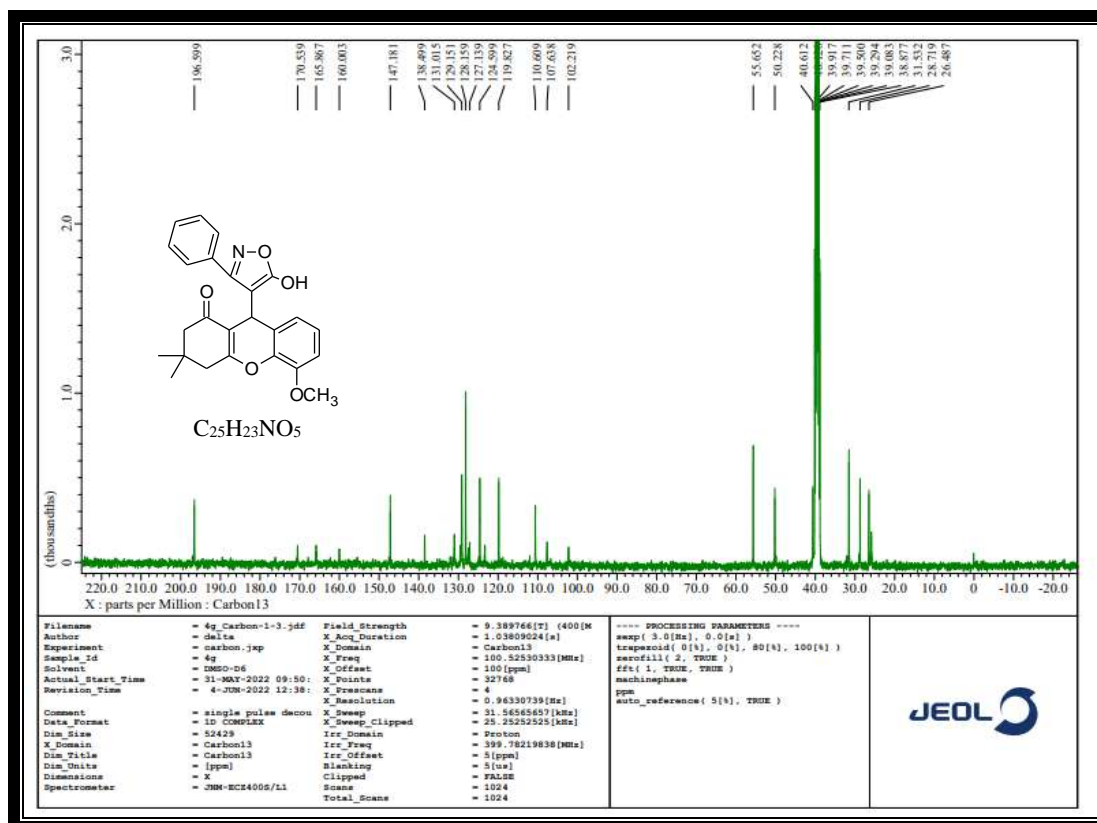
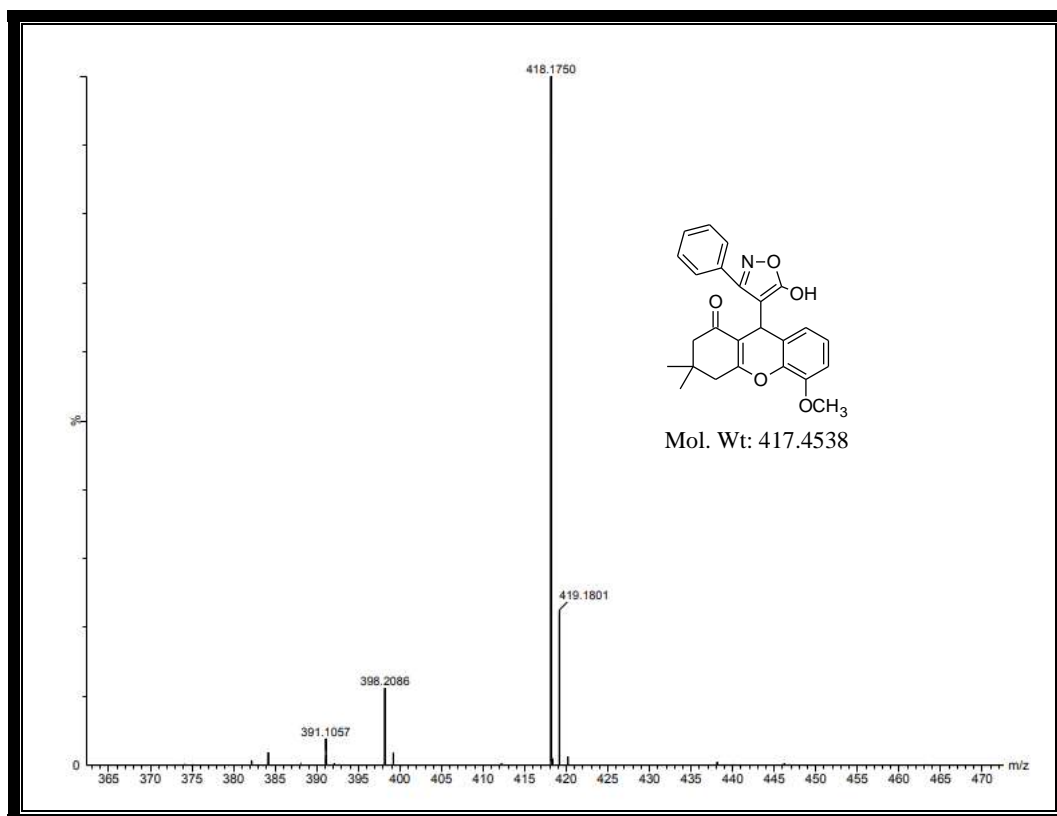
¹H NMR spectrum of compound 4f

**¹³C NMR spectrum of compound 4f****MASS spectrum of compound 4f**



IR spectrum of compound 4g

¹H NMR spectrum of compound 4g

 ^{13}C NMR spectrum of compound 4g

MASS spectrum of compound 4g

4B.3. 2D ^1H - ^{13}C HSQC NMR

The ^1H NMR spectrum of compound **4g** exhibited two singlet peaks at δ 0.96 (H_1) and 1.04 (H_2) ppm corresponds to methyl protons (s, 6H, CH_3), four singlet peaks at δ 2.09, 2.25 (H_3) and 2.29, 2.52 (H_4) ppm corresponds to CH_2 protons (s, 4H, CH_2). A singlet peak at δ 3.81 (H_5) ppm correspond to methoxy protons (s, 3H, OCH_3) and another singlet peak at δ 4.84 (H_6) ppm due to CH proton (s, 1H, CH). A doublet peaks at δ 6.35-6.37 (H_7), 6.88-6.90 (H_8) & 6.94-6.96 (H_9) ppm which corresponds to three aromatic protons (d, $J=8$ Hz, 3H, Ar-H) and two singlet peaks at δ 7.62 (H_{11} - H_{13}) & δ 7.94 (H_{10} & H_{14}) ppm corresponds to five aromatic protons (s, 5H, Ar-H). The ^{13}C NMR spectrum of compound **4g** exhibited peaks at δ 26.48 (C_6) ppm correspond to CH carbon, 28.71 (C_1) & 31.53 (C_2) ppm correspond to CH_3 carbons and 40.61 (C_4) & 50.22 (C_3) ppm due to CH_2 carbons and 55.65 (C_5) ppm correspond to OCH_3 carbon. Peaks at δ 110.60 (C_8), 119.82 (C_7) & 124.59 (C_9) ppm corresponds to three aromatic carbons. Another peaks at δ 128.15 (C_{10} & C_{14}), 129.15 (C_{11} - C_{13}) ppm corresponds to five aromatic carbons.

HSQC of compound **4g** explained that, ^1H - ^{13}C correlation between H_1 (δ 0.96) & C_1 (δ 28.71), H_2 (δ 1.04) & C_2 (δ 31.53), H_3 (δ 2.09, 2.25) & C_3 (δ 50.22), H_4 (δ 2.29, 2.52) & C_4 (δ 40.61), H_5 (δ 3.81) & C_5 (δ 55.65), H_6 (δ 4.84) & C_6 (δ 26.48), H_7 (δ 6.35) & C_7 (δ 119.82), H_8 (δ 6.88) & C_8 (δ 110.60), H_9 (δ 6.94) & C_9 (δ 124.59), H_{10} , H_{14} (δ 7.94) & C_{10} , C_{14} (δ 128.15), H_{11-13} (δ 7.62) & C_{11-13} (δ 129.15). In addition, δ 12.23 ppm which does not shows HSQC correlation to any carbon indicates the OH proton and remaining carbon peaks do not show HSQC correlations to other protons. This confirmed the structure of 3,4-dihydro-9-(5-hydroxy-3-phenylisoxazol-4-yl)-5-methoxy-3,3-dimethyl-2H-xanthen-1(9H)-one (**Fig. 1**).

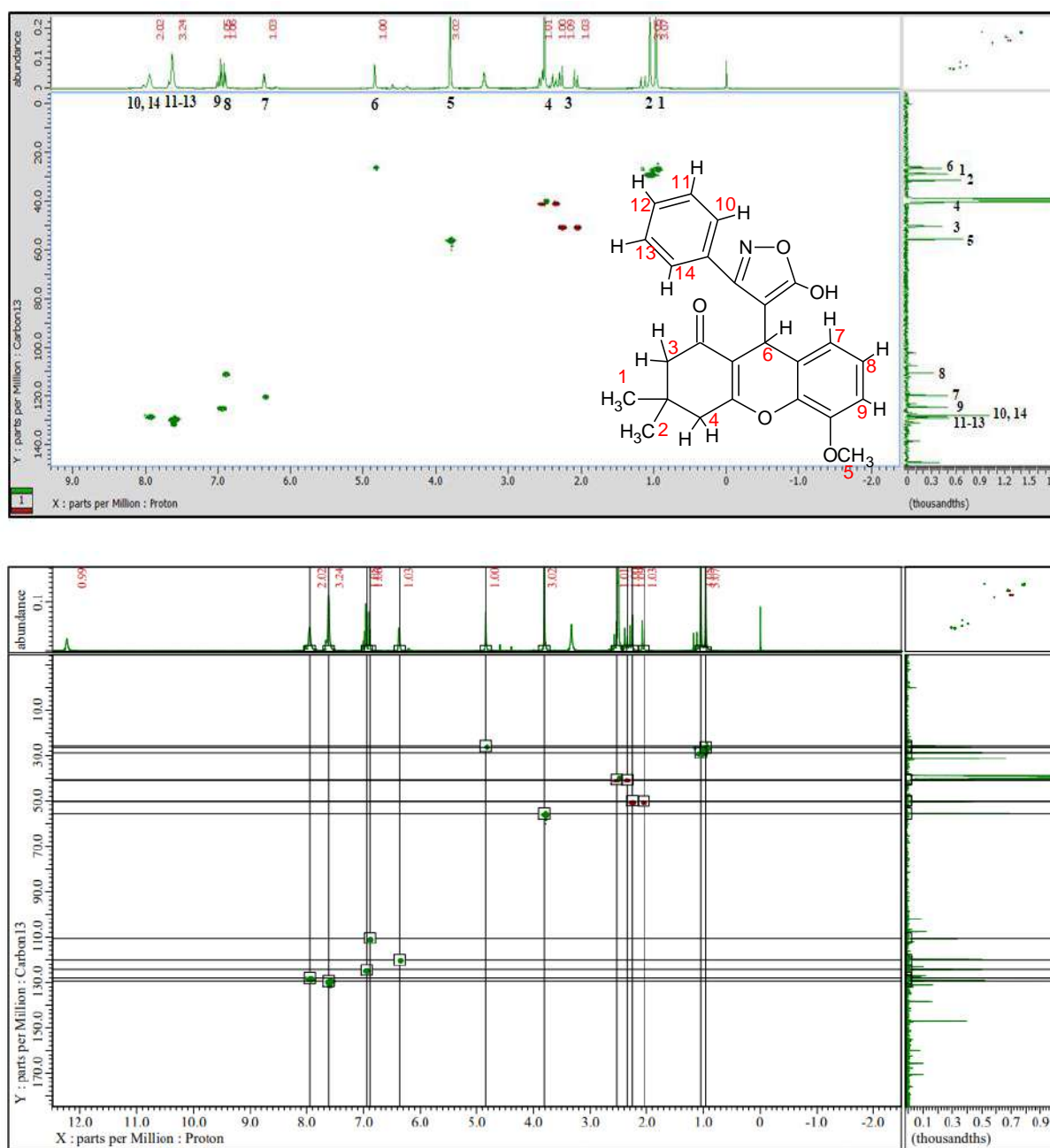


Fig. 1. 2D ^1H - ^{13}C HSQC NMR spectrum of compound **4g** recorded in DMSO- d_6 solvent.

4B.4. Experimental

4B.4.1. General information:

In **Chapter-2A** (section 2A.3.1) and **Chapter-4A** (section 4A.4.1), we have been explained the detailed general information regarding the different solvents, chemicals and instruments.

4B.4.2. Procedure for synthesis of substituted-(5-hydroxy-3-phenylisoxazol-4-yl)-3,3-dimethyl-2H-xanthen-1(9H)-one derivatives **4(f-j)**:

A mixture of dimedone (**1**, 1 mmol), substituted salicylaldehyde/2-hydroxy-naphthaldehyde (**2**, 1 mmol) and *p*-TSA (10 mol %) in ethanol/water (1:1) was stirred under refluxed condition. After 5 min, 3-phenyl-5-isoxazolone (**3**, 1 mmol) was added to it and refluxed temperature with constant stirring for about 3-4 h and followed by according to procedure [36] to afford pure solid products **4(f-j)**.

3,4-Dihydro-9-(5-hydroxy-3-phenylisoxazol-4-yl)-3,3-dimethyl-2H-xanthen-1(9H)-one (4f):

Yellow solid; Yield: 90 %; MP: 220-222 °C; Mol. Formula: C₂₄H₂₁NO₄; UV (nm) λ_{max} (log ε): 410 (3.96) & 318 (4.17); FTIR (ν cm⁻¹): 3483 (OH), 2887 (CH), 1697 (C=O) & 1580 (C=N); ¹H NMR (δ ppm): 12.20 (s, 1H, OH), 7.91 (s, 1H, Ar-H), 7.76-7.61 (m, 3H, Ar-H), 7.02 (s, 1H, Ar-H), 6.99-6.92 (m, 3H, Ar-H), 6.86 (s, 1H, Ar-H), 4.86 (s, 1H, CH), 2.49 (s, 1H, CH), 2.21 (s, 2H, CH), 2.11 (s, 1H, CH), 1.17 (s, 3H, CH₃), 1.03 (s, 3H, CH₃); ¹³C NMR (δ ppm): 192.22, 166.30, 161.69, 155.61, 144.65, 142.89, 128.28, 126.71, 126.62, 124.95, 124.61, 124.28, 123.90, 121.82, 120.63, 118.54, 114.84, 111.95, 103.71, 45.94, 36.30, 27.29, 27.20, 24.44; HRMS: m/z 388.1162 [M⁺+1]; Anal. Calcd: C 74.40, H 5.46, N 3.62 %, Found: C 74.37, H 5.42, N 3.59 %.

3,4-Dihydro-9-(5-hydroxy-3-phenylisoxazol-4-yl)-5-methoxy-3,3-dimethyl-2H-xanthen-1(9H)-one (4g):

White solid; Yield: 86 %, MP: 204-206 °C; Mol. Formula: C₂₅H₂₃NO₅; UV (nm) λ_{\max} (log ϵ): 325 (4.25); FTIR (ν cm⁻¹): 3464 (OH), 2937 (CH), 2854 (OCH₃), 1763 (C=O) & 1599 (C=N); ¹H NMR (δ ppm): 12.23 (s, 1H, OH), 7.94 (s, 2H, Ar-H), 7.62 (s, 3H, Ar-H), 6.96-6.94 (d, J = 8 Hz, 1H, Ar-H), 6.90-6.88 (d, J = 8 Hz, 1H, Ar-H), 6.37-6.35 (d, J = 8 Hz, 1H, Ar-H), 4.84 (s, 1H, CH), 3.81 (s, 3H, OCH₃), 2.52 (s, 1H, CH), 2.29 (s, 1H, CH), 2.25 (s, 1H, CH), 2.09 (s, 1H, CH), 1.04 (s, 3H, CH₃), 0.96 (s, 3H, CH₃); ¹³C NMR (δ ppm): 196.59, 170.53, 165.86, 160.00, 147.18, 138.49, 131.01, 129.15, 128.15, 127.13, 124.59, 119.82, 110.60, 107.63, 102.21, 55.65, 50.22, 40.61, 31.53, 28.71, 26.48; HRMS: m/z 418.1750 [M⁺+1]; Anal. Calcd: C 71.93, H 5.55, N 3.36 %, Found: C 71.90, H 5.51, N 3.32 %.

3,4-Dihydro-12-(5-hydroxy-3-phenylisoxazol-4-yl)-3,3-dimethyl-2H-benzo[b]xanthen-1(12H)-one (4h):

White solid; Yield: 88 %, MP: 214-216 °C; Mol. Formula: C₂₈H₂₃NO₄; UV (nm) λ_{\max} (log ϵ): 355 (4.03) & 325 (3.89); FTIR (KBr, ν cm⁻¹): 3406 (OH), 2910 (CH), 1715 (C=O) & 1588 (C=N); ¹H NMR (δ ppm): 12.22 (s, 1H, OH), 8.99-8.93 (m, 3H, Ar-H), 8.62-8.60 (d, J = 8 Hz, 1H, Ar-H), 8.26-8.24 (d, J = 8 Hz, 1H, Ar-H), 8.09-8.07 (d, J = 8 Hz, 1H, Ar-H), 7.72-7.61 (m, 5H, Ar-H), 4.84 (s, 1H, CH), 2.44 (s, 1H, CH), 2.32 (s, 1H, CH), 2.24 (s, 1H, CH), 2.09 (s, 1H, CH), 1.19 (s, 3H, CH₃), 1.04 (s, 3H, CH₃); ¹³C NMR (δ ppm): 194.26, 168.48, 162.54, 155.72, 153.46, 149.01, 146.29, 135.37, 130.60, 129.31, 125.70, 124.91, 124.62, 124.55, 124.27, 124.11, 121.89, 118.33, 116.94, 112.39, 108.49, 52.84, 44.20, 30.29, 28.32, 25.44; HRMS: m/z 438.1885 [M⁺+1]; Anal. Calcd: C 76.87, H 5.30, N 3.20 %, Found: C 76.85, H 5.27, N 3.16 %.

3,4-Dihydro-9-(5-hydroxy-3-phenylisoxazol-4-yl)-3,3-dimethyl-7-nitro-2H-xanthen-1(9H)-one (4i):

White solid; Yield: 80 %; MP: 188-190 °C; Mol. Formula: C₂₄H₂₀N₂O₆; UV (nm) λ_{\max} (log ϵ): 326 (3.98); FTIR (ν cm⁻¹): 3410 (OH), 2921 (CH), 1698 (C=O) & 1599 (C=N); ¹H NMR (δ ppm): 12.24 (s, 1H, OH), 7.95 (s, 1H, Ar-H), 7.68-7.66 (d, J = 8 Hz, 2H, Ar-H), 7.09 (s, 1H, Ar-H), 6.95-6.90 (m, 3H, Ar-H), 6.88 (s, 1H, Ar-H), 4.85 (s, 1H, CH), 2.52 (s, 1H, CH), 2.28 (s, 2H, CH), 2.13 (s, 1H, CH), 1.23 (s, 3H, CH₃), 1.12 (s, 3H, CH₃); ¹³C NMR (δ ppm): 191.98, 165.38, 162.85, 158.66, 146.64, 142.55, 128.36, 126.80, 126.25, 124.98, 124.36, 122.86, 120.68, 118.88, 114.92, 111.99, 103.75, 50.89, 45.98, 28.94, 27.33, 24.48; HRMS: m/z 432.2482 [M⁺]; Anal. Calcd: C 66.66, H 4.66, N 6.48 %, Found: C 66.62, H 4.62, N 6.45 %.

7-Bromo-3,4-dihydro-9-(5-hydroxy-3-phenylisoxazol-4-yl)-3,3-dimethyl-2H-xanthen-1(9H)-one (4j):

Orange solid; Yield: 81 %; MP: 198-200 °C; Mol. Formula: C₂₄H₂₀BrNO₄; UV (nm) λ_{\max} (log ϵ): 312 (3.98); FTIR (ν cm⁻¹): 3402 (OH), 2908 (CH), 1663 (C=O) & 1595 (C=N); ¹H NMR (δ ppm): 12.40 (s, 1H, OH), 7.89 (s, 1H, Ar-H), 7.63-7.61 (d, J = 8 Hz, 2H, Ar-H), 7.13 (s, 1H, Ar-H), 6.99-6.94 (m, 3H, Ar-H), 6.82 (s, 1H, Ar-H), 4.81 (s, 1H, CH), 2.48 (s, 1H, CH), 2.22 (s, 2H, CH), 2.15 (s, 1H, CH), 1.19 (s, 3H, CH₃), 1.06 (s, 3H, CH₃); ¹³C NMR (δ ppm): 192.38, 165.46, 162.89, 158.73, 146.88, 142.72, 128.57, 126.62, 126.30, 124.64, 124.58, 122.96, 121.18, 118.92, 114.98, 112.56, 103.80, 52.26, 45.66, 31.25, 29.42, 26.46; HRMS: m/z 466.2088 [M⁺] & 467.1028 [M⁺⁺¹]; Anal. Calcd: C 61.81, H 4.32, N 3.00 %, Found: C 61.78, H 4.28, N 2.98 %.

4B.5. Electronic absorption study

The UV-Vis spectra of the obtained compounds **4(f-j)** was done by HR 4000 UV-Visible Spectrophotometer using six different solvents *viz* methanol, ethanol, acetonitrile, DMSO, 1,4-dioxane and chloroform at 10^{-5} M concentration. The absorption maxima and molar absorption coefficient values are appended in **Table 1** and spectras of the compounds were displayed in **Fig. 2**. Compounds **4f** & **4h** exhibited two absorption maxima in all the solvents in the range 304-325 nm corresponds to first absorption maxima and 352-410 nm corresponds to second absorption maxima due to the π - π^* & n - π^* transitions. Also, most of the compounds displayed maximum bathochromic/redshift towards the longer wavelength in DMSO solvent. It suggested that, as the polarity of the solvent increases, the absorption maxima (λ_{max}) is shift towards a longer wavelength due to the effective interaction between the solvent molecules and the lone pair of electrons [37]. Apart from these, the compounds **4f** & **4i** displayed a large redshift at 318, 410 nm & 326 nm compared to other compounds.

Table 1. Electronic absorption data of the synthesized compounds **4(f-j)** in six different solvents.

Compd.	Solvents											
	Methanol		Ethanol		Acetonitrile		DMSO		1, 4-dioxane		Chloroform	
	$\lambda_{\max}(\text{nm})$	Log ϵ	$\lambda_{\max}(\text{nm})$	Log ϵ	$\lambda_{\max}(\text{nm})$	Log ϵ	$\lambda_{\max}(\text{nm})$	Log ϵ	$\lambda_{\max}(\text{nm})$	Log ϵ	$\lambda_{\max}(\text{nm})$	Log ϵ
4f	308	4.14	304	4.18	307	4.12	318	4.17	309	4.17	311	4.13
	402	3.85	406	3.77	404	3.56	410	3.96	387	3.91	399	3.86
4g	307	4.11	305	4.13	315	4.20	325	4.25	309	4.13	318	4.18
	-	-	-	-	-	-	-	-	-	-	-	-
4h	323	3.79	322	3.97	323	4.01	325	3.89	315	4.04	325	3.99
	355	3.90	354	4.08	355	4.10	355	4.03	352	4.03	358	4.08
4i	303	3.96	306	4.02	323	3.90	326	3.98	313	4.06	318	4.14
	-	-	-	-	-	-	-	-	-	-	-	-
4j	308	4.07	300	4.09	306	4.07	312	3.98	300	3.93	300	3.83
	-	-	-	-	-	-	-	-	-	-	-	-

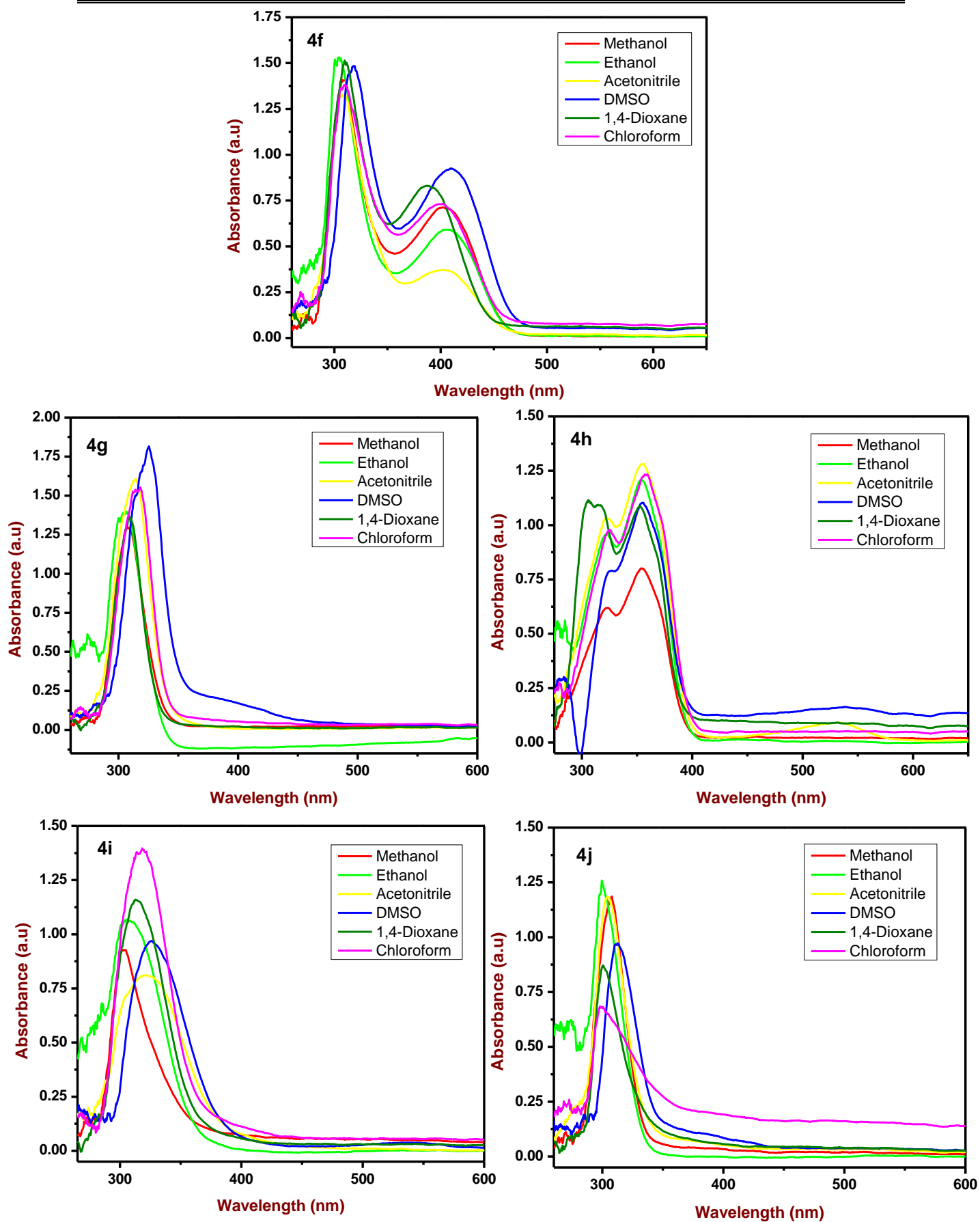


Fig. 2. A graph of UV-Visible spectras of the synthesized compounds **4(f-j)** in six different solvents.

4B.6. Powder-XRD analysis

Powder X-ray diffraction method was used to study the crystalline nature and lattice parameters of compounds and it has been done at 2θ range of $5-80^\circ$ and wavelength 1.5406 \AA . The compound **4g** showed 10 reflections at the range of $10-80^\circ$ with the intense peaks and lattice parameters associated with compounds and have been determined by the h, k and l of miller indices values [38]. The crystalline size was calculated using Debye-Scherrer equation has been shown below.

$$D = 0.9\lambda/\beta\cos\theta$$

Where β is the full width at half maxima in radians, λ is the wavelength of $\text{CuK}\alpha$ X-ray radiation used ($\lambda = 0.154 \text{ nm}$) and θ is the Bragg's diffraction angle in degrees [39].

Fig. 3 shows P-XRD of the compound **4g** and it has sharp intense peaks, this confirmed the crystalline nature and it gives sharp peaks at 100 and 210 which indicate a monocyclic crystalline structure. From the graph considering the intense peaks, the unit cell parameters and miller indices have been calculated and calculation shows **4g** compound is monocyclic and crystalline in nature. Calculated parameters are listed in **Table 2**.

Table 2. Calculated Powder-XRD structural data of synthesized compound **4g**.

Compd.	Peak	2θ	$\theta/2$	$\text{Sin } \theta$	$\text{Sin}^2 \theta$	$\text{Sin}^2 \theta \times 1000$	$h^2+k^2+l^2$	h.k.l
4g	1	9.29	4.64	0.080	0.006	6.54	1	100
	2	14.98	7.49	0.130	0.016	16.99	2.54	110
	3	19.11	9.55	0.165	0.027	27.52	4.02	200
	4	20.40	10.20	0.177	0.031	31.35	4.79	210
	5	21.96	10.98	0.190	0.036	36.27	5.54	211
	6	24.14	12.07	0.209	0.043	43.72	6.68	221
	7	25.70	12.85	0.222	0.049	49.96	7.56	222
	8	28.16	14.08	0.243	0.059	59.04	9.04	300
	9	30.61	15.30	0.263	0.069	69.62	10.64	310
	10	31.90	15.95	0.274	0.075	75.51	11.54	311

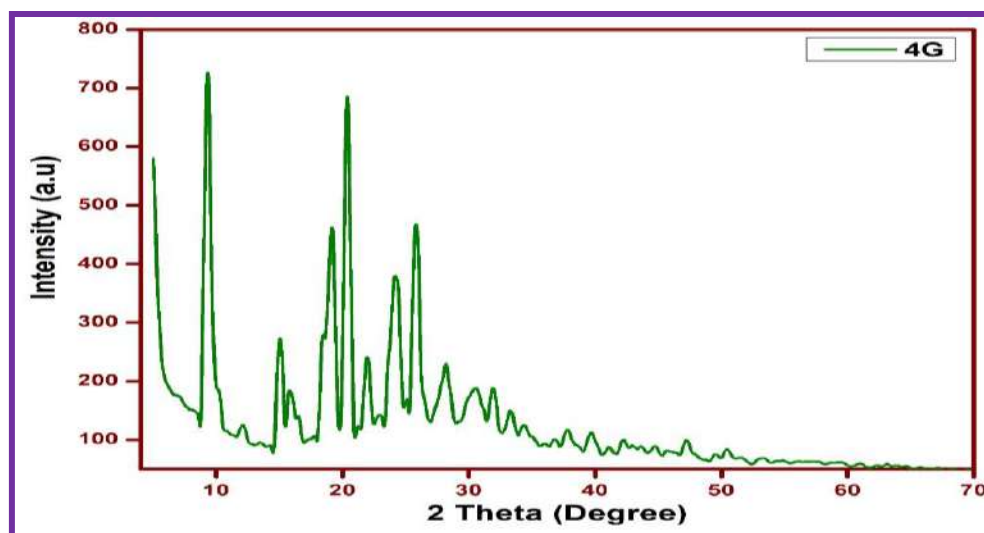


Fig. 3. Powder-XRD structures of synthesized compounds **4g**.

4B.7. Pharmacological studies

In-vitro cytotoxicity, anti-mycobacterial activity, *in silico* molecular docking, molecular dynamic simulation and DFT studies has been explained previously in the experimental section 4A.7 of **Chapter-4A**.

4B.8. Results and discussion

4B.8.1. Cytotoxicity study

The *in vitro* cytotoxicity of the synthesized compounds **4(f-j)** was evaluated against MCF-7 cell line and results indicates that, tested compounds showed very good selectivity and cytotoxic effect against MCF-7. In that, compound **4h** possessed significant cytotoxicity with an IC_{50} value of 0.15 ± 0.08 $\mu\text{g/mL}$ and the rest of the compounds displayed IC_{50} values in the range of 19.17 ± 2.10 to 134.9 ± 12.09 $\mu\text{g/mL}$ compared to reference standards anastrozole and folic acid (99.47 ± 1.57 & 139.2 ± 1.42 $\mu\text{g/mL}$). The compound **4h** demonstrated highly promising cell viability at 6.25 $\mu\text{g/mL}$ concentration due to presence of an additional phenyl nucleus was supposed to be the reason for the superior activity. A graph of % of cell viability at different concentration and IC_{50} value of synthesized compounds were shown in **Fig. 4 & 5**. The cytotoxicity results were tabulated in **Table 3**.

Table 3. % of cell viability against MCF-7 cell line of the synthesized compounds **4(f-j)**.

Compd.	Mean cell viability of MCF-7 Concentration in $\mu\text{g/mL}$							IC ₅₀ in $\mu\text{g/mL}$
	NC	6.25	12.5	25	50	100	200	
4f	100	69.37 \pm 1.35	50.00 \pm 0.33	43.78 \pm 0.33	39.47 \pm 1.68	38.28 \pm 0.67	36.39 \pm 0.70	21.96 \pm 2.06
4g		77.99 \pm 1.35	73.92 \pm 1.01	71.53 \pm 1.01	54.30 \pm 2.36	41.86 \pm 1.01	34.21 \pm 1.01	69.17 \pm 4.85
4h		41.15 \pm 0.67	38.51 \pm 1.01	36.12 \pm 0.33	34.69 \pm 0.34	33.73 \pm 0.33	32.77 \pm 0.33	0.15 \pm 0.08
4i		60.05 \pm 1.01	51.19 \pm 0.67	44.97 \pm 0.67	42.34 \pm 0.33	41.39 \pm 0.34	40.91 \pm 0.34	19.17 \pm 2.10
4j		88.04 \pm 1.35	83.25 \pm 0.67	81.10 \pm 1.01	79.66 \pm 1.01	72.48 \pm 1.68	44.73 \pm 1.01	134.9 \pm 12.09
Std^a		74.60 \pm 1.39	72.24 \pm 0.27	69.68 \pm 1.11	66.93 \pm 1.11	55.71 \pm 1.95	30.90 \pm 1.39	99.47 \pm 1.57
Std^b		85.82 \pm 1.11	82.48 \pm 0.83	78.15 \pm 1.38	74.01 \pm 1.67	61.02 \pm 0.56	36.61 \pm 0.55	139.2 \pm 1.42

Std^a- Anastrozole (AZ), **Std^b**- Folic acid (FA), **NC**- Negative control
 Values are Mean \pm SE, N=3, *P<0.01 vs. Control

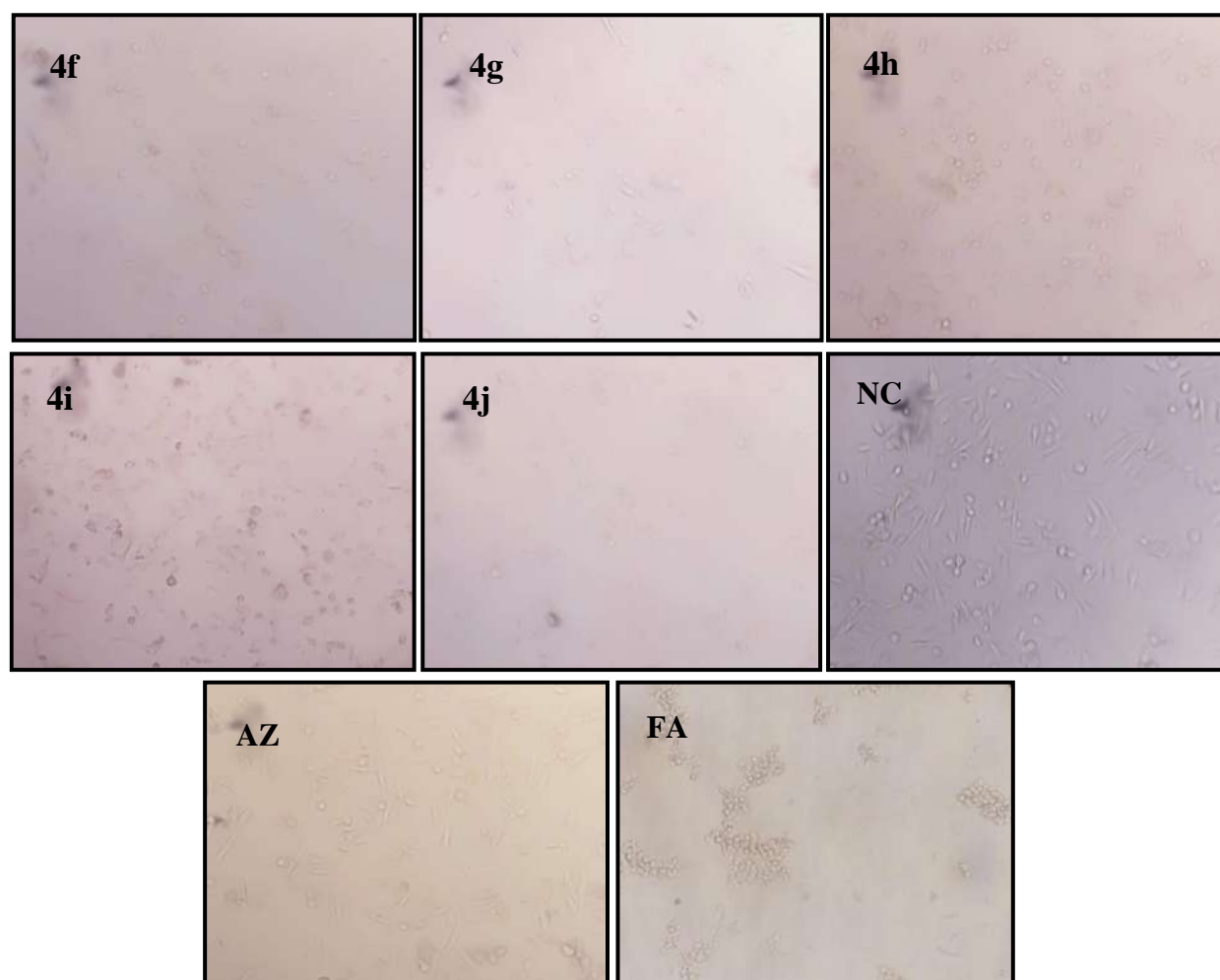


Fig. 4. Images of anticancer activity of the synthesized compounds **4(f-j)**, standard drugs (**AZ**-Anastrozole, **FA**-Folic acid) and Negative control (**NC**).

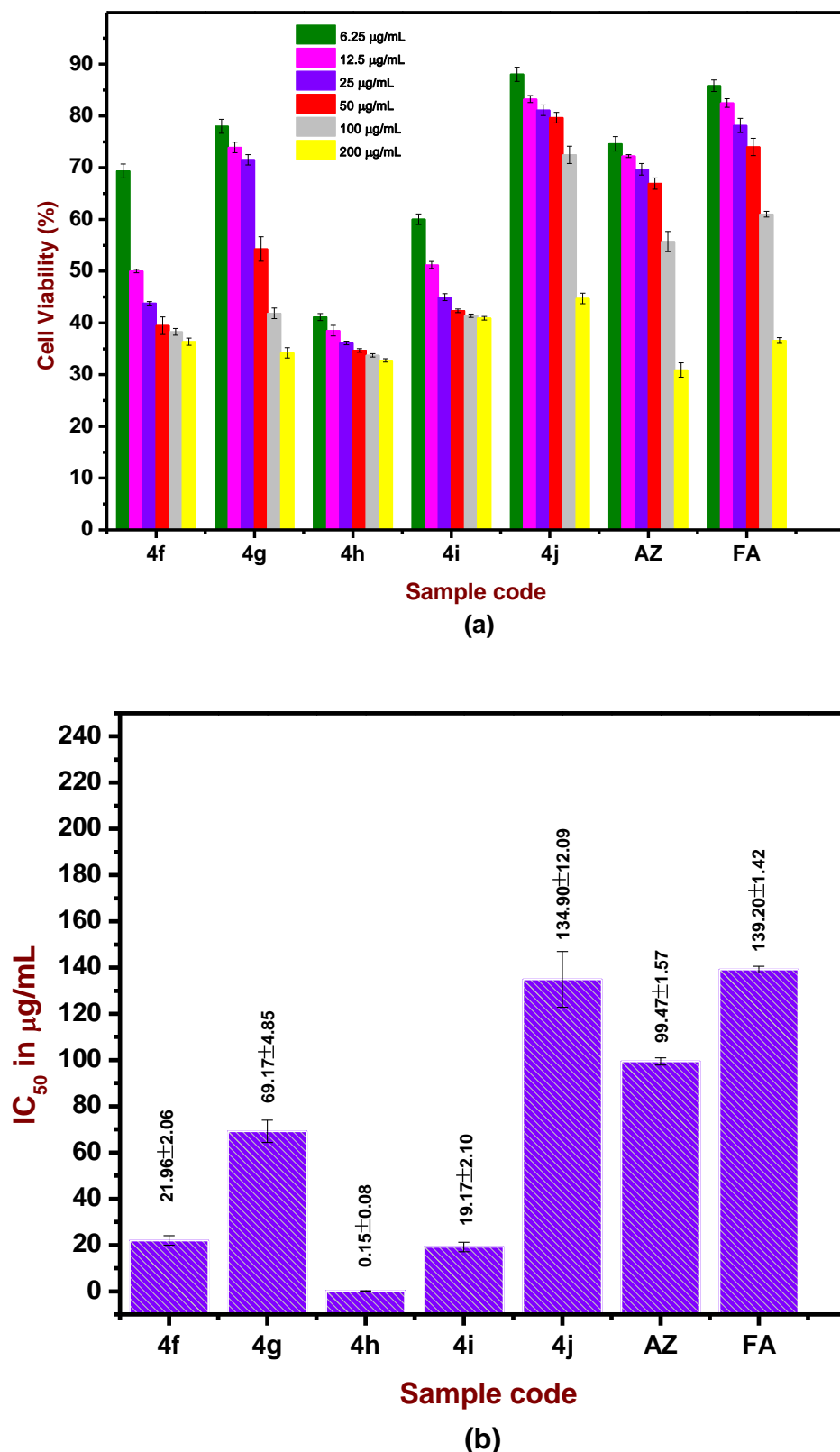


Fig. 5. A graph of % of survival cells of synthesized compounds **4(f-j)** at different concentration (a); a graph of IC₅₀ value of compounds **4(f-j)** against MCF-7 cell line (b).

4B.8.2. Anti-tubercular activity

The anti-TB activity of targeted compounds were evaluated against H37RV strain and results indicates that, the compound **4h** exhibited effective anti-TB sensitivity with a MIC value of 3.12 $\mu\text{g/mL}$ and it has sensitivity almost similar to the reference standard Pyrazinamide (MIC= 3.2 $\mu\text{g/mL}$). Compound **4i** also showed good sensitivity at MIC of 12.5 $\mu\text{g/mL}$ and the remaining compounds displayed considerable sensitivity with MIC value in the range of 25-100 $\mu\text{g/mL}$ as compared to reference standards Isoniazid, Ethambutol, Pyrazinamide, Rifampicin & Streptomycin having MIC values of 1.6, 1.6, 3.12, 0.8, 0.8 $\mu\text{g/mL}$ respectively. Anti-TB results and image was shown in **Table 4** and **Fig. 6**.

Table 4. Anti-tubercular activity results of synthesized compounds **4(f-j)**.

Compd.	Concentration in $\mu\text{g/mL}$							
	100	50	25	12.5	6.25	3.12	1.6	0.8
4f	S	S	S	R	R	R	R	R
4g	S	S	S	R	R	R	R	R
4h	S	S	S	S	S	S	R	R
4i	S	S	S	S	R	R	R	R
4j	S	S	R	R	R	R	R	R
Std^a	S	S	S	S	S	S	S	R
Std^b	S	S	S	S	S	S	S	R
Std^c	S	S	S	S	S	S	R	R
Std^d	S	S	S	S	S	S	S	S
Std^e	S	S	S	S	S	S	S	S

S-Sensitive, **R**-Resistant, **Std^a**- Isoniazid, **Std^b**- Ethambutol, **Std^c**- Pyrazinamide, **Std^d**- Rifampicin, **Std^e**- Streptomycin.

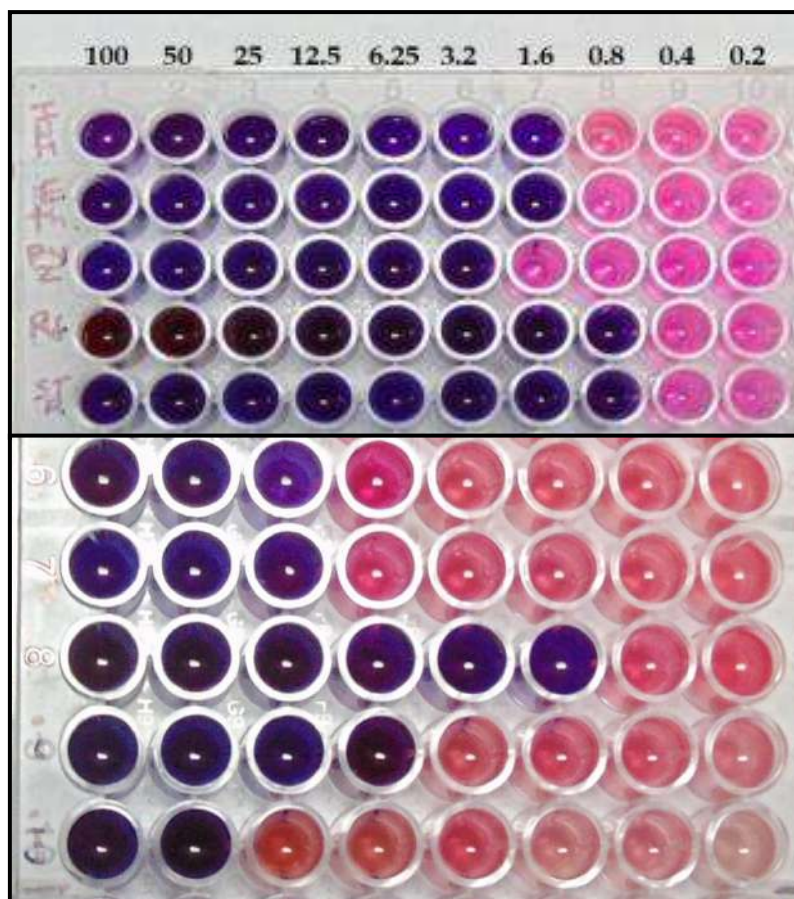


Fig. 6. Image of anti-TB activity results of the synthesized compounds **4(f-j)**.

4B.8.3. SAR Study

SAR study was performed on synthesized compounds **4(f-j)** and compounds exhibited good anticancer and anti-TB activity. Among the tested compounds, **4h** displayed outstanding anticancer and anti-TB activity with least IC_{50} value and MIC compared to standard drugs. The presence of an additional phenyl nucleus in the **4h** compound is supposed to be the main reason for the superior anticancer and anti-TB activity.

4B.8.4. *in silico* molecular docking study

The synthesized compounds **4(f-i)** were docked to binding pocket of P38 MAP kinase. Among the docked structures, compound **4h** demonstrated the least binding energy of -9.9 kcal/mol forming one hydrogen bond with GLY170. Compounds **4f**, **4g** & **4i** exhibited binding energies of -9.1, -8.6 & -9.2 kcal/mol by forming three to four hydrogen bonds with

amino acid residues compared with folic acid and anastrozole which demonstrated binding energies of -8.7 kcal/mol and -7.0 kcal/mol respectively (**Table 5**).

The interactions of synthesized compounds **4h** & **4i** with InhA-Enoyl-Acyl Carrier Protein demonstrated that, **4h** & **4i** shows binding energies of -11.0 & -9.0 kcal/mol respectively by forming three hydrogen bonds with GLY14, ILE95, GLY96, SER152, ARG153 & PRO156. The interactions were compared with Isoniazid (-5.8 kcal/mol), Pyrazinamide (-5.1 kcal/mol), Rifampicin (-8.0 kcal/mol) and Streptomycin (-8.4 kcal/mol). Binding interactions were tabulated in **Table 6**.

Table 5. Molecular interactions between synthesized compounds & standards with P38 MAP kinase protein.

Compd.	Binding energy in kcal/mol	H-bonds	Interacting Residues
4f	-9.1	03	ARG149, LEU171, ARG70
4g	-8.6	04	ARG149, TYR200, LEU171, ALA172
4h	-9.9	01	GLY170
4i	-9.2	04	ARG149, GLY170, LEU171, HIS148
Anastrozole	-7.0	03	TYR35, LYS53, MET109
Folic acid	-8.7	-	-

Table 6. Molecular interactions between synthesized compounds & standards with InhA-Enoyl-Acyl Carrier Reductase Protein.

Compd.	Binding energy in kcal/mol	H-bonds	Interacting Residues
4h	-11.0	03	GLY96, GLY14, ILE95
4i	-9.0	03	SER152, ARG153, PRO156
Isoniazid	-5.8	02	VAL65, LEU63
Pyrazinamide	-5.1	05	ILE21, ALA22, SER94, GLY96, GLY14
Rifampicin	-8.0	04	ARG225, MET155, LEU268, LEU 217
Streptomycin	-8.4	05	GLY14, ILE15, PHE41, ILE95, SER94

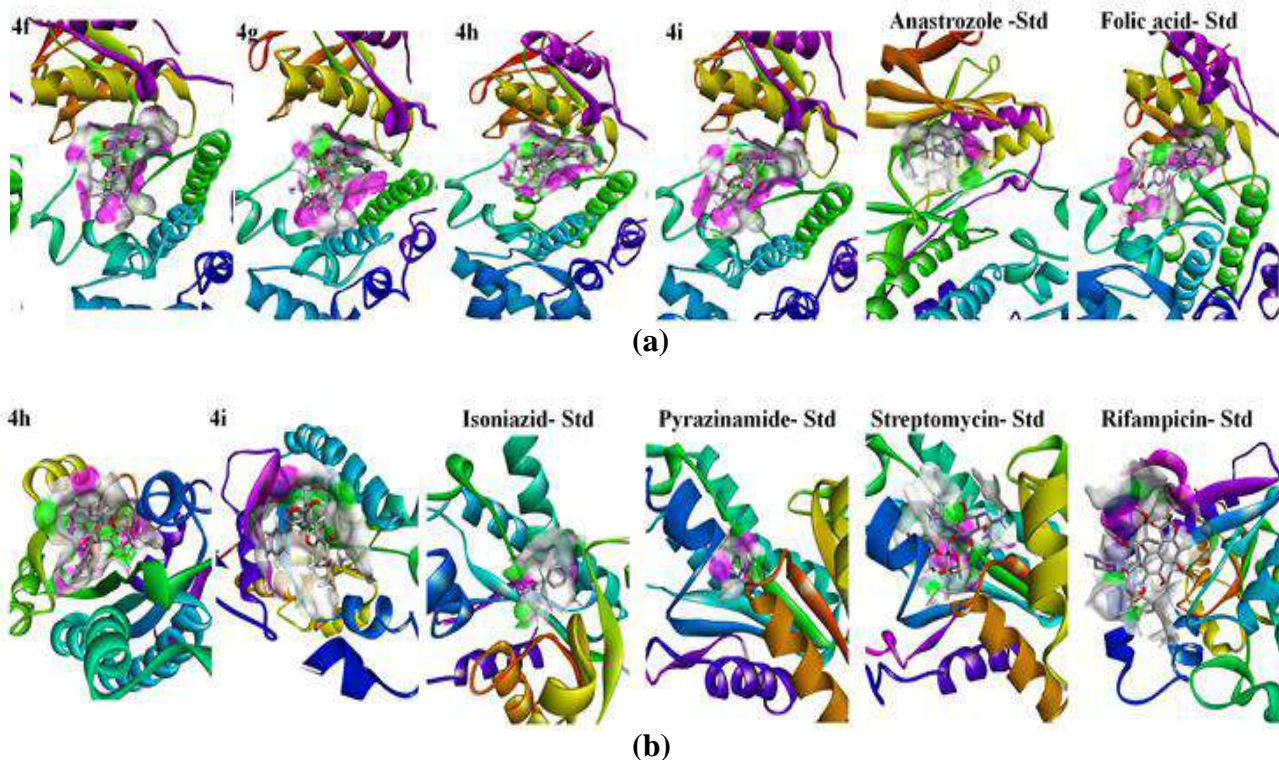


Fig. 7. Molecular interaction of synthesized compounds **4(f-i)** & standards with P38 MAP kinase (a); **4h, 4i** & standards with InhA-Enoyl-Acyl Carrier Protein Reductase (b).

4B.8.5. Molecular dynamics simulation

MD simulation was used to study the conformational changes of tested compounds upon binding to respective targets [40]. Among the docked structures, **4h** was selected for the MD simulation study due to least binding energy. Thus, the compound **4h** bound structure of InhA-Enoyl-Acyl Carrier Protein Reductase was selected. The MD simulated structures displayed stable conformational changes acquired by the target protein upon binding with the ligand (**Fig. 8**).

The conformational variations imposed by the synthesized compound **4h** upon binding with InhA-Enoyl-Acyl Carrier Protein Reductase was compared with its native structure along with the binding of standard drug pyrazinamide. The average potential energy of the synthesized compound **4h** bound InhA structure was -0.7610×10^{-6} kJ/mol compared to pyrazinamide-bound (-0.7618×10^{-6} kJ/mol) and unbound structure (-0.7385×10^{-6} kJ/mol)

(Table 8). The MD trajectory analysis for RMSD and RMSF revealed that the compound **4h** imposed fewer RMS deviations and RMS fluctuations with an average value of 0.1264 nm and 0.0741 nm respectively, whereas the pyrazinamide-bound structure displayed an average RMSD of 0.1485 nm and an average RMSF of 0.0826 nm respectively. The Rg and SASA plots also supported the conformational stability attained by the macromolecule upon binding with the synthetic compound **4h**.

The interactions of compound **4h** with InhA-Enoyl-Acyl Carrier Protein Reductase was found to have binding free energy value of -96.842 kJ/mol, while the standard compound pyrazinamide displayed a binding free energy value of -29.209 kJ/mol. The energy terms associated with binding free energy calculations are detailed in Table 7.

Table 7. Calculated MD parameters of compound **4h** and **Pyrazinamide** for native and ligand-bound InhA-Enoyl-Acyl Carrier Protein Reductase along with binding energies and the contributing energy terms calculated using g_mmpbsa module.

		InhA-Enoyl-Acyl Carrier Protein Reductase		
Gromacs Modules		Native Protein	Compound 4h	Pyrazinamide-Standard
	Potential Energy (x 10 ⁻⁶) (kJ/mol)	-0.7385	-0.7610	-0.7618
	RMSD (nm)	0.2079	0.1264	0.1485
	RMSF (nm)	0.1102	0.0741	0.0826
	Rg (nm)	1.7985	1.8252	1.8191
	SASA (nm ²)	129.238	128.40	129.01
MMPBSA Module	Binding Energy (kJ/mol)	-	-96.842	-29.209
	SASA Energy (kJ/mol)	-	-19.438	-7.654
	Polar Solvation Energy (kJ/mol)	-	100.042	72.604
	Electrostatic Energy (kJ/mol)	-	-11.536	-35.85
	van der WAALS Energy (kJ/mol)	-	-165.909	-58.344

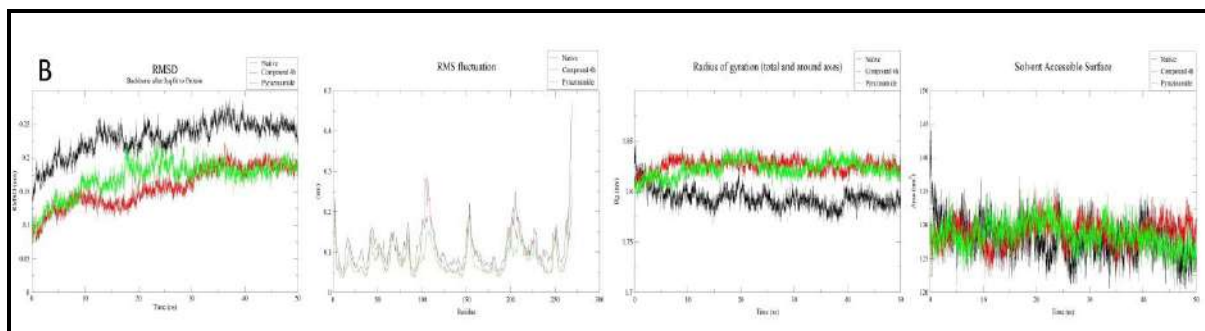


Fig. 8. RMSD, RMSF, Rg, and SASA, plots obtained from MD trajectories analysis of **4h** and **Pyrazinamide** for unbound and bound structures of InhA-Enoyl-Acyl Carrier Protein Reductase.

4B.8.6. DFT study

The HOMO-LUMO energy gap, electrostatic potential map, chemical functional descriptors (CFDs) and optimized structures of synthesized compounds are shown in **Fig. 9**, **10**, **11** & **12**. The calculated HOMO-LUMO energies and global reactivity parameters of the synthesized compounds **4(f-j)** are displayed in **Table 8**. Lesser the HOMO-LUMO energy gap (ΔE) softer the molecule, while larger the gap harder will be the molecule. A lower energy gap, lesser chemical hardness and more softness values indicate that molecule with more chemically and biologically active with low kinetic stability [41].

DFT results reveal that, the energy gap (ΔE) of compounds **4(f-j)** in the range of 3.97 eV to 4.87 eV. In that, the compound **4i** shows less energy gap at 3.97 eV and more softness value (0.50 eV). Hence, compound **4i** is chemically more reactive compared to other molecules. Also, **4i** compound has more electronegative value of 4.40 eV, due to the presence of an electron-withdrawing nitro group on phenyl ring and electron-donating hydroxyl group on isoxazole nucleus. Therefore, it has greater tendency to attract a bonding electron pair compared to other molecules.

Table 8. Chemical parameters of synthesized compounds 4(f-j).

Compd.	E_{HOMO} (eV)	E_{LUMO} (eV)	ΔE $E_{\text{HOMO}} - E_{\text{LUMO}}$ (eV)	I (eV)	A (eV)	η (eV)	σ (eV)	χ (eV)	μ (eV)	ω (eV)	D (Debye)
4f	-6.01	-1.14	4.87	6.01	1.14	2.43	0.41	3.57	-3.57	2.62	3.46
4g	-5.76	-1.05	4.71	5.76	1.05	2.35	0.42	3.40	-3.40	2.45	4.71
4h	-5.77	-1.29	4.48	5.77	1.29	2.24	0.44	3.53	-3.53	2.78	3.40
4i	-6.39	-2.42	3.97	6.39	2.42	1.98	0.50	4.40	-4.40	4.88	7.33
4j	-6.19	-1.38	4.81	6.19	1.38	2.40	0.41	3.78	-3.78	2.97	5.24

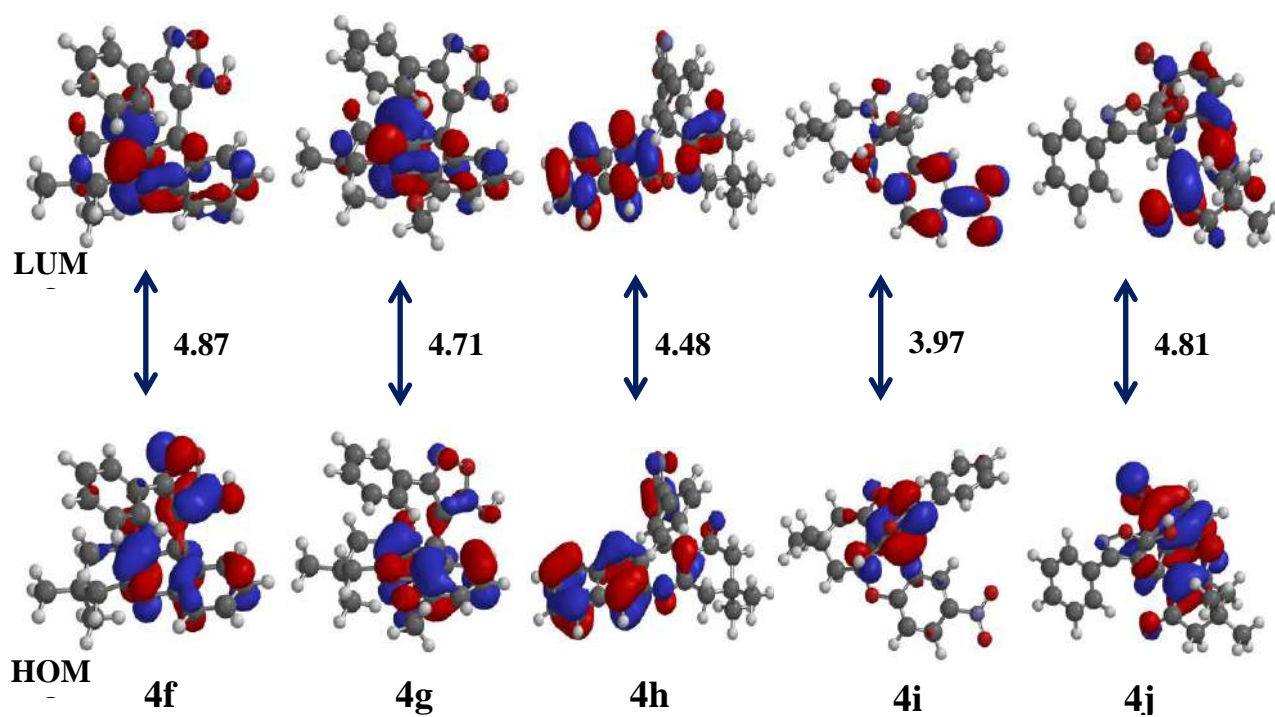


Fig. 9. FMO orbitals & HOMO-LUMO energy gap of the synthesized compounds 4(f-j).

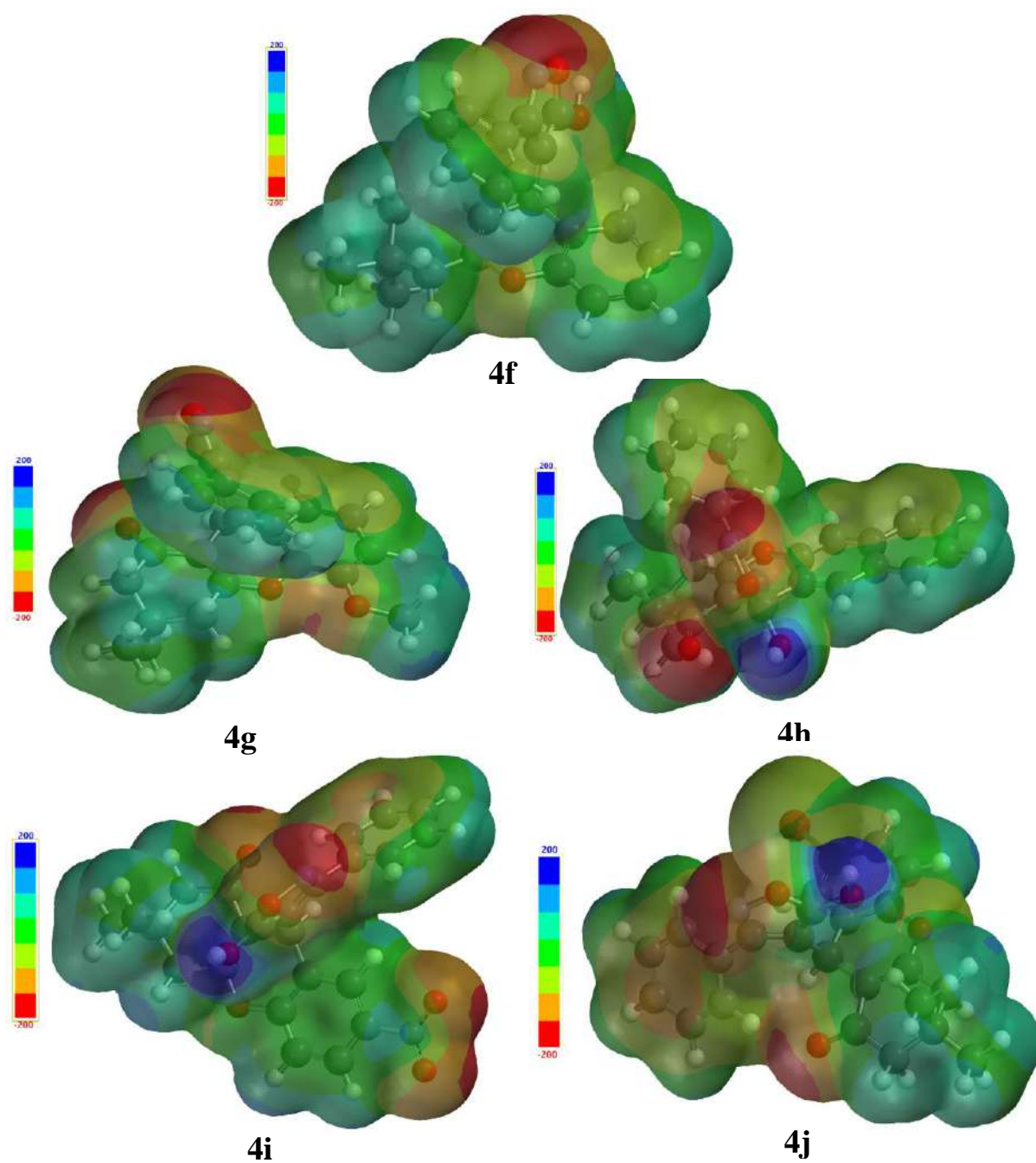


Fig. 10. Images of molecular electrostatic potential map (-200 to +200 kJ) of the synthesized compounds **4(f-j)**.

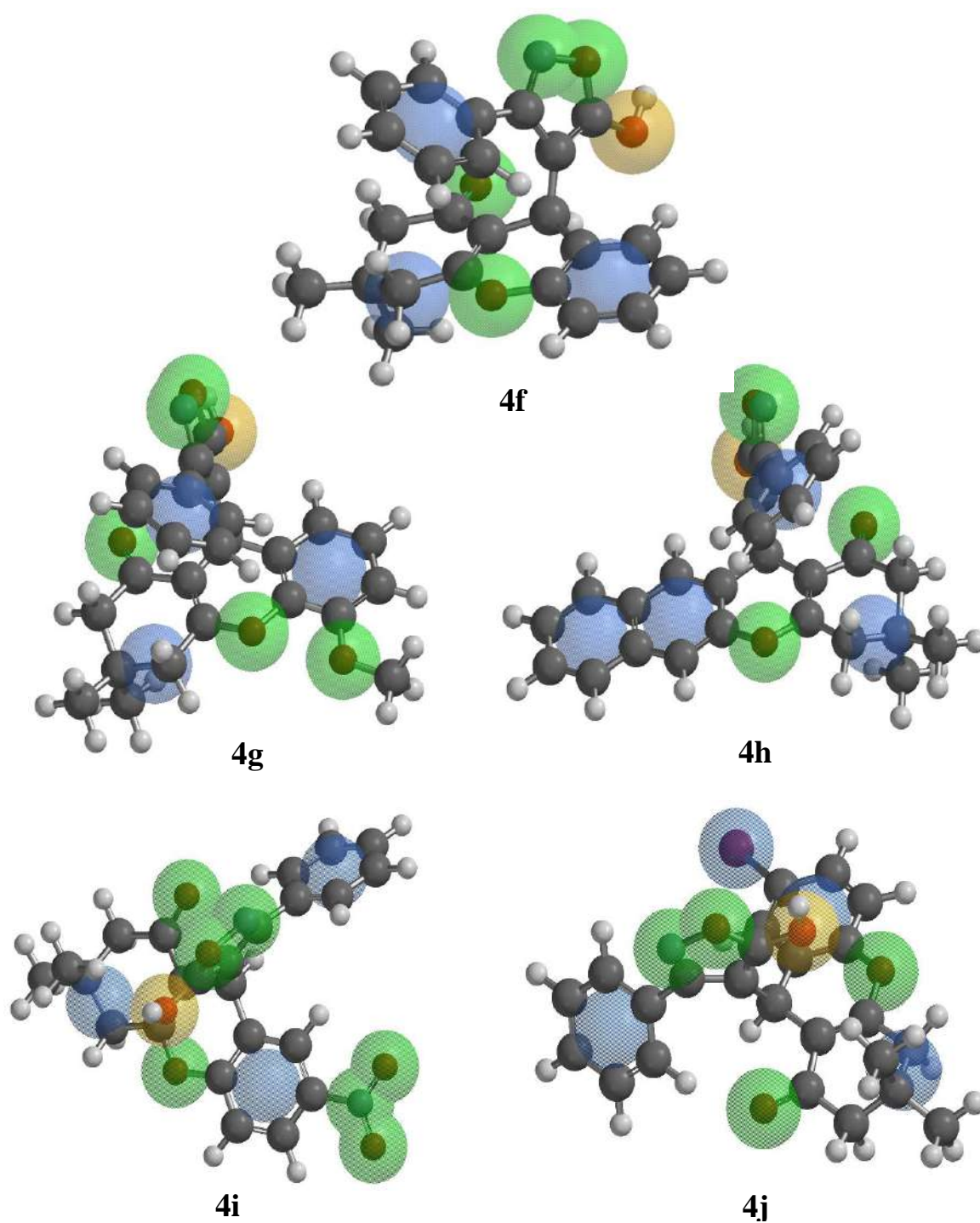


Fig. 11. Images of chemical functional descriptors (CFDs) of the synthesized compounds 4(f-j).

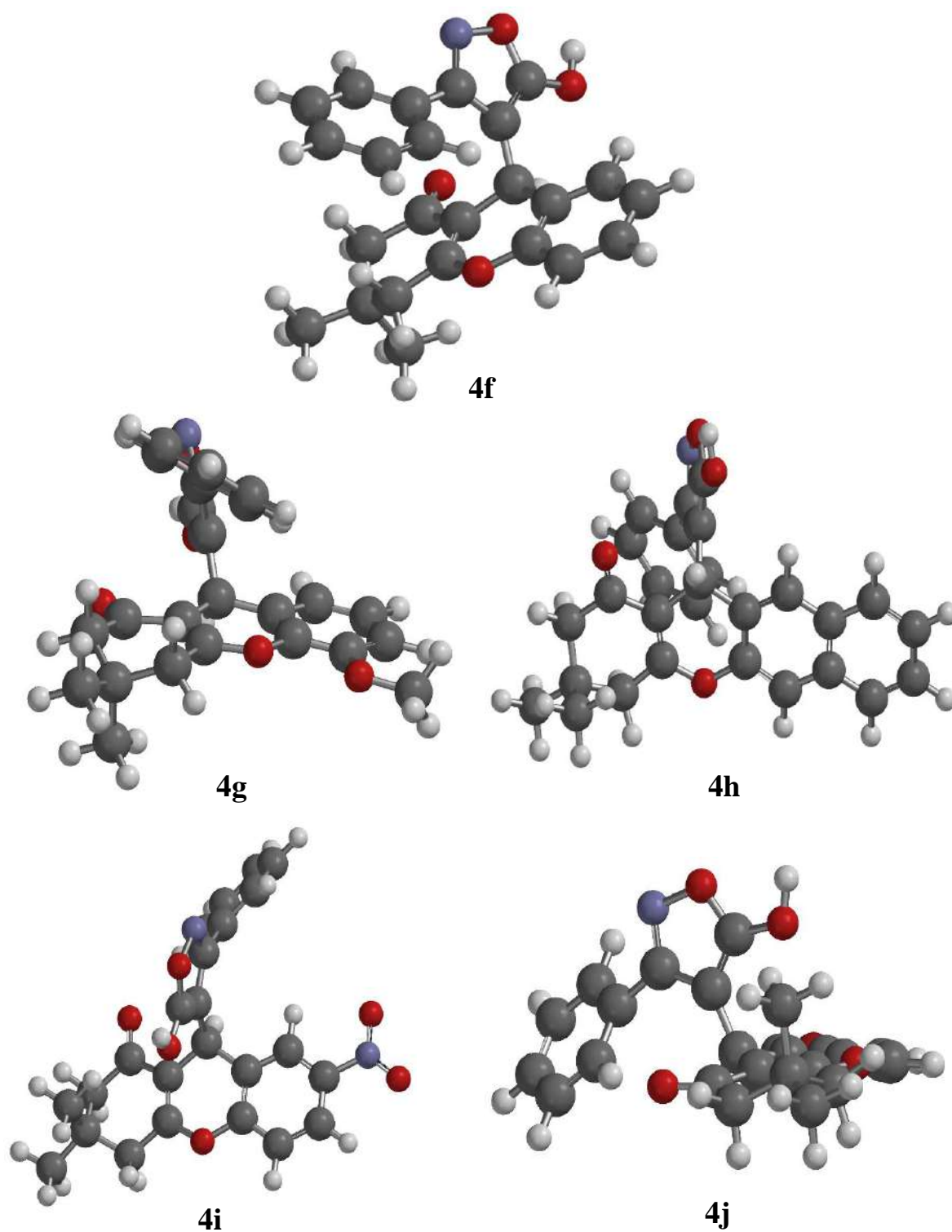


Fig. 12. Optimized structures of the synthesized compounds **4(f-j)**.

4B.9. Conclusion

In summary, we reported some new substituted-(5-hydroxy-3-phenylisoxazol-4-yl)-3,3-dimethyl-2*H*-xanthen-1(9*H*)-one derivatives and evaluated their pharmacological and computational studies. From the absorption study, most of the compounds exhibited a maximum bathochromic shift towards the longer wavelength in DMSO solvent. Cytotoxicity results suggested that, compound **4h** possessed significant efficacy with an IC₅₀ value of 0.15±0.08 µg/mL and anti-TB activity results shows, **4h** compound exhibited good sensitivity at 3.12 µg/mL. The *in silico* molecular interaction studies and structural stability studies also corroborated these findings. Molecular docking study suggested that, the compound **4h** showed least binding energy of -9.9 and -11.0 kcal/mol with P38 MAPk & InhA-Enoyl-Acyl Carrier Protein Reductase respectively. From the DFT study, the compounds are chemically and biologically more reactive with low kinetic stability due to less energy gap.

4B.10. References

1. M. Vadivelu, S. Sampath, K. Muthu, K. Karthikeyan, C. Praveen, *J. Org. Chem.*, **2019**, 84, 13636-13645.
2. V. Guguloth, N.S. Thirukovela, S. Paidakula, R. Vadde, *Russ. J. Gen. Chem.*, **2020**, 90, 470-475.
3. R. Naresh Kumar, G. Jitender Dev, N. Ravikumar, D. Krishna Swaroop, B. Debanjan, G. Bharath, B. Narsaiah, S. Nishant Jain, A. Gangagni Rao, *Bioorg. Med. Chem. Lett.*, **2016**, 26, 2927-2930.
4. J. Trivedi, A. Parveen, F. Rozy, A. Mitra, C. Bal, D. Mitra, A. Sharon, *Eur. J. Med. Chem.*, **2019**, 183, 1-9.
5. B. Manjunatha, Y.D. Bodke, R. Sandeep kumar Jain, T.N. Lohith, M.A. Sridhar, *J. Mol. Struct.*, **2021**, 1244, 1-9.
6. E.K.A. Abdelall, *Bioorg. Chem.*, **2020**, 94, 1-42.
7. S. Colleoni, A.A. Jensen, E. Landucci, E. Fumagalli, P. Conti, A. Pinto, M. De Amici, D.E. Pellegrini-Giampietro, C. De Micheli, T. Mennini, M. Gobbi, *J. Pharmacol. Exp. Ther.*, **2008**, 326, 646-656.
8. L. Joseph and M. George, *Br. J. Pharm. Res.*, **2016**, 9, 1-7.
9. L. Yu, W. Tueckmantel, J.B. Eaton, B. Caldarone, A. Fedolak, T. Hanania, D. Brunner, R.J. Lukas, A.P. Kozikowski, *J. Med. Chem.*, **2012**, 55, 812-823.
10. Y. Zhang, B.W. Wei, L.N. Zou, M.L. Kang, H.Q. Luo, X.L. Fan, *Tetrahedron*, **2016**, 72, 2472-2475.
11. X. Xia, Q. Zhu, J. Wang, J. Chen, W. Cao, B. Zhu, X.Y. Wu, *J. Org. Chem.*, **2018**, 83, 14617-14625.
12. B. Holzer, B. Stoger, P. Kautny, G. Reider, C. Hametner, J. Frohlich, D. Lumpi, *Cryst. Eng. Comm.*, **2018**, 20, 12-16.
13. M. Tanaka, T. Haino, K. Ideta, K. Kubo, A. Mori, Y. Fukazawa, *Tetrahedron*, **2007**, 63, 652-665.
14. K. Koyama, M. Takahashi, M. Oitate, N. Nakai, H. Takakusa, S. Miura, O. Okazaki, *Antimicrob. Agents Chemother.*, **2009**, 53, 4845-4851.
15. D. Kumar, P. Sharma, H. Singh, K. Nepali, G.K. Gupta, S.K. Jain, F. Ntie-Kang, *RSC Adv.*, **2017**, 7, 36977-36999.
16. X. Fan, D. Feng, Y. Qu, X. Zhang, J. Wang, P.M. Loiseau, E. De Clercq, *Bioorg. Med. Chem. Lett.*, **2010**, 20, 809-813.

17. M.D. Aytemir, U. Calis, M. Ozalp, *Arch. Pharm.*, **2004**, 337, 281-289.
18. R. Sakhuja, S.S. Panda, L. Khanna, S. Khurana, S.C. Jain, *Bioorg. Med. Chem. Lett.*, **2011**, 21, 5465-5469.
19. V.J. Ram, A. Goel, P.K. Shukla, A. Kapil, *Bioorg. Med. Chem. Lett.*, **1997**, 7, 3101-3106.
20. D. Kumar, G. Singh, P. Sharma, A. Qayum, G. Mahajan, M.J. Minto, G.K. Gupta, *Anti-Cancer Agents Med. Chem.*, **2018**, 18, 57-73.
21. A. Defant, I. Mancini, R. Tomazzolli, J. Balzarini, *Arch. Pharm.*, **2015**, 348, 23-33.
22. A.I. Almansour, R.S. Kumar, N. Arumugam, D. Sriram, *Eur. J. Med. Chem.*, **2012**, 53, 416-423.
23. L. Abrunhosa, M. Costa, F. Areias, A. Venâncio, F. Proenca, *J. Ind. Microbiol. Biotechnol.*, **2007**, 34, 787-795.
24. N. Vaddiraju, M. Ajitha, K. Rajnarayana, G. Ramreddy, *Res. J. Pharm. Technol.*, **2022**, 15, 591-597.
25. L.A. Reiter, R.P. Robinson, K.F. McClure, C.S. Jones, M.R. Reese, P.G., Mitchell, M.L. Vaughn-Bowser, *Bioorg. Med. Chem. Lett.*, **2004**, 14, 3389-3395.
26. T.V. Mourik, M. Buhl, M.P. Gaigeot, *Phil. Trans. R. Soc. A*, **2014**, 372, 1-7.
27. F. Erdemir, D.B. Celepci, A. Aktas, Y. Gok, *J. Mol. Struct.*, **2020**, 1204, 1-25.
28. A. Pandith, Y.J. Seo, *J. Inorg. Biochem.*, **2020**, 203, 1-41.
29. T. Venkatesh, K. Upendranath, Y.A. Nayaka, *J. Solid State Electrochem.*, **2021**, 25, 1237-1244.
30. V. Krishnakumar, B.K. Mandal, F.R.N. Khan, E.D. Jeong, *Tetrahedron Lett.*, **2014**, 55, 3717-3720.
31. L. Suresh, P.S.V. Kumar, G.V.P. Chandramouli, *J. Mol. Struct.*, **2017**, 1134, 51-58.
32. A. Singh, K.R. Ansari, D.S. Chauhan, M.A. Quraishi, S. Kaya, *Sustain. Chem. Pharm.*, **2020**, 16, 1-11.
33. U.S. Rai, A.M. Isloor, A.M. Vijesh, N. Prabhu, S. Isloor, M. Thiageeswaran, H.K. Fun, *Eur. J. Med. Chem.*, **2010**, 45, 2695-2699.
34. F.S. Abu El-Azm, M.M. El-Shahawi, A.S. Elgubbi, H.M. Madkour, *Synth. Commun.*, **2020**, 50, 669-683.
35. S. Poola, M.S. Shaik, M. Sudileti, S. Yakkate, V. Nalluri, A. Chippada, S.R. Cirandur, *J. Chin. Chem. Soc.*, **2020**, 67, 805-820.
36. S.H. Sukanya, T. Venkatesh, S.A. Rao, A. Pandith, *J. Mol. Struct.*, **2022**, 1267, 1-28.
37. O. Nagaraja, Y.D. Bodke, I. Pushpavathi, S. Ravi Kumar, *Heliyon*, **2020**, 6, 1-11.

38. K. Upendranath, T. Venkatesh, Y.A. Nayaka, M. Shashank, G. Nagaraju, *Inorg. Chem. Commun.*, **2022**, 139, 1-14.
39. G. Ramesh, S. Daravath, N. Ganji, A. Rambabu, K. Venkateswarlu, *J. Mol. Struct.*, **2020**, 1202, 1-41.
40. S.J. Aditya Rao and P. Nandini Shetty, *Life Sci.*, **2021**, 281, 1-11.
41. J. George, J.C. Prasana, S. Muthu, T.K. Kuruvilla, S. Savanthi, R.S. Saji, *J. Mol. Struct.*, **2018**, 1171, 268-278.

5.1. Introduction

Isoxazole analogs have been recognized as key moieties in the field of pharmaceuticals and they are found in many natural products which include ibotenic acid, muscimol etc. [1] and found in synthetic drugs [2]. Moreover, previous reports suggested that, isoxazole fused other biologically active heterocyclic compounds are exhibited as anti-HIV [3], anti-tuberculosis [4], anti-inflammatory [5], anti-diabetic [6], anticancer [7], antidepressant [8], antimicrobial [9], dipeptidyl peptidase IV inhibitors [10] and as protein tyrosine phosphatase-1B inhibitors etc [11]. Because of its enormous biological applications, isoxazoles creates great interest of researchers to develop methodologies for the preparation of drugs in the medicinal field.

Diabetes and cancer diseases are more common nowadays around the globe due to their inappropriate metabolism of carbohydrates, fat and proteins [12] and uncontrolled cell divisions [13]. One of the important therapeutic approaches for treating diabetes is to decrease of postprandial hyperglycemia. This can be achieved by hindering the absorption of glucose by the inhibition of carbohydrate hydrolyzing enzymes, such as α -amylase and α -glucosidase in the gastrointestinal track [14]. Lung cancer is the most prominent cause of carcinoma deaths. The high mortality rate of this disease is due to tobacco smoking or cigarette smoking in human beings. Besides surgery and radiotherapy, chemotherapy is the most effective method for the treatment of diabetic and cancer diseases [15, 16]. The importance of isoxazole-based compounds are available in the market as shown in **Fig. 1** and some reported biologically important isoxazole-containing derivatives have been discussed below.

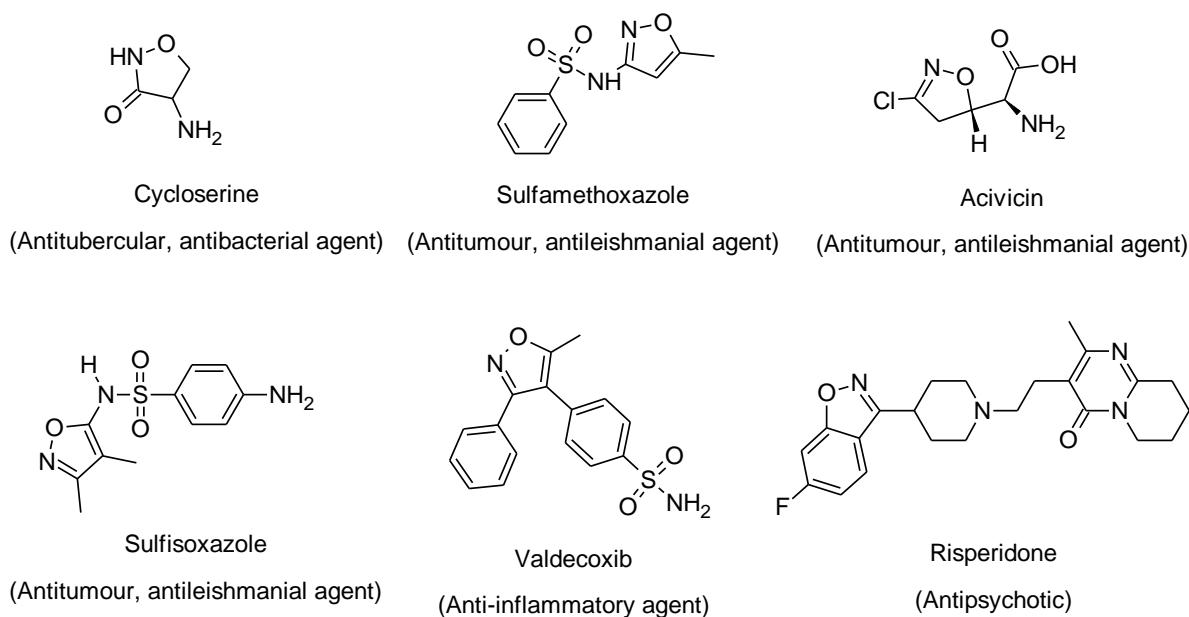
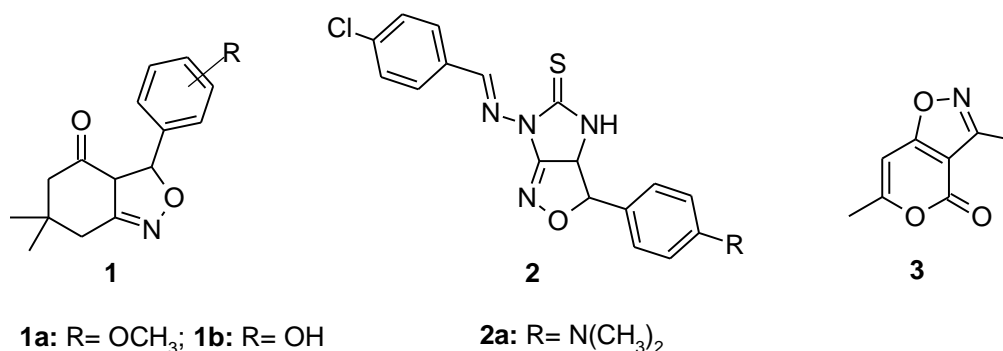


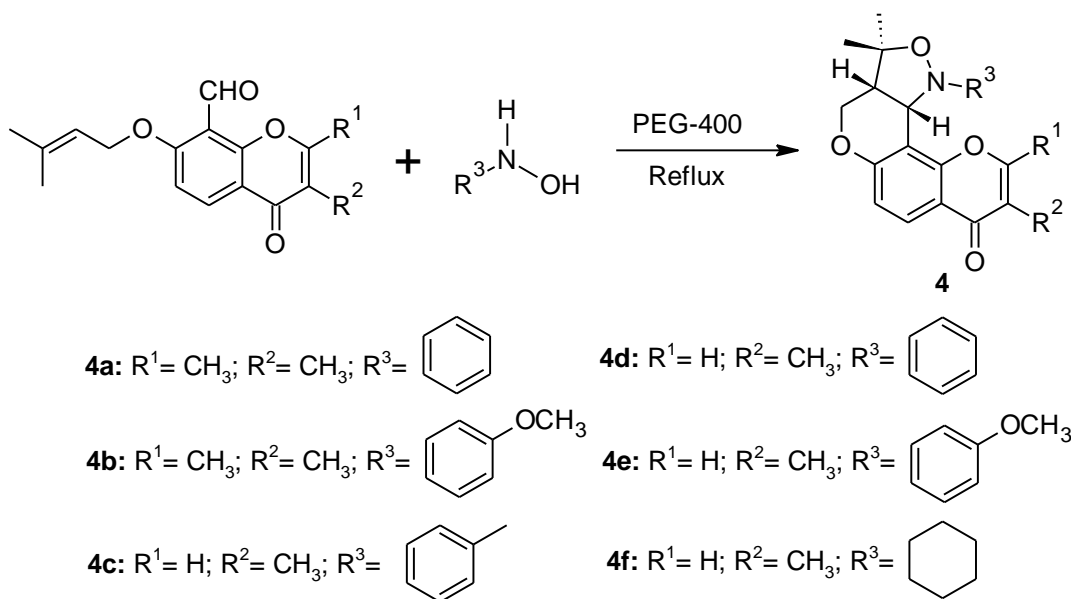
Fig. 1. Some of the drugs containing isoxazole nucleus.

V.V. Dabholkar and F.Y. Ansari reported a cyclocondensation of fused isoxazole derivatives (**1** & **2**) as a potent antibacterial agent. Compound **1a** showed zone of inhibition 16 & 10 mm against *S. aureus* and *C. diphtheria*. Compound **1b** exhibited inhibition 10 & 10 mm against *E. coli* and *P. aeruginosa* respectively. **2a** showed a good zone of inhibition of 21 & 17 mm towards *S. aureus* and *C. diphtheria*, respectively [17]. In 1995, L. Somogyi *et. al.*, have been reported a 3,6-dimethyl-4*H*-pyrano[3,4-*d*][1,2]oxazol-4-one (**3**) from the acylhydrazones [18].

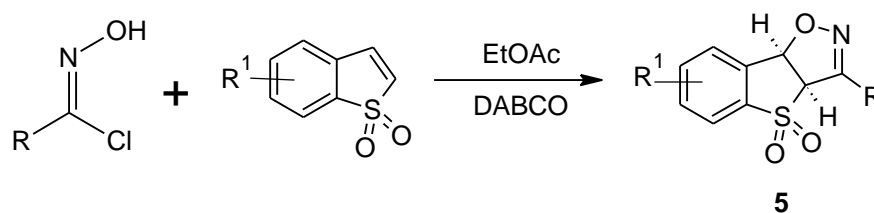


A series of chromeno-annulated cis-fused pyrano[4,3-*c*]isoxazole derivatives (**4**) was reported by N.K. Bejjanki and co-authors *via* intramolecular nitronc cycloaddition and their

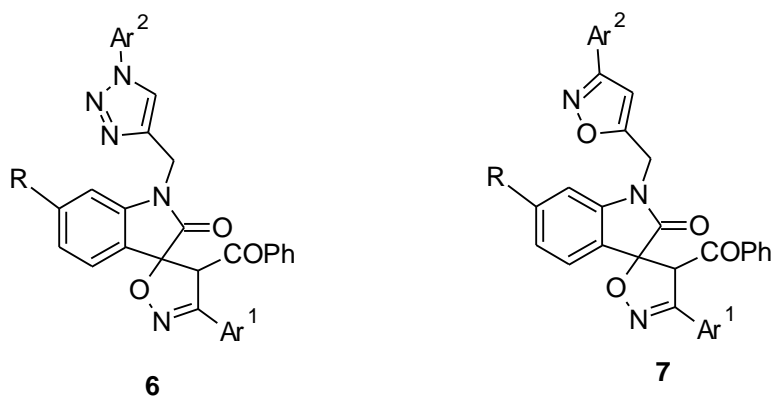
cytotoxicity evaluation. Compounds **4a**, **4b** & **4c** displayed potent inhibitory activity against breast cancer cell line with IC_{50} values of 5.78, 5.59 & 5.3 μM and compounds **4d** & **4e** exhibited significant activity against HeLa cell line with IC_{50} values of 6.61 & 6.54 μM . Compound **4f** was found to have the most promising cytotoxicity against lung cancer cell line with an IC_{50} value of 0.194 μM [19].



In 2020, Tricyclic isoxazole-fused benzo[*b*]thiophene 1,1-dioxide derivatives (**5**) have been reported by K.K. Wang *et. al.*, via 1,3-dipolar cycloaddition [20].

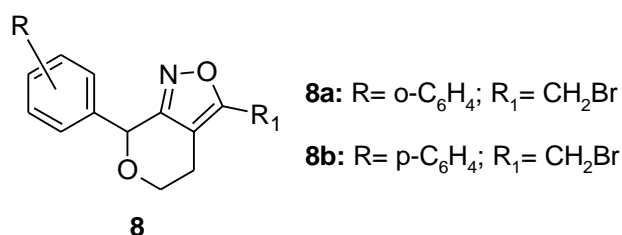


R. Sakly *et. al.*, reported a spirooxindole-fused isoxazoline/triazole (**6**) and isoxazoline/isoxazole derivatives (**7**) from 1,3-dipolar cycloaddition as a potent antimicrobial agent. The compound **6a** exhibited excellent bacterial activity with MIC value of 15.62 $\mu\text{g/mL}$ against *E. coli* strain and compound **7a** showed a MIC of 31.25 $\mu\text{g/mL}$ against *P. aeruginosa* strain. **6b** compound showed MIC value of 15.62 $\mu\text{g/mL}$ against *S. aureus* and compound **6c** exhibits MIC value of 62.5 $\mu\text{g/mL}$ against *S. pyogenes* [21].

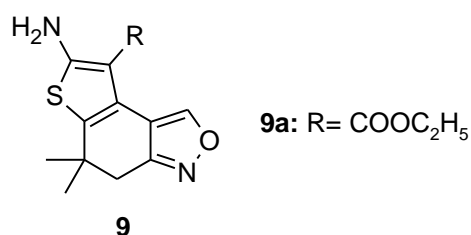


- 6a:** R= Br; Ar¹= p-CH₃-C₆H₄; Ar²= p-Cl-C₆H₄ **7a:** R= Br; Ar¹= p-CH₃-C₆H₄; Ar²= p-Cl-C₆H₄
6b: R= Br; Ar¹= CH₃-C₆H₄; Ar²= p-NO₂-C₆H₄
6c: R= Br; Ar¹= CH₃-C₆H₄; Ar²= p-OCH₃-C₆H₄

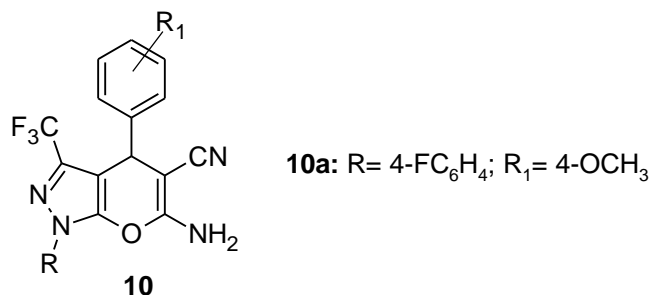
H.J. Kim and co-workers synthesized 4,5-dihydro-7H-pyrano[3,4-c]isoxazole derivatives (**8**) as a fungicidal agents. The compounds **8a** & **8b** shows higher % of inhibition against all the fungal strains *viz* *P. Oryzae*, *R. Solani*, *B. Cinerea*, *P. Infestants*, *P. Recondite* & *E. Graminis* [22].



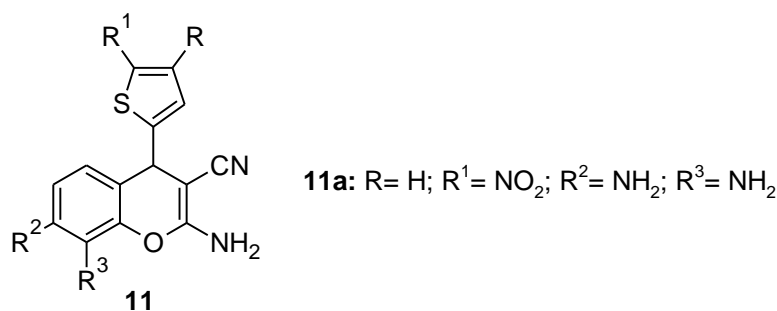
In 2020, R.M. Mohareb *et. al.*, synthesized a 5,5-dimethyl-4,5-dihydrothieno[3,2-*e*][2,1]benzoxazol-7-amines (**9**) as a potent anticancer agent and tyrosine kinase inhibitors. Compound **9a** shows the most cytotoxic effect against all the six cell lines with IC₅₀ values of 1.28, 1.63, 0.79, 0.83, 1.63 & 0.92 μM respectively and also exhibits good inhibitions toward Pim-1 kinase [23].



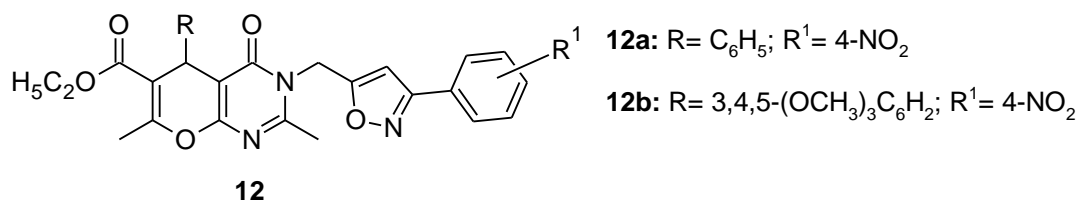
S. Bhavanarushi and co-authors synthesized a novel pyrano[2,3-*c*]pyrazole analogs (**10**) and screened for *in vitro* cytotoxicity against lung cancer (A549), non-lung cancer cells (MRC-5) and cervical cancer (HeLa) cell lines. Among them, compound **10a** exhibited the best cytotoxicity against a lung cancer line with an IC_{50} value of $10.3 \pm 0.89 \mu\text{M}$ [24].



A series of 4*H*-chromene-3-carbonitrile derivatives (**11**) have been synthesized by Z. Saffari *et. al.*, and evaluated for their anticancer activity against five cancer cell lines. The compound **11a** exhibited least IC_{50} values of 58.64 ± 6.1 , 48.39 ± 3.2 , 81.42 ± 6.1 , 46.86 ± 2.4 & $100.53 \pm 7.4 \mu\text{M}$ for human ductal breast epithelial carcinoma, human breast epithelial carcinoma, human glioblastoma carcinoma, rat brain fibroblast carcinoma and mouse fibroblast carcinoma cell lines respectively [25].



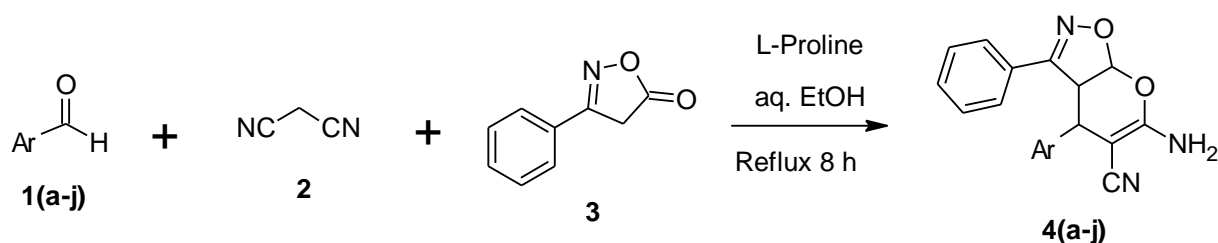
In 2017, a series of novel ethyl 2,7-dimethyl-4-oxo-5-phenyl-3-[(3-phenylisoxazol-5-yl)methyl]-3,5-dihydro-4*H*-pyrano[2,3-*d*]pyrimidine-6-carboxylates derivatives (**12**) as antibacterial agent and was reported by B.S. Kumar *et. al.* Compounds **12a** & **12b** shows excellent activity against bacterial strains *S. aureus*, *P. aeruginosa*, *E. coli* and *K. pneumonia* with MIC value of 38, 36, 38, 38 $\mu\text{g/mL}$ and 33, 28, 30, 29 $\mu\text{g/mL}$ respectively [26].



From the above findings, we encouraged to synthesizing pyrano-isoxazole derivatives and evaluated their anti-diabetic and cytotoxicity. This study also extends to predict the binding interactions of synthesized compounds against the target enzymes α -D-glucosaminidase and P38 MAP kinase proteins along with their *in silico* ADME investigations.

5.2. Present work

In this chapter, we explained one-pot synthesis of 6-amino-4-substituted-pyrano[3,2-*d*]isoxazole-5-carbonitrile derivatives **4(a-j)** through Knoevenagel condensation reaction of aromatic aldehyde (**1**), malononitrile (**2**) and 3-phenyl-5-isoxazolone (**3**) in aqueous ethanol using L-Proline as a catalyst and the reaction pathway has been given in **Scheme 6**.



Compd.	Ar	Compd.	Ar
4a	C ₆ H ₅	4f	2-OH C ₆ H ₄
4b	4-OH C ₆ H ₄	4g	5-Br 2-OH C ₆ H ₃
4c	4-OCH ₃ C ₆ H ₄	4h	3-OC ₂ H ₅ 4-OH C ₆ H ₃
4d	4-CN C ₆ H ₄	4i	
4e	3-NO ₂ C ₆ H ₄	4j	

Scheme 6. Synthesis of 6-amino-4-substituted-pyrano[3,2-*d*]isoxazole-5-carbonitrile derivatives **4(a-j)**.

The synthetic strategy involves in the following steps:

- The 6-amino-4-substituted-pyrano[3,2-*d*]isoxazole-5-carbonitrile derivatives were synthesized initially, L-Proline abstract the hydrogen from malononitrile (**2**) to form carbanion (**I**).
- It attacks the carbonyl group of the aromatic aldehyde (**1**) to form an intermediate **II** & **III**, it undergoes Knoevenagel condensation to afford a cyano-olefin (**IV**) intermediate.
- Then, 3-phenyl-5-isoxazolone (**3**) was attacked on cyano-olefin to afford intermediates **V** and **VI**. Further intermediate **VI** undergoes an intramolecular nucleophilic cyclisation to afford **VII**.
- Finally, 1,3-hydrogen shift takes place from intermediate **VII** to form desired product **4(a-j)**. The possible mechanism as shown below (**Fig. 2**).

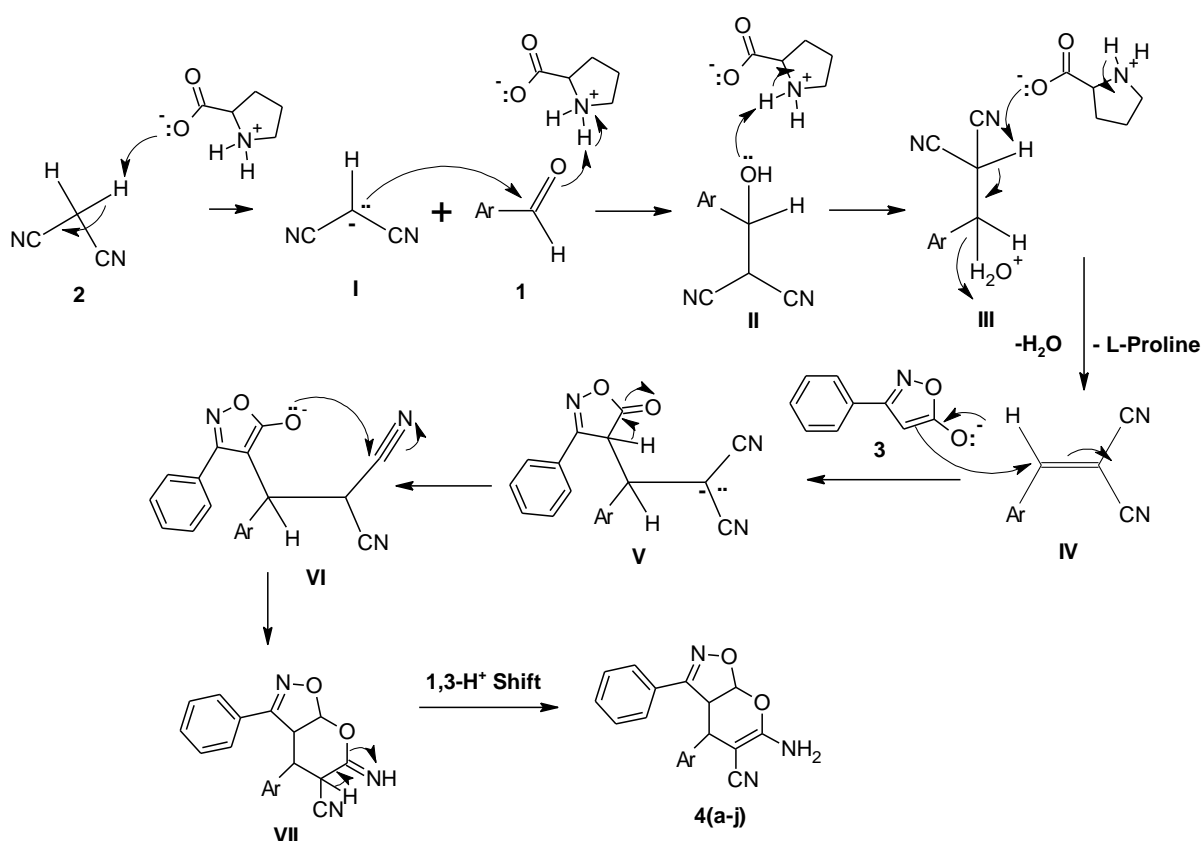


Fig. 2. Possible mechanism of synthesized compounds **4(a-j)**.

Here, we studied the effect of catalyst on this reaction. In the previous reports, this method was carried out in the presence of different catalysts such as TEBA, HTMAB, B(OH)₃, Et₃N, PS-PTSA, Nano TiO₂, ZnS NPs, piperidine and also in the absence of catalyst (**Table 1**). We selected L-Proline as a catalyst to find the progress of the reaction as well as on the increase of the product yield by using different mol % i.e., 5, 10, 15 and 20 was examined on the compound **4a**. 10 mol % L-Proline was preferred in this reaction due to short reaction time and good yield, whereas a further increase in the quantity of catalyst does not affect the reaction kinetics (**Table 2**).

Table 1. Effect of catalysts on synthesized compound **4a**.

Entry	Catalyst	Solvent	Temperature (°C)	Time	Yield (%)
1	L-Proline	EtOH	Reflux	8 h	90-92
2	-	CH ₃ CN	RT	12 h	58-79 ^[27]
3	TEBA	H ₂ O	Reflux	6-10 h	90-99 ^[28]
4	HTMAB	H ₂ O	Reflux	8 h	79-91 ^[29]
5	B(OH) ₃	H ₂ O	Reflux	10-20 min	70-85 ^[30]
6	Et ₃ N	EtOH	Reflux	15 min	47-75 ^[31]
7	PS-PTSA	H ₂ O	Reflux	15-25 min	82-94 ^[32]
8	Nano TiO ₂	-	RT	2-6 min	81-96 ^[33]
9	ZnS NPs	Grinding	RT	5-21 min	87-97 ^[34]
10	Piperidine	EtOH	Reflux	1 h	85 ^[35]

Table 2. Effect of mol % of L-Proline catalyst on synthesized compound **4a**.

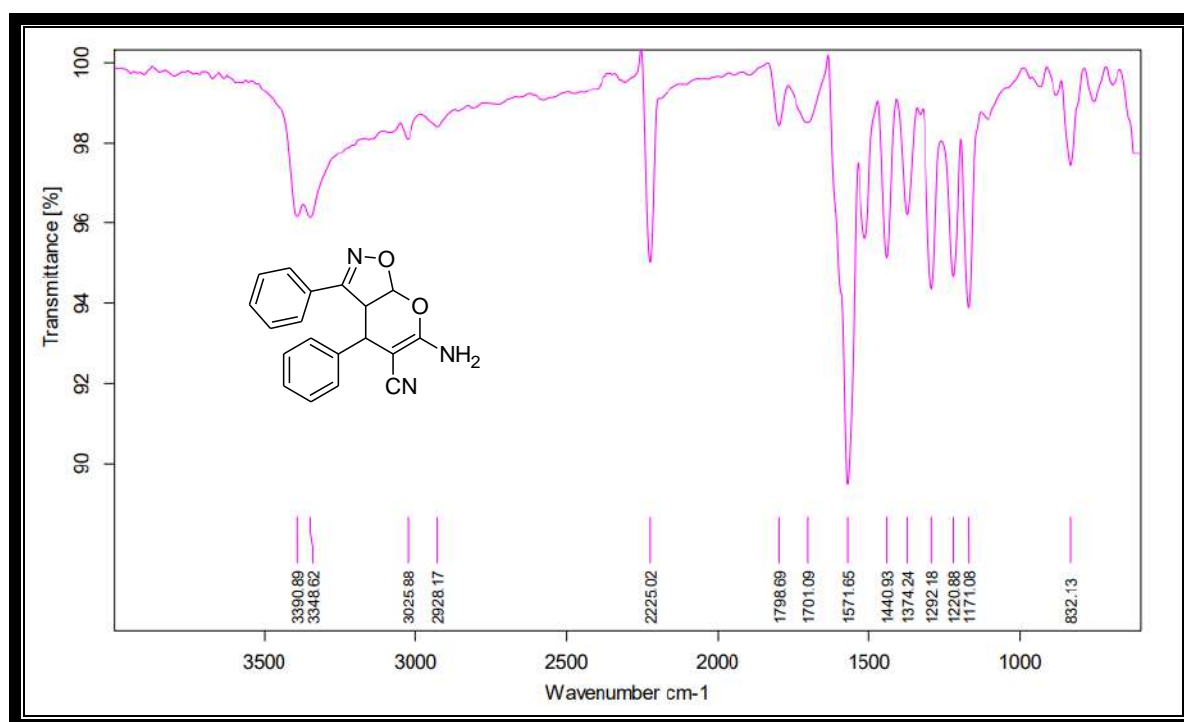
Entry	Catalyst	Solvent	Mol (%)	Time	Yield (%)
1	-	EtOH	-	14 h	50-54
2	L-Proline	EtOH	5	10 h	70-72
3	L-Proline	EtOH	10	8 h	90-92
4	L-Proline	EtOH	15	8 h	88-90
5	L-Proline	EtOH	20	8 h	86-89

The structures of the 6-amino-4-substituted-pyrano[3,2-*d*]isoxazole-5-carbonitrile derivatives **4(a-j)** were confirmed by different spectroscopic techniques such as IR, ¹H NMR, ¹³C NMR and mass spectrometry.

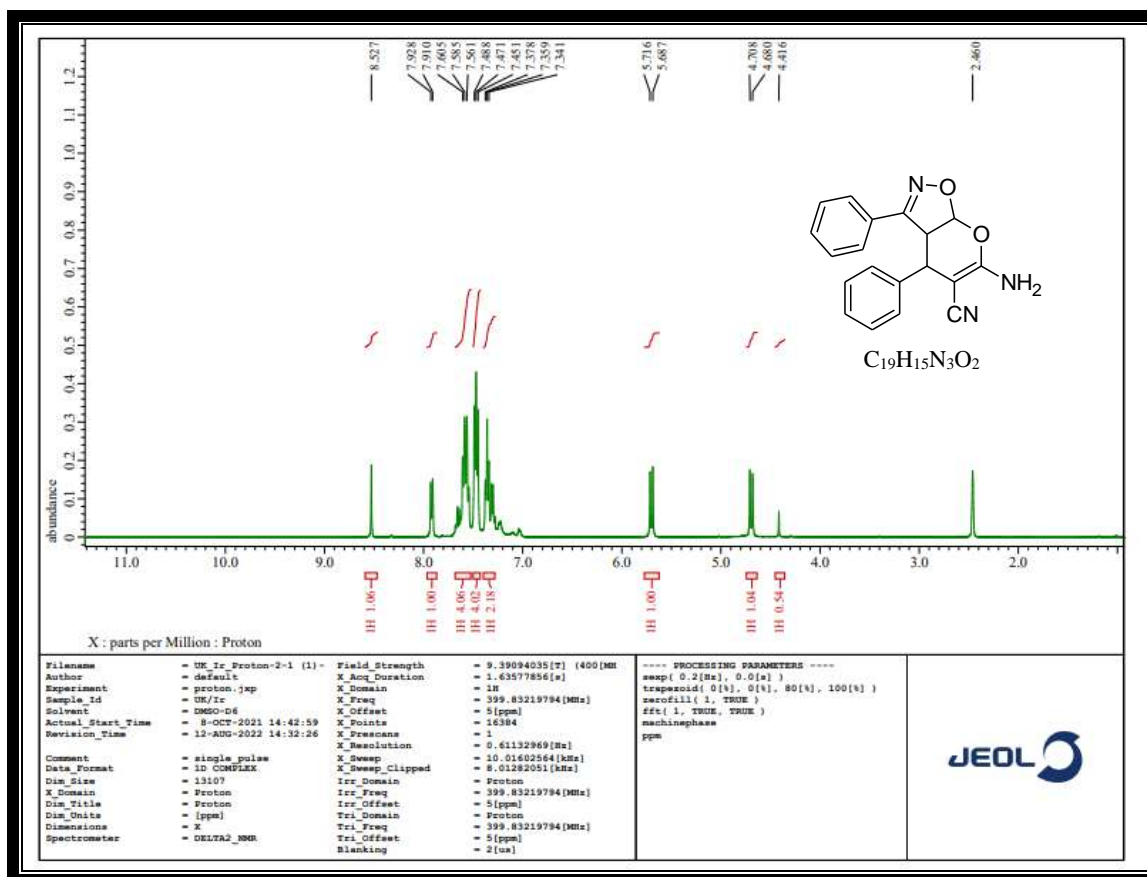
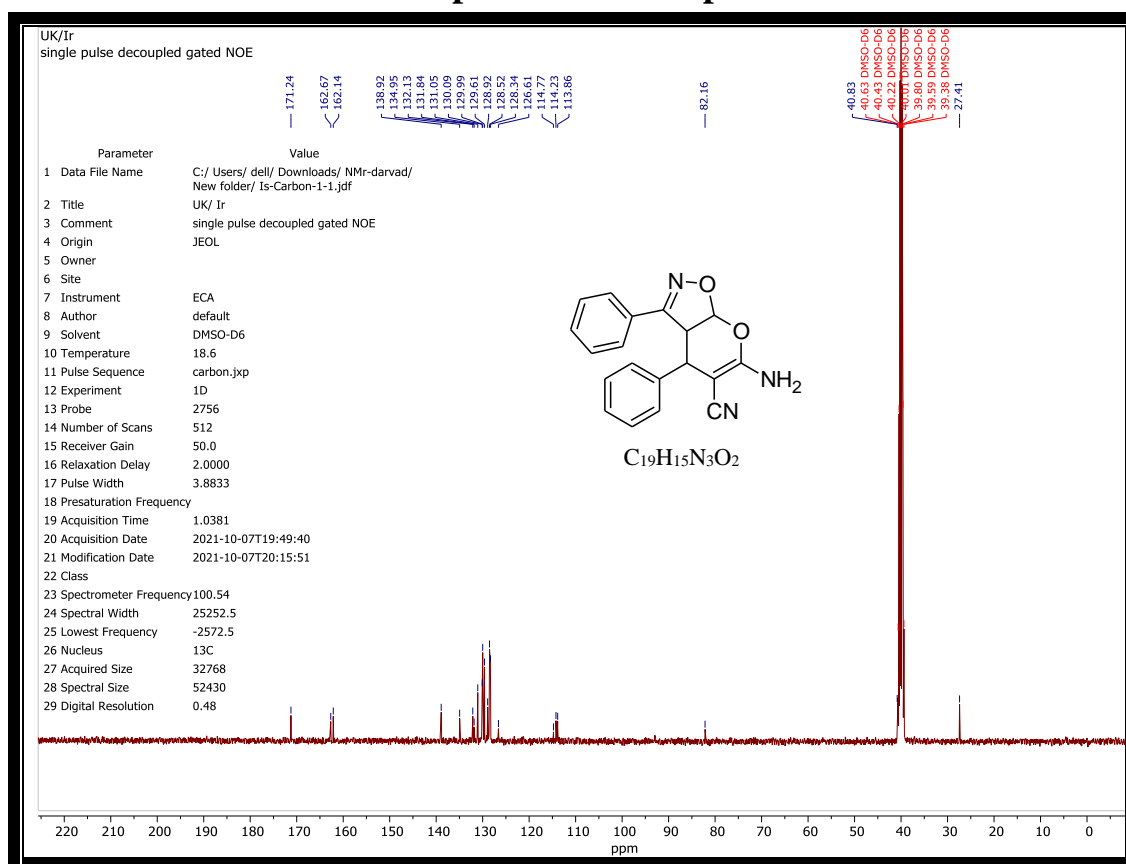
The IR spectrum of compound **4a** showed the absorption band in the region of 3390 cm⁻¹ is attributed to the NH stretching vibration and another strong absorption band at 2225

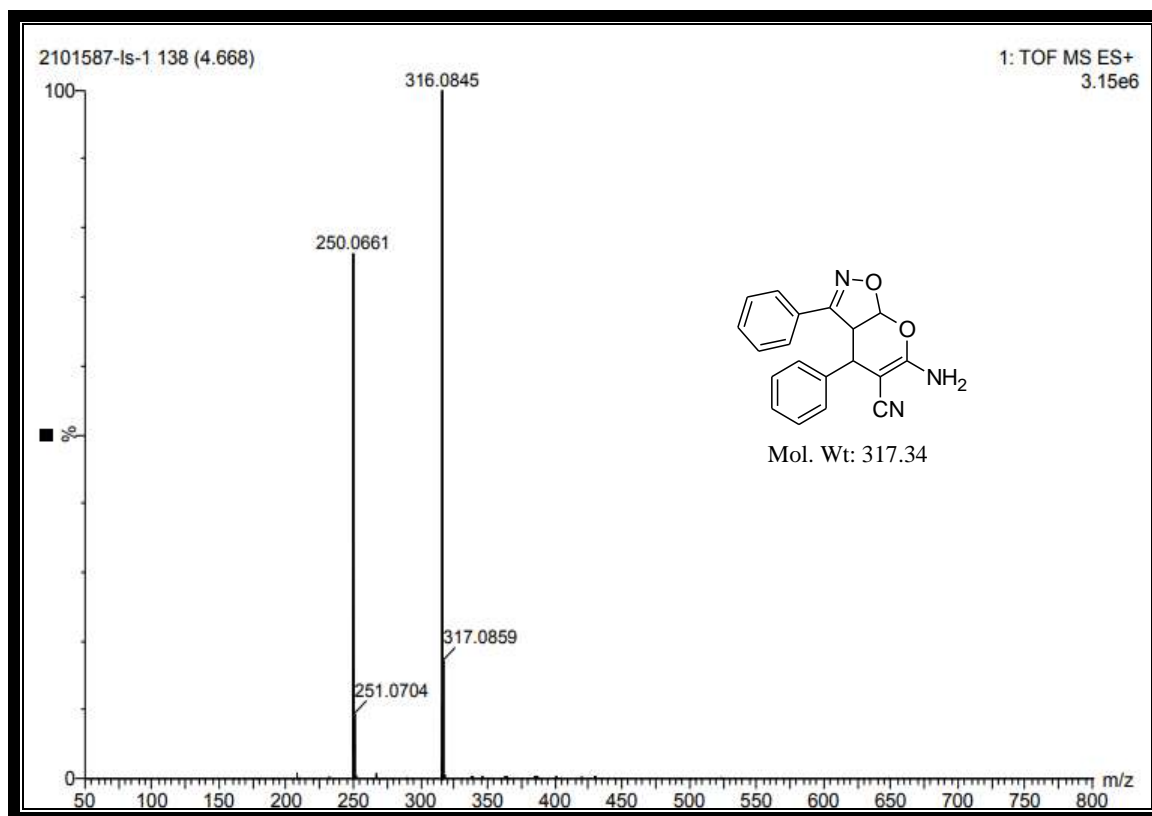
cm^{-1} correspond to $\text{C}\equiv\text{N}$ functionality. The band at 1571 cm^{-1} correspond to the azomethine group ($\text{C}=\text{N}$). The ^1H NMR spectrum of compound **4a** exhibited a singlet peak at δ 8.52 ppm which correspond to aromatic proton (s, 1H, Ar-H) and multiplet peaks in the range at δ 7.93-7.34 ppm which corresponds to aromatic along with amine protons (m, 11H, Ar-H+ NH_2). A doublet peaks at δ 5.71-5.69 & 4.70-4.68 ppm corresponds to two CH protons of isoxazole nucleus (d, $J=8\text{ Hz}$, 2H, CH). And a singlet peak at δ 4.42 ppm due to CH proton (s, 1H, CH). In addition, ^{13}C NMR spectrum of compound **4a** exhibited peaks at δ 138.92, 134.95, 132.13, 131.84, 131.05, 130.09, 129.99, 129.61, 128.92 & 128.34 ppm correspond to $\text{C}=\text{C}$ carbons of phenyl rings and 82.16 ppm due to CH carbon. The mass spectrum showed a molecular ion peak m/z at 316.0845 [M^+-1], which correspond to the molecular weight of compound **4a**.

Characterization:

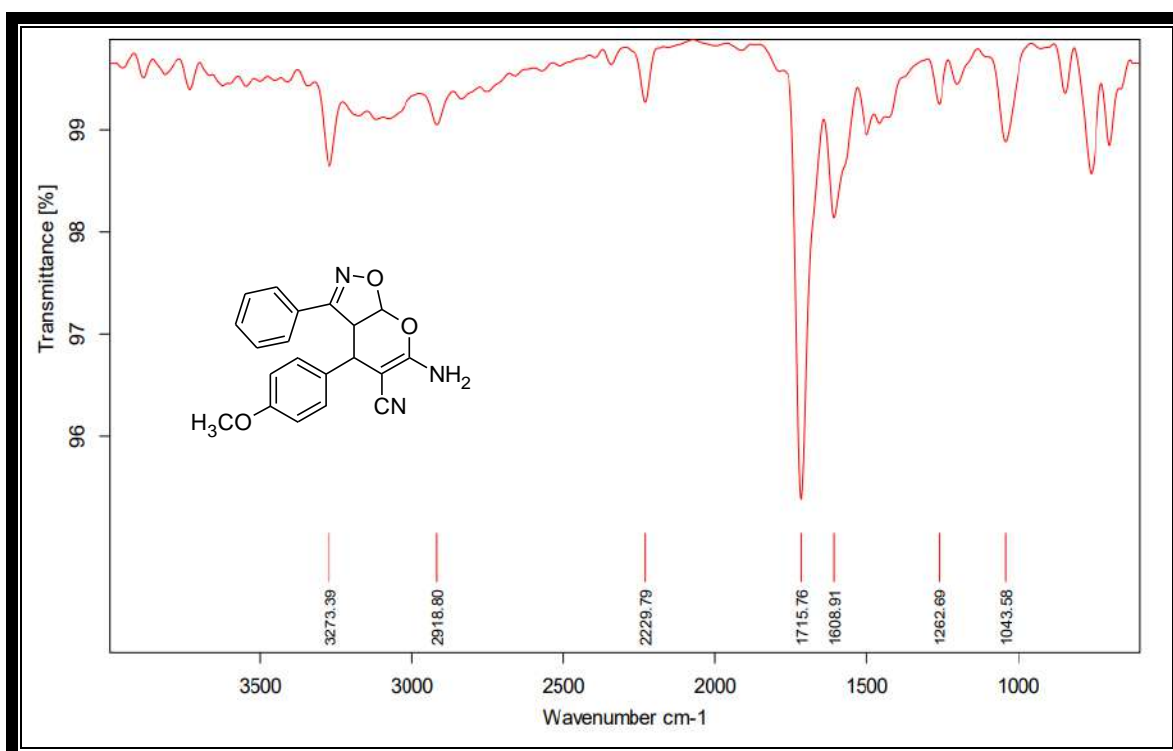


IR spectrum of compound **4a**

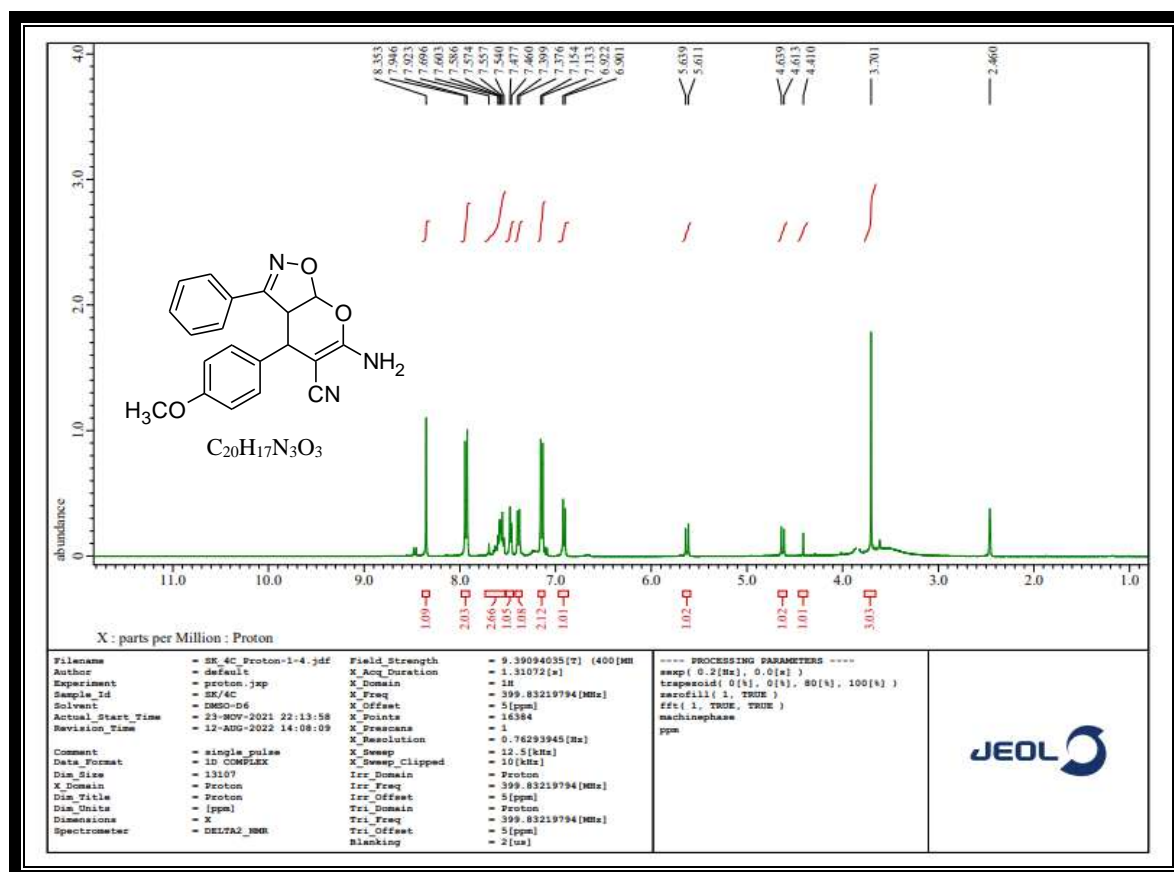
¹H NMR spectrum of compound 4a¹³C NMR spectrum of compound 4a



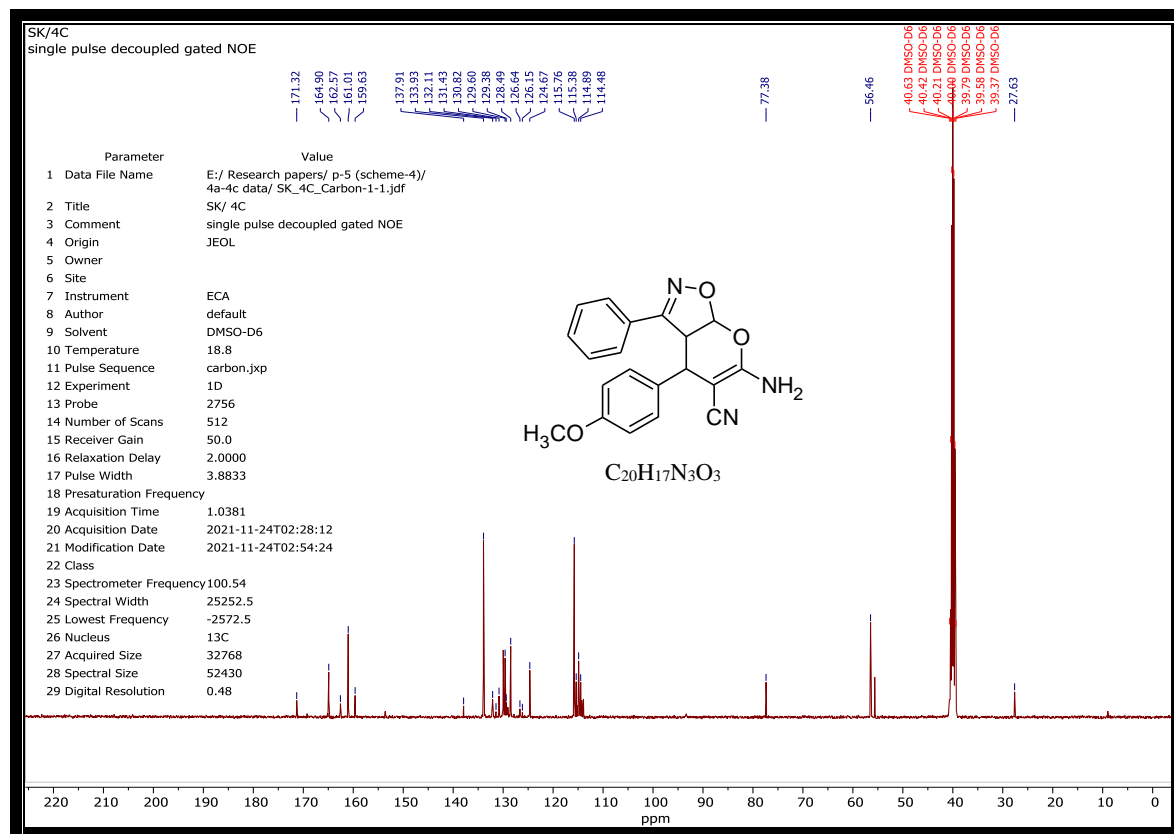
MASS spectrum of compound 4a



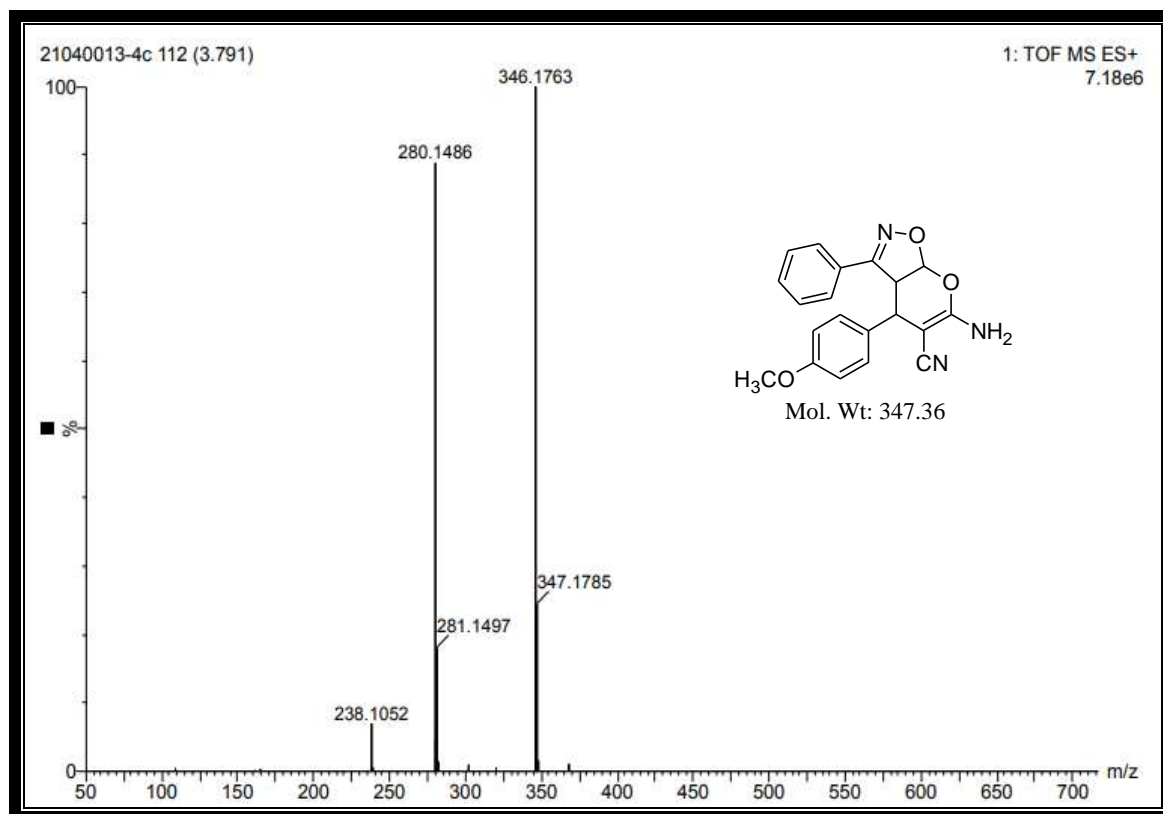
IR spectrum of compound 4c



¹H NMR spectrum of compound 4c



¹³C NMR spectrum of compound 4c



MASS spectrum of compound 4c

5.3. Experimental

5.3.1. General information:

The general information regarding the different solvents, reagents and instruments etc., used for the analysis has been discussed in the experimental section (2A.3.1) of **Chapter-2A**. The cytotoxicity was carried out in the Dept. of Microbiology, Maratha Mandal's NGH Institute of Dental Sciences & Research Centre, Belgaum, Karnataka. The diabetic activity was carried out in LAYA Workstation, Haveri and Alekhya agro solutions, Mysore.

5.3.2. Procedure for synthesis of novel 6-amino-4-substituted-pyrano[3,2-*d*]isoxazole-5-carbonitrile derivatives 4(a-j):

A mixture of equimolar quantity of aromatic aldehydes (**1**, 1 mmol), malononitrile (**2**, 1 mmol) and 3-phenyl-5-isoxazolone (**3**, 1 mmol) using 10 mol % of L-Proline as a catalyst in 20 mL of aqueous ethanol was refluxed with constant stirred at 80-82 °C for about 8 h. At the

same time, the reaction mixture was monitored by TLC (Ethyl acetate & Pet ether). After completion of the reaction, the reaction mixture was cooled at room temperature and poured into the 100 mL ice flake with vigorous stirring to get solid precipitate. Then, it was filtered, washed, dried and recrystallized from methanol to afford pure solid products **4(a-j)**.

6-Amino-3,4-diphenyl-3a,7a-dihydro-4H-pyrano[3,2-d]isoxazole-5-carbonitrile (4a):

White solid; Yield: 95 %; MP: 168-170 °C; Mol. Formula: C₁₉H₁₅N₃O₂; UV (nm) λ_{max} (log ε) 358 (3.72) & 354 (3.57); FTIR (ν cm⁻¹): 3390 (NH), 3025 (CH), 2225 (C≡N) & 1571 (C=N); ¹H NMR (δ ppm): 8.52 (s, 1H, Ar-H), 7.93-7.91 (d, *J*= 8 Hz, 1H, Ar-H), 7.60-7.56 (m, 4H, Ar-H), 7.48-7.45 (m, 4H, NH₂+Ar-H), 7.37-7.34 (m, 2H, Ar-H), 5.71-5.69 (d, *J*= 8 Hz, 1H, CH), 4.70-4.68 (d, *J*= 8 Hz, 1H, CH), 4.42 (s, 1H, CH); ¹³C NMR (δ ppm): 171.24, 162.67, 162.14, 138.92, 134.95, 132.13, 131.84, 131.05, 130.09, 129.99, 129.61, 128.92, 128.34, 126.61, 114.77, 114.23, 113.86, 82.16, 40.83 & 27.41; HRMS: *m/z* 316.0845 [M⁺-1]; Anal. Calcd: C 71.91, H 4.76, N 13.24 %, Found: C 71.86, H 4.72, N 13.20 %.

6-Amino-4-(4-hydroxyphenyl)-3-phenyl-3a,7a-dihydro-4H-pyrano[3,2-d]isoxazole-5-carbonitrile (4b):

Yellow solid; Yield: 80 %; MP: 146-148 °C; Mol. Formula: C₁₉H₁₅N₃O₃; UV (nm) λ_{max} (log ε) 352 (3.75) & 352 (3.74); FTIR (ν cm⁻¹): 3452 (OH), 3257 (NH), 2904 (CH), 2220 (C≡N) & 1580 (C=N); ¹H NMR (δ ppm): 11.06 (s, 1H, OH), 8.41-8.39 (d, *J*= 8 Hz, 1H, Ar-H), 8.27 (s, 1H, Ar-H), 7.86-7.84 (d, *J*= 8 Hz, 2H, Ar-H), 7.62-7.45 (m, 2H, Ar-H), 7.27-7.25 (d, *J*= 8 Hz, 1H, Ar-H), 6.95-6.89 (m, 3H, NH₂+Ar-H), 6.72-6.70 (d, *J*= 8 Hz, 1H, Ar-H), 5.57-5.55 (d, *J*= 8 Hz, 1H, CH), 4.54-4.52 (d, *J*= 8 Hz, 1H, CH), 4.41 (s, 1H, CH); ¹³C NMR (δ ppm): 164.43, 161.08, 138.61, 134.44, 129.97, 129.77, 129.58, 129.38, 128.46, 123.33, 117.17, 116.70, 116.22, 115.65, 114.74, 75.63 & 28.26; HRMS: *m/z* 332.1556 [M⁺-1]; Anal. Calcd: C 68.46, H 4.54, N 12.61 %, Found: C 68.41, H 4.51, N 12.55 %.

6-Amino-4-(4-methoxyphenyl)-3-phenyl-3a,7a-dihydro-4H-pyranof[3,2-d]isoxazole-5-carbonitrile (4c):

Yellow solid; Yield: 82 %; MP: 120-122 °C; Mol. Formula: C₂₀H₁₇N₃O₃; UV (nm) λ_{max} (log ε) 354 (3.36) & 353 (3.30), 282 (3.32); FTIR (ν cm⁻¹): 3273 (NH), 2918 (CH), 2854 (OCH₃), 2229 (C≡N) & 1608 (C=N); ¹H NMR (δ ppm): 8.35 (s, 1H, Ar-H), 7.94-7.92 (d, J= 8 Hz, 2H, Ar-H), 7.69-7.54 (m, 3H, NH₂+Ar-H), 7.48-7.46 (d, J= 8 Hz, 1H, Ar-H), 7.39-7.37 (d, J= 8 Hz, 1H, Ar-H), 7.15-7.13 (d, J= 8 Hz, 2H, Ar-H), 6.92-6.90 (d, J= 8 Hz, 1H, Ar-H), 5.63-5.61 (d, J= 8 Hz, 1H, CH), 4.63-4.61 (d, J= 8 Hz, 1H, CH), 4.41 (s, 1H, CH), 3.70 (s, 3H, OCH₃); ¹³C NMR (δ ppm): 171.32, 164.90, 162.57, 161.01, 159.63, 137.91, 133.93, 132.11, 131.43, 130.82, 129.60, 129.38, 128.49, 126.15, 124.67, 115.38, 114.48, 77.38, 56.46 & 27.63; HRMS: m/z 346.1763 [M⁺-1]; Anal. Calcd: C 69.15, H 4.93, N 12.10 %, Found: C 69.09, H 4.89, N 12.06 %.

6-Amino-4-(4-cyanophenyl)-3-phenyl-3a,7a-dihydro-4H-pyranof[3,2-d]isoxazole-5-carbonitrile (4d):

Cream white solid; Yield: 90 %; MP: 180-182 °C; Mol. Formula: C₂₀H₁₄N₄O₂; UV (nm) λ_{max} (log ε) 366 (3.20), 296 (3.17) & 359 (3.14), 295 (3.11); FTIR (ν cm⁻¹): 3255 (NH), 2902 (CH), 2220 (C≡N) & 1601 (C=N); ¹H NMR (δ ppm): 8.52 (s, 1H, Ar-H), 7.93-7.91 (d, J= 8 Hz, 1H, Ar-H), 7.66-7.56 (m, 4H, Ar-H), 7.49-7.45 (t, 2H, Ar-H), 7.38-7.30 (m, 3H, NH₂+Ar-H), 5.71-5.68 (d, J= 12 Hz, 1H, CH), 4.70-4.67 (d, J= 12 Hz, 1H, CH), 4.41 (s, 1H, CH); ¹³C NMR (δ ppm): 171.31, 162.66, 162.08, 138.81, 134.89, 132.06, 131.92, 130.99, 130.17, 129.78, 129.44, 129.09, 128.47, 128.37, 126.58, 114.71, 114.01, 113.88, 82.11, 40.82 & 27.36; HRMS: m/z 341.1794 [M⁺-1]; Anal. Calcd: C 70.17, H 4.12, N 16.37 %, Found: C 70.13, H 4.08, N 16.31 %.

6-Amino-4-(3-nitrophenyl)-3-phenyl-3a,7a-dihydro-4H-pyranof[3,2-d]isoxazole-5-carbonitrile (4e):

Yellow solid; Yield: 92 %; MP: 160-162 °C; Mol. Formula: C₁₉H₁₄N₄O₄; UV (nm) λ_{\max} (log ϵ) 343 (3.46) & 340 (3.96); FTIR (ν cm⁻¹): 3320 (NH), 2919 (CH), 2223 (C≡N) & 1577 (C=N); ¹H NMR (CDCl₃, δ ppm): 8.36 (s, 1H, Ar-H), 8.26-8.24 (d, J = 8 Hz, 1H, Ar-H), 7.88-7.86 (d, J = 8 Hz, 1H, Ar-H), 7.70-7.59 (m, 5H, Ar-H), 7.45-7.43 (d, J = 8 Hz, 2H, Ar-H), 7.25 (s, 2H, NH₂), 5.30-5.27 (d, J = 12 Hz, 1H, CH), 4.42-4.39 (d, J = 12 Hz, 1H, CH), 4.32 (s, 1H, CH); ¹³C NMR (CDCl₃, δ ppm): 171.40, 164.26, 148.82, 138.60, 133.97, 132.94, 130.99, 130.17, 127.97, 124.80, 124.46, 123.10, 111.68, 111.39, 76.80, 42.59 & 26.21; HRMS: m/z 361.1749 [M⁺-1]; Anal. Calcd: C 62.98, H 3.89, N 15.46 %, Found: C 62.94, H 3.83, N 15.41 %.

6-Amino-4-(2-hydroxyphenyl)-3-phenyl-3a,7a-dihydro-4H-pyrano[3,2-d]isoxazole-5-carbonitrile (4f):

Yellow solid; Yield: 92 %; MP: 142-144 °C; Mol. Formula: C₁₉H₁₅N₃O₃; UV (nm) λ_{\max} (log ϵ) 340 (3.77) & 339 (3.39); FTIR (ν cm⁻¹): 3420 (OH), 3290 (NH), 2912 (CH), 2226 (C≡N) & 1608 (C=N); ¹H NMR (δ ppm): 11.02 (s, 1H, OH), 7.99-7.97 (d, J = 8 Hz, 1H, Ar-H), 7.92 (s, 1H, Ar-H), 7.88-7.86 (d, J = 8 Hz, 3H, Ar-H), 7.64-7.49 (m, 2H, Ar-H), 7.29-7.27 (d, J = 8 Hz, 1H, Ar-H), 6.92-6.74 (m, 3H, NH₂+Ar-H), 5.61-5.59 (d, J = 8 Hz, 1H, CH), 4.57-4.55 (d, J = 8 Hz, 1H, CH), 4.43 (s, 1H, CH), ¹³C NMR (δ ppm): 164.47, 161.12, 138.65, 134.48, 129.99, 129.79, 129.61, 129.43, 128.51, 123.39, 117.22, 116.75, 116.28, 115.71, 114.82, 76.72 & 24.98; HRMS: m/z 333.3423 [M⁺]; Anal. Calcd: C 68.46, H 4.54, N 12.61 %, Found: C 68.42, H 4.50, N 12.57 %.

6-Amino-4-(5-bromo-2-hydroxyphenyl)-3-phenyl-3a,7a-dihydro-4H-pyrano[3,2-d]isoxazole-5-carbonitrile (4g):

Cream white solid; Yield: 84 %; MP: 126-128 °C; Mol. Formula: C₁₉H₁₄BrN₃O₃; UV (nm) λ_{\max} (log ϵ) 340 (3.84) & 336 (3.80); FTIR (ν cm⁻¹): 3418 (OH), 3298 (NH), 2923 (CH), 2231 (C≡N) & 1601 (C=N); ¹H NMR (δ ppm): 11.02 (s, 1H, OH), 7.90 (s, 1H, Ar-H), 7.84-

7.82 (d, $J = 8$ Hz, 3H, Ar-H), 7.50-7.45 (m, 2H, Ar-H), 7.26-7.24 (d, $J = 8$ Hz, 1H, Ar-H), 6.84-6.71 (m, 3H, NH₂+Ar-H), 5.55-5.53 (d, $J = 8$ Hz, 1H, CH), 4.53-4.51 (d, $J = 8$ Hz, 1H, CH), 4.44 (s, 1H, CH); ¹³C NMR (δ ppm): 163.38, 162.25, 138.62, 134.51, 129.62, 129.58, 128.52, 128.38, 121.39, 117.32, 116.90, 115.30, 114.68, 113.62, 75.42 & 25.85; HRMS: m/z 412.2308 [M⁺]; Anal. Calcd: C 55.36, H 3.42, N 10.19 %, Found: C 55.31, H 3.38, N 10.14 %.

6-Amino-4-(3-ethoxy-4-hydroxyphenyl)-3-phenyl-3a,7a-dihydro-4H-pyrano[3,2-d]isoxazole-5-carbonitrile (4h):

Pale yellow solid; Yield: 88 %; MP: 130-132 °C; Mol. Formula: C₂₁H₁₉N₃O₄; UV (nm) λ_{\max} (log ϵ) 345 (4.13), 302 (4.14) & 342 (3.71), 299 (3.70); FTIR (ν cm⁻¹): 3390 (OH), 3220 (NH), 2911 (CH), 2230 (C \equiv N) & 1603 (C=N); ¹H NMR (δ ppm): 11.08 (s, 1H, OH), 7.72 (s, 1H, Ar-H), 7.68-7.66 (d, $J = 8$ Hz, 2H, Ar-H), 6.39-7.99 (m, 7H, NH₂+Ar-H), 5.10-5.08 (d, $J = 8$ Hz, 1H, CH), 4.44-4.42 (d, $J = 8$ Hz, 1H, CH), 4.35 (s, 1H, CH), 3.12 (s, 3H, CH₃), 2.21 (s, 2H, CH₂); ¹³C NMR (δ ppm): 171.12, 163.24, 162.46, 138.57, 134.23, 129.46, 129.45, 128.96, 128.12, 121.46, 117.85, 116.72, 115.64, 114.98, 113.42, 76.52, 32.00, 29.86 & 24.46; HRMS: m/z 377.3909 [M⁺]; Anal. Calcd: C 66.83, H 5.07, N 11.13 %, Found: C 66.79, H 5.02, N 11.09 %.

6-Amino-4-(3-methyl-2-thienyl)-3-phenyl-3a,7a-dihydro-4H-pyrano[3,2-d]isoxazole-5-carbonitrile (4i):

Brown solid; Yield: 90 %; MP: 136-138 °C; Mol. Formula: C₁₈H₁₅N₃O₂S; UV (nm) λ_{\max} (log ϵ) 335 (4.07) & 337 (3.77); FTIR (ν cm⁻¹): 3270 (NH), 2921 (CH), 2217 (C \equiv N) & 1574 (C=N); ¹H NMR (CDCl₃, δ ppm): 7.92 (s, 1H, Ar-H), 7.77-7.75 (d, $J = 8$ Hz, 1H, Ar-H), 7.67-7.65 (d, $J = 8$ Hz, 2H, Ar-H), 7.55-7.45 (m, 3H, NH₂+Ar-H), 7.25 (s, 1H, Ar-H), 7.06-7.04 (d, $J = 8$ Hz, 1H, Ar-H), 3.81 (s, 1H, CH), 2.44 (s, 3H, CH₃), 2.41 (s, 1H, CH), 2.32 (s, 1H, CH); ¹³C NMR (CDCl₃, δ ppm): 174.90, 163.22, 162.72, 150.50, 149.27, 132.33, 131.32,

131.01, 129.43, 129.34, 128.62, 126.71, 114.59, 113.34, 76.83, 34.19 & 14.91; HRMS: m/z 338.0639 [$M^{+}+1$]; Anal. Calcd: C 64.08, H 4.48, N 12.45 %, Found: C 64.03, H 4.42, N 12.42 %.

6-Amino-4-(3a,7a-dihydro-1H-indol-2-yl)-3-phenyl-3a,7a-dihydro-4H-pyrano[3,2-d]isoxazole-5-carbonitrile (4j):

Yellow solid; Yield: 92 %; MP: 174-176 °C; Mol. Formula: $C_{21}H_{16}N_4O_2$; UV (nm) λ_{max} ($\log \epsilon$) 335 (3.89) & 336 (3.77); FTIR (ν cm^{-1}): 3289 (NH), 2915 (CH), 2252 ($C\equiv N$) & 1599 ($C=N$); 1H NMR (δ ppm): 12.94 (s, 1H, indole NH), 7.90-7.82 (m, 3H, Ar-H), 7.57-7.55 (d, $J=8$ Hz, 2H, Ar-H), 7.33-7.31 (d, $J=8$ Hz, 2H, Ar-H), 6.94-6.92 (d, $J=8$ Hz, 2H, Ar-H), 6.78-6.22 (m, 3H, NH_2+Ar-H), 5.50-5.48 (d, $J=8$ Hz, 1H, CH), 4.64-4.62 (d, $J=8$ Hz, 1H, CH), 4.39 (s, 1H, CH); ^{13}C NMR (δ ppm): 171.14, 163.38, 162.25, 146.62, 134.54, 129.59, 129.23, 128.96, 128.52, 124.39, 121.39, 120.86, 117.32, 116.98, 115.45, 114.46, 113.98, 113.56, 112.98, 77.32 & 32.13; HRMS: m/z 356.3704 [M^{+}]; Anal. Calcd: C 70.77, H 4.53, N 15.72 %, Found: C 70.74, H 4.49, N 15.67 %.

5.4. Absorption property

The absorption properties of the target compounds **4(a-j)** were recorded in DMSO & DMF solvents at 10^{-5} M concentration using a UV-Vis Spectrophotometer. The λ_{max} and molar absorption coefficient values were appended in **Table 3** and UV-Vis spectra of the compounds are shown in **Fig. 3**. All the synthesized compounds exhibited absorption maxima (λ_{max}) in the range of 335-366 nm in DMSO and 336-359 nm in DMF solvents due to the $\pi-\pi^*$ & $n-\pi^*$ transitions. Among the synthesized compounds, **4d** compound exhibited maximum bathochromic/red shift towards the longer wavelength of 366 nm in DMSO & 359 nm in DMF solvent. Most of the compounds show higher absorption maxima in DMSO solvent due to high polarity of the solvent. Increase in polarity of the solvent absorption maxima also

increases at higher wavelength. This is due to effective interaction between solvent molecules and the lone pair of electrons in compounds [36].

Table 3. Electronic absorption data of the synthesized compounds **4(a-j)** in DMSO & DMF solvents.

Compd.	DMSO		DMF	
	$\lambda_{\max}(\text{nm})$	Log ϵ	$\lambda_{\max}(\text{nm})$	Log ϵ
4a	358	3.72	354	3.57
4b	352	3.75	352	3.74
4c	354	3.36	282	3.32
			353	3.30
4d	296	3.17	295	3.11
	366	3.20	359	3.14
4e	343	3.46	340	3.96
4f	340	3.77	339	3.39
4g	340	3.84	336	3.80
4h	302	4.14	299	3.70
	345	4.13	342	3.71
4i	335	4.07	337	3.77
4j	335	3.89	336	3.77

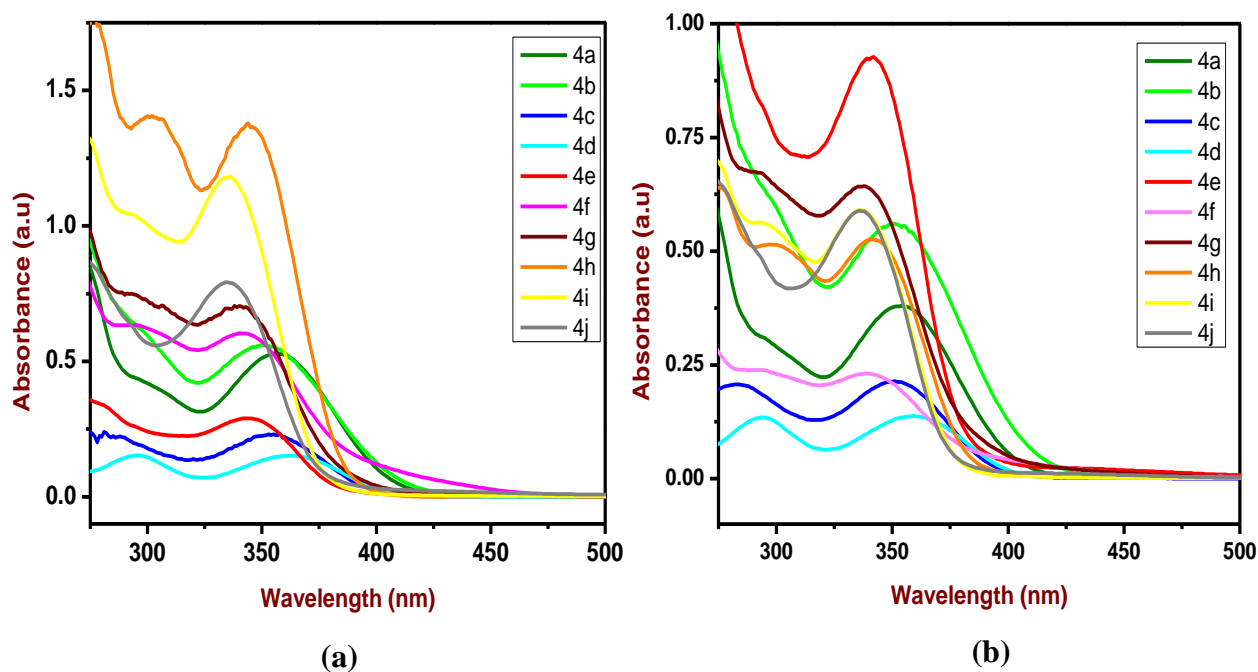


Fig. 3. A graph of UV-Visible spectra of the synthesized compounds **4(a-j)** in DMSO (a) & DMF (b) solvents.

5.5. Pharmacological studies

5.5.1. *In vitro* α -amylase & α -glucosidase inhibitory assay

The evaluation of *in vitro* α -amylase & α -glucosidase inhibitory efficacy of synthesized compounds were carried out according to the reported procedure Ademiluyi A O *et. al.* with minor modification [37]. In a test tube, reaction mixture containing 500 μ L phosphate buffer (100 mM, pH = 6.8), 100 μ L α -amylase/ α -glucosidase (2 U/mL) and 200 μ L of compounds of different concentration from 25 to 100 μ g/mL was pre-incubated at 37 °C for 20 min. Then, the 200 μ L of 1% soluble starch (100 mM phosphate buffer pH 6.8) was added as a substrate and incubated further at 37 °C for 30 min; 1 mL of the DNS color reagent was then added and kept on water bath for 10 min. The absorbance of the resulting mixture was measured at 540 nm using UV spectrophotometer (Biorad, USA). Acarbose (25-100 μ g/mL) was used as a standard. Without test sample substance was set up in parallel as control and each experiment was performed in triplicates. The results were expressed as percentage inhibition, which was calculated by using the formula,

$$\% \text{ inhibition} = (A_s/A_c) \times 100$$

Where, A_s is the absorbance in the presence of test substance and A_c is the absorbance of control. IC_{50} value was calculated by using the percentage scavenging activities at different concentrations of the synthesized compounds.

5.5.2. *In vitro* cytotoxicity

The detailed experimental procedure for *in vitro* cytotoxicity of the synthesized compounds has been discussed in the experimental section 2B.5.2 of **Chapter-2B** using A549 (Human Lung cancer) cell line and Doxorubicin as standard.

5.5.3. *in silico* molecular docking study

In docking study, exo- β -D-glucosaminidase and P38 MAP kinase proteins are used by automated docking by employing the Autodock Vina program [38]. The co-crystallized

structure of *exo*- β -D-glucosaminidase (PDB ID: 2x05) and P38 MAP kinase (PDB ID: 1OUK) were retrieved from the protein databank and their substrate binding sites were identified using pdbsum server [39]. A grid box of dimensions 25 x 25 x 25 Å with X, Y & Z coordinates at 50.995, 42.447 and 71.445 for *exo*- β -D-glucosaminidase and 25 x 25 x 25 Å with X, Y & Z coordinates at 43.699, 33.538 and 32.807 for P38 MAPk. Biovia Discovery Studio Visualizer V.20.1 was used to visualize the binding interactions of the compounds.

5.5.4. *in silico* oral bioavailability assessment and ADME studies

Various physicochemical features and pharmacokinetic descriptors were calculated through the online web tool SwissADME [40]. The oral bioavailability of the synthesized compounds (**4a-j**) was predicted using the Lipinski rule-of-five (RO5) filter [41] to derive the candidate drug's pharmacokinetic (PK) [42]. The structural properties used in the RO5 filter are derived using Osiris Data warrior V.4.4.3 software [43]. The bioavailability scores were predicted using the molinspiration server [44].

5.6. Results and discussion

5.6.1. *In vitro* α -amylase and α -glucosidase inhibitory activity

All the obtained compounds **4(a-j)** was used to studied the *in vitro* α -amylase & α -glucosidase inhibitory assay using three different concentrations (25, 50 and 100 μ g/mL) and acarbose was used as a standard for comparison. Percentage of inhibition and IC₅₀ values of enzyme activity has been tabulated in **Table 4 & 5**. The α -amylase enzyme activity results showed that, the obtained compounds **4(a-j)** possessed significant efficacy ranging from 12.45 \pm 0.49 to 32.60 \pm 0.84, 13.50 \pm 0.56 to 53.10 \pm 0.98, 43.50 \pm 0.56 to 75.90 \pm 0.98 % with respect to their concentration 25, 50 and 100 μ g/mL respectively. The potencies of IC₅₀ values vary from 46.51 \pm 1.26 to 112.59 \pm 1.24 μ g/mL. Among them, compound **4c** exhibited the most effective % inhibition with least IC₅₀ value of 46.51 \pm 1.26 μ g/mL and compounds **4g** & **4j** showed good % inhibition with IC₅₀ values of 83.47 \pm 1.47 & 81.99 \pm 1.15 μ g/mL

respectively. Rest of the compounds also exhibit moderate inhibition with considerable IC₅₀ values as compared to standard drug acarbose (44.95±0.78 µg/mL) (Fig. 4).

Based on the α-amylase inhibitory activity results, we selected **4c**, **4g** & **4j** compounds for α-glucosidase enzyme activity and the results revealed that, all three compounds possessed significant IC₅₀ values varying from 50.07±0.53 to 75.75±1.41 µg/mL. Out of three compounds, **4c** exhibited good % inhibition with least IC₅₀ value of 50.07±0.53 µg/mL as compared to standard drug acarbose (50.53±1.59 µg/mL) and as shown in Fig. 5.

Table 4. α-amylase enzyme activity results (%) at different concentrations and IC₅₀ values of the synthesized compounds **4(a-j)**.

Compd.	Concentration in µg/mL			IC ₅₀ in µg/mL
	25	50	100	
4a	12.60±0.84	26.80±0.84	47.10±0.98	105.86±1.48
4b	16.10±0.98	13.50±0.56	43.70±0.70	111.49±1.15
4c	32.60±0.84	53.10±0.98	75.90±0.98	46.51±1.26
4d	14.75±0.63	21.90±0.42	48.45±0.63	102.44±0.84
4e	15.85±0.49	22.70±0.56	43.50±0.56	112.59±1.24
4f	14.55±0.49	24.85±0.49	46.40±0.56	107.05±0.44
4g	12.45±0.49	32.70±0.56	58.65±0.63	83.47±1.47
4h	13.45±0.63	23.65±0.49	48.65±0.63	102.57±1.46
4i	14.45±0.49	34.45±0.63	51.80±0.42	95.30±1.49
4j	23.70±0.70	37.85±0.49	56.95±0.77	81.99±1.15
Acarbose	39.55±0.63	52.50±0.42	81.45±0.63	44.95±0.78

Values are Mean ±SE, N=3, *P<0.01 vs. Control

Table 5. α-glucosidase enzyme activity results (%) at different concentrations and IC₅₀ values of the synthesized compounds **4(a-j)**.

Compd.	Concentration in µg/mL			IC ₅₀ in µg/mL
	25	50	100	
4c	30.70±0.84	49.80±0.56	77.55±0.77	50.07±0.53
4g	15.80±0.84	36.80±0.56	62.60±0.42	74.61±0.19
4j	24.70±0.56	37.80±0.84	61.75±0.35	75.75±1.41
Acarbose	34.65±0.49	49.55±0.63	76.40±0.56	50.53±1.59

Values are Mean ±SE, N=3, *P<0.01 vs. Control

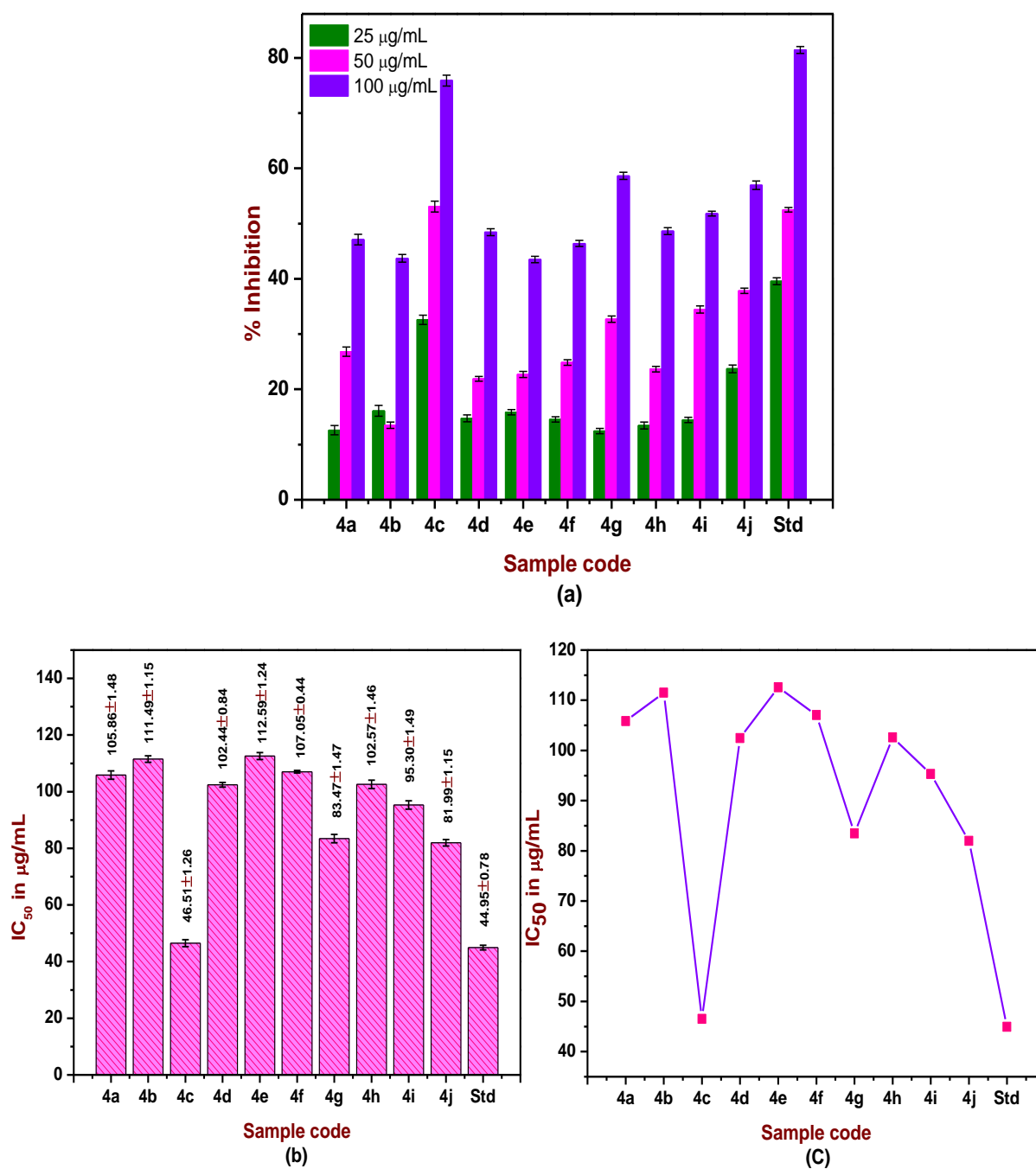


Fig. 4. *In vitro* α -amylase inhibitory activity of the synthesized compounds **4(a-j)**; A graph of % inhibition of synthesized compounds at different concentration (a); A graph of IC₅₀ value of compounds (b & c).

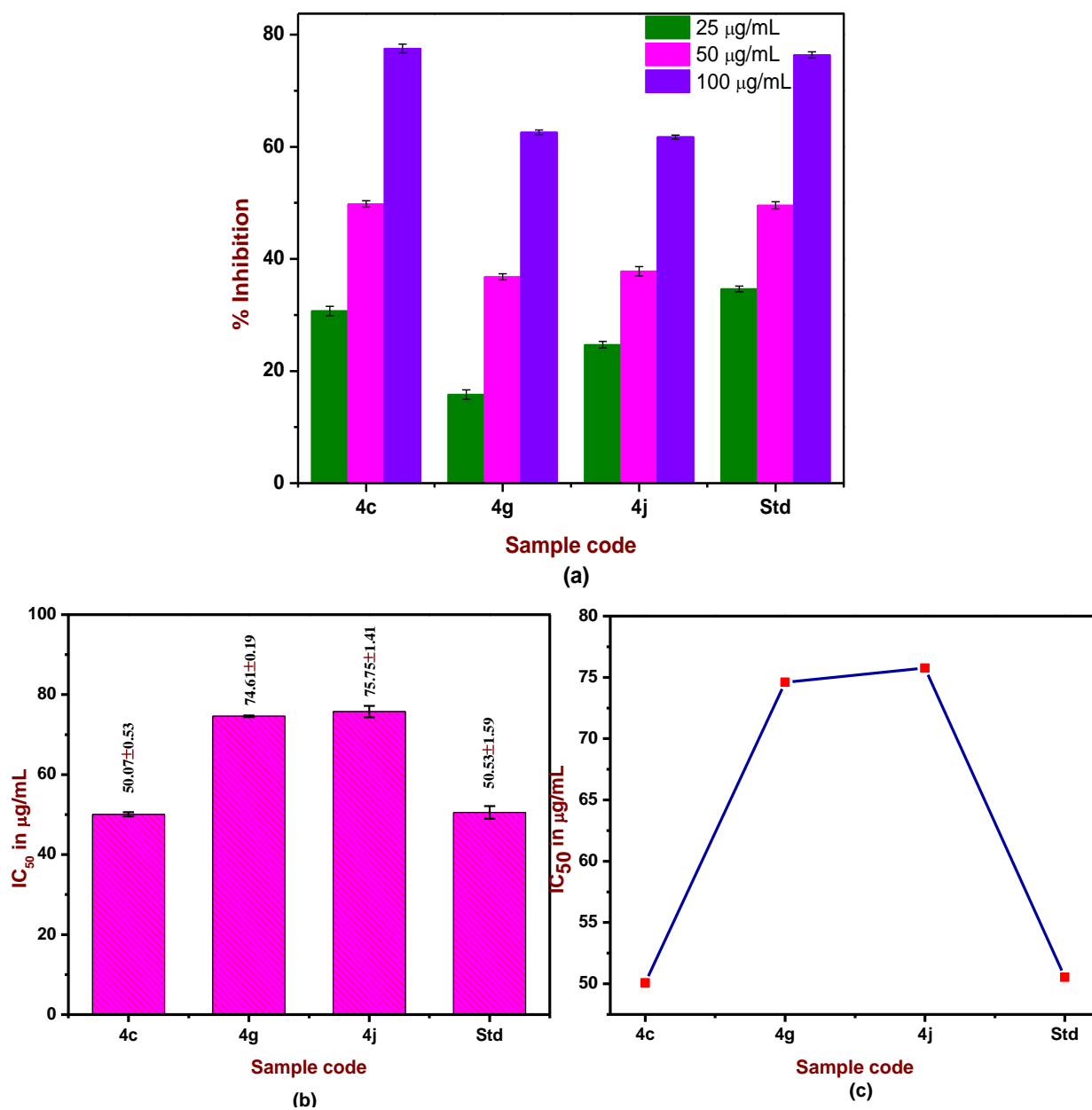


Fig. 5. *In vitro* α -glucosidase inhibitory activity of the synthesized compounds (4c, 4g & 4j); A graph of % inhibition of synthesized compounds at different concentration (a); A graph of IC_{50} value of compounds (b & c).

5.6.2. *In vitro* cytotoxicity

The *in vitro* cytotoxicity results suggested that, synthesized targets **4(a-j)** were exhibited good selectivity against the A549 cell line with IC₅₀ values ranging from 21.62±0.01 to 101.85±4.60 µg/mL. Among them, compound **4h** exhibited a significant cytotoxic effect with least IC₅₀ value of 21.62±0.01 µg/mL and compounds **4b**, **4e** & **4f** also possessed good cytotoxicity with IC₅₀ values of 30.29±2.20, 35.76±1.04 & 33.47±0.73 µg/mL respectively, and the rest of the compounds displayed moderate cytotoxic effect with an IC₅₀ value in the range of 36.38±0.87 to 101.85±4.60 µg/mL as compared to reference standard doxorubicin (7.56±0.08 µg/mL). % of cell viability and IC₅₀ values of the targets was shown in **Fig. 6 & 7** and results were listed in **Table 6**.

Table 6. % of cell viability against A549 cell line of the synthesized compounds **4(a-j)**.

Compd.	Mean cell Viability of A549 (Human Lung cancer)							IC ₅₀ in µg/mL
	Concentration in µg/mL							
	NC	3.125	6.25	12.5	25	50	100	
4a	100	95.46±0.40	90.93±1.20	89.23±0.80	85.41±0.20	73.79±1.80	42.06±0.60	101.85±4.60
4b		73.50±0.60	71.81±1.00	62.88±0.79	54.38±0.40	44.61±2.20	40.65±1.40	30.29±2.20
4c		93.34±1.00	81.15±0.60	74.07±0.20	71.24±1.00	44.75±0.40	28.75±0.19	42.90±0.81
4d		87.67±1.00	72.66±0.19	70.96±0.19	64.30±0.80	61.18±2.00	42.63±1.00	52.96±2.79
4e		82.57±0.60	79.88±1.20	78.47±1.20	67.13±0.40	36.68±2.20	24.92±0.79	35.76±1.04
4f		83.28±1.20	70.25±0.80	57.36±0.19	56.51±0.19	55.52±0.80	35.83±1.40	33.47±0.73
4g		94.75±0.99	88.38±0.80	72.09±0.60	67.84±2.20	52.68±0.40	48.01±1.00	59.03±2.38
4h		82.29±2.20	67.70±0.80	64.72±0.20	50.70±1.20	28.89±0.39	25.63±1.00	21.62±0.01
4i		81.15±0.60	62.74±0.20	57.92±1.80	56.08±0.40	54.24±0.20	49.99±3.40	36.38±0.87
4j		81.86±0.79	66.42±0.60	58.77±0.60	56.65±0.79	54.95±0.40	50.98±0.40	39.42±1.65
Std			48.57±0.60	42.77±0.79	40.65±1.40	38.52±0.79	34.84±0.39	32.15±1.00

Std-Doxorubicin, **NC**- Negative control

Values are Mean ±SE, N=3, *P<0.01 vs. Control

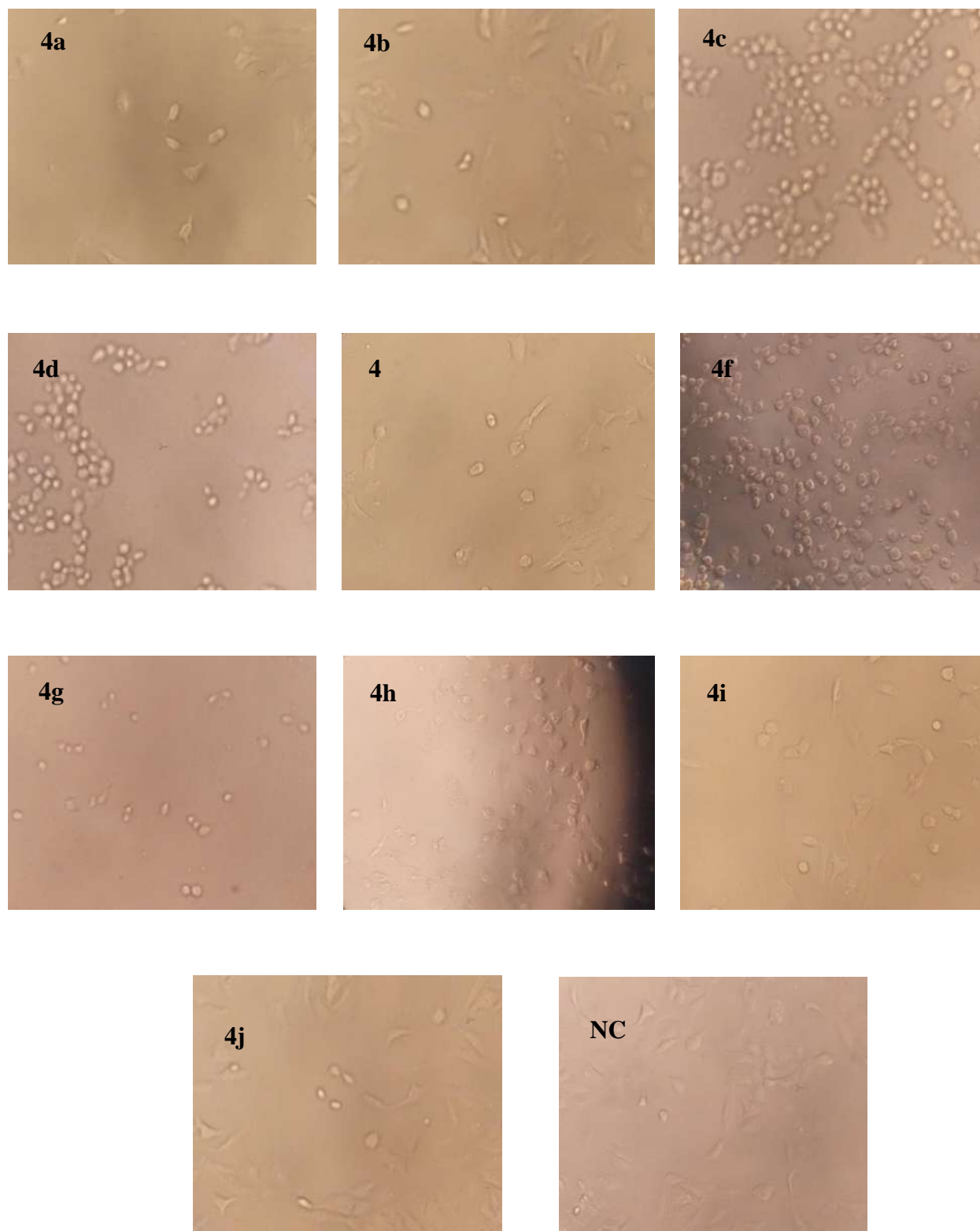


Fig. 6. Images of cytotoxicity of the synthesized compounds **4(a-j)** and Negative control (NC).

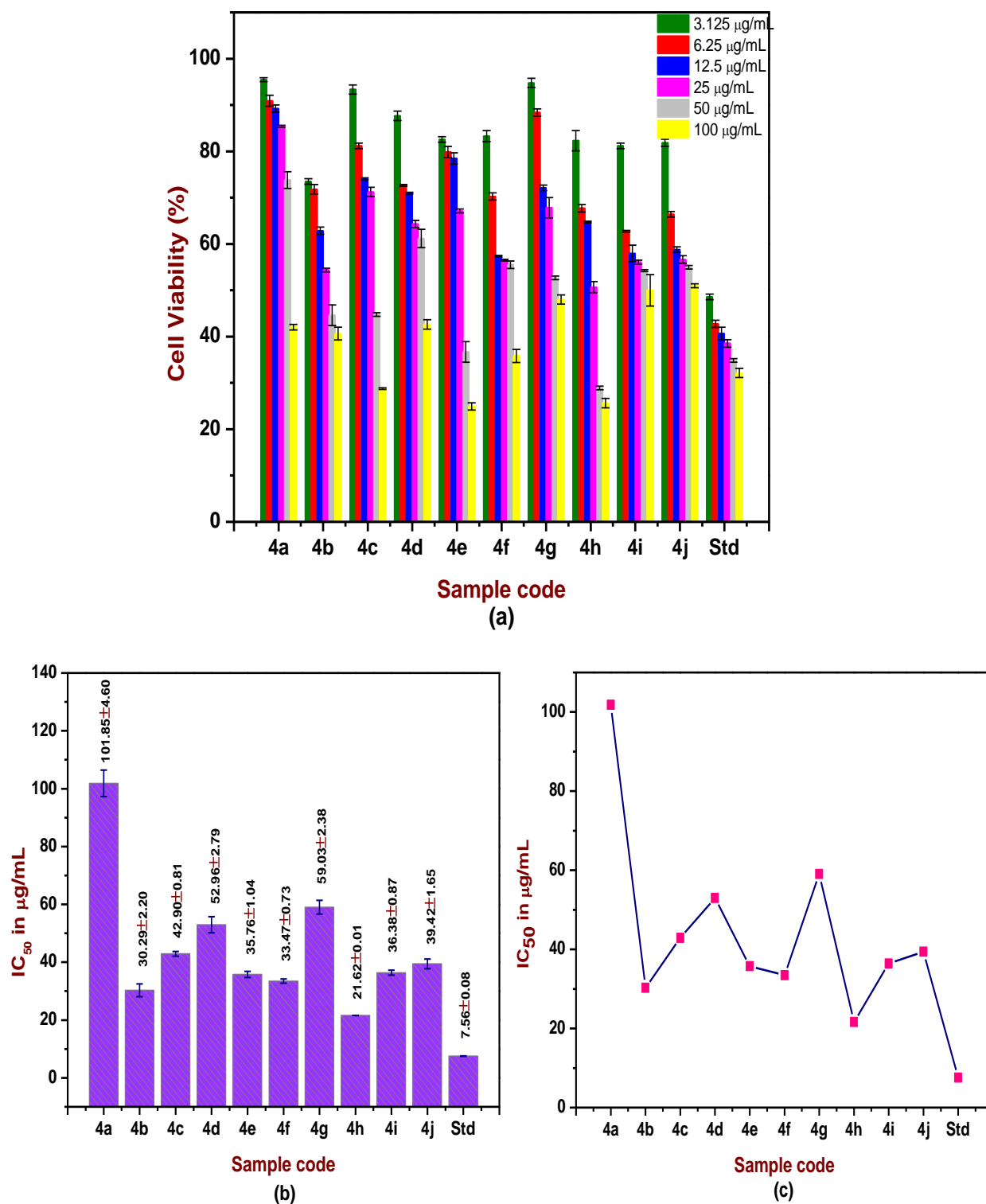


Fig. 7. A graph of % of surviving cells of synthesized compounds **4(a-j)** at different concentration against A549 cell line (a); A graph of IC₅₀ value of compounds **4(a-j)** against A549 cell line (b & c).

5.6.3. Structure-activity relationship

Synthesized compounds have been conducted by SAR study. All compounds exhibited good α -amylase, α -glucosidase and cytotoxicity. Among them, **4c**, **4g** & **4j** compounds exhibited significant anti-diabetic property with effective IC_{50} values. Although, the compound **4c** having an electron withdrawing methoxy group at para position exhibited the most effective inhibitory assay [45]. **4b**, **4e**, **4f** & **4h** compounds show significant cytotoxic effect with effective IC_{50} values. In that, compound **4h** having an electron donating OH group at para position and an electron-withdrawing ethoxy group at the meta position shows a significant cytotoxic effect as compared to other compounds, which was supposed to be the reason for the admirable cytotoxicity.

5.6.4. *in silico* molecular docking

in silico molecular docking study was helps to predict the favoured binding modes and binding energies of the targeted compounds with active sites of the enzymes. The docking receptors of α -D-glucosaminidase (**Fig. 8**) and P38 MAP kinase (**Fig. 9**) with synthesized compounds **4(a-j)** and standards exhibited well-established binding energies in the active pockets was tabulated in **Table 7 & 8**. In this study, α -D-glucosaminidase has been selected as the active site for anti-diabetic activity because it plays a vital role in the decrease of postprandial hyperglycemia; it achieved by slow down the absorption of glucose by the inhibition of the carbohydrate hydrolysing enzyme α -glucosidase in the digestive track [14]. It can delay the liberation and absorption of glucose from the diet or increase the efficacy in glycemic control as a result decrease the postprandial plasma glucose levels [46]. Similarly, P38 MAP kinase has been selected as the active site for anticancer study because the inhibition of P38 MAP kinase is likely to affect cellular proliferation accounting for cell toxicity. Hence, it is used as a measure of mitochondrial respiration, indirectly corresponding to cellular toxicity [47].

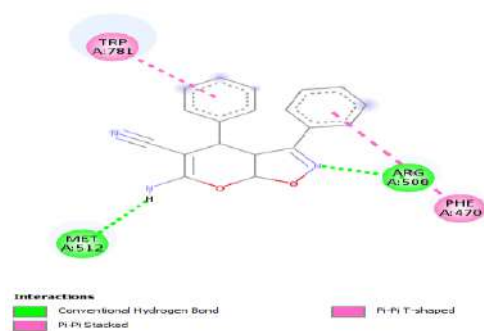
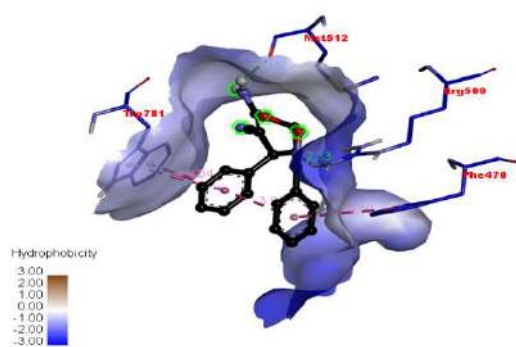
The docking results of anti-diabetic and cytotoxicity investigations revealed that, the synthesized compounds **4(a-j)** had significant binding modes with docking scores in the range of -7.6 to -8.4 kcal/mol and -7.2 to -8.1 kcal/mol with respect to standards Acarbose (-7.8 kcal/mol) and Doxorubicin (-8.4 kcal/mol) respectively. Among the docked structures with α -D-glucosaminidase, compound **4a** established the least binding energy of -8.4 kcal/mol forming two hydrogen bonds with amino acid residues ARG500 & MET512. **4c**, **4g** & **4j** compounds also displayed moderate binding energies (-7.8, -8.1 & -8.3 kcal/mol) with two or three hydrogen bonds with amino acid residues ARG500, MET512 & GLU431. The docked structures with P38 MAP kinase protein revealed that, the compound **4j** demonstrated the least binding energy of -8.1 kcal/mol forming one hydrogen bond with amino acid residue MET109 and compounds **4b**, **4e**, **4f** & **4h** displayed moderate binding energies (-7.6, -7.6, -7.4 & -7.2 kcal/mol) with one or two hydrogen bonds with amino acid residues TYR35, MET109, LYS53 & ASP168. The remaining compounds also established moderate binding energies with hydrogen bonds in their active pockets.

Table 7. Molecular interactions synthesized compounds **4(a-j)** & standard **Acarbose** with α -D-glucosaminidase protein.

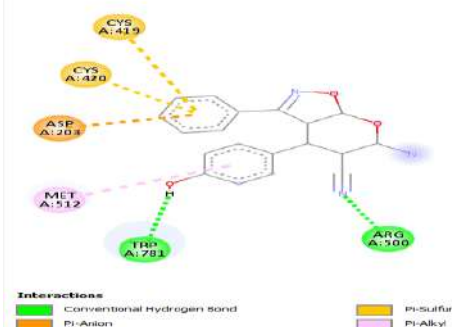
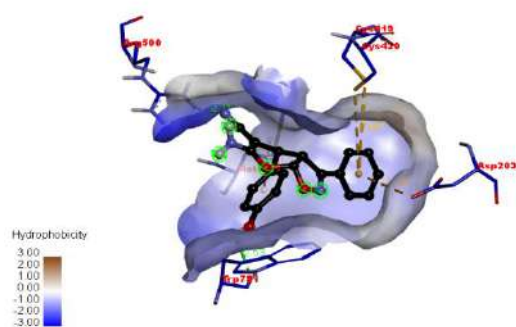
Compd.	Binding affinity (kcal/mol)	Hydrogen bond interaction	Hydrogen bond length in Å	Hydrophobic and other interactions
4a	-8.4	ARG500, MET512	2.32, 2.14	TRP781, PHE470
4b	-8.0	ARG500, TRP781	2.10, 2.52	ASP203, CYS419, CYS420, MET512
4c	-7.8	ARG500, MET512	2.27, 2.08	TRP781, PHE470
4d	-8.2	ARG500, MET512	2.24, 1.97	TRP781
4e	-8.2	ARG500, MET512	2.29, 1.99	TRP781, PHE470
4f	-7.6	-	-	TRP781, PHE470
4g	-8.1	ARG500, GLU431 MET512	2.31, 2.59, 2.71	TRP781, PHE470
4h	-7.8	ARG500, TYR516 MET512	2.28, 2.78, 2.58	TRP781, PHE470
4i	-8.3	ARG500, MET512	2.21, 2.00	TRP781, PHE470
4j	-8.3	ARG500, MET512	2.33, 2.45	TRP781, PHE470
Acarbose	-7.8	GLU431, GLU431, MET512, MET512, ARG500, ARG500 ARG500	2.45, 2.65, 2.54, 2.89, 2.23, 2.85, 2.64	ASP469, CYS420, MET512, SER580, ILE202, TRP781

Table 8. Molecular interactions of synthesized compounds **4(a-j)** & standard **Doxorubicin** with P38 MAP kinase protein.

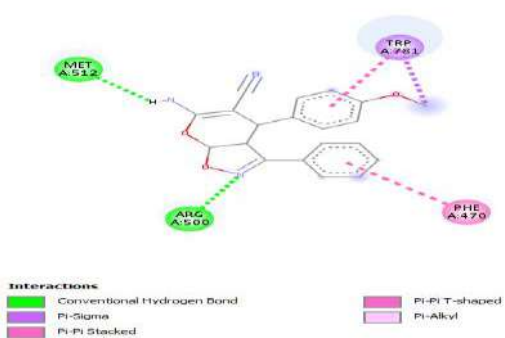
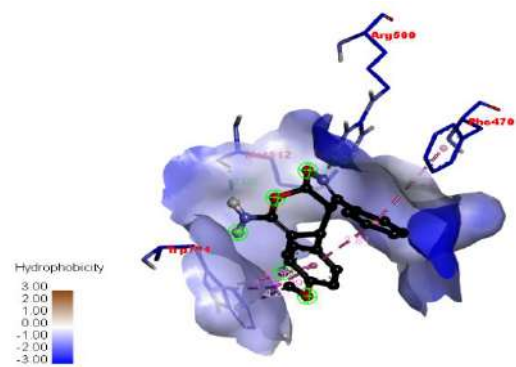
Compd.	Binding affinity (kcal/mol)	Hydrogen bond interaction	Hydrogen bond length in Å	Hydrophobic and other interactions
4a	-7.5	MET109	2.07	THR106, VAL38, ALA51, LYS53
4b	-7.6	TYR35, MET109	2.21, 2.61	VAL38, ALA51, LYS53, LEU167
4c	-7.4	ASP168, LYS53	2.50, 2.83	ASP112, VAL38, ALA51
4d	-7.9	ASP168, LYS53	1.89, 2.81	VAL38, ALA51
4e	-7.6	LYS53, MET109	2.52, 2.15	THR106, VAL38, ALA51
4f	-7.4	-	-	THR106, VAL38, ALA51, LYS53
4g	-7.3	TYR35	2.57	VAL30, VAL38, ALA51, LEU167,
4h	-7.2	ASP168	2.48	ALA51, LEU167, VAL30, MET109
4i	-7.4	-	-	THR106, LEU167, ALA51, LYS53, VAL38,
4j	-8.1	MET109	2.31	ALA51, VAL38,
Doxorubicin	-8.4	ASP168, VAL30, LYS53	2.38, 2.80, 2.95	LYS53, LEU75, ILE84, VAL38, LEU167, VAL38, LYS53, LEU167, LYS53, TYR35



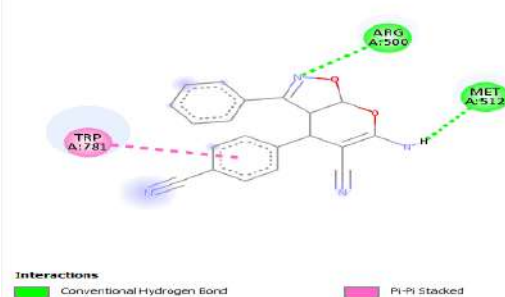
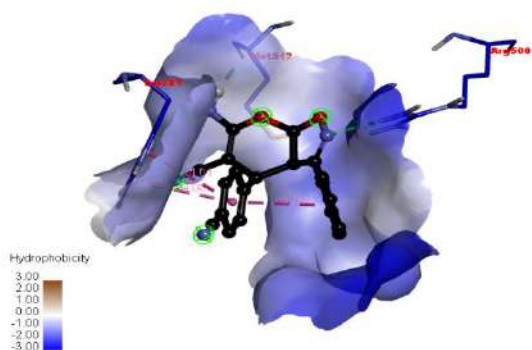
4a



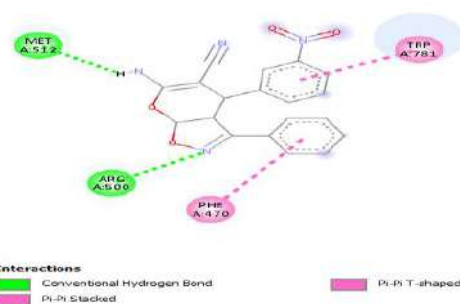
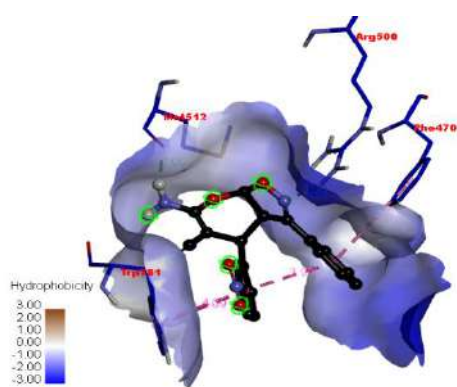
4b



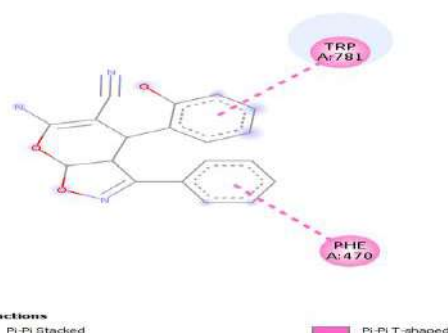
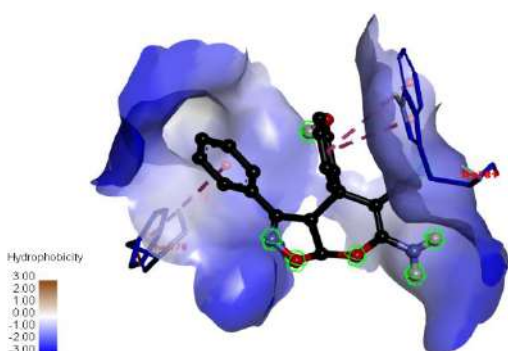
4c



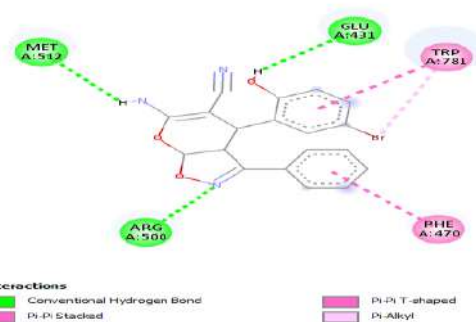
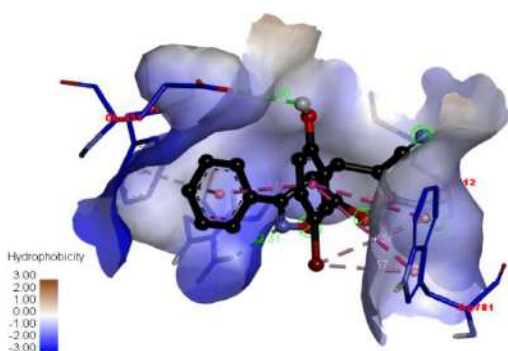
4d



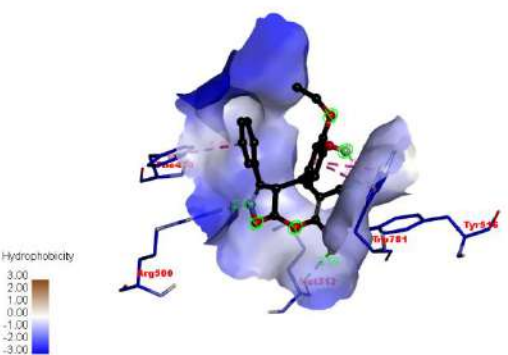
4e



4f



4g



4h

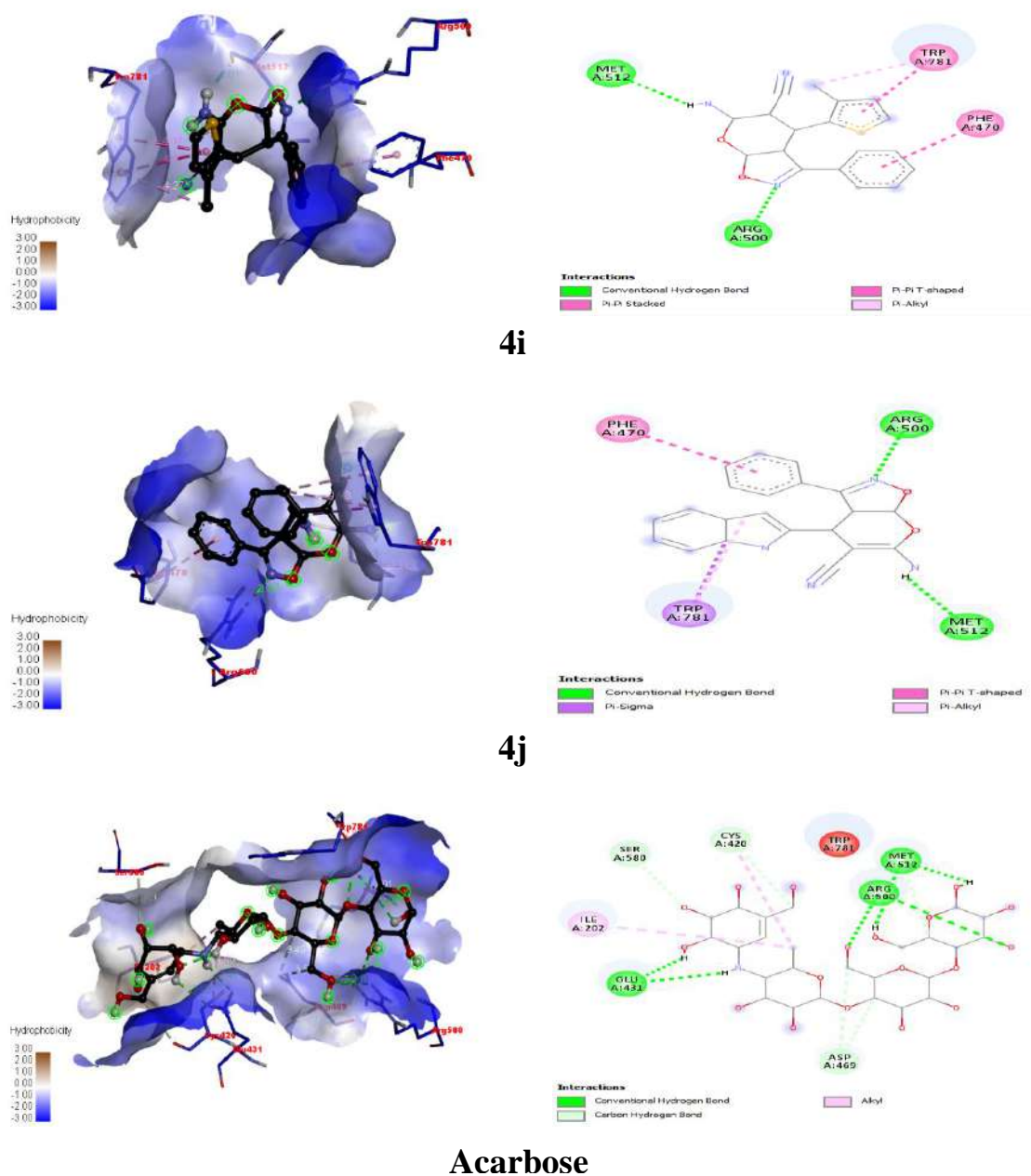
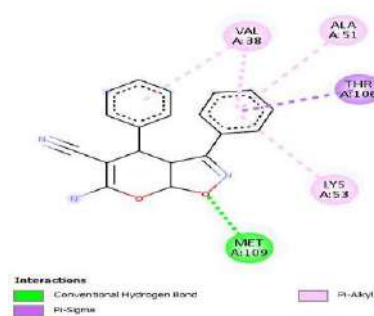
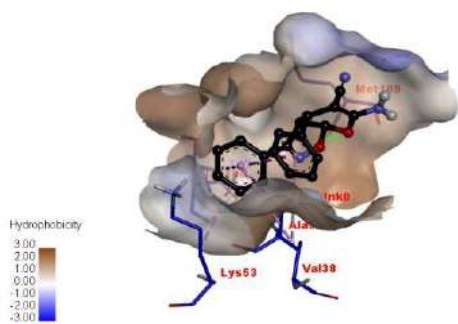
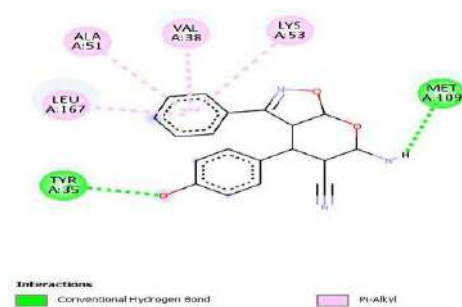
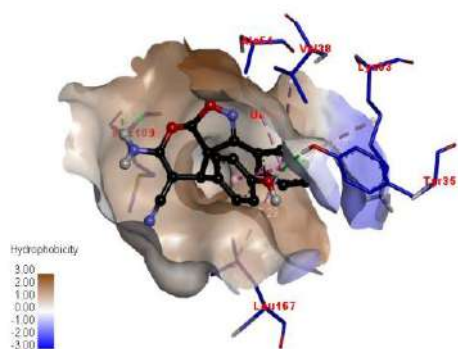


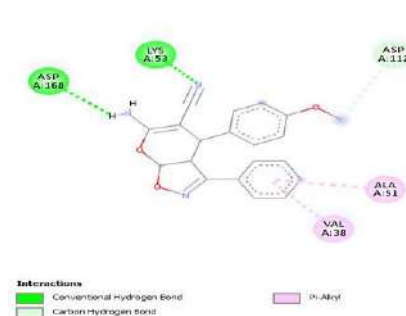
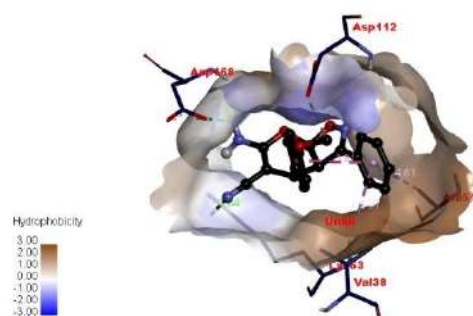
Fig. 8. 3D and 2D representation of molecular interactions between exo- β -D-glucosaminidase with synthesized compounds 4(a-j) and standard drug **Acarbose**.



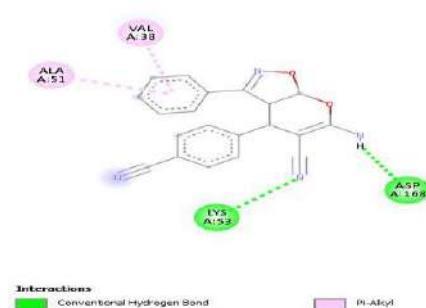
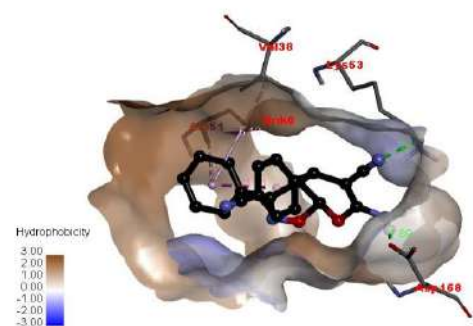
4a



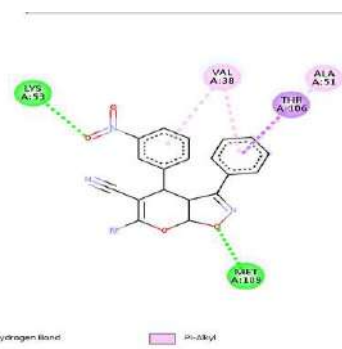
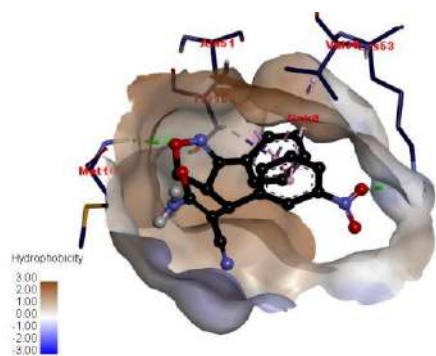
4b



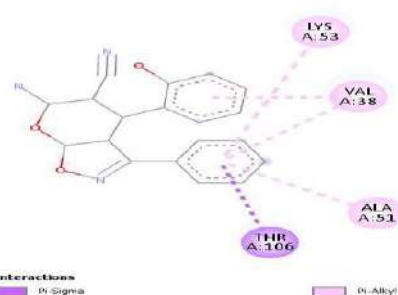
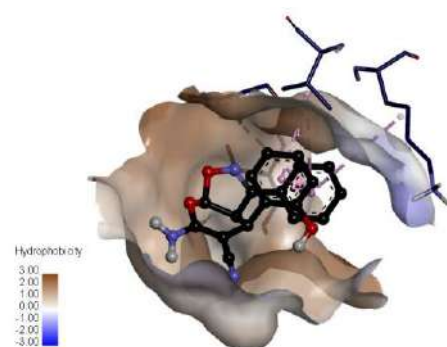
4c



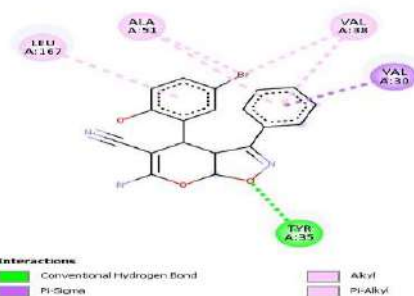
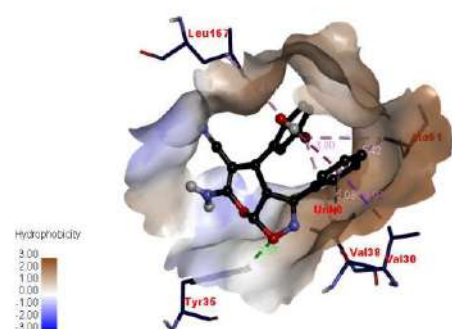
4d



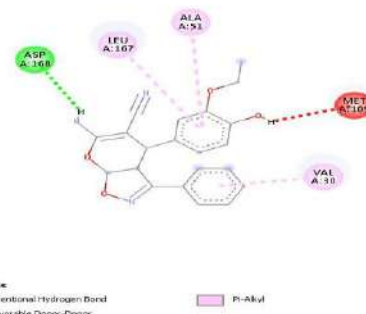
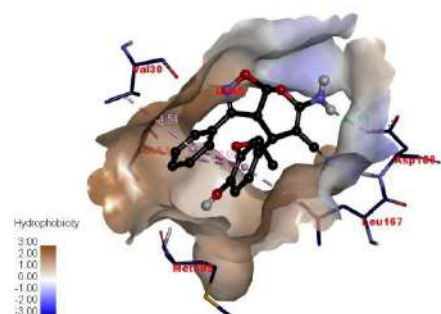
4e



4f



4g



4h

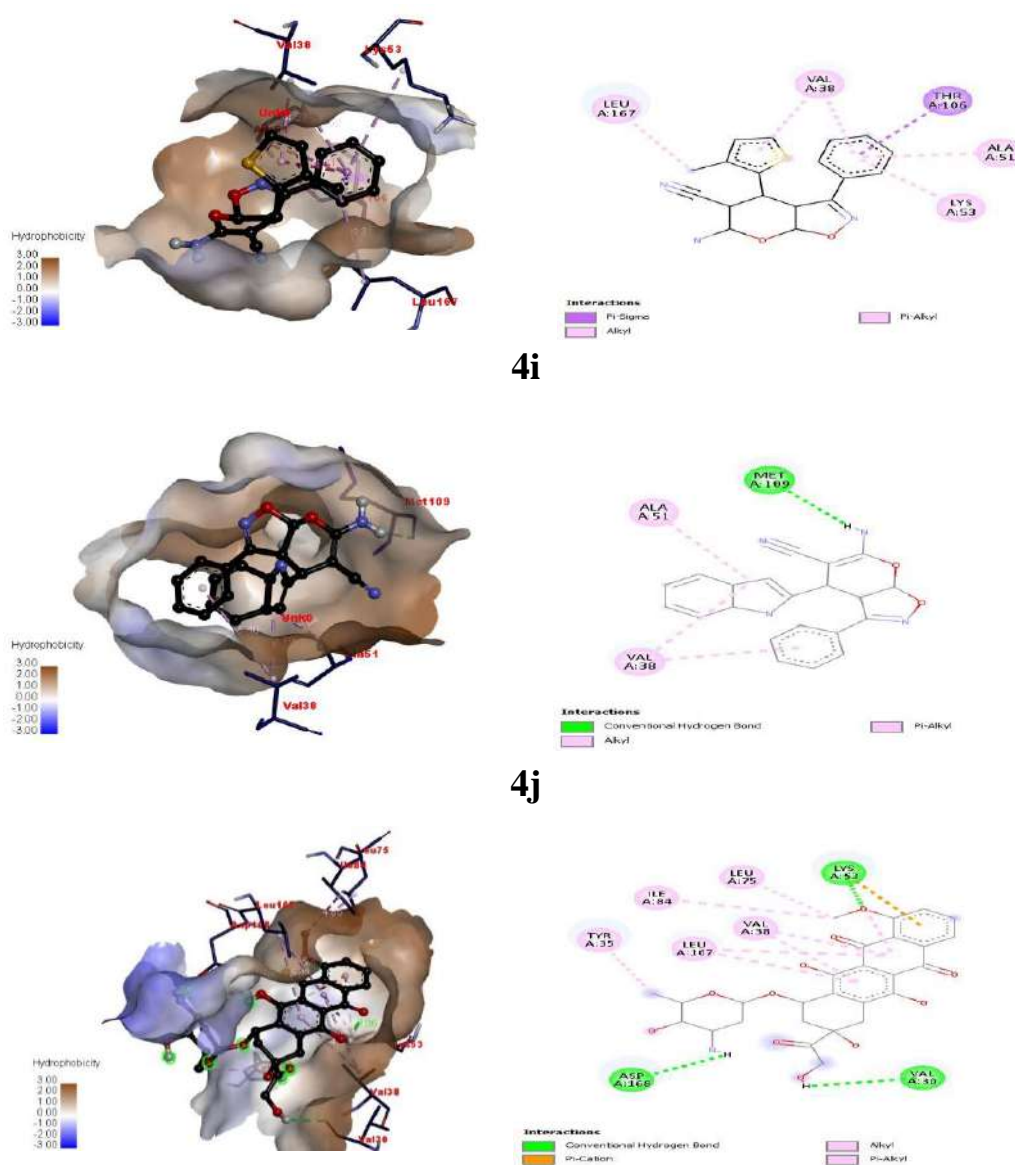


Fig. 9. 3D and 2D representation of molecular interactions between P38 MAP kinase with synthesized compounds **4(a-j)** and standard drug **Doxorubicin**.

5.6.5. *in silico* oral bioavailability assessment and ADME

in silico, oral bioavailability assessment and ADME studies are necessary for the drug design of new molecules. The drug-likeness outline can be evaluated through parameters such as molecular weight, number of heavy atoms, hydrogen bond acceptors, hydrogen bond donors, rotatable bonds, molar refractivity and TPSA. These parameters were calculated for synthesized compounds **4(a-j)** and as tabulated in **Table 9**. The drug-likeness profiles were calculated based on Lipinski, Ghose, Veber, Egan and Muegge rules [48, 49]. The rule-based score defines the compounds into four probability score classes, i.e. 11 %, 17 %, 55 % and 85 %. The acceptable probability score is 55 %, which indicates that it passed the rule of five [50, 51]. All synthesized compounds showed a score of 55 % indicating of compounds obeyed all five rules without any violations of good bioavailability. Further, the synthetic accessibility of the compounds was assessed to quantify the complexity of the molecular structure. The results showed that the synthetic accessibility scores were in the range of 4.71 to 5.39. It shows that all compounds do not have complex synthetic routes (**Table 10**).

Table 9. Physicochemical properties of the synthesized compounds **4(a-j)**.

Compd.	Mol. Formula	Mol. Weight	No. Heavy atoms	HBA	HBD	Rotatable bonds	Fraction Csp3	Molar Refractivity	TPSA (Å ²)
4a	C ₁₉ H ₁₅ N ₃ O ₂	317.34	24	4	1	2	0.16	91.67	80.63
4b	C ₁₉ H ₁₅ N ₃ O ₃	333.34	25	5	2	2	0.16	93.70	100.86
4c	C ₂₀ H ₁₇ N ₃ O ₃	347.37	26	5	1	3	0.20	98.16	89.86
4d	C ₂₀ H ₁₄ N ₄ O ₂	342.35	26	5	1	2	0.15	96.39	104.42
4e	C ₁₉ H ₁₄ N ₄ O ₄	362.34	27	6	1	3	0.16	100.49	126.45
4f	C ₁₉ H ₁₅ N ₃ O ₃	333.34	25	5	2	2	0.16	93.70	100.86
4g	C ₁₉ H ₁₄ BrN ₃ O ₃	412.24	26	5	2	2	0.16	101.40	100.86
4h	C ₂₁ H ₁₉ N ₃ O ₄	377.39	28	6	2	4	0.24	104.99	110.09
4i	C ₁₈ H ₁₅ N ₃ O ₂ S	337.40	24	4	1	2	0.22	94.52	108.87
4j	C ₂₁ H ₁₆ N ₄ O ₂	356.37	27	4	2	2	0.24	106.71	92.66

Table 10. Drug likeness, bioactivity and synthetic accessibility score of the synthesized compounds **4(a-j)**.

Compd.	Lipinski	Ghose	Veber	Egan	Muegge	Bioactivity Score	Synthetic accessibility
4a	Yes	Yes	Yes	Yes	Yes	0.55	4.72
4b	Yes	Yes	Yes	Yes	Yes	0.55	4.71
4c	Yes	Yes	Yes	Yes	Yes	0.55	4.78
4d	Yes	Yes	Yes	Yes	Yes	0.55	4.76
4e	Yes	Yes	Yes	Yes	Yes	0.55	4.77
4f	Yes	Yes	Yes	Yes	Yes	0.55	4.76
4g	Yes	Yes	Yes	Yes	Yes	0.55	4.78
4h	Yes	Yes	Yes	Yes	Yes	0.55	4.93
4i	Yes	Yes	Yes	Yes	Yes	0.55	4.75
4j	Yes	Yes	Yes	Yes	Yes	0.55	5.39

The mean predicted lipophilicity parameters were evaluated to study the solubility of the compounds either in an aqueous or in non-aqueous media and they were calculated by considering the consensus log Po/w. According to this, if the log Po/w values are more negative, then the molecules are more soluble in nature [52]. The results showed that, all the compounds had positive log Po/w values hence they were less soluble in non-aqueous medium. Consensus log S (if log S < -10: poorly soluble, < -6: moderately soluble, < -4: soluble, < -2: very soluble, and < 0: highly soluble). **Table 11** indicated that, our synthesized compounds were in the range of -4.13 to -5.04 log S values. This shows compounds were moderately soluble in aqueous medium.

Table 11. Predicted lipophilicity parameters of the synthesized compounds **4(a-j)**.

Compd.	Consensus Log Po/w	Consensus Log S	Solubility Class
4a	2.60	-4.27	Moderately soluble
4b	2.20	-4.13	Moderately soluble
4c	2.58	-4.34	Moderately soluble
4d	2.36	-4.22	Moderately soluble
4e	1.83	-4.33	Moderately soluble
4f	2.22	-4.13	Moderately soluble
4g	2.81	-5.04	Moderately soluble
4h	2.52	-4.44	Moderately soluble
4i	2.85	-4.41	Moderately soluble
4j	2.13	-4.26	Moderately soluble

The pharmacokinetic parameters like absorption, skin permeation, distribution, metabolism and excretion were predicted. According to this predictive model, if a molecule fall in the white region, it indicates passive gastrointestinal absorption, whereas in the yellow region indicates passive brain permeation [53]. Predicted absorption & distribution parameters of the compounds have shown in **Table 12** and it suggested that, all the synthesized compounds **4(a-j)** have high gastrointestinal absorption with no blood-brain permeant. Hence there was no possibility of causing harmful toxicants in the brain and bloodstream. If the molecules have a more negative log Kp value, they are said to be less skin

permeant [54]. Our synthesized compounds have a log K_p value in the range of -5.73 to -6.12 cm/s. Therefore, these compounds are less skin permeant.

Table 12. Predicted absorption & distribution parameters of the compounds **4(a-j)**.

Compd.	GI absorption	BBB permeant	Log K _p (cm/s)
4a	High	No	-5.73
4b	High	No	-6.08
4c	High	No	-5.93
4d	High	No	-6.08
4e	High	No	-6.12
4f	High	No	-6.08
4g	High	No	-6.07
4h	High	No	-6.11
4i	High	No	-5.80
4j	High	No	-6.04

Drug metabolism plays an important role in the bioavailability of drugs as well as drug-drug interactions [55]. Certain metabolism parameters are important to understand whether the compounds act as substrate (inhibitors) or non-substrate (non-inhibitors) of certain proteins. Hence, all the synthesized compounds were evaluated for metabolism parameters and results show that, synthesized compounds (except **4b** & **4h**) were found to be non-substrate of permeability glycoprotein (P-gp). The P-gp, an efflux membrane transporter, is widely distributed throughout the body and is responsible for limiting cellular uptake and the distribution of xenobiotic and toxic substances [56]. The compounds (except **4d** & **4i**) were found to be non-substrates of CYP1A2 inhibitors. The compounds **4a**, **4c**, **4e**, **4g** & **4i** were found to be substrates of CYP2C19 inhibitors and the remaining compounds were non-substrates of CYP2C19 inhibitors. All compounds were found to be substrates of CYP2C9 inhibitors. Compounds (except **4c**) were found to be non-substrates to CYP2D6 inhibitors. The compounds (except **4h**) were found to be non-substrates of CYP3A4 inhibitors and the data was tabulated in **Table 13**.

Table 13. Predicted metabolism parameters of the synthesized compounds **4(a-j)**.

Compd.	P-gp	CYP1A2 inhibitor	CYP2C19 inhibitor	CYP2C9 inhibitor	CYP2D6 inhibitor	CYP3A4 inhibitor
4a	No	No	Yes	Yes	No	No
4b	Yes	No	No	Yes	No	No
4c	No	No	Yes	Yes	Yes	No
4d	No	Yes	No	Yes	No	No
4e	No	No	Yes	Yes	No	No
4f	No	No	No	Yes	No	No
4g	No	No	Yes	Yes	No	No
4h	Yes	No	No	Yes	No	Yes
4i	No	Yes	Yes	Yes	No	No
4j	No	No	No	Yes	No	No

5.7. Conclusion

In summary, we have reported an easy and efficient protocol of the synthesized some novel 6-amino-4-substituted-pyrano[3,2-*d*]isoxazole-5-carbonitrile derivatives **4(a-j)** through one-pot reaction and screened for their pharmacological and *in silico* investigations. The activity results suggested that, compound **4c** exhibited the most effective % inhibition for α -amylase & α -glucosidase assays and the compound **4h** displayed a significant cytotoxic effect. *In silico* docking studies suggested that, synthesized compounds were interacted effectively with exo- β -D-glucosaminidase and P38 MAP kinase proteins with good binding energy. ADME profiles shows that, synthesized compounds obeyed all the five rules with good bioavailability. Pharmacokinetic parameters suggested that, the compounds have high GI absorption, no blood-brain barrier, less skin permeant and no possibility of causing harmful toxicants.

5.8. References

1. R. Pajkert, H. Koroniak, P. Kafarski, G.V. Roschenthaler, *Org. Biomol. Chem.*, **2021**, 19, 4871-4876.
2. N. Agrawal, P. Mishra, *Med. Chem. Res.*, **2018**, 27, 1309-1344.
3. J. Trivedi, A. Parveen, F. Rozy, A. Mitra, C. Bal, D. Mitra, A. Sharon, *Eur. J. Med. Chem.*, **2019**, 183, 1-9.
4. B. Manjunatha, Y.D. Bodke, R. Sandeepkumar Jain, T.N. Lohith, M.A. Sridhar, *J. Mol. Struct.*, **2021**, 1244, 1-9.
5. E.K.A. Abdelall, *Bioorg. Chem.*, **2020**, 94, 1-42.
6. I. Saidi, M. Manachou, M. Znati, J. Bouajilac, H.B. Jannet, *J. Mol. Struct.*, **2022**, 1247, 1-16.
7. S.R. Pedada, N.S. Yarla, P.J. Tambade, D.B. Lakkappa, A. Bishayee, K.M. Arunasree, G.H. Philip, G. Dharmapuri, G. Aliev, S. Putta, G. Rangaiah, *Eur. J. Med. Chem.*, **2016**, 1-33.
8. M.A. Barmade, P.R. Murumkar, M. Kumar Sharma, M. Ram Yadav, *Curr. Top. Med. Chem.*, **2016**, 16, 2863-2883.
9. V.V. Dabholkar, F.Y. Ansari, *J. Serb. Chem. Soc.*, **2009**, 74, 1219-1228.
10. W.T. Ashton, R.M. Sisco, H. Dong, K.A. Lyons, H. He, G.A. Doss, B. Leiting, R.A. Patel, J.K. Wu, F. Marsilio, N.A. Thornberry, A.E. Weber, *Bioorg. Med. Chem. Lett.*, **2005**, 15, 2253-2258.
11. A. Kumar, P. Ahmad, R.A. Maurya, A.B. Singh, A.K. Srivastava, *Eur. J. Med. Chem.*, **2009**, 44, 109-116.
12. H. Laoufi, N. Benariba, S. Adjdir, R. Djaziri, *J. Appl. Pharm. Sci.*, **2017**, 2, 191-198.
13. S.H. Sukanya, T. Venkatesh, S.A. Rao, A. Pandith, *J. Mol. Struct.*, **2022**, 1267, 1-28.
14. P.S. Kumar, S. Sudha, *Int. Res. J. Pharm.*, **2012**, 3, 128-130.
15. J. Dhuguru, R. Skouta, *Molecules*, **2020**, 25, 1615-1640.
16. M.M. Ghorab, M.G.E. Gazzar, M.S. Alsaid, *Int. J. Mol. Sci.*, **2014**, 15, 5582-5595.
17. V.V. Dabholkar and F.Y. Ansari, *J. Serb. Chem. Soc.*, **2009**, 74, 1219-1228.
18. L. Somogyi and P. Sohar, *Liebigs Annalen*, **1995**, 10, 1903-1906.
19. N.K. Bejjanki, A. Venkatesham, J. Madda, N. Kommu, S. Pombala, C.G. Kumar, J.B. Nanubolu, *Bioorg. Med. Chem. Lett.*, **2013**, 23, 4061-4066.
20. K.K. Wang, Y.L. Li, W. Zhang, S.S. Zhang, T.T. Qiu, X. Ma, *Tetrahedron Lett.*, **2020**, 61, 1-7.

21. R. Sakly, H. Edziri, M. Askri, M. Knorr, K. Louven, C. Strohmann, M. Mastouri, *J. Heterocycl. Chem.*, **2017**, 54, 3554-3564.
22. H.J. Kim, J.Y. Jang, K.H. Chung, J.H. Lee, *Biosci. Biotechnol. Biochem.*, **1999**, 63, 494-499.
23. R.M. Mohareb, F.M. Manhi, M.A.A. Mahmoud, A. Abdelwahab, *Med. Chem. Res.*, **2020**, 29, 1536-1551.
24. S. Bhavanarushi, V. Kanakaiah, E. Yakaiah, V. Saddanapu, A. Addlagatta, J.V. Rani, *Med. Chem. Res.*, **2013**, 22, 2446-2454.
25. Z. Saffari, H. Aryapour, A. Akbarzadeh, A. Foroumadi, N. Jafari, M.F. Zarabi, A. Farhangi, *Tumor Biology*, **2014**, 35, 5845-5855.
26. B.S. Kumar, P.V.A. Lakshmi, B.S. Veena, E. Sujatha, *Russ. J. Gen. Chem.*, **2017**, 87, 829-836.
27. A. Shaabani, A. Sarvary, A.H. Rezayan, S. Keshipour, *Tetrahedron*, **2009**, 65, 3492-3495.
28. D. Shi, J. Mou, Q. Zhuang, L. Niu, N. Wu, X. Wang, *Synth. Commun.*, **2004**, 34, 4557-4563.
29. T.S. Jin, A.Q. Wang, Z.L. Cheng, J.S. Zhang, T.S. Li, *Synth. Commun.*, **2005**, 35, 137-143.
30. A.R. Moosavi-Zare, H. Afshar-Hezarkhani, M.M. Rezaei, *Polycycl. Aromat. Compd.*, **2020**, 40, 150-158.
31. Y.M. Litvinov, A.A. Shestopalov, L.A. Rodinovskaya, A.M. Shestopalov, *J. Comb. Chem.*, **2009**, 11, 914-919.
32. M.A. Chaudhari, J.B. Gujar, D.S. Kawade, N.R. Jogdand, M.S. Shingare, *Cogent Chem.*, **2015**, 1, 1-10.
33. H.R. Shaterian, K. Azizi, *Res. Chem. Intermed.*, **2014**, 40, 661-667.
34. A.V. Borhade, B.K. Uphade, *J. Iran. Chem. Soc.*, **2015**, 12, 1107-1113.
35. A.K. Elziaty, O.E.A. Mostafa, E.A. El-Bordany, M. Nabil, H.M.F. Madkour, *Int. J. Sci. Eng. Res.*, **2014**, 5, 727-735.
36. O. Nagaraja, Y.D. Bodke, I. Pushpavathi, K.S. Ravi, *Heliyon*, **2020**, 6, 1-11.
37. A.O. Ademiluyi, G. Oboh, *Exp. Toxicol. Pathol.*, **2013**, 65, 305-309.
38. O. Trott, A.J. Olson, *J. Comput. Chem.*, **2010**, 31, 455-461.
39. S.J. Aditya Rao, C.K. Ramesh, S. Raghavendra, M. Paramesha, *Curr. Comput. Aided Drug Des.*, **2020**, 16, 231-237.

40. G.K. Swamy, G. Ramesh, K. Pruthviraj, S. Banu, B. Roopa, H.J. Preritha, B.S. Rajeshwari, M. Ravikumar, P.R. Shetty, D.B. Aruna Kumar, S. Sreenivasa, *Chem. Data Collect.*, **2020**, 28, 1-23.
41. C.A. Lipinski, F. Lombardo, B.W. Dominy, P.J. Feeney, *Adv. Drug Deliv. Rev.*, **1997**, 23, 1-25.
42. S. Raghavendra, S.J. Aditya Rao, V. Kumar, C.K. Ramesh, *Comput. Biol. Chem.*, **2015**, 59, 81-86.
43. T. Sander, J. Freyss, M. Von Korff, C. Rufener, *J. Chem. Inf. Model*, **2015**, 55, 460-473.
44. A. Jarrahpour, M. Motamedifar, M. Zarei, M.H. Youssoufi, M. Mimouni, Z.H. Chohan, *Phosphorus Sulfur Silicon Relat. Elem.*, **2010**, 185, 491-497.
45. M. Nawaz, M. Taha, F. Qureshi, N. Ullah, M. Selvaraj, S. Shahzad, S. Chigurupati, A. Waheed, F.A. Almutairi, *BMC Chem.*, **2020**, 14, 1-11.
46. H. Mechchate, I. Es-safi, A. Louba, A.S. Alqahtani, F.A. Nasr, O.M. Noman, M. Farooq, M.S. Alharbi, A. Alqahtani, A. Bari, H. Bekkari, D. Bousta, *Molecules*, **2021**, 26, 293-303.
47. S.J. Aditya Rao, S.M. Shivayogi, J.K. Satyanarayana, R.C. Kumaran, *Bioimpacts*, **2021**, 11, 187-197.
48. C.A. Lipinski, *Drug Discov. Today Technol.*, **2004**, 1, 337-341.
49. I. Muegge, *Med. Res. Rev.*, **2003**, 23, 302-321.
50. R.B. Breemen van, Y. Li, *Expert. Opin. Drug Metab. Toxicol.*, **2005**, 1, 175-185.
51. S. Alam, F. Khan, *Sci. Reports*, **2018**, 8, 1-16
52. Y. Rohitash, I. Mohammed, D. Puneet, K.C. Dheeraj, H. Shailendra, *J. Biomol. Struct. Dyn.*, **2021**, 39, 6617-6632.
53. P.P. Shinoj Kumar, G. Krishnaswamy, N.R. Desai, S. Sreenivasa, D.B. Aruna Kumar, *Chem. Data Collect.*, **2020**, 31, 1-19.
54. S. Mishra, R. Dahima, *J. Drug Deliv. Ther.*, **2019**, 9, 366-369.
55. G.K. Swamy, G. Ramesh, K. Pruthviraj, S. Banu, B. Roopa, H.J. Preritha, B.S. Rajeshwari, M. Ravikumar, P. Raghuram Shetty, D.B. Aruna Kumar, S. Sreenivasa, *Chem. Data Collect.*, **2020**, 28, 1-23.
56. Md. Lutful Amin, *Drug Target Insights*, **2013**, 7, 27-34.

6A.1. Introduction

Azaheterocycles are a very important class of heterocyclic compounds. In that, diazines containing two nitrogen atoms (1,2-diazine, 1,3-diazine and 1,4-diazine). They are found in many natural products, alkaloids, flavors and fragrances etc., due to their unique chemical and biological properties, they have found great importance in organic field. Among them, 1,3-diazine i.e., pyrimidine and their derivatives play a vital role in drug discovery processes. The pyrimidine structural skeleton is a fundamental constituent of nucleic bases and alkaloids [1] and they are the building blocks of many natural compounds such as vitamins, liposacharides, antibiotics, DNA and RNA [2] as well as synthetic drugs such as gemcitabine, 5-fluorouracil, floxuridine, aronixil, buspirone, risperidone, stavudine etc [3]. Pyrimidine nucleus present in many classes of chemotherapeutic agents and is in clinical use as an anticancer [4], antibacterial [5], antiviral [6], antifungal [7], antimalarial [8] anti-HIV [9], anti-tuberculosis [10], anti-inflammatory [11], anti-diabetic agents [12] and also act as enzyme inhibitors [13]. Due to their broad spectrum of biological applications, researchers are attaining more attention to pyrimidine derivatives.

Diabetes diseases are characterized by high glucose level in the blood, which has becomes a serious problem nowadays. So, the main goal of the researchers is to develop treatment or medication for diabetes by controlling the blood glucose level [14]. Cancer is the second leading cause of death worldwide (about 8.2 million deaths per year as estimated by the World Health Organization). It is a multistep process involving multiple mutations, leading to uncontrolled cell growth and proliferation as well as genomic and chromosomal instability [15]. Uncontrolled cell divisions are regulated by chemotherapy, it is the most effective tool for the treatment of cancer because it controls the cancer spread across the body [16, 17]. The treatment modes and medicines are still having some side effects; to overcome these problems further investigation of novel drugs is needed for the treatment. Pyrimidine

derivatives have properties that are potentially useful in the fight against cancer and diabetic diseases. Some of the reported biologically important pyrimidine heterocyclic compounds have been appended in **Fig. 1**.

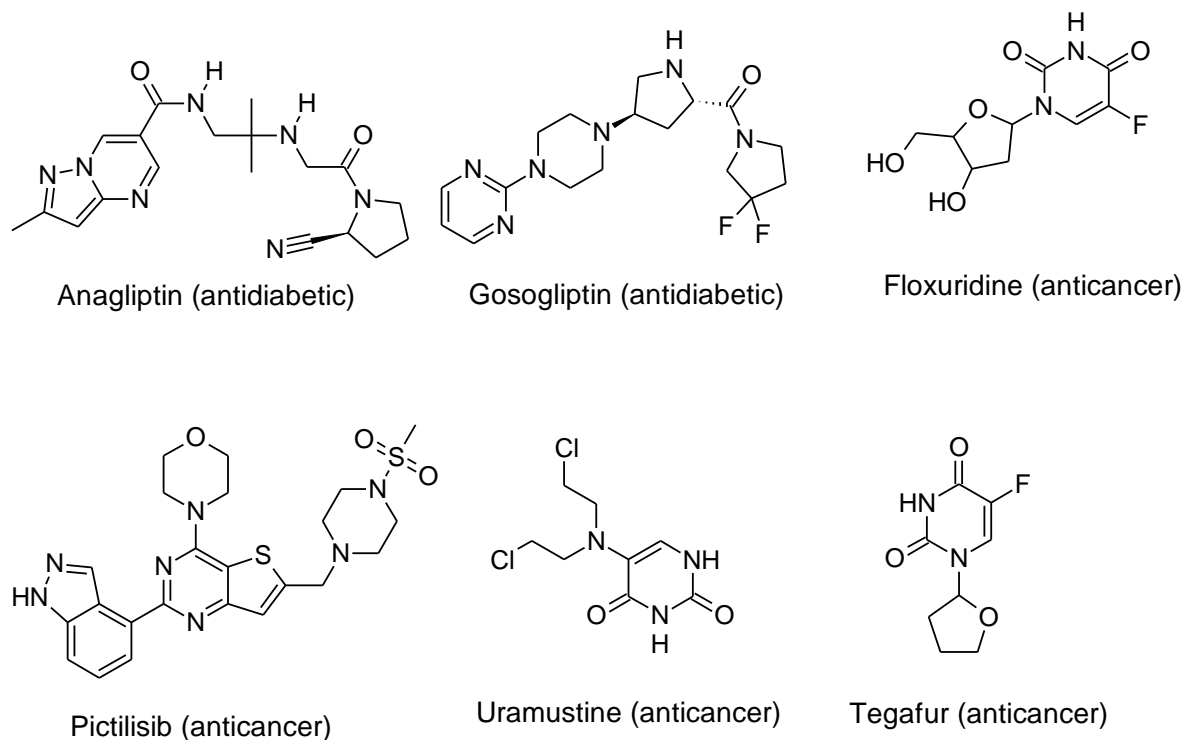
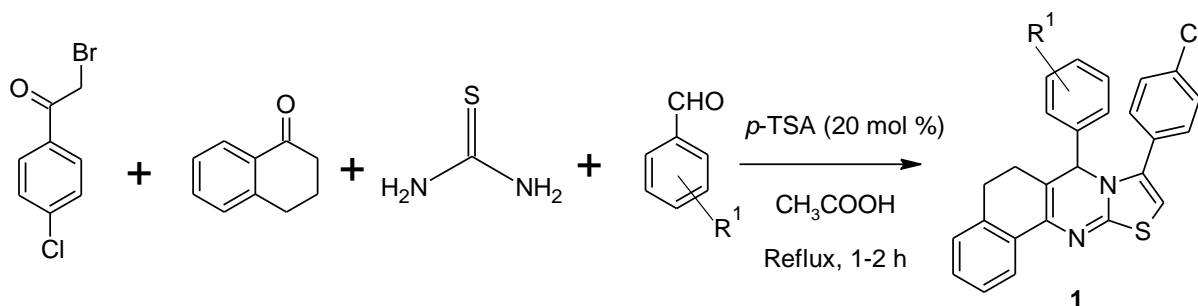
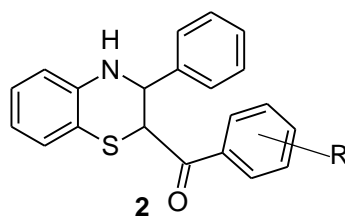


Fig. 1. Some of the drugs containing pyrimidine nucleus.

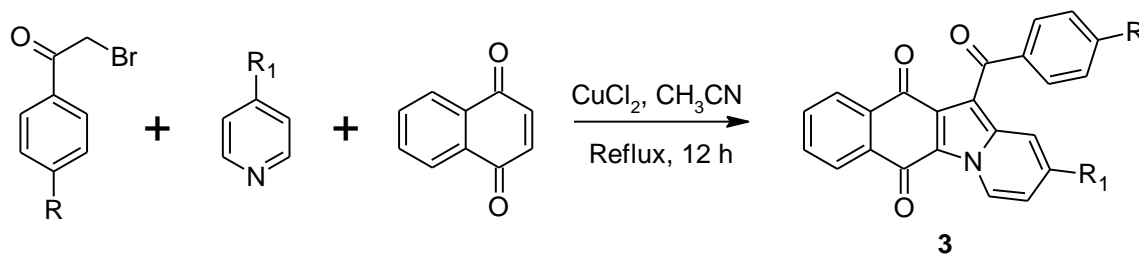
B. Sakram *et. al.*, have discussed one-pot tandem protocol for the preparation of 7,9-disubstituted-6,7-dihydro-5*H*-benzo[*h*]thiazolo[2,3-*b*]quinazoline derivatives (**1**) by using *p*-TSA as a catalyst [18].



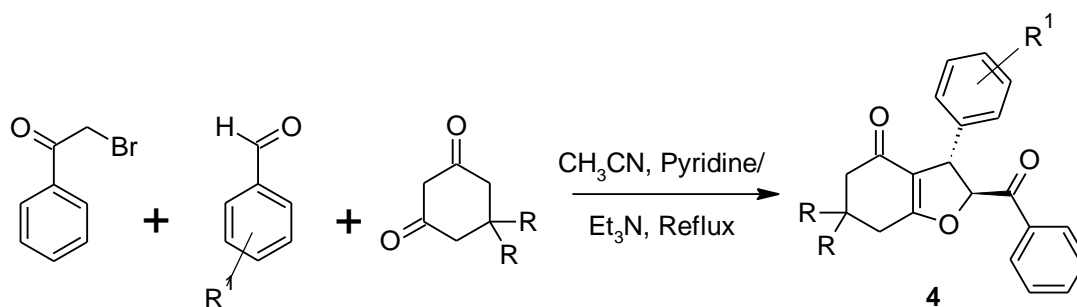
In 2019, D.K. Jangid and S. Dhadda reported a series of phenyl (3-phenyl-3,4-dihydro-4*H*-benzo[*b*][1,4]thiazin-2-yl)methanone derivatives (**2**) [19].



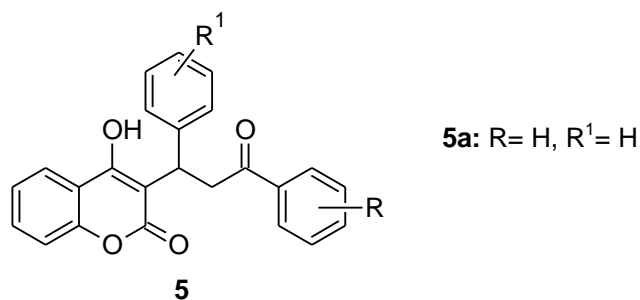
A novel series of benzo[*f*]pyrido[1,2-*a*]indole-6,11-dione derivatives (**3**) has been reported by Y. Liu and J.W. Sun using CuCl_2 as a catalyst [20].



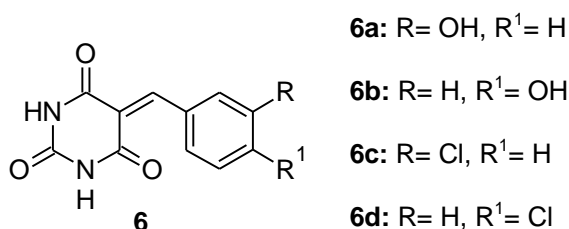
In 2009, Q.F. Wang *et. al.*, have developed an efficient synthetic methodology for the preparation of fused 2,3-dihydrofuran derivatives (**4**) in the presence of pyridine and triethylamine as a catalyst [21].



J.W. Xie and co-authors developed a chiral anticoagulant drug, (*S*)-warfarin/4-hydroxy-3-(3-oxo-1,3-diphenylpropyl)-2*H*-chromen/xanthene-2-one derivatives (**5**) in the presence of TFA as an additives with good yield. The compound **5a** shows potent anticoagulant activity compared to other compounds [22].



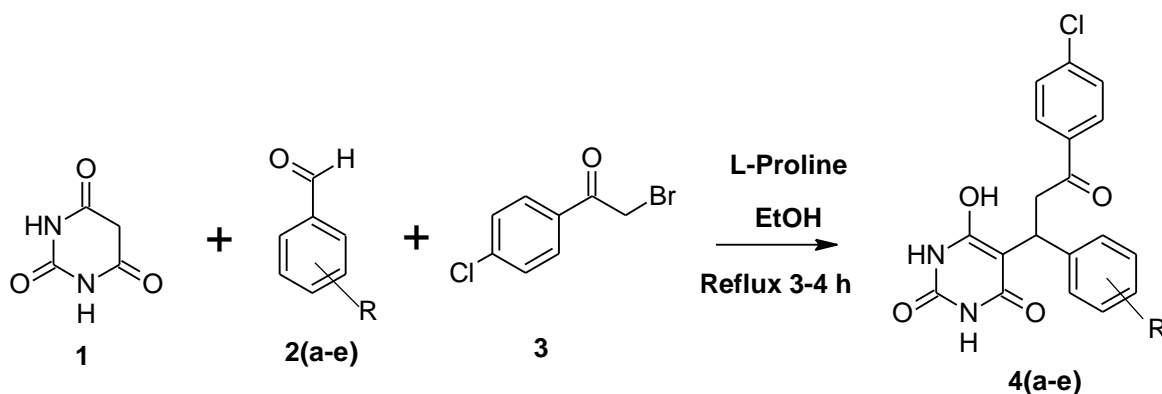
N. Irshad *et. al.*, has reported a substituted 5-benzylidenepyrimidine-2,4,6(1*H*,3*H*,5*H*)-trione derivatives (**6**) as antihypertensive agents. Among the series, the compounds **6a**, **6b**, **6c** and **6d** increased the urinary output in rats and inhibited the human platelet aggregation with IC₅₀ values of 37, 93, 31 & 23 μM respectively [23].



Based on these findings, we reported a simple method for synthesizing new 5-[3-(4-chlorophenyl)-substituted-6-hydroxypyrimidine-2,4(1*H*,3*H*)-dione] derivatives and investigate their anti-diabetic and anticancer activities. Further, to predict the binding interactions of targets using *exo*-β-D-glucosaminidase and P38 MAP kinase along with their *in silico* ADME investigations.

6A.2. Present work

In this chapter, we described an effective protocol for the synthesis of novel 5-[3-(4-chlorophenyl)-substituted-6-hydroxypyrimidine-2,4(1*H*,3*H*)-dione] derivatives **4(a-e)** via multicomponent reaction of barbituric acid (**1**), substituted aromatic aldehydes (**2**) and 2-bromo-4-chloroacetophenone (**3**) in aqueous ethanol using L-Proline as a catalyst and the reaction pathway has been given in **Scheme 7**.



Compd.	R
4a	H
4b	4-OH
4c	4-OCH ₃
4d	4-CN
4e	3-NO ₂

Scheme 7. Synthesis of 5-[3-(4-chlorophenyl)-substituted-6-hydroxypyrimidine-2,4(1*H*,3*H*)-dione derivatives 4(a-e).

The synthetic strategy involves in the following steps:

- 5-[3-(4-chlorophenyl)-substituted-6-hydroxypyrimidine-2,4(1*H*,3*H*)-dione derivatives was synthesized initially by the reaction of barbituric acid (1) and aromatic aldehydes (2) in presence of L-Proline as a catalyst undergo Knoevenagel condensation reaction to afford an intermediate [24].
- Then it undergoes Michael addition with 2-bromo-4-chloroacetophenone (3) to afford the desired product 4(a-e). The possible mechanism is shown below (Fig. 2).

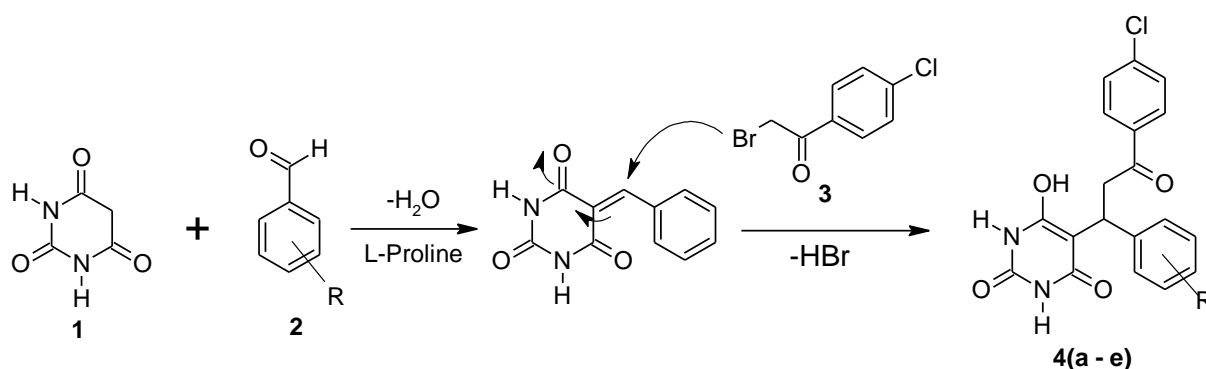


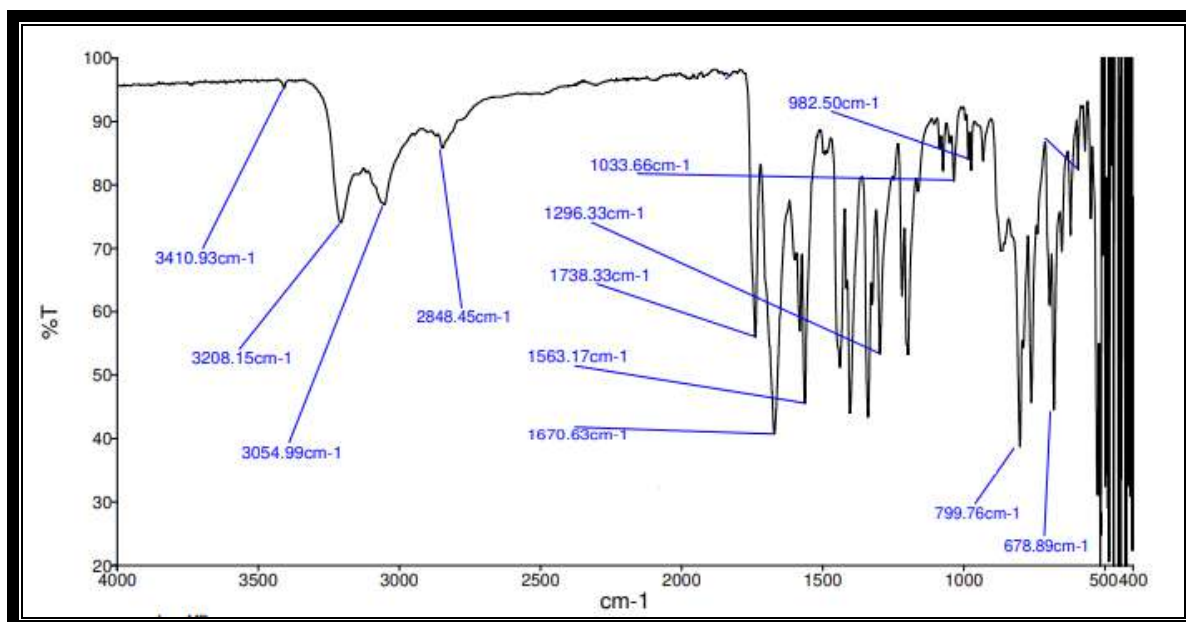
Fig. 2. Possible mechanism of synthesized compounds 4(a-e).

The structures of 5-[3-(4-chlorophenyl)-substituted-6-hydroxypyrimidine-2,4(1*H*,3*H*)-dione derivatives **4(a-e)** were confirmed by recording their IR, ¹H NMR, ¹³C NMR and Mass spectral data.

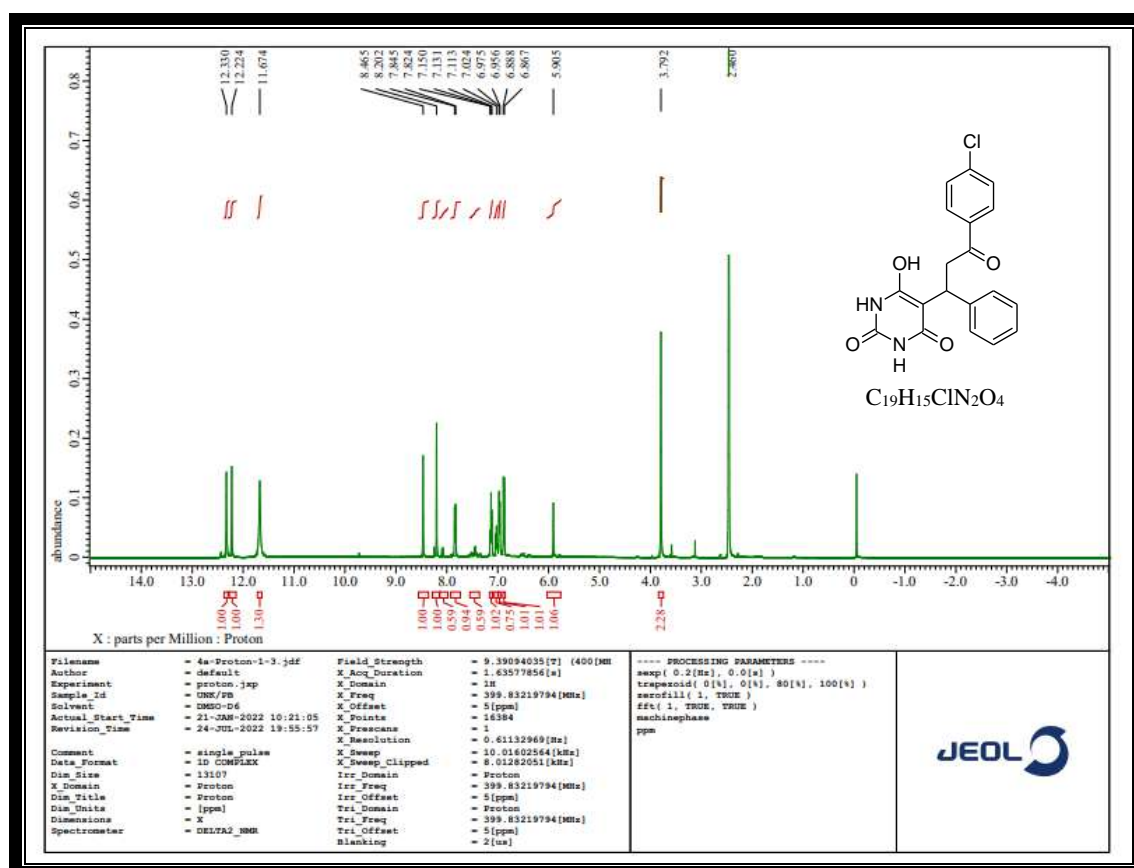
In IR spectrum of compound **4a** showed the absorption band in the region of 3410 cm⁻¹ is attributed to the hydroxyl stretching frequency, 3208 cm⁻¹ correspond to amide functionality, 3054 cm⁻¹ correspond to aromatic CH group, 1670 cm⁻¹ correspond to C=O functionality and another stretching vibrational band at 799 cm⁻¹ correspond to C-Cl functionality. The ¹H NMR spectrum of compound **4a** exhibited two singlet peaks at δ 12.33 & 12.23 ppm which corresponds to two NH protons of barbituric acid nucleus (s, 2H, NH) and another singlet peak at δ 11.68 ppm which correspond to OH proton (s, 1H, OH) and δ range from 8.47-6.87 ppm corresponds to nine aromatic protons (9H, Ar-H). A singlet peak at δ 5.91 ppm due to CH proton (s, 1H, CH) and δ 3.79 ppm due to CH₂ protons (s, 2H, CH₂). In addition, the ¹³C NMR spectrum of compound **4a** exhibited peaks at δ 163.55 and 163.03 ppm which correspond to carbonyl carbons.

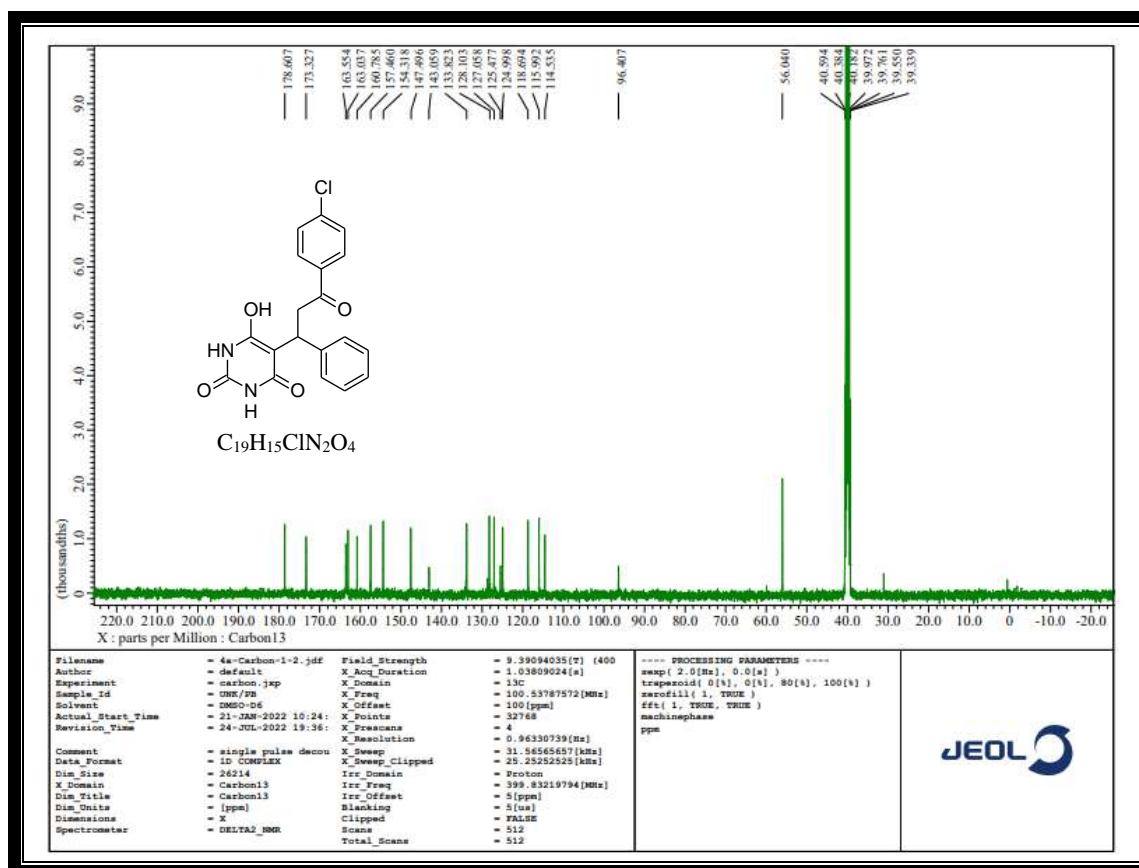
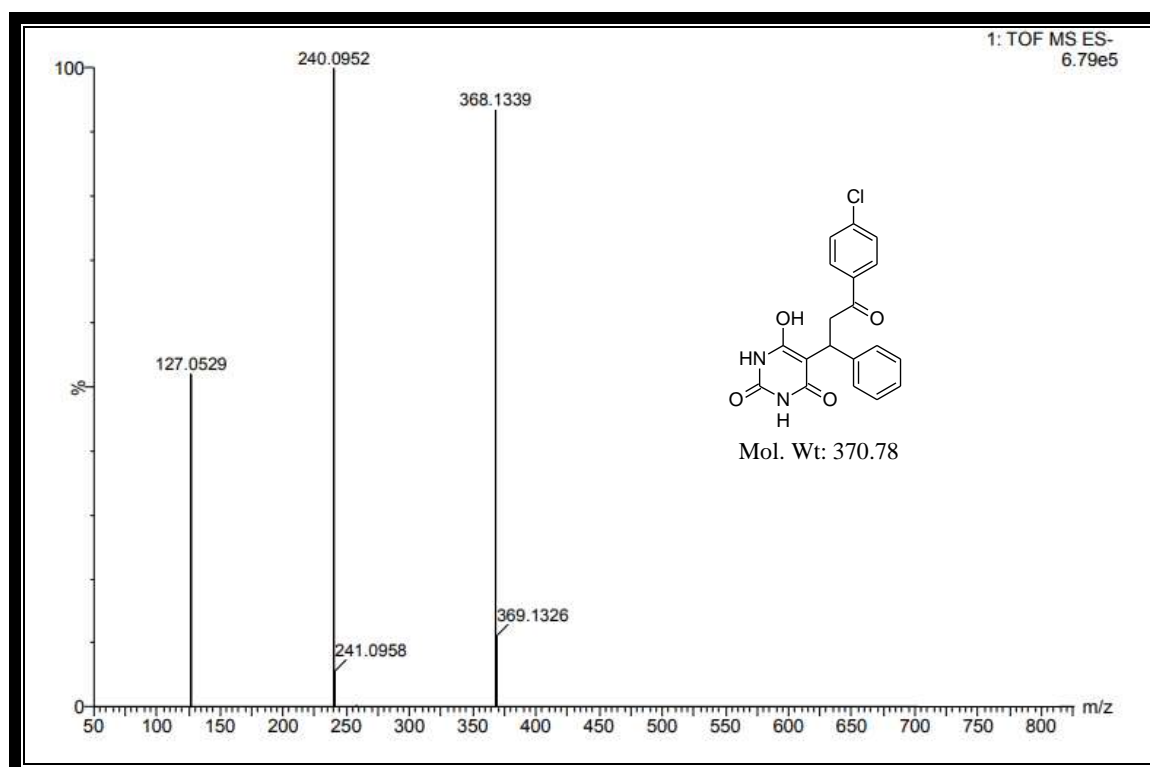
The mass spectrum showed a molecular ion peak m/z at 369.1326 [M⁺-1] & 368.1339 [M⁺-2], which corresponds to the molecular weight of compound **4a**.

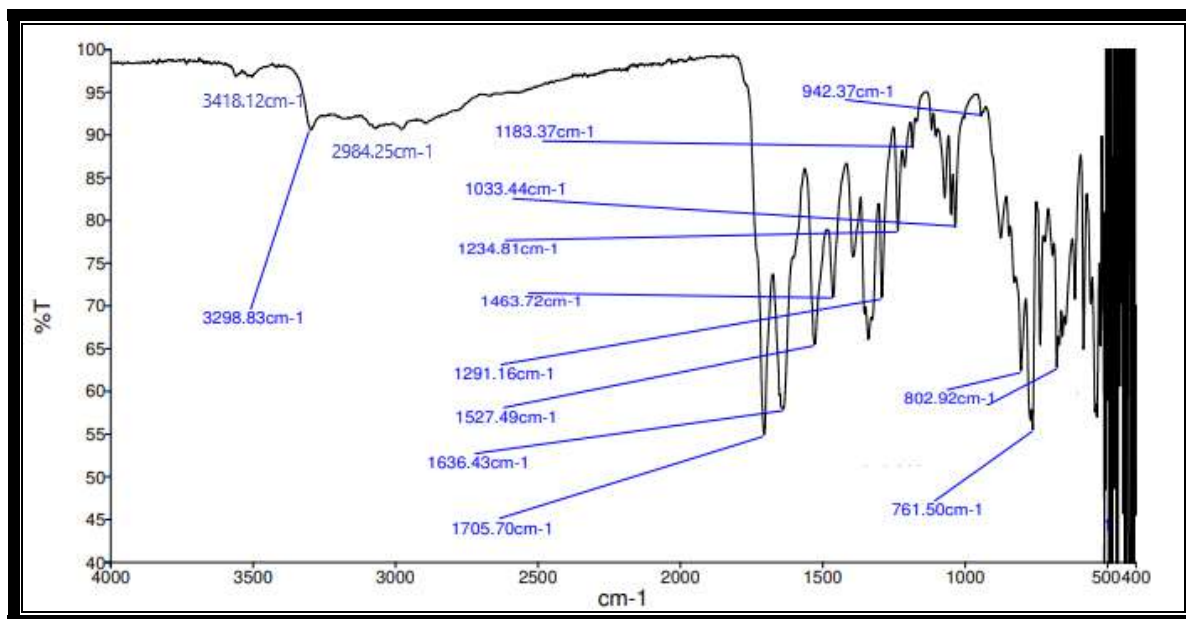
Characterization:



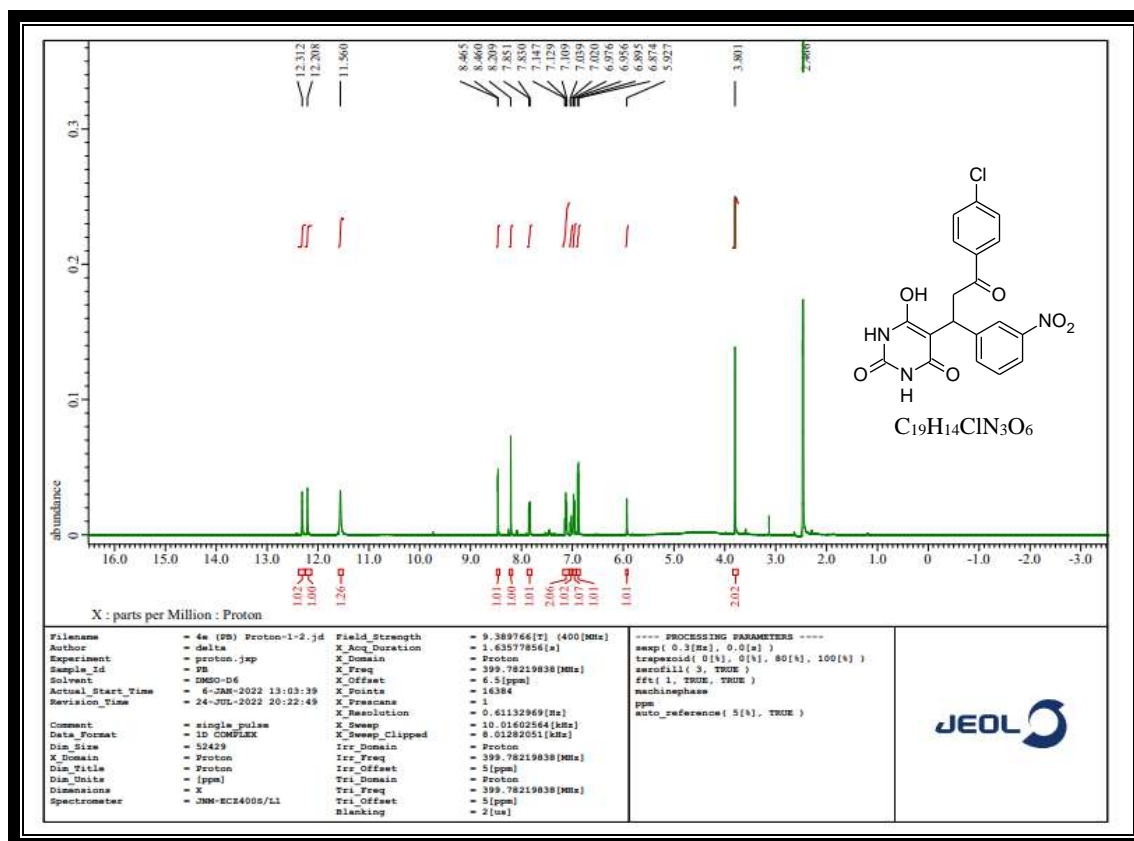
IR spectrum of compound 4a

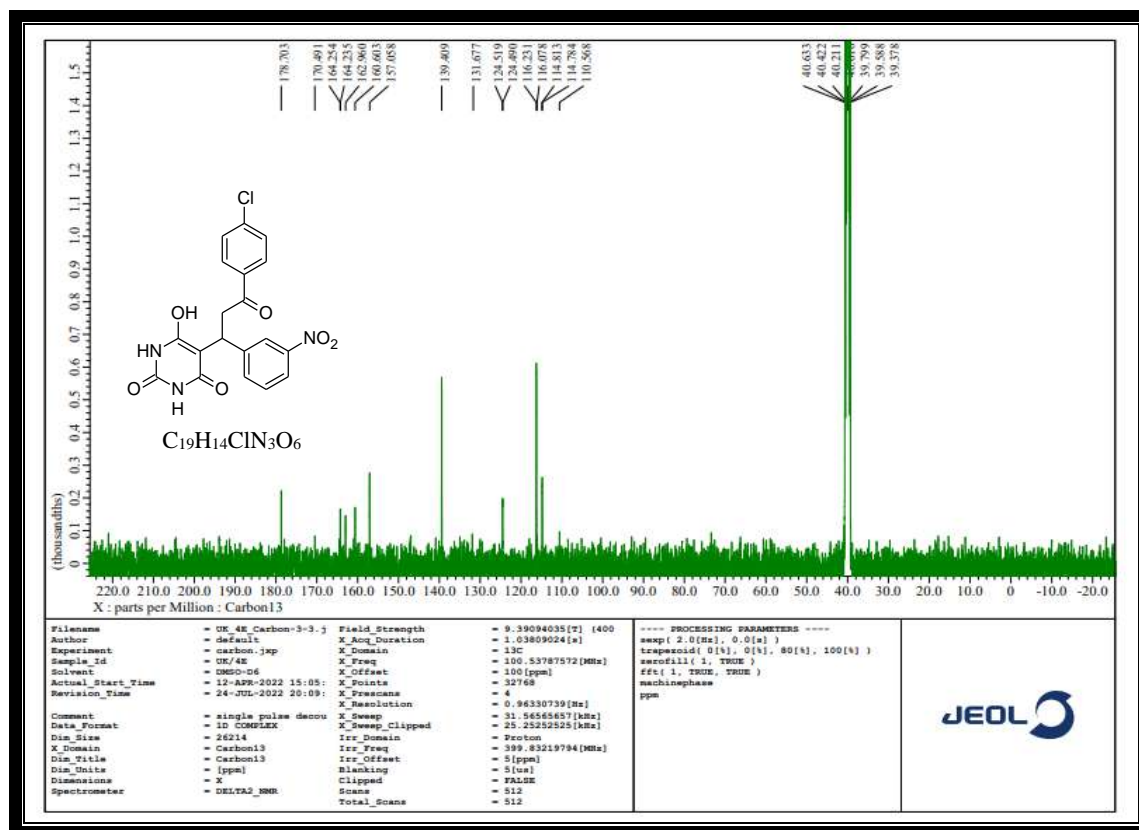
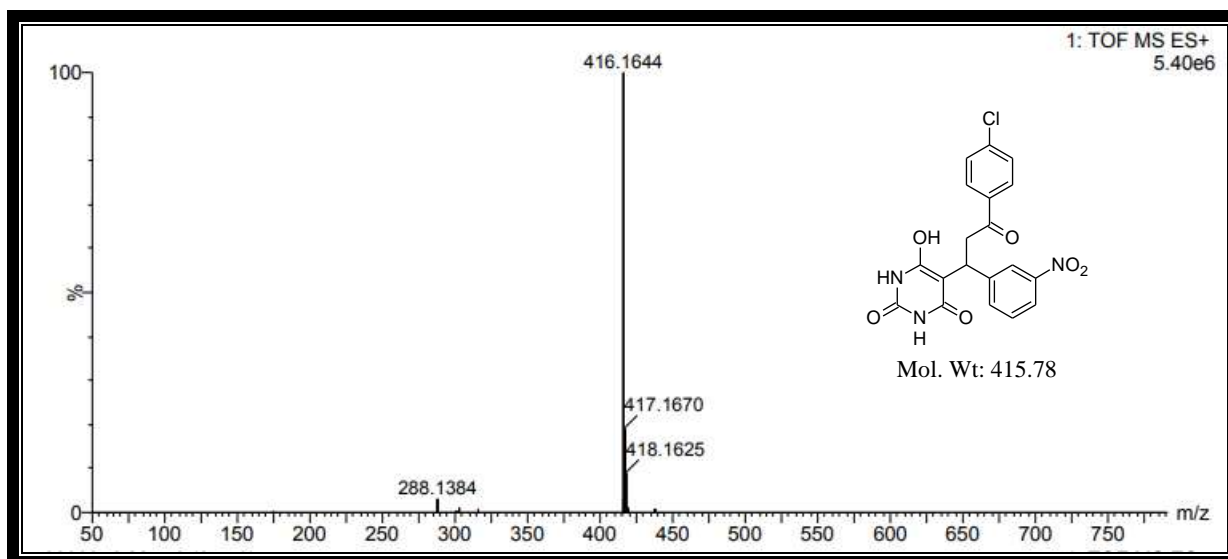
¹H NMR spectrum of compound 4a

 **^{13}C NMR spectrum of compound 4a****MASS spectrum of compound 4a**



IR spectrum of compound 4e

 ^1H NMR spectrum of compound 4e

 ^{13}C NMR spectrum of compound 4e

MASS spectrum of compound 4e

6A.3. Experimental

6A.3.1. General information:

The general information regarding the different solvents, reagents and instruments etc., used for the analysis has been discussed in the experimental section 2A.3.1 & 5.3.1 of Chapter-2A & Chapter-5.

6A.3.2. General procedure for synthesis of some novel 5-[3-(4-chlorophenyl)-substituted-6-hydroxypyrimidine-2,4(1H,3H)-dione derivatives 4(a-e):

An equimolar quantity of barbituric acid (**1**, 1 mmol) and aromatic aldehydes (**2**, 1 mmol) using 10 mol % of L-Proline as a catalyst in aqueous ethanol was stirred under refluxed condition. After 10 min, 2-bromo-4-chloroacetophenone (**3**, 1 mmol) was added to it and refluxed at 80-82 °C with constant stirring for about 5-6 hour. Simultaneously, the reaction was monitored by TLC (ethyl acetate and pet ether). After completion of the reaction, the reaction mixture was cooled to room temperature and poured into the 100 mL ice flake with vigorous stirring to obtain a solid precipitate. Then, it was filtered, washed, dried and recrystallized from methanol to afford pure solid products **4(a-e)**.

5-[3-(4-Chlorophenyl)-3-oxo-1-phenylpropyl]-6-hydroxypyrimidine-2,4(1H,3H)-dione (4a):

White solid; Yield: 92 %; MP: 212-214 °C; Mol. Formula: C₁₉H₁₅ClN₂O₄; UV (nm) λ_{max} (log ε): 325 (3.42) & 323 (3.70); FTIR (ν cm⁻¹): 3410 (OH), 3208 (NH), 3054 (CH), 1670 (C=O) & 799 (C-Cl); ¹H NMR (δ ppm): 12.33 (s, 1H, NH), 12.22 (s, 1H, NH), 11.67 (s, 1H, OH), 8.46 (s, 1H, Ar-H), 8.20 (s, 1H, Ar-H), 8.09-8.07 (d, *J*= 8 Hz, 1H, Ar-H), 7.84-7.82 (d, *J*= 8 Hz, 1H, Ar-H), 7.45-7.43 (d, *J*= 8 Hz, 1H, Ar-H), 7.15-7.11 (t, *J*= 16 Hz, 1H, Ar-H), 7.04-7.00 (t, *J*= 16 Hz, 1H, Ar-H), 6.97-6.95 (d, *J*= 8 Hz, 1H, Ar-H), 6.88-6.86 (d, *J*= 8 Hz, 1H, Ar-H), 5.90 (s, 1H, CH), 3.79 (s, 2H, CH₂); ¹³C NMR (δ ppm): 178.60, 173.32, 163.55, 163.03, 160.78, 157.46, 154.31, 147.49, 143.05, 133.82, 128.10, 127.05, 125.47, 124.99,

118.69, 115.99, 114.53, 96.40 & 56.04; HRMS: m/z 369.1326 [M^+-1] & 368.1339 [M^+-2];
Anal. Calcd: C 61.55, H 4.08, N 7.56 %, Found: C 61.51, H 4.05, N 7.52 %.

5-[3-(4-Chlorophenyl)-1-(4-hydroxyphenyl)-3-oxopropyl]-6-hydroxypyrimidine-2,4(1H,3H)-dione (4b):

Yellow solid; Yield: 90 %; MP: 289-291 °C; Mol. Formula: $C_{19}H_{15}ClN_2O_5$; UV (nm) λ_{max} (log ϵ): 316 (2.57) & 322 (3.81), 412 (3.56), 492 (3.23); FTIR (ν cm^{-1}): 3475 (OH), 3240 (NH), 2904 (CH), 1672 (C=O) & 792 (C-Cl); 1H NMR (δ ppm): 12.32 (s, 1H, NH), 12.22 (s, 1H, NH), 10.94 (s, 2H, OH), 8.38-8.36 (d, $J=8$ Hz, 4H, Ar-H), 8.22 (s, 1H, CH), 6.90-6.88 (d, $J=8$ Hz, 4H, Ar-H), 3.16 (s, 2H, CH_2); ^{13}C NMR (δ ppm): 161.11, 159.70, 158.99, 155.48, 151.98, 151.44, 151.35, 146.95, 129.53, 121.65, 121.57, 121.38, 117.11, 116.29, 114.97, 114.85, 114.68, 110.88 & 55.42; HRMS: m/z 389.1286 [M^++1] & 388.1273 [M^++2];
Anal. Calcd: C 59.00, H 3.91, N 7.24 %, Found: C 58.96, H 3.88, N 7.19 %.

5-[3-(4-Chlorophenyl)-1-(4-methoxyphenyl)-3-oxopropyl]-6-hydroxypyrimidine-2,4(1H,3H)-dione (4c):

Yellow solid; Yield: 80 %; MP: 204-206 °C; Mol. Formula: $C_{20}H_{17}ClN_2O_5$; UV (nm) λ_{max} (log ϵ): 386 (2.63) & 326 (3.86), 392 (3.77), 491 (2.92); FTIR (ν cm^{-1}): 3420 (OH), 3198 (NH), 2984 (CH), 2854 (OCH_3), 1705 (C=O) & 781 (C-Cl); 1H NMR (δ ppm): 12.28 (s, 1H, NH), 12.18 (s, 1H, NH), 11.45 (s, 1H, OH), 8.36-8.34 (d, $J=8$ Hz, 2H, Ar-H), 8.28-8.12 (m, 2H, Ar-H), 6.84-6.82 (d, $J=8$ Hz, 2H, Ar-H), 6.72-6.70 (d, $J=8$ Hz, 1H, Ar-H), 6.50-6.48 (d, $J=8$ Hz, 1H, Ar-H), 5.85 (s, 1H, CH), 3.84 (s, 3H, OCH_3), 3.18 (s, 2H, CH_2); ^{13}C NMR (δ ppm): 163.46, 162.22, 161.78, 157.94, 156.37, 148.56, 142.05, 134.82, 128.64, 127.23, 125.66, 124.45, 113.89, 112.59, 111.53, 84.24 & 58.22; HRMS: m/z 401.1245 [M^++1] & 402.1108 [M^++2]; Anal. Calcd: C 59.93, H 4.28, N 6.99 %, Found: C 59.89, H 4.25, N 6.95 %.

4-[3-(4-Chlorophenyl)-1-(6-hydroxy-2,4-dioxo-1,2,3,4-tetrahydropyrimidin-5-yl)-3-oxopropyl]benzotrile (4d):

White solid; Yield: 83 %; MP: 274-276 °C; Mol. Formula: C₂₀H₁₄ClN₃O₄; UV (nm) λ_{max} (log ε): 318 (3.02) & 316 (3.11); FTIR (ν cm⁻¹): 3415 (OH), 3201 (NH), 2974 (CH), 1652 (C=O) & 785 (C-Cl); ¹H NMR (δ ppm): 12.30 (s, 1H, NH), 12.20 (s, 1H, NH), 11.80 (s, 1H, OH), 8.24-8.22 (d, *J* = 8 Hz, 1H, Ar-H), 7.86-7.84 (d, *J* = 8 Hz, 2H, Ar-H), 7.32-7.30 (d, *J* = 8 Hz, 1H, Ar-H), 7.25-7.23 (d, *J* = 8 Hz, 2H, Ar-H), 7.14-7.12 (d, *J* = 8 Hz, 1H, Ar-H), 7.00-6.98 (d, *J* = 8 Hz, 1H, Ar-H), 5.88 (s, 1H, CH), 3.48 (s, 2H, CH₂); ¹³C NMR (δ ppm): 162.86, 162.25, 161.88, 158.46, 156.31, 146.56, 146.05, 138.82, 126.89, 126.05, 124.47, 122.93, 116.69, 114.99, 113.53, 89.40 & 48.04; HRMS: *m/z* 396.1288 [M⁺+1] & 397.1274 [M⁺+2]; Anal. Calcd: C 60.69, H 3.57, N 10.62 %, Found: C 60.65, H 3.54, N 10.58 %.

5-[3-(4-Chlorophenyl)-1-(3-nitrophenyl)-3-oxopropyl]-6-hydroxypyrimidine-2,4(1H,3H)-dione (4e):

White solid; Yield: 88 %; MP: 180-182 °C; Mol. Formula: C₁₉H₁₄ClN₃O₆; UV (nm) λ_{max} (log ε): 312 (3.43) & 314 (3.43); FTIR (ν cm⁻¹): 3418 (OH), 3298 (NH), 2984 (CH), 1705 (C=O) & 802 (C-Cl); ¹H NMR (δ ppm): 12.31 (s, 1H, NH), 12.20 (s, 1H, NH), 11.56 (s, 1H, OH), 8.46 (s, 1H, Ar-H), 8.20 (s, 1H, Ar-H), 7.85-7.83 (d, *J* = 8 Hz, 1H, Ar-H), 7.14-7.10 (t, *J* = 12 Hz, 2H, Ar-H), 7.04-7.01 (t, *J* = 12 Hz, 1H, Ar-H), 6.97-6.95 (d, *J* = 8 Hz, 1H, Ar-H), 6.89-6.87 (d, *J* = 8 Hz, 1H, Ar-H), 5.92 (s, 1H, CH), 3.80 (s, 2H, CH₂); ¹³C NMR (δ ppm): 178.70, 170.49, 164.25, 164.23, 162.96, 160.60, 157.05, 139.40, 131.67, 124.51, 124.49, 116.23, 116.07, 114.81, 114.78, 110.56 & 66.77; HRMS: *m/z* 416.1644 [M⁺+1] & 417.1670 [M⁺+2]; Anal. Calcd: C 54.88, H 3.39, N 10.11 %, Found: C 54.85, H 3.34, N 10.06 %.

6A.4. Absorption property

The UV-Vis spectra of compounds **4(a-e)** were recorded in two different solvents (DMSO & DMF) at 10^{-5} M concentration using UV-Vis Spectrophotometer. The λ_{\max} and molar absorption coefficient values were appended in **Table 1**. All the synthesized compounds exhibited absorption maxima (λ_{\max}) in the range of 312-386 nm in DMSO and 314-492 nm in DMF solvents due to the π - π^* & n - π^* transitions (**Fig. 3**). Among them, **4b** and **4c** compounds displayed three absorption maxima at 322, 412, 492 nm & 326, 392, 491 nm in DMF respectively.

Table 1. Electronic absorption data of the synthesized compounds **4(a-e)** in DMSO & DMF solvents.

Compd.	DMSO		DMF	
	$\lambda_{\max}(\text{nm})$	Log ϵ	$\lambda_{\max}(\text{nm})$	Log ϵ
4a	325	3.42	323	3.70
4b	316	2.57	322	3.81
			412	3.56
			492	3.23
4c	386	2.63	326	3.86
			392	3.77
			491	2.92
4d	318	3.02	316	3.11
4e	312	3.43	314	3.43

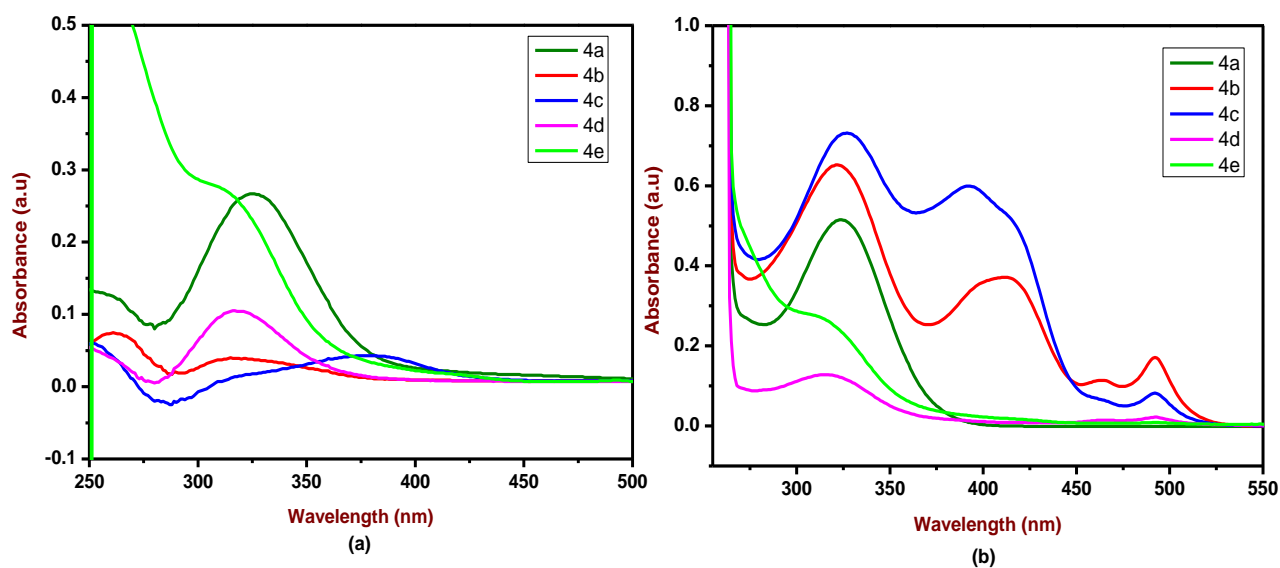


Fig. 3. A graph of UV-Visible spectra of the synthesized compounds **4(a-e)** in DMSO (a) and DMF (b) solvents.

6A.5. Pharmacological studies

6A.5.1. *In vitro* α -amylase & α -glucosidase inhibitory assay

In vitro α -amylase & α -glucosidase inhibitory activity of pooled fractions was carried out according to the reported procedure by Ademiluyi A O *et. al.* [25]. It has been previously explained in the experimental section (5.5.1) of **Chapter-5**.

6A.5.2. *In vitro* cytotoxicity

In vitro cytotoxicity was assessed by MTT assay method [26] against MCF-7 (Breast cancer) cell line. It has been previously explained in the experimental section (2B.5.2) of **Chapter-2B**.

6A.5.3. *in silico* molecular docking and ADME study

in silico molecular docking and ADME study has been explained in experimental section (5.5.3 and 5.5.4) of **Chapter-5**.

6A.6. Results and discussion

6A.6.1. *In vitro* α -amylase and α -glucosidase inhibitory activity

The α -amylase enzyme activity results revealed that, the obtained compounds **4(a-e)** possessed significant efficacy ranging from 42.70 ± 1.27 to 46.90 ± 1.27 , 52.45 ± 1.06 to 56.15 ± 0.91 , 60.15 ± 0.49 to 64.45 ± 0.63 & 72.05 ± 0.63 to 73.60 ± 1.27 % with respect to their concentration 25, 50, 75 & 100 $\mu\text{g/mL}$. The potencies of IC_{50} values vary from 35.62 ± 4.46 to 42.73 ± 3.11 $\mu\text{g/mL}$. All the compounds exhibited outstanding % inhibition with IC_{50} values as compare to standard drug acarbose (51.28 ± 0.67 $\mu\text{g/mL}$) (**Fig. 4**). Among all compounds, **4d** exhibited the least IC_{50} value of 35.62 ± 4.46 $\mu\text{g/mL}$ and results have been shown in **Table 2**.

The α -glucosidase inhibitory activity results expelled that, all the compounds show excellent % inhibition ranging from 52.35 ± 0.77 to 56.35 ± 0.77 , 59.80 ± 1.13 to 63.35 ± 0.77 , 70.10 ± 0.56 to 78.10 ± 0.28 & 80.25 ± 0.49 to 82.00 ± 0.98 % with respect to their concentration

of 25, 50, 75 & 100 $\mu\text{g/mL}$. The potencies of IC_{50} values vary from 22.62 ± 0.70 to 24.36 ± 0.37 $\mu\text{g/mL}$. All compounds exhibited almost similar IC_{50} values, in that compound **4e** showed least IC_{50} value of 22.62 ± 0.70 $\mu\text{g/mL}$ as compared to standard drug acarbose (37.69 ± 0.53 $\mu\text{g/mL}$) (**Fig. 5**) and results have been shown in **Table 3**.

Table 2. α -amylase enzyme activity results of the synthesized compounds **4(a-e)**.

Compd.	Concentration in $\mu\text{g/mL}$				IC_{50} in $\mu\text{g/mL}$
	25	50	75	100	
4a	42.70 ± 1.27	53.55 ± 0.91	64.35 ± 1.06	72.95 ± 1.34	41.90 ± 2.07
4b	46.20 ± 0.98	52.60 ± 1.13	60.90 ± 1.27	73.60 ± 1.27	39.87 ± 4.35
4c	44.35 ± 0.77	56.15 ± 0.91	61.30 ± 0.70	72.35 ± 0.63	37.14 ± 2.20
4d	46.90 ± 1.27	54.20 ± 0.98	60.15 ± 0.49	72.05 ± 0.63	35.62 ± 4.46
4e	44.35 ± 0.77	52.45 ± 1.06	64.45 ± 0.63	72.40 ± 1.13	42.73 ± 3.11
Acarbose	26.00 ± 0.70	49.30 ± 0.84	68.65 ± 0.77	78.90 ± 0.84	51.28 ± 0.67

Values are Mean \pm SE, N=3, *P<0.01 vs. Control

Table 3. α -glucosidase enzyme activity results of the synthesized compounds **4(a-e)**.

Compd.	Concentration in $\mu\text{g/mL}$				IC_{50} in $\mu\text{g/mL}$
	25	50	75	100	
4a	52.35 ± 0.77	59.80 ± 1.13	72.00 ± 0.70	80.25 ± 0.49	24.36 ± 0.37
4b	54.15 ± 0.77	60.95 ± 1.06	74.50 ± 0.84	80.70 ± 0.98	23.22 ± 0.31
4c	54.10 ± 0.56	61.10 ± 0.42	78.10 ± 0.28	82.00 ± 0.98	23.33 ± 0.16
4d	54.30 ± 0.56	63.35 ± 0.77	70.10 ± 0.56	80.60 ± 0.84	23.11 ± 0.48
4e	56.35 ± 0.77	60.65 ± 0.91	73.85 ± 0.49	80.40 ± 0.70	22.62 ± 0.70
Acarbose	39.20 ± 0.56	60.30 ± 0.56	74.05 ± 0.63	86.20 ± 0.42	37.69 ± 0.53

Values are Mean \pm SE, N=3, *P<0.01 vs. Control

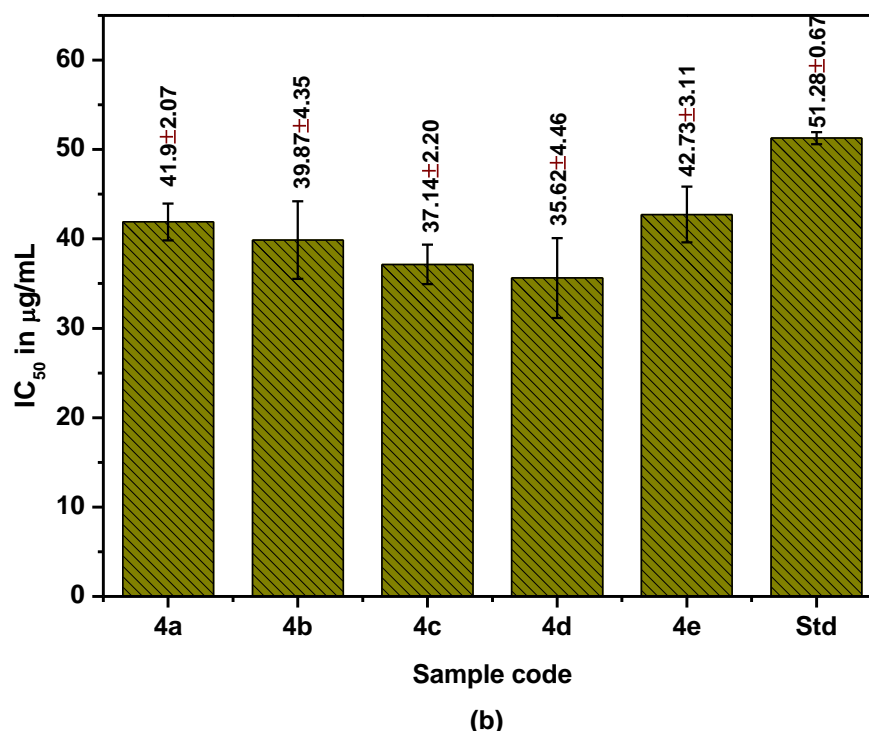
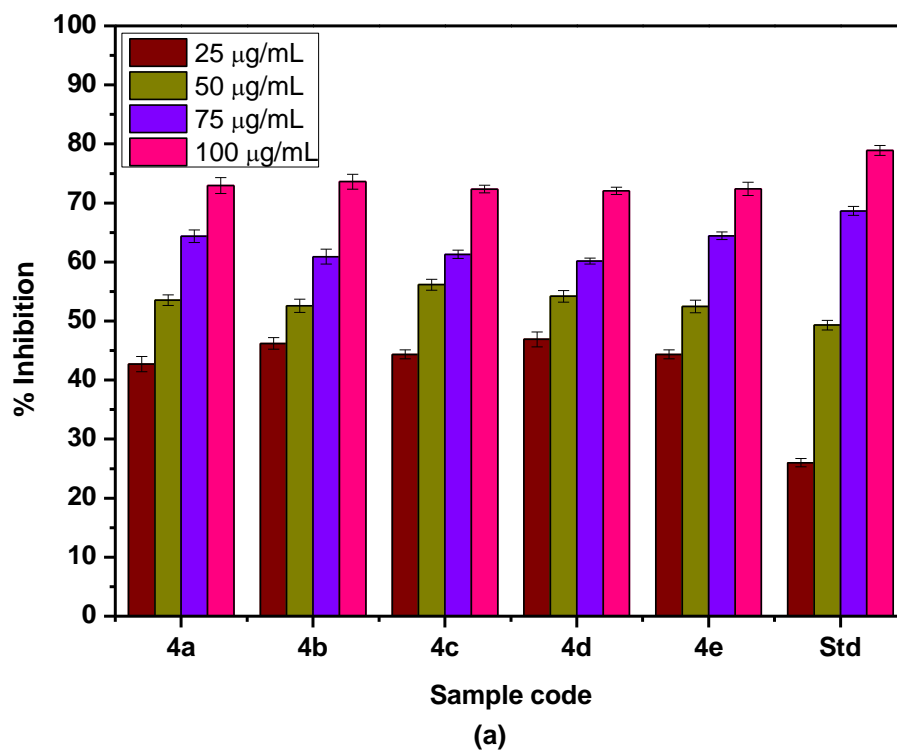


Fig. 4. *In vitro* α -amylase inhibitory activity of the synthesized compounds **4(a-e)**; A graph of % inhibition of synthesized compounds at different concentration (a); A graph of IC₅₀ value of compounds (b).

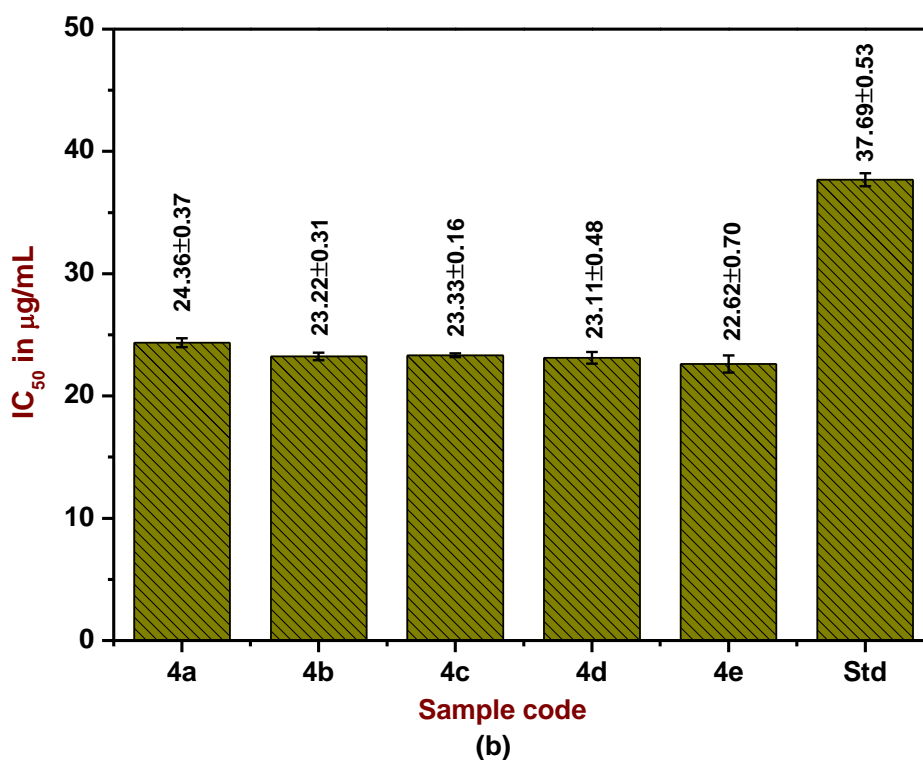
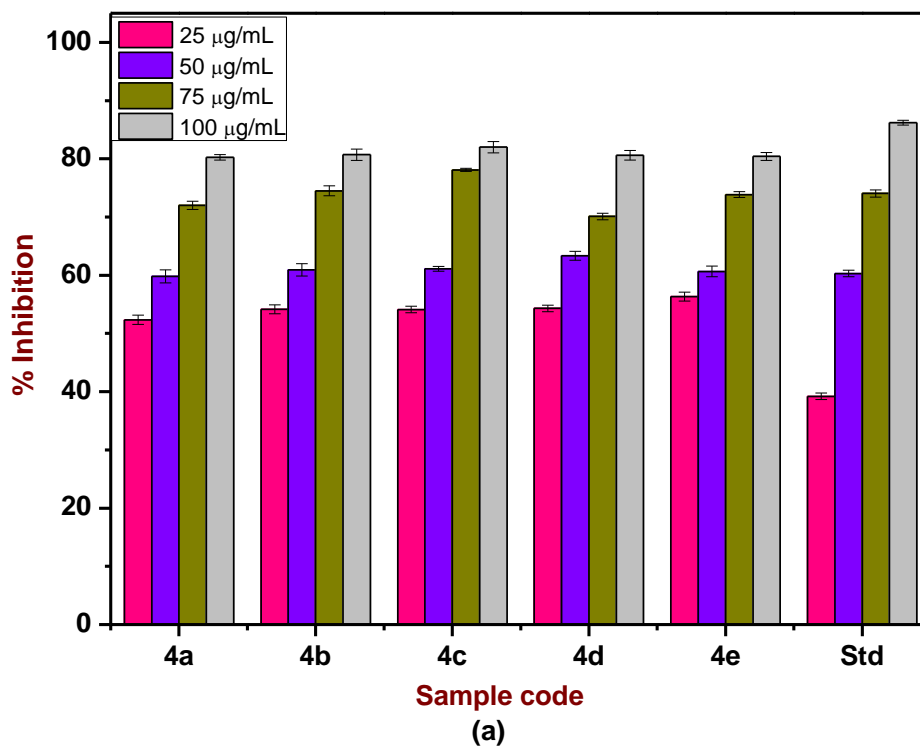


Fig. 5. *In vitro* α -glucosidase inhibitory activity of the synthesized compounds **4(a-e)**; A graph of % inhibition of synthesized compounds at different concentration (a); A graph of IC₅₀ value of compounds (b).

6A.6.2. *In vitro* cytotoxicity

In vitro cytotoxicity of the synthesized compounds **4(a-e)** was evaluated against MCF-7 cell line. A graph describing the concentration versus cell viability and IC₅₀ value of the compounds was plotted (**Fig. 6**). Doxorubicin was used as reference standard for comparison. The activity results revealed that, synthesized compounds exhibited good selectivity against the MCF-7 cell line with IC₅₀ values ranging from 9.90±0.18 to 112±0.90 µg/mL. Among them, compound **4c** showed a significant cytotoxic effect with least IC₅₀ value of 9.90±0.18 µg/mL and rest of the compounds displayed moderate cytotoxic effects with an IC₅₀ values in the range of 43.80±0.77 to 112±0.90 µg/mL as compared to reference standard doxorubicin (3.16±0.10 µg/mL) and the obtained results were listed in **Table 4**.

Table 4. Percentage of cell viability against MCF-7 cell line results of the synthesized compounds **4(a-e)**.

Compd.	Mean cell Viability of MCF-7 (Human breast cancer)							IC ₅₀ in µg/mL
	NC	3.125	6.25	12.5	25	50	100	
4a	100	94.49±0.98	85.97±0.53	84.37±0.53	82.36±0.80	77.68±0.37	40.49±1.11	96.72±1.69
4b		87.33±1.08	84.48±0.36	79.45±0.36	75.07±0.26	70.22±0.54	62.81±0.44	112.0±0.90
4c		89.28±0.89	82.00±0.62	27.65±0.54	14.86±0.54	11.60±0.54	11.18±0.47	9.90±0.18
4d		97.86±0.47	94.73±1.00	83.30±0.17	79.87±0.73	67.26±1.53	42.86±0.67	87.15±2.95
4e		96.56±0.27	94.72±0.81	89.99±0.44	81.40±1.08	30.07±0.97	15.98±0.17	43.80±0.77
Std		33.80±0.93	30.57±1.14	28.93±0.42	27.53±0.37	26.16±0.16	23.69±0.53	3.16±0.10

Std-Doxorubicin, **NC**- Negative control

Values are Mean ±SE, N=3, *P<0.01 vs. Control

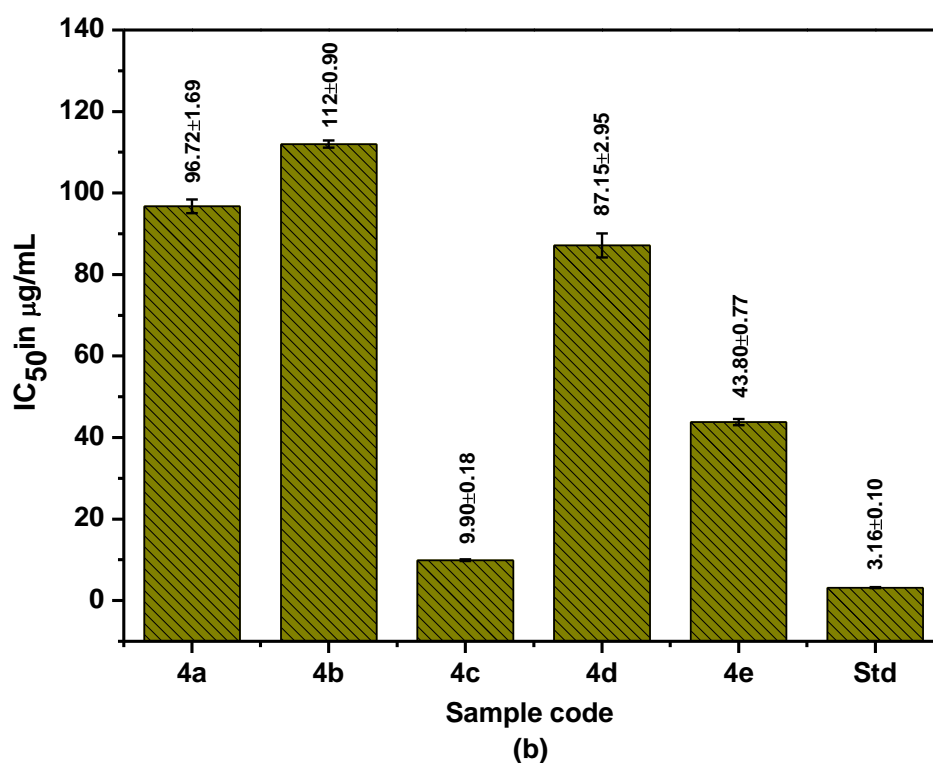
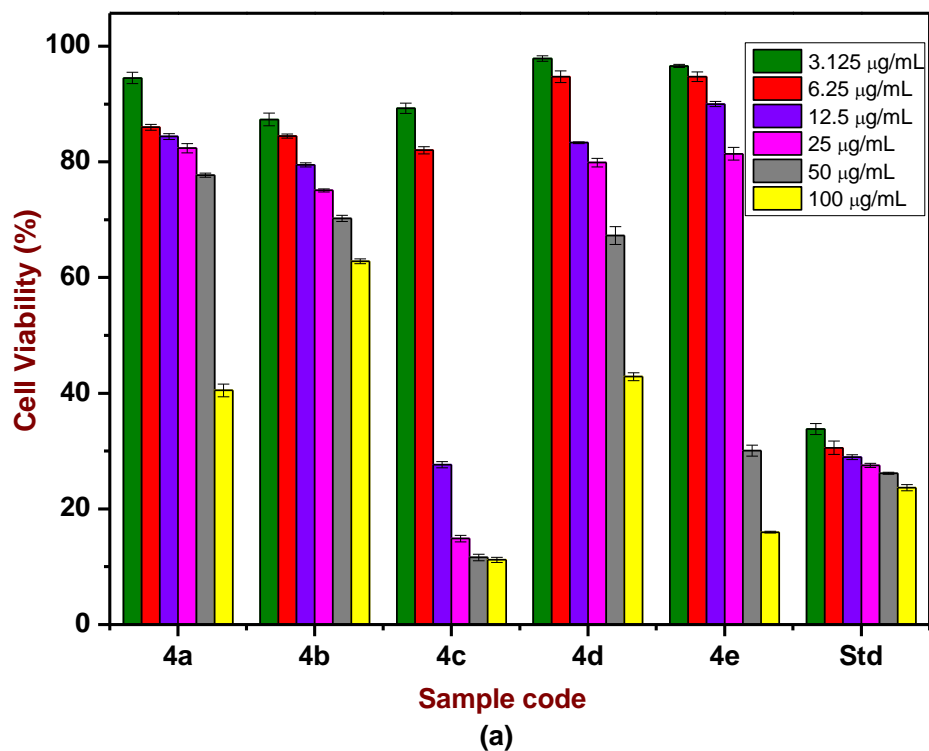


Fig. 6. A graph of % of surviving cells of synthesized compounds **4(a-e)** at different concentration against MCF-7 cell line (a); A graph of IC₅₀ value of compounds **4(a-e)** against MCF-7 cell line (b).

6A.6.3. Structure-activity relationship

A SAR study has been conducted on the newly synthesized compounds **4(a-e)**. All the five compounds exhibited considerable α -amylase, α -glucosidase and cytotoxicity with significant IC_{50} values. Among them, **4d** & **4e** show excellent α -amylase, α -glucosidase inhibitory activity due to the presence of electron-withdrawing nitro and chloro groups in their ring structures, which may be the possible reason for their admirable anti-diabetic activity [27]. The compound **4c** shows a significant cytotoxic effect due to the presence of electron-withdrawing methoxy and chloro groups in their ring structure. It may be the possible reason for the admirable anticancer activity [28].

6A.6.4. *in silico* molecular docking study

The study of intermolecular interactions between synthesized compounds **4(a-e)** and enzymes is necessary for the development of novel therapeutic drugs [29]. Therefore, we have screened the synthesized compounds for *in silico* molecular docking studies; it helps to predict the binding modes of the compounds with enzymes. From the results of docking study, synthesized compounds established good binding modes with docking receptors of α -D-glucosaminidase (**Fig. 7**) and P38 MAP kinase (**Fig. 8**) in the active pockets, respectively.

The docking of anti-diabetic and cytotoxicity investigations revealed that, the synthesized compounds **4(a-e)** had significant docking scores in the range of -8.3 to -8.8 kcal/mol and -8.1 to -8.9 kcal/mol with respect to standards Acarbose (-7.8 kcal/mol) and Doxorubicin (-8.4 kcal/mol) respectively. The docked structures with α -D-glucosaminidase results suggested that, the compound **4e** established the least binding energy of -8.8 kcal/mol forming four hydrogen bonds with amino acid residues CYS420, GLU431 TRP204 & TRP642. And the remaining compounds also established good binding modes and three hydrogen bonds with amino acid residues TRP204, TRP642, ASP469, MET512,

CYS420, GLU431 & ARG500 (**Table 5**). The docked structures with P38 MAP kinase protein results revealed that, the compounds **4b** & **4e** demonstrated the least binding energy of -8.9 kcal/mol forming four & two hydrogen bonds with amino acid residues LYS53, MET109, MET109 & LEU104. Remaining compounds were also established encouraging binding energies and forming two or more hydrogen bonds with amino acid residues in their active pockets and the results were tabulated in **Table 6**.

Table 5. Molecular interactions of synthesized compounds **4(a-e)** & standard drug **acarbose** against α -D-glucosaminidase protein.

Compd.	Binding affinity (kcal/mol)	Hydrogen bond interaction	Hydrogen bond length in Å	Hydrophobic and other interactions
4a	-8.6	TRP204, TRP642, ASP469	2.26, 2.06, 2.61	ASP203, GLU541, TYR516, TRP781, MET512
4b	-8.5	MET512, TRP204, TRP642	1.98, 2.31, 2.25	CYS420, ASP203, GLU431, GLU541, CYS419, CYS420, TYR516, LYS432, CYS420, MET512
4c	-8.3	ASP469, TRP204, TRP642	2.29, 2.21, 2.37	CYS420, ASP203, ASP203, GLU431, ASP469, GLU541, CYS419, CYS420, CYS420, TYR516 LYS432, MET512, MET512
4d	-8.5	CYS420, TRP204, TRP642	2.42, 2.26, 2.29	CYS420, ASP203, ASP203, GLU431, ASP469, GLU541, CYS419, CYS420, CYS420, TYR516, MET512
4e	-8.8	CYS420, GLU431 TRP204, TRP642	2.83, 2.19, 1.98, 2.43	ASP203, ASP203, CYS419, CYS420, CYS420, TYR516, MET512, TYR516
Acarbose	-7.8	GLU431, GLU431, MET512, MET512, ARG500, ARG500 ARG500	2.45, 2.65, 2.54, 2.89, 2.23, 2.85, 2.64	ASP469, CYS420, MET512, SER580, ILE202, TRP781

Table 6. Molecular interactions of synthesized compounds **4(a-e)** & standard drug **Doxorubicin** against P38 MAP kinase protein.

Compd.	Binding affinity (kcal/mol)	Hydrogen bond interaction	Hydrogen bond length in Å	Hydrophobic and other interactions
4a	-8.1	LYS53, LEU104	2.44, 2.02	THR106, LYS53, LEU104, VAL38, ALA51, VAL38
4b	-8.9	LYS53, MET109, MET109, LEU104	1.83, 2.13, 3.02, 2.34	ASP168, THR106, TYR35, TYR35, VAL38, ALA51, ALA51, LYS53
4c	-8.7	LYS53, MET109, LEU104	1.84, 2.37, 2.27	THR106, TYR35, LEU108, TYR35, VAL38, ALA51, LYS53
4d	-8.8	LYS53, MET109, LEU104	1.84, 2.34, 2.31	THR106, TYR35, TYR35, VAL38, ALA51, LYS53, ILE84
4e	-8.9	LEU104, LYS53	2.26, 1.84	ASP168, THR106, TYR35, VAL38, ALA51, ALA51, LYS53, TYR35
Doxorubicin	-8.4	ASP168, VAL30, LYS53	2.38, 2.80, 2.95	LYS53, LEU75, ILE84, VAL38, LEU167, VAL38, LYS53, LEU167, LYS53, TYR35

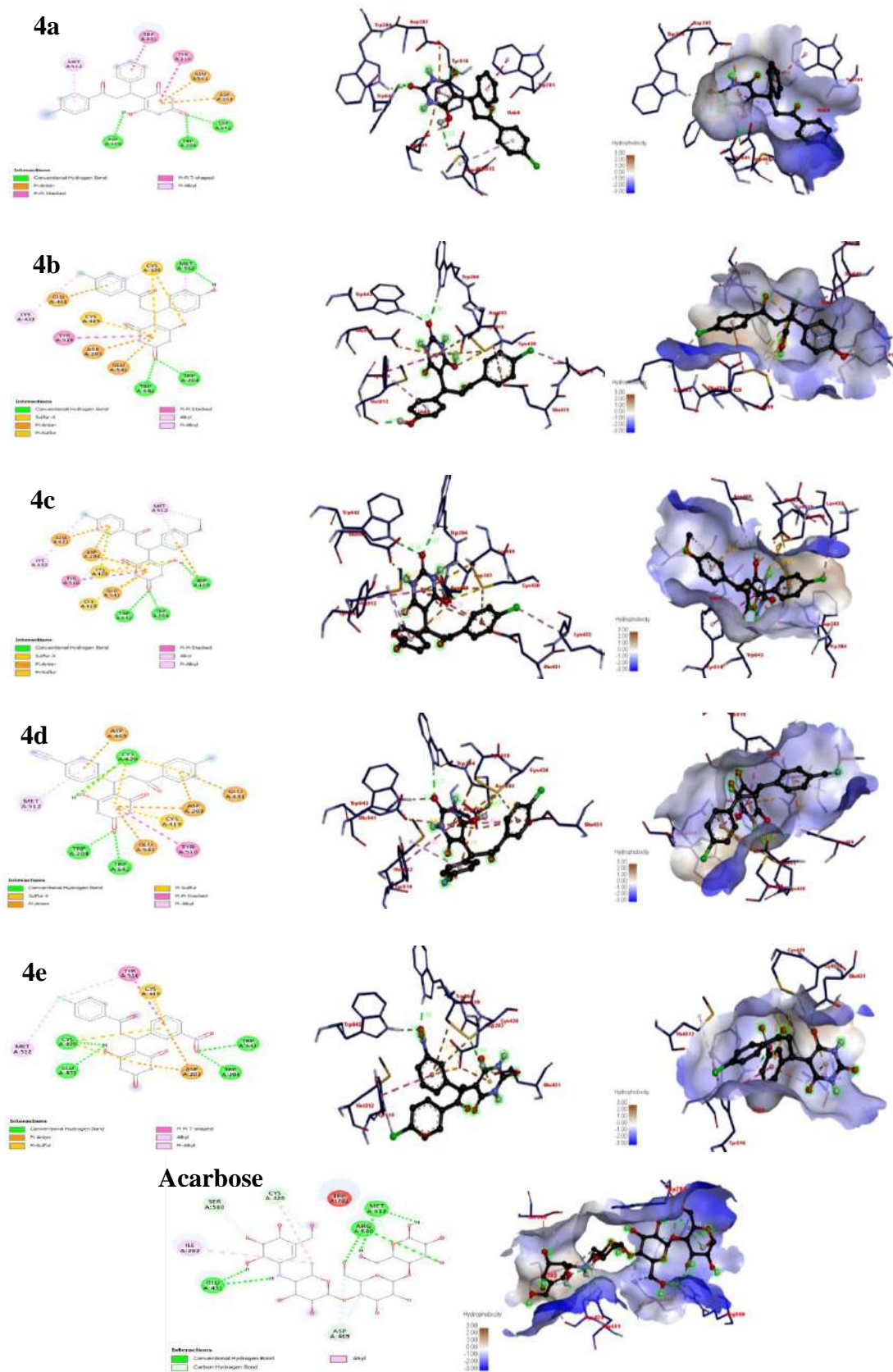


Fig. 7. 2D, 3D & hydrophobic representation of molecular interactions between *exo*- β -D-glucosaminidase with synthesized compounds **4(a-e)** and standard drug **Acarbose**.

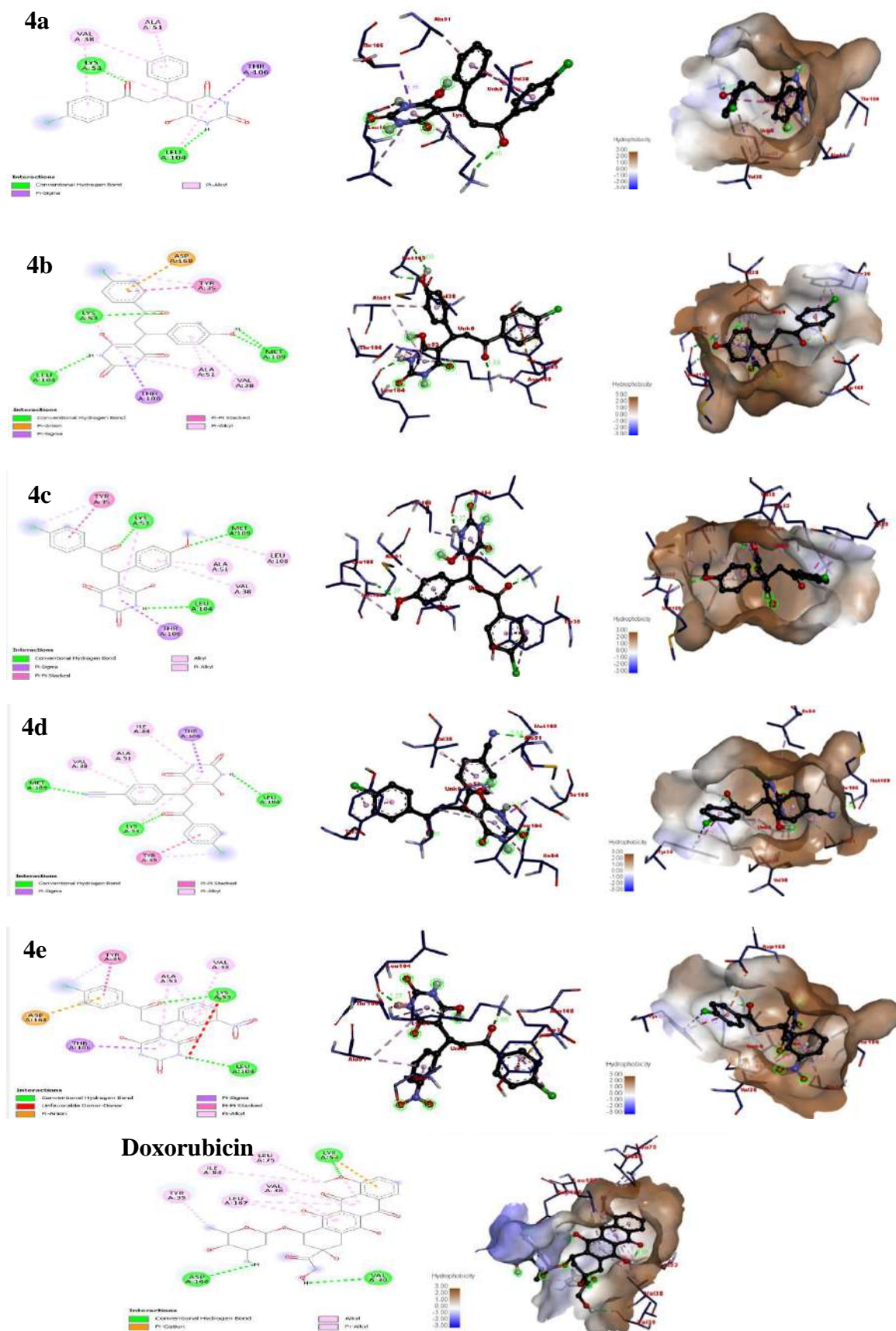


Fig. 8. 2D, 3D & hydrophobic representation of molecular interactions between P38 MAP kinase with synthesized compounds **4(a-e)** and standard drug **Doxorubicin**.

6A.6.5. *in silico* oral bioavailability assessment and ADME study

Physicochemical descriptors can be evaluated through parameters such as molecular weight, number of heavy atoms, hydrogen bond acceptors, hydrogen bond donors, rotatable bonds, molar refractivity and topological polar surface area (TPSA). These parameters were subjected to synthesized compounds **4(a-e)** and the results were tabulated in **Table 7**.

Table 7. Physicochemical properties of the synthesized compounds **4(a-e)**.

Compd.	Mol. Formula	Molecular Weight (g/mol)	No. Heavy atoms	H B A	H B D	Rotatable bonds	Fraction Csp3	Molar Refractivity	TPSA (Å ²)
4a	C ₁₉ H ₁₅ ClN ₂ O ₄	370.79	26	4	3	5	0.11	98.69	103.02
4b	C ₁₉ H ₁₅ ClN ₂ O ₅	386.79	27	5	4	5	0.11	100.71	123.25
4c	C ₂₀ H ₁₇ ClN ₂ O ₅	400.81	28	5	3	6	0.15	105.18	112.25
4d	C ₂₀ H ₁₄ ClN ₃ O ₄	395.80	28	5	3	5	0.10	103.41	126.81
4e	C ₁₉ H ₁₄ ClN ₃ O ₆	415.78	29	6	3	6	0.11	107.51	148.84

The drug-likeness profiles were calculated based on Lipinski's (MW ≤ 500; HBA ≤ 10 and HBD ≤ 5) [30], Ghose (MW between 160 & 480; log P between -0.4 & 5.6; molar refractivity between 40 & 130 and total number of atoms between 20 & 70), Veber (rotatable bonds ≤ 10 and TPSA ≤ 140), Egan (TPSA ≤ 131.6 Å²) and Muegge (MW between 200 & 600; log P between -2 & 5; TPSA ≤ 150; number of aromatic rings ≤ 7; number of rotatable bonds ≤ 15; HBA ≤ 10 and HBD ≤ 5) [31]. All the synthesized compounds obeyed Lipinski, Ghose, Veber, Egan & Muegge rule. The rule-based score defines the compounds into four probability score classes i.e. 11 %, 17 %, 55 % and 85 %. The acceptable probability score is 55% which indicates that it passed the rule of five [32, 33]. Our synthesized compounds **4(a-e)** received a score of 55 %, indicating that they followed all five rules without any violations and had good bioavailability. Further, synthetic accessibility of the compounds were assessed to quantify the complexity of the molecular structure. The results showed that the synthetic accessibility score were in the range of 3.22 to 3.37, it shows that all compounds do not have a complex synthetic route (**Table 8**).

Table 8. Drug likeness, bioactivity and synthetic accessibility score of the synthesized compounds **4(a-e)**.

Compd.	Lipinski	Ghose	Veber	Egan	Muegge	Bioactivity Score	Synthetic accessibility
4a	Yes	Yes	Yes	Yes	Yes	0.55	3.22
4b	Yes	Yes	Yes	Yes	Yes	0.55	3.23
4c	Yes	Yes	Yes	Yes	Yes	0.55	3.31
4d	Yes	Yes	Yes	Yes	Yes	0.55	3.34
4e	Yes	Yes	No	No	Yes	0.55	3.37

The predicted lipophilicity parameters were evaluated to study the solubility of the compounds either in an aqueous or in a non-aqueous media and they were calculated by considering the consensus log Po/w. According to this, if the log Po/w values are more negative, then the molecules are more soluble in nature [34]. The results showed that, all the compounds have positive log Po/w values hence they were less soluble in non-aqueous medium. Consensus log S (if log S is between -10 to -6: poorly soluble, -6 to -4: moderately soluble, -4 to -2: soluble, -2 to 0: very soluble and less than 0: highly soluble). Our synthesized compounds **4(a-e)** in the range of -3.78 to -3.99 log S value; this shows compounds were soluble in aqueous medium and result were tabulated in **Table 9**.

Table 9. Predicted lipophilicity parameters of the synthesized compounds **4(a-e)**.

Compd.	Consensus Log Po/w	Consensus Log S	Solubility Class
4a	2.94	-3.93	Soluble
4b	2.61	-3.78	Soluble
4c	3.02	-3.99	Soluble
4d	2.71	-3.86	Soluble
4e	2.18	-3.97	Soluble

The pharmacokinetic parameters like absorption, skin permeation, distribution, metabolism and excretion were predicted. Predicted absorption & distribution parameters of the compounds have shown in **Table 10** and it suggested that, all the synthesized compounds **4(a-e)** have high gastrointestinal absorption (except **4e**) with no blood-brain permeant. Hence there was no possibility of causing harmful toxicants in the brain and bloodstream. If the

molecules have more negative log Kp value, they are said to be less skin permeant [35]. Our synthesized compounds have more negative log Kp values in the range of -6.75 to -7.15 cm/s. Therefore, our synthesized compounds are less skin permeant.

Table 10. Predicted absorption & distribution parameters of the synthesized compounds **4(a-e)**.

Compd.	GI absorption	BBB permeant	Log Kp (cm/s)
4a	High	No	-6.75
4b	High	No	-7.10
4c	High	No	-6.96
4d	High	No	-7.11
4e	Low	No	-7.15

Metabolism plays an important role in the bioavailability of drugs as well as drug-drug interactions [36]. Metabolism parameters are important to understand whether the compounds act as a substrates or non-substrates of certain proteins. Hence, all the synthesized compounds were screened for metabolism parameter and results showed that, the compounds **4(a-e)** were found to be non-substrate of permeability glycoprotein (P-gp), CYP1A2, CYP2C19, CYP2D6 & CYP3A4 inhibitors. The P-gp an efflux membrane transporter, is widely distributed throughout the body and is responsible for limiting cellular uptake and the distribution of xenobiotic and toxic substances [37]. The compounds **4a**, **4b** & **4d** were found to be non-substrates of CYP2C9 inhibitor and the remaining compounds **4c** & **4e** were found to be substrates of CYP2C9 inhibitor & the results were tabulated in **Table 11**.

Table 11. Predicted metabolism parameters of the synthesized compounds **4(a-e)**.

Compd.	P-gp	CYP1A2 inhibitor	CYP2C19 inhibitor	CYP2C9 inhibitor	CYP2D6 inhibitor	CYP3A4 inhibitor
4a	No	No	No	No	No	No
4b	No	No	No	No	No	No
4c	No	No	No	Yes	No	No
4d	No	No	No	No	No	No
4e	No	No	No	Yes	No	No

6A.7. Conclusion

In this chapter, we have developed a simple and eco-friendly protocol for the synthesis of some new 5-[3-(4-chlorophenyl)-substituted-6-hydroxypyrimidine-2,4(1*H*,3*H*)-dione derivatives **4(a-e)** through concerted reaction and screened for their pharmacological and *in silico* investigations. The activity results suggested that, all compounds displayed good pharmacological activity. Among them, the compounds **4d** & **4e** exhibited least IC₅₀ values of 35.62±4.46 & 22.62±0.70 µg/mL for α-amylase and α-glucosidase activity respectively. The compound **4c** shows least IC₅₀ values of 9.90±0.18 µg/mL for anticancer activity. The *in silico* molecular interaction study suggested that, the compounds show well-established binding modes. In that, **4e** compound established least binding energy of -8.8 and -8.9 kcal/mol with docking receptors of exo-β-D-glucosaminidase and P38 MAP kinase respectively. ADME profiles indicated that, our synthesized compounds obeyed all the five rules with good bioavailability. Pharmacokinetic parameters suggested that, our compounds have high GI absorption, no blood-brain permeant and less skin permeant. Hence, there was no possibility of causing harmful toxicants.

6A.8. References

1. G. Zarren, N. Shafiq, U. Arshad, N. Rafiq, S. Parveen, Z, *J. Mol. Struct.*, **2021**, 1227, 1-40.
2. R. Jyoti, K. Sanjiv, S. Monika, M. Jyoti, K.V. Prabhakar, *Res. Chem. Intermed.*, **2016**, 42, 6777-6804.
3. D.H. Matthew and M. Mohammad, *Chem. Eur. J.*, **2008**, 14, 6836-6844.
4. T. Venkatesh, Y.D. Bodke and S.J. Aditya Rao, *Chem. Data Collect.*, **2020**, 25, 1-13.
5. S. Triloknadh, C.V. Rao, K. Nagaraju, N.H. Krishna, C.V. Ramaiah, W. Rajendra, Y. Suneetha, *Bioorg. Med. Chem. Lett.*, **2018**, 28, 1663-1669.
6. D. Kang, H. Zhang, Z. Wang, T. Zhao, T. Ginex, F.J. Luque, X. Liu, *J. Med. Chem.*, **2019**, 62, 1484-1501.
7. W. Wu, M. Chen, R. Wang, H. Tu, M. Yang, G. Ouyang, *Chem. Pap.*, **2019**, 73, 719-729.
8. S.S. Maurya, A. Bahuguna, S.I. Khan, D. Kumar, R. Kholiya, D.S. Rawat, *Eur. J. Med. Chem.*, **2019**, 162, 277-289.
9. B. Huang, D. Kang, Y. Tian, D. Daelemans, E. De Clercq, C. Pannecouque, X. Liu, *Chem. Biol. Drug Des.*, **2021**, 97, 67-76.
10. P. Modi, S. Patel, M. Chhabria, *Bioorg. Chem.*, **2019**, 87, 240-251.
11. K. Thirumurugan, S. Lakshmanan, D. Govindaraj, D.S.D. Prabu, N. Ramalakshmi, S.A. Antony, *J. Mo Struct.*, **2018**, 1171, 541-550.
12. B.N. Reddy, R.R. Ruddaraju, G. Kiran, M. Pathak, A.R.N. Reddy, *ChemistrySelect*, **2019**, 4, 10072-10078.
13. K.R. Abdellatif, R.B. Bakr, *Med. Chem. Res.*, **2021**, 30, 31-49.
14. F. Bassyouni, M. Tarek, A. Salama, B. Ibrahim, S. Salah El Dine, N. Yassin, M. Abdel-Rehim, *Molecules*, **2021**, 26, 1-20.
15. M. Massaro, G. Barone, V. Barra, P. Cancemi, A. Di Leonardo, G. Grossi, S. Riela, *Int. J. Pharm.*, **2021**, 599, 1-10.
16. J. Dhuguru, R. Skouta, *Molecules*, **2020**, 25, 1615-1640.
17. M.M. Ghorab, M.G.E. Gazzar, M.S. Alsaied, *Int. J. Mol. Sci.*, **2014**, 15, 5582-5595.
18. B. Sakram, B. Sonyanaik, K. Ashok, S. Rambabu, S.K. Johnmiya, *Res. Chem. Intermed.* **2016**, 42, 1699-1705.
19. D.K. Jangid and S. Dhadda, *IntechOpen*, **2019**, 1-17.
20. Y. Liu and J.W. Sun, *J. Org. Chem.*, **2012**, 77, 1191-1197.

21. Q.F. Wang, H. Hou, L. Hui, C.G. Yan, *J. Org. Chem.*, **2009**, 74, 7403-7406.
22. J.W. Xie, L. Yue, W. Chen, W. Du, J. Zhu, J.G. Deng, Y.C. Chen, *Org. Lett.*, **2007**, 9, 413-415.
23. N. Irshad, A.U. Khan & M.S. Iqbal, *Biomed. Pharmacother.*, **2021**, 139, 1-15.
24. S.H. Sukanya, T. Venkatesh, S.J. Aditya Rao, M.N. Joy, *J. Mol. Struct.*, **2021**, 1247, 1-13.
25. A.O. Ademiluyi, G. Oboh, *Exp. Toxicol. Pathol.*, **2013**, 65, 305-309.
26. S.H. Sukanya, T. Venkatesh, S.J. Aditya Rao, A. Pandith, *J. Mol. Struct.*, **2022**, 1267, 1-28.
27. M. Faisal, A. Saeed, D. Shahzad, T.A. Fattah, B. Lal, P.A. Channar, F.A. Larik, *Eur. J. Med. Chem.*, **2017**, 141, 386-403.
28. R.S. Cheke, V.M. Patil, S.D. Firke, J.P. Ambhore, I.A. Ansari, H.M. Patel, M. Snoussi, *Pharmaceuticals*, **2022**, 15, 1-34.
29. A.A. Haredi, M.M. Eldeeb, M. El-Naggar, H. Temairk, M.A. Mohamed, *Front. Mol. Biosci.*, **2020**, 7, 1-19.
30. C.A. Lipinski, *Drug Discov. Today Technol.*, 2004, 1, 337-341.
31. I. Muegge, *Med. Res. Rev.*, **2003**, 23, 302-321.
32. R.B. Breemen van and Y. Li, *Expert. Opin. Drug Metab. Toxicol.*, **2005**, 1, 175-185.
33. S. Alam and F. Khan, *Sci. Reports*, **2018**, 8, 1-16.
34. Y. Rohitash, I. Mohammed, D. Puneet, K.C. Dheeraj, H. Shailendra, *J. Biomol. Struct. Dyn.*, **2021**, 39, 6617-6632.
35. S. Mishra, R. Dahima, *J. drug Deliv. Ther.*, **2019**, 9, 366-369.
36. G.K. Swamy, G. Ramesh, K. Pruthviraj, S. Banu, B. Roopa, H.J. Preritha, B.S. Rajeshwari, M. Ravikumar, P. Raghuram Shetty, D.B. Aruna Kumar, S. Sreenivasa, *Chem. Data Collect.*, **2020**, 28, 1-23.
37. Md. Lutful Amin, *Drug Target Insights*, **2013**, 7, 27-34.

6B.1. Introduction

German chemist, Adolf von Baeyer [1] was first discovered the barbituric acid (**1**) in 1864 [2]. It was synthesized through a condensation of urea with malonic acid/diethyl malonate. The derivatives of barbituric acid, commonly known as barbiturates, have a special importance in pharmaceutical field because of their wide variety of biological activities such as hypnotic [3], sedative [4], anticonvulsant [5], antimicrobial [6], anaesthetic [7], anticancer and antitumor properties [8, 9]. Barbital (**2**) was the first barbiturate and it is used as a sedative, hypnotic, sleeping aid and anxiolytic [10]. Phenobarbital (**3**) is another medication recommended by the World Health Organization for the treatment of certain types of seizure disorders [11]. Merbarone (**4**) was a derivative of barbituric acid and represented a unique class of antineoplastic agents against leukaemia and murine tumours [12]. Bucolome (**5**) used as an analgesic, anti-inflammatory and CYP2CP inhibitors. Secobarbital (**6**) is used for the treatment of insomnia and also possesses anaesthetic, anticonvulsant, anxiolytic, sedative and hypnotic properties [13] (**Fig. 1**). Moreover, barbituric acid and its derivatives have been used as dye-sensitized solar cells [14]. Barbituric acid has the capability to make keto-enol form, due to its unique potential to be used as a valuable building block in various organic reactions.

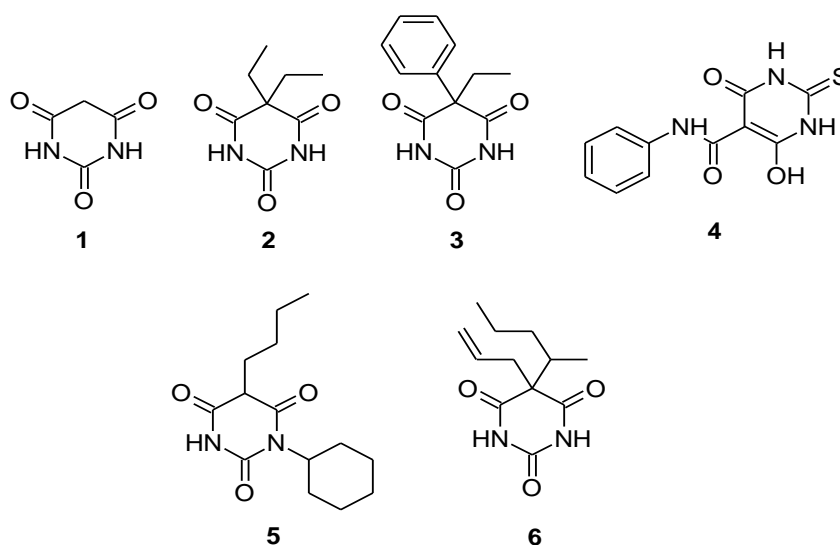
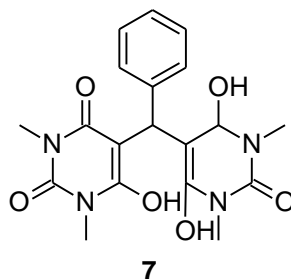
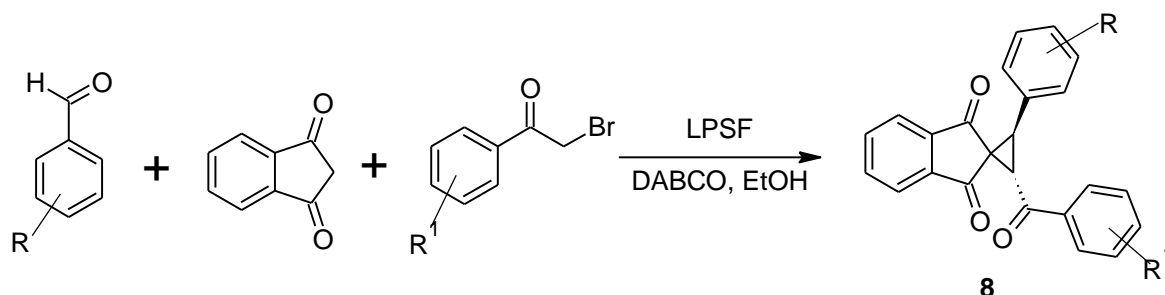


Fig. 1. Biologically active barbituric acid derivatives.

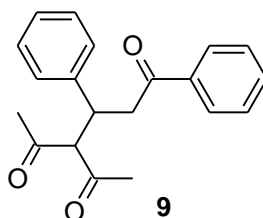
F. Nemati *et. al.*, reported a 5,5-dimethyl-2-((4,4-dimethyl-2,6-dioxocyclohexyl)(phenyl) methyl) cyclohexane-1,3-dione (**7**) using $\text{Fe}_3\text{O}_4@\text{SiO}_2\text{-SO}_3\text{H}$ nano-catalyst [15].



A series of *trans*-2,3-dihydro-spiro[2-aryl-3-aryl-cyclopropane]1,2-indene-1,3-dione derivatives (**8**) has been reported by R. Firouzi- Haji and Maleki using DABCO as a co-catalyst and $\text{Fe}_3\text{O}_4@\text{SiO}_2\text{-propyltriethoxysilane-L-proline}$ (LPSF) as a nanomagnetic organocatalyst [16].

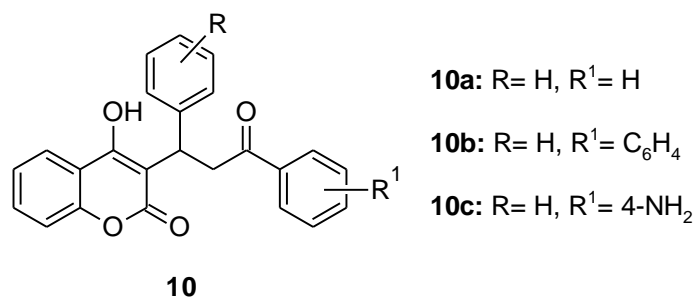


In 2006, P. Kotrusz and S. Toma reported a L-Proline catalysed Michael addition of different active methylene compounds to α -enones in ionic liquid media ($[\text{bmim}]\text{PF}_6$) to offer a 4-acetyl-1,3-diphenylhexane-1,5-dione derivatives (**9**) [17].

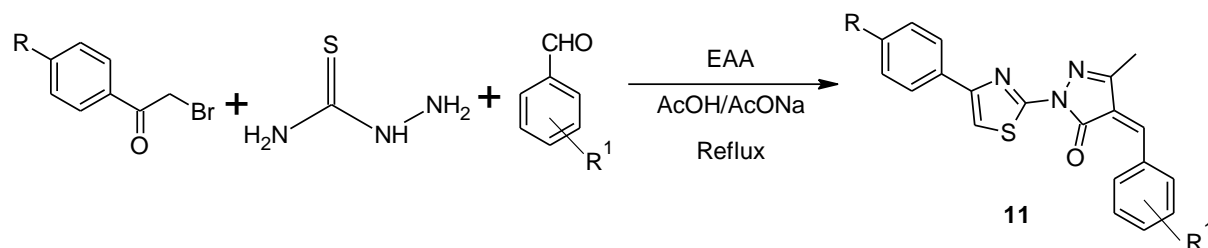


In 2022, a series of 4-hydroxy-3-(3-oxo-1,3-diphenylpropyl)-2*H*-chromen-2-one (**10**) derivatives has been synthesized by Z. Afzal *et. al.*, and reported as anticoagulant and antimicrobial activity. Among the series, compound **10a** showed excellent anticoagulant

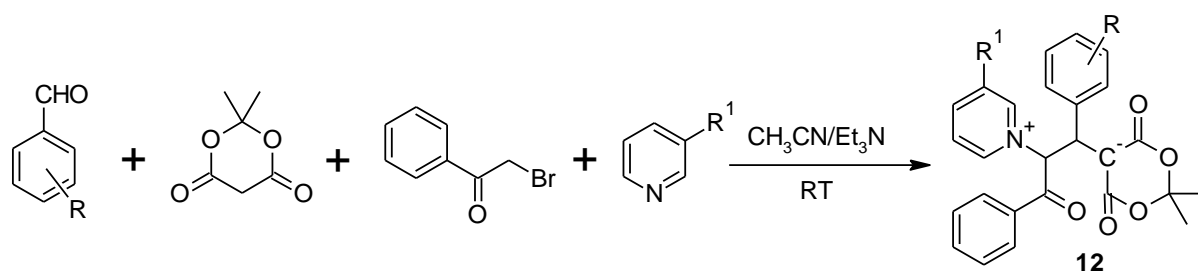
activity with IC_{50} value of 249.88 μ M, **10b** showed 68 % inhibition against *S. aureus* and compound **10c** showed 70 % inhibition against *C. albicans* [18].



C.S. Venkata *et. al.*, reported a novel 4-arylidene-3-methyl-1-(4-arylthiazol-2-yl)-1H-pyrazol-5(4H)-ones (**11**) by Knoevenagel reaction of ethylacetoacetate and aryl aldehydes, then Michel addition of phenacyl bromide [19].



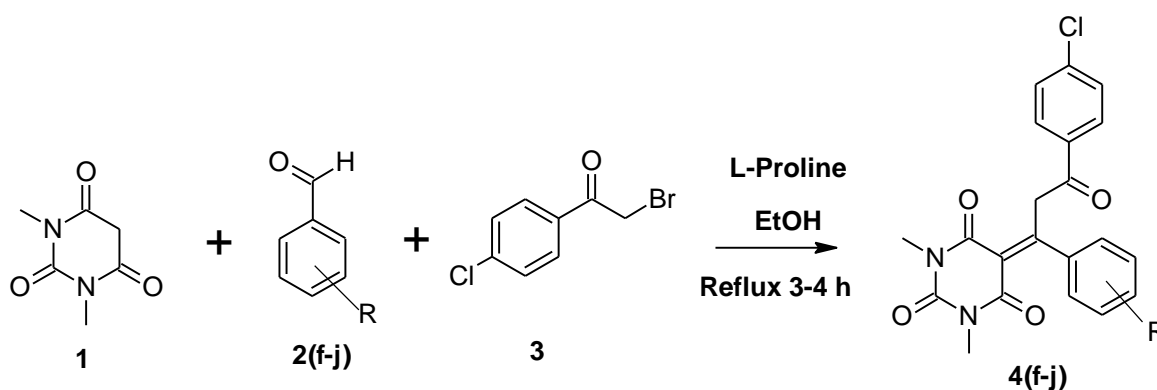
Q.F. Wang and co-authors reported a zwitterionic salt of pyridinium-meldrum acid derivatives (**12**) by the reaction of aromatic aldehyde, meldrum acid, phenacyl bromide and in the presence of an excess of substituted pyridine [20].



Based on the above investigation, we have synthesized a some new 5-[3-(4-chlorophenyl)-substituted-1,3-dimethylpyrimidine-2,4,6(1H,3H,5H)-trione derivatives and screened for different biological activities, *in silico* molecular docking and ADME studies.

6B.2. Present work

In this chapter, we explained synthesis of 5-[3-(4-chlorophenyl)-substituted-1,3-dimethylpyrimidine-2,4,6(1*H*,3*H*,5*H*)-trione derivatives **4(f-j)** via Knoevenagel condensation reaction of 1,3-dimethylbarbituric acid (**1**), substituted aromatic aldehydes (**2**) and 2-bromo-4-chloroacetophenone (**3**) in aqueous ethanol using L-Proline as a catalyst and synthetic route has been given in **Scheme 8**.



Compd.	R
4f	H
4g	4-OH
4h	4-OCH ₃
4i	4-CN
4j	3-NO ₂

Scheme 8. Synthesis of 5-[3-(4-chlorophenyl)-substituted-1,3-dimethylpyrimidine-2,4,6(1*H*,3*H*,5*H*)-trione derivatives **4(f-j)**.

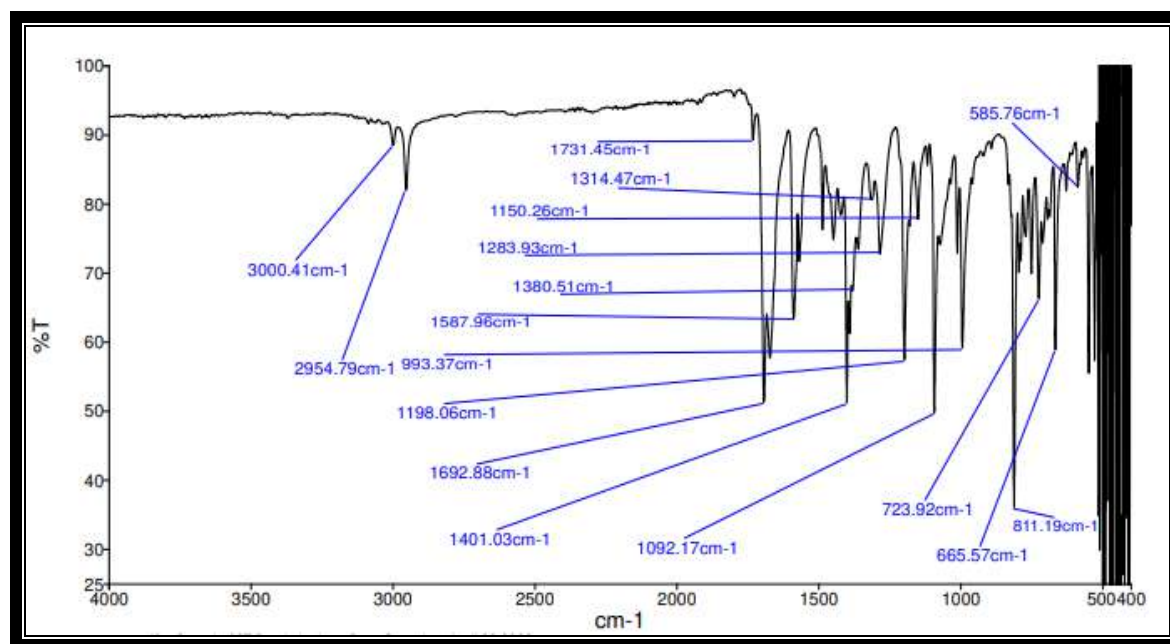
The structures of 5-[3-(4-chlorophenyl)-substituted-1,3-dimethylpyrimidine-2,4,6(1*H*,3*H*,5*H*)-trione derivatives **4(f-j)** were confirmed by recording their IR, ¹H NMR, ¹³C NMR and Mass spectral data.

In IR spectrum of compound **4f** showed the absorption band in the region of 3000 cm⁻¹ is attributed to aromatic CH group, 1692 cm⁻¹ correspond to C=O functionality and another stretching vibrational band at 811 cm⁻¹ correspond to C-Cl functionality. The ¹H NMR spectrum of compound **4f** exhibited a singlet peak at δ 8.34 ppm correspond to aromatic

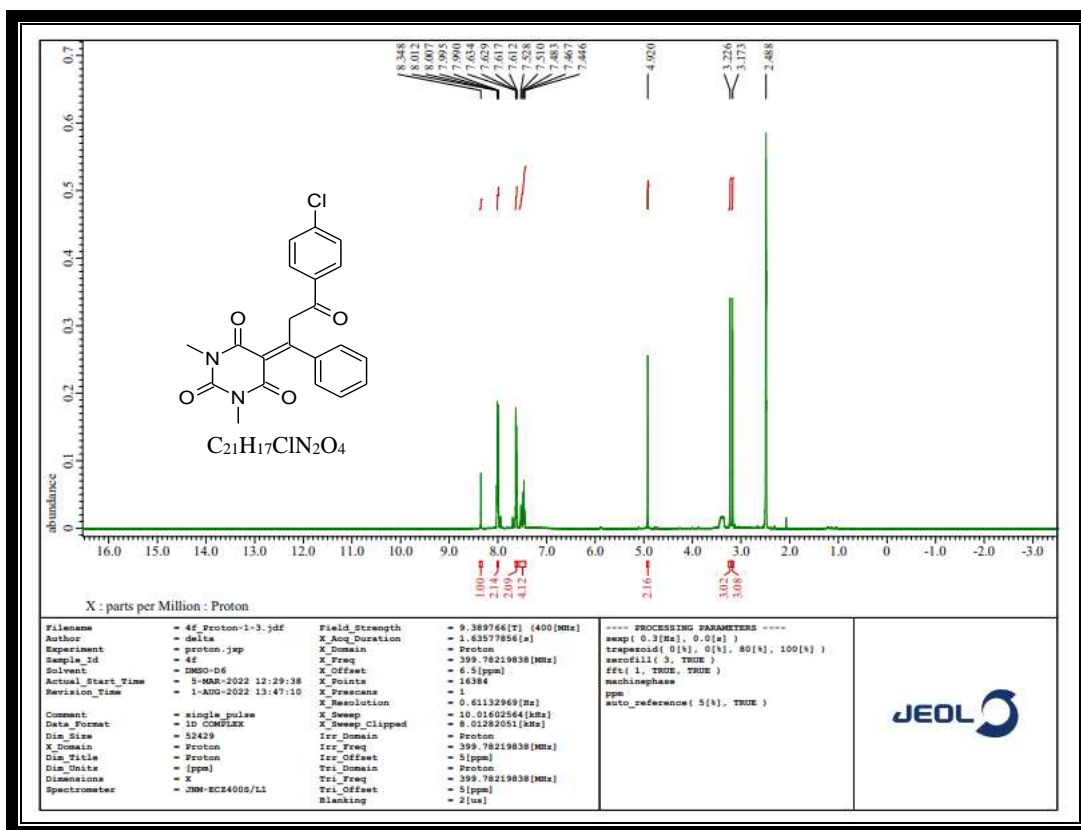
proton (s, 1H, Ar-H). Two doublet of doublet peaks at δ 7.99-8.01 & 7.61-7.63 ppm which corresponds to four aromatic protons (dd, $J=8$ Hz, 4H, Ar-H) and multiplet peaks at δ 7.44-7.54 ppm corresponds to aromatic protons (m, 4H, Ar-H). A singlet peak at δ 4.92 ppm due to CH_2 protons (s, 2H, CH_2) and two singlets at δ 3.22 & 3.17 corresponds to two CH_3 protons (s, 6H, 2 CH_3). In addition, ^{13}C NMR spectrum of compound **4f** exhibited peaks at δ 159.76 and 159.68 ppm which correspond to carbonyl carbons.

The mass spectrum showed molecular ion peak m/z at 397.1353 [M^++1] & 399.1322 [M^++3], which corresponds to the molecular weight of the compound **4f**.

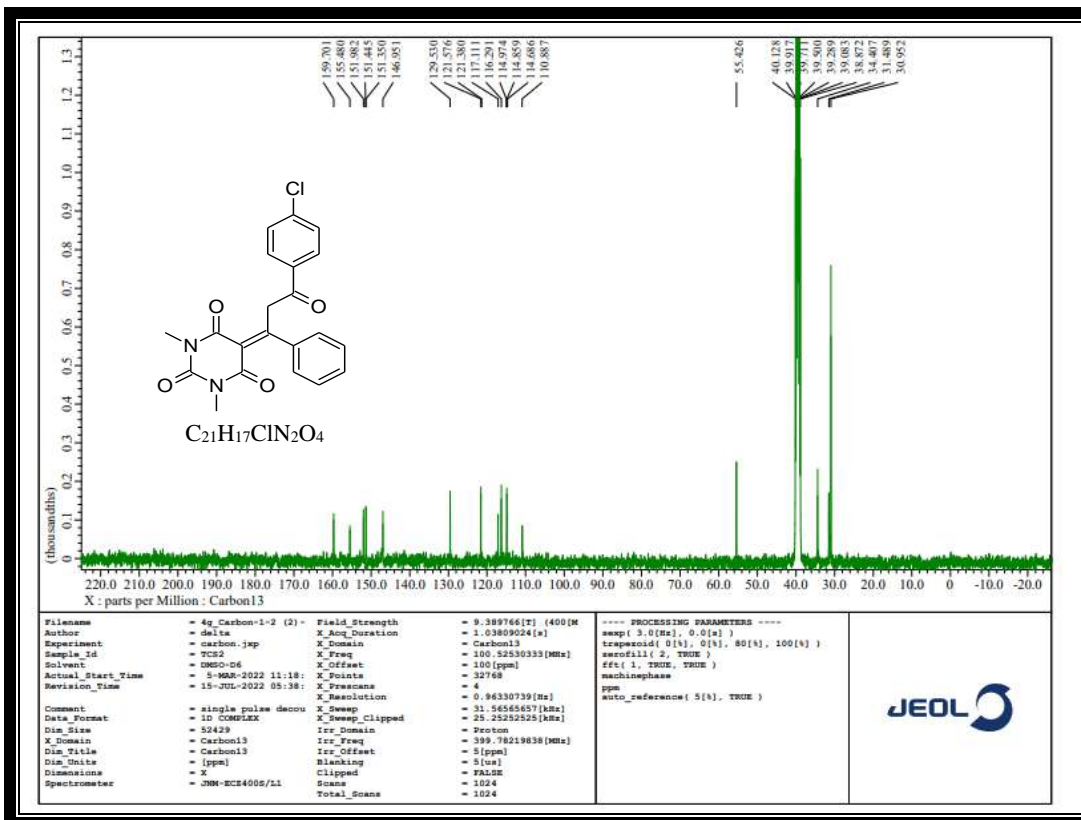
Characterization:



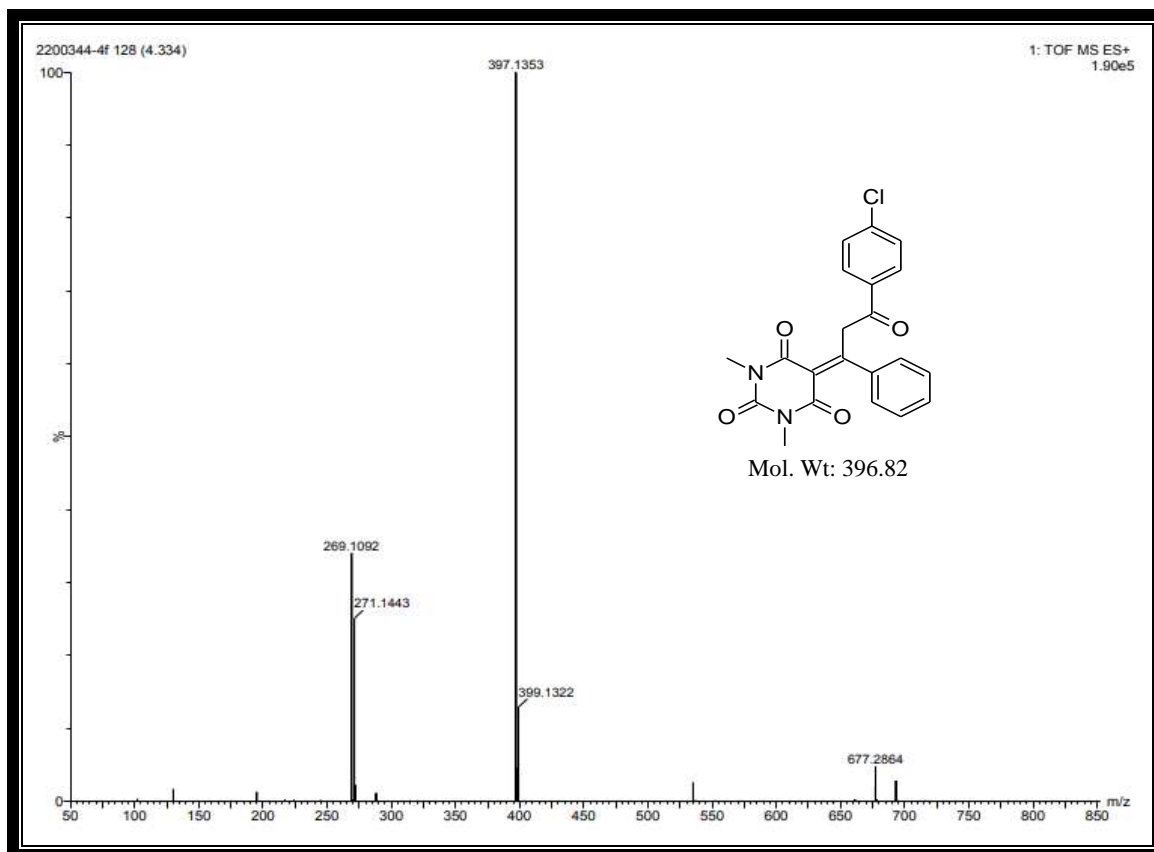
IR spectrum of compound **4f**



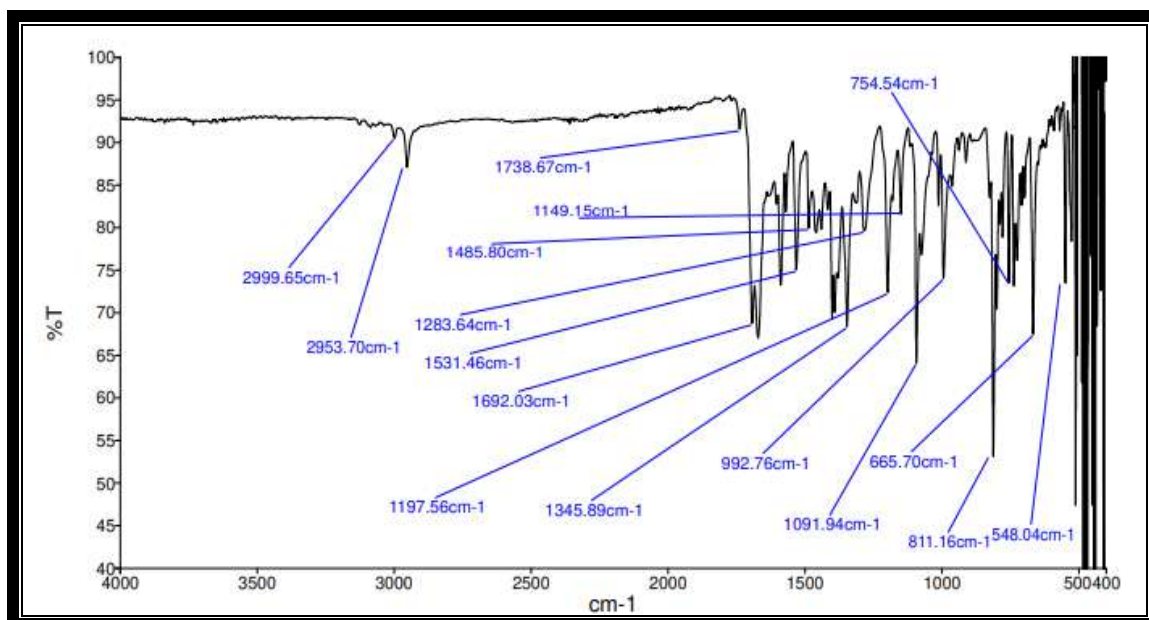
¹H NMR spectrum of compound 4f



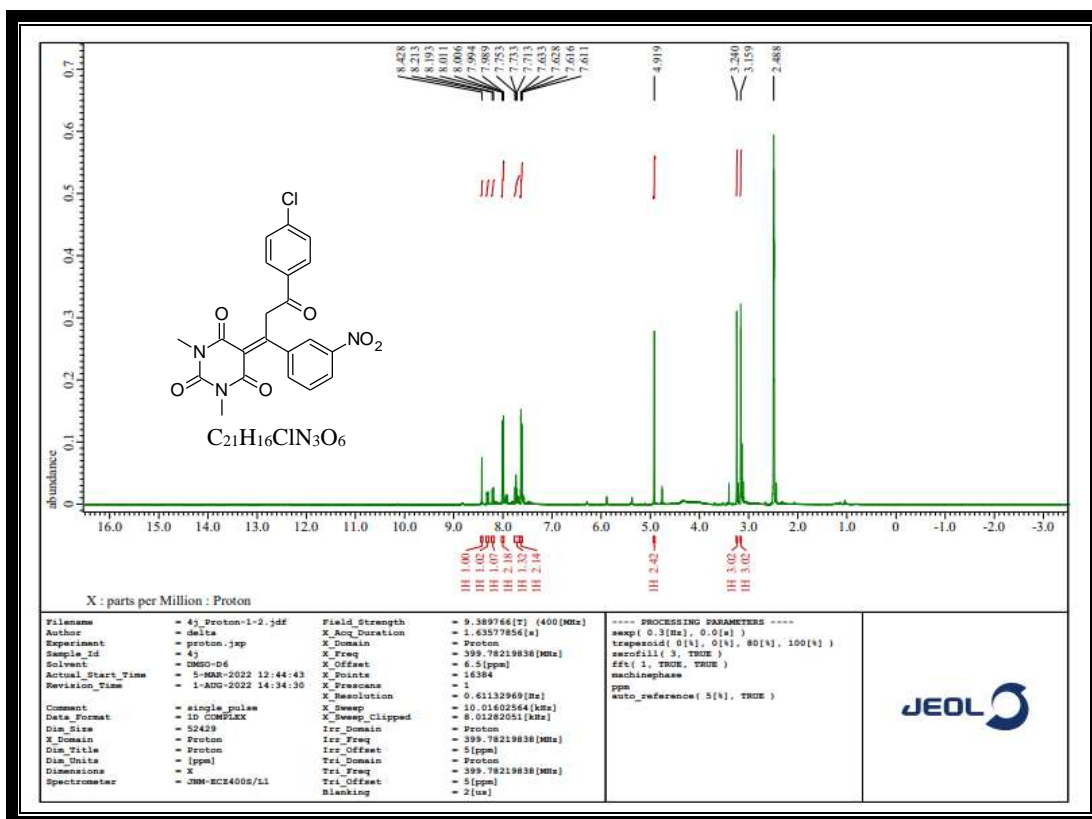
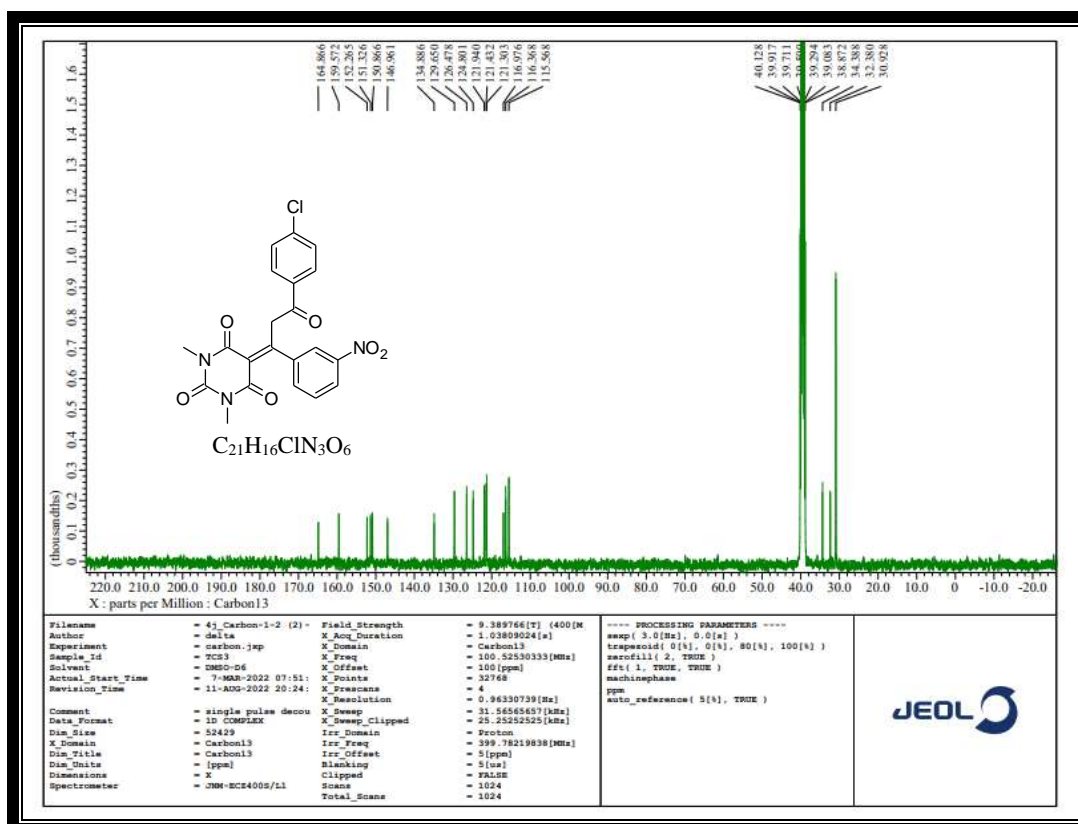
¹³C NMR spectrum of compound 4f

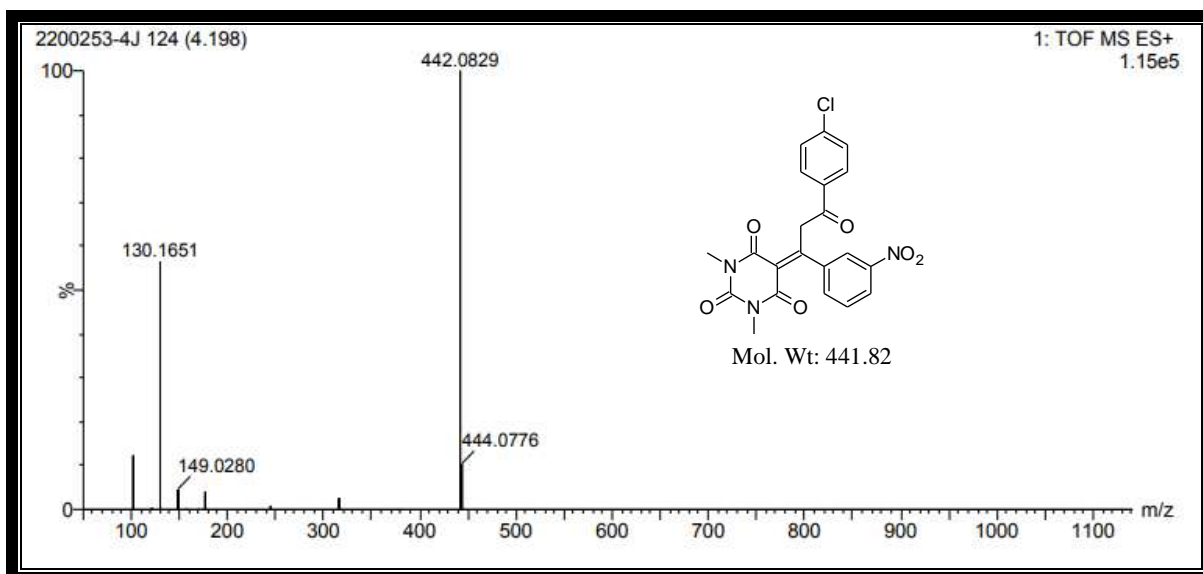


MASS spectrum of compound 4f



IR spectrum of compound 4j

 ^1H NMR spectrum of compound 4j ^{13}C NMR spectrum of compound 4j



MASS spectrum of compound 4j

6B.3. Experimental

6B.3.1. General information:

The general information regarding the different solvents, reagents and instruments etc., used for the analysis has been previously discussed in the experimental section 2A.3.1 & 5.3.1 of **Chapter-2A** & **Chapter-5**.

6B.3.2. Procedure for synthesis of some novel 5-[3-(4-chlorophenyl)-substituted-1,3-dimethylpyrimidine-2,4,6(1*H*,3*H*,5*H*)-trione derivatives 4(f-j):

An equimolar quantity of 1,3-dimethylbarbituric acid (**1**, 1 mmol), aromatic aldehydes (**2**, 1 mmol) and 10 mol% of L-Proline as catalyst in aqueous ethanol was stirred under refluxed condition. After 10 min, 2-bromo-4-chloroacetophenone (**3**, 1 mmol) was added to it and refluxed at 80-82 °C with constant stirring for about 5-6 h and followed by according to the previous procedure of **Chapter-6A** (section 6A.3.2) afford pure solid products **4(f-j)**.

5-[3-(4-Chlorophenyl)-3-oxo-1-phenylpropylidene]-1,3-dimethylpyrimidine-2,4,6(1*H*,3*H*,5*H*)-trione (**4f**):

White solid; Yield: 89 %; MP: 168-170 °C; Mol. Formula: C₂₁H₁₇ClN₂O₄; UV (nm) λ_{max} (log ε) 229 (4.55) & 322 (3.80); FTIR (ν cm⁻¹): 3000 (CH), 2954 (N-CH₃), 1692 (C=O)

& 811 (C-Cl); ^1H NMR (δ ppm): 8.34 (s, 1H, Ar-H), 8.01-7.99 (dd, J = 8 Hz, 2H, Ar-H), 7.63-7.61 (dd, J = 8 Hz, 2H, Ar-H), 7.54-7.44 (m, 4H, Ar-H), 4.92 (s, 2H, CH_2), 3.22 (s, 3H, CH_3), 3.17 (s, 3H, CH_3); ^{13}C NMR (δ ppm): 159.76, 159.68, 159.58, 151.90, 151.34, 148.46, 146.94, 129.65, 129.52, 129.39, 121.58, 117.10, 116.50, 117.10, 116.28, 114.97, 110.54, 34.38, 31.18 & 30.93. HRMS: m/z 397.1353 [M^++1] & 399.1322 [M^++3]; Anal. Calcd: C 63.56, H 4.32, N 7.06 %, Found: C 63.52, H 4.28, N 7.03 %.

5-[3-(4-Chlorophenyl)-1-(4-hydroxyphenyl)-3-oxopropylidene]-1,3-dimethylpyrimidine-2,4,6(1H,3H,5H)-trione (4g):

Yellow solid; Yield: 90 %; MP: 218-220 °C; Mol. Formula: $\text{C}_{21}\text{H}_{17}\text{ClN}_2\text{O}_5$; UV (nm) λ_{max} (log ϵ) 325 (3.43) & 325 (3.87); FTIR (ν cm^{-1}): 3398 (OH), 2988 (CH), 2854 (N- CH_3), 1689 (C=O) & 812 (C-Cl); ^1H NMR (δ ppm): 10.78 (s, 1H, OH), 8.29-8.27 (dd, J = 8 Hz, 2H, Ar-H), 7.99-7.97 (dd, J = 8 Hz, 2H, Ar-H), 7.62-7.60 (dd, J = 8 Hz, 2H, Ar-H), 6.87-6.85 (dd, J = 8 Hz, 2H, Ar-H), 4.90 (s, 2H, CH_2), 3.20 (s, 3H, CH_3), 3.18 (s, 3H, CH_3); ^{13}C NMR (δ ppm): 159.70, 155.48, 151.98, 151.44, 151.35, 151.07, 146.95, 129.53, 121.57, 121.38, 117.11, 116.29, 114.97, 114.85, 114.68, 110.88, 55.42, 34.40, 31.48 & 30.95; HRMS: m/z 412.1825 [M^+] & 414.1794 [M^++2]; Anal. Calcd: C 61.10, H 4.15, N 6.79 %, Found: C 61.05, H 4.10, N 6.74 %.

5-[3-(4-Chlorophenyl)-1-(4-methoxyphenyl)-3-oxopropylidene]-1,3-dimethylpyrimidine-2,4,6(1H,3H,5H)-trione (4h):

Yellow solid; Yield: 91 %; MP: 160-162 °C; Mol. Formula: $\text{C}_{22}\text{H}_{19}\text{ClN}_2\text{O}_5$; UV (nm) λ_{max} (log ϵ) 259 (4.29) & 313 (4.28); FTIR (ν cm^{-1}): 2973 (CH), 2897 (N- CH_3), 2854 (OCH_3), 1632 (C=O) & 785 (C-Cl); ^1H NMR (δ ppm): 8.04-8.02 (d, J = 8 Hz, 2H, Ar-H), 7.98-7.96 (dd, J = 8 Hz, 2H, Ar-H), 7.50-7.48 (d, J = 8 Hz, 2H, Ar-H), 6.89-6.87 (dd, J = 8 Hz, 2H, Ar-H), 4.98 (s, 2H, CH_2), 3.89 (s, 3H, OCH_3), 3.18 (s, 3H, CH_3), 3.15 (s, 3H, CH_3); ^{13}C NMR (δ ppm): 162.86, 162.23, 161.89, 158.94, 157.37, 147.56, 146.05, 132.82, 128.34, 126.23,

125.98, 124.66, 114.89, 112.89, 112.20, 89.24, 58.22, 36.89, 35.33, 34.96 & 34.42; HRMS: m/z 426.1278 [M^+] & 428.1268 [$M^+ + 2$]; Anal. Calcd: C 61.90, H 4.49, N 6.56 %, Found: C 61.86, H 4.44, N 6.52 %.

4-[3-(4-Chlorophenyl)-1-(1,3-dimethyl-2,4,6-trioxotetrahydropyrimidin-5(2H)-ylidene)-3-oxopropyl]benzotrile (4i):

White solid; Yield: 94 %; MP: 174-176 °C; Mol. Formula: $C_{22}H_{16}ClN_3O_4$; UV (nm) λ_{max} (log ϵ) 259 (4.44) & 315 (4.13); FTIR (ν cm^{-1}): 2986 (CH), 2850 (N-CH₃), 1662 (C=O) & 788 (C-Cl); ¹H NMR (δ ppm): 8.22-8.20 (dd, J = 8 Hz, 2H, Ar-H), 7.88-7.86 (dd, J = 8 Hz, 2H, Ar-H), 7.60-7.58 (dd, J = 8 Hz, 2H, Ar-H), 6.84-6.82 (dd, J = 8 Hz, 2H, Ar-H), 4.98 (s, 2H, CH₂), 3.18 (s, 3H, CH₃), 3.14 (s, 3H, CH₃); ¹³C NMR (δ ppm): 162.62, 162.11, 159.66, 157.46, 156.39, 146.56, 142.05, 132.82, 127.22, 126.05, 124.47, 123.93, 117.69, 115.99, 113.53, 88.40, 49.04, 37.24, 36.71, 34.92 & 34.12; HRMS: m/z 421.2230 [M^+] & 423.1220 [$M^+ + 2$]; Anal. Calcd: C 62.64, H 3.82, N 9.96 %, Found: C 62.60, H 3.78, N 9.91 %.

5-[3-(4-Chlorophenyl)-1-(3-nitrophenyl)-3-oxopropylidene]-1,3-dimethylpyrimidine-2,4,6(1H,3H,5H)-trione (4j):

White solid; Yield: 84 %; MP: 136-138 °C; Mol. Formula: $C_{21}H_{16}ClN_3O_6$; UV (nm) λ_{max} (log ϵ) 258 (4.52) & 371 (4.23); FTIR (ν cm^{-1}): 2999 (CH), 2953 (N-CH₃), 1692 (C=O) & 811 (C-Cl); ¹H NMR (400 MHz, DMSO- d_6 , δ ppm): 8.42 (s, 1H, Ar-H), 8.32-8.30 (d, J = 8 Hz, 1H, Ar-H), 8.21-8.19 (d, J = 8 Hz, 1H, Ar-H), 8.01-7.99 (dd, J = 8 Hz, 2H, Ar-H), 7.75-7.67 (m, 1H, Ar-H), 7.63-7.61 (dd, J = 8 Hz, 2H, Ar-H), 4.91 (s, 2H, CH₂), 3.24 (s, 3H, CH₃), 3.15 (s, 3H, CH₃); ¹³C NMR (100 MHz, DMSO- d_6 , δ ppm): 164.86, 159.57, 152.26, 151.32, 150.86, 146.96, 134.88, 129.65, 126.47, 124.80, 121.94, 121.43, 121.30, 116.97, 116.36, 115.56, 34.38, 32.38 & 30.92; HRMS: m/z 442.0829 [$M^+ + 1$] & 444.0776 [$M^+ + 3$]; Anal. Calcd: C 57.09, H 3.65, N 9.51 %, Found: C 57.04, H 3.62, N 9.47 %.

6B.4. Absorption property

The UV-Vis spectra of the compounds **4(f-j)** were recorded in two different solvents (DMSO & DMF) at 10^{-5} M concentration using UV-Vis Spectrophotometer. The λ_{\max} and molar absorption coefficient values were appended in **Table 1**. All the synthesized compounds exhibited absorption maxima (λ_{\max}) in the range of 229-325 nm in DMSO and 313-371 nm in DMF solvents due to the $\pi-\pi^*$ & $n-\pi^*$ transitions (**Fig. 2**). The compound **4g** shows a higher absorption maximum at 325 nm in DMSO and **4j** shows higher absorption maxima at 371 nm in DMF solvent.

Table 1. Electronic absorption data of the synthesized compounds **4(f-j)** in DMSO & DMF solvents.

Compd.	DMSO		DMF	
	$\lambda_{\max}(\text{nm})$	Log ϵ	$\lambda_{\max}(\text{nm})$	Log ϵ
4f	229	4.55	322	3.80
4g	325	3.43	325	3.87
4h	259	4.29	313	4.28
4i	259	4.44	315	4.13
4j	258	4.52	371	4.23

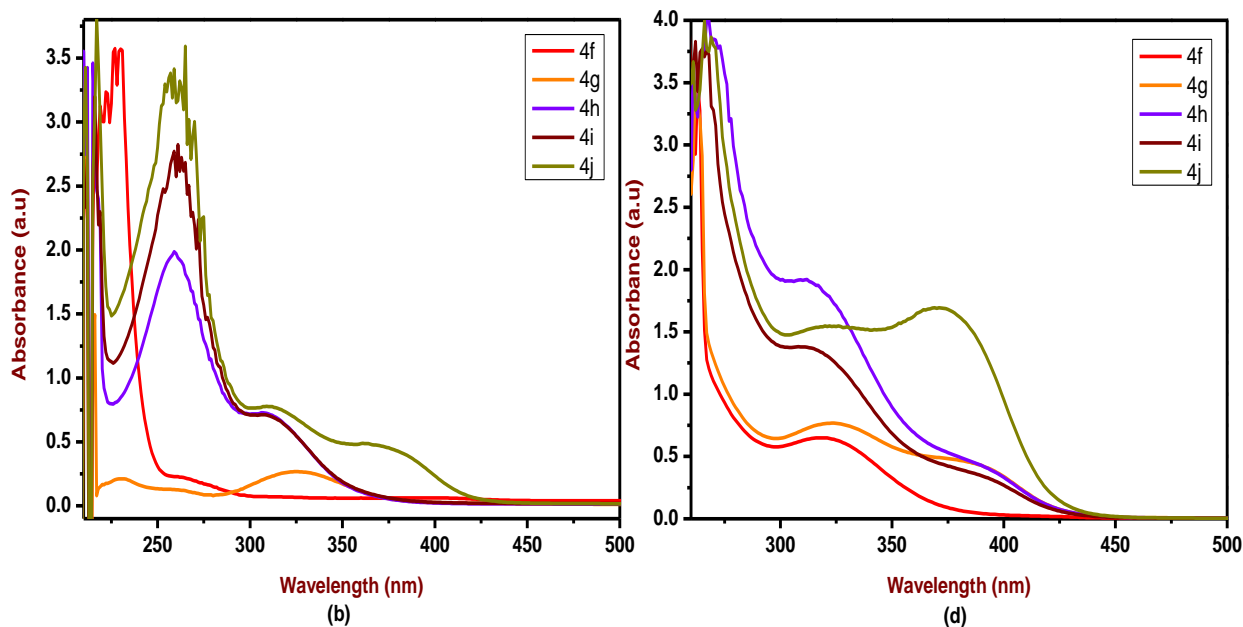


Fig. 2. A graph of UV-Visible spectra of the synthesized compounds **4(f-j)** in DMSO (a) and DMF (b) solvents.

6B.5. Pharmacological studies

In-vitro α -amylase & α -glucosidase inhibitory assay, *in-vitro* cytotoxicity, *in silico* molecular docking and ADME study has been previously explained in the experimental section (6.2.5) of **Chapter-6A** [21-24].

6B.6. Results and discussion

6B.6.1. *In vitro* α -amylase and α -glucosidase inhibitory activity

All the synthesized compounds **4(f-j)** were screened for *in vitro* α -amylase & α -glucosidase inhibitory activity using different concentrations (25, 50, 75 & 100 $\mu\text{g/mL}$) and calculated IC_{50} values of enzyme activity and acarbose was used as a standard for comparison. The α -amylase enzyme activity results revealed that, the obtained compounds possessed significant efficacy ranging from 42.35 ± 0.63 to 51.25 ± 0.63 , 54.30 ± 0.84 to 59.60 ± 0.84 , 64.10 ± 0.70 to 72.65 ± 1.20 & 71.00 ± 1.13 to 81.10 ± 0.84 % with respect to their concentration 25, 50, 75 & 100 $\mu\text{g/mL}$. The potencies of IC_{50} values vary from 24.53 ± 0.27 to 41.25 ± 1.52 $\mu\text{g/mL}$. All the compounds exhibited outstanding % inhibition with IC_{50} values as compare to standard drug acarbose (51.28 ± 0.67 $\mu\text{g/mL}$) (**Fig. 3**). Among all the compounds, **4j** exhibited least IC_{50} value of 24.53 ± 0.27 $\mu\text{g/mL}$ and results have been shown in **Table 2**.

The α -glucosidase inhibitory activity results expelled that, all the compounds show excellent % inhibition ranging from 54.15 ± 0.63 to 56.35 ± 0.63 , 60.65 ± 0.91 to 66.35 ± 0.49 , 74.25 ± 0.77 to 81.80 ± 0.56 & 82.10 ± 0.56 to 90.60 ± 0.84 % with respect to their concentration of 25, 50, 75 & 100 $\mu\text{g/mL}$. The potencies of IC_{50} values vary from 22.18 ± 0.16 to 23.38 ± 0.09 $\mu\text{g/mL}$. All compounds exhibited almost similar IC_{50} values, in that the compound **4j** showed the least IC_{50} value of 22.18 ± 0.16 $\mu\text{g/mL}$ as compared to standard drug acarbose (37.69 ± 0.53 $\mu\text{g/mL}$) (**Fig. 4**) and results have been shown in **Table 3**.

Table 2. α -amylase enzyme activity results (%) at different concentrations and IC₅₀ values of the synthesized compounds **4(f-j)**.

Compd.	Concentration in $\mu\text{g/mL}$				IC ₅₀ in $\mu\text{g/mL}$
	25	50	75	100	
4f	44.45 \pm 0.63	54.45 \pm 0.91	64.10 \pm 0.70	71.00 \pm 1.13	39.18 \pm 1.65
4g	42.35 \pm 0.63	54.30 \pm 0.84	68.50 \pm 0.84	76.50 \pm 0.84	41.25 \pm 1.52
4h	44.60 \pm 0.84	56.35 \pm 0.77	68.85 \pm 1.20	76.55 \pm 0.77	36.79 \pm 1.71
4i	48.15 \pm 0.91	56.25 \pm 0.77	70.95 \pm 1.34	80.70 \pm 0.98	31.65 \pm 2.27
4j	51.25 \pm 0.63	59.60 \pm 0.84	72.65 \pm 1.20	81.10 \pm 0.84	24.53 \pm 0.27
Acarbose	26.00 \pm 0.70	49.30 \pm 0.84	68.65 \pm 0.77	78.90 \pm 0.84	51.28 \pm 0.67

Values are Mean \pm SE, N=3, *P<0.01 vs. Control

Table 3. α -glucosidase enzyme activity results (%) at different concentrations and IC₅₀ values of the synthesized compounds **4(f-j)**.

Compd.	Concentration in $\mu\text{g/mL}$				IC ₅₀ in $\mu\text{g/mL}$
	25	50	75	100	
4f	56.60 \pm 0.84	60.65 \pm 0.91	74.25 \pm 0.77	82.10 \pm 0.56	22.56 \pm 0.15
4g	54.15 \pm 0.63	64.10 \pm 0.56	74.50 \pm 0.56	82.40 \pm 0.56	23.38 \pm 0.09
4h	56.05 \pm 0.49	66.00 \pm 0.56	75.75 \pm 0.63	83.80 \pm 0.56	22.23 \pm 0.76
4i	56.35 \pm 0.63	66.35 \pm 0.49	80.30 \pm 0.56	90.60 \pm 0.84	22.56 \pm 0.62
4j	56.00 \pm 0.56	65.90 \pm 0.42	81.80 \pm 0.56	90.45 \pm 0.63	22.18 \pm 0.16
Acarbose	39.20 \pm 0.56	60.30 \pm 0.56	74.05 \pm 0.63	86.20 \pm 0.42	37.69 \pm 0.53

Values are Mean \pm SE, N=3, *P<0.01 vs. Control

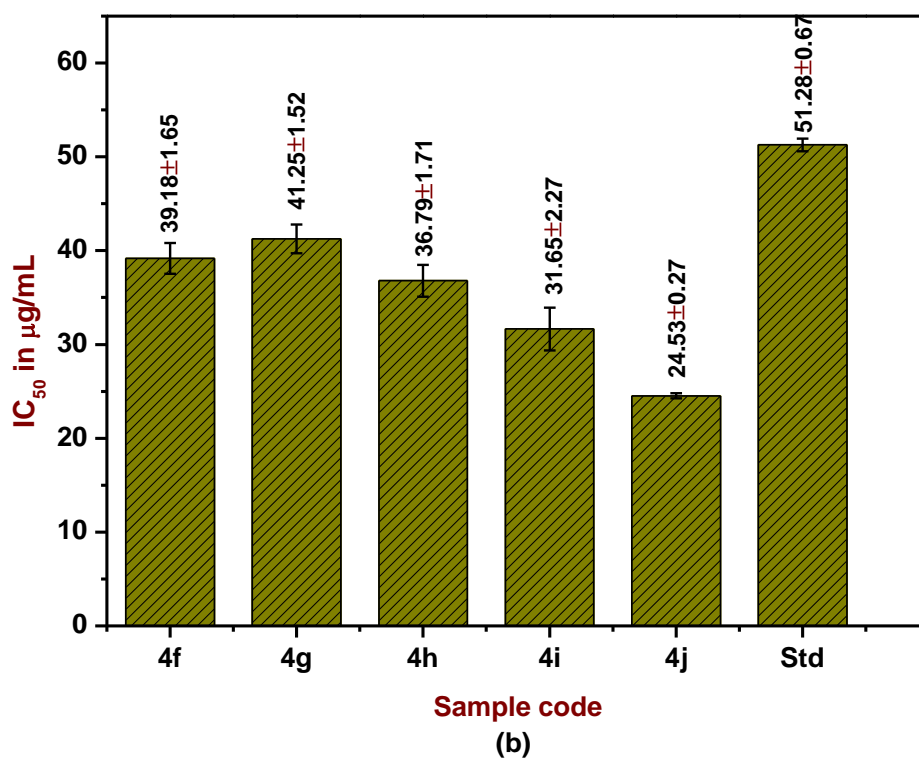
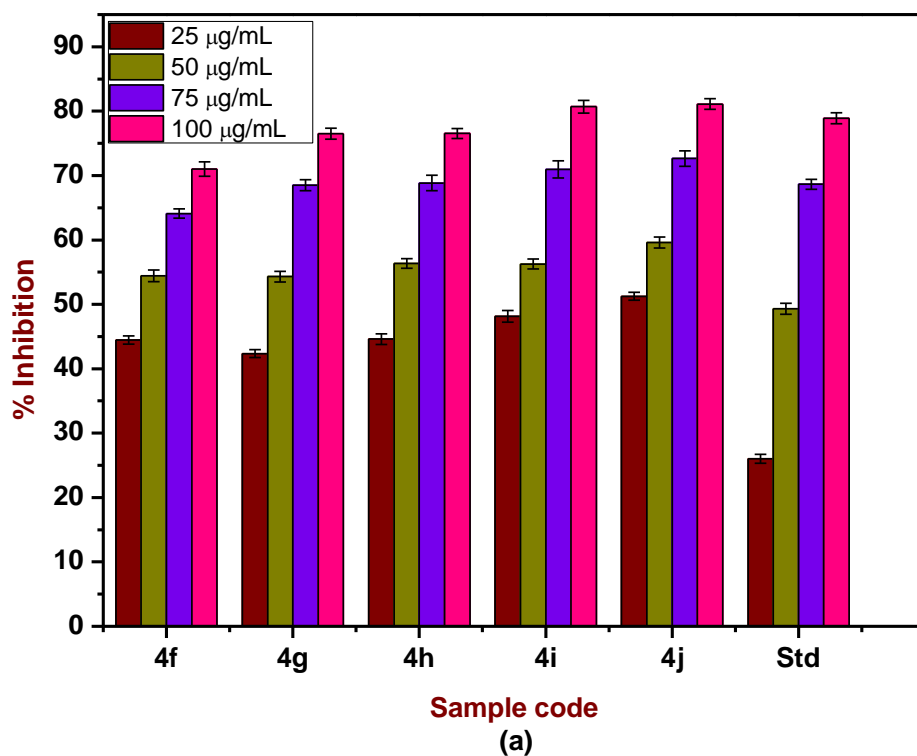


Fig. 3. *In vitro* α -amylase inhibitory activity of the synthesized compounds (**4a-j**); A graph of % inhibition of synthesized compounds at different concentration (**a**); A graph of IC₅₀ value of compounds **4(f-j)** (**b**)

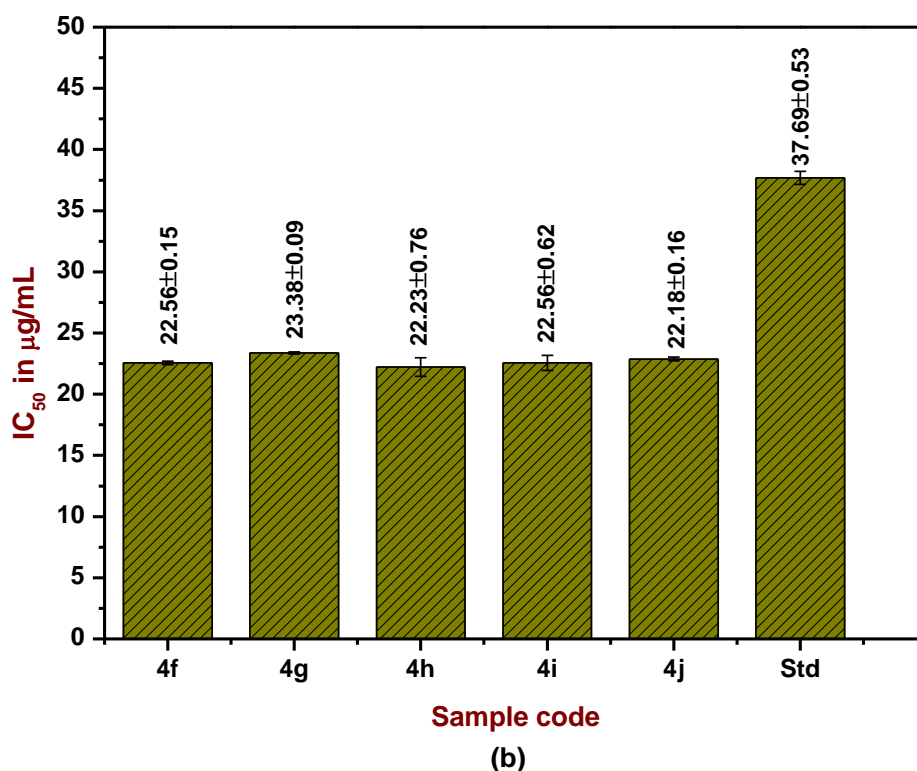
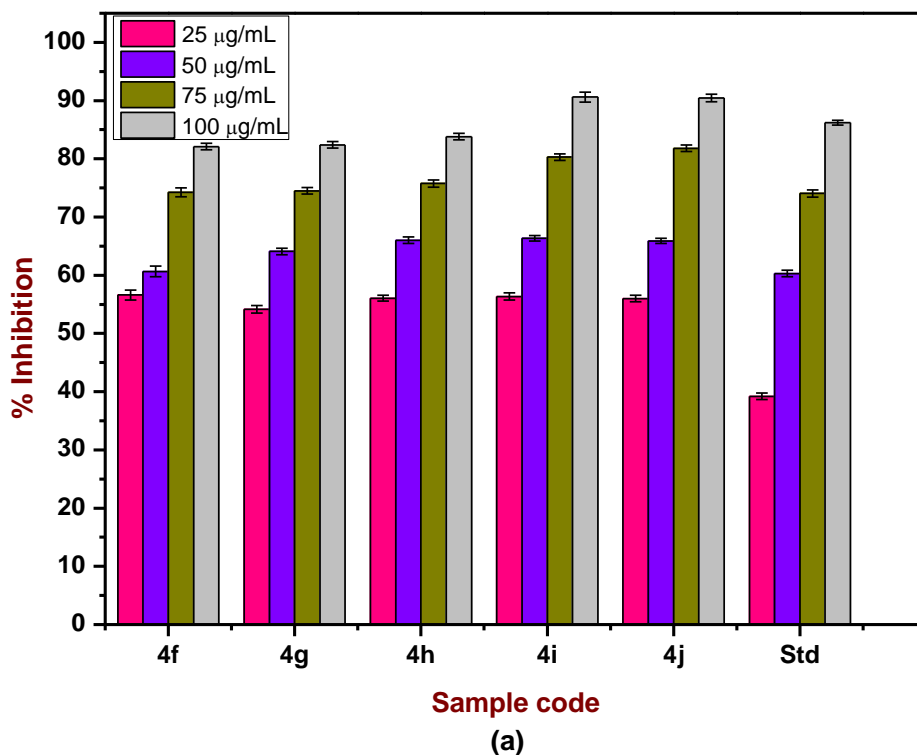


Fig. 4. *In vitro* α -glucosidase inhibitory activity of the synthesized compounds (**4a-j**); A graph of % inhibition of synthesized compounds at different concentration (**a**); A graph of IC₅₀ value of compounds (**b**)

6B.6.2. *In vitro* cytotoxicity

In vitro cytotoxicity of the synthesized compounds **4(f-j)** was evaluated against MCF-7 cell line. A graph describing the concentration versus cell viability and IC₅₀ value of the compounds was plotted (**Fig. 5**). Doxorubicin was used as a reference standard for comparison. The activity results revealed that, synthesized compounds exhibited good selectivity against the MCF-7 cell line with IC₅₀ values ranging from 6.68±0.06 to 20.97±0.31 µg/mL. Among them, compound **4j** shows a significant cytotoxic effect with least IC₅₀ value of 6.68±0.06 µg/mL and rest of the compounds displayed a moderate cytotoxic effects with IC₅₀ values in the range of 7.31±0.21 to 20.97±0.31 µg/mL as compared to reference standard doxorubicin (3.16±0.10 µg/mL) and the obtained results were listed in **Table 4**.

Table 4. Percentage of cell viability against MCF-7 cell line of the synthesized compounds **4(f-j)**.

Compd.	Mean cell Viability of MCF-7 Concentration in µg/mL							IC ₅₀ in µg/mL
	NC	3.125	6.25	12.5	25	50	100	
4f	100	63.76±0.47	46.89±0.77	44.94±1.38	27.88±0.64	12.37±0.67	11.48±0.27	7.31±0.21
4g		81.29±0.89	63.76±0.17	32.32±1.45	15.27±0.35	10.54±0.73	9.41±1.08	8.10±0.18
4h		91.53±0.36	85.02±0.57	78.98±1.07	41.80±0.91	11.66±0.62	9.88±0.40	20.97±0.31
4i		99.11±0.46	79.69±0.44	41.74±0.63	16.81±0.26	12.73±0.40	11.78±0.20	12.10±0.12
4j		67.44±1.51	46.77±0.83	38.07±0.44	22.26±0.56	13.02±0.57	11.30±0.67	6.68±0.06
Std		33.80±0.93	30.57±1.14	28.93±0.42	27.53±0.37	26.16±0.16	23.69±0.53	3.16±0.10

Std-Doxorubicin, **NC**- Negative control

Values are Mean ±SE, N=3, *P<0.01 vs. Control

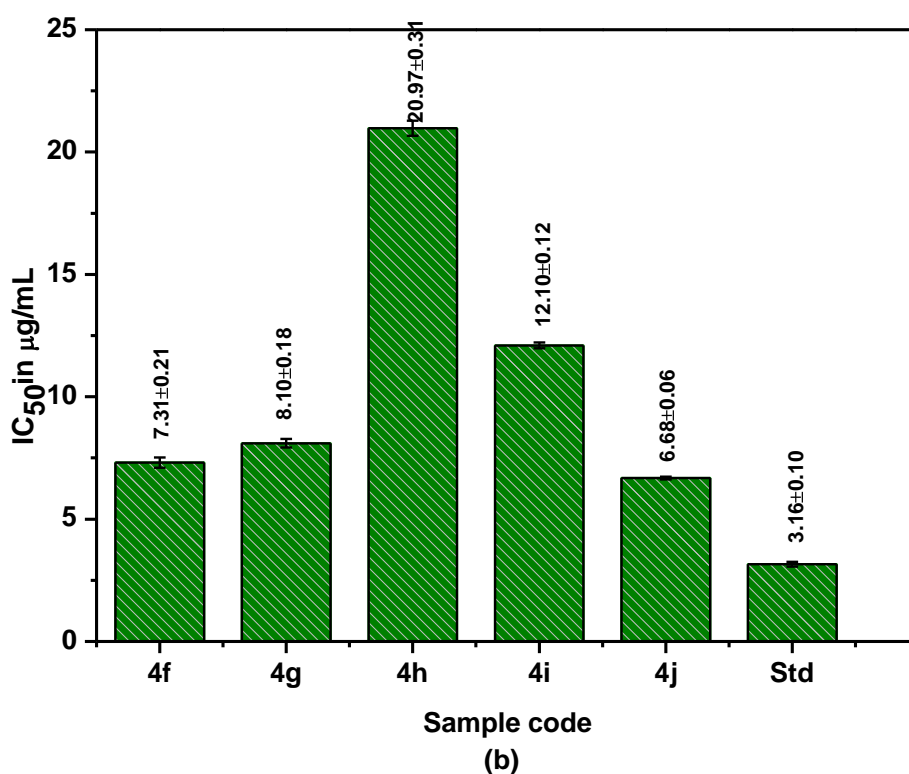
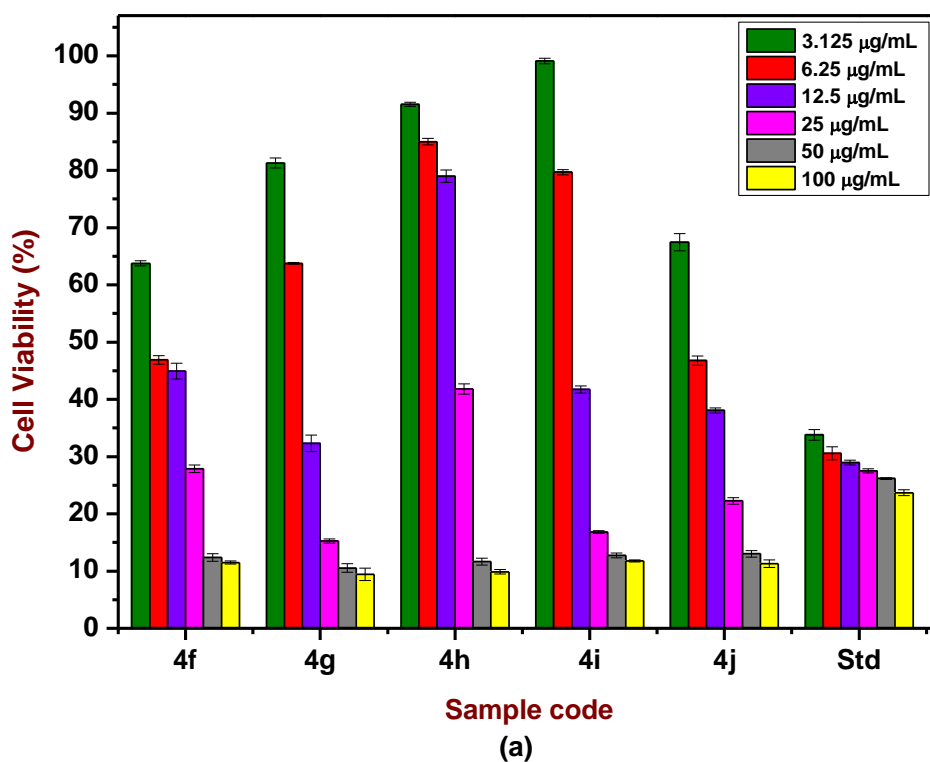


Fig. 5. A graph of % of surviving cells of synthesized compounds **4(f-j)** at different concentration against MCF-7 cell line (a); A graph of IC₅₀ value of compounds **4(f-j)** against MCF-7 cell line (b).

6B.6.3. SAR study

SAR study has been carried out for the newly synthesized compounds **4(f-j)**. All compounds exhibited excellent α -amylase, α -glucosidase and cytotoxicity with significant IC_{50} values. Among all the synthesized compounds, **4j** shows outstanding α -amylase, α -glucosidase inhibition and cytotoxicity with a remarkable IC_{50} value. The compound **4j** has an electron withdrawing nitro and chloro groups in their ring structures; it may be the possible reason for the admirable anti-diabetic and cytotoxic activity [25]. The *in silico* molecular interaction study also supported these findings.

6B.6.4. *in silico* molecular docking study

The study of intermolecular interactions between synthesized compounds **4(f-j)** and enzyme is a necessary for the development of novel therapeutic drugs [26]. Therefore, we have screened the synthesized compounds for *in silico* molecular docking studies; it helps to predict the binding modes of the compounds with enzymes. From the results of docking study, synthesized compounds established good binding modes with docking receptors of α -D-glucosaminidase (**Fig. 6**) and P38 MAP kinase (**Fig. 7**) in the active pockets, respectively.

The docking of anti-diabetic and cytotoxicity investigations revealed that, the synthesized compounds **4(f-j)** had significant docking scores in the range of -8.6 to -9.6 kcal/mol and -8.2 to -9.2 kcal/mol with respect to standards Acarbose (-7.8 kcal/mol) and Doxorubicin (-8.4 kcal/mol) respectively. The docked structures with α -D-glucosaminidase results suggested that, the compound **4j** established the least binding energy of -9.6 kcal/mol forming two hydrogen bonds with amino acid residues TRP204 & TRP642 and remaining compounds also established good binding modes with amino acid residues TRP204, TRP642 & ARG500 (**Table 5**). The docked structures with P38 MAP kinase protein results revealed that, the compounds **4g** & **4j** demonstrated the least binding energy of

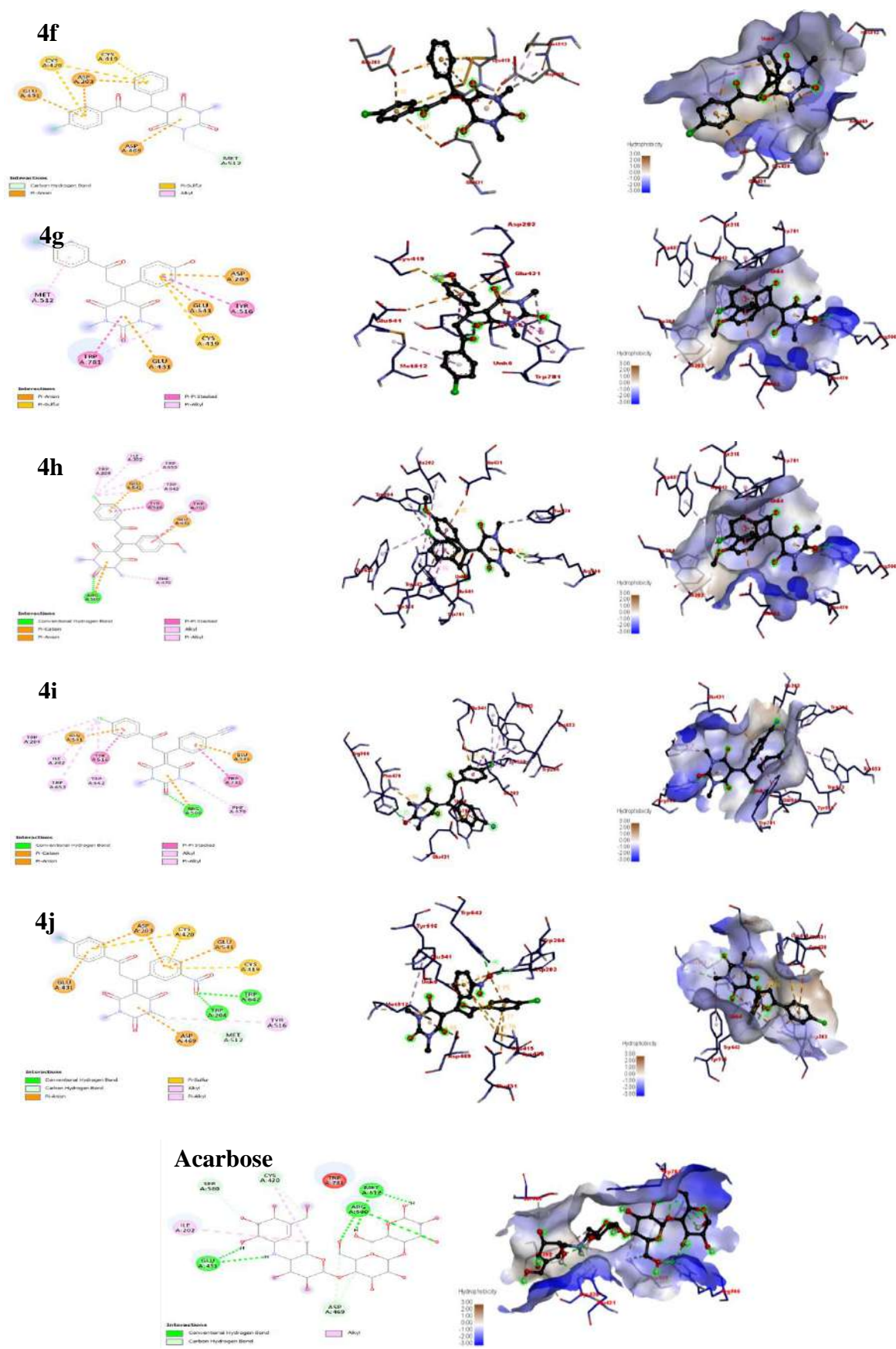
-9.2 kcal/mol forming three & two hydrogen bonds with amino acid residues LYS53, MET109 & LEU104 and the results were tabulated in **Table 6**.

Table 5. Molecular interactions synthesized compounds **4(f-j)** & standard **acarbose** with α -D-glucosaminidase protein.

Compd.	Binding affinity (kcal/mol)	Hydrogen bond interaction	Hydrogen bond length in Å	Hydrophobic and other interactions
4f	-8.9	--	--	MET512, ASP203, ASP203, GLU431, ASP469, CYS419, CYS420, CYS420, MET512
4g	-8.7	--	--	ASP203, GLU431, GLU541, CYS419, TRP781, TYR516, TRP781, MET512, TRP781
4h	-8.6	ARG500	2.36	ARG500, GLU431, GLU541, TYR516, TRP781, ILE202, TRP204, PHE470, TRP642, TRP642, TRP653
4i	-9.0	ARG500	2.35	ARG500, GLU431, GLU541, TRP781, TYR516, ILE202, TRP204, PHE470, TRP642, TRP642, TRP653
4j	-9.6	TRP204, TRP642	1.85, 2.45	MET512, ASP203, ASP203, GLU431, ASP469, GLU541, CYS419, CYS420, CYS420, MET512, TYR516
Acarbose	-7.8	GLU431, GLU431, MET512, MET512, ARG500, ARG500, ARG500	2.45, 2.65, 2.54, 2.89, 2.23, 2.85, 2.64	ASP469, CYS420, MET512, SER580, ILE202, TRP781

Table 6. Molecular interactions of synthesized compounds **4(f-j)** & standard **Doxorubicin** with P38 MAP kinase protein.

Compd.	Binding affinity (kcal/mol)	Hydrogen bond interaction	Hydrogen bond length in Å	Hydrophobic and other interactions
4f	-8.8	LYS53	2.23	ASP168, TYR35, TYR35, LEU171, LEU75, ILE84, PHE169, LEU75, ILE84, LEU167, VAL38, ALA51
4g	-9.2	LYS53, MET109, MET109	2.16, 2.00, 2.85	ASP168, TYR35, TYR35, LEU171, LEU75, ILE84, PHE169, LEU75, ILE84, LEU167, VAL38, ALA51
4h	-8.2	-	-	ASP168, THR106, LEU75, LEU86, LEU104, TYR35, VAL38, ALA157, ALA51, LYS53
4i	-8.6	--	--	ASP168, THR106, TYR35, TYR35, VAL38, ALA51, LYS53, VAL38
4j	-9.2	LYS53, MET109	2.21, 1.88	SER154, ASP168, ASP168, TYR35, TYR35, LEU171, LEU75, ILE84, PHE169, LEU75, ILE84, LEU167, VAL38, ALA51
Doxorubicin	-8.4	ASP168, VAL30, LYS53	2.38, 2.80, 2.95	LYS53, LEU75, ILE84, VAL38, LEU167, VAL38, LYS53, LEU167, LYS53, TYR35



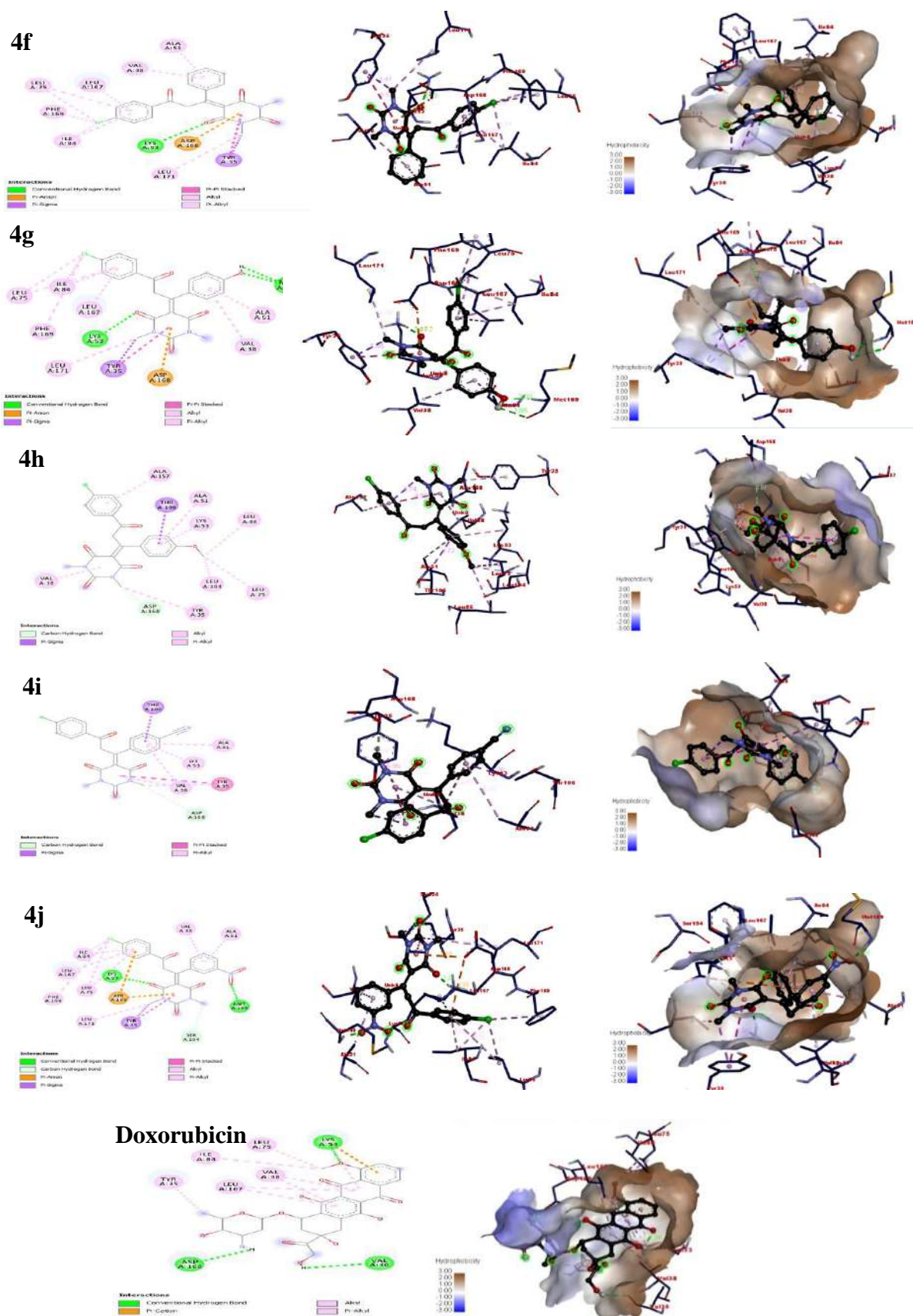


Fig. 7. 2D, 3D & hydrophobic representation of molecular interactions between P38 MAP kinase with synthesized compounds **4(f-j)** and standard drug **Doxorubicin**.

6B.6.5. *in silico* oral bioavailability assessment and ADME study

Molecular weight, number of heavy atoms, hydrogen bond acceptors, hydrogen bond donors, rotatable bonds, molar refractivity and topological polar surface area parameters are used for the evaluation of physicochemical properties of compounds and results are appended in **Table 7**.

Table 7. Physicochemical properties of the synthesized compounds **4(f-j)**.

Compd.	Mol. Formula	Mol. Weight (g/mol)	No. Heavy atoms	H B A	H B D	Rotatable bonds	Fraction Csp3	Molar Refractivity	TPSA (Å ²)
4f	C ₂₁ H ₁₇ Cl N ₂ O ₄	396.82	28	4	0	4	0.14	112.60	74.76
4g	C ₂₁ H ₁₇ Cl N ₂ O ₅	412.82	29	5	1	4	0.14	114.62	94.99
4h	C ₂₂ H ₁₉ Cl N ₂ O ₅	426.85	30	5	0	5	0.18	119.09	83.99
4i	C ₂₂ H ₁₆ Cl N ₃ O ₄	421.83	30	5	0	4	0.14	117.31	98.55
4j	C ₂₁ H ₁₆ Cl N ₃ O ₆	441.82	31	6	0	5	0.14	121.42	120.58

The drug-likeness profiles were calculated based on Lipinski's [27], Ghose, Veber, Egan and Muegge rules [28]. All the synthesized compounds obeyed all the five rules. The acceptable probability score is 55% which indicates that it passed the rule of five [29, 30]. Our synthesized compounds **4(f-j)** showed a score of 55 % indicating compounds obeyed all five rules without any violations with good bioavailability. Further, synthetic accessibility of the compounds were assessed to quantify the complexity of the molecular structure. The results showed that the synthetic accessibility score was in the range of 2.98 to 3.23, which shows that all compounds do not have complex synthetic routes (**Table 8**).

Table 8. Drug likeness, bioactivity and synthetic accessibility score of the synthesized compounds **4(f-j)**.

Compd.	Lipinski	Ghose	Veber	Egan	Muegge	Bioactivity Score	Synthetic accessibility
4f	Yes	Yes	Yes	Yes	Yes	0.55	3.02
4g	Yes	Yes	Yes	Yes	Yes	0.55	2.98
4h	Yes	Yes	Yes	Yes	Yes	0.55	3.06
4i	Yes	Yes	Yes	Yes	Yes	0.55	3.16
4j	Yes	Yes	Yes	Yes	Yes	0.55	3.23

Solubility of the compounds was predicted based on lipophilicity parameters, it is used to study the solubility of the compounds either in an aqueous or in a non-aqueous media and they were calculated by considering the consensus log Po/w. According to this, if the log Po/w values are more negative, then the molecules are more soluble in nature [31]. The results showed that, all the compounds had positive log Po/w values hence they were less soluble in non-aqueous medium. Consensus log S (if log S is between -10 to -6: poorly soluble, -6 to -4: moderately soluble, -4 to -2: soluble, -2 to 0: very soluble and less than 0: highly soluble). Our synthesized compounds **4(f-j)** in the range of -4.42 to -4.63 log S value; this shows compounds were moderately soluble in aqueous medium (**Table 9**).

Table 9. Predicted lipophilicity parameters of the synthesized compounds **4(f-j)**.

Compd.	Consensus Log Po/w	Consensus Log S	Solubility Class
4f	2.95	-4.55	Moderately soluble
4g	2.48	-4.42	Moderately soluble
4h	2.97	-4.63	Moderately soluble
4i	2.68	-4.51	Moderately soluble
4j	2.21	-4.63	Moderately soluble

Absorption, skin permeation, distribution, metabolism and excretion were predicted and have been shown in **Table 10**. The synthesized compounds have high GI absorption with no blood-brain permeant. Hence, there was no possibility of causing harmful toxicants in the brain and blood stream. If the molecules have more negative log Kp value, they are said to be

less skin permeant [32]. Our synthesized compounds have more negative log Kp values in the range of -6.24 to -6.64 cm/s. Therefore, our synthesized compounds are less skin permeant.

Table 10. Predicted absorption & distribution parameters of the compounds **4(f-j)**.

Compd.	GI absorption	BBB permeant	Log Kp (cm/s)
4f	High	Yes	-6.24
4g	High	No	-6.59
4h	High	No	-6.45
4i	High	No	-6.59
4j	High	No	-6.64

Metabolism parameters are important to understanding whether the compounds act as substrates or non-substrates of certain proteins. Hence, all the synthesized compounds were evaluated for metabolism parameter and results showed that, the compounds **4(f-j)** were found to be non-substrate of permeability glycoprotein (P-gp), CYP1A2 & CYP2D6 inhibitors and they were found to be a substrate of CYP2C19, CYP2C9 & CYP3A4 inhibitors and the results were tabulated in **Table 11**.

Table 11. Predicted metabolism parameters of the synthesized compounds **4(f-j)**.

Compd.	P-gp	CYP1A2 inhibitor	CYP2C19 inhibitor	CYP2C9 inhibitor	CYP2D6 inhibitor	CYP3A4 inhibitor
4f	No	No	Yes	Yes	No	Yes
4g	No	No	Yes	Yes	No	Yes
4h	No	No	Yes	Yes	No	Yes
4i	No	No	Yes	Yes	No	Yes
4j	No	No	Yes	Yes	No	Yes

6B.7. Conclusion

In this report, we have developed a simple and eco-friendly protocol for the synthesis of some new 5-[3-(4-chlorophenyl)-substituted-1,3-dimethylpyrimidine-2,4,6(1*H*,3*H*,5*H*)-trione derivatives **4(f-j)** through one-pot reaction and evaluated for their pharmacological and *in silico* investigations. The activity results suggested that, the compound **4j** exhibited the lowest IC₅₀ values of 24.53±0.27, 22.18±0.16 & 6.68±0.06 µg/mL for α-amylase, α-glucosidase & cytotoxic activity. The SAR study suggested that, the compound **4j** having electron withdrawing nitro and chloro groups in their ring structure increases the potency of the bioactivity of the compound and *in silico* molecular interaction study also supported these findings. The docking study suggested that, the compounds shows well-established binding modes with docking receptors of exo-β-D-glucosaminidase and P38 MAP kinase. ADME profiles explained that, our synthesized compounds obeyed all five rules with good bioavailability. Pharmacokinetic parameters suggested that, our compounds have high GI absorption, no blood-brain permeant and less skin permeant. Hence, there was no possibility of causing harmful toxicants.

6B.8. References

1. Adolf von Baeyer, *Annalen der Chemie*, **1864**, 130, 129-175.
2. G.M. Ziarani, F. Aleali & N. Lashgari, *RSC Adv.*, **2016**, 6, 50895-50922.
3. H. Shonle and A. Moment, *J. Am. Chem. Soc.*, **1923**, 45, 243-249.
4. C.L. Kliethermes, P. Metten, J.K. Belknap, K.J. Buck and J.C. Crabbe, *Brain Res.*, **2004**, 1009, 17-25.
5. Archana, V.K. Srivastava and A. Kumar, *Bioorg. Med. Chem.*, **2004**, 12, 1257-1264.
6. B.D. Dhorajiya, B.Z. Dholakiya and R.M. Mohareb, *Med. Chem. Res.*, **2014**, 23, 3941-3952.
7. F. Sandberg, *Acta Physiol. Scand.*, **1951**, 24, 7-26.
8. P. Singh, M. Kaur and P. Verma, *Bioorg. Med. Chem. Lett.*, **2009**, 19, 3054-3058.
9. O.M. Ashour, F.N. Naguib, M.M. Khalifa, M.H. Abdel-Raheem, R.P. Panzica and M.H. Kouni, *Cancer Res.*, **1995**, 55, 1092-1098.
10. L. Deng, A.M. Shi & Q. Wang, *J. Sci. Food Agric.*, **2018**, 98, 4885-4894.
11. N.B. Ilangaratne, N.N. Mannakkara, G.S. Bell and J.W. Sander, *Bull. World Health Organ.*, **2012**, 90, 871-872.
12. A. Glover, H.G. Chun, L.M. Kleinman, D.A. Cooney, J. Plowman, C.K. Grieshaber, L. Malspeis and B. Leyland-Jones, *Invest. New Drugs*, **1987**, 5, 137-143.
13. A. Barakat, H.A. Ghabbour, A.M. Al-Majid, R. Imad, K. Javaid, N.N. Shaikh & A. Wadood, *J. Chem.*, **2016**, 1-12.
14. R.A. Irgashev, G.A. Kim, G.L. Rusinov and V.N. Charushin, *ARKIVOC*, **2014**, 123-131.
15. F. Nemati, M.M. Heravi & R.S. Rad, *Chinese J. Catal.*, **2012**, 33, 1825-1831.
16. R. Firouzi- Haji and A. Maleki, *ChemistrySelect*, **2019**, 4, 853-857.
17. P. Kotrusz and S. Toma, *ARKIVOC*, **2006**, 100-109.
18. Z. Afzal, N. Rashid, H. Nadeem, A. Khan, *Research square*, **2022**, 1-22.
19. C.S. Venkata and V.R. Rao, *Phosphorus Sulfur Silicon Relat. Elem.*, **2011**, 186, 489-495.
20. Q.F. Wang, L. Hui, H. Hou, C.G. Yan, *J. Comb. Chem.*, **2010**, 12, 260-265.
21. A.O. Ademiluyi, G. Oboh, *Exp. Toxicol. Pathol.*, **2013**, 65, 305-309.
22. S.H. Sukanya, T. Venkatesh, S.J. Aditya Rao, M.N. Joy, *J. Mol. Struct.*, **2021**, 1247, 1-13.
23. O. Trott and A.J. Olson, *J. Comput. Chem.*, **2010**, 31, 455-461.

24. G.K. Swamy, G. Ramesh, K. Pruthviraj, S. Banu, B. Roopa, H.J. Preritha, B.S. Rajeshwari, M. Ravikumar, P.R. Shetty, D.B. Aruna Kumar, S. Sreenivasa, *Chem. Data Collect.*, **2020**, 28, 1-23.
25. R.S. Cheke, V.M. Patil, S.D. Firke, J.P. Ambhore, I.A. Ansari, H.M. Patel, M. Snoussi, *Pharmaceuticals*, **2022**, 15, 1-34.
26. A.A. Haredi, M.M. Eldeeb, M. El-Naggar, H. Temairk, M.A. Mohamed, *Front. Mol. Biosci.*, **2020**, 7, 1-19.
27. C.A. Lipinski, *Drug Discov. Today Technol.*, 2004, 1, 337-341.
28. I. Muegge, *Med. Res. Rev.*, **2003**, 23, 302-321.
29. R.B. Breemen van and Y. Li, *Expert. Opin. Drug Metab. Toxicol.*, **2005**, 1, 175-185.
30. S. Alam and F. Khan, *Sci. Reports*, **2018**, 8, 1-16.
31. Y. Rohitash, I. Mohammed, D. Puneet, K.C. Dheeraj, H. Shailendra, *J. Biomol. Struct. Dyn.*, **2021**, 39, 6617-6632.
32. S. Mishra, R. Dahima, *J. drug Deliv. Ther.*, **2019**, 9, 366-369.

7.1. Introduction

In 1818, Brugnatelli [1] synthesized the first pyrimidine derivative i.e., alloxan (**1**) by oxidative degradation of uric acid with nitric acid and it exhibited a variety of biological activities mainly recognized as a diabetogenic agent [2]. Pyrimidines are the bases of nucleic acid, DNA and RNA. Uracil (**2**), thymine (**3**) and cytosine (**4**) are the three important constituents of nucleic acids that contain the pyrimidine nucleus [3] (**Fig. 1**). Pyrimidine and their derivatives are considered to be the significant in the preparation of drugs [4], agricultural chemicals [5], latent fingerprints (LFPs) [6] opto-electronics [7], fluorescence sensors [8], energy materials [9] etc. They also serve as reactive moieties in pharmaceutical field due to their diverse medicinal properties, such as anticancer [10], antibacterial [11], antiviral [12], antifungal [13], antimalarial [14] anti- HIV [15], anti-tuberculosis [16], anti- inflammatory [17], anti-diabetic [18] tyrosine kinase inhibitors [19], COX-2 inhibitors [20] and antihypertensive [21] etc. Due to these biological and photophysical applications, researchers are more focused on pyrimidine derivatives.

2-Bromoacetophenones are major building blocks for the preparation of heterocyclic moieties and industrially active intermediates, which serve as key intermediates for the development of different bioactive compounds as well as natural products [22]. Phenacyl bromides were mainly obtained from acetophenones with liquid bromine in the presence of protic and Lewis acids [23] and it is serving as versatile synthons in heterocyclic synthesis. This led to an interest on these compounds in the construction of heterocyclic compounds [24].

The growth of pathogenic microorganisms causes a rapid increase in bacterial or fungal infections, leading to serious health problems [25]. While many factors contributed to microbial genome mutations, it has been widely demonstrated that improper antibiotic use was one of them. In order to overcome these problems, novel antibiotic drugs are essential

[26]. This creates an interest in antimicrobial research; hence, we have screened antibacterial and anti-diabetic activity of obtained compounds. Some of the reported biologically active heterocyclic compounds have been discussed below.

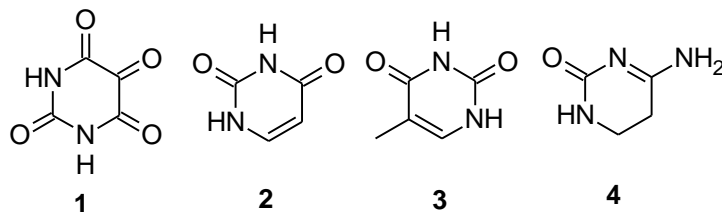
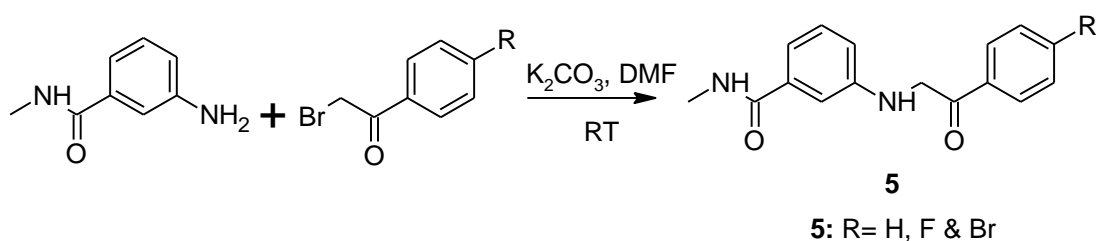
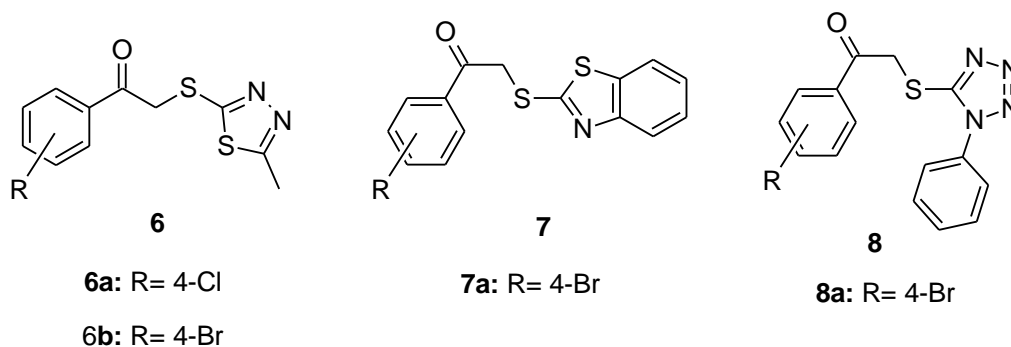


Fig. 1. Some of the bioactive compounds containing pyrimidine nucleus

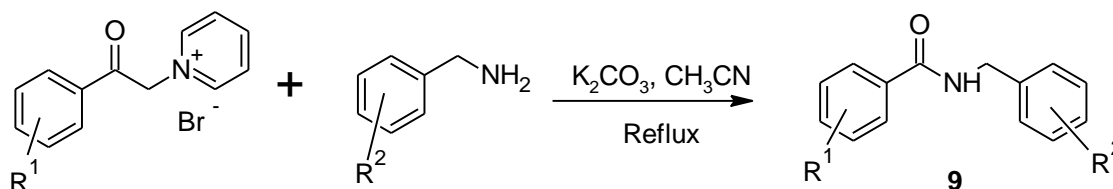
A.M. Qandil & L.I. Fakhouri was synthesized a series of *N*-methyl-3-[(2-oxo-2-phenylethyl) amino]benzamide derivatives (**5**) by the reaction of 4-substituted-phenacylbromide with aniline undergoes monoalkylation to afford anilinoketones [27].



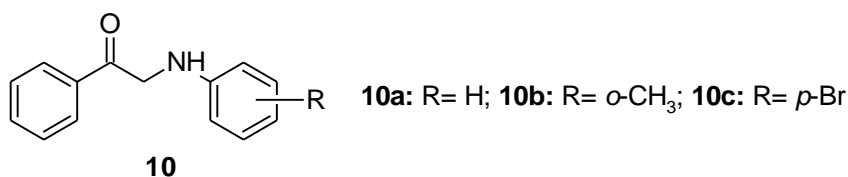
S. Chitra *et al.*, have been reported a 2-[(5-methyl-1,3,4-thiadiazol-2-yl)sulfanyl]-1-phenylethanones (**6**), 2-(1,3-benzothiazol-2-ylsulfanyl)-1-phenylethanones (**7**) and 1-phenyl-2-[(1-phenyl-1*H*-tetrazol-5-yl)sulfanyl]ethanones (**8**) and reported as anti-TB and cytotoxicity. The compounds **6a**, **6b**, **7a** & **8a** are shows good anti-TB efficacy with MIC value of 3.5, 3.2, 5.9 & 23.3 μ M respectively. The compounds **6a** & **6b** shows good cytotoxicity with IC_{50} values of 1263 & 2050 μ M respectively [28].



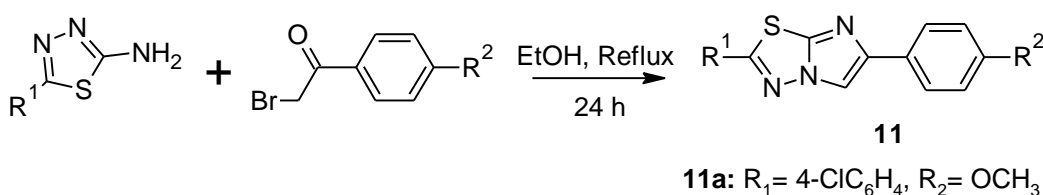
K.L. Manasa and co-authors have synthesized a *N*-benzylbenzamide derivatives (**9**) by the reaction of amides/esters with pyridinium salts of phenacyl bromides *via* oxidative cleavage of a C–C bond followed by formation of a new C–N/C–O bond in the presence of K_2CO_3 as a catalyst [29].



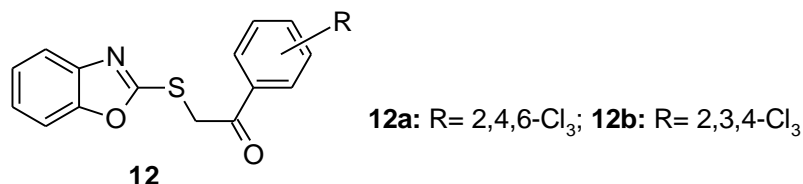
A series of 1-phenyl-2-(phenylamino)ethanone derivatives (**10**) has been prepared by Gupta *et. al.*, and screened for antimicrobial activity. The compound **10b** shows highest zone of inhibition of 18 & 12 mm for *S. aureus* & *P. aeruginosa* and **10a** & **10c** exhibited maximum zone of inhibition of 10 & 18 mm for *K. Pneumonia* & *P. Mirabilis* strains respectively [30].



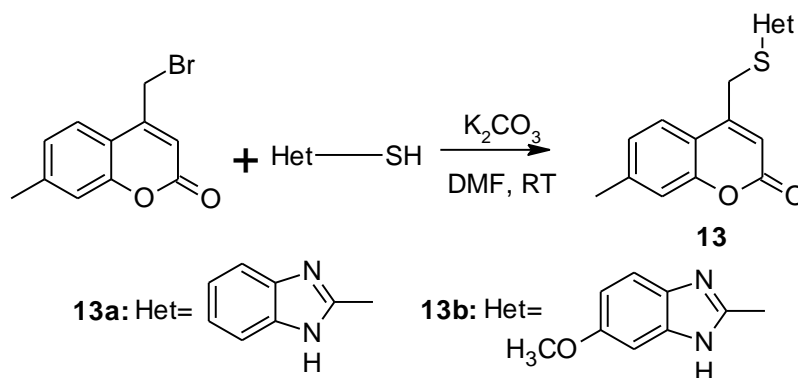
In 2015, J. Ramprasad and co-workers synthesized a 2,6-diphenylimidazo[2,1-*b*][1,3,4]thiadiazole derivatives (**11**) and evaluated their antimicrobial activity. Among them, **11a** compound displayed highest zone of inhibition of 13±0.5, 14±0.1, 13±0.1 & 15±0.3 mm against bacterial strains *S. aureus*, *E. coli*, *P. aeruginosa* and *S. typhi* respectively and 6±0.2, 5±0.2 & 6±0.1 mm for fungal strains *A. flavus*, *C. keratinophilum* and *C. albicans* respectively [31].



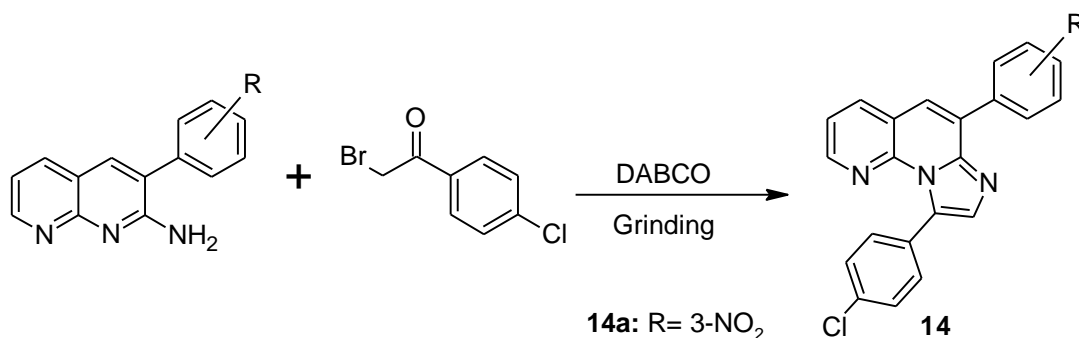
In 2021, M. Staniszevska *et. al.*, was reported a 2-(1,3-benzoxazol-2-ylsulfanyl)-1-phenylethanone derivatives (**12**) as antifungal agent against *C. albicans* & *C. glabrata* strains. Compounds **12a** & **12b** exhibited as most active compounds with % of inhibition value of 64.2 ± 10.6 & 53.0 ± 3.5 at 16 $\mu\text{g/mL}$ against fungal strains *C. albicans* & *C. glabrata* respectively [32].



In 2022, B. Manjunatha and co-authors synthesized some coumarin-thioether derivatives (**13**) and investigated antimycobacterial activity. The compounds **13a** and **13b** showed good inhibition with MIC value of 1.6 $\mu\text{g/mL}$ due to presence of thio-benzimidazole moiety, while the remaining coumarin conjugates also exhibited significant potency with MIC values ranging from 25 to 50 $\mu\text{g/mL}$ [33].



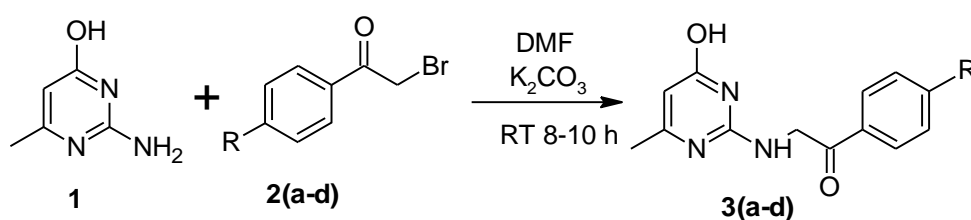
In 2018, a series of fused imidazo[1,2-*a*] [1,8]naphthyridine derivatives (**14**) has been developed by S. Banoth *et. al.* and reported as antibacterial and fungal activity. The compound **14a** demonstrated highest zone of inhibition value of 29, 30, 29 & 28 mm at 35 $\mu\text{g/mL}$ against *S. aureus*, *E. coli*, *A. niger* and *C. metapsilosis* respectively [34].



Based on the above investigations, we reported a 2-[(4-hydroxy-6-methylpyrimidin-2-yl)amino]-1-(4-substituted)ethanone derivatives and screened for their anti-bacterial, anti-diabetic, *in silico* molecular docking and ADME studies using DNA gyrase and exo- β -D-glucosaminidase proteins as target enzymes respectively.

7.2. Present work

In this chapter, we described a new 2-[(4-hydroxy-6-methylpyrimidin-2-yl)amino]-1-(4-substituted)ethanone derivatives **3(a-d)** were carried out by the reaction of 2-amino-4-hydroxy-6-methyl pyrimidine (**1**) with 2-bromo-4-substituted-acetophenone (**2**) in the presence of DMF and K_2CO_3 as a catalyst and the reaction pathway have been given in **Scheme 9**.



Compd.	R
3a	Cl
3b	NO_2
3c	OCH_3
3d	CH_3

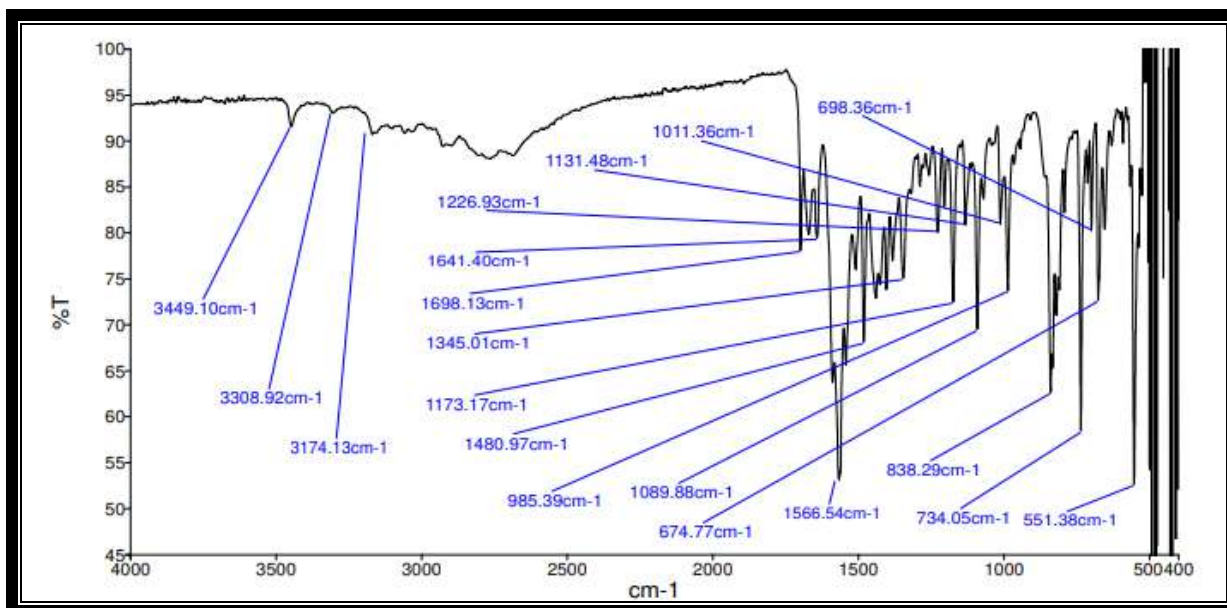
Scheme 9. Synthesis of 2-[(4-hydroxy-6-methylpyrimidin-2-yl)amino]-1-(4-substituted)ethanone derivatives **3(a-d)**.

The structures of 2-[(4-hydroxy-6-methylpyrimidin-2-yl)amino]-1-(4-substituted) ethanone derivatives **3(a-d)** were confirmed by recording their IR, ^1H NMR, ^{13}C NMR and Mass spectral data.

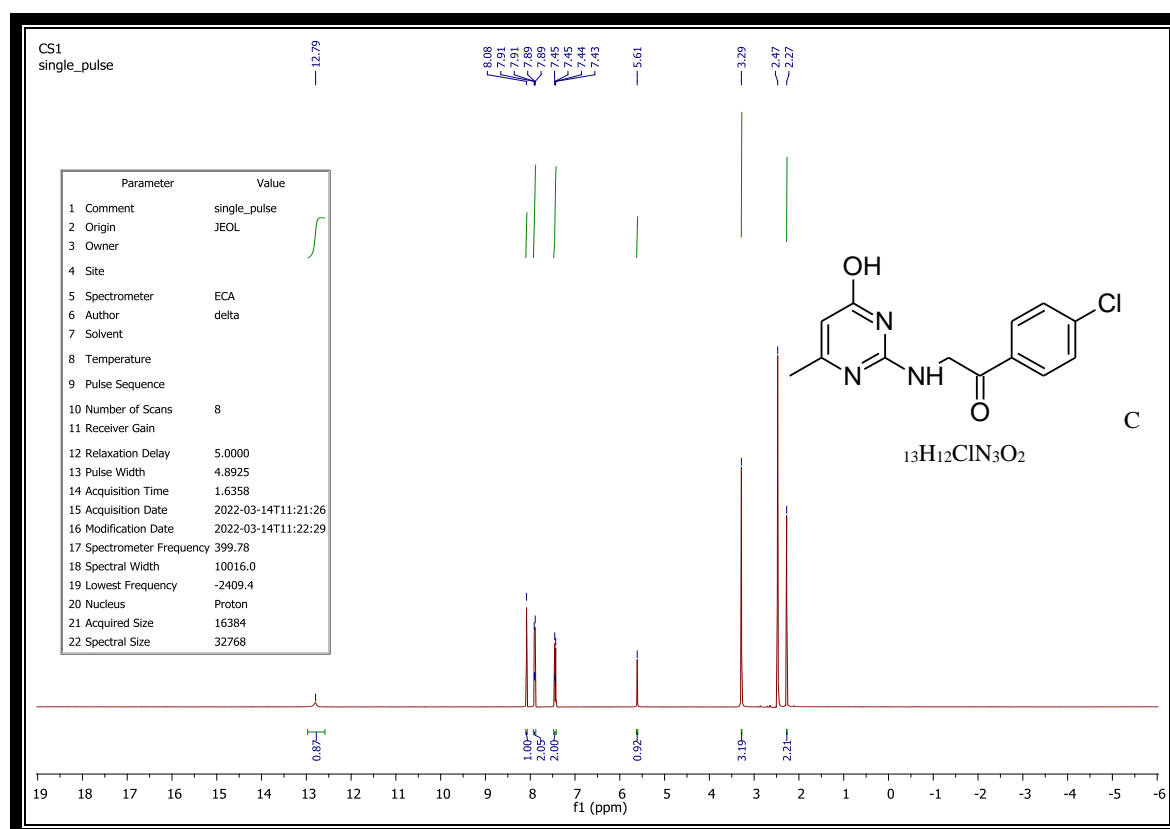
In IR spectrum of compound **3a** showed the absorption band in the region of 3449 cm^{-1} is attributed to the OH stretching frequency, 3174 cm^{-1} correspond to NH functionality, 1698 cm^{-1} correspond to C=O functionality, 1566 cm^{-1} correspond to C=N group and another stretching vibrational band at 734 cm^{-1} correspond to C-Cl functionality. The ^1H NMR spectrum of compound **3a** exhibited a singlet peak at δ 12.79 ppm which correspond to OH proton (s, 1H, OH) and another singlet peak at δ 8.08 ppm due to NH proton (s, 1H, NH) and two doublet of doublet peaks at δ 7.91-7.89 & 7.45-7.43 ppm corresponds to four aromatic protons (dd, $J= 8\text{ Hz}$, 4H, Ar-H). A singlet peak at δ 5.61 ppm due to aromatic proton of pyrimidine nucleus (s, 1H, Ar-H) and two singlet peaks at δ 3.29 & 2.27 ppm due to methyl & CH_2 protons (s, 5H, CH_3 & CH_2) respectively. In addition, ^{13}C NMR spectrum of compound **3a** exhibited peaks at δ 169.43 ppm which correspond to carbonyl carbon and 23.77 ppm due to CH_3 carbon.

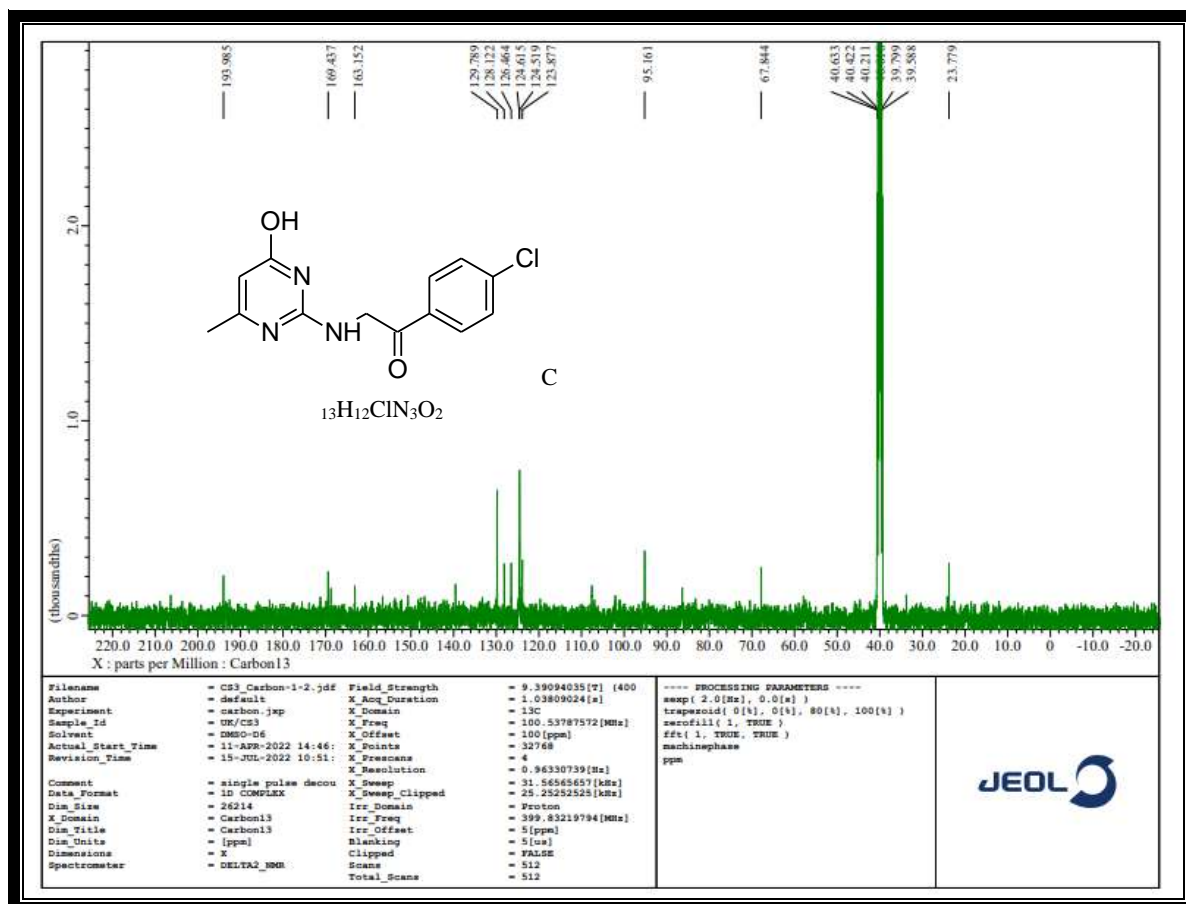
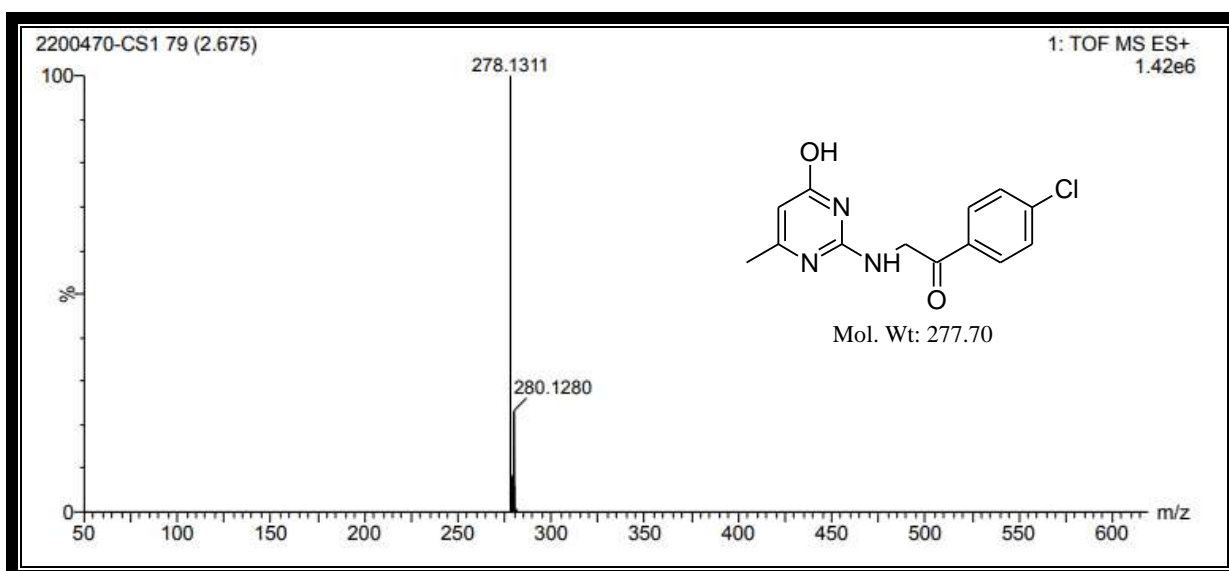
The mass spectrum showed molecular ion peak m/z at 278.1311 [M^++1] & 280.1280 [M^++3] which corresponds to the molecular weight of compound **3a**.

Characterization:

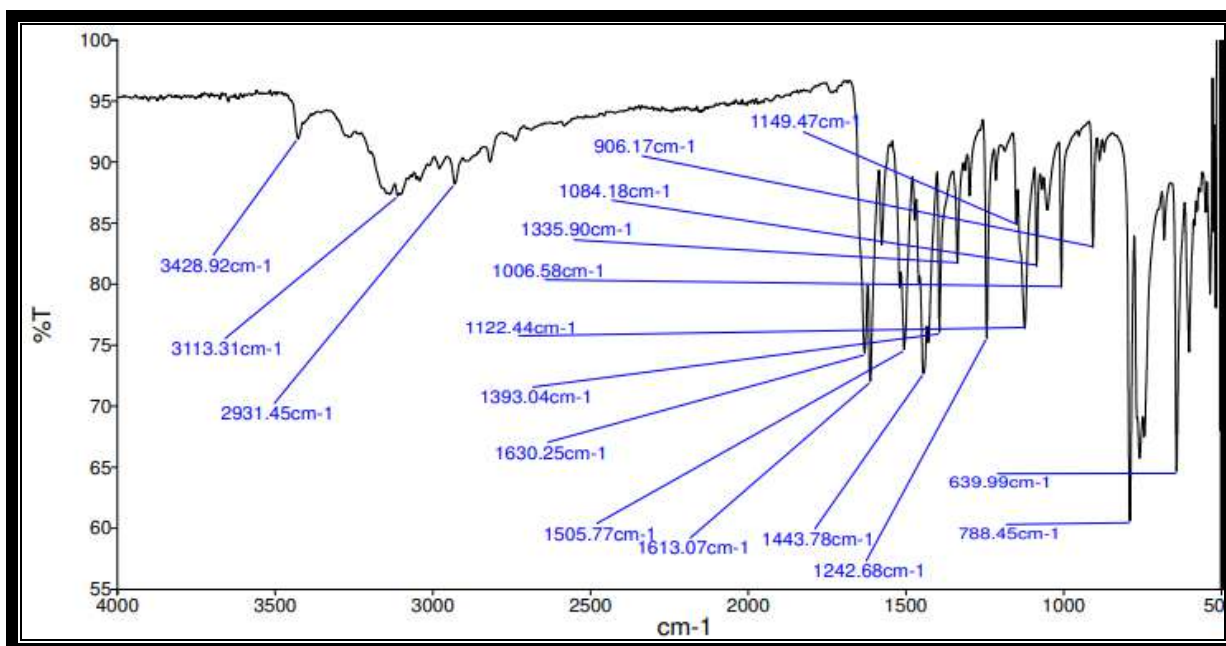


IR spectrum of compound 3a

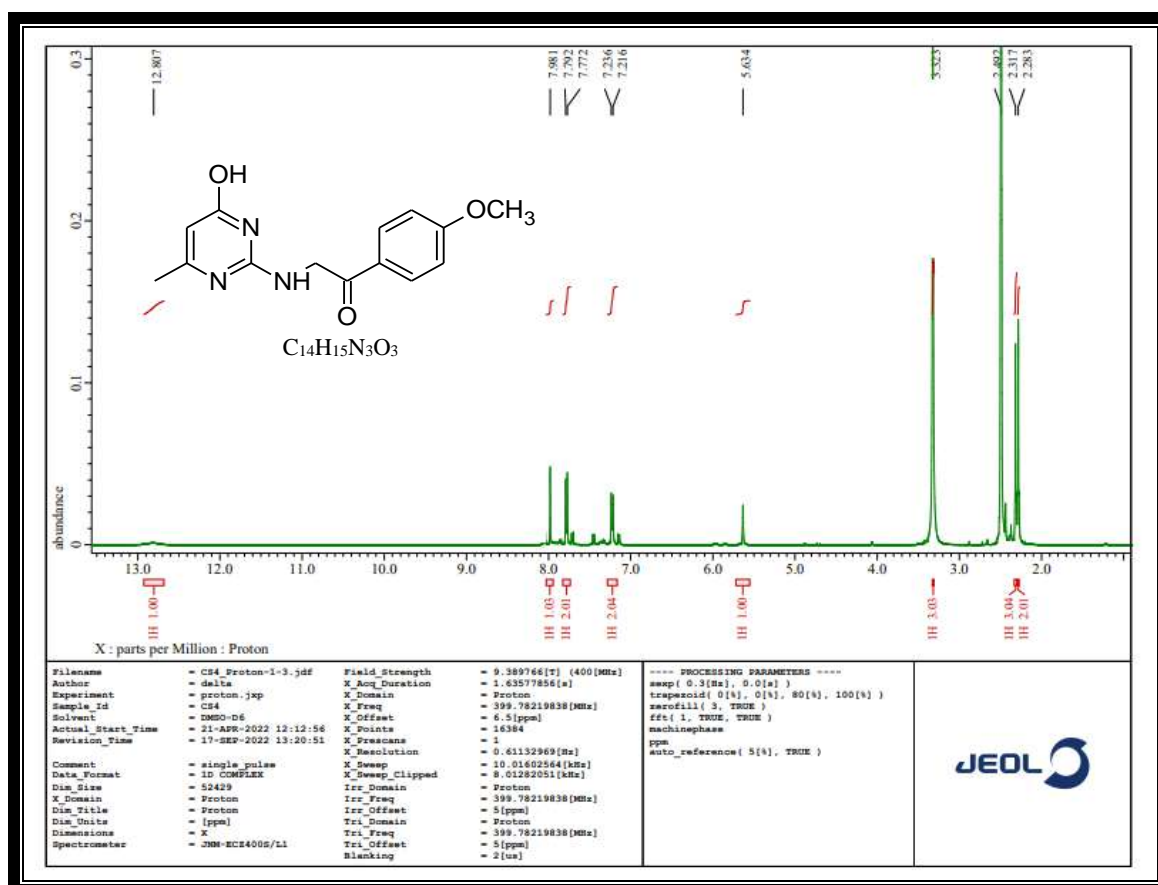
¹H NMR spectrum of compound 3a

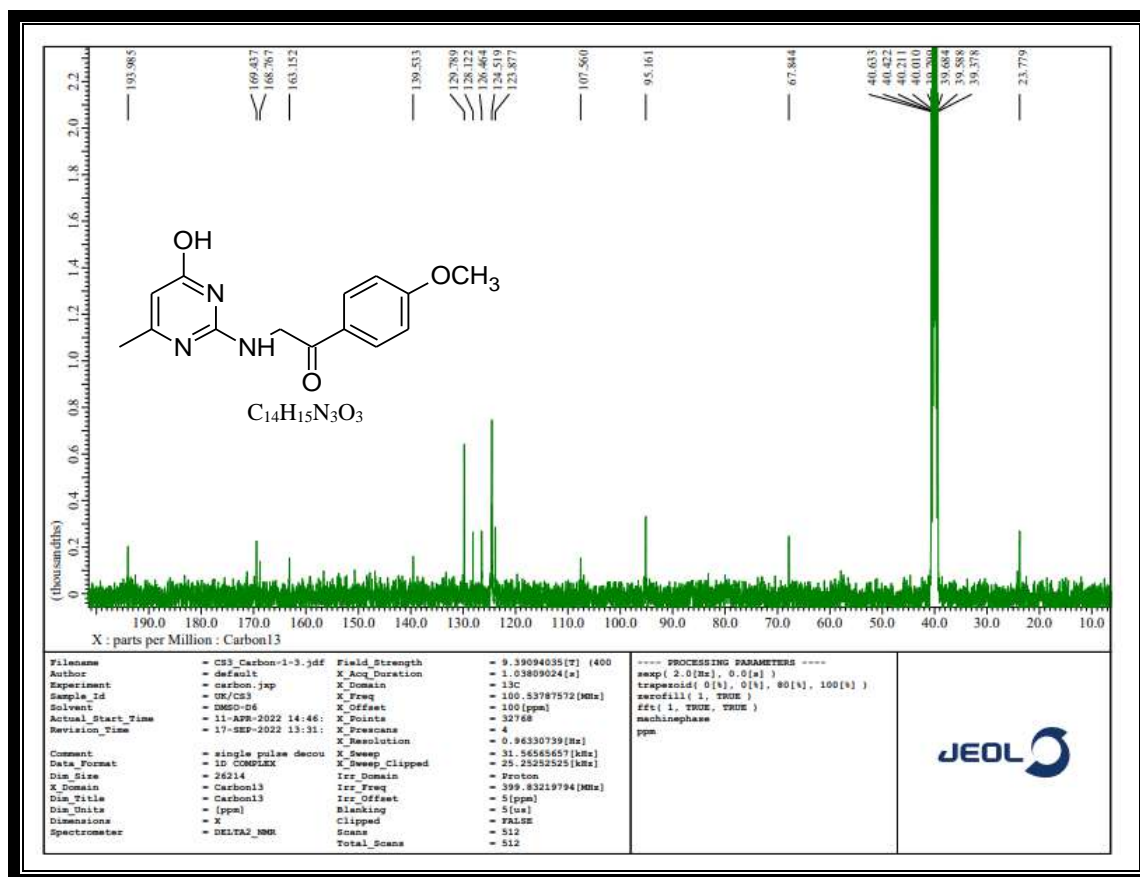
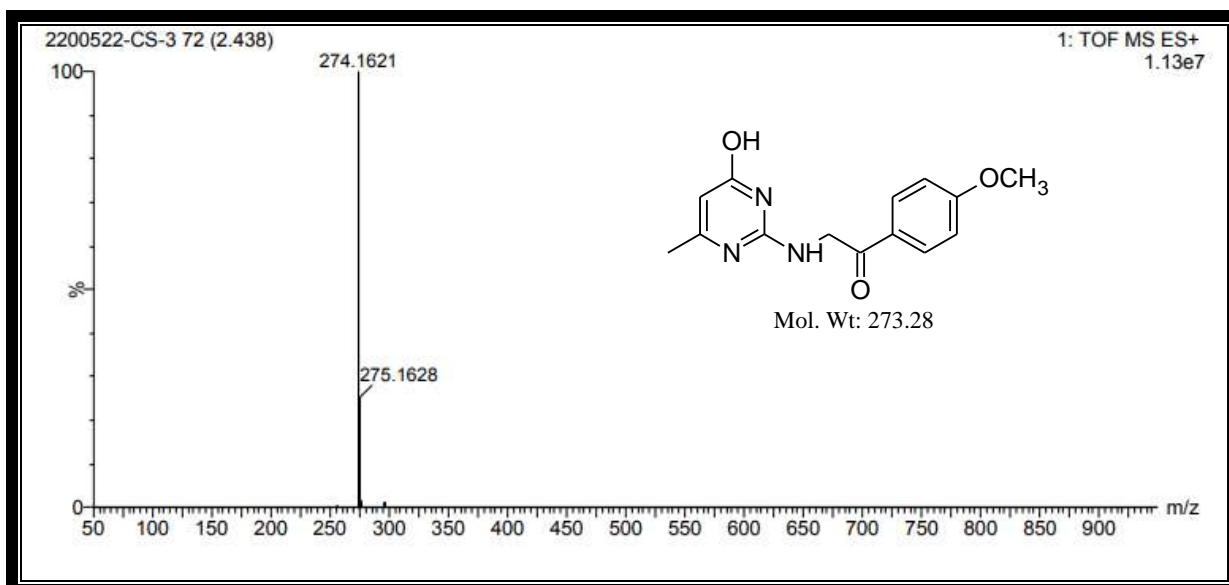
 ^{13}C NMR spectrum of compound 3a

MASS spectrum of compound 3a



IR spectrum of compound 3c

¹H NMR spectrum of compound 3c

 ^{13}C NMR spectrum of compound 3c

MASS spectrum of compound 3c

7.3. Experimental

7.3.1. General information:

The detailed general information regarding the reagents, solvents and instruments etc., used for the analysis has been discussed in the experimental section 2A.3.1 & 5.3.1 of Chapter-2A & Chapter-5.

7.3.2. Synthesis of some new 2-[(4-hydroxy-6-methylpyrimidin-2-yl)amino]-1-(4-substituted)ethanone derivatives 3(a-d):

A mixture of 2-amino-4-hydroxy-6-methyl pyrimidine (**1**, 1 mmol) and 2-bromo-4-substituted-acetophenone (**2**, 1 mmol) in the presence of K_2CO_3 as a catalyst in DMF and stirred for 8-10 hours under RT condition. Simultaneously, the reaction was monitored by TLC (Ethyl acetate & Pet ether). After completion of the reaction, the reaction mixture was cooled and poured into an ice flake with vigorous stirring to get solid precipitate. Then, it was filtered, washed, dried and recrystallized from methanol to afford pure solid products **3(a-d)**.

1-(4-Chlorophenyl)-2-[(4-hydroxy-6-methylpyrimidin-2-yl)amino]ethanone (3a):

White solid; Yield: 88 %; MP: 268-270 °C; Mol. Formula: $C_{13}H_{12}ClN_3O_2$; FTIR (ν cm^{-1}): 3449 (OH), 3174 (NH), 1698 (C=O), 1566 (C=N) & 734 (C-Cl); 1H NMR (δ ppm): 12.79 (s, 1H, OH), 8.08 (s, 1H, NH), 7.91-7.89 (dd, $J=8$ Hz, 2H, Ar-H), 7.45-7.43 (dd, $J=8$ Hz, 2H, Ar-H), 5.61 (s, 1H, Ar-H), 3.29 (s, 3H, CH_3) & 2.27 (s, 2H, CH_2); ^{13}C NMR (δ ppm): 193.98, 169.43, 163.15, 129.78, 128.78, 128.12, 126.46, 124.61, 124.51, 123.87, 95.16, 67.84 & 23.77; HRMS: m/z 278.1311 [M^++1] & 280.1280 [M^++3]; Anal. Calcd: C 56.22, H 4.36, N 15.13 %, Found: C 56.18, H 4.31, N 15.08 %.

2-[(4-Hydroxy-6-methylpyrimidin-2-yl)amino]-1-(4-nitrophenyl)ethanone (3b):

Yellow solid; Yield: 86 %; MP: 242-244 °C; Mol. Formula: $C_{13}H_{12}N_4O_4$; FTIR (ν cm^{-1}): 3410 (OH), 3210 (NH), 2930 (CH), 1678 (C=O) & 1586 (C=N); 1H NMR (δ ppm): 12.58

(s, 1H, OH), 7.95 (s, 1H, NH), 7.59-7.57 (d, $J=8$ Hz, 2H, Ar-H), 7.41-7.33 (m, 2H, Ar-H), 6.78 (s, 1H, Ar-H), 2.84 (s, 3H, CH₃) & 2.68 (s, 2H, CH₂); ¹³C NMR (δ ppm): 167.54, 165.70, 164.90, 163.03, 162.83, 162.71, 131.62, 128.63, 128.13, 122.62, 122.37, 43.61 & 36.31; HRMS: m/z 289.1398 [M^++1]; Anal. Calcd: C 54.17, H 4.20, N 19.44 %, Found: C 54.13, H 4.15, N 19.40 %.

2-[(4-Hydroxy-6-methylpyrimidin-2-yl)amino]-1-(4-methoxyphenyl)ethanone (3c):

Pale yellow solid; Yield-90 %; MP: 190-192 °C; Mol. Formula: C₁₄H₁₅N₃O₃; FTIR (ν cm⁻¹): 3428 (OH), 3113 (NH), 2931 (CH), 2821 (OCH₃), 1630 (C=O) & 1613 (C=N); ¹H NMR (δ ppm): 12.80 (s, 1H, OH), 7.98 (s, 1H, NH), 7.79-7.77 (d, $J=8$ Hz, 2H, Ar-H), 7.23-7.21 (d, $J=8$ Hz, 2H, Ar-H), 5.63 (s, 1H, Ar-H), 3.32 (s, 3H, OCH₃), 2.31 (s, 3H, CH₃) & 2.28 (s, 2H, CH₂); ¹³C NMR (δ ppm): 193.98, 169.43, 168.76, 163.15, 139.53, 129.78, 128.12, 126.46, 124.51, 123.87, 107.56, 95.16, 67.84 & 23.77; HRMS: m/z 274.1621 [M^++1]; Anal. Calcd: C 61.53, H 5.53, N 15.38 %, Found: C 61.48, H 5.49, N 15.32 %.

2-[(4-Hydroxy-6-methylpyrimidin-2-yl)amino]-1-(4-methylphenyl)ethanone (3d):

White solid; Yield: 87 %; MP: 223-225 °C; Mol. Formula: C₁₄H₁₅N₃O₂; FTIR (ν cm⁻¹): 3410 (OH), 3161 (NH), 2915 (CH), 1684 (C=O) & 1570 (C=N); ¹H NMR (δ ppm): 12.83 (s, 1H, OH), 7.96 (s, 1H, NH), 7.77-7.75 (d, $J=8$ Hz, 2H, Ar-H), 7.22-7.20 (d, $J=8$ Hz, 2H, Ar-H), 5.62 (s, 1H, Ar-H), 3.30 (s, 3H, CH₃), 2.30 (s, 3H, CH₃) & 2.26 (s, 2H, CH₂); ¹³C NMR (δ ppm): 171.06, 161.80, 161.73, 161.67, 150.62, 150.45, 150.36, 148.78, 129.40, 128.63, 117.95, 85.80 & 29.24; HRMS: m/z 256.1484 [M^+-1]; Anal. Calcd: C 65.35, H 5.88, N 16.33 %, Found: C 65.30, H 5.82, N 16.29 %.

7.4. Pharmacological studies

The detailed procedure for antibacterial activity, *in-vitro* α -amylase & α -glucosidase inhibitory assay and ADME study has been discussed in the experimental section 2B.5.1 & 5.5.1 of **Chapter-2B** & **Chapter-5**.

7.4.1. *in silico* molecular docking study

The molecular interactions of the synthesized compounds with binding pocket of DNA gyrase for antibacterial and exo- β -D-glucosaminidase for anti-diabetic activity were studied using automated docking by employing the Autodock Vina program [35]. The co-crystallized structure of DNA gyrase (PDB ID: 1KZN) and exo- β -D-glucosaminidase (PDB ID: 2x05) were retrieved from the protein databank and their substrate binding sites were identified using pdbsum server [36]. A grid box of dimensions 20 x 20 x 20 Å with X, Y & Z coordinates at 21.57, 30.764 and 36.764 for DNA gyrase and 25 x 25 x 25 Å with X, Y & Z coordinates at 50.995, 42.447 and 71.445 for exo- β -D-glucosaminidase were created respectively. The grid box was set around the residues forming the active pocket. The binding interactions were visualized using Biovia Discovery Studio Visualizer V.20.1.

7.5. Results and discussion

7.5.1. Antibacterial activity

The *in vitro* antibacterial activity of the synthesized compounds **3(a-d)** were evaluated against four Gram negative bacterial strains *viz.* *P. aeruginosa*, *E. coli*, *Shigella* and *Salmonella* at four different concentrations 25, 50, 75 & 100 μ g/mL (**Fig. 2**) and the results were expressed as zone of inhibition in mm as shown in **Table 1**. Gentamycin was used as a standard drug for comparison. The activity results revealed that, the obtained compounds displayed an outstanding zone of inhibition against all bacterial strains. These compounds showed appreciable antibacterial activity with a varied zone of inhibition in the range of 6 \pm 0.12 to 14 \pm 1.19, 11 \pm 1.41 to 14 \pm 1.15, 12 \pm 0.23 to 14 \pm 0.97 and 15 \pm 0.43 to 16 \pm 0.45 mm with

respect to their concentration of 25, 50, 75 & 100 $\mu\text{g/mL}$. Among them, the compound **3d** exhibited the highest zone of inhibition of 16 ± 0.17 , 16 ± 0.45 , 15 ± 0.79 and 15 ± 0.74 mm against *P. aeruginosa*, *E. coli*, *Shigella* and *Salmonella* respectively, at a concentration of 100 $\mu\text{g/mL}$. The rest of the compounds showed a considerable zone of inhibition as compared to the standard drug Gentamycin.

Table 1. Antibacterial activity results of synthesized compounds **3(a-d)**.

Compd.	Zone of inhibition in mm (mean \pm SD)				
	Conc. in ($\mu\text{g/mL}$)	<i>P. aeruginosa</i>	<i>E. coli</i>	<i>Shigella</i>	<i>Salmonella</i>
3a	25	6 ± 0.12	8 ± 0.25	6 ± 0.23	7 ± 1.26
	50	11 ± 0.15	12 ± 0.71	11 ± 0.86	11 ± 1.41
	75	14 ± 0.41	13 ± 0.43	12 ± 0.57	14 ± 0.93
	100	15 ± 0.54	15 ± 0.43	13 ± 0.26	14 ± 0.84
3b	25	6 ± 0.45	8 ± 0.71	12 ± 0.87	7 ± 1.14
	50	14 ± 1.19	14 ± 0.36	14 ± 0.67	14 ± 1.29
	75	14 ± 0.47	14 ± 0.99	14 ± 1.15	14 ± 0.85
	100	14 ± 0.86	15 ± 0.53	14 ± 1.14	15 ± 0.89
3c	25	7 ± 0.55	9 ± 1.41	12 ± 0.91	8 ± 1.18
	50	14 ± 1.12	14 ± 1.11	14 ± 1.21	14 ± 1.20
	75	14 ± 0.85	14 ± 0.88	14 ± 0.97	14 ± 0.51
	100	14 ± 0.89	15 ± 0.88	15 ± 1.20	14 ± 0.42
3d	25	8 ± 0.71	9 ± 1.41	14 ± 1.19	8 ± 1.14
	50	13 ± 1.09	14 ± 1.19	14 ± 1.21	14 ± 1.12
	75	13 ± 0.27	14 ± 0.75	14 ± 0.54	14 ± 0.84
	100	16 ± 0.17	16 ± 0.45	15 ± 0.79	15 ± 0.74
Gentamycin	25	8 ± 1.10	9 ± 1.11	8 ± 1.12	8 ± 1.11
	50	15 ± 0.88	16 ± 1.23	15 ± 0.94	15 ± 0.98
	75	15 ± 0.96	16 ± 0.97	15 ± 0.31	15 ± 0.87
	100	15 ± 0.93	16 ± 0.91	15 ± 0.71	15 ± 0.39

Each value is the mean of three replicate determinations \pm standard deviation

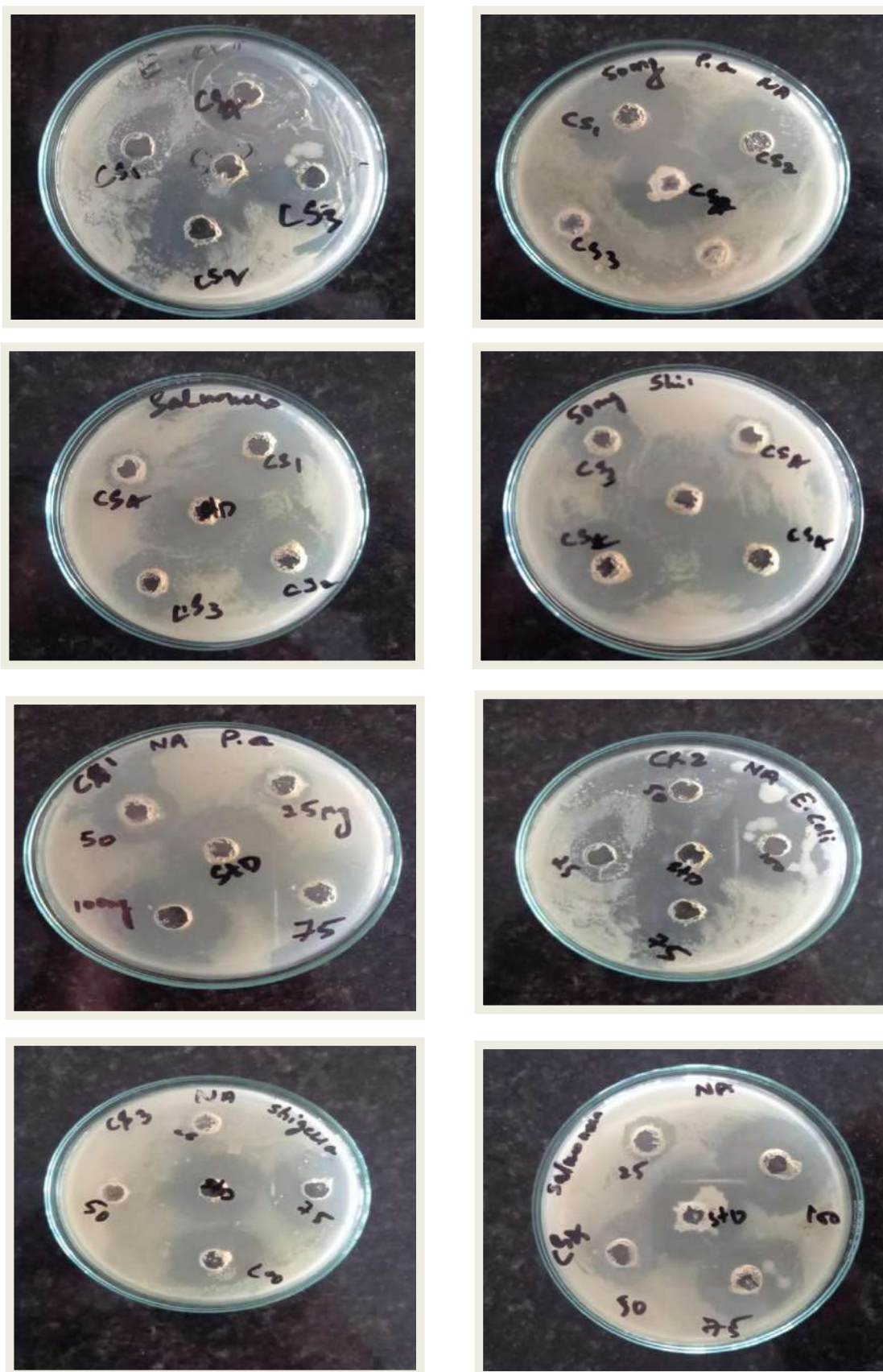


Fig. 2. Images of antibacterial activity of the synthesized compounds 3(a-d).

7.5.2. *In vitro* α -amylase and α -glucosidase inhibitory activity

In vitro α -amylase & α -glucosidase inhibitory activity results were expressed in terms of % inhibition and IC₅₀ values as shown in **Table 2** & **3**. From the α -amylase activity results, compounds possessed significant efficacy ranging from 30±0.98 to 81±0.63 % with respect to concentration (25, 50, 75 & 100 μ g/mL). In that, **3c** exhibited least IC₅₀ value of 29.19±2.20 μ g/mL as compared to standard acarbose (50.81±0.67 μ g/mL). The potencies of IC₅₀ values varied from 29.19±2.20 to 70.70±2.07 μ g/mL and remaining compounds exhibited good % inhibition with considerable IC₅₀ values (**Fig. 3a**).

The α -glucosidase inhibitory activity results displayed that, the compounds showed % inhibition ranging from 42±0.77 to 86±0.84 %. The potencies of IC₅₀ values vary from 23.33±0.48 to 77.45±0.37 μ g/mL. All compounds exhibited well to considerable IC₅₀ values, in that compounds **3c** & **3d** showed best IC₅₀ values of 23.33±0.48 & 24.75±0.16 μ g/mL as compared to standard acarbose (38.18±0.53 μ g/mL) as shown in **Fig. 3b**.

Table 2. α -amylase enzyme activity results (%) at different concentrations and IC₅₀ values of the synthesized compounds **3(a-d)**.

Compd.	Concentration in μ g/mL				IC ₅₀ in μ g/mL
	25	50	75	100	
3a	39±1.27	44±0.91	51±1.06	56±1.34	70.70±2.07
3b	30±0.98	46±1.13	52±1.27	54±1.27	64.83±4.35
3c	49±0.77	56±0.91	72±0.70	81±0.63	29.19±2.20
3d	46±1.27	54±0.98	70±0.49	79±0.63	36.97±4.46
Acarbose	22±0.70	49±0.84	69±0.77	85±0.84	50.81±0.67

Values are Mean \pm SE, N=3, *P<0.01 vs. Control

Table 3. α -glucosidase enzyme activity results (%) at different concentrations and IC_{50} values of the synthesized compounds **3(a-d)**.

Compd.	Concentration in $\mu\text{g/mL}$				IC_{50} in $\mu\text{g/mL}$
	25	50	75	100	
3a	42 \pm 0.77	46 \pm 1.13	49 \pm 0.70	60 \pm 0.49	77.45 \pm 0.37
3b	42 \pm 0.82	46 \pm 1.06	51 \pm 0.84	62 \pm 0.98	71.40 \pm 0.31
3c	54 \pm 0.56	63 \pm 0.77	75 \pm 0.56	86 \pm 0.84	23.33 \pm 0.48
3d	51 \pm 0.89	61 \pm 0.42	75 \pm 0.28	85 \pm 0.98	24.75 \pm 0.16
Acarbose	39 \pm 0.56	60 \pm 0.56	74 \pm 0.63	86 \pm 0.42	38.18 \pm 0.53

Values are Mean \pm SE, N=3, *P<0.01 vs. Control

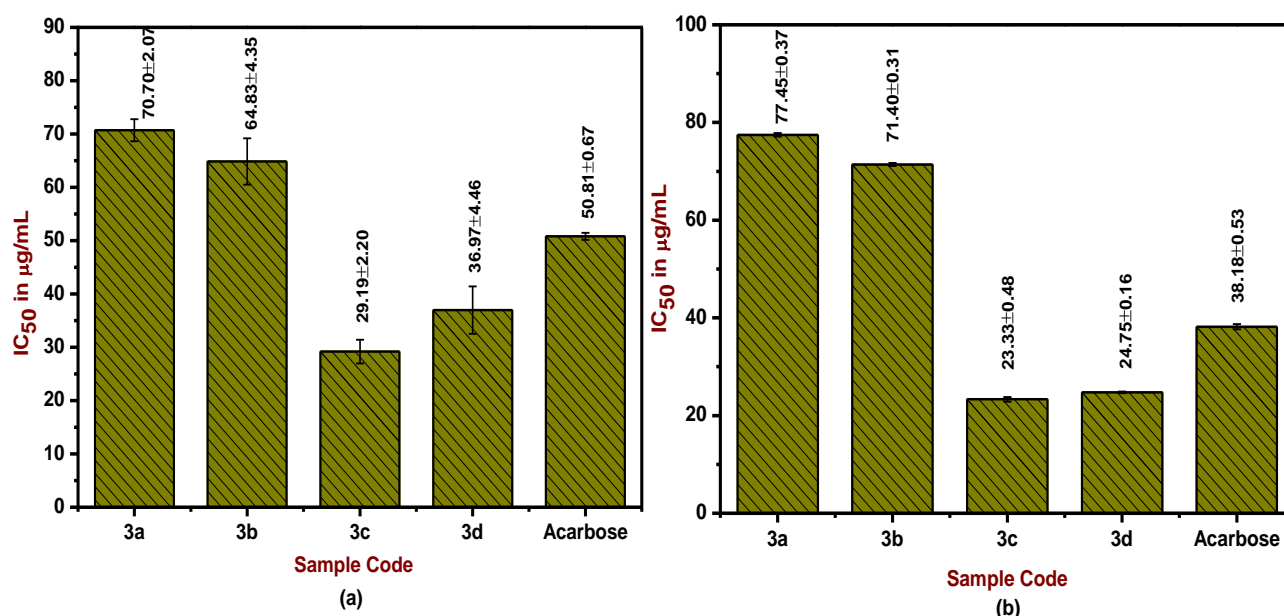


Fig. 3. A graph of IC_{50} value of compounds **3(a-d)** for α -amylase inhibitory activity (a); A graph of IC_{50} value of compounds for α -glucosidase inhibitory activity (b).

7.5.3. SAR study

SAR study has been carried out for obtained compounds; they exhibited good antibacterial and anti-diabetic activity with significant IC_{50} values. Compound **3d** shows the highest zone of inhibition due to the presence of an electron-donating methyl group at the para position; it may be reason for the admirable antibacterial activity [37]. The compound **3c** shows excellent anti-diabetic activity due to the presence of electron withdrawing methoxy groups in their ring structure [38].

7.5.4. *in silico* molecular docking study

For *in silico* molecular docking study DNA gyrase and exo- β -D-glucosaminidase proteins were selected for antibacterial and anti-diabetic activity. Target structures with DNA gyrase and exo- β -D-glucosaminidase proteins were shown in **Fig. 4 & 5**. Docking investigation shows, obtained targets established good binding interaction with docking receptors.

The docked structures with DNA gyrase receptor suggested that, targets had significant docking scores in the range of -7.2 to -7.6 kcal/mol with respect to standard Gentamycin (-8.8 kcal/mol). In that, compound **3d** shows the least binding energy of -7.6 kcal/mol by forming three hydrogen bonds with amino acid residues ASN46, ARG76 and GLY77 in their active pockets (**Table 4**). From the docked structures with exo- β -D-glucosaminidase, compound **3c** established good binding energy of -7.5 kcal/mol by forming two hydrogen bonds with amino acid residues ASP469 & GLU394. Remaining compounds also established good binding modes in the range of -7.2 to -7.4 kcal/mol as compared to standard Acarbose (-7.8 kcal/mol) and the results were tabulated in **Table 5**.

Table 4. Molecular interactions of synthesized compounds **3(a-d)** & standard drug **Gentamycin** with DNA gyrase protein.

Compd.	Binding affinity (kcal/mol)	Hydrogen bond interaction	Hydrogen bond length in Å	Hydrophobic and other interactions
3a	-7.4	ASN46, ARG136	2.15, 2.43	ASN46, VAL71, GLU50, THR165, VAL43, VAL71, VAL167, ALA47, ILE78, PRO79
3b	-7.5	ASN46, GLY77, VAL167, GLY77	2.26, 2.7, 2.8, 2.42	GLU50, GLY77, ILE78, PRO79, ALA47, ILE78, ILE78, PRO79
3c	-7.2	ASN46, GLY77, GLU50	2.27, 2.77, 1.9	ASP73, THR165, GLU50, GLY77, ILE78, ALA47, VAL71, PRO79, ALA47, ILE78, ILE78, PRO79
3d	-7.6	ASN46, ARG76, GLY77	2.26, 2.82, 2.25	ASN46, GLU50, THR165, VAL43, VAL71, VAL167, ALA47, ILE78, PRO79
Gentamycin	-8.8	ASN24, ARG47, GLY90, SER92	2.21, 2.31, 2.37, 2.45	AGLY22, LEU91

Table 5. Molecular interactions of synthesized compounds **3(a-d)** & standard drug **Acarbose** with *exo-β-D-glucosaminidase* protein.

Compd.	Binding affinity (kcal/mol)	Hydrogen bond interaction	Hydrogen bond length in Å	Hydrophobic and other interactions
3a	-7.2	ASP469	2.06	GLU541, TYR516, PHE583, TRP653, TRP781, CYS419
3b	-7.4	TRP204, ARG500, ARG500, TRP642	2.00, 2.24, 2.11, 1.86	ASP469, GLU541, TYR516, PHE470
3c	-7.5	ASP469, GLU394	1.97, 2.79	ASP203, GLU541, TYR516, PHE583, TRP653, MET512, CYS419
3d	-7.3	ASP469, GLU394	2.07, 2.79	GLU541, TRP781, TYR516, TRP781, PHE583, TRP653, TRP781, CYS419
Acarbose	-7.8	GLU431, GLU431, MET512, MET512, ARG500, ARG500, ARG500	2.45, 2.65, 2.54, 2.89, 2.23, 2.85, 2.64	ASP469, CYS420, MET512, SER580, ILE202, TRP781

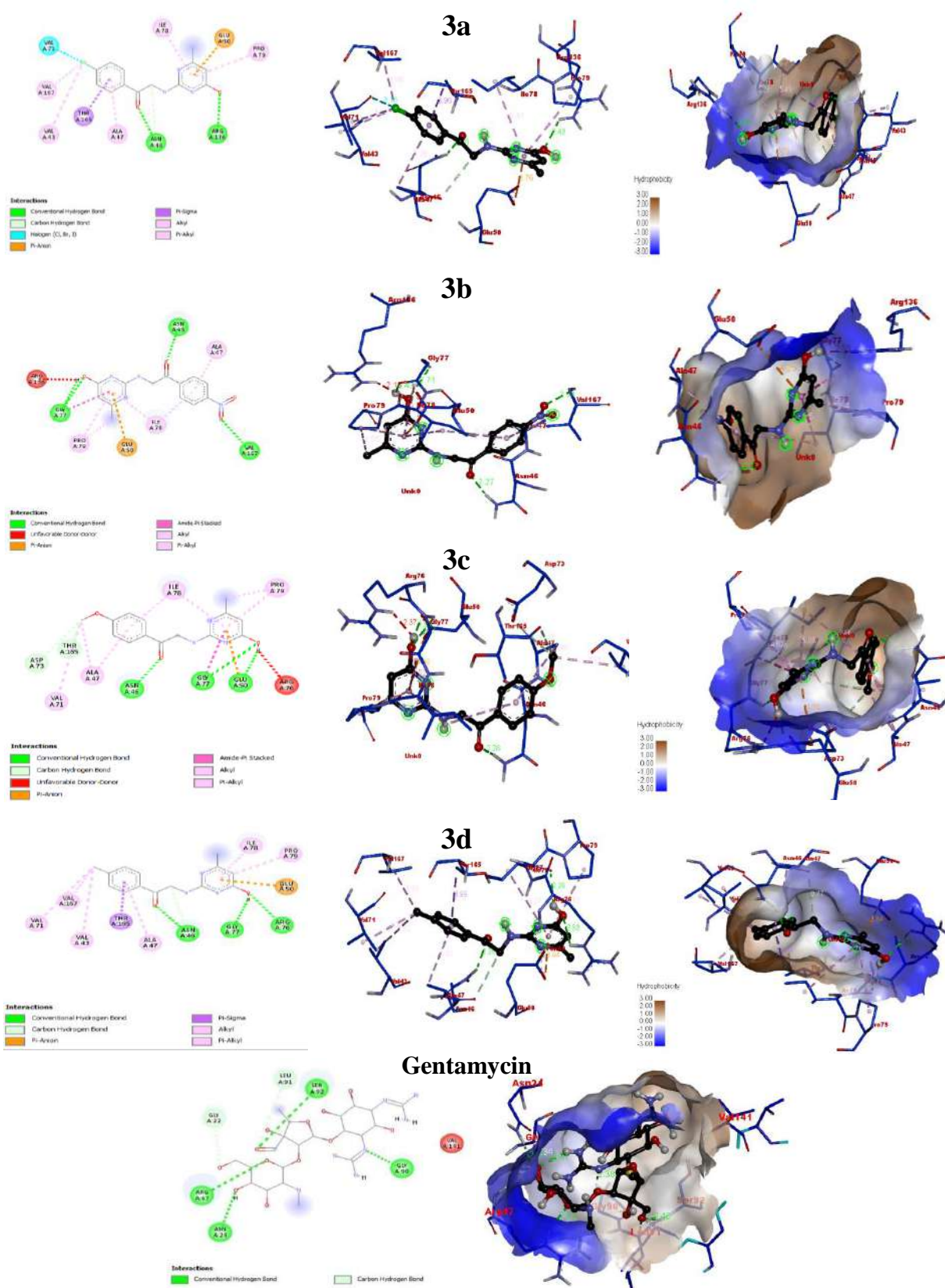


Fig. 4. 2D, 3D & hydrophobic representation of molecular interactions between DNA gyrase protein with synthesized compounds **3(a-d)** and standard drug **Gentamycin**.

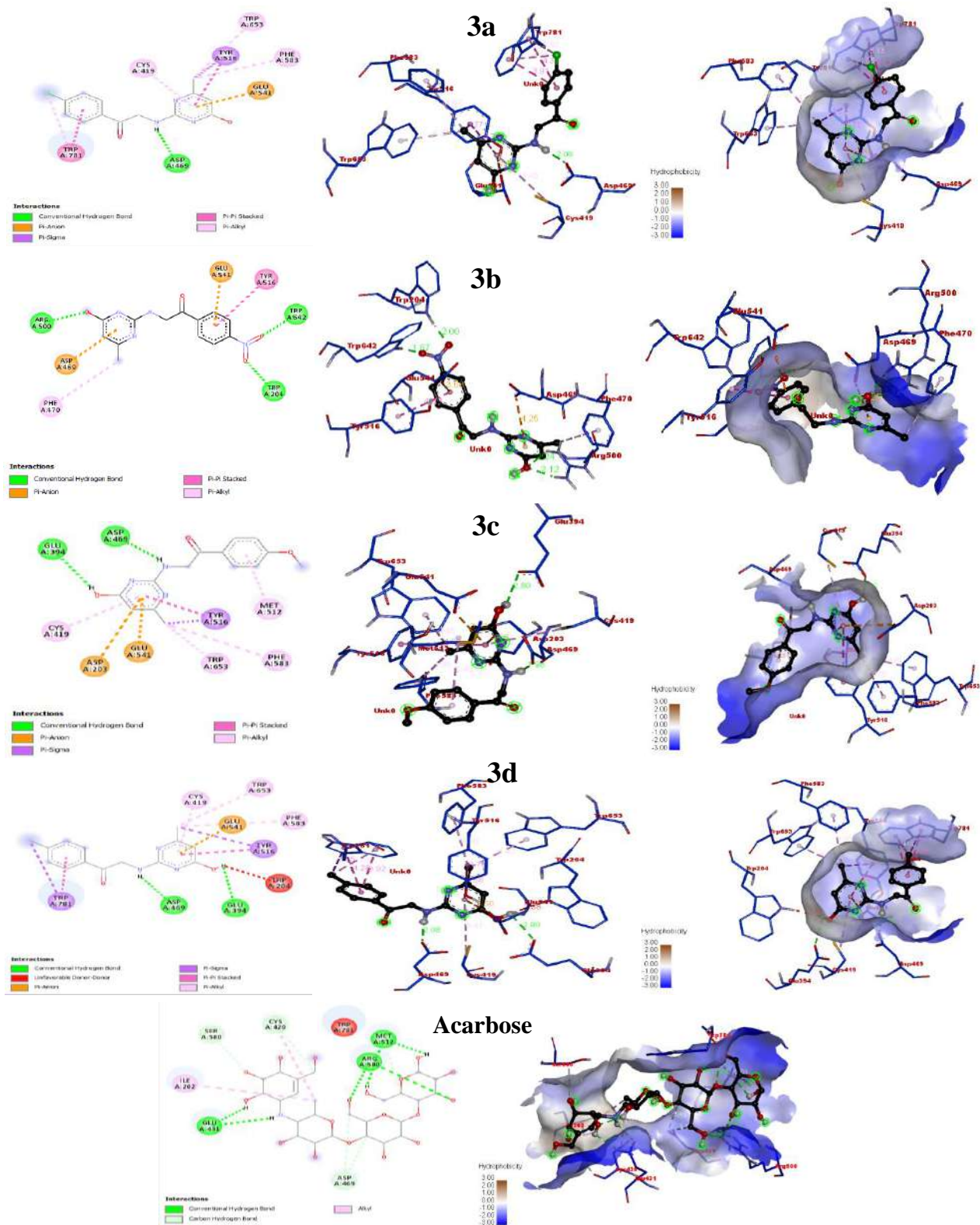


Fig. 5. 2D, 3D & hydrophobic representation of molecular interactions between exo-β-D-glucosaminidase with synthesized compounds **3(a-d)** and standard drug **Acarbose**.

7.5.5. *in silico* oral bioavailability assessment and ADME

Drug-likeness outline can be evaluated through parameters such as molecular weight, number of heavy atoms, hydrogen bond acceptors, hydrogen bond donors, rotatable bonds, molar refractivity and TPSA. These parameters were calculated for synthesized compounds **3(a-d)** and as tabulated in **Table 6**. The drug-likeness profiles were calculated based on Lipinski, Ghose, Veber, Egan and Muegge rules [39, 40].

Drug-likeness table indicated that, all the synthesized compounds showed a bioactivity score of 55 %. Hence, the compounds obeyed all the five rules without any violations of good bioavailability. The synthetic accessibility score is in the range of 2.19 to 2.37 which indicates that, the compounds do not have complex synthetic routes (**Table 7**).

From the results of lipophilicity parameters, consensus log Po/w and log S values indicated that, compounds are soluble in non-aqueous and aqueous medium (if log S < -10: poorly soluble, < -6: moderately soluble, < -4: soluble, < -2: very soluble, and < 0: highly soluble). Our obtained compounds in the range of -3.07 to -3.62, therefore compounds were soluble in nature (**Table 8**).

Absorption, skin permeation, distribution, metabolism and excretion parameters were predicted for obtained compounds and results indicates that, the compounds have high GI absorption with no blood-brain permeant. Therefore, there is no possibility of causing harmful toxicants in the brain and bloodstream. Due to the presence of negative log Kp values, compounds are less skin permeable (**Table 9**).

Metabolism parameters suggested that, the synthesized compounds **3(a-d)** were found to be non-substrate or non-inhibitor of permeability glycoprotein (P-gp), CYP2C19, CYP2C9, CYP2D6 and CYP3A4 inhibitors. Hence, all compounds were found to be substrate of CYP1A2 inhibitor and data was tabulated in **Table 10**.

Table 6. Physicochemical properties of the synthesized compounds **3(a-d)**.

Compd.	Mol. Formula	Molecular Weight	No. Heavy atoms	HBA	HBD	Rotatable bonds	Fraction Csp3	Molar Refractivity	TPSA in Å ²
3a	C ₁₃ H ₁₂ ClN ₃ O ₂	277.71	19	4	2	4	0.15	73.05	75.11
3b	C ₁₃ H ₁₂ N ₄ O ₄	288.26	21	6	2	5	0.15	76.86	120.93
3c	C ₁₄ H ₁₅ N ₃ O ₃	273.29	20	5	2	5	0.21	74.53	84.34
3d	C ₁₄ H ₁₅ N ₃ O ₂	257.29	19	4	2	4	0.21	73.01	75.11

Table 7. Drug likeness, bioactivity and synthetic accessibility score of the synthesized compounds **3(a-d)**.

Compd.	Lipinski	Ghose	Veber	Egan	Muegge	Bioactivity Score	Synthetic accessibility
3a	Yes	Yes	Yes	Yes	Yes	0.55	2.19
3b	Yes	Yes	Yes	Yes	Yes	0.55	2.37
3c	Yes	Yes	Yes	Yes	Yes	0.55	2.27
3d	Yes	Yes	Yes	Yes	Yes	0.55	2.27

Table 8. Predicted lipophilicity parameters of the synthesized compounds **3(a-d)**.

Compd.	Consensus Log Po/w	Consensus Log S	Solubility Class
3a	2.29	-3.62	Soluble
3b	0.99	-3.07	Soluble
3c	1.76	-3.08	Soluble
3d	2.07	-3.32	Soluble

Table 9. Predicted absorption & distribution parameters of the compounds **3(a-d)**.

Compd.	GI absorption	BBB permeant	Log Kp (cm/s)
3a	High	Yes	-5.91
3b	High	No	-6.54
3c	High	No	-6.35
3d	High	Yes	-5.97

Table 10. Predicted metabolism parameters of the synthesized compounds **3(a-d)**.

Compd.	P-gp	CYP1A2 inhibitor	CYP2C19 inhibitor	CYP2C9 inhibitor	CYP2D6 inhibitor	CYP3A4 inhibitor
3a	No	Yes	No	No	No	No
3b	No	Yes	No	No	No	No
3c	No	Yes	No	No	No	No
3d	No	Yes	No	No	No	No

7.6. Conclusion

In summary, we have reported a some new 2-[(4-hydroxy-6-methylpyrimidin-2-yl)amino]-1-(4-substituted)ethanone derivatives **3(a-d)** and evaluation of antibacterial, anti-diabetic and *in silico* investigations. Antibacterial activity results suggested that, the compound **3d** exhibited highest zone of inhibition of 16 ± 0.17 , 16 ± 0.45 , 15 ± 0.79 & 15 ± 0.74 mm against *P. aeruginosa*, *E. coli*, *Shigella* & *Salmonella* respectively. Anti-diabetic activity results disclosed that, **3c** exhibited least IC_{50} value of 29.19 ± 2.20 $\mu\text{g/mL}$ for α -amylase assay and compounds **3c** & **3d** shows least IC_{50} values of 23.33 ± 0.48 & 24.75 ± 0.16 $\mu\text{g/mL}$ for α -glucosidase assay. *In silico* molecular docking results suggested that, **3d** & **3c** compounds exhibits least binding energy of -7.6 & -7.5 kcal/mol for DNA gyrase and $\text{exo-}\beta\text{-D}$ -glucosaminidase proteins respectively. ADME profiles explained that, our synthesized compounds obeyed all five rules, high GI absorption, no blood-brain barrier and less skin permeant.

7.7. References

1. G. Brugnattelli, "Sopra i cangiamenti che avvengono nell' ossiurico (ac. urico) trattato coll' ossissettonoso (ac. nitroso)" 2nd series, **1818**, 1, 117-129.
2. O.M. Ighodaro, A.M. Adeosun, O.A. Akinloye, *Medicina*, **2017**, 53, 365-374.
3. M.D. Hill, M. Movassaghi, *Chem. Eur. J.*, **2008**, 14, 6836-6844.
4. K. Oukoloff, B. Lucero, K.R. Francisco, K.R. Brunden, C. Ballatore, *Eur. J. Med. Chem.*, **2019**, 165, 332-346.
5. M. Kidwai, S. Saxena, S. Rastogi, R. Venkataramanan, *Sci. World J.*, **2003**, 2, 269-286.
6. K. Upendranath, T. Venkatesh, M. Shashank, G. Nagaraju, K.M. Pasha, *J. Mol. Struct.*, **2022**, 1250, 1-13.
7. S. Achelle & C. Baudequin, *Targets Heterocycl. Syst.*, **2013**, 17, 1-34.
8. V.D. Suryawanshi, A.H. Gore, P.R. Dongare, P.V. Anbhule, S.R. Patil, G.B. Kolekar, *Spectrochim. Acta A Mol. Biomol. Spectrosc.*, **2013**, 114, 681-686.
9. R. Komatsu, H. Sasabe, J. Kido, *J. Photonics Energy*, **2018**, 8, 1-18.
10. T. Venkatesh, Y.D. Bodke and S.J. Aditya Rao, *Chem. Data Collect.*, **2020**, 25, 1-13.
11. S. Triloknadh, C.V. Rao, K. Nagaraju, N.H. Krishna, C.V. Ramaiah, W. Rajendra, Y. Suneetha, *Bioorg. Med. Chem. Lett.*, **2018**, 28, 1663-1669.
12. D. Kang, H. Zhang, Z. Wang, T. Zhao, T. Ginex, F.J. Luque, X. Liu, *J. Med. Chem.*, **2019**, 62, 1484-1501.
13. W. Wu, M. Chen, R. Wang, H. Tu, M. Yang, G. Ouyang, *Chem. Pap.*, **2019**, 73, 719-729.
14. S.S. Maurya, A. Bahuguna, S.I. Khan, D. Kumar, R. Kholiya, D.S. Rawat, *Eur. J. Med. Chem.*, **2019**, 162, 277-289.
15. B. Huang, D. Kang, Y. Tian, D. Daelemans, E. De Clercq, C. Pannecouque, X. Liu, *Chem. Biol. Drug Des.*, **2021**, 97, 67-76.
16. P. Modi, S. Patel, M. Chhabria, *Bioorg. Chem.*, **2019**, 87, 240-251.
17. K. Thirumurugan, S. Lakshmanan, D. Govindaraj, D.S.D. Prabu, N. Ramalakshmi, S.A. Antony, *J. Mol. Struct.*, **2018**, 1171, 541-550.
18. B.N. Reddy, R.R. Ruddaraju, G. Kiran, M. Pathak, A.R.N. Reddy, *ChemistrySelect*, **2019**, 4, 10072-10078.
19. R. Frey, N. Wishart, *J. Med. Chem.*, **2005**, 48, 6066-6083.
20. G.J. Reddy, S. Sailaja, K. Srinivasa Rao, *Indian J. Chem.*, **2005**, 44B, 204-206.

21. A.M. Farghaly, O.M. Aboul Wafa, Y.A. Elshaier, W.A. Badawi, H.H. Haridy, H.A. Mubarak, *Med. Chem. Res.*, **2019**, 28, 360-379.
22. R.H. Vekariya, K.D. Patel, N.P. Prajapati, H.D. Patel, *Synth. Commun.*, **2018**, 48, 1505-1533.
23. Q. Jiang, W. Sheng, C. Guo, *Green Chem.*, **2013**, 15, 2175-2179.
24. A.W. Erian, S.M. Sherif, H.M. Gaber, *Molecules*, **2003**, 8, 793-865.
25. M. Saleh, S. Abbott, V. Perron, C. Lauzon, C. Penney, B. Zacharie, *Bioorg. Med. Chem. Lett.*, **2010**, 20, 945-949.
26. D. Sanglard, & F.C. Odds, *Lancet Infect. Dis.*, **2002**, 2, 73-85.
27. A.M. Qandil, L.I. Fakhouri, *Pharmaceuticals*, **2012**, 5, 591-612.
28. S. Chitra, N. Paul, S. Muthusubramanian, P. Manisankar, P. Yogeewari, D. Sriram, *Eur. J. Med. Chem.*, **2011**, 46, 4897-4903.
29. K.L. Manasa, Y. Tangella, N.H. Krishna, M. Alvala, *Beilstein J. Org. Chem.*, **2019**, 15, 1864-1871.
30. G.K. Gupta, V. Saini, R. Khare, V. Kumar, *Med. Chem. Res.*, **2014**, 23, 4209-4220.
31. J. Ramprasad, N. Nayak, U. Dalimba, P. Yogeewari, D. Sriram, S.K. Peethambar, H.S. Kumar, *Eur. J. Med. Chem.*, **2015**, 95, 49-63.
32. M. Staniszevska, L. Kuryk, A. Gryciuk, J. Kawalec, M. Rogalska, J. Baran, A. Kowalkowska, *Molecules*, **2021**, 26, 1-19.
33. B. Manjunatha, Y.D. Bodke, H.M. Kumaraswamy, K.M. Pasha, N. Prashanth, *J. Mol. Struct.*, **2022**, 1254, 1-12.
34. S. Banoth, S. Perugu, S. Boda, *J. Heterocycl. Chem.*, **2018**, 55, 709-715.
35. O. Trott, A.J. Olson, *J. Comput. Chem.*, **2010**, 31, 455-461.
36. S.J. Aditya Rao, C.K. Ramesh, S. Raghavendra, M. Paramesha, *Curr. Comput. Aided Drug Des.*, **2020**, 16, 231-237.
37. K. Paulrasu, A. Duraikannu, M. Palrasu, A. Shanmugasundaram, M. Kuppusamy, B. Thirunavukkarasu, *Org. Biomol. Chem.*, **2014**, 12, 5911-5921.
38. R.S. Cheke, V.M. Patil, S.D. Firke, J.P. Ambhore, I.A. Ansari, H.M. Patel, M. Snoussi, *Pharmaceut.*, **2022**, 15, 272-280.
39. C.A. Lipinski, *Drug Discov. Today Technol.*, **2004**, 1, 337-341.
40. I. Muegge, *Med. Res. Rev.*, **2003**, 23, 302-321.

List of papers published/communicated

1. Efficient L-Proline catalyzed synthesis of some new (4-substituted-phenyl)-1,5-dihydro-2*H*-pyrimido[4,5-*d*][1,3]thiazolo[3,2*a*]-pyrimidine-2,4(3*H*)-diones bearing thiazolopyrimidine derivatives and evaluation of their pharmacological activities, *Journal of Molecular Structure*, 1247 (2021) 1-13, <https://doi.org/10.1016/j.molstruc.2021.131324>.

S.H. Sukanya, Talavara Venkatesh*, S.J. Aditya Rao, Muthipeedika Nibin Joy.

2. Facile TiO₂ NPs catalysed synthesis of substituted-4-hydroxy/methoxy benzylidene derivatives as potent antioxidant and anti-tubercular agents, *Chemical Data Collections*, 33 (2021) 1-16, <https://doi.org/10.1016/j.cdc.2021.100713>.

S.H. Sukanya, Talavara Venkatesh*, S.R. Kumar, Y.D. Bodke.

3. Facile synthesis of some 5-(3-substituted-thiophene)-pyrimidine derivatives and their pharmacological and computational studies, *Chimica Techno Acta*, 8 (2021) 1-13, <https://doi.org/10.15826/chimtech.2021.8.4.01>.

S.H. Sukanya, Talavara Venkatesh*, S.J. Aditya Rao, N. Shivakumara, Muthipeedika Nibin Joy.

4. An efficient *p*-TSA catalyzed synthesis of some new substituted-(5-hydroxy-3-phenylisoxazol-4-yl)-1,3-dimethyl-1*H*-chromeno[2,3-*d*]pyrimidine-2,4(3*H*,5*H*)-dione/3,3-dimethyl-2*H*-xanthen-1(9*H*)-one scaffolds and evaluation of their pharmacological and computational investigations, *Journal of Molecular Structure*, 1267 (2022) 133587, <https://doi.org/10.1016/j.molstruc.2022.133587>.

S.H. Sukanya, Talavara Venkatesh*, S.J. Aditya Rao, Anup Pandith.

5. Synthesis, *in-vitro* evaluation and docking studies of novel 6-amino-4-substituted-pyrano[3,2-*d*]isoxazole-5-carbonitrile derivatives as potential anti-diabetic and anticancer agents. *Pharmaceutical Chemistry Journal* (Under review).

S.H. Sukanya, Talavara Venkatesh*, K. Upendranath, H. Shanavaz, O. Nagaraj.

6. Synthesis, *in-vitro* and *in-silico* studies of novel 5-[3-(4-chlorophenyl)-substituted-6-hydroxypyrimidine-2,4(1*H*,3*H*)-dione derivatives as potential anti-diabetic and anticancer agents. *Structural Chemistry* (Communicated).

S.H. Sukanya, Talavara Venkatesh*, K. Upendranath, H. Shanavaz.

7. Synthesis, characterization, *in-vitro* and *in-silico* investigation of novel 5-[3-(4-chlorophenyl)-substituted-1,3-dimethylpyrimidine-2,4,6(1*H*,3*H*,5*H*)-trione derivatives as potential anti-diabetic and anticancer agents. *Journal of Molecular Structure* (Communicated).

S.H. Sukanya, Talavara Venkatesh*, K. Upendranath, H. Shanavaz.

8. Synthesis, characterization and biological evaluation of some new 2-[(4-hydroxy-6-methylpyrimidin-2-yl)amino]-1-(4-substituted)ethanone derivatives. *Chemistryselect* (Communicated).

S.H. Sukanya, Talavara Venkatesh*, H. Shanavaz.

Articles (Co-Author)

1. Synthesis of some new substituted 5-phenyl-3,4-dihydro-1*H*,2*H*-3,4-bipyrazole derivatives and evaluation for their biological activities, *Chemical Data Collections*, 42 (2022) 100952, <https://doi.org/10.1016/j.cdc.2022.100952>.

R.S. Priya Rani, Talavara Venkatesh*, **S.H. Sukanya**, K. Upendranath, N.D. Satyanarayan.

2. Facile synthesis and *in-vitro* cytotoxicity study of some 5-(4-substituted phenyl)-7-hydroxy-9-methyl-2-thioxo-2,3-dihydro-1*H*-dipyrimido[1,2-*a*:4',5'-*d*]pyrimidin-4(5*H*)-one derivatives and their Optoelectronic, DFT and LFPs applications. *Journal of Molecular Structure* (Under Revision).

K. Upendranath, Talavara Venkatesh*, **S.H. Sukanya**, H. Shanavaz.

Paper presented at National/International Conferences

1. “TiO₂ NPs catalyzed Knoevenagel condensation of synthesis of substituted-4-hydroxy/methoxy benzylidene derivatives and evaluation of their pharmacological activities” in Two day’s International Webinar on “*Current trends and alternative approaches to target COVID-19*” Organized by the Department of Chemistry in Co-ordination with IQAC, held at Sahyadri Science College, Shivamogga on 7th & 8th August 2021. **(Poster presentation)**

S.H. Sukanya, Talavara Venkatesh*

2. “An efficient *p*-TSA catalyzed synthesis of some new isoxazole scaffolds and their biological and molecular modeling studies” in “*40th Annual National conference of Indian Council of Chemists held at Department of Chemistry, Satavahana University, Karimnagar (T.S.)*” on 29th & 30th December 2021 in Virtual Mode. **(Oral presentation)**

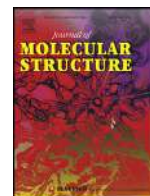
S.H. Sukanya, Talavara Venkatesh*

3. “An efficient H₂O₂: HCl catalyzed synthesis of some 5-(3-substituted-thiophene)-pyrimidine derivatives and its biological interest” in the two-day National conference on “*Impact of Chemistry and Biology to the Society and Industry*” (ICBSI-2022) held on 20th & 21st May 2022, at Dept. of Industrial Chemistry, Kuvempu University, Shankarghatta, Shivamogga, Karnataka. **(Poster presentation)**

S.H. Sukanya, Talavara Venkatesh*

4. “*International Webinar on Empowering Diversity in Science*” (GWB-2022) on 16th February 2022 organized by Department of Chemistry, Kamla Nehru Mahavidyalaya, Nagpur, Association of Chemistry Teachers (ACT) Mumbai.

S.H. Sukanya, Talavara Venkatesh*



Efficient L-Proline catalyzed synthesis of some new (4-substituted-phenyl)-1,5-dihydro-2H-pyrimido[4,5-d][1,3]thiazolo[3,2a]-pyrimidine-2,4(3H)-diones bearing thiazolopyrimidine derivatives and evaluation of their pharmacological activities

S.H. Sukanya^a, Talavara Venkatesh^{a,*}, S.J. Aditya Rao^{b,*}, Muthipeedika Nibin Joy^c

^a Department of PG Studies and Research in Chemistry, Jnanasahyadri, Kuvempu University, Shankaraghatta, Karnataka 577451, India

^b Plant Cell Biotechnology Department, CSIR-Central Food Technological Research Institute, Mysore, Karnataka 570020, India

^c Innovation Center for Chemical and Pharmaceutical Technologies, Institute of Chemical Technology, Ural Federal University, 19 Mira Street, Yekaterinburg 620002, Russia

ARTICLE INFO

Article history:

Received 21 June 2021

Revised 13 August 2021

Accepted 15 August 2021

Available online 17 August 2021

Keywords:

Thiazole-pyrimidine derivatives

Cytotoxicity

Anti-inflammatory

SAR

ADME-toxicology study

Molecular docking

ABSTRACT

In the present study, a simple and efficient protocol has been developed to synthesize a series of new (4-substituted-phenyl)-1,5-dihydro-2H-pyrimido[4,5-d][1,3]thiazolo[3,2a]-pyrimidine-2,4(3H)-dione derivatives (4a-g) through L-proline-catalyzed reaction of 2-amino-4-(4-substituted-phenyl)thiazole (1), substituted benzaldehyde (2), and barbituric/thiobarbituric acid (3) at a refluxed temperature in aqueous ethanol under mild and metal-free conditions. The obtained compounds were evaluated for *in vitro* cytotoxicity and anti-inflammatory effects. The *in silico* docking studies provided the probable interactions of synthesized compounds with P38 MAP kinase and MMP-9 proteins. The structures of all the synthesized compounds were confirmed using analytical and spectroscopic techniques. The *in vitro* cytotoxicity studies revealed the potential cytotoxic effects of the compounds 4f and 4g. The anti-inflammatory studies suggested the prominent anti-inflammatory effects of the compounds 4a and 4g. The SAR studies showed the importance of electron-withdrawing groups in enhancing the potency among the tested compounds. The results of *in silico* studies supported our findings from *in vitro* analysis in terms of drug-likeness of the synthesized compounds and their effective interactions with P38 MAP kinase and MMP-9 proteins envisaging their use as prominent therapeutic agents.

© 2021 Elsevier B.V. All rights reserved.

1. Introduction

Multicomponent one-step reactions (MCRs) are upstanding as a valuable tool for synthesizing polyfunctional molecules with high competence over multistep synthesis. Globally, it has been explored as an efficient tool for preparing several active drugs [1]. MCRs offer many advantages as they avoid unnecessary expensive purification, high atom economy, toxic reagents, and solvents consumption [2].

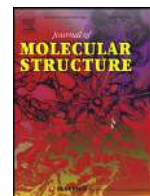
Proline is a bifunctional chiral homogenous organocatalyst that is cost-effective, efficient, and readily available than any other catalyst [3]. L-Proline has both acidic (–COOH) and basic (–NH) functionality and catalyzes chemical transformations similar to enzyme

catalysis [4]. It is efficient in catalyzing various organic transformations [5], Knoevenagel-type condensation [6], Biginelli reaction [7], Mannich [8], Michael [9], Diels-Alder [10], α -amination reaction [11] and asymmetric Hantzsch reaction [12].

Heterocyclic compounds, mainly polyfunctionalized heterocycles (PFHs), are widespread in bioactive natural compounds and marketed pharmaceuticals, food and paints, agrochemicals, dyes and pigments, electrochemicals, optoelectronic, fluorescence sensors, and many other application-oriented resources [13–15]. Therefore, investigations on the synthesis of PFHs have received particular attention. Among the privileged class of various heterocyclic compounds, thiazole and pyrimidine are key moieties in medicinal chemistry. The significant pharmacological potential of these molecules includes antimicrobial, antioxidant, anti-tubercular, anti-inflammatory, antiviral, and anticancer properties [16,17].

* Corresponding author.

E-mail addresses: venkateshatalwar@gmail.com (T. Venkatesh), adityaraosj@gmail.com (S.J. Aditya Rao).



An efficient *p*-TSA catalyzed synthesis of some new substituted-(5-hydroxy-3-phenylisoxazol-4-yl)-1,3-dimethyl-1*H*-chromeno[2,3-*d*]pyrimidine-2,4(3*H*,5*H*)-dione/3,3-dimethyl-2*H*-xanthen-1(9*H*)-one scaffolds and evaluation of their pharmacological and computational investigations

S H Sukanya^a, Talavara Venkatesh^{a,*}, S J Aditya Rao^b, Anup Pandith^{c,d}

^a Department of PG Studies and Research in Chemistry, Jnanasahyadri, Kuvempu University, Shankaraghatta, Karnataka 577451, India

^b Kimberlite chemicals India Pvt. Ltd, KIADB III Phase, Doddaballapur, Bangalore, Karnataka 561203, India

^c Department of Chemistry, Kyung Hee University, Seoul, South Korea

^d College of Biomedical Engineering, Taipei Medical University, Wuxing St, Xinyi, Taipei city 11031, Taiwan (R. O. C.)

ARTICLE INFO

Article history:

Received 9 December 2021

Revised 9 June 2022

Accepted 23 June 2022

Available online 25 June 2022

Keywords:

Isoxazole derivatives

Absorption

Cytotoxicity

Anti-TB

SAR

in silico molecular docking and

Computational study

ABSTRACT

We have developed an easy and efficient protocol for the synthesis of a series of some novel substituted-(5-hydroxy-3-phenylisoxazol-4-yl)-1,3-dimethyl-1*H*-chromeno[2,3-*d*]pyrimidine-2,4(3*H*,5*H*)-dione/3,3-dimethyl-2*H*-xanthen-1(9*H*)-one derivatives (4a–j) via *p*-TSA catalyzed reaction of 1,3-dimethylbarbituric acid/dimedone, substituted salicylaldehyde/2-hydroxy-nepthaldehyde and 3-phenyl-5-isoxazolone was administered in refluxed temperature in the presence of aqueous ethanol. All the obtained compounds were evaluated for their therapeutic effect using pharmacological and computational investigations, and structures were confirmed using analytical and spectroscopic techniques. Absorption spectra were recorded in six different solvents such as polar protic, polar aprotic, and nonpolar solvents, λ_{\max} of all the compounds are appeared at bathochromic shift towards the longer wavelength due to the π - π^* & n - π^* transitions. The results of pharmacological investigations revealed that the compounds 4c, 4e, and 4h possess excellent cytotoxicity efficacy, and compounds 4c, 4d, 4h, and 4i have shown better anti-TB efficiency. The SAR study shows the importance of the electron-withdrawing group and additional phenyl nucleus enhancing the biological potency of the compounds. The results of the *in silico* molecular docking studies revealed that the compounds 4c and 4h effectively interacted with P38 MAP kinase (-10.9 kcal/mol) and InhA-Enoyl-Acyl Carrier Protein Reductase (-11.0 kcal/mol), respectively. Further, the molecular dynamics (MD) simulation studies revealed that the compounds 4c and 4h stabilized the macromolecular structures in terms of RMSD, RMSF, the Radius of gyration, and SASA compared to their unbound and standard compound bound structures. DFT study suggested that the compounds are chemically and biologically more reactive due to less energy gap.

© 2022 Elsevier B.V. All rights reserved.

1. Introduction

Multi-component reactions (MCRs) afford an exceptionally valuable tool within the field of synthetic chemistry, also as medicinal chemistry. These reactions are characterized by their convergence, simplicity of implementation, high yield, effectiveness, reducing waste, and atom economy. Insight of increasing knowledge within the synthesis of fused heterocyclic compounds. The progress of the

latest and unnaturally valuable multi-component reactions remains a challenge along with academic and industrial research [1–4].

Previous reports revealed that isoxazole is an important heterocyclic nucleus, commonly found in various pharmacologically active natural products, clinical drugs, and lead compounds [5]. Isoxazole derivatives are paid attention in the development of heterocyclic chemistry due to their broad spectrum of biological activities such as antimicrobial [6], anticancer [7], anti-HIV [8], anti-tuberculosis [9], anti-inflammatory [10], neuroprotective [11], anti-diabetic [12] and antidepressant activities [13]. On the other hand, isoxazole and its derivatives have also been recognized as important and useful synthons in organic synthesis [14,15] and as organic materials in optoelectronics [16,17]. Because of its

* Corresponding author.

E-mail address: venkateshatalwar@gmail.com (T. Venkatesh).



Contents lists available at ScienceDirect

Chemical Data Collections

journal homepage: www.elsevier.com/locate/cdc

Data Article

Facile TiO₂ NPs catalysed synthesis of substituted-4-Hydroxy/methoxy benzylidene derivatives as potent antioxidant and anti-tubercular agents

S.H. Sukanya^a, Talavara Venkatesh^{a,*}, Ravi Kumar S^b, Yadav D. Bodke^a^a Department of P.G. Studies and Research in Chemistry, Jnanasahyadri, Kuvempu University, Shankaraghatta, 577451, Karnataka, India^b Department of P.G. Studies and Research in Biotechnology, Jnanasahyadri, Kuvempu University, Shankaraghatta, 577451, Karnataka, India

ARTICLE INFO

Article history:

Received 30 March 2021

Revised 30 April 2021

Accepted 1 May 2021

Available online 7 May 2021

Keywords:

TiO₂ NPs

Knoevenagel condensation

Antioxidant activity

Anti-tubercular activity

Molecular docking study

ABSTRACT

In this work, we report a facile synthesis of a series of substituted-4-hydroxy/methoxy benzylidene derivatives (**3a-i**) via Knoevenagel condensation reaction of different active methylene compounds (**1**) with 4-hydroxy/methoxy benzaldehyde (**2**) under reflux condition in aq. EtOH using catalytic amount of TiO₂ NPs. The structures of all the obtained compounds were confirmed by analytical and spectroscopic methods and screened for their antioxidant and anti-tubercular activities. Antioxidant activity results revealed that, the compound **3e** with IC₅₀ value 105.48 µg/mL showed very effective DPPH scavenging activity and compound **3h** with IC₅₀ value 129.72 µg/mL exhibited most effective nitric oxide radical scavenging activity compared to the reference standard BHT and ascorbic acid respectively. From the results of anti-TB activity, compound **3b** displayed a more sensitivity at 25 µg/mL. Furthermore, synthesized compounds were assessed for molecular docking studies on the target enzymes Human peroxiredoxin 5 and enoyl-ACP reductase and they were emerged has an active antioxidant and anti-TB agents with least binding energy -5.8 and -8.0 kJ mol⁻¹ respectively.

© 2021 Elsevier B.V. All rights reserved.


Specifications Table

Subject area	Bioorganic Chemistry,
Compounds	Substituted-4-hydroxy/methoxy benzylidene derivatives
Data category	Spectral and Biological data
Data acquisition format	UV-visible, IR, NMR and Mass spectra
Data type	Analysed
Procedure	Series of substituted-4-hydroxy/methoxy benzylidene derivatives were synthesized through Knoevenagel reaction in presence of TiO ₂ NPs and characterized by spectroscopic analysis. Compounds were screened for their biological study.

* Corresponding author:

E-mail address: venkateshatalwar@gmail.com (T. Venkatesh).

Facile synthesis of some 5-(3-substituted-thiophene)-pyrimidine derivatives and their pharmacological and computational studies

S.H. Sukanya ^a, Talavara Venkatesh ^{a*} , S.J. Aditya Rao ^b, N. Shivakumara ^c, Muthipeedika Nibin Joy ^d

- a: Department of P.G. Studies and Research in Chemistry, Jnanasahyadri, Kuvempu University, Shankaraghatta 577451, Karnataka, India
b: Plant Cell Biotechnology Department, CSIR-Central Food Technological Research Institute, Mysore 570020, Karnataka, India
c: Department of Chemistry, Ramaiah Institute of Technology, Bangalore 560054, India
d: Innovation Center for Chemical and Pharmaceutical Technologies, Institute of Chemical Technology, Ural Federal University, 19 Mira St., Yekaterinburg 620002, Russia
* Corresponding author: venkateshatalwar@gmail.com

This article belongs to the regular issue.

© 2021, The Authors. This article is published in open access form under the terms and conditions of the Creative Commons Attribution (CC BY) license (<http://creativecommons.org/licenses/by/4.0/>).



Abstract

A series of 5-(3-substituted-thiophene)-pyrimidine derivatives (**3a-d**) were synthesized *via* Knoevenagel condensation reaction in aqueous ethanol using H₂O₂:HCl as a catalyst. Their pharmacological effects were evaluated. Analytical and spectroscopic methods confirmed the structures of the target molecules. The antibacterial activity studies revealed that compounds **3b** and **3d** exhibited the most effective zone of inhibition against bacterial strains *E. coli* and *S. aureus*, respectively. The *in vitro* cytotoxicity was carried out by MTT assay against MCF-7 cell line. The results showed the excellent selectivity for all four compounds, among which the compound **3a** exhibited remarkable cytotoxicity with a minimum cell viability range of 23.68 to 44.16%. The interaction of compounds with calf thymus DNA was determined using UV-absorption spectroscopy. The results confirmed that all the synthesized compounds interacted strongly with CT DNA through electrostatic or groove binding. *In silico* ADME-toxicology studies indicated that all the molecules under investigation are non-toxic with good oral bioavailability. The drug-likeness score indicated that they are suitable as drug-leads. *In silico* molecular docking the specified compound **3b** binds with GlcN-6-P and P38 MAPk with a minimum binding energy of -7.9 and -6.4 kcal/mol, respectively. DFT study demonstrated that the compound **3d** was chemically and biologically more reactive due to less energy gap.

Keywords

biological studies
DNA binding
ADME-toxicology study
SAR study
molecular docking and DFT studies

Received: 02.09.2021

Revised: 11.10.2021

Accepted: 12.10.2021

Available online: 15.10.2021

1. Introduction

Heterocyclic compounds play a predominant role in medicinal chemistry and synthetic organic chemistry due to their massive biological importance. The synthesis of nitrogen and sulphur containing fused heterocyclic compounds with multi-structures in one molecule has attracted the attention of medicinal chemists and researchers due to their multifaceted pharmacological activities [1-2]. Among them, pyrimidine and thiophene have been recognized as key scaffolds owing to their important biological

significances and interesting therapeutic properties including anti-tubercular [3], anticancer [4], anti-HIV [5], antibacterial [6], antifungal [7], antitumor [8], also used as potent EGFR inhibitor [9, 10], protein kinase inhibitors [11-14] and 5-HT₇ receptors [15].

Moreover, the heterocyclic compounds increase the strength of the molecules by forming hydrogen bonds with DNA. Hence, the interactive study of heterocyclic moieties with DNA is essential for estimating their anticancer activity and elucidates the viable mechanism of their action. Therefore, DNA binding is considered as an essential ex-

Document Information

Analyzed document	KU-RTH-CHE-SUKANYA-SH-22.pdf (D149206433)
Submitted	11/10/2022 6:41:00 AM
Submitted by	Walmiki R H
Submitter email	walmiki_rh@rediffmail.com
Similarity	6%
Analysis address	walmiki_rh.kuvempu@analysis.arkund.com

Sources included in the report

SA	Bharathiar University, Coimbatore / Bharathi. R.pdf Document Bharathi. R.pdf (D120908344) Submitted by: rspani1967@gmail.com Receiver: rspani1967.bhauhi@analysis.arkund.com	25
SA	Kishore thesis-Dr. G. Brahmeshwari , ku.pdf Document Kishore thesis-Dr. G. Brahmeshwari , ku.pdf (D141849908)	6
SA	Kuvempu University, Jnanasahyadri / KU-TH-IC-TALAVARA-17.pdf Document KU-TH-IC-TALAVARA-17.pdf (D29333890) Submitted by: walmiki_rh@rediffmail.com Receiver: walmiki_rh.kuvempu@analysis.arkund.com	23
SA	Chitkara University, Patiala / An appraisal on synthetic and medicinal aspects of Pyrimidines as anti neoplastic agents (Autosaved).docx Document An appraisal on synthetic and medicinal aspects of Pyrimidines as anti neoplastic agents (Autosaved).docx (D110789167) Submitted by: anju.goyal@chitkara.edu.in Receiver: anju.goyal.chitka@analysis.arkund.com	1
SA	Bharathiar University, Coimbatore / Kulandai Therese. S.docx Document Kulandai Therese. S.docx (D35949595) Submitted by: bulib_librarian@yahoo.co.in Receiver: bulib_librarian.bhauni@analysis.arkund.com	8
SA	Kuvempu University, Jnanasahyadri / KU-RTH-IC-NAGARAJ-O-21.pdf Document KU-RTH-IC-NAGARAJ-O-21.pdf (D109830991) Submitted by: walmiki_rh@rediffmail.com Receiver: walmiki_rh.kuvempu@analysis.arkund.com	16
SA	Doctor Harisingh Gour Vishwavidyalaya, Sagar / THESIS.docx Document THESIS.docx (D18674122) Submitted by: anuragmlis@gmail.com Receiver: anuragmlis.dhgsu@analysis.arkund.com	2
SA	Kuvempu University, Jnanasahyadri / KU-TH-CHE-MANJUNATHA-B-22.pdf Document KU-TH-CHE-MANJUNATHA-B-22.pdf (D145684138) Submitted by: walmiki_rh@rediffmail.com Receiver: walmiki_rh.kuvempu@analysis.arkund.com	9

LIBRARIAN
KUVEMPU UNIVERSITY
Jnana Sahyadri
Shankaragatta-577 451

KUVEMPU  **UNIVERSITY**

Department of P.G. Studies and Research in Chemistry,
Jnanasahyadri, Shankaraghatta-577451

Thesis submitted to the Faculty of Science, Kuvempu University

For the award of

DOCTOR OF PHILOSOPHY IN CHEMISTRY

**“Synthesis and biological evaluation of some new
heterocyclic compounds containing Nitrogen and Oxygen
atoms”**

Submitted by

Ms. Sukanya S.H. M.Sc.

Research Scholar

Department of P.G. Studies and Research in Chemistry,
Kuvempu University, Jnanasahyadri,
Shankaraghatta-577451

Under the guidance of

Dr. Talavara Venkatesh M.Sc., Ph.D.

Assistant Professor

Department of P.G. Studies and Research in Chemistry,
Kuvempu University, Jnanasahyadri,
Shankaraghatta-577451

2022

“Individual chapters need to be referred for conclusion”